Topics in Organometallic Chemistry 59

Philippe Kalck *Editor*

Homo- and Heterobimetallic Complexes in Catalysis

Cooperative Catalysis

Springer

59
Topics in Organometallic Chemistry

Aims and Scope

The series *Topics in Organometallic Chemistry* presents critical overviews of research results in organometallic chemistry. As our understanding of organometallic structure, properties and mechanisms increases, new ways are opened for the design of organometallic compounds and reactions tailored to the needs of such diverse areas as organic synthesis, medical research, biology and materials science. Thus the scope of coverage includes a broad range of topics of pure and applied organometallic chemistry, where new breakthroughs are being achieved that are of significance to a larger scientific audience.

The individual volumes of *Topics in Organometallic Chemistry* are thematic. Review articles are generally invited by the volume editors. All chapters from Topics in Organometallic Chemistry are published OnlineFirst with an individual DOI. In references, Topics in Organometallic Chemistry is abbreviated as Top Organomet Chem and cited as a journal.

More information about this series at http://www.springer.com/series/3418

Philippe Kalck
Editor

Homo- and Heterobimetallic Complexes in Catalysis

Cooperative Catalysis

With contributions by

J.K. Bera · E. Bodio · I. Dutta · R.G. Fernando · L. Gan · M. Garland · C.D. Gasery · M. Iglesias · D. Jennings · A.K. Jones · J. Laureanti · P. Le Gendre · B.A. Messerle · M.D. Moulis · L.A. Oro · M.J. Page · M. Picquet · G. Sengupta · E. Sola · G.G. Stanley · D.B. Walker

Springer

Editor
Philippe Kalck
Equipe C “Catalyse et Chimie Fine”
Laboratoire de Chimie de Coordination du CNRS
Toulouse Cedex
France

ISSN 1436-6002 ISSN 1616-8534 (electronic)
Topics in Organometallic Chemistry
ISBN 978-3-319-34182-8 ISBN 978-3-319-34184-2 (eBook)
DOI 10.1007/978-3-319-34184-2

Library of Congress Control Number: 2016941598

Printed on acid-free paper

This Springer imprint is published by Springer Nature
The registered company is Springer International Publishing AG Switzerland

Preface

Καταλυσις, as coined by Berzelius in an 1835 report to the Swedish Academy of Sciences, concerns the capacity of a substance to start a reaction without taking part in it and not being consumed.[1] After many studies and interpretations, Ostwald in 1894 stated that the exclusive role of the catalyst is to accelerate the reaction rate, and in 1901, one year before patenting the process for the production of nitric oxide by catalytic oxidation of ammonia, he gave this definition: "A catalyst is a substance that alters a chemical reaction rate without being part of the final products." In the "Institut de Chimie" created in 1906 in Toulouse by Paul Sabatier, we can mention the analysis of Senderens and Sabatier that nickel, and more generally a catalyst, gives the origin of a true chemical reaction.[2] Their discovery from 1902 of the methanation process from CO_2 and H_2, known as the *Sabatier process*, is still used in space stations to recycle CO_2 and mainly to produce water.[3]

$$CO_2 + 4\ H_2 \rightarrow CH_4 + H_2O/\text{finely divided nickel},\ 300^{\circ}C$$

Today we know that a catalyst decreases the activation energy not only of the reaction but also of each step. Thus it is possible by adjusting the catalyst composition to follow preferentially a chemical pathway in order to combine a high activity (measured by the turnover frequency), a complete chemoselectivity to obtain only one product, a great regioselectivity to have a privileged access to an isomer, and in many cases an important enantioselectivity to favor one enantiomer or diastereoisomer. Moreover, it is important to have a long-lived catalyst, which is

[1] S. Califano, Pathways to Modern Chemical Physics, **2012**, Springer.

[2] P. Sabatier, J.-B. Senderens, Comptes Rendus Hebdomadaires de l'Académie des Sciences, **1897**, *124*, 616–618 and 1358–1361.

[3] P. Sabatier, J.-B. Senderens, Comptes Rendus Hebdomadaires de l'Académie des Sciences, **1902**, *134*, 514–516.

measured by the turnover number (TON), especially for industrial applications (up to 10^6–10^7!). Around 80% of the chemical products elaborated in the chemical industry are produced with at least one step involving a catalyst. For the more recent processes, 90% of the products are in contact with a catalyst during their elaboration. Indeed numerous compounds or intermediates for the efficient synthesis of pharmaceuticals, natural products, agrochemicals, fine chemicals, plastics, synthetic fibers, dyes, perfumes, etc.,[4] require the presence of a catalyst. In addition, the same statement prevails for the crude oil processing in petrochemistry and the purification of exhaust gas from automobiles or off-gas from many industrial plants.[5]

Among the three main catalytic domains, which include heterogeneous and homogeneous systems and biocatalysts, homogeneous transition metal complexes account for around 15%. Many organometallic complexes have been synthesized during the last years, and the various steps of a catalytic cycle are in many cases well understood. It is now possible to adjust the electronic effects of the ligands, as well as their steric hindrance, and to coordinate them to a metal center, most of the time a transition metal, in order to obtain good catalytic performances. Various in situ infrared and NMR studies, performed at the temperature and pressure of catalytic conditions, have allowed to identify all the steps and among them to discriminate the rate-determining step. In this *coordination catalysis* domain, the coordination sphere of the metal needs to be flexible enough in order to coordinate the substrates, to activate them, to induce the reaction between the appropriate activated fragments, and in time to eliminate the expected product and recover the active species. Mostly, this catalysis involves mononuclear complexes containing sophisticated ligands, adjusted with reacting fragments such as carbon monoxide, and hydride, alkyl, and acyl groups, to achieve the electron density at the right time (step) and at the right position.

In addition, dinuclear complexes have recently been shown to be an elegant way to manage these variations of electron flexibility along all the catalytic cycle, one metal center being able to produce the classical and expected activation of one reactant whereas the other center being able to provide the required flexibility. In some cases, the second metal complex is able to unblock a step in which the activation energy is too high, most of the time inducing the decoordination of a ligand.

Thus, this issue is especially dedicated to dinuclear (homo- as well as hetero-dinuclear complexes) entities which are clearly more active than the mononuclear counterparts and for which the dinuclear framework is maintained along all the catalytic cycle.

[4] F. Hartwig, Organotransition Metal Chemistry – From Bonding to Catalysis, 2010, University Science Books.

[5] H.-J. Arpe, Industrial Organic Chemistry, 5th Edition, **2010**, Wiley-VCH.

The first contribution from Georges G. Stanley and his group, entitled "Bimetallic Homogeneous Hydroformylation," shows that binuclear rhodium complexes bearing the tetraphosphine *rac-et,ph-P4* ligand are active hydroformylation catalysts when they are dicationic. Whereas in acetone their activity is somewhat short due to the fragmentation in monometallic less active species, in acetone/water mixtures these complexes are monocationic, making them far more resistant to fragmentation. Infrared, NMR studies, and DFT calculations are consistent with the prominent role of **15r** to coordinate the alkene, on the left d^8 Rh(I) metal center by substitution of a CO ligand, after the reductive elimination of the aldehyde from the right d^6 Rh(III) leading to **14r** with a Rh–H bond.

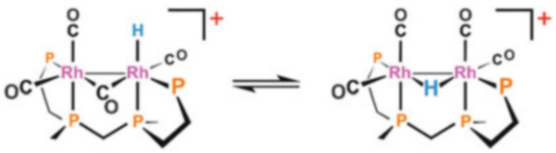

14r 15r

The second contribution from Luis A. Oro and co-workers "Binuclear Iridium Complexes in Catalysis" deals with the demonstration that the *trans*-influence of the ligands operates through the bridging ligands or intermetallic bonds and governs the reactivity of the diiridium framework.

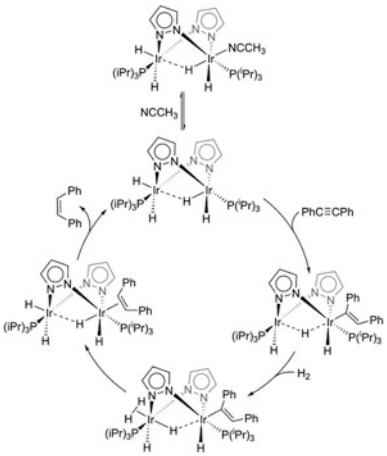

Thus, in the dinuclear d^6-d^6 iridium (III) complex, bridged by two pyrazolyl ligands, the intermetallic *trans*-influence of the terminal hydride ligand on the bridging hydride is crucial for decoordination of acetonitrile and activation of diphenylacetylene. The transmission of the *trans*-effect along the binuclear backbone results in the selectivity of the hydrogenation into *cis*-stilbene. On the contrary, when the reaction operates on a mononuclear center, the rates are lower and the resulting product is 1,2-diphenylethane

The third chapter, entitled "Reactivity and Catalysis at Sites *Trans* to the [Ru–Ru] Bond" is from Jitendra K. Bera and two co-workers. After analyzing the effects of the various axial donors on the paddlewheel $[Ru_2(CO)_4]^{2+}$ core of $\sigma^2\pi^4\delta^2\delta^{*2}\pi^{*4}$ electronic configuration, the authors exploit the axial reactivity for stoichiometric C–H bond activation and C–C bond formation.

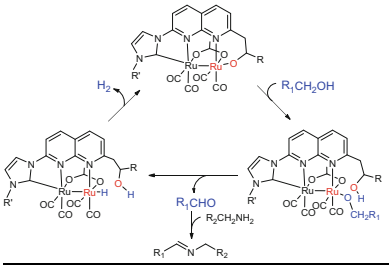

The effect of a hydroxyl unit at the axial position of a [Ru–Ru] core, placed through the agency of a naphthyridyl-functionalized NHC, is examined for catalytic acceptorless dehydrogenation to aldehyde and subsequent coupling with amine to form exclusively imine products

Here the R_1CH_2OH alcohol adds to the Ru–O bond allowing the formation of Ru-alkoxide, which undergoes β-hydride elimination to produce the R_1CHO aldehyde. The inability of the aldehyde to bind at the metal center, owing to the strong effect of the *trans*-NHC ligand, is credited for selective imine formation.

The fourth review by Barbara A. Messerle and co-workers is dedicated to the "Alkyne Activation Using Bimetallic Catalysts." Two metal centers can induce activation of the triple bond in a variety of different coordination modes as shown below:

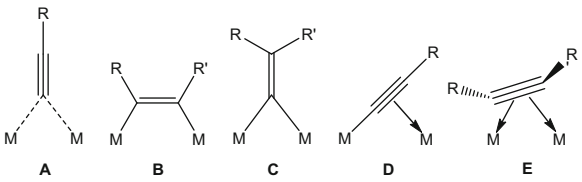

Various situations are analyzed where the two metal centers play a role in one of the coordination modes A–E. There are many cases in which bimetallic catalysis can occur with the two metals acting cooperatively, for instance, in the dimerization of alkynes at two ruthenium metal centers, where a ruthenium-vinylidene species is formed, which is able to subsequently activate the second alkyne reactant through a C–H cleavage on the second ruthenium center. The coupling of these two moieties occurs on this dinuclear platform to provide the enyne product molecule. Examples are also presented where bimetallic catalysts cooperatively activate substituted alkynes in the catalyzed formation of heterocycles.

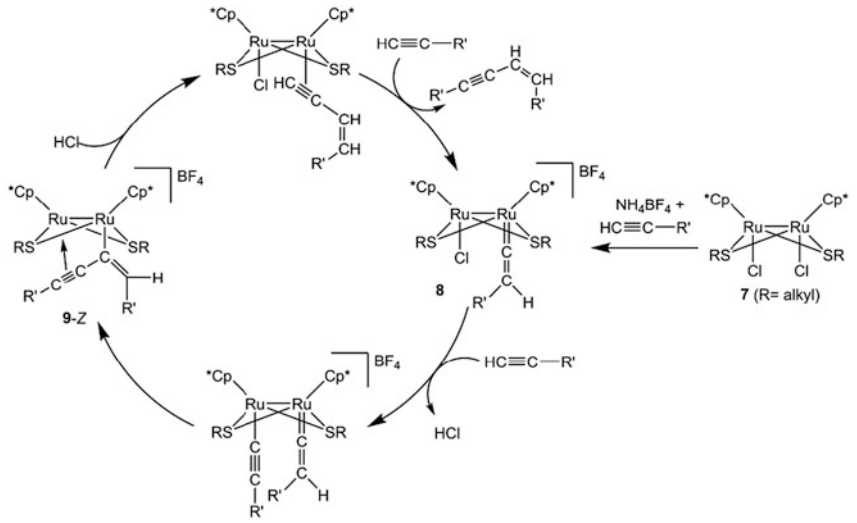

In a fifth contribution, Pierre Le Gendre et al. review the catalytic performances of early-late bimetallic complexes. After an introduction dealing with bifunctional and cooperative dual catalysis in which the cooperative effects arise from two catalytic functions present in the same or two different molecules, this paper focuses on an inventory of early-late heterobimetallic complexes in catalysis. It includes those where the two metal centers belong to the same complex, with bridging ligands as in the following example in which the chiral information is provided by the titanium metal center:

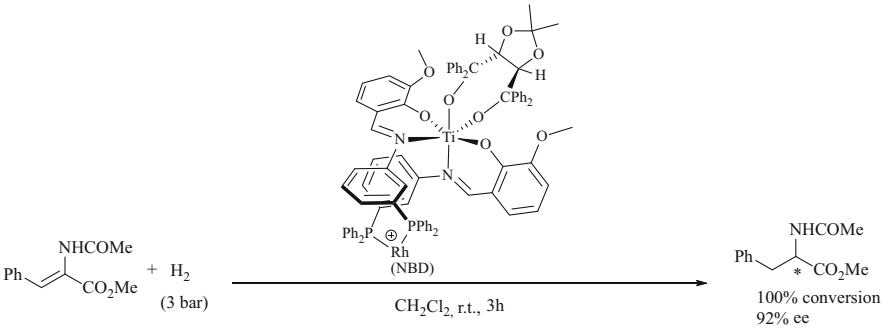

The two metals can operate successively in a concerted manner but with two different roles in catalysis. The following example shows clearly that the cobalt complex produces α-alkenes from ethylene which are incorporated into the polyethylene chain (from[6]):

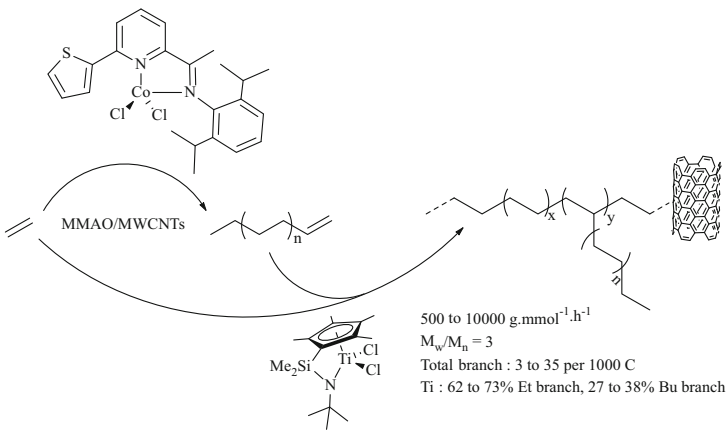

In the sixth chapter, Marc Garland analyzes in detail the cooperativity or synergism in metal-mediated *homogeneous* catalysis and focuses on the *actual* reaction mechanism, arising from the application of 1 or 2 metallic elements in the catalytic system. This system exhibits either an unusual rate dependence or an unusual selectivity pattern that has its origin(s) in the structure of the reaction mechanism and not in some secondary effect due to physicochemical issues such as transport. This chapter is dedicated to the catalytic binuclear elimination reaction (CBER) in which both mononuclear and dinuclear organometallic intermediates act in a synchronized and bicyclic reaction topology, each set of mononuclear intermediates carrying an organic ligand which will eventually be part of the organic product. In situ Fourier transformed infrared (FTIR) and kinetics are necessary to access the real mechanism.

[6] A. Toti, G. Gambastiani, C. Bianchini, A. Meli, S. Bredeau, P. Dubois, D. Bonduel, M. Claes, *Chem. Mater*. **2008**, *20*, 3092–3098.

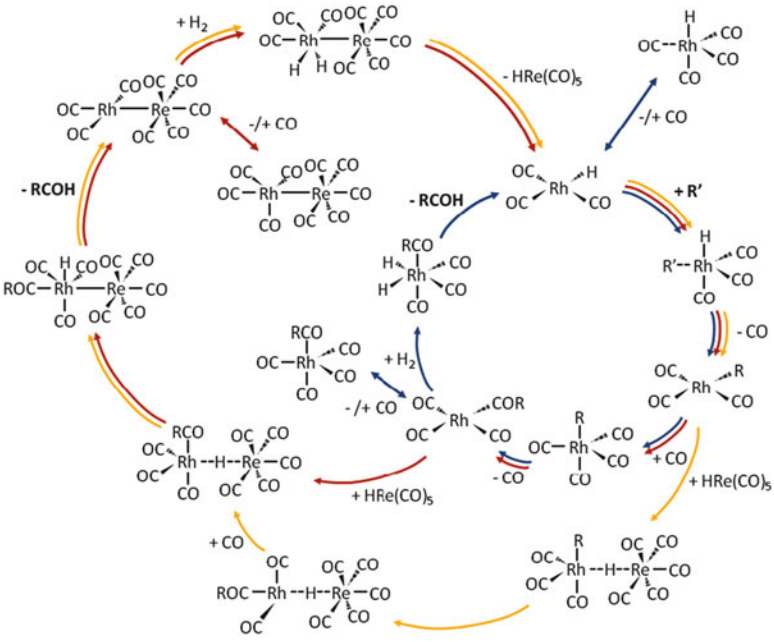

For instance in the double catalytic cycle shown below, and for which the reaction rate depends both on the mono- and dinuclear systems ($r = \{k_1 + k_2[\mathrm{Re(H)(CO)_5}]\}[\mathrm{Rh(COR)(CO)_4}]$), the rhenium hydride $[\mathrm{Re(H)(CO)_5}]$ is ca 1,000 times more effective than molecular hydrogen toward attack on the acyl rhodium species $[\mathrm{Rh(COR)(CO)_4}]$.

To demonstrate that a cooperative bimetallic catalysis is operating, such fine kinetics and in situ analyses are essential to discriminate a bimetallic mechanism from a monometallic one where the second metallic species is poorly efficient or just a spectator.

In the seventh and last chapter, Anne Katherine Jones and her co-workers start from the description of [FeFe]- and [NiFe]-hydrogenases which are very efficient biological enzymes for hydrogen oxidation and production. These proteins operate at high rates ($k_{cat} \sim 10^4\ s^{-1}$) and are highly reversible. The authors describe also carbon monoxide dehydrogenases with [MoCu] and [NiFe] active sites to transform CO into CO_2 or the reverse and formate dehydrogenases which catalyze the two-electron reduction of CO_2 to formate with a mononuclear Mo or W active site. The authors survey recent efforts that have been done to produce biologically inspired catalysts for proton and CO_2 reduction. If monometallic complexes of the first row of transition metals are active in the catalytic proton reduction, examples are given of diiron complexes to perform the photocatalytic production of hydrogen

(see below left) or dipalladium complexes to activate CO_2 and produce CO (below right).

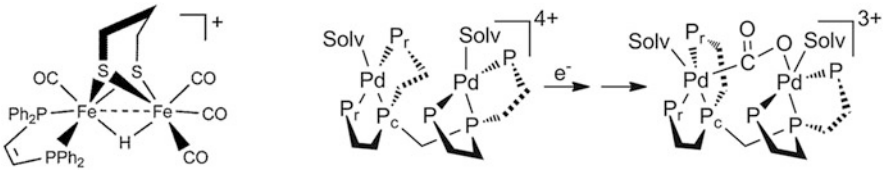

These seven contributions do not cover all the bimetallic catalytic systems which show efficiency in organic synthesis, especially in biocatalysis, but they represent the key points to transpose the high activity of biological enzymes and approach synthetic tools from homogeneous catalysis using transition metals and if possible non-noble metals. Industrial catalytic conversions have been recently reviewed in a modern perspective.[7] Similarly, cooperative catalysis involving Lewis-Brønsted base or Lewis base or ligand associations and cooperation of carbophilic metal centers or of artificial oligopeptides have been described in a recent book.[8]

Presumably, *coordination catalysis* and *biocatalysis* will be more interconnected in the very near future, and we can imagine for the multistep synthesis of an elaborated product the successive intervention of both these strategies. This volume would be helpful to academic and industrial researchers who are involved in the fields of coordination chemistry, homogeneous catalysis, and organic synthesis, in order to develop efficient tools to have the access to fine chemicals from abundant and low-cost substrates.

Finally, as volume editor, I would like to thank all the contributors for their participation in this project and for their enthusiastic efforts to present a synthetic view of the domain. I can anticipate that their contributions will stimulate further studies in the field. I would like also to offer my warm thanks to the Springer team for their continuous support and their efficiency.

[7] M. Beller, A. Renken, R.A. van Santen, Catalysis, from Principles to Applications, 2012, Wiley-VCH.

[8] R. Peters, Cooperative Catalysis, Designing Efficient catalysts for Synthesis, 2015, Wiley-VCH.

Contents

Top Organomet Chem (2016) 59: 1–30
DOI: 10.1007/3418_2015_147

Published online: 18 February 2016

Bimetallic Homogeneous Hydroformylation

Ranelka G. Fernando, Ciera D. Gasery, Marshall D. Moulis, and George G. Stanley

Abstract A dirhodium hydrido-carbonyl catalyst system based on a binuclating tetraphosphine ligand is discussed. Spectroscopic and DFT computational studies support the formulation of the key catalyst complex in acetone solvent as $[Rh_2(\mu\text{-}H)_2(CO)_2(rac\text{-}P4)]^{2+}$, which is highly active and regioselective for producing linear aldehydes under mild conditions. This dicationic catalyst suffers from facile fragmentation reactions in acetone that lead to inactive monometallic and bimetallic complexes. The addition of water to the acetone solvent leads to deprotonation from the dicationic catalyst to form monocationic dirhodium catalyst species that are far less susceptible to deactivation. Spectroscopic and DFT computational studies indicate that the key monocationic catalyst is $[Rh_2(\mu\text{-}H)(CO)_3(rac\text{-}P4)]^{+}$. Although the monocationic bimetallic catalyst is less active on a per molecule basis relative to the dicationic catalyst, there is a higher concentration present producing better overall catalyst rates and selectivity.

Keywords Bimetallic cooperativity • DFT calculations • Hydrides • Hydroformylation (oxo) • Phosphines • Rhodium • Spectroscopic studies

Contents

R.G. Fernando, C.D. Gasery, M.D. Moulis, and G.G. Stanley (✉)
Department of Chemistry, Louisiana State University, Baton Rouge, LA 70803-1804, USA
e-mail: gstanley@lsu.edu

1 Introduction: Hydroformylation and Polymetallic Cooperativity

Hydroformylation is the process for reacting alkenes, typically 1-alkenes, with H_2 and CO to produce aldehydes (Scheme 1). Hydroformylation, also known as "oxo," is one of the largest homogeneous catalytic processes carried out in industry with over 10 million metric tons of aldehydes produced each year (cf. [1–5]). The linear aldehyde product is usually the more valuable, especially for commodity chemicals, so the linear to branched (l:b) regioselectivity is important and ranges from 2:1 to 20:1 in commercial processes.

Although all current industrial hydroformylation catalysts are based on monometallic hydride-carbonyl complexes, usually with phosphine ligands, there has been considerable interest in exploring the utility of polymetallic complexes in homogeneous catalysis ever since Muetterties proposed the cluster-surface analogy in 1975 [6–9]. Of the many areas of homogeneous catalysis, hydroformylation has had the largest number of reports concerning the use of polymetallic complexes as catalysts.

In 1961 Heck proposed what is now generally considered to be the correct monometallic mechanism for $[HCo(CO)_4]$-catalyzed hydroformylation [10]. He also proposed, but did not favor, a bimetallic pathway involving an intermolecular hydride transfer between $[HCo(CO)_4]$ and $[Co(acyl)(CO)_4]$ to eliminate aldehyde product (Scheme 2). Most proposals concerning polymetallic cooperativity in hydroformylation have, therefore, centered on the use of inter- or *intra*molecular hydride transfers to accelerate the elimination of aldehyde product. Bergman, Halpern, Norton, and Marko have all performed elegant stoichiometric mechanistic studies demonstrating that intermolecular hydride transfers can indeed take place between metal-hydride and metal-acyl species to eliminate aldehyde products [11–14]. The monometallic $[HCo(CO)_4]$ pathway involving reaction of the acyl intermediate with H_2, however, has been repeatedly shown to be the dominant catalytic mechanism for 1-alkenes and cyclohexane [15, 16].

Pittman and coworkers, for example, reported in 1977 that 1-pentene could be hydroformylated by the intact cobalt clusters **1** and **2** [17]. These clusters gave linear to branched aldehyde ratios of between 1 and 5:1 (~2.5 being typical) at

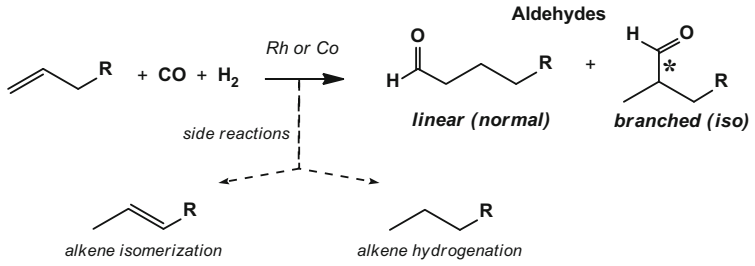

Scheme 1 Hydroformylation reaction

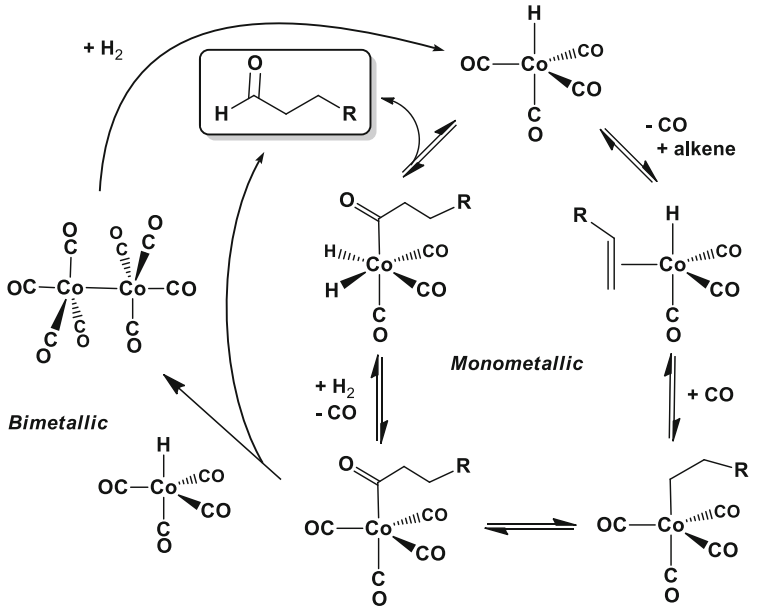

Scheme 2 $HCo(CO)_4$ catalyzed hydroformylation cycle

temperatures of 90–150°C and pressures of 400–1,100 psig. The highest linear aldehyde regioselectivities were found, as with monometallic cobalt catalysts, at lower temperatures and higher pressures. One important piece of evidence that fragmentation to $[HCo(CO)_4]$ was not occurring was obtained from the influence of phosphine ligands on the chemoselectivity of the catalysis. The addition of 2–4 equivalents of PPh_3 improved the stability of the cluster (similar to the monometallic catalysts), but did not increase hydrogenation activity to produce alcohol products, quite unlike monometallic $[HCo(CO)_3(PR_3)]$ catalysts [18]. High-pressure IR studies of phosphine-substituted analogs of **2** show that there was no observable cluster fragmentation under catalytic conditions (150°C, 600 psi), even over a 2-day period [19].

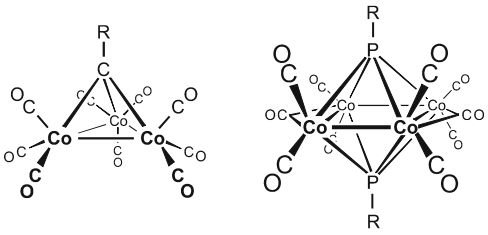

1 **2**

Sanger and coworkers also reported in 1977 the unusual effect of certain diphosphine ligands, $Ph_2P(CH_2)_nPPh_2$, on the activity of $[HRh(CO)(PPh_3)_2]$ hydroformylation catalysts [20]. The addition of 0.25 equivalents of $Ph_2P(CH_2)_nPPh_2$ ($n = 2$–4) per equivalent of $[HRh(CO)(PPh_3)_2]$, for example, caused an increase in the catalytic activity by 90–150%. Addition of more than 0.3 equivalents, however, caused a decrease in the activity relative to the starting $[HRh(CO)(PPh_3)_2]$ catalyst. Di- and polyphosphine-bridged rhodium species such as **3** and **4** were spectroscopically identified at about the same time.

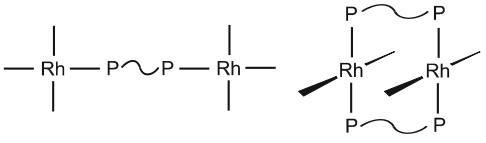

3 **4**

This led to the proposal that tethering the two rhodium centers together via longer chain-length diphosphine ligands, which had less of a preference for chelating a single metal atom, was producing some sort of bimetallic cooperativity between the two metal centers. An *intra*molecular hydride transfer, analogous to the intermolecular hydride transfer proposed by Heck (Scheme 2), enhanced by the proximity of the two metal centers, seemed a very likely possibility.

Fragmentation has been a major and continuing problem in polymetallic catalyst systems. Longoni and coworkers reported in 1984 that the $[Co_5Rh_2(CO)_{12}]$ mixed-metal cluster was more active for hydroformylation than either the parent $[Co_4(CO)_{12}]$ or $[Rh_4(CO)_{12}]$ cluster species [21]. The higher activity was proposed to be caused by heterobimetallic cooperativity between the Co and Rh centers in the homogeneous cluster. Garland, however, showed that the higher activity of the $[Co_5Rh_2(CO)_{12}]$ mixed-metal cluster was simply due to the more facile fragmentation of this cluster into reactive $[HRh(CO)_4]$ monometallic catalyst species [22]. Fragmentation reactions to produce highly active monometallic species also turned out to be occurring in Kalck's thiolate-bridged rhodium complex $[Rh_2(\text{-}\mu\text{-}SR)_2(CO)_2(PR_3)_2]$ bimetallic hydroformylation catalyst [23, 24].

2 Dirhodium Tetraphosphine Hydroformylation Catalysts

Our work into bimetallic cooperativity in homogeneous catalysis has concentrated on the binucleating tetraphosphine ligands *meso*- and *racemic*-et,ph-P4, shown in Scheme 3 [25, 26]. These ligands are designed to chelate two metal centers via a single, conformationally flexible, methylene bridge.

We have characterized both "open-mode" bimetallic complexes where the metal centers are separated by 5–7 Å [26] and "closed-mode" systems where the metals

Scheme 3 Tetraphosphine diastereomers studied

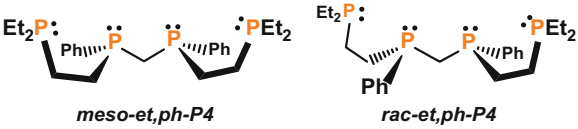

Table 1 Hydroformylation results on 1-hexene (90 psig, 1:1 H_2/CO, 90°C, acetone solvent, 1 mM catalyst, 1 M 1-hexene)

Catalyst precursor	Initial TO/min[a]	Aldehyde l:b ratio[b]	Alkene isomerization (%)	Alkene hydrogenation (%)
$[Rh_2(nbd)_2$(*rac*-et,ph-P4)$](BF_4)_2$	20	28:1	2.5	3.4
$Rh(CO)_2$(acac) + 0.82 M PPh_3	9	17:1	1	0.5
$[Rh_2(nbd)_2$(*meso*-et,ph-P4)$](BF_4)_2$	0.9	14:1	24	10

[a]Turnovers per min (# moles product/# moles catalyst); initial rate is the initial linear part of the uptake curve representing the highest catalytic rate
[b]Linear to branched aldehyde product ratio based on GC and NMR analysis

are bonded to one another or in close contact (M-M < 3 Å) [27]. *Rac*-et,ph-P4 reacts in very high yield with 2 equivalents of $[Rh(nbd)_2]BF_4$ (nbd = norbornadiene) to produce $[Rh_2(nbd)_2$(*rac*-et,ph-P4)$](BF_4)_2$, **5r**, which is a precursor for an active and highly regioselective bimetallic hydroformylation catalyst [28].

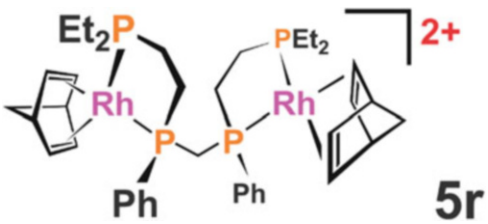

We have used 1-hexene as our standard alkene, but the results presented are typical for 1-alkenes. In comparing **5r** to the commercial Rh/PPh_3 catalyst (Table 1), we find that **5r** is faster and has a higher linear to branched aldehyde regioselectivity. The rate and selectivity of Rh/PPh_3 hydroformylation catalysts are quite dependent on the concentration of PPh_3. Industry typically runs with a minimum PPh_3 concentration of 0.4 M (1 mM rhodium catalyst), which represents a 400:1 PPh_3/Rh ratio. The higher the PPh_3 concentration, the slower the catalysis, but the higher the L:B aldehyde ratio. The 0.82 M PPh_3 concentration used in our study is about midway for PPh_3 concentrations used in industry.

The *meso* catalyst precursor, on the other hand, generates a considerably poorer hydroformylation catalyst. The *racemic* catalyst is 22 times faster than the *meso*

catalyst and gives considerably higher overall product selectivities (Table 1), particularly with respect to the undesirable alkene isomerization and hydrogenation side reactions.

In contrast with virtually all other aryl phosphine or phosphite coordinated rhodium hydroformylation catalysts, **5r** does not require any excess phosphine ligand in order to maintain its selectivity or stability. In fact, adding excess *rac*-P4 ligand deactivates the bimetallic catalyst. The need for excess phosphine in monometallic rhodium catalysts arises from the relatively weak Rh–PPh_3 (or phosphite) bonding. In order to maintain the coordination of two phosphine ligands, which are required for good regioselectivity, a large excess of PPh_3 is required to force the dissociation equilibrium to favor [$HRh(CO)(PPh_3)_2$] [29–31]. In **5r**, the chelating and electron-donating et,ph-P4 phosphine ligand coordinates strongly enough to the rhodium centers so that excess phosphine is not needed. But as we have subsequently found out, the chelate effect is not strong enough to maintain stability of the bimetallic complex, which will be discussed further below.

The following observations support the proposed bimetallic cooperativity. Model monometallic [$Rh(nbd)(P_2)$](BF_4) ($P_2 = Et_2PCH_2CH_2PEt_2$, $Et_2PCH_2CH_2PMePh$, $Et_2PCH_2CH_2PPh_2$, or $Ph_2PCH_2CH_2PPh_2$) catalyst precursors generate terrible hydroformylation catalysts for 1-hexene from both a rate and regioselectivity viewpoint (1–2 turnovers/h, 3:1 linear to branched aldehyde regioselectivity, 50–70% alkene isomerization and hydrogenation side reactions). Tethering together two extremely poor monometallic hydroformylation catalysts with our *rac*-et,ph-P4 ligand to form a highly active and selective hydroformylation catalyst is strong evidence for the presence of effective bimetallic cooperativity in this system.

Further persuasive evidence for bimetallic cooperativity came from bimetallic model systems where the central methylene group in the et,ph-P4 ligand has been replaced by *p*-xylylene (**6**) or propyl groups (**7**), thus limiting the ability of the two rhodium centers to interact with one another.

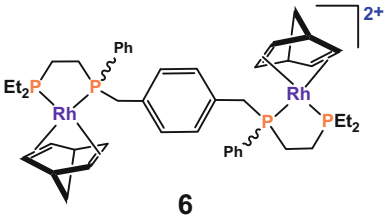

6

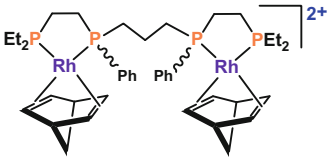

7

These "spaced" bimetallic precursors, **6** and **7**, are also extremely poor hydroformylation catalysts (1/2–6 turnovers/h, 3:1 linear to branched aldehyde regioselectivity, 50–70% alkene isomerization and hydrogenation side reactions). Complex **7**, however, is about three times faster than the monometallic analogs, consistent with Sanger's proposal (vide supra) of some bimetallic cooperativity

occurring in his $Ph_2P(CH_2)_4PPh_2$/Rh hydroformylation catalysts [20]. Just as in Sanger's systems, **7** has very low regio- and chemoselectivity.

The most internally self-consistent check, however, is that the *racemic* bimetallic catalyst is 22 times faster for the hydroformylation of 1-hexene than the *meso*catalyst and gives higher product regioselectivity and far fewer side reactions. The higher rate of the *racemic* system was proposed to arise from its ability to form a double-bridged hydrido-carbonyl intermediate, which favors the intramolecular hydride transfer step that leads to aldehyde elimination. The *meso*catalyst can do an intramolecular hydride transfer, but cannot make the lower energy double-bridged edge-sharing bioctahedral structure.

3 Dicationic Dirhodium Catalyst in Acetone Solution

The in situ FT-IR and NMR studies on the catalyst system have been extremely important in identifying the nature of the catalytic species [32]. As indicated from the IR spectra (using a Spectratech Circle Reaction Cell) in Fig. 1, the very poor hydroformylation catalyst generated from neutral $[Rh_2(\eta^3\text{-allyl})_2(rac\text{-et,ph-P4})]$, **8r**, has carbonyl stretching frequencies that are 100 cm^{-1} lower in energy relative to those for the highly active and regioselective catalyst generated from dicationic **5r** (D_2/CO labeling studies confirm that all the bands in the IR spectra shown are due to carbonyls).

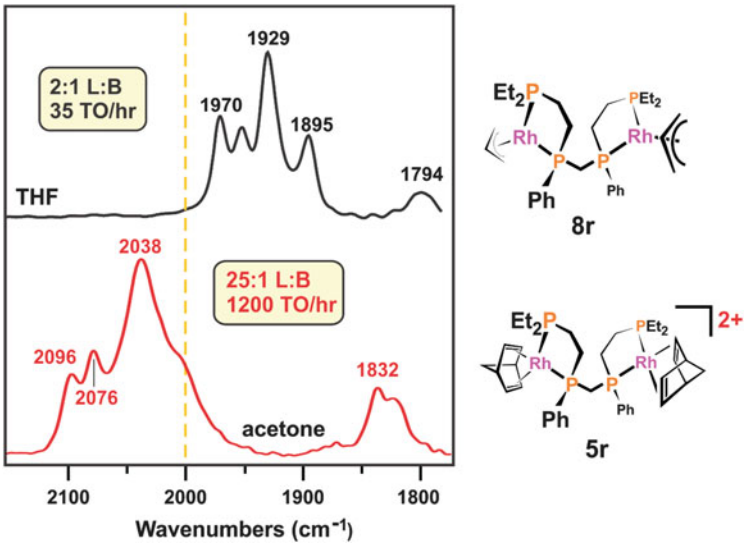

Fig. 1 In situ FT-IR spectra of the hydroformylation catalysts generated from the indicated precursor species. Conditions: 1 mM Rh_2 catalyst, 1 M 1-hexene, 90°C, 90 psig, 1:1 H_2/CO. Hydroformylation activities and L:B aldehyde regioseletivities for 1-hexene are shown

Figure 1 quite clearly demonstrates that the bimetallic complexes generated from the dicationic precursor **5r** have considerably lower electron densities on the rhodium atoms, as indicated by the ~100 cm^{-1} higher ν_{CO} stretching frequencies, relative to the electron-rich neutral bimetallic hydrido-carbonyl species formed from the reaction of **8r** with H_2/CO.

The nature of the active catalyst species was studied by in situ FT-IR using the dicationic precursors **5r** and $[Rh_2(CO)_4(rac\text{-et,ph-P4})](BF_4)_2$, **9r**, which generate the same catalytically active species and give identical spectroscopic results [32]. The FT-IR spectra of **9r** under 1 bar CO (22°C) are shown in Fig. 2a. The ν_{CO} IR bands observed for **9r** (2,058 and 2,006 cm^{-1}) compare well to other known $[Rh(CO)_2(P_2)]^+$ (P_2 = chelating phosphine) complexes. The ^{31}P NMR spectrum of **9r** is completely consistent with the proposed chelated symmetrical structure.

The reaction of **9r** with up to 90 psig of CO produces the bimetallic pentacarbonyl $[Rh_2(CO)_5(rac\text{-et,ph-P4})]^{2+}$ (**10r**, Fig. 2b), which has been crystallographically characterized (Fig. 3). The structure shows the expected open-mode conformation with a 4-coordinate 16e- square-planar Rh center, the other Rh being 5-coordinate, 18e-, and approximately trigonal bipyramidal. The addition of one carbonyl ligand causes a higher than expected shift to higher energies (by 37 cm^{-1}) for the carbonyl bands. ^{31}P NMR studies support a very facile CO-pressure-dependent equilibrium and an averaged symmetrical open-mode structure.

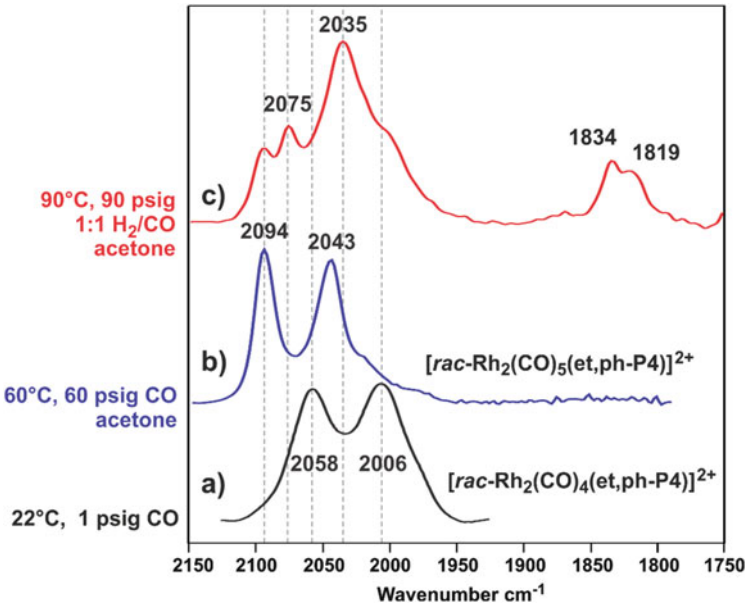

Fig. 2 In situ FT-IR spectra: (*a*) $[Rh_2(CO)_4(rac\text{-et,ph-P4})]^{2+}$, **9r** (22°C, 14 psi CO); (*b*) $[Rh_2(CO)_5(rac\text{-et,ph-P4})]^{2+}$, **10r**, formed when **9r** is placed under 90 psig of CO at 60°C; (*c*) spectrum formed when **9r** is placed under 90 psig of H_2/CO at 60°C

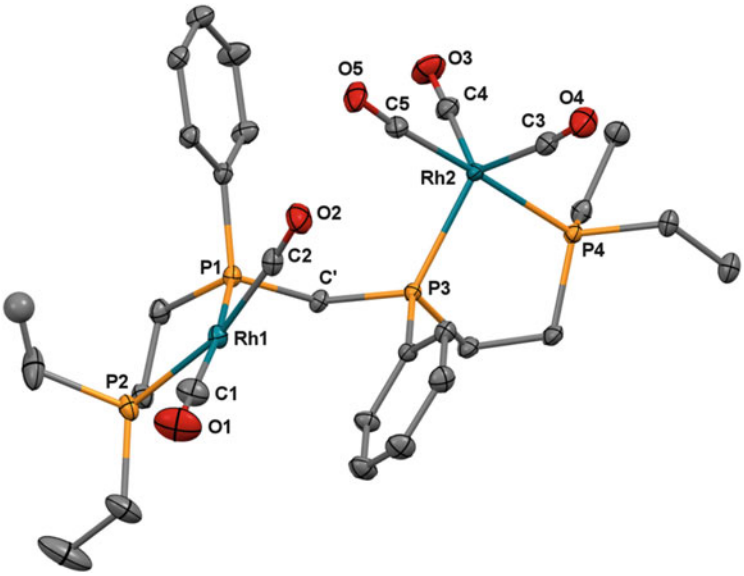

Fig. 3 ORTEP plot (50% ellipsoids) of $[Rh_2(CO)_5(rac\text{-et,ph-P4})]^{2+}$, **10r**. Hydrogens, two BF_4 counter anions, and disordered CH_2Cl_2 solvent omitted for clarity

Surprisingly, the pentacarbonyl **10r** does not seem to react with more CO to form the hexacarbonyl complex, $[Rh_2(CO)_6(rac\text{-et,ph-P4})]^{2+}$, at pressures less than 90 psig.

Density functional theory (DFT) calculations on the pentacarbonyl complex **10r** demonstrate that a sixth CO ligand barely coordinates with a long Rh-CO distance of 2.31 Å (other Rh-CO distances average 1.98 Å), consistent with the FT-IR data. Placing **9r**/**10r** under H_2/CO (90 psig, 20–90°C) generates a new equilibrium mixture that contains **10r** and new hydride species as indicated by ^1H, ^{31}P NMR, and FT-IR spectroscopy. Most notable in the FT-IR (Fig. 3c) is the presence of bridging CO bands at 1,834 and 1,819 cm^{-1}. The hydroformylation activity of the catalyst appears to track with the relative intensity of the bridging CO bands in a variety of solvents unless water is present. The bridging CO bands in CH_2Cl_2 solvent, for example, are considerably weaker and the hydroformylation activity is only about 25% of that observed in acetone.

The in situ $^{31}P\{^1H\}$ NMR of **5r** (or **9r**/**10r**) under H_2/CO at 22°C and 280 psig clearly demonstrate that it is initially composed of complex **10r** along with two broad resonances at 66 and 74 ppm. Over the course of 24 h at room temperature, a number of additional resonances grow in as shown in Fig. 4. The same ^{31}P NMR spectrum can be generated in an hour when the catalyst solution in acetone is heated at 60°C.

The ^1H NMR (Fig. 5) indicates the presence of three major hydride species, two of which result from fragmentation of the $[Rh_2(rac\text{-et,ph-P4})]^{2+}$ carbonyl and carbonyl-hydride complexes. The temperature-independent hydride resonances at

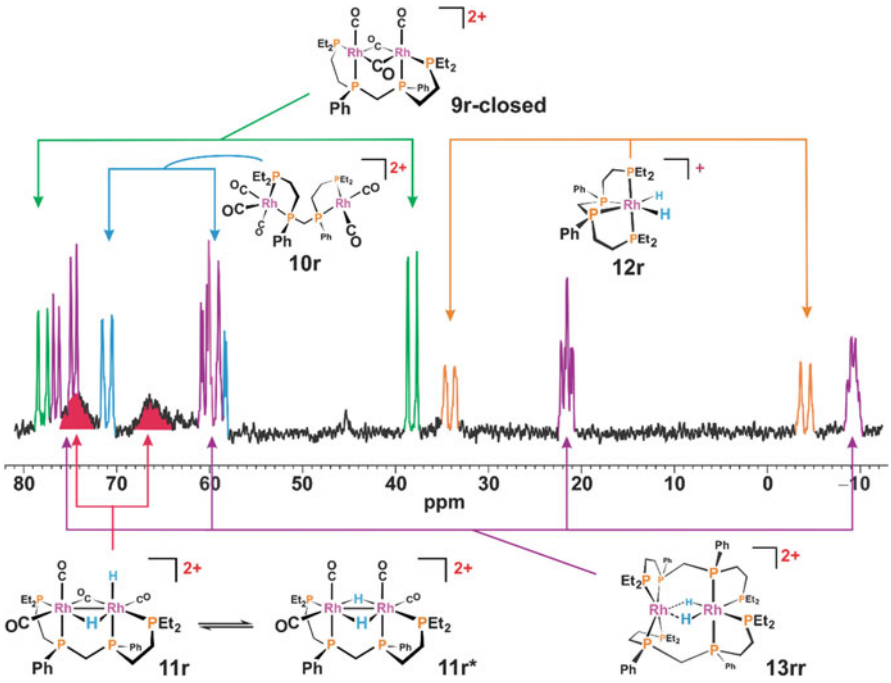

Fig. 4 $^{31}P\{^{1}H\}$ NMR of **5r** under 280 psig 1:1 H_2/CO in d_6-acetone after 24 h at room temperature. Proposed assignments are shown

−5.6 and −15.1 ppm are due to the two fragmentation species. Although we have not isolated the Rh(III) monometallic dihydride complex, $[RhH_2(\kappa^4\text{-}rac\text{-et,ph-P4})]^+$, **12r**, we have prepared and fully characterized the dichloride analog, $[RhCl_2(\kappa^4\text{-}rac\text{-et,ph-P4})]^+$,which has a very similar ^{31}P NMR [33]. $[RhH_2(\kappa^4\text{-}rac\text{-et,ph-P4})]^+$, **12r**, is the only hydride species that remains after depressurization and flushing with N_2. It is a very stable and unreactive 18e- complex. Attempts to prepare **12r** from the dichloride analog have failed as the dichloride is also extremely stable and unreactive. The lack of H_2 reductive elimination activity from **12r** arises from the expanded H-Rh-H angle, which is *trans* to the highly compressed four-membered chelate ring and extremely stable octahedral Rh(III) structure.

Fragmentation of $[Rh_2(rac\text{-et,ph-P4})]^{2+}$ also produces, in the relatively high concentrations of the NMR tube experiment, the double-ligand coordinated complex, $[Rh_2H_2(rac\text{-et,ph-P4})_2]^{2+}$, **13rr**. We mistakenly assigned the hydride resonances for this complex at −5.5 ppm to the catalyst species due to the initial ^{31}P decoupling experiments that indicated that the 164 Hz coupling was not due to any of the phosphines [32], which left us with an unusual Rh-H coupling assignment. Subsequent ^{31}P decoupling studies did eventually show that the 164 Hz hydride coupling was indeed due to the ^{31}P resonance at −9 ppm. COSY NMR experiments demonstrate that the hydrides are coupled to the phosphorus resonances at −9,

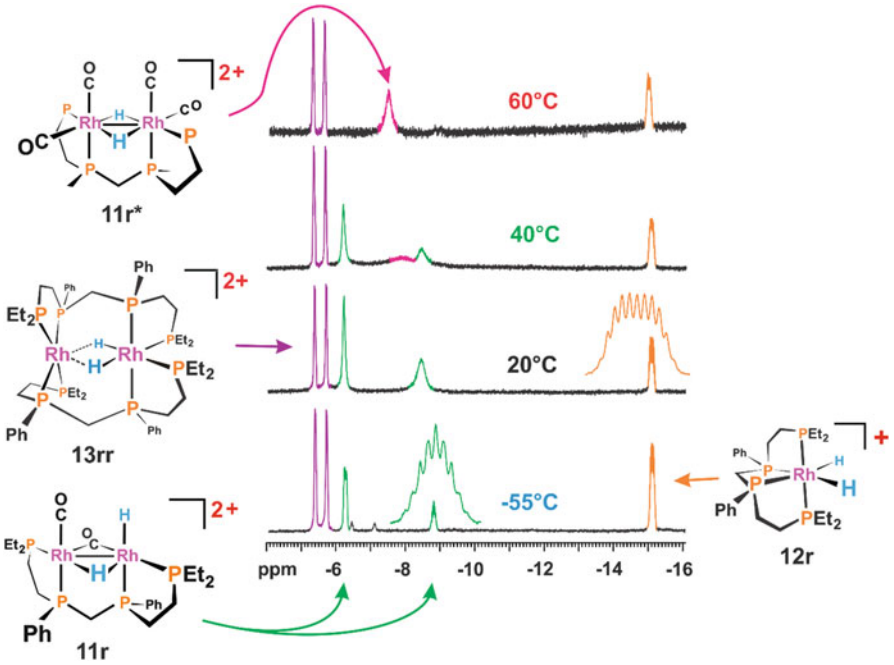

Fig. 5 Variable temperature ^{1}H showing the hydride region of **5r** under 280 psig H_2/CO in d_6-acetone along with proposed assignments. Expansions of two of the resonances are shown

60, and 75 ppm, but not the resonance at 21 ppm, which we assign to the *cis*-coordinated chemically equivalent phosphines.

We propose the unusual mixed-valence, semi-hydride-bridged Rh(I)/Rh(III) structure for **13rr** due to the considerable difference in ^{31}P chemical shifts between the two halves of the complex. The ^{31}P resonances centered at 60 and 75 ppm have large *trans* P-P couplings of 280 Hz, consistent with *trans* nonchemically equivalent phosphines in a square-planar-like cationic Rh(I) environment. The Rh(III) resonances at 21 and −9 ppm are oriented *cis* to one another with smaller coupling constants. ^{31}P COSY experiments demonstrate that the 75 ppm resonance is strongly coupled to the 60 ppm resonance, consistent with the *trans* coupling pathway. The 60 ppm resonance is also coupled to the 21 ppm resonance. Finally, the 21 and −9 ppm resonances are coupled. This coupling pattern is consistent with the proposed structure for **13rr**.

The broad ^{31}P resonances at 66 and 74 ppm correspond to the broadened hydride resonances at −6.2 and −8.5 ppm at 20°C. These are assigned to the hydride-containing bimetallic hydroformylation catalyst species. At −55°C these two hydride resonances start to resolve, with the resonance at −8.8 ppm forming what appears to be a pseudo-nonet, while the resonance at −6.3 ppm is only partially resolved. We assign this to the dirhodium species with one terminal and one bridging hydride, $[Rh_2(H)(\mu\text{-}H)(\mu\text{-}CO)(CO)_x(rac\text{-et,ph-P4})]^{2+}$, **11r**, where $x = 1$–3.

The terminal carbonyls that are oriented approximately opposite the Rh–Rh bond are considered to be exceptionally labile due to the dicationic charge that contracts the Rh d-orbitals and reduces π-backbonding.

As the temperature is increased from −55°C to 60°C, these two resonances broaden and coalesce to form a new single hydride resonance at −7.5 ppm. This can be assigned to one of two symmetrical bimetallic dihydride isomers of **11r**, either the bridged species, $[Rh_2(\mu\text{-}H)_2(CO)_x(rac\text{-et,ph-P4})]^{2+}$, **11r***, where $x = 2$–4, or the terminal dihydride with bridging carbonyls, $[Rh_2H_2(\mu\text{-}CO)_2(CO)_x(rac\text{-et,ph-P4})]^{2+}$, **11r****, where $x = 1$–2. DFT calculations (B3LYP, 3-21G on Rh, 6-311G** on all other atoms, methyl groups on phosphines) on these three dihydride isomers order them with relative energies shown in Fig. 6 (all optimized with four carbonyl ligands).

11r and **11r*** have essentially the same energies within the error of the DFT calculation, which is about 2 kcal. The terminal dihydride, **11r****, is a fair bit higher in energy using either total relative energy or ΔG energy values. Experimentally, the low-temperature ^{1}H NMR clearly indicates that the unsymmetrical dihydride, **11r**, is the lowest energy species and a reference point for our assignments. The question is which symmetrical dihydride is formed at higher temperatures and is acting as the primary hydroformylation catalyst. Because of the vast amount of work on monometallic hydride complexes, there is a strong bias toward favoring a terminal hydride for the key alkene-hydride migratory insertion step. We, therefore, proposed for many years the terminal dihydride complex **11r**** as a key catalyst intermediate [32], but based on the DFT studies and a re-examination of the experimental data, we now favor **11r*** as the primary hydride catalyst for hydroformylation.

The mechanistic steps parallel that of monometallic hydroformylation cycles. Oxidative addition of H_2 to the 16e- four-coordinate Rh side of **10r** generates the transient intermediate species **A**. We do not have any spectroscopic data directly supporting any of the complexes labeled with letters in Fig. 7. DFT calculations on all the species in Fig. 7, along with all likely isomers, support the indicated structures. The optimized structures from the DFT calculations generally have somewhat unsymmetrical bridging ligands (hydrides or carbonyls) and more distorted structures than those drawn here for clarity. Complex **A** rapidly closes up to form the hydride and carbonyl-bridged complex **11r**, which is the

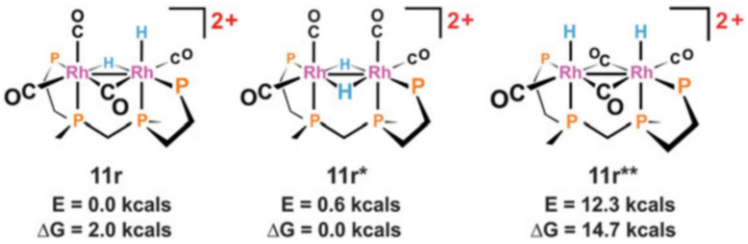

Fig. 6 DFT relative energies for the three closed-mode dihydride isomers

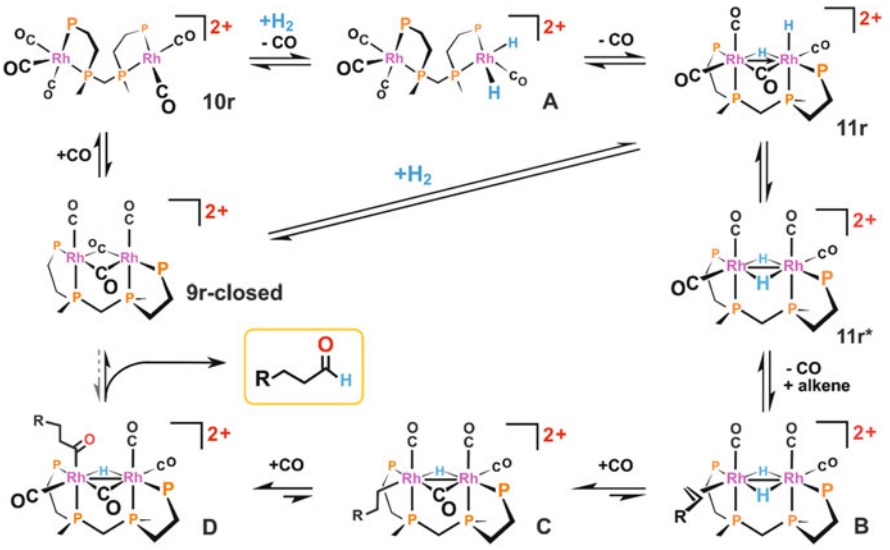

Fig. 7 Proposed bimetallic hydroformylation cycle based on DFT calculations using **11r*** as the catalytically active hydride species

experimentally observed low-energy structure at −55°C in our NMR studies. Hydroformylation occurs at higher temperatures that favor a symmetrical hydride structure, shown in Fig. 7 as the bridging dihydride **11r***. The terminal CO ligands are very labile, allowing coordination of the alkene substrate to form **B**, which does a migratory insertion to form the alkyl **C**, followed by CO coordination and another migratory insertion to form the acyl complex **D**. The acyl complex **D** has a bridging hydride present in a cisoidal position and is set up for a facile reductive elimination to produce aldehyde and the Rh(I)-bridged carbonyl complex **9r-closed**. The final steps have **9r-closed** reacting with CO to open up and reform **10r** or reacting directly with H_2 to form a dihydride species, most likely **11r**.

Although still preliminary, the most recent (and still ongoing) DFT computational results point to the dihydride-bridged bimetallic complex **11r*** as the most likely catalyst for hydroformylation. The DFT computed mechanism based on **11r*** is shown in Fig. 8.

Not only are the various complexes in the catalytic cycle based on **11r***, once alkene coordinates, lower in energy compared to cycles based on **11r****, but the calculated activation barriers for most of the reaction steps are also lower in energy. DFT calculates the activation energy for **B** going to **C** based on the terminal dihydride **11r**** as 23.1 kcal. The same alkene-hydride migratory insertion step for the double-bridged dihydride complex **11r*** shown in Fig. 7 is only 8 kcal. Based on the DFT calculations and the spectroscopic data, especially the FT-IR, we propose that the rate determining step is either the CO migratory insertion to make the acyl intermediate or the reductive elimination of aldehyde. Both have essentially the activation barriers based on the DFT calculations.

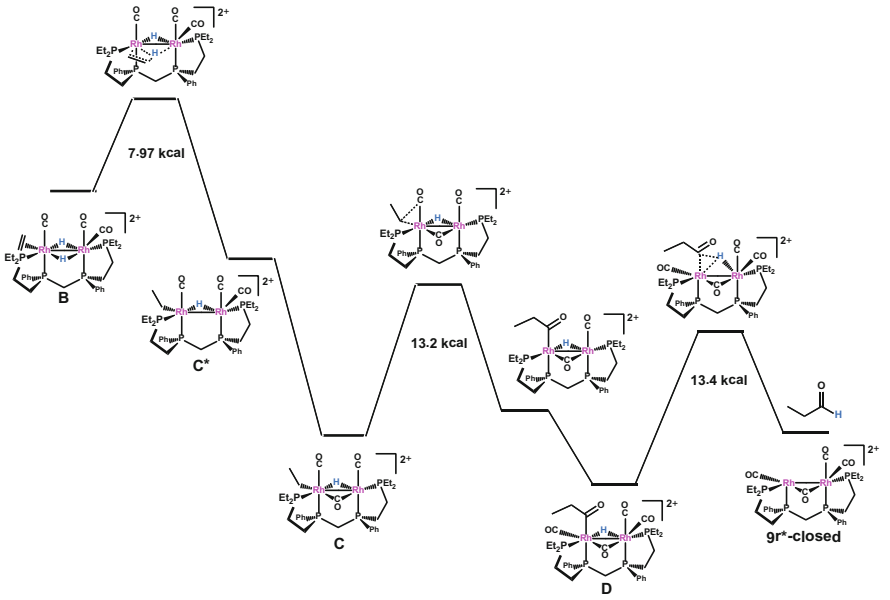

Fig. 8 Relative energies and activation barriers for key catalytic steps based on DFT calculations using **11r*** as the catalytically active hydride species

The presence of two bridging carbonyl peaks in the IR spectra at higher temperatures and the apparent activity dependence on these bridging bands, however, would seem to argue for the terminal dihydride species **11r**** as the main catalyst. But we are quite sure that there is facile phosphine arm dissociation occurring for species **11r**, **11r***, and **11r**** if it exists, based on the broad resonances in the ^{31}P and ^{1}H NMR at room temperature and above. The equilibrium between **11r** and **11r** with an external phosphine dissociated should show up in the IR as two separate species. DFT calculations show **11r** has one long Rh–$P_{external}$ distance of 2.51 Å indicating weaker Rh–P bonding. Calculations for the phosphine arm-on and arm-off complexes of **11r** show that the bridging CO bands have different stretching frequencies and should lead to the two bridging IR bands observed experimentally.

The dicationic charge and unusual Rh(+2) oxidation state offers an ideal explanation for the remarkable hydroformylation activity and regioselectivity of **11r**/**11r***. There are, for example, no other examples of active and highly regioselective hydroformylation catalysts that have mainly alkylated, strongly donating phosphine ligands (like et,ph-P4). The reason for this is well understood. The presence of two electron-donating alkylated phosphine ligands increases the electron density on the rhodium atom leading to increased π-back-donation and stronger Rh–CO bonding. This stronger Rh–CO bonding stabilizes the unreactive 18 e^- five-coordinate complexes $[RhH(CO)_2(P_2)]$ or $[Rh(acyl)(CO)_2(P_2)]$ (P_2 = two monodentate or one chelating bisphosphine). Facile CO (or phosphine) dissociation is needed to

generate the catalytically active four-coordinate 16 e^- complexes, which are needed to coordinate alkene or H_2 to start and/or finish the hydroformylation catalytic cycle. The fact that our bimetallic catalyst is *dicationic* and has the rhodium centers in the +2 oxidation state compensates for the strongly donating, mainly alkylated et,ph-P4 ligand.

The +2 oxidation state and d^7 electronic configuration enables Rh–Rh covalent bonding, which is supported by the DFT calculations (Rh–Rh = 2.886 Å for **11r**, 2.969 Å for **11r***, and 2.892 Å for **11r****). The Rh–Rh bond, in turn, keeps the Rh centers in close proximity supporting the bridging ligands that are important for the cooperativity and intramolecular transfers between metal centers. The combination of the Rh–Rh bonding and bridging ligands creates a well-defined binding site that produces the high aldehyde regioselectivity. Key aspects of this are discussed in the binding site section.

The weakness of our dicationic bimetallic catalyst is the fact that it readily fragments in acetone or other polar organic solvents into inactive monometallic (**12r**) and double-P4 coordinated bimetallic (**13rr**) complexes. The proposed fragmentation pathway is shown in Fig. 9 and starts with the dissociation of one of the external phosphine chelate arms.

The broadness of the phosphine resonances assigned to the catalyst in Fig. 4 is due to the exchange between the different dihydride isomers **11r** and **11r***, discussed earlier, and the phosphine arm-on/arm-off equilibrium. Once one of the external phosphines dissociates, CO can coordinate to form **E**. The replacement of a σ-donating alkylated phosphine with a π-backbonding CO reduces the electron density on that Rh center. This will promote reductive elimination of the two hydrides to produce the Rh(I) bimetallic complex **F**. The CO saturation of the one Rh center leads to loss of $[Rh(CO)_4]^+$, which probably goes on to form unreactive cluster complexes and monometallic species **G**. Under low-concentration autoclave conditions (catalyst concentration equal to 1 mM),

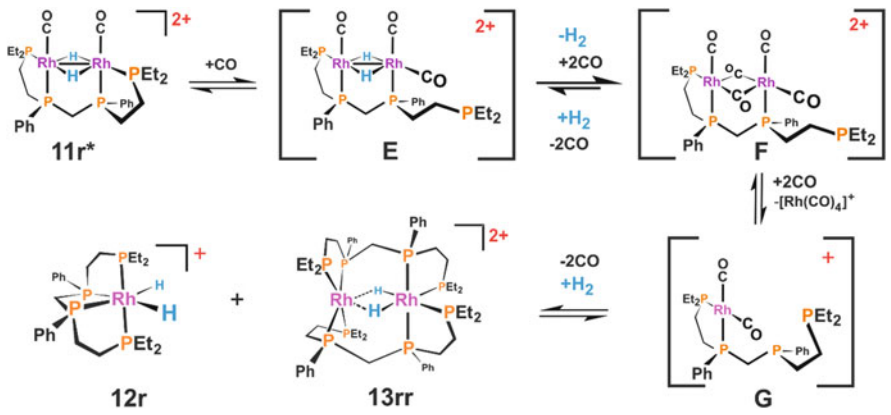

Fig. 9 Proposed fragmentation pathway using **11r*** as the starting species. 16e- species are shown for **11r***, **E**, **F**, and **G**. Additional CO ligands could coordinate to these complexes

the primary product is the inert 18e- monometallic product **12r**. In our higher-concentration NMR tube studies (Figs. 4 and 5), **G** can also dimerize to form **13rr**.

There are two electronic factors that favor phosphine dissociation. The first is that while there are many examples of metal-metal-bonded dinuclear Rh(+2) compounds ([34] and references therein), edge-sharing bioctahedral structures are quite rare. The two most closely related dinuclear Rh(+2) oxidation state complexes are Cotton's $[Rh_2(\mu\text{-}CO)(\mu\text{-}Cl)Cl_2(dppm)_2(MeOH)]^+$, which has been structurally characterized and needs one additional terminal ligand to reach full edge-sharing bioctahedral coordination geometry[35–37], and Bianchini's $[Rh_2H_2(\mu\text{-}H)_2(tripod)_2]$ (tripod = $MeC(CH_2PPh_2)_3$) that has been proposed to have a full edge-sharing bioctahedral structure, but for which there is scant spectroscopic or structural data [38]. There are also several examples of Rh(+2) complexes with one or three bridging hydrides [39–41]. $[Rh_2(\mu\text{-}H)_3(H)(PR_3)_4]$ (R = O-*i*Pr and *i*Pr) complexes have been characterized, but both have been assigned as mixed valent Rh(+1)/Rh(+3) compounds [42, 43]. It is important to note that none of these other Rh(+2), or mixed valent, hydride complexes have been demonstrated to be efficient hydroformylation catalysts.

The vast majority of Rh(+2) dimers have a D_{4h}-like "lantern" coordination geometry. These systems have weakly coordinated axial ligands oriented *trans* to the Rh–Rh bond. Transforming the D_{4h}-like structure with weakly coordinated axial ligands into the edge-sharing bioctahedral structure, as shown in Fig. 10, spreads out the axial ligand lability to the four coordination sites that are opposite the M–M bond. The metal-ligand bond weakening effect for these locations promotes carbonyl lability, which is good, but also weakens the Rh–P bonding, which leads to fragmentation and deactivation of the bimetallic catalyst. The presence of bridging hydrides with a strong *trans*-σ-donor labilizing effect further enhances the possibility for phosphine chelate arm dissociation.

The other Rh–P bond weakening effect is the electrostatic repulsion between the phosphorus and rhodium atoms. The phosphorus atoms have a considerable amount of partial positive charge for the complexes in the catalytic cycle ranging from +0.4 to +0.6 based on the DFT calculations. Although the rhodium centers with hydride ligands usually have small partial negative charges (−0.1 to −0.3), the alkyl, acyl, and carbonyl-only dicationic complexes have partial positive charges (+0.1 to +0.3) consistent with their cationic natures and σ-donor ligands weaker than hydride.

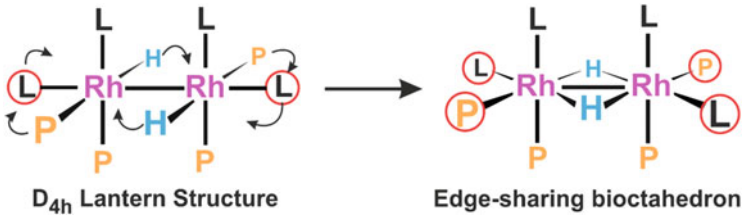

Fig. 10 The electronic lability of the *trans* ligands in the D_{4h}-like dimer is transferred and spread out over all four coordination sites for the edge-sharing bioctahedral structure

When the rhodium and phosphorus atoms have partial positive charges, the electrostatic repulsion will work to weaken the Rh–P bonding. While this is probably not a large effect, it does contribute to the Rh–P dissociation problem.

4 Hydroformylation in Water/Acetone: Formation of a Monocationic Dirhodium Catalyst

The addition of 30% water by volume to the acetone solvent causes a dramatic improvement in hydroformylation as shown in Table 2 [44]. The most dramatic improvement, however, is in the stability of the catalyst. A common test for the stability of monometallic Rh-phosphine hydroformylation catalysts is to let them sit under H_2/CO at operating conditions without alkene. Most monometallic Rh-phosphine catalysts will deactivate within 24 h, usually quite a bit more quickly depending on the phosphine and amount of excess present. Our bimetallic catalyst in pure acetone deactivates completely via the fragmentation reactions described earlier after 80 min at the conditions shown in Table 2. In marked contrast, using 30% water/acetone as the solvent, the bimetallic catalyst only loses 10% of its hydroformylation activity after 120 min.

Although we initially proposed that the water was inhibiting the phosphine ligand dissociation and bimetallic fragmentation from generating inactive **12r** and **13rr** [44], the actual situation is quite different. The dicationic dihydride catalyst **11r/11r*** can easily deprotonate to form a new monocationic monohydride dirhodium catalyst. This is supported by in situ FT-IR, NMR, the acidity of the catalyst solution, and DFT computational studies. A 1 mM catalyst solution in 30% water/acetone after exposure to H_2/CO has a pH of 3.1, while a 10 mM solution has a pH of 2.2 – consistent with a strong monoprotic acidic species.

The in situ FT-IR of the bimetallic catalyst in acetone and water/acetone are shown in Fig. 11 along with the tetra- and pentacarbonyl complexes, **9r** and **10r**. There are several significant differences between the carbonyl bands in acetone and water/acetone solvent. The first is the very small amount of the 2,094 cm^{-1} band

Table 2 Hydroformylation of 1-hexene by $[Rh_2(nbd)_2(rac\text{-et,ph-P4})](BF_4)_2$ using the solvent system indicated (90 psig, 1:1 H_2/CO, 90°C, 1 mM catalyst, 1 M 1-hexene)

Solvent	Initial TO/min[a]	Aldehyde l:b ratio[b]	Alkene isomerization (%)	Alkene hydrogenation (%)
Acetone	20	28:1	2.5	3.4
30% water/ acetone	30	33:1	1	>1

[a]Turnovers per min (# moles product/# moles catalyst); initial rate is the initial linear part of the uptake curve representing the highest catalytic rate

[b]Linear to branched aldehyde product ratio based on GC and NMR analysis

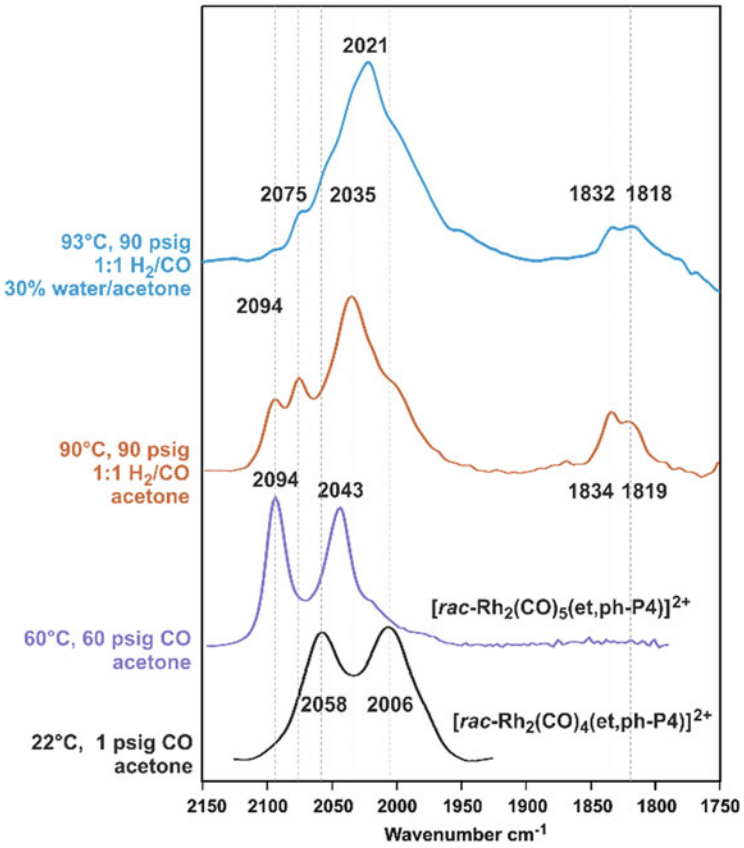

Fig. 11 FT-IR spectra of $[Rh_2(nbd)_2(rac\text{-et,ph-P4})]^{2+}$ under catalytic conditions (*top two spectra*). Reference carbonyl complexes shown on *bottom two spectra*

present in water/acetone, which corresponds to the open-mode dicationic pentacarbonyl complex **10r**. The second is the general shifting of the terminal carbonyl bands to lower wave numbers, consistent with a monocationic charge and more π-backbonding to the carbonyl ligands. The two bridging CO bands in water/acetone likely represent the presence of dicationic **11r** in equilibrium with the phosphine arm dissociated complex.

DFT calculations have proven to be of great importance in understanding the monocationic bimetallic catalyst system. Our initial structural proposals involved double-bridged complexes similar to the dicationic system. DFT optimizations on these starting hydride-carbonyl structures, however, consistently produced bimetallic complexes with only a single CO or hydride bridge, $[Rh_2(H)(\mu\text{-CO})(CO)_3(rac\text{-et,ph-P4})]^+$, **14r**, and $[Rh_2(\mu\text{-H})(CO)_4(rac\text{-et,ph-P4})]^+$, **15r**. Although DFT calculates **14r** as the lower energy structure, **15r** is only 1.8 kcal higher in energy.

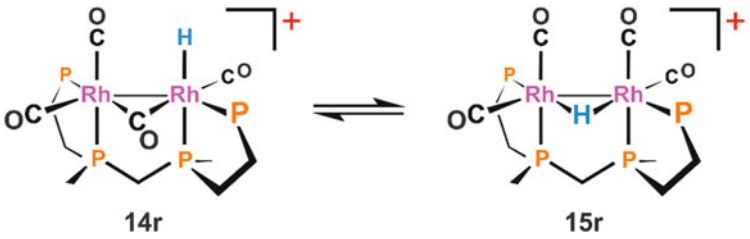

Experimentally, **14r** and **15r** have similar energies as indicated by broadened peaks indicating dynamic exchange in the in situ ^{1}H and ^{31}P NMR spectra (90 psig, 30% water/d_6-acetone) shown in Fig. 12. The ^{1}H NMR of the hydride region at 60°C only shows a single broadened resonance at −10.7 ppm, consistent with a dynamic exchange between these **14r** and **15r**. Although we propose that dicationic **11r** and **11r*** are also present, the hydride resonances for these around −7.8 ppm are not observed, most likely because their concentrations are too low or the resonance is broadened out due to exchange via deprotonation.

Note that there is only a small amount of bimetallic catalyst fragmentation occurring to form the monometallic complex $[RhH_2(\kappa^4\text{-}rac\text{-et,ph-P4})]^+$, **12r**, and no observable double-P4 ligand complex **13rr**. The ^{31}P NMR at 25°C also shows a symmetrical pattern consistent with a dynamic exchange between **14r** and **15r**.

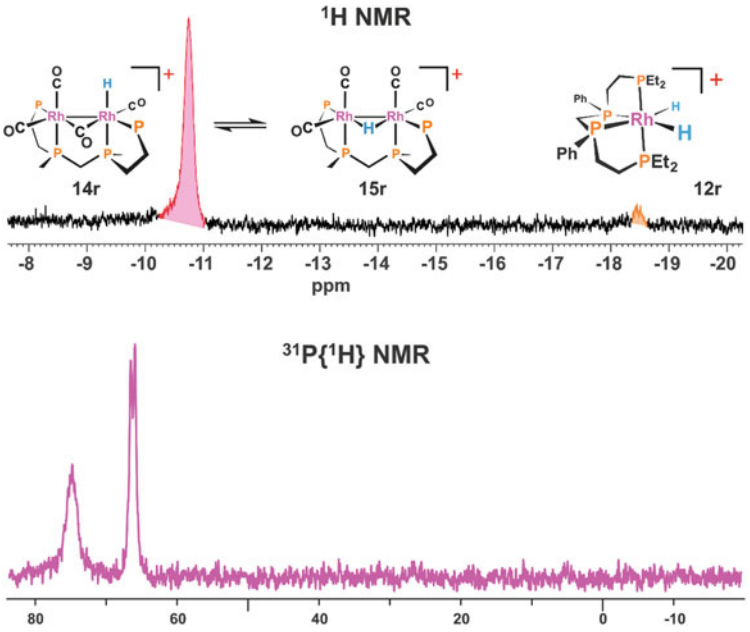

Fig. 12 ^{1}H and ^{31}P NMR spectra of $[Rh_2(nbd)_2(rac\text{-et,ph-P4})]^{2+}$ in 30% water/d_6-acetone producing an exchanging mixture of the monocationic dirhodium species **14r** and **15r**

Comparing this spectrum with that of the fragmentation-prone dicationic system in acetone (Fig. 4) reveals the dramatically improved stability of the monocationic bimetallic catalyst toward deactivation.

DFT calculations indicate that **15r** is the preferred monocationic catalyst for hydroformylation since it has lower activation barriers and energies relative to starting with **14r** as the catalyst. Additionally, the IR spectrum of the catalyst solution in water/acetone only shows low-intensity bridging CO bands that we assign to dicationic **11r/11r*** and **11r/11r*** with one phosphine dissociated. So there is clearly some reprotonation of the monocationic catalysts to regenerate the dicationic catalyst system, as one might expect. The differences in hydroformylation activity and selectivity between the water/acetone and acetone solvent systems indicate that the monocationic bimetallic system is the primary catalyst in water/acetone. The bridging CO for **14r** is likely to occur at 1,790 cm^{-1}, based on in situ FT-IR studies in THF, but is difficult to observe in water/acetone due to its low intensity and acetone solvent carbonyl band subtraction artifacts.

The proposed bimetallic hydroformylation mechanism for **15r** is shown in Fig. 13 and is based on our DFT calculations. In many ways the mechanistic steps parallel those for the dicationic catalyst, and bimetallic cooperativity once

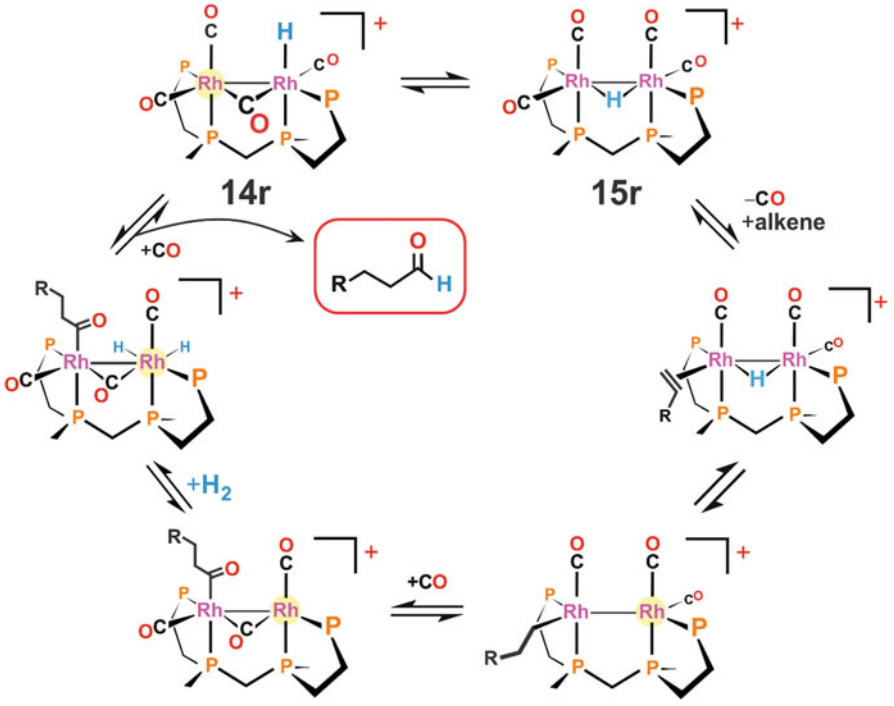

Fig. 13 Proposed monocationic bimetallic hydroformylation cycle based on **15r** and DFT calculations. Rh atoms shaded *yellow* have a localized cationic charge helping to labilize the carbonyls on that *center*

again plays an important role. One significant difference is that most of this cycle operates using Rh(+1) oxidation state bimetallic complexes versus the Rh(+2) oxidation state complexes for the dicationic cycle. DFT indicates an Rh–Rh covalent bond for **15r** and most of the species shown in Fig. 12, consistent with the common electron-counting method where a bridging hydride or CO is considered a 1e- donor to each metal center, leading to odd electron counts on the Rh(+1) d^8 atoms and the formation of a covalent bond between the metal centers. This is important in stabilizing the bimetallic closed-mode structure.

Another key point is that for most of the complexes shown in Fig. 13, one of the rhodium centers is formally cationic, which helps labilize the CO ligands to keep the bimetallic catalyst from becoming saturated. Since **15r** is monocationic and more electron-rich, we believe that on a per molecule basis it is less active compared to the dicationic catalyst **11r**/**11r***. But it is far more resistant to fragmentation reactions, which increases the concentration of the active catalyst in solution producing higher overall activity.

The DFT calculated energetics for the main hydroformylation reaction steps based on **15r** starting with the **15r**-alkene complex are shown in Fig. 14. The two largest activation barriers are for the initial alkene-hydride migratory insertion step (16.8 kcal/mol) and for the final reductive elimination of the acyl and hydride (21.6 kcal/mol). The computational prediction, therefore, is that the final aldehyde reductive elimination is the rate determining step for the monocationic catalyst **15r**. The largest activation barrier for the dicationic dirhodium catalyst (Fig. 8) is only 13 kcal/mol, indicating that the monocationic dirhodium catalyst should be less active on a per molecule basis, which is completely consistent with the impact of

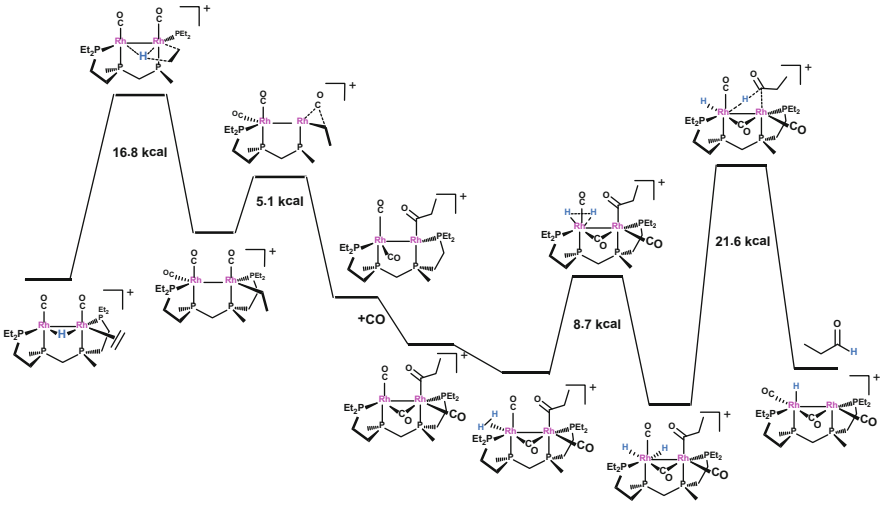

Fig. 14 Main part of proposed bimetallic monocationic hydroformylation cycle energetics based on DFT calculations using **15r**-**alkene** starting species. One of the phosphine chelates is not shown (or only partially) in several of the structures for clarity

stronger Rh-CO π-backbonding for more electron-rich hydroformylation catalysts. The higher overall activity of the monocationic dirhodium catalyst species in water/acetone solvent is due to the higher concentration of active catalyst present due to considerably reduced catalyst fragmentation and deactivation that occurs for the dicationic catalyst **11r/11r***.

Although the computed bimetallic mechanisms for the monocationic and dicationic catalysts follow an analogous series of fundamental reaction steps and rely heavily on bimetallic cooperativity throughout each cycle, there are some substantial differences in the energetics of the reactions steps. For example, the activation barrier for the initial alkene-hydride migratory insertion step for the dicationic catalyst **11r*** is about half (8 vs. 17 kcal) that for the monocationic catalyst **15r**. The dicationic alkyl intermediate **C** is quite a bit more stable than the corresponding species for the monocationic system. The other dramatic difference between the two systems is that the CO migratory insertion step for the monocationic catalyst has a very small barrier of 5 kcal vs. a 13 kcal barrier for the dicationic catalyst.

The other significant difference between the two bimetallic catalysts is that the monocationic monohydride dirhodium catalyst needs to oxidatively add H_2 in order to gain the hydride(s) to allow the reductive elimination of aldehyde. The dicationic dihydride system has the second hydride already present and "ready to go" for the acyl reductive elimination step. H_2 then oxidatively adds to the dicationic catalyst to regenerate the dihydride **11r/11r***. But since the monocationic catalyst system has a low activation barrier for H_2 oxidative addition (8.7 kcal), this is not a bottleneck in the catalysis cycle.

The need to oxidatively add H_2 to enable the reductive elimination of aldehyde makes the monocationic dirhodium catalyst **15r** somewhat similar to monometallic hydroformylation catalysts that have the same requirement. The presence of a formal cationic charge, however, helps compensate for the strongly donating, mainly alkylated phosphine ligands present that would normally dramatically reduce the activity of a monometallic hydroformylation catalyst via too strong coordination of the CO ligands and saturation of the metal center. Most of the proposed and computed intermediates in the cycle based on **15r** have a localized cationic charge residing on a single Rh center, weakening the Rh–CO bonding and enabling coordination and oxidative addition of H_2.

We believe that the presence of free H^+ in the acetone/water solvent system plays a role in the monocationic system. The rate determining step, once again, is the reductive elimination of aldehyde with a calculated barrier of 21.6 kcal (Fig. 14). Protonation of the monocationic dirhodium acyl is an alternate and likely pathway for eliminating aldehyde and forming the dicationic dirhodium catalyst **11r**. Due to the very low activation barrier for the monocationic alkyl-CO migratory insertion step, protonation of Rh-alkyl species to produce alkane is far less likely and consistent with the much lower alkane side reactions for **15r**.

Addition of 2 equivalents of NEt_3 to either the dicationic catalyst in acetone or the monocationic catalyst in water/acetone dramatically slows the hydroformylation. In acetone the initial TOF is reduced by ~34%, while in water/acetone

it is decreased by 80%. Part of the effect of base, especially with the dramatic effect on the monocationic system, is to deprotonate **14r/15r** to make neutral Rh_2 complexes that are extremely poor hydroformylation catalysts [45]. But we also believe that the H^+ concentration plays a role in the monocationic system for protonating the acyl to aldehyde. Addition of 5 equivalents of HBF_4 to the bimetallic catalyst system in water/acetone, however, also slows the hydroformylation and increases alkene isomerization. We believe that this generates more dicationic catalyst and enhances the catalyst fragmentation and deactivation.

Although the monocationic dirhodium catalyst **14r/15r** is far more resistant to fragmentation and deactivation relative to the dicationic species **11r/11r***, the in situ NMR spectroscopy still shows some fragmentation of **14r/15r** to the inactive monometallic complex, $[RhH_2(\kappa^4\text{-et,ph-P4})]^+$, **12r** (Fig. 9). This may be via a reprotonation of **14r/15r** to the dicationic system or via a much slower fragmentation directly from **14r/15r** also due to phosphine chelate arm dissociation intrinsic to the monocationic complexes. A variant of the catalyst fragmentation equilibria shown in Fig. 9 likely affects **14r/15r**, most likely via phosphine arm dissociation. Hydroformylation studies using variable H_2/CO ratios with water/acetone solvent support this and are shown in Table 3 [46].

The fragmentation equilibrium shown in Fig. 9 is highly dependent on the partial pressure of CO and H_2. More CO promotes fragmentation of the dirhodium complex. Higher H_2 pressures or ratios favor the active hydride-containing complexes. Reducing both the H_2 and CO partial pressures in Table 3 (experiment 2) leads to the expected reduction in turnover frequency, but note the increase in aldehyde linear to branched regioselectivity (33:1 to 55:1). The lower CO-pressure favors coordination of the phosphine chelate, which maximizes the steric directing effects and higher l:b aldehyde selectivity. Raising the H_2 partial pressure while

Table 3 Hydroformylation using $[Rh_2(nbd)_2(rac\text{-et,ph-P4})]^{2+}$ and variable ratio H_2/CO studies in 30% water/acetone (partial pressures of H_2 and CO in psig)

H_2/CO	pH_2	pCO	TOF	TON	l:b	% Linear	Isomerization
1:1	45.0	45.0	30(2)	1,000	33:1	97.1	1%
1:1	22.5	22.5	20(1)	1,000	55:1	98.2	1%
2:1	45.0	22.5	27(2)	1,000	64:1	98.5	1%
3:1	67.5	22.5	30(2)	1,000	75:1	98.7	1%
4:1	88.0	22.5	46(1)	1,000	152:1	99.3	7.7%[a]
1:4	22.5	82.5	–	0	–		–
1:3	22.5	67.5	–	0	–		–

Conditions: 90°C, 1 M 1-hexene (1,000 equivalents), 1 mM Rh catalyst, solvent = 30% H_2O in acetone for all tested systems, constant pressure conditions, 1,000 rpm stirring; pressures listed as psig, TOF = initial turnover frequency with standard deviation based on four consistent runs, TON = total turnover number (alkene reactant converted to products), l:b = aldehyde linear to branched regioselectivity, Isom = alkene isomerization, there is less than 1% alkene hydrogenation for all runs

[a]ca. 5% n-heptanol produced

keeping the CO partial pressure at 22.5 psig causes dramatic increases in turnover frequency and aldehyde l:b regioselectivity.

One factor to note is that a constant pressure was maintained in the autoclaves with the H_2/CO ratio indicated. But the hydroformylation reaction only consumed 1:1 H_2/CO. Thus, as the reaction proceeded, the H_2/CO ratio for experiments with higher H_2 partial pressures also increased. This is most clearly indicated by the 4:1 H_2/CO experiment where considerable CO depletion occurred leading to enhanced alkene isomerization and some hydrogenation of the aldehyde to alcohol. The remarkably strong inhibitory effect of CO is clearly shown by the last two experiments in Table 3 where 1:4 and 1:3 H_2/CO experiments did no hydroformylation.

The effect of increased H_2/CO ratios on monometallic hydroformylation catalysts is similar regarding increases in initial turnover frequency and aldehyde l:b regioselectivity. Monometallic Rh catalysts based on Naphos, Bisbi, and Xantphos chelating ligands were also tested, and those results are shown in Table 4 [46]. The general trends for the Naphos and Bisbi ligand-based monometallic hydroformylation catalyst are quite similar to what we see for our bimetallic system: lowering the overall pressure with a 1:1 H_2/CO ratio results in lower initial TOF, an increase in aldehyde l:b regioselectivity, and a small increase in alkene

Table 4 H_2/CO ratio hydroformylation runs using $Rh(CO)_2(acac)$ and phosphine ligand shown

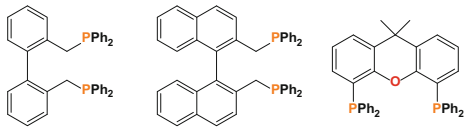

Rh catalyst	H_2/CO	pH_2	pCO	TOF	TON	l:b	% Linear	Isom
Naphos	1:1	45.0	45.0	35(1)	1,000	120:1	99.2	2.2%
Naphos	1:1	22.5	22.5	27(2)	950	160:1	99.4	3%
Naphos	3:1	67.5	22.5	48(7)	700	360:1	99.7	4%
Naphos	4:1	88.0	22.5	87(7)	810	360:1	99.7	3%
Bisbi	1:1	45.0	45.0	37(1)	1,000	80:1	98.8	2%
Bisbi	1:1	22.5	22.5	24(1)	975	90:1	98.9	3%
Bisbi	3:1	67.5	22.5	61(7)	550	150:1	99.3	2%
Bisbi	4:1	88.0	22.5	26(3)	530	162:1	99.4	3%
Xantphos	1:1	45.0	45.0	28(1)	1,000	60:1	98.4	<1%
Xantphos	1:1	22.5	22.5	26(4)	900	55:1	98.2	1.5%
Xantphos	3:1	67.5	22.5	21(2)	750	49:1	98.0	2%
Xantphos	4:1	88.0	22.5	20(2)	845	40:1	97.6	5%

Conditions: 90°C, 1 M 1-hexene (1,000 equivalents), 1 mM Rh catalyst, 5 equivalent of phosphine ligand, solvent = 30% H_2O in acetone for all tested systems, constant pressure conditions, 1,000 rpm stirring; pressures listed as psig, TOF = initial turnover frequency with standard deviation based on four consistent runs, TON = total turnover number (alkene reactant converted to products), l:b = aldehyde linear to branched regioselectivity, Isom = alkene isomerization – there is less than 1% alkene hydrogenation for all runs

isomerization. Increasing the H_2/CO ratio while maintaining a low CO partial pressure increases the initial TOF substantially along with the aldehyde l:b ratio.

But all the monometallic catalysts deactivate before they can complete the 1,000 turnovers (100% conversion of alkene). This is tied into Rh-induced phosphine orthometalations and P–Ph or P–benzyl bond cleavage reactions that lead to monometallic catalyst deactivation [4]. Bisbi is especially susceptible to deactivation under these conditions, barely making it past 50% conversion of the alkene. The mainly alkylated et,ph-P4 ligand does not seem to suffer from Rh-induced phosphine fragmentations under these conditions, but does tend to lose a rhodium center and "fragment" losing the bimetallic cooperativity.

The Xantphos-based monometallic hydroformylation catalyst also deactivates before converting all the alkene to aldehyde under reduced CO pressures but behaves differently in that both the initial TOF and aldehyde l:b regioselectivity decreases with higher H_2/CO ratios while keeping the CO partial pressure low. We believe the reason for this is that the Xantphos ligand can coordinate to the Rh center via the central oxygen atom, but this is a weaker interaction than the Rh–P bonds. At low CO partial pressures, the Xantphos favors the κ^3-mode using the phosphines and central oxygen atom leading to less reactive and selective catalysts. Higher CO pressures favor dissociation of the Xantphos oxygen leading to a more active catalyst with a folded Xantphos configuration that is more sterically directing relative to the flatter Xantphos structure when the oxygen atom is coordinated to the rhodium [47, 48].

5 Catalyst Binding Site Considerations

The high product aldehyde regioselectivity observed for our bimetallic catalyst, either dicationic or monocationic, is a result of the relatively rigid dinuclear structure of **11r/11r*/15r** and the proper arrangement of steric effects on the et, ph-P4 ligand/catalyst. When an alkene coordinates to a typical monometallic square-planar hydroformylation catalyst, the other ligands will bend away to form a trigonal bipyramid or square pyramid, which is the least congested coordination geometry (Fig. 15). This geometric reorganization results from electronic orbital rehybridization on the metal center and causes the steric directing groups on the phosphine ligands to swing away from the incoming alkene substrate. This, in turn, reduces the steric effectiveness of the phosphine for orienting the alkene to insert properly into the Rh–H bond to give the desired linear alkyl intermediate species.

The bimetallic catalysts, however, cannot distort this way on alkene coordination because the Rh–Rh bond and bridging ligand(s) prevents any significant movement of the ligand environment away from the alkene. Minimizing the geometric reorganization about the rhodium maximizes the steric effect of the et, ph-P4 ligand, directing the alkene insertion into the M–H bond to form a linear alkyl group, which goes on to form the linear aldehyde product.

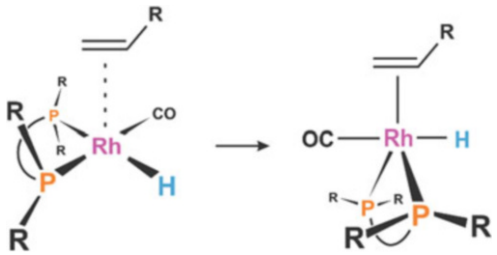

Fig. 15 Electronically driven transformation of ligand environment from square planar to 5-coordinate upon coordination of alkene

We believe that the Rh–Rh bond and bridging ligand(s) plays a critical role in defining and enhancing the steric factors present in our alkene binding site. There are no regioselective monometallic hydroformylation catalysts with phosphine ligands that have the small R-groups present in et,ph-P4 (an ethyl and phenyl). Except for a minor increase at 1-hexene, dicationic **11r/11r*** has essentially constant linear to branched regioselectivity across a fairly broad series of alkenes in acetone solvent: propylene (20:1), 1-butene (20:1), 1-pentene (23:1), 1-hexene (28:1), 1-heptene (21:1), and 1-octene (21:1). We haven't studied this entire series with monocationic **15r** yet, but believe it will exhibit higher regioselectivities with minimal variations between alkenes as it has a similarly well-defined binding site. This behavior is quite unusual compared to monometallic hydroformylation catalysts that show a considerably larger regioselectivity range that increases with longer chain alkene substrates.

6 Future Studies

The facile fragmentation and deactivation of the dicationic dirhodium catalyst in acetone was disappointing as we specifically designed the et,ph-P4 ligand to be a strong chelator and to minimize bimetallic fragmentation – a problem that has plagued multimetallic homogeneous catalysts. Although the monocationic bimetallic hydroformylation catalyst has considerably improved stability relative to the dicationic dirhodium system, a better binucleating ligand to generate even more robust but active catalysts was needed. The next-generation binucleating tetraphosphine has been designed with 1,2-phenylene-linked chelates, one of the strongest chelators known in transition metal chemistry. The *rac*- and *meso*-et,ph-P4-Ph ligands are shown below.

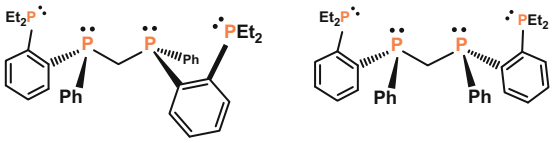

***rac*-et,ph-P4-Ph** ***meso*-et,ph-P4-Ph**

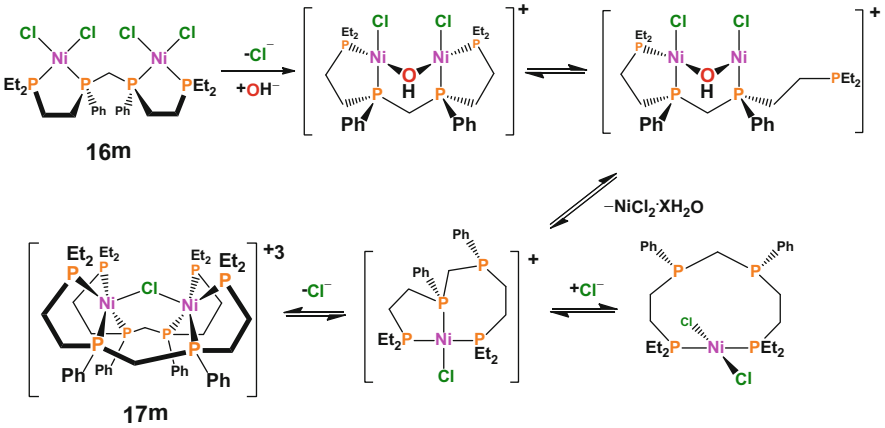

Scheme 4 Facile fragmentation of Ni_2Cl_4(et,ph-P4), **16m**, in the presence of water at room temperature

The ligand synthesis, characterization, and dinickel tetrachloride complexes based on this new P4 ligand have been reported [49]. Our unpublished work on comparisons between the new P4-Ph chelated bimetallic complexes and similar systems based on the "old" P4 ligand clearly demonstrate that the P4-Ph ligand is a much stronger chelator and dramatically minimizes fragmentation reactions of bimetallic complexes based on it. For example, *rac*- and *meso*-[Ni_2Cl_4(et,ph-P4)] complexes, **16**, fragment readily at room temperature when water is added to acetonitrile, acetone, or DMSO. The proposed fragmentation equilibrium for the *meso*-[Ni_2Cl_4(et,ph-P4)] complex, **16m**, is shown in Scheme 4.

After 24–48 h at room temperature with 15% water present, **16m** completely converts to the double-P4 coordinated dinickel complex **17m**, which has been crystallographically characterized and is isostructural with [Pt_2(μ-Cl)(*meso*-ph,ph-P4)]$^{3+}$ prepared by Anderson and coworkers [50]. Heating **17m** in the absence of water and two equivalents of $NiCl_2$ plus some extra chloride will reform **16m**. The ease of fragmentation for this dinickel system appears to be clearly tied into a facile chelate arm dissociation, as proposed for the dicationic dirhodium hydroformylation catalyst **11r/11r*** (or even **11r****).

Ongoing reaction studies on the new more strongly chelated P4-Ph bimetallic nickel complexes, *rac*- and *meso*-[Ni_2Cl_4(et,ph-P4-Ph)], with water show that the bridged hydroxide complex, [Ni_2(μ-OH)Cl_2(*meso*-et,ph-P4-Ph)]$^+$, forms but without any subsequent fragmentation even at elevated temperatures (60°C). [Ni_2(μ-OH)Cl_2(*meso*-et,ph-P4-Ph)]$^+$ has been crystallographically characterized. Furthermore, the bridged hydroxide is the primary molecular ion when either *rac*- or *meso*-[Ni_2Cl_4(et,ph-P4-Ph)] is analyzed by LC-MS using a methanol/water/formic acid mobile phase. The considerably higher stability of the bridged

hydroxide dinickel complexes with the new P4-Ph ligand supports the much stronger chelating ability and that it appears to favor closed-mode bimetallic complexes.

We are about to start hydroformylation studies using the dirhodium bis-norbornadiene catalyst precursor based on the new *rac*-et,ph-P4-Ph ligand. This new more strongly chelated catalyst should be dramatically more resistant to deactivating fragmentation reactions for the highly active dicationic catalyst. These studies will be reported in due course.

Acknowledgments This research has been supported over the years by NSF, the Louisiana Board of Regents through their Industrial Ties programs, and the following companies: Hoechst Celanese, Arco Chemical, Albemarle, Ferro, Eastman Chemical, Sasol North America, and current funding from Dow Chemical. Additionally, the team leader had excellent discussions and interactions with hydroformylation experts at Union Carbide (now Dow), ExxonMobil, and Shell Chemical.

References

1. Cornils B (1980) In: Falbe J (ed) New syntheses with carbon monoxide. Springer, Berlin
2. Tkatchenko I (1982) In: Wilkinson G, Stone FGA, Abel EW (eds) Comprehensive organometallic chemistry. Pergamon, Oxford
3. Stanley GG (1994) In: King B (ed) Encyclopedia of inorganic chemistry. Wiley, New York
4. van Leeuwen PWNM, Claver C (eds) (2000) Rhodium catalyzed hydroformylation. Kluwer, Dordrecht
5. Börner A (2012) Chem Rev 112:5675. doi:10.1021/cr3001803
6. Muetterties EL (1975) Bull Soc Chim Belg 84:959. doi:10.1002/bscb.19750841006
7. Muetterties EL (1976) Bull Soc Chim Belg 85:451. doi:10.1002/bscb.19760850701
8. Muetterties EL (1978) Angew Chem Int Ed Engl 17:545. doi:10.1002/anie.197805453
9. Muetterties EL, Krause MJ (1983) Angew Chem Int Ed Engl 22:135. doi:10.1002/anie.198301351
10. Heck RF, Breslow DS (1961) J Am Chem Soc 83:4023. doi:10.1021/ja01480a017
11. Jones WD, Huggins JM, Bergman RG (1981) J Am Chem Soc 103:4415. doi:10.1021/ja00405a022
12. Nappa MJ, Santi R, Halpern J (1985) Organometallics 4:34. doi:10.1021/om00120a007
13. Martin BD, Warner KE, Norton JR (1986) J Am Chem Soc 108:33. doi:10.1021/ja00261a008
14. Ungváry F, Markó L (1983) Organometallics 2:1608. doi:10.1021/om50005a021
15. Mirbach MF (1984) J Organomet Chem 265:205. doi:10.1016/0022-328X(84)80075-3
16. Moser WR (1992) In: Moser WR, Slocum DW (eds) Homogeneous transition metal catalyzed reactions. ACS advances in chemistry series, vol 230. ACS, Washington, p 14, Chapter 1
17. Ryan RC, Pittman CU Jr, O'Connor JP (1977) J Am Chem Soc 99:1986. doi:10.1021/ja00448a057
18. Pittman CU Jr, Wilemon GM, Wilson WD, Ryan RC (1980) Angew Chem Int Ed Engl 19:478. doi:10.1002/anie.198004781
19. Don M-J, Richmond MG (1992) J Mol Catal 73:181. doi:10.1016/0304-5102(92)80071-N
20. Sanger AR (1983) In: Pignolet LH (ed) Homogeneous catalysis with metal phosphine complexes. Plenum, New York, pp 228–233, Chapter 6
21. Ceriotti A, Garlaschilli L, Longoni G, Malatesta MC, Strumolo D, Fumagalli A, Martinengo S (1984) J Mol Catal 24:309. doi:10.1016/0304-5102(84)85118-4
22. Garland M (1993) Organometallics 12:535. doi:10.1021/om00026a041

23. Kalck P (1988) Polyhedron 7:2441. doi:10.1016/S0277-5387(00)86365-2
24. Davis R, Epton JW, Southern TG (1992) J Mol Catal 77:159. doi:10.1016/0304-5102(92)80196-N
25. Laneman SA, Fronczek FR, Stanley GG (1988) J Am Chem Soc 110:5585. doi:10.1021/ja00224a061
26. Laneman SA, Fronczek FR, Stanley GG (1989) Inorg Chem 28:1872. doi:10.1021/ic00309a021
27. Laneman SA, Fronczek FR, Stanley GG (1989) Inorg Chem 28:1206. doi:10.1021/ic00306a003
28. Broussard ME, Juma B, Train SG, Peng WJ, Laneman SA, Stanley GG (1993) Science 260:1784. doi:10.1126/science.260.5115.1784
29. Pruett RL, Smith JA (1969) J Org Chem 34:327. doi:10.1021/jo01254a015
30. Kastrup RV, Merola JS, Oswald AA (1982) In: Alyea EC, Meek DW (eds) Catalytic aspects of metal phosphine complexes, vol 196, Advances in chemistry series. American Chemical Society, Washington, Chap. 3
31. Brown JM, Kent AG (1987) J Chem Soc Perkin Trans 1597. Doi:10.1039/p29870001597
32. Matthews RC, Howell DK, Peng WJ, Train SG, Treleaven WD, Stanley GG (1996) Angew Chem Int Ed Engl 35:2253. doi:10.1002/anie.199622531
33. Hunt C Jr, Fronczek FR, Billodeaux DR, Stanley GG (2001) Inorg Chem 40:5192. doi:10.1021/ic010003s
34. Cotton FA, Walton RA (1993) Multiple bonds between metal atoms. Clarendon Press/Oxford University Press, Oxford/New York, pp 431–501
35. Cotton FA, Eagle CT, Price AC (1988) Inorg Chem 27:4362. doi:10.1021/ic00297a007
36. Tortorelli LJ, Tinsley PW, Woods C, Janke CJ (1988) Polyhedron 7:315. doi:10.1016/S0277-5387(00)80473-8
37. Woods C, Tortorelli LJ (1988) Polyhedron 7:1751. doi:10.1016/S0277-5387(00)80407-6
38. Bianchini C, Meli A, Laschi F, Ramirez JA, Zanello P, Vacca A (1988) Inorg Chem 27:4429. doi:10.1021/ic00297a019
39. Sutherland BR, Cowie M (1984) Inorg Chem 23:1290. doi:10.1021/ic00177a023
40. Bianchini C, Laschi F, Masi D, Mealli C, Meli A, Ottaviani FM, Proserpio DM, Sabat M, Zanello P (1989) Inorg Chem 28:2552. doi:10.1021/ic00312a011
41. Schiavo SL, Bruno G, Nicolo F, Piraino P, Faraone F (1985) Organometallics 4:2091. doi:10.1021/om00131a004
42. Sivak AJ, Muetterties EL (1979) J Am Chem Soc 101:4878. doi:10.1021/ja00511a016
43. Thorn DL, Ibers JA (1982) Adv Chem Ser 196:117. doi:10.1021/ba-1982-0196.ch007
44. Aubry DA, Bridges NN, Ezell K, Stanley GG (2003) J Am Chem Soc 125:11180. doi:10.1021/ja035926w
45. Peng W-J, Train SG, Howell DK, Fronczek FR, Stanley GG (1996) Chem Commun 2607. Doi:10.1039/CC9960002607
46. Barker BL (2005) LSU dissertation. http://etd.lsu.edu/docs/available/etd-04132005-131235/unrestricted/Barker_dis.pdf
47. Sandee AJ, Reek ANH, van Leeuwen PWMN (1999) Angew Chem Int Ed 38:3231. doi:10.1002/(SICI)1521-3773(19991102)
48. Zuiedveld MA, van Leeuwen PWMN (2002) J Chem Soc Dalton Trans 2308. Doi: 10.1039/B111596K
49. Schreiter WJ, Monteil AR, Kalachnikova K, Peterson MA, Gasery CD, McCandless GT, Fronczek FR, Stanley GG (2014) Inorg Chem 53:10036. doi:10.1021/ic5019345
50. Nair P, White CP, Anderson GK, Rath NP (2006) J Organomet Chem 691:529. doi:10.1016/j.jorganchem.2005.09.021

Top Organomet Chem (2016) 59: 31–58
DOI: 10.1007/3418_2015_145

Published online: 26 August 2015

Binuclear Iridium Complexes in Catalysis

Manuel Iglesias, Eduardo Sola, and Luis A. Oro

Abstract In this chapter, recent progresses in the use of binuclear iridium complexes as catalysts for the preparation of value-added organic molecules and the catalytic cycles involved in these reactions are presented. The reactivity of these complexes toward a variety of substrates and the intermetallic cooperation mechanisms that differentiate binuclear entities from their mononuclear counterparts are reviewed and analyzed in detail. Oxidative addition and reductive elimination reactions usually occur at one of the iridium centers followed by ligand migration to the vicinal iridium atom or to bridging positions, although cooperative activation of various substrates has been proposed in the literature. The close proximity of two metal centers in binuclear complexes, and their ability to cooperate, brings about new reactivity patterns that very often differ from those expected for related monometallic systems. Especially noteworthy is the transmission of ligands *trans* effects (or influences) via bridging ligands or intermetallic bonds, together with the facile migration of hydrides between metals and the interaction between iridium centers in $Ir_2^{I,I}$ dimers, which seem to govern the chemistry of diiridium complexes. In this regard, it is worth noting that single-site activation does not exclude a cooperative bimetallic cycle. Most of the reported catalytic cycles based on bimetallic iridium complexes follow inner sphere mechanisms, but the presence of outer sphere pathways cannot be excluded as exemplified by recent reports on ionic or dimetal–ligand bifunctional mechanisms; therefore, bimetallic iridium catalysis may show one or more cooperation mechanism.

Keywords Binuclear complexes, Bond activation, Homogeneous catalysis, Intermetallic cooperation, Iridium, Ligand migration, *Trans* effect

M. Iglesias (✉), E. Sola, and L.A. Oro (✉)
Department of Inorganic Chemistry, ISQCH, University of Zaragoza-CSIC, Pedro Cerbuna 12, 50009 Zaragoza, Spain
e-mail: miglesia@unizar.es; oro@unizar.es

Contents

1 Introduction

Metal cooperation is a widely used concept in enzyme catalysis, often invoked in order to rationalize activities and selectivity patterns inaccessible by action of a single metal center [1–13]. An illustrative example is the enzyme tyrosinase, which catalyzes the hydroxylation of tyrosine to DOPA (3,4-dihydroxyphenylalanine) and its subsequent oxidation to the corresponding quinone. Tyrosinase makes use of an active site based on a bimetallic copper complex that activates molecular oxygen. The deoxy form consists of a [Cu(I) Cu(I)] core, while the oxygenated site presents a μ-η^2:η^2-peroxide (O_2^{2-}) bridge: [Cu(I)O_2Cu(I)]. According to the generally accepted catalytic cycle (Scheme 1), the binuclear nature of the catalyst is required, not only for the activation of molecular oxygen but also for the transfer of the oxygen atom in the hydroxylation of tyrosinase, as well as for the two-electron oxidation of DOPA [14–21].

Despite the vast number of outstanding examples of enzymatic catalysis that rely on the collaboration of two or more vicinal metal centers hitherto disclosed, the design and development of efficient binuclear organometallic complexes able to enhance the performance of mononuclear catalyst by means of an intermetallic cooperative process remains widely unexplored [22–24]. In fact, the formation of bi- or polynuclear complexes has been often described as a catalyst deactivation pathway [25–30]. However, the availability of more electron density at the active site, extra coordination positions, and the possibility to develop more preorganized systems that allow for (enantio)selective reactions shows great promise for an improved catalytic performance [9].

Binuclear rhodium complexes in particular have met with great success as catalysts for various transformations, especially remarkable are the Rh (II) examples reported by Doyle et al. [31] (and references therein) and Stanley's system for hydroformylation [32–38]. The latter showed an excellent regioselectivity for the hydroformylation of 1-hexene with remarkable turnover numbers (ca. 12,000 cycles) and frequencies (73 min^{-1}). The enhanced activity and

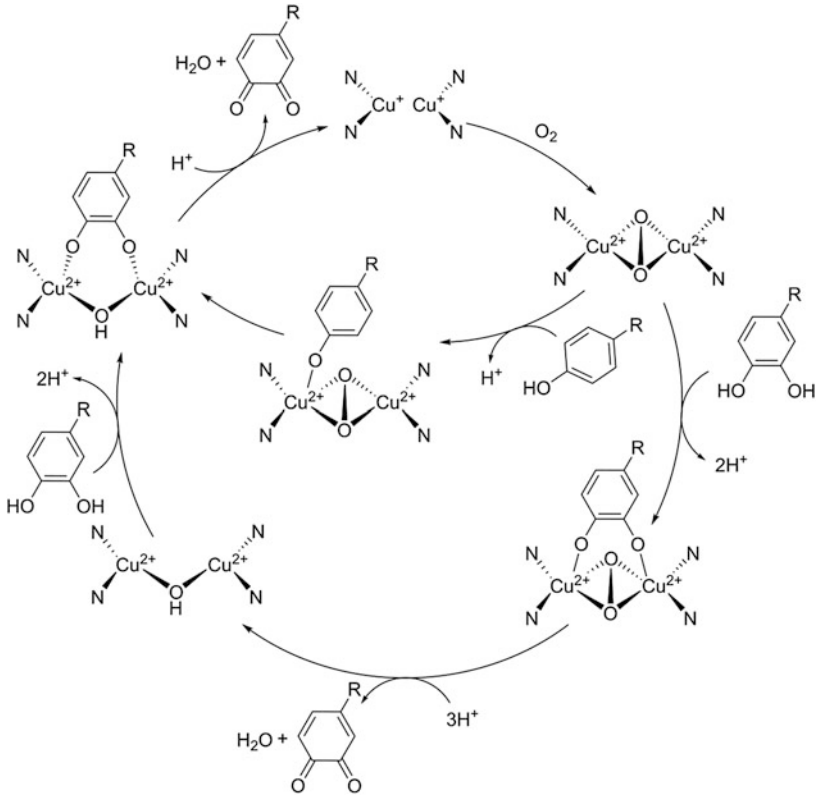

Scheme 1 Catalytic cycle for the hydroxylation of tyrosine and the oxidation of DOPA. N = histidine residues (axial ligands at the coppers were omitted for clarity); R = alanine

selectivity compared to its mononuclear analogue has been attributed to (i) the intramolecular hydride transfer, which facilitates the reductive elimination of the aldehyde, thus improving the reactivity, and (ii) the rigid structure of the bimetallic core, which directs the selectivity of the process (Scheme 2).

2 Elementary Steps in Binuclear Catalysis

Elementary steps in binuclear catalysis can differ significantly from those described for mononuclear complexes due to the proximity of a second metal center. A brief description of binuclear oxidative addition, reductive elimination, ligand migration, and migratory insertion will be made in order to facilitate the understanding of the mechanisms discussed in this chapter.

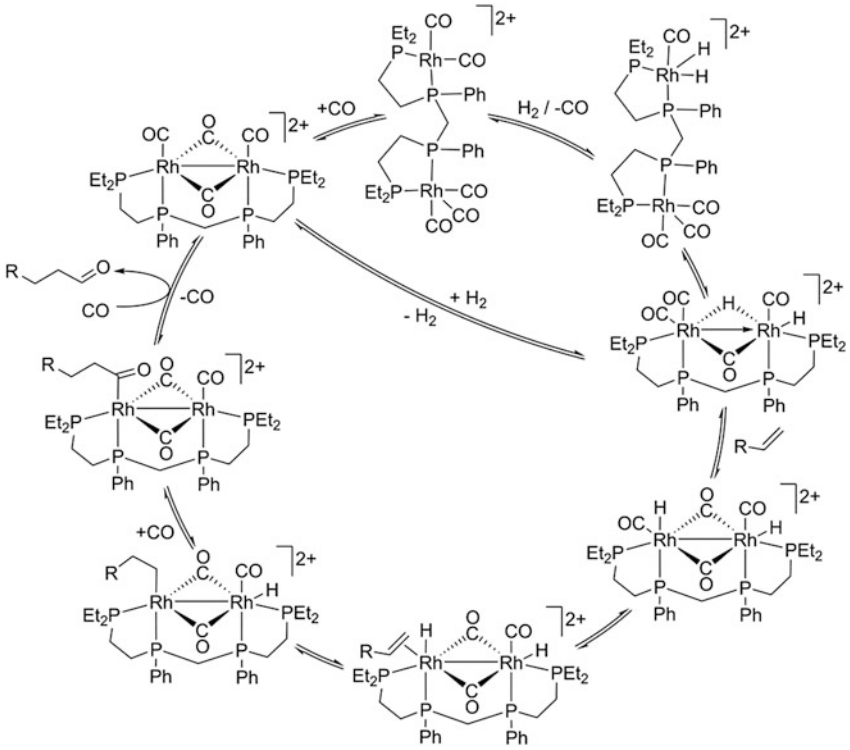

Scheme 2 Hydroformylation of 1-hexene catalyzed by Stanley's system

2.1 Oxidative Addition/Reductive Elimination

Several mechanisms can be envisaged for the oxidative addition or reductive elimination in binuclear systems, which may depend on the nature of the substrate and the metallic core. Intuitively, the mechanism for the oxidative addition of molecular hydrogen and its microscopic reverse reaction may be proposed to occur by a concerted symmetric mechanism (least-motion pathway; Scheme 3a). However, theoretical calculations have revealed that this pathway is spin forbidden and leads to prohibitive activation energies [39]. The most generally accepted mechanism (non-least-motion pathway; Scheme 3b) entails (i) initial coordination of molecular hydrogen to one of the metal centers, followed by (ii) oxidative addition of H_2 to give $M_2(\mu\text{-H})(H)$, and, finally, (iii) migration of the bridging hydride over the other metal center.

Step (ii) could take place by two different routes (Scheme 4): the oxidative addition may happen over one of the metal centers, as it would be expected to occur for a mononuclear complex, or in a cooperative fashion, i.e., aided by the second metal. The resulting mixed-valent complex features a dative metal–metal bond, where the metal in a lower formal oxidation state donates electron density to the

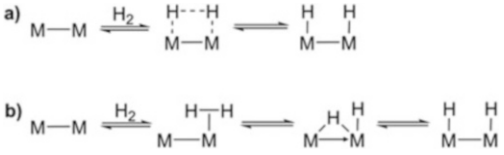

Scheme 3 Least-motion (**a**) and non-least-motion (**b**) pathways for the binuclear oxidative addition of molecular hydrogen

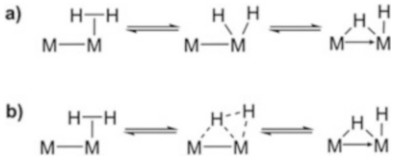

Scheme 4 Oxidative addition of H_2: (**a**) at a single metal center and (**b**) aided by the second metal

second (in a higher formal oxidation state). This type of species has been postulated as intermediates in binuclear catalytic cycles and, what is more, characterized and isolated [40–48]. Although no conclusive data permits to establish whether the oxidative addition takes place thanks to metal–metal cooperation or via a single-site process, the fact that challenging oxidative additions for mononuclear species occur under relatively mild conditions for binuclear complexes suggests that the latter may occur at least in these cases [49–53].

2.2 *Migratory Insertion, β-Hydrogen Elimination, and Ligand Migration*

Little has been reported on the β-hydrogen elimination [54] or migratory insertion [41, 55–58] at binuclear systems, and, therefore, no irrefutable reactivity trends or mechanisms can be established from the available data. Noteworthy, several examples show that the reaction rates for β-hydrogen elimination in binuclear complexes are higher than those obtained for mononuclear analogues. For instance, β-hydrogen elimination at (dppe)EtPt–$MoCp(CO)_3$, (dppe)EtPt–$WCp(CO)_3$, and (dppe)EtPt–$CoCp(CO)_4$ takes place significantly faster than that at PtEtCl (dppe) [54].

Migratory insertion reactions seem to occur at a single site, similar to what would be expected for a mononuclear complex, although the facile migration of ligands (including hydrides, alkyl groups, or carbonyl ligands) from one metal to the other in binuclear complexes contributes to achieve the right ligand disposition for the insertion to happen. Consequently, the migrating ligand and the vacant coordination site do not need to reside in the same metal center [41, 57]. Similarly, the vacancy generated by the migratory insertion may end at the other side of the bimetallic complex, thus enabling subsequent reactions not possible for mononuclear entities [59].

The extended coordination possibilities offered by the bridging positions may also turn into reactivity advantages, as proposed for one of the rare examples of

imine insertion into metal–hydride bonds [60]. The same concept was applied to alkyne insertions leading to bridging alkenyls, in this case aiming to explain unusual stereoselectivities in stoichiometric [61] or catalytic [62] reactions.

3 *Trans* Effect in Bimetallic Complexes

The *trans* effect/influence in binuclear complexes brings about two main phenomena that are not observed in mononuclear complexes: (i) the position of the bridging ligands is determined by the *trans* influences of ligands in both metals, and (ii) the *trans* effect/influence of a terminal ligand in one of the metal centers can be transmitted to the adjacent metal center via a bridging hydride or an intermetallic bond.

3.1 Position of Bridging Ligands

Hydrides are one of the most commonly found bridging ligands in iridium homobimetallic complexes. The symmetry or asymmetry of the hydride bridge is usually determined by the nature of the *trans*-ligands in both metal centers. For example, the complexes depicted in Fig. 1 feature asymmetric hydride bridges in solution and in the solid state. Although the position of the bridging hydrides obtained from X-ray diffraction must be examined with care due to the limited accuracy of the technique for these situations, this assumption has been also supported by NMR studies in solution [63, 64].

The asymmetry of the bridge has been attributed to the different *trans* influence of the ligands in *trans* positions to the bridging hydrides. For example, the μ-H ligand in complex $[Ir_2((CH_3)_2CO)(CO)_2(H)(\mu\text{-}H)(\mu\text{-}1,8\text{-}(NH)_2naphtha)(P^iPr_3)_2)][CF_3SO_3]_2$ presents two *trans*-ligands that possess very different *trans* influences, namely, an acetone and a hydride ligand. For that reason, the μ-hydride is closer to the metal that contains the *trans*-ligand with the weakest *trans* effect, in this case acetone.

3.2 Intermetallic Trans *Effect/Influence*

The intermetallic *trans* influence in L–Au–Au–L′ complexes has been postulated in order to explain the Au–L′ bond length, which changes depending on the *trans* influence of L, while the Au–Au distance remains unaltered [65, 66]. Focusing on the chemistry of homobimetallic iridium complexes, several illustrative cases of intermetallic *trans* effect can be found. For example, complexes $[Ir_2(CH_3CN)(H)_3(\mu\text{-}H)(\mu\text{-}Pz)_2(P^iPr_3)_2]$ and $[Ir_2(CH_3CN)(Cl)(H)_2(\mu\text{-}H)(P^iPr_3)_2(\mu\text{-}Pz)_2]$ (Fig. 2)

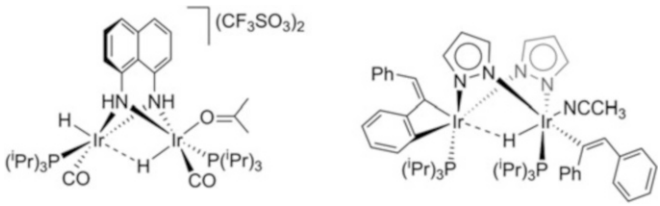

Fig. 1 Depiction of complexes $[Ir_2((CH_3)_2CO)(CO)_2(H)(\mu\text{-}H)(\mu\text{-}1,8\text{-}(NH)_2naphtha)(P^iPr_3)_2][CF_3SO_3]_2$ [63] (*left*) and $[Ir_2\{\kappa C\text{-}C_6H_4\text{-}2\text{-}[\kappa C\text{-}(Z)\text{-}C{=}CHPh]\}\{(Z)\text{-}C(Ph){=}CHPh\}(CH_3CN)(\mu\text{-}H)(\mu\text{-}Pz)_2(P^iPr_3)_2]$ [64] (*right*)

show very different reactivity toward the substitution on the acetonitrile ligand. The former readily losses the CH_3CN ligand giving rise to a rich substitution chemistry, whereas the latter is inert toward good ligands such as pyrazole, CO, or ethylene. A plausible explanation for this drastically different behavior rests in the transmission of the *trans* effect from one metal to the other through the hydride bridge. This postulation would be in agreement with the strong σ-orbital mixing along the H_a–Ir–H_b–Ir–$NCCH_3$ axis suggested by theoretical calculations. Moreover, X-ray and ^{1}H-NMR data of both complexes show clarifying structural information that reveals the different nature of the hydride bridge in the H- and Cl-derivatives. The strong *trans* influence of H_a brings about an enlargement of the Ir–H_b distance, which pushes H_b closer to the second metal center, whereas the chloride derivative features a symmetric hydride bridge equidistant from both metal centers. Consequently, the proximity of H_b to the second iridium center translates into an enhanced *trans* effect, i.e., lability of the acetonitrile ligand compared to its chloride analogue [59, 67].

The *trans* effect can also be transmitted via an intermetallic bond as shown in Scheme 5, where a strong *trans*-labilizing methyl group leads to reversible coordination of carbon monoxide. The parent isomer, on the other hand, which presents a P^iPr_3 in *trans* to the vacant coordination site, affords the stable CO adduct [68].

4 Homobimetallic Iridium Complexes: Reactivity and Catalysis

This section will focus on the reactivity and catalytic applications of homobimetallic iridium complexes containing the two metal centers in close proximity, purposely excluding examples of heterobimetallic systems that contain an iridium center, since their rich chemistry makes it impossible to deliver a comprehensive description within the scope of this chapter. However, for the interested reader, catalytic cooperativity in heterobimetallic complexes has been recently reviewed [69].

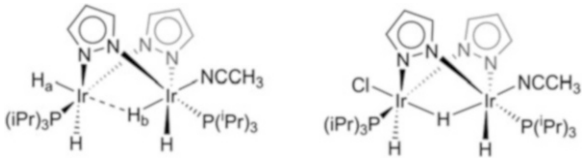

Fig. 2 Complexes $[Ir_2(CH_3CN)(H)_3(\mu\text{-}H)(P^iPr_3)_2(\mu\text{-}Pz)_2]$ (*left*) and $[Ir_2(CH_3CN)(Cl)(H)_2(\mu\text{-}H)(P^iPr_3)_2(\mu\text{-}Pz)_2]$ (*right*)

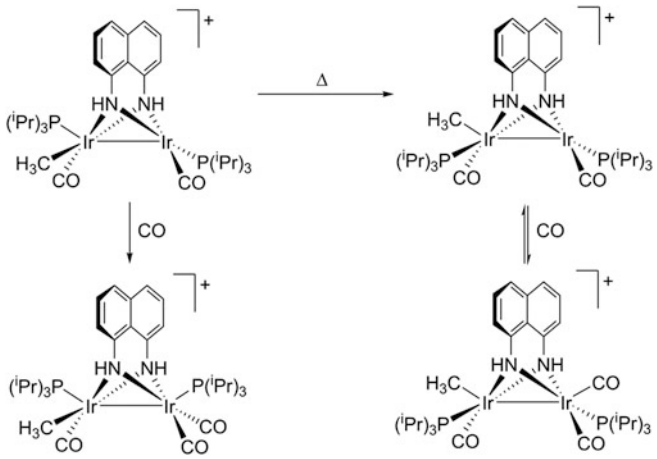

Scheme 5 Intermetallic *trans* effect transmitted via a metal–metal bond

4.1 Bond Activation by Homobimetallic Iridium Complexes

The stoichiometric chemistry of binuclear iridium complexes with reagents such as molecular hydrogen, halocarbons, alkynes, and alkenes has provided a wealth of interesting examples that have shed light on the reactivity trends and potential for substrate activation of this type of species, which often diverge from those of their mononuclear analogues [68]. As a typical example, there are precedents of Ir (I) dimers inactive toward the oxidative addition of molecular hydrogen that need to be oxidized in order to become active [63, 70]. This sharply contrasts with the behavior expected for mononuclear iridium complexes, where the ability to undergo oxidative addition increases when the metal centers are in low oxidation states.

Theoretical calculations on the concerted binuclear addition of H_2 to Ir d^8–d^8 complexes propose that the formation of a diradical that needs to reorganize previous to metal–metal bond formation is required, which leads to high energy barriers [71]. Besides, concerted symmetric mechanism are spin forbidden (vide supra) [39]. These studies, together with experimental evidences, suggest that in the rare cases where H_2 oxidative addition takes place at $Ir_2^{I,I}$ systems, this is initiated at one of the metal centers [72, 73]. Detailed NMR studies on the *A-frame* system $[Ir_2(CO)_2(dppm)_2(\mu\text{-}S)]$ (dppm = $Ph_2PCH_2CH_2PPh_2$) support a single-site oxidative addition followed by a hydride migration to the other Ir center. The oxidative

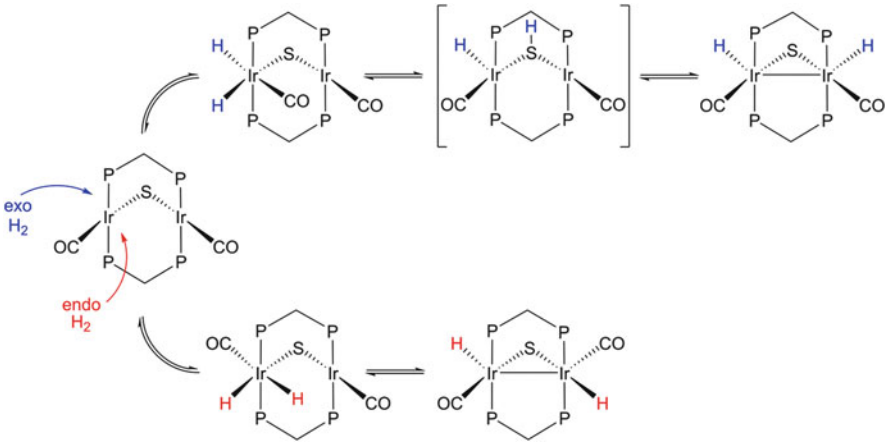

Scheme 6 Mechanism proposed for the oxidative addition of H_2 to $[Ir_2(CO)_2(dppm)_2(\mu\text{-}S)]Cl$

addition may take place according to two different geometries, *exo* or *endo*, depending on where the attack of the dihydrogen molecule occurs relative to the cavity generated by the ligand system. The migration has been proposed to happen via the bridging sulfide ligand to give the thermodynamic symmetric product (*exo* addition) or directly to afford the kinetic product (*endo* addition) (Scheme 6).

Similar bis(dppm)bridged Ir(I) complexes, such as $[Ir_2(\mu\text{-}Cl)(CO)_2(dppm)_2]BF_4$ and $[Ir_2(CO)_2(dppm)_2(X)_2]$ (X = Cl or I), have also proved to be able to undergo H_2 activation according to analogous mechanisms [40, 74, 75]. Noteworthy, the latter generates a vacant orbital usable for hydrogen coordination [76].

Besides the above *A-frame* systems, the activation of hydrogen has been reported for a handful of iridium dimers with *open-book* structures. For the bis(thiolate) complex $[Ir(CO)(PR_3)(\mu\text{-}S^tBu)]_2$ [77, 78], the oxidative addition is proposed to occur at one of the iridium centers, which subsequently transfers one of the hydrides to the second iridium to give the Ir(II)–Ir(II) complex $[[Ir(CO)(H)_2(PR_3)(\mu\text{-}S^tBu)]$ (Scheme 7). The same process is initiated in the symmetric phosphido-bridged complex $[\{Ir(PH^tBu_2)(CO)\}_2(\mu\text{-}H)(\mu\text{-}P^tBu_2)]$ to form the nonsymmetric product $[\{Ir(CO)(H)(PH^tBu_2)\}(\mu\text{-}H)_2(\mu\text{-}P^tBu_2)\{Ir(CO)(PH^tBu_2)\}]$, but the transferred hydride does not go beyond the bridging position, thus allowing the oxidative addition to be reversed [79]. Another noteworthy d^8–d^8 diiridium(I) system capable of dihydrogen activation is that reported by Stobart and co-workers, where the splitting of the H_2 molecule by complex $[Ir_2(CO)_2(PPh_3)_2(\mu\text{-}Pz)_2]$ was described to be sluggish at room temperature but proceeds rapidly at temperatures above 70°C [80].

The scarcity of Ir(I) dinuclear complexes able to activate H_2 has been attributed to the rigidity of such complexes, which prevents the distortion of the square-planar geometry and, consequently, the appearance of the empty metal orbital required for the coordination of the dihydrogen molecule [81–83]. In the particular case of open-book structures, theoretical calculations support a weak metal–metal interaction

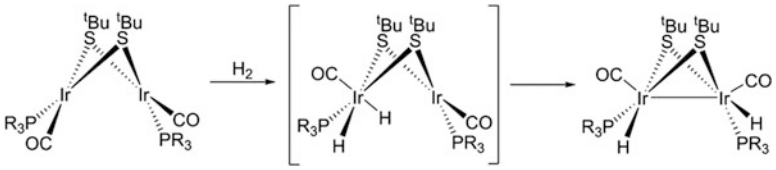

Scheme 7 Oxidative addition of H_2 to *open-book* complex $[Ir(CO)(PR_3)(\mu\text{-}S^tBu)]_2$

that stabilizes the bent geometry [84], further hampering H_2 coordination. Against this, however, the ability of bridging ligands to dissociate and adopt terminal positions may generate the necessary vacant sites, thus accounting for dihydrogen activation at certain complexes [40, 74–76]. Besides, the functional contributions of ligands such as thiolates might account for the success of some of the previously described systems. Actually, the thiolates present in the cysteine-rich active site of hydrogenases have been proposed to assist the heterolytic activation of dihydrogen [85–89]. Also, similar bifunctional heterolytic activations of dihydrogen have been recognized for mononuclear Ir-thiolate complexes [90, 91] and, remarkably, also for a binuclear (d^8–d^8) Rh system (Fig. 3) [92].

$Ir_2^{I,I}$ systems may also become active toward H_2 addition via disproportionation. The reaction sequence depicted in Scheme 8 illustrates how the transformation of an $Ir_2^{I,I}$ symmetric structure (d^8–d^8 system) into its related mixed-valence $Ir_2^{0,II}$ complex (d^7–d^9 system) results in the generation of an empty orbital at the Ir(II) (d^7 metal center) that permits H_2 coordination and subsequent oxidative addition [44, 46].

In spite of their relative inertness for H_2 activation, the Ir(I) dinuclear complexes are still electron-rich entities and, therefore, capable of undergoing oxidative additions via an S_N2 mechanism. This is the case of complex $[Ir_2(CO)_2(\text{-}\mu\text{-}1,8\text{-}(NH)_2naphtha)(PiPr_3)_2]$, which does not react with molecular hydrogen but readily undergoes the binuclear oxidative addition of (pseudo)halocarbons and strong acids to form products that display a metal–metal bond (Scheme 9) [70].

An analogous reaction between methyl iodide and complex $[Ir(CN^tBu)_2(\mu\text{-}Pz)]_2$ (Pz = pyrazolate) consumes two equivalents of the reagent to give the $Ir_2^{III,III}$ complex $[\{Ir(CN^tBu)_2(Me)(\mu\text{-}Pz)\}_2(\mu\text{-}I)]I$ (Scheme 10) [93].

The latter $Ir_2^{I,I}$ complex is also capable of undergoing binuclear oxidative addition of chloroalkanes such as $MeCOCH_2Cl$ and $MeCO_2CH_2Cl$ to form the $Ir_2^{II,II}$ complexes $[Ir(CH_3COCH_2)(Cl)(CN^tBu)_2(\mu\text{-}Pz)]_2$ and $[Ir(CH_3CO_2CH_2)(Cl)(CN^tBu)_2(\mu\text{-}Pz)]_2$, which are in equilibrium with their related $Ir_2^{I,III}$ isomers (Scheme 11) [94].

In contrast with haloalkanes, diiodine has been proposed to react with $[Ir(CN^tBu)_2(\mu\text{-}Pz)]_2$ by a two-electron transfer process that affords cation $[Ir(\mu\text{-}Pz)(CN^tBu)_2]_2^{2+}$ and two iodide ions, which are subsequently incorporated into the coordination sphere of the iridium centers to give the $Ir_2^{II,II}$ complex $[Ir(CN^tBu)_2(I)_2(\mu\text{-}Pz)]_2$ (Scheme 12) [95]. Analogous oxidation processes have been described for other similar Ir(I) d^8–d^8 systems (e.g., see [80, 96–100])

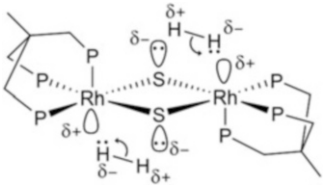

Fig. 3 Heterolytic activation of H_2 by a binuclear $Rh_2^{I,I}$ system as proposed by Mealli et al.

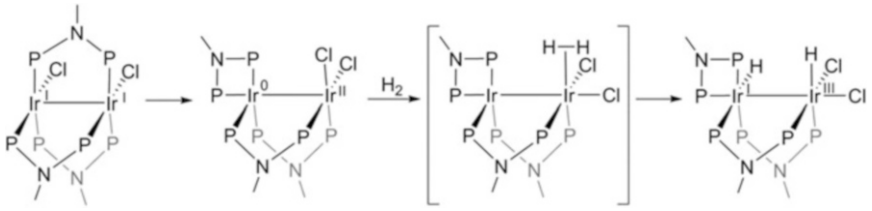

Scheme 8 Example of dihydrogen activation over a mixed-valence $Ir_2^{0,II}$ complex formed by disproportionation of the parent (inactive) $Ir_2^{I,I}$ system ($P = P(OCH_2CF_3)_2$)

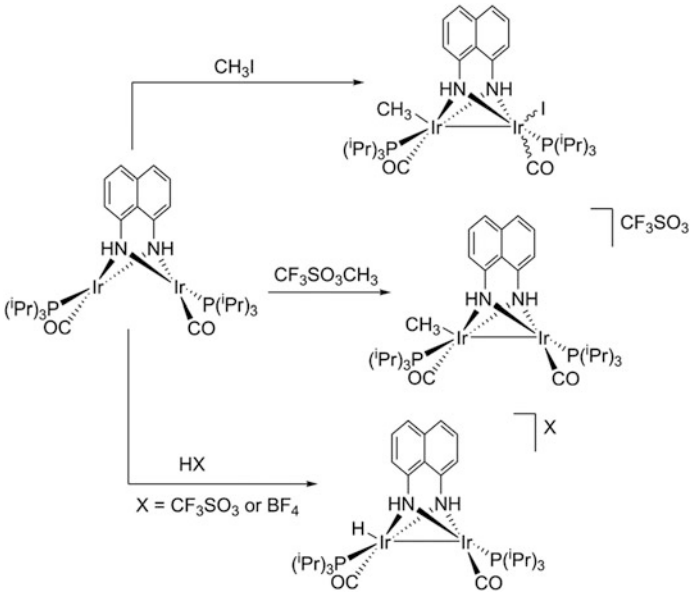

Scheme 9 Reactivity of $[Ir_2(CO)_2(\mu\text{-}1,8\text{-}(NH)_2naphtha)(PiPr_3)_2]$ against (pseudo)halocarbons and strong acids

In what can be considered a genuine characteristic of these binuclear systems, the $Ir_2^{I,I}$ complexes often become active toward the oxidative addition of H–H or C–H bonds after oxidation to $Ir_2^{II,II}$ (d^7–d^7 system) or $Ir_2^{I,III}$ (d^6–d^8 system) systems. As described above, $Ir_2^{I,I}$ complexes can be oxidized by (i) S_N2 oxidative addition of strong acids or (pseudo)halocarbons or (ii) two-electron transfer process with

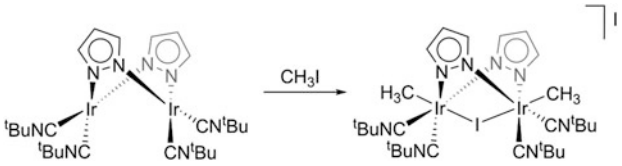

Scheme 10 Reactivity of $[\{Ir(\mu\text{-}Pz)(CN^tBu)_2\}_2]$ with methyl iodide

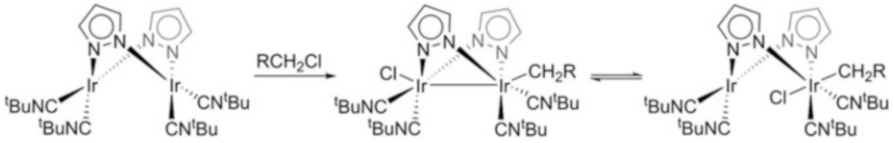

Scheme 11 Oxidative addition of RCH_2Cl to $[Ir(CN^tBu)_2(\mu\text{-}Pz)]_2$ (R = MeCO or $MeCO_2$)

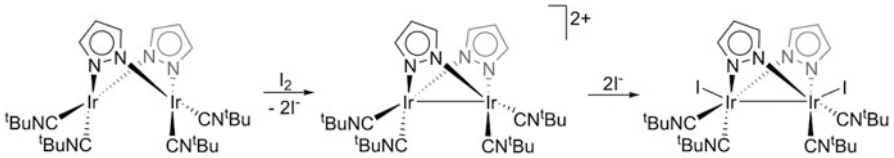

Scheme 12 Reactivity of $[Ir(CN^tBu)_2(\mu\text{-}Pz)]_2$ with diiodine

oxidants such as I_2 or $[FeCp_2]O_3SCF_3$. Either of such oxidations leads to a disruption of the rigid d^8–d^8 system that enables the modification of the orbital architecture and permits substrate coordination [68]. Besides, in $Ir_2^{I,III}$ compounds, the Lewis acidity of the Ir(I) center is enhanced due to the weak intermetallic bond, which, to some extent, equilibrates the electron density between both metal centers. This favors the coordination of σ-donors and even anionic nucleophiles such as iodide. Consequently, the coordination and subsequent oxidative addition of dihydrogen is possible in the new oxidized species, while the parent $Ir_2^{I,I}$ compound was inert toward H_2 (Scheme 13) [84].

Along with the example of Scheme 13, other $Ir_2^{I,III}$ and $Ir_2^{II,II}$ compounds show analogous reactivity patterns toward H_2 (Scheme 14). Remarkably, the formation of a hydride bridge that replaces the metal–metal bond is observed in all cases, which may be due to the existence of a common mechanism for the activation of dihydrogen by these complexes (Schemes 13 and 14). A concerted pathway that entails coordination of the dihydrogen molecule in *cis* position to the intermetallic bond as first step has been postulated. Subsequently, single-site oxidative addition assisted by a shift of the electron density at the metal–metal bond would result in the formation of a hydride-bridged bimetallic complex.

A similar reactivity trend has been reported for the oxidative addition of C–H bonds by binuclear iridium complexes. In fact, the $Ir_2^{I,III}$ compound $[Ir_2(CO)_2(H)(\mu\text{-}1,8\text{-}(NH)_2naphtha)(P^iPr_3)_2]^+$ also undergoes the C–H bond oxidative addition of phenylacetylene to give a $\mu\text{-}\kappa C,\eta^2$-alkynyl-bridged complex, which, in this case,

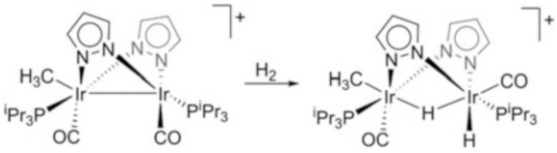

Scheme 13 Oxidative addition of H_2 over $Ir_2^{I,III}$ cation $[Ir_2(CH_3)(CO)_2(P^iPr_3)_2(\mu\text{-}Pz)_2]^+$

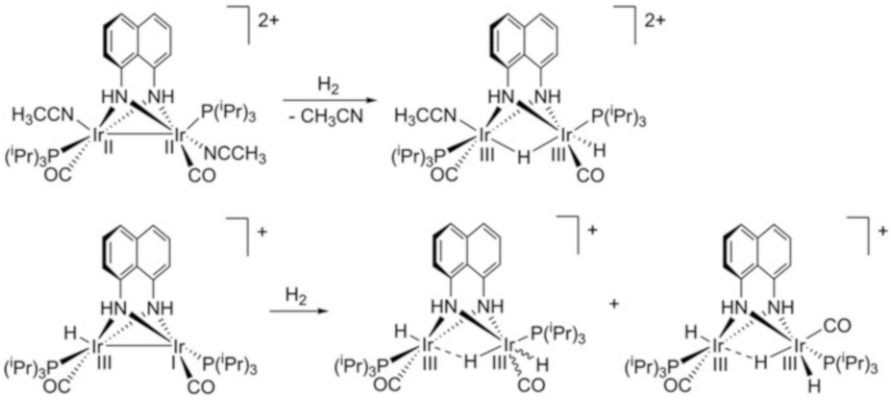

Scheme 14 Reactivity of cations $[Ir_2(CH_3CN)_2(CO)_2(\mu\text{-}1,8\text{-}(NH)_2naphtha)(P^iPr_3)_2]^{2+}$ (*top*) and $[Ir_2(CO)_2(H)(\mu\text{-}1,8\text{-}(NH)_2naphtha)(P^iPr_3)_2]^+$ (*down*) with dihydrogen

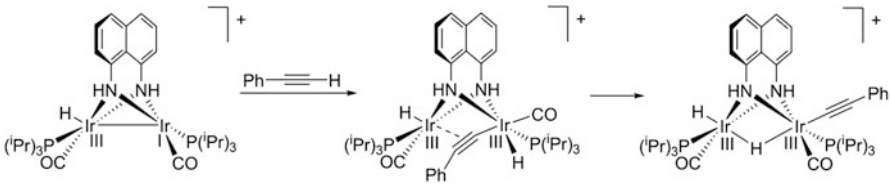

Scheme 15 Reactivity of $[Ir_2(CO)_2(H)(\mu\text{-}1,8\text{-}(NH)_2naphtha)(P^iPr_3)_2]^+$ with phenylacetylene

slowly isomerizes to the hydride-bridged complex (Scheme 15). However, as it was described for dihydrogen reactivity (vide supra), the parent $Ir_2^{I,I}$ complex is inert toward the oxidative addition of alkynes.

The parent $Ir_2^{II,II}$ complexes showed a similar reactivity toward phenylacetylene, but, in this case, the bridged complex was not observed; instead, the unsaturated dicationic $Ir_2^{III,III}$ complex $[Ir_2(C{\equiv}CPh)(CO)_2(H)(\mu\text{-}1,8\text{-}(NH)_2naphtha)(P^iPr_3)_2][CF_3SO_3]_2$ was isolated when the reaction was carried out in dichloromethane. Noteworthy, when this compound was refluxed for long reaction times, a new complex featuring a bridging vinylidene ligand was formed (Scheme 16).

When acetone was used as solvent, a significant change in reactivity occurs, as a deprotonated $Ir_2^{II,II}$ compound $[Ir_2(C{\equiv}CPh)(CO)_2(\mu\text{-}1,8\text{-}(NH)_2naphtha)(P^iPr_3)_2]CF_3SO_3$ is obtained. This compound is able to react with a new molecule of alkyne

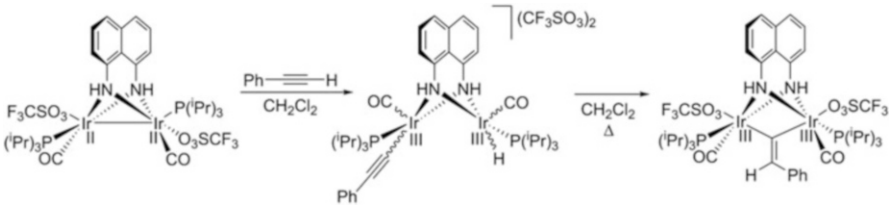

Scheme 16 Reactivity of $[Ir_2(CF_3SO_3)_2(CO)_2(\mu\text{-}1,8\text{-}(NH)_2naphtha)(P^iPr_3)_2]^+$ with phenyl acetylene in CH_2Cl_2

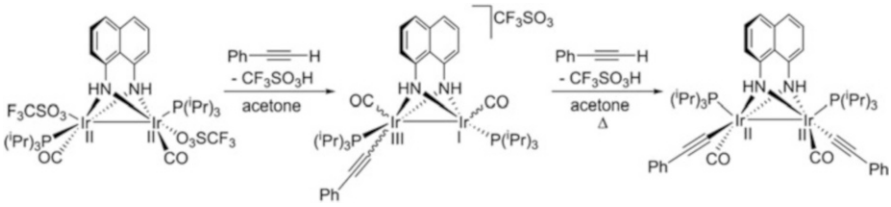

Scheme 17 Reactivity of $[Ir_2(CF_3SO_3)_2(CO)_2(\mu\text{-}1,8\text{-}(NH)_2naphtha)(P^iPr_3)_2]^+$ with phenylacetylene in acetone

to give $Ir_2^{II,II}$ complex $[Ir_2(C{\equiv}CPh)_2(CO)_2(\mu\text{-}1,8\text{-}(NH)_2naphtha)(P^iPr_3)_2]$ (Scheme 17) [101].

Further support for the prerequisite of $Ir_2^{I,I}$ oxidation is well exemplified by the C–H activation of 2-butene in complex $[Ir_2(2\text{-butene})_2(\mu\text{-}1,8\text{-}(NH)_2naphtha)(P^iPr_3)_2]$ to give the corresponding hydride-allyl $Ir_2^{III,III}$ product, which occurs via an $Ir_2^{II,II}$ species formed upon oxidation of the precursor with $[FeCp_2][CF_3SO_3]$ (Scheme 18) [102].

The activation of C–H bonds has also been reported for various other systems containing oxidized $Ir_2^{I,III}$ or $Ir_2^{II,II}$ cores. Selected examples are depicted in Schemes 19, 20, and 21. The binuclear iridium complexes reported by Yamaguchi et al. are capable of C–H activation for a variety of aromatic compounds [42, 103, 104]. The cooperation of a second metal center for the cleavage of the C–H bond is proposed (Scheme 19).

The binuclear complexes derived from the dimerization of Cp*(η^3-allyl)hydride iridium fragments (Cp* = η^5-pentamethylcyclopentadienyl) reported by Bergman provide noteworthy examples of CSp^3–H bond activation (Scheme 20) [105].

The group of Jones has described the desulfurization of thiophene and benzothiophene using $[Ir_2(Cp^*)_2(H)_2(\mu\text{-}H)]$ with excess TBE (*t*-butylethylene) or $[Ir(Cl)(Cp^*)(H)]_2$ in the presence of H_2 [53, 106]. The reactions eventually afford diiridium complexes with sulfide and $\eta^2{:}\eta^2$-butadiene bridges and seem to proceed via two consecutive carbon–sulfur bond cleavages that require more than one metal center and the ability to form bridging thiolate intermediates (Scheme 21) [107].

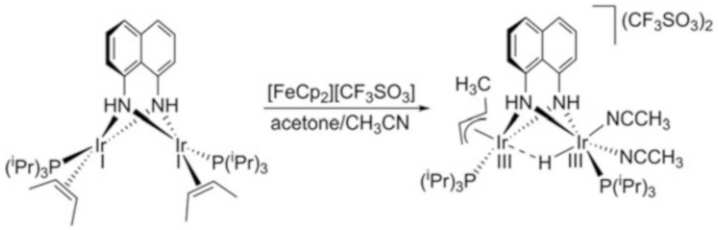

Scheme 18 Oxidation-promoted C–H activation at binuclear complex $[Ir_2(CH_3CH{=}CHCH_3)_2(\text{-}\mu\text{-}1,8\text{-}(NH)_2naphtha)(P^iPr_3)_2]$

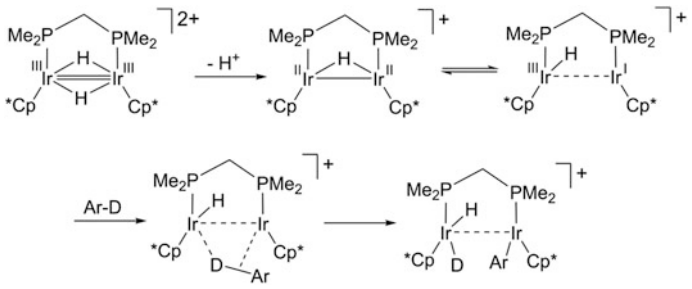

Scheme 19 Activation mechanism proposed by Yamaguchi et al. for the activation of aromatic compounds

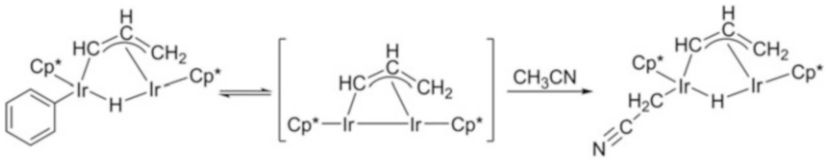

Scheme 20 Acetonitrile C–H activation by species $[Ir_2(Cp^*)_2(\mu\text{-}\eta^1,\eta^3\text{-}CHCHCH_2)]$

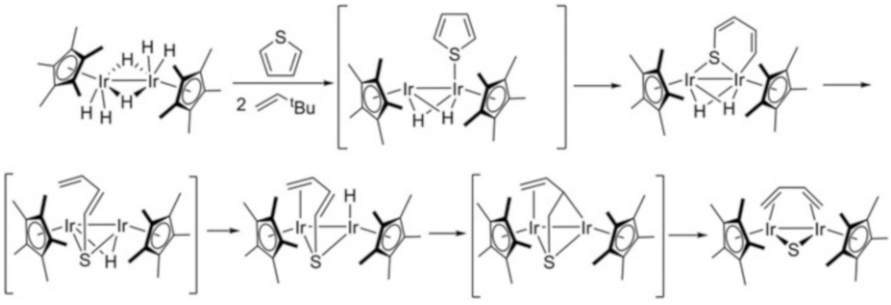

Scheme 21 Desulfurization of thiophene by homobinuclear iridium complexes

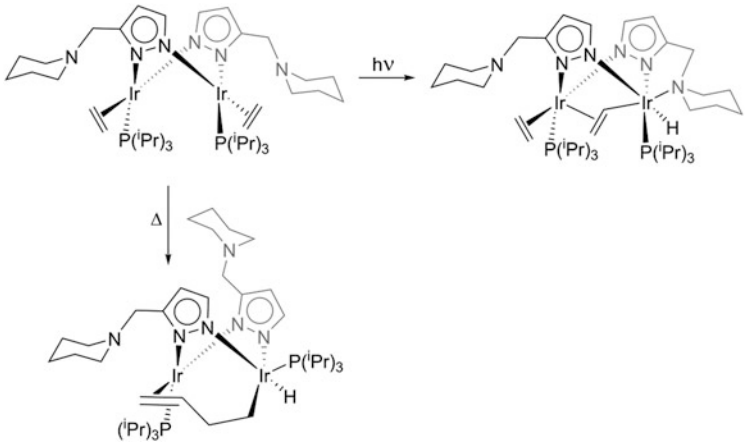

Scheme 22 Thermal and UV irradiation-driven C–H activation of ethylene by the 3-(piperidinemethyl)pyrazolate $Ir_2^{I,I}$ system

Several C–H-activating systems seem to constitute an exception for the pre-oxidation requisite, since they can work in the $Ir_2^{I,I}$ form. The 3-(piperidinemethyl)pyrazolate $Ir_2^{I,I}$ system depicted in Scheme 22 has been found to activate the C–H bond of an ethylene ligand after UV irradiation or thermal induction [108]. Although the mechanisms that govern these reactions are still unclear, according to the structure of the final products, the thermal C–H bond activation seems to happen at an iridium center not protected by piperidinemethyl substituents. This suggests that the C–H activation requires a previous reorganization of the pyrazolate bridges within the dimer, from head-to-tail to head-to-head. Such a process resembles other pre-activations discussed in the previous lines, such as oxidation with strong acids or disproportionation, in the sense that it breaks the symmetry of the $Ir_2^{I,I}$ dimer and may help to generate available orbitals, full or empty, in each of the individual metal centers.

Another thoroughly studied example of a $Ir_2^{I,I}$ system able to promote C–H bond activations is also nonsymmetric. The cationic *A-frame* complex $[Ir_2(CH_3)(CO)_2(dppm)_2][CF_3SO_3]$ accomplishes a double geminal C–H activation of butadiene to form the hydride–vinylvinylidene-bridged complex $[Ir_2(CH_3)(\mu\text{-}C{=}C(H)C(H){=}CH_2)(CO)_2(dppm)_2(H)(\mu\text{-}H)][CF_3SO_3]$ (Scheme 23) [109, 110]. The proposed mechanism involves the activation of one of the geminal bonds to form an alkynyl complex with a bridging hydride, followed by a μ-H inversion [109], to end with the second C–H activation.

This nonsymmetric cationic precursor also carries out the rare case of regioselective C–F activation of fluoroolefins reported by Cowie et al. [50, 51]. This is a prominent example of cooperative activation, as the reactivity of the substrate is significantly boosted when bridging two metal centers. The $\mu\text{-}\eta^1{:}\eta^2\text{-}C_2F_3$-coordinated olefin readily undergoes a second C–F activation to

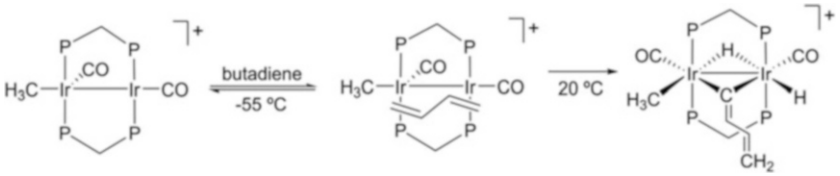

Scheme 23 Activation of butadiene by $[Ir_2(CH_3)(CO)_2(dppm)_2][CF_3SO_3]$

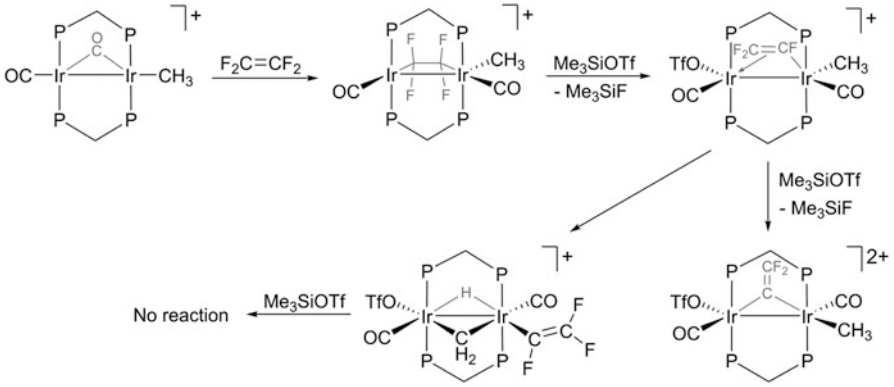

Scheme 24 Examples of activation of the C–F bond of fluoroolefins (bridge vs. terminal) by homobinuclear iridium complexes

afford complex $[Ir_2(\mu\text{-}C{=}CF_2)(CF_3SO_3)(CH_3)(CO)_2(dppm)_2][CF_3SO_3]_2$; however, a η^1-C_2F_3 coordination mode precludes further fluoride abstraction (Scheme 24).

4.2 Catalysis by Homobimetallic Iridium Complexes

As mentioned above, complex $[Ir_2(CH_3CN)(H)_3(\mu\text{-}H)(P^iPr_3)_2(\mu\text{-}Pz)_2]$ features a labile acetonitrile ligand as a consequence of the intermetallic *trans* effect exerted by the hydride, occupying the axial coordination position (H_a in Fig. 2, right). The transmission of the *trans* effect along the binuclear backbone plays a crucial role in the catalytic hydrogenation of ethylene [59] and diphenylacetylene [64]. The acetonitrile ligand can be easily displaced by ethylene or diphenylacetylene, which then undergoes similar catalytic cycles (Scheme 25). After the migratory insertion of the substrate into the hydride bond, diphenylacetylene in Scheme 25, a new vacant is generated at the adjacent iridium center, probably due to fast migration of the hydride ligands along the bimetallic frame. Coordination of dihydrogen leads to formation of a nonclassical hydride complex followed by reductive elimination of *cis*-stilbene and subsequent hydride reorganization.

Noteworthy, dissociation of the coordinated stilbene to regenerate the active species and restart the catalytic cycle is favored again by the intermetallic *trans*

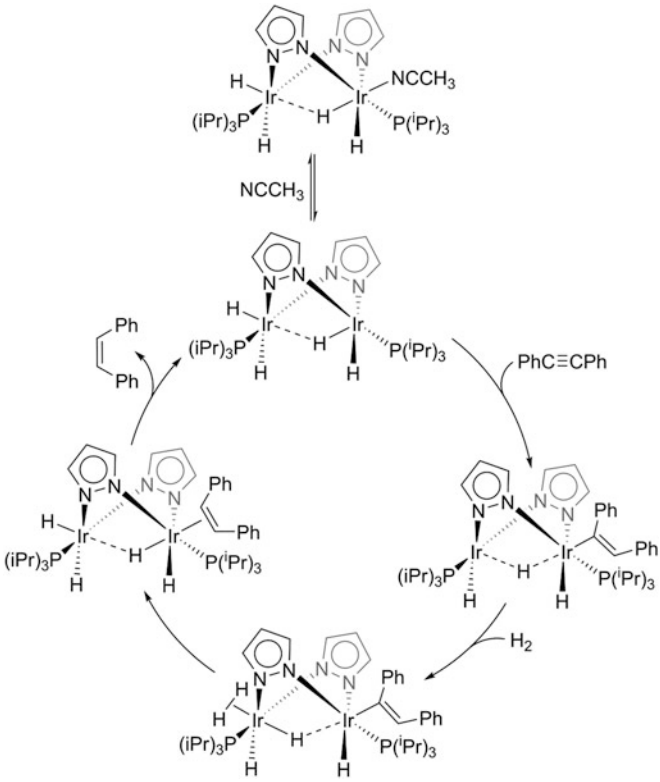

Scheme 25 Catalytic cycle proposed for the hydrogenation of diphenylacetylene to *cis*-stilbene by $Ir_2^{III,III}$ complex $[Ir_2(CH_3CN)(H)_3(\mu\text{-}H)(P^iPr_3)_2(\mu\text{-}Pz)_2]$

effect exerted by the hydride ligand. When one of the positions *trans* to the bridging hydride is blocked, namely, by orthometallation of a vinyl ligand, the reaction operates by a mononuclear catalytic cycle [64]. This results in a new product selectivity since 1,2-diphenylethane is obtained instead of stilbene (vide supra). The formation of 1,2-diphenylethane has been rationalized as a consequence of the thwarted dissociation of stilbene, which does not experience the *trans* labilization effect of the hydride ligand across the bimetallic core described above for its precursor (Scheme 26). This hindered release of the alkene in the mononuclear mechanism also explains the higher reaction rates obtained for the analogous binuclear mechanism.

The activity of complex $[Ir_2(CH_3CN)(H)_3(\mu\text{-}H)(P^iPr_3)_2(\mu\text{-}Pz)_2]$ as a catalyst for the hydrogenation of diphenylacetylene and ethylene contrasts with its inactivity when employed in the hydrogenation of *N*-benzylideneaniline. However, when transformed into its protonated derivative, for example, $[Ir_2(CH_3CN)(H)_2(H_2)(\mu\text{-}H)(P^iPr_3)_2(\mu\text{-}Pz)_2]BF_4$ by reaction with HBF_4, the new complex becomes a very active catalyst for C=N hydrogenation [111]. The catalytic cycle involves fast elementary steps of hydride and proton transfer according to an ionic outer sphere mechanism that takes place at one of the iridium centers of the binuclear complex (Scheme 27).

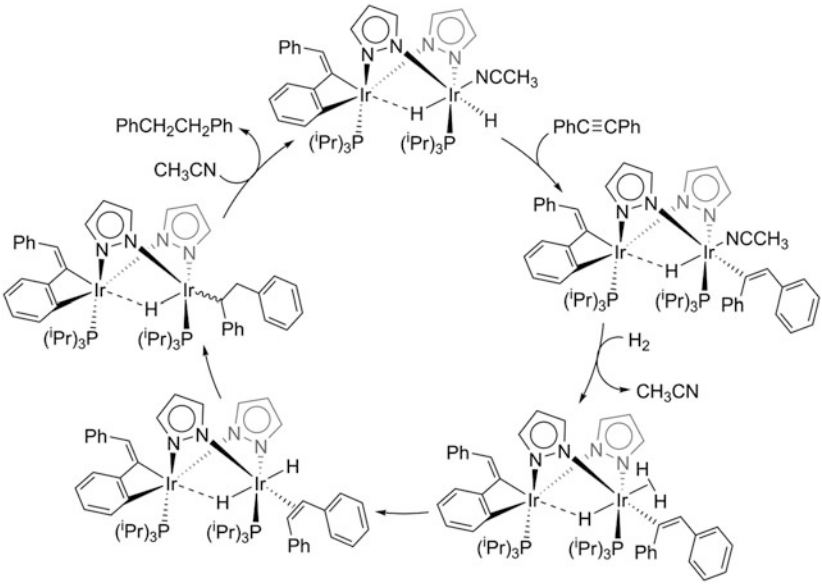

Scheme 26 Mononuclear mechanism for the hydrogenation of diphenylacetylene catalyzed by $[Ir_2\{\eta^1\text{-}C_6H_4\text{-}2\text{-}[\eta^1\text{-}(Z)\text{-}C{=}CHPh]\}(CH_3CN)(H)(\mu\text{-}H)(P^iPr_3)_2(\mu\text{-}Pz)_2]$

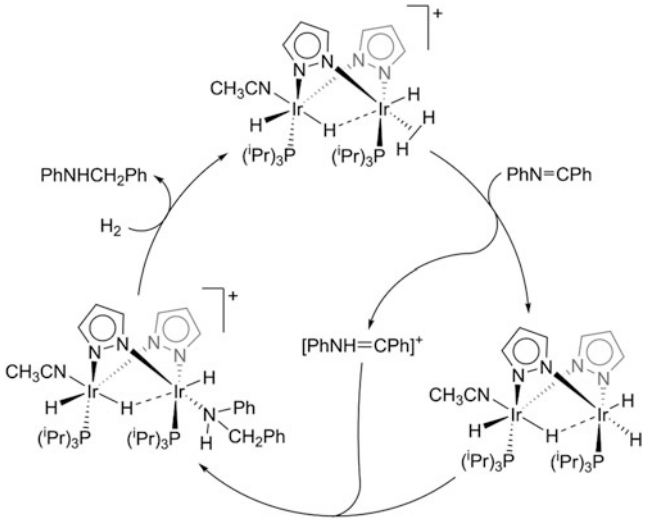

Scheme 27 Hydrogenation of imines by catalysts $[Ir_2(CH_3CN)(H)_2(H_2)(\mu\text{-}H)(P^iPr_3)_2(\mu\text{-}Pz)_2]BF_4$

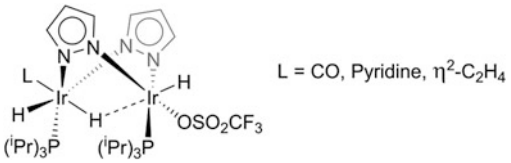

Fig. 4 Catalysts with different axial ligands (L) at the expectator iridium center

Although the mechanism takes place exclusively at one of the metal sites, the ligand at the spectator iridium center occupying the position *trans* to the bridging hydride (L) effectively influences the catalytic activity of the binuclear system. Therefore, the intermetallic communication and, consequently, the binuclear nature of the complex play a crucial role on the performance of the catalyst even when the second metal is not directly involved in the catalytic cycle (Fig. 4).

The reaction of the $Ir_2^{III,III}$ complex $[Ir_2(CH_3CN)(H)_3(\mu\text{-}H)(\mu\text{-}1,8\text{-}(NH)_2naphtha)(P^iPr_3)_2]$ with an excess of internal alkyne affords its reduced $Ir_2^{I,I}$ analogues $[Ir_2(\mu\text{-}1,8\text{-}(NH)_2naphtha)(\eta^2\text{-}cis\text{-}olefin)_2(P^iPr_3)_2]$ upon hydrogenation of the C≡C bonds. This reaction occurs via nonsymmetric alkenyl complexes, which subsequently undergo two C–H reductive eliminations to afford the corresponding bis-*Z*-alkene diiridium(I) complexes. The reaction of silyl-substituted internal alkynes with $[Ir_2(CH_3CN)(H)_3(\mu\text{-}H)(\mu\text{-}1,8\text{-}(NH)_2naphtha)(P^iPr_3)_2]$ leads selectively to the formation of bis(vinylidene) derivatives, for example, reaction with trimethylsilyl-1-propyne affords complex $[Ir_2\{\eta^2\text{-}CH_2{=}C(Me)SiMe_3\}_2\{\mu\text{-}1,8\text{-}(NH)_2C_{10}H_6\}(P^iPr_3)_2]$ as the final product. Despite the similar migrating ability of H and SiR_3, the analogous reaction with terminal alkynes gives rise to the formation of various iridium-containing species and organic compounds resulting from alkyne dimerization and trimerization (Scheme 28).

Remarkably, the diiridium(I) complexes show excellent regio- and stereoselectivities for alkyne dimerization and trimerization reactions, giving a single hexadienyne trimer and exclusive formation of head-to-head *Z*-butenyne (Scheme 29) [112].

The catalytic C–C coupling of alkynes has been widely reported for rhodium and ruthenium complexes (e.g., see [113–120]); however, examples of iridium catalysts are less frequent [121–123]. The low activity observed for Ir complexes could be attributed to the greater tendency of rhodium and ruthenium to form vinylidene complexes [124–127], since it is generally accepted that the formation of *Z*-enynes occurs via vinylidene intermediates [117–120]. In this regard, the intermetallic cooperation makes it possible to form the Ir-vinylidene intermediates required for the formation of *Z*-enynes and, ultimately, C–C coupling reactions.

Diiridium(II) complexes have often been proposed as inactive species formed by the deactivation of Ir(I) catalysts [25–30]. This contrasts with the extensive use of $Rh_2^{II,II}$ complexes in catalysis, the work by Doyle et al. being an outstanding contribution to the field ([31] and references therein). An example of a catalyst based on an iridium(II) species is binuclear complex $[Ir(C_5Me_5)(\mu\text{-}H)]_2$ reported by

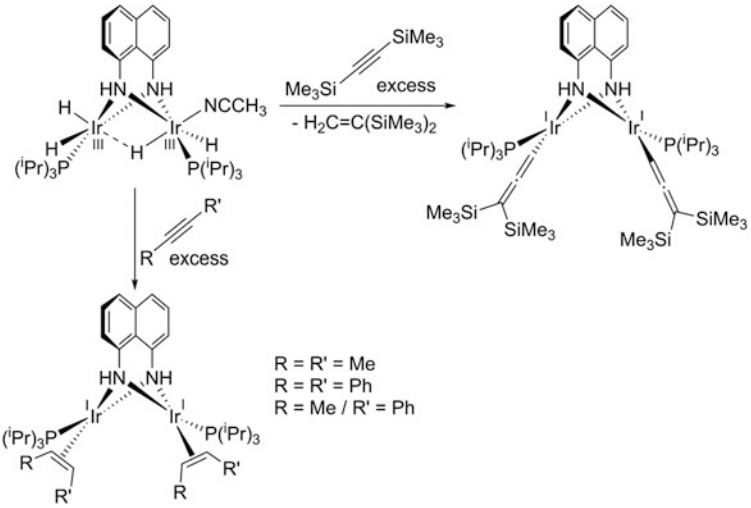

Scheme 28 Reactivity of $[Ir_2(CH_3CN)(H)_3(\mu\text{-}H)(\mu\text{-}1,8\text{-}(NH)_2naphtha)(P^iPr_3)_2]$ with alkynes

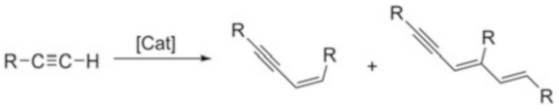

Scheme 29 C–C coupling of alkynes catalyzed by $[Ir_2(\mu\text{-}1,8\text{-}(NH)_2naphtha)]$ complexes

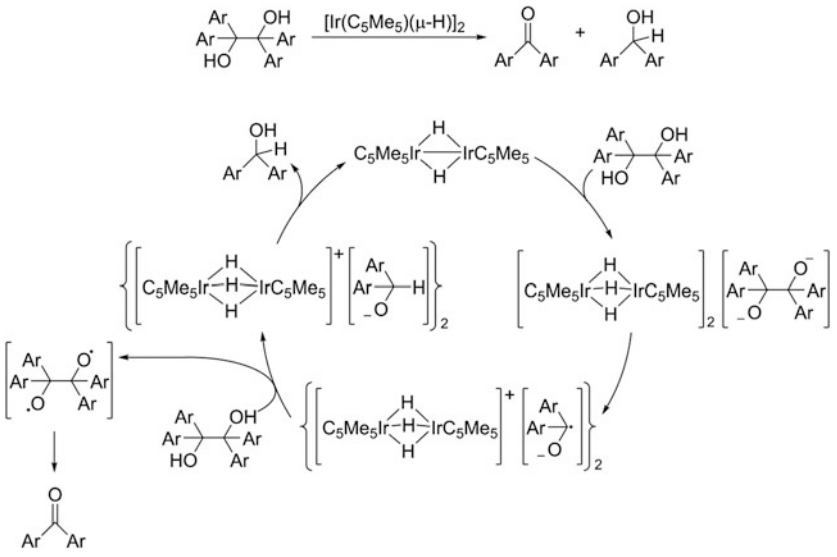

Scheme 30 Catalytic cycle proposed for the cleavage of 1,2-diols by $[Ir(C_5Me_5)(\mu\text{-}H)]_2$

Wakatsuki and co-workers [128]. This complex is able to reversibly deprotonate acidic organic compounds, which makes possible a novel catalytic reaction for the cleavage of the C–C bond in aromatic 1,2-diols (Scheme 30). Besides, this complex is able to reversibly deprotonate acidic methylenic protons and act as a catalyst for Michael addition reactions under neutral conditions.

A new example of a binuclear Ir(II) catalyst is complex [{Ir(μ-κC_{NHC},η^6_{Dipp}-IDipp)(H)}$_2$][BF_4]$_2$, which efficiently promotes the hydroalkynylation of imines [129]. The $Ir_2^{II,II}$ compound is remarkably stable in the presence of air or moisture, even at high temperatures in the presence of imines. Addition of one equivalent of alkyne to [{Ir(μ-κC_{NHC},η^6_{Dipp}-IDipp)(H)}$_2$][BF_4]$_2$ results in the formation of a non-identified hydride complex in low yields. However, when excess alkyne is added, the C–C coupling reaction takes place to give a mixture of organic compounds (dimerization, trimerization, and cyclotrimerization) and the initial binuclear complex. The proposed reaction mechanism, substantiated by theoretical calculations at the DFT level, entails (i) single-site oxidative addition of the alkyne's C–H bond to give the alkynyl–trihydride complex, in agreement with the reactivity described above for terminal alkynes (vide supra); (ii) deprotonation of the binuclear complex by the imine to give the protonated imine and the corresponding dihydride $Ir_2^{I,III}$ compound with the end-on coordinated alkynyl ligand; (iii) coordination of the protonated imine by the C=N bond and subsequent migratory insertion into the Ir–C(alkynyl) bond; and to end with, (iv) the release of the propargyl amine with the concomitant formation of the $Ir_2^{II,II}$ active species, which restarts the catalytic cycle (Scheme 31).

Noteworthy, the arene ligands undergo multiple hapticity changes during the course of the proposed catalytic cycle, which regulates the activity and stability of the catalyst by providing the vacant coordination sites required for substrate coordination while, at the same time, maintains the integrity of the bimetallic entity.

As already mentioned in Sect. 4.1, the use of binuclear $Ir_2^{I,I}$ complexes for hydrogenation reactions is not favored. In particular, $Ir_2^{I,I}$ complexes, containing binucleating N-donor ligands presenting open-book structures, are usually inactive toward molecular hydrogen activation. However, a binuclear $Ir_2^{I,I}$ complex containing bridging amido ligands of formula [{Ir(cod)(μ-NH_2)}$_2$] is an active homogeneous catalyst for the transfer hydrogenation of acetophenone to 1-phenylethanol, using ^{i}PrOH as hydrogen donor. The unusual activity of this $Ir_2^{I,I}$ system has been attributed to the cooperation between the two Ir centers and the non-innocent amido ligand [130]. The proposed reaction mechanism, substantiated by experimental observations and theoretical calculations at the DFT level, is shown in Scheme 32.

The process is initiated by an unusual metalacycle opening to yield [(cod)Ir(μ-NH_2)Ir(NH_2)(cod)] species that promotes the concerted dehydrogenation of isopropanol and simultaneous transference of two hydrogen atoms to form a diiridium hydride intermediate [(cod)(H)Ir(μ-NH_2)Ir(NH_3)(cod)] containing a bridging amido ligand. This is followed by the concerted hydrogenation of acetophenone, by simultaneous transference of two hydrogen atoms to the C=O bond, to yield 1-phenylethanol. The concerted dehydrogenation of isopropanol, and

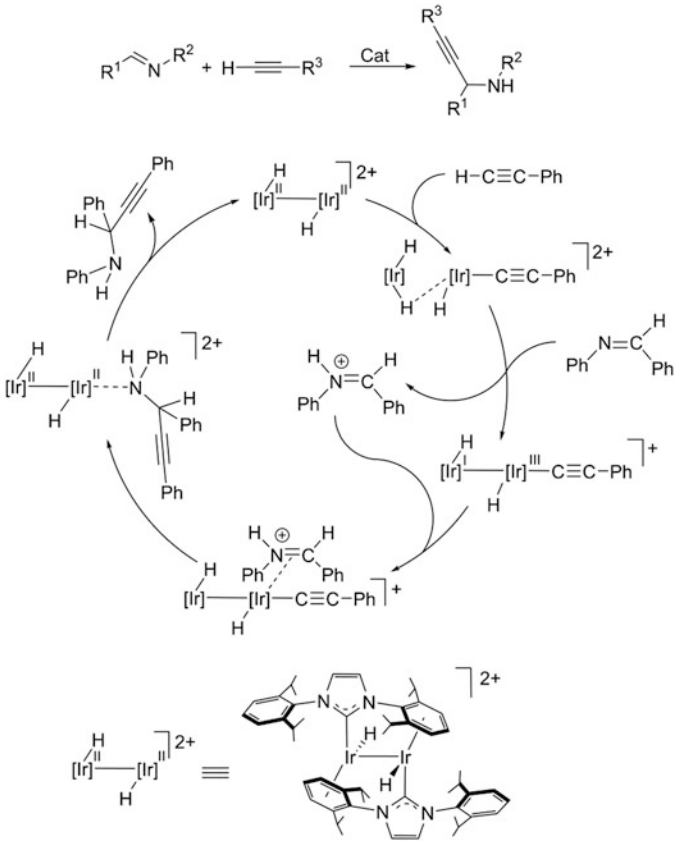

Scheme 31 Proposed catalytic cycle for the hydroalkynylation of imines

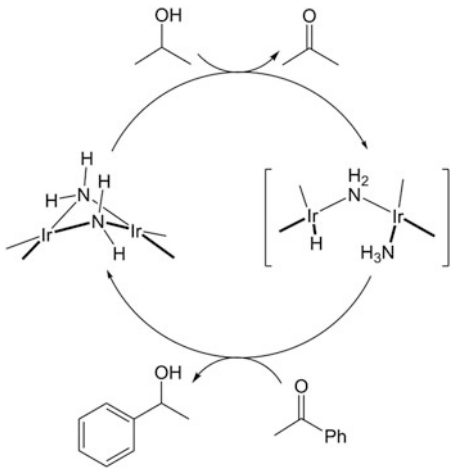

Scheme 32 Proposed catalytic cycle for the transfer hydrogenation of acetophenone by $Ir_2^{I,I}$ complex $[Ir(cod)(\mu\text{-}NH_2)]_2$

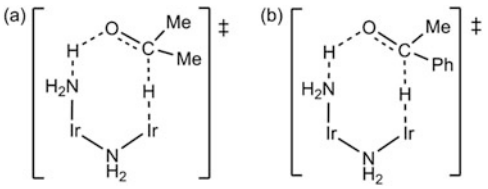

Fig. 5 Eight-membered-ring transition state for (**a**) concerted dehydrogenation of isopropanol and (**b**) concerted hydrogenation of acetophenone

hydrogenation of acetophenone, takes place through an eight-membered-ring pericyclic mechanism, which presents similarities to the metal–ligand bifunctional mechanism proposed by Noyori [131, 132], in such a way that both hydrogen atoms are transferred simultaneously to the Ir and NH_2 ligand. However, owing to the starting bimetallic ring structure and the steric hindrance enforced by the cyclooctadiene ligands, cooperative participation of the NH_2–Ir–NH_2–Ir moiety is required. Figure 5 shows the proposed transition states for the concerted process.

Finally, a noteworthy reaction due to its present significance and future potential is the oxidation of water by organometallic catalysts. The benefits of bimetallic cooperation in water oxidation catalysts (WOCs) based on molecular systems, in particular for ruthenium complexes, are well established, although comprehensive mechanistic studies are exceptionally challenging owing to the multi-electron and multi-proton transfer steps involved in this reaction [133–135]. An interesting example of metal cooperation in iridium WOCs has been recently reported by Albrecht et al. In this case, the close proximity of two triazolylidene–iridium complexes linked by an aliphatic chain has proved to enhance the catalytic activity of WOCs at low catalyst concentrations compared to their monometallic analogues, which seems to support the fact that a binuclear mechanism operates under dilute conditions [136].

5 Concluding Remarks

The cooperation between metals in binuclear complexes indubitably brings about distinctive reactivity patterns, although the origin and mechanism of such cooperation still remains vaguely defined or unknown in many instances. Significantly, the study of iridium bimetallic complexes has contributed to identify and understand phenomena that can give rise to intermetallic cooperation beyond those exploiting the extended possibilities of bridging sites for bond activations and insertions. Thus, the transmission of ligands *trans* effects (or influences) via bridging ligands or intermetallic bonds, together with the facile migration of hydrides between metals, allow a joint and synchronized use of vacant sites in both metal centers with a single catalytic purpose. Yet, the interaction between iridium centers seems to hamper the reactivity of many $Ir_2^{I,I}$ dimers toward H–H and C–H bond activation, in contrast with a hallmark of their mononuclear counterparts. A wealth of evidence, however, suggests that the mere breaking of the symmetry of the dimer is enough to generate

bond-activating species. Such active complexes have proved able to exploit both intermetallic and metal–ligand bifunctional contributions to achieve catalysis.

References

1. Maret W, Li Y (2009) Chem Rev 109:4682
2. Kaila VRI, Verkhovsky MI, Wilkstrom M (2010) Chem Rev 110:7062
3. Magnus KA, Tonthat H, Carpenter JE (1994) Chem Rev 94:727
4. Valentine AM, Stahl SS, Lippard SJ (1999) J Am Chem Soc 121:3876
5. Wirstam M, Lippard SJ, Friesner RA (2003) J Am Chem Soc 125:3980
6. Wu AJ, Penner-Hahn JE, Pecoraro VL (2004) Chem Rev 104:903
7. Siegbahn PEM, Tye JW, Hall MB (2007) Chem Rev 107:4414
8. Hetterscheid DGH, Chikkali SH, de Bruin B, Reek JNH (2013) ChemCatChem 5:2785
9. Kuwata S, Ikariya T (2010) Dalton Trans 39:2984
10. McCollum DG, Bosnich B (1998) Inorg Chim Acta 270:13
11. Qin CJ, Gavrilova A, Bosnich B (2001) Pure Appl Chem 73:221
12. Gautrona S, Lassauque N, Le Berre C, Azam L, Giordano R, Serp P, Laurenczy G, Thiébaut D, Kalck P (2006) Top Catal 40:83
13. Gautrona S, Lassauque N, Le Berre C, Azam L, Giordano R, Serp P, Laurenczy G, Daran JC, Duhayon C, Thiébaut D, Kalck P (2006) Organometallics 25:5894
14. Solomon EI, Sundaram UM, Machonkin TE (1996) Chem Rev 96:2563
15. Wilcox DE, Porras AG, Hwang YT, Lerch K, Winkler ME, Solomon EI (1985) J Am Chem Soc 107:4015
16. Ross PK, Solomon EI (1990) J Am Chem Soc 112:5871
17. Ross PK, Solomon EI (1991) J Am Chem Soc 113:3246
18. Matoba T, Kumagai A, Yamamoto H, Yoshitsu M, Sugiyama J (2006) Biol Chem 281:8981
19. Tepper AWJW, Lonardi E, Bubacco L, Canters GW (2010) In: Messerschmidt A (ed) Handbook of metalloproteins. Wiley, Chichester
20. Nadine Hamann J, Tuczek F (2014) Chem Commun 50:2298
21. Decker H, Schweikardt T, Tuczek F (2006) Angew Chem Int Ed 45:4546
22. Adams RA, Cotton FA (eds) (1998) Catalysis by di and polynuclear metal clusters. Wiley-VCH, New York
23. van der Beuken EK, Feringa BL (1998) Tetrahedron 54:12985
24. Chaloner PA, Esteruelas MA, Joó F, Oro LA (1993) Homogeneous hydrogenation. Kluwer, Dordrecht, 56 p
25. Kolychev EL, Kronig S, Brandhorst K, Freytag M, Jones PG, Tamm M (2013) J Am Chem Soc 135:12448
26. Bianchi D, Bortolo R, Aloisio RD, Querci C, Ricci M (1999) In: Delmon B, Forments GF (eds) Catalyst deactivation. Elsevier, Amsterdam, 481 pp
27. Heller D, De Vries AHM, De Vries JG (2008) Catalyst inhibition and deactivation in homogeneous hydrogenation. In: de Vries JG, Elsevier CJ (eds) The handbook of homogeneous hydrogenation. Wiley-VCH, Weinheim, p 1483
28. Pfaltz A, Blankenstein J, Hilgraf R, Hormann E, McIntyre S, Menges F, Schonleber M, Smidt SP, Wustenberg B, Zimmermann N (2003) Adv Synth Catal 345:33
29. Xu Y, Michael D, Mingos P, Brown JM (2008) Chem Commun 199
30. Li H, Lu G, Jiang J, Huang F, Wang Z-X (2011) Organometallics 30:2349
31. Xu X, Doyle MP (2014) Acc Chem Res 47:1396
32. Laneman SA, Fronczek FR, Stanley GG (1988) J Am Chem Soc 110:5585
33. Broussard ME, Juma B, Train SG, Peng WJ, Laneman SA, Stanley GG (1993) Science 260:1784

34. Peng WJ, Train SG, Howell DK, Fronczek FR, Stanley GG (1996) Chem Commun 2607
35. Matthews RC, Howell DK, Peng WJ, Train SG, Treleaven WD, Stanley GG (1996) Angew Chem 108:2402
36. Matthews RC, Howell DK, Peng WJ, Train SG, Treleaven WD, Stanley GG (1996) Angew Chem Int Ed Engl 35:2253
37. Hunt C Jr, Nelson BD, Harmon EG, Fronczek FR, Watkins SF, Billodeaux DR, Stanley GG (2000) Acta Crystallogr C 56:546
38. Aubry DA, Bridges NN, Ezell K, Stanley GG (2003) J Am Chem Soc 125:11180
39. Trinquier G, Hoffmann R (1984) Organometallics 3:370
40. Vaartstra BA, Cowie M (1989) Inorg Chem 28:3138
41. Samant RG, Trepanier SJ, Wigginton JR, Xu L, Bierenstiel M, McDonald R, Ferguson MJ, Cowie M (2009) Organometallics 28:3407
42. Patureau FW, De Boer S, Kuil M, Meeuwissen J, Breuil PAR, Siegler MA, Spek AL, Sandee AJ, De Bruin B, Reek JNH (2009) J Am Chem Soc 131:6683
43. Nocera DG (2009) Inorg Chem 48:10001
44. Gray TG, Veige AS, Nocera DG (2004) J Am Chem Soc 126:9760
45. Esswein AJ, Veige AS, Piccoli PMB, Schultz AJ, Nocera DG (2008) Organometallics 27:1073
46. Veige AS, Gray TG, Nocera DG (2005) Inorg Chem 44:17
47. Heyduk AF, Nocera DG (2000) J Am Chem Soc 122:9415
48. Heyduk AF, Nocera DG (2001) Science 293:1639
49. Fujita K-I, Takahashi Y, Nakaguma H, Hamada T, Yamaguchi R (2008) J Organomet Chem 693:3375
50. Anderson DJ, McDonald R, Cowie M (2007) Angew Chem 2007(119):3815
51. Anderson DJ, McDonald R, Cowie M (2007) Angew Chem Int Ed 46:3741
52. Fujita K, Nakaguma H, Hamada T, Yamaguchi R (2003) J Am Chem Soc 125:12368
53. Vicic DA, Jones WD (1994) J Am Chem Soc 116:198
54. Komiya S, Yasuda T, Fukuoka A, Hirano M (2000) J Mol Catal A 159:63
55. Wang L-S, Cowie M (1995) Organometallics 14:2374
56. Antwi-Nsiah FH, Oke O, Cowie M (1996) Organometallics 15:1042
57. Trepanier SJ, McDonald R, Cowie M (2003) Organometallics 22:2638
58. Rowsell BD, McDonald R, Cowie M (2004) Organometallics 23:3873
59. Sola E, Bakhmutov VI, Torres F, Elduque A, López JA, Lahoz FJ, Werner H, Oro LA (1998) Organometallics 17:683
60. Fryzuk MD, Piers WE (1990) Organometallics 9:986
61. Shima T, Suzuki H (2000) Organometallics 19:2420
62. Martín M, Sola E, Lahoz FJ, Oro LA (2002) Organometallics 21:4027
63. Jiménez MV, Sola E, López JA, Lahoz FJ, Oro LA (1998) Chem Eur J 4:1398
64. Torres F, Sola E, Elduque A, Martínez AP, Lahoz FJ, Oro LA (2000) Chem Eur J 6:2120
65. Murray HH, Flacker JP Jr, Trzcinska-Bankroft B (1998) Organometallics 17:1449
66. Laguna A, Laguna M, Jiménez J, Lahoz FJ, Olmos E (1992) J Organomet Chem 435:235
67. Sola E, Torres F, Jiménez MV, López JA, Ruiz SE, Lahoz FJ, Elduque A, Oro LA (2001) J Am Chem Soc 123:11925
68. Oro LA, Sola E (2001) In: Poli R, Peruzzini M (eds) Recent advances in hydride chemistry. Elsevier, Oxford, 299 p
69. Mata JA, Hahn FE, Peris E (2014) Chem Sci 5:1723
70. Jiménez MV, Sola E, Egea MA, Huet A, Francisco AC, Lahoz FJ, Oro LA (2000) Inorg Chem 39:4868
71. Sevin A, Hengtai Y, Chaquin P (1984) J Organomet Chem 3:391
72. McDonald R, Cowie M (1993) Inorg Chem 32:1671
73. Oldham SM, Houlis JF, Sleigh CJ, Duckett SB, Eisenberg R (2000) Organometallics 19:2985
74. Sutherland BR, Cowie M (1985) Organometallics 4:1801
75. Poilblanc R (1982) Inorg Chim Acta 62:75

76. Sutherland BR, Cowie M (1985) Organometallics 4:1637
77. Bonnet JJ, Thorez A, Maisonnat A, Poilblanc R (1979) J Am Chem Soc 101:5940
78. Bonnet JJ, Thorez A, Maisonnat A, Galy J, Poilblanc R (1983) Organometallics 2:1123
79. Arif AM, Heaton DE, Jones RA, Kidd KB, Wright TC, Whittlesey BR, Atwood JL, Hunter WE, Zhangt H (1987) Inorg Chem 26:4065
80. Brost RD, Bushnell GW, Harrison DG, Stobart SR (2002) Inorg Chem 41:1412
81. Aullón G, Ujaque G, Lledós A, Alvarez S, Alemani P (1998) Inorg Chem 37:804
82. Aullón G, Ujaque G, Lledós A, Alvarez S (1999) Chem Eur J 5:1391
83. Lichtenberger DL, Copenhaver AS, Gray HB, Marshall JL, Hopkins MD (1988) Inorg Chem 27:4488
84. Oro LA, Sola E, López JA, Torres F, Elduque A, Lahoz FJ (1998) Inorg Chem Commun 1:64
85. Niu S, Thomson LM, Hall MB (1999) J Am Chem Soc 121:4000
86. Amara P, Volbeda A, Fontecilla-Camps JC, Field MJ (1999) J Am Chem Soc 121:4468
87. Maroney MJ, Bryngelson PA (2001) J Biol Inorg Chem 6:453
88. Sellmann D, Prakash R, Heinemann FW, Moll M, Klimowicz M (2004) Angew Chem Int Ed 43:1877
89. Sellmann D, Geipel F, Moll M (2000) Angew Chem Int Ed 39:561
90. Ohki Y, Sakamoto M, Tatsumi K (2008) J Am Chem Soc 130:11610
91. Tao J, Li S (2010) Dalton Trans 39:857
92. Ienco A, Calhorda MJ, Reinhold J, Reineri F, Bianchini C, Maurizio P, Vizza F, Mealli C (2004) J Am Chem Soc 126:11954
93. Tejel C, Ciriano MA, Edwards AJ, Lahoz FJ, Oro LA (1997) Organometallics 16:45
94. Tejel C, Ciriano MA, López JA, Lahoz FJ, Oro LA (2000) Organometallics 19:4977
95. Tejel C, Ciriano MA, López JA, Lahoz FJ, Oro LA (1997) Organometallics 16:4718
96. Ciriano MA, Viguri F, Oro LA, Tiripicchio A, Tiripicchio-Camellini M (1987) Angew Chem Int Ed Engl 26:444
97. Ciriano MA, Sebastián S, Oro LA, Tiripicchio A, Tiripicchio-Camellini M, Lahoz FJ (1988) Angew Chem Int Ed Engl 27:402
98. Tejel C, Ciriano MA, Eva Villarroya B, Gelpi R, López JA, Lahoz FJ, Oro LA (2001) Angew Chem Int Ed 40:4084
99. Tejel C, Ciriano MA, Villarroya BE, López JA, Lahoz FJ, Oro LA (2003) Angew Chem Int Ed 42:530
100. Villarroya BE, Tejel C, Rohmer M-M, Oro LA, Ciriano MA, Bénard M (2005) Inorg Chem 44:6536
101. Jiménez MV, Sola E, Martínez AP, Lahoz FJ, Oro LA (1999) Organometallics 18:1125
102. Jiménez MV, Sola E, Caballero J, Lahoz FJ, Oro LA (2002) Angew Chem Int Ed 41:1208
103. Fujita K, Hamada T, Yamaguchi R (2000) J Chem Soc Dalton Trans 1931
104. Fujita K, Nakaguma H, Hanasaka F, Yamaguchi R (2002) Organometallics 21:3749
105. McGhee WD, Bergman RG (1986) J Am Chem Soc 108:5622
106. Jones WD, Chin RM (1997) Organometallics 16:1912
107. Topsøe H, Clausen BS, Massoth FE (1996) Hydrotreating catalysis. Springer, Berlin
108. Yuan Y, Jiménez MV, Sola E, Lahoz FJ, Oro LA (2002) J Am Chem Soc 124:752
109. Burkhart BJ, DeKock RL (2012) Comput Theor Chem 994:1
110. Ristic-Petrovic D, Torkelson JR, Hilts RW, McDonald R, Cowie M (2000) Organometallics 19:4432
111. Martín M, Sola E, Tejero S, López JA, Oro LA (2006) Chem Eur J 12:4057
112. Jiménez MV, Sola E, Lahoz FJ, Oro LA (2005) Organometallics 24:2722
113. Werner H, Schäfer M, Wolf J, Peters K, von Schnering HG (1995) Angew Chem Int Ed Engl 34:191
114. Bianchini C, Frediani P, Masi D, Peruzzini M, Zanobini F (1994) Organometallics 13:4616
115. Burrows AD, Green M, Jeffery JC, Lynam JM, Mahon MF (1999) Angew Chem Int Ed 38:3043
116. Nishiura M, Hou Z (2004) J Mol Catal A Chem 213:101

117. Bruneau C, Dixneuf P (1999) Acc Chem Res 32:311
118. Werner H (2004) Coord Chem Rev 248:1693
119. Katayama H, Ozawa F (2004) Coord Chem Rev 248:1703
120. Qü J-P, Masui D, Ishii Y, Hidai M (1998) Chem Lett 1003
121. Jun C-H, Lu Z, Crabtree RH (1992) Tetrahedron Lett 33:7119
122. Ohmura T, Yorozuya S-I, Yamamoto Y, Miyaura N (2000) Organometallics 19:365
123. Chin CS, Won G, Chong D, Kim M, Lee H (2002) Acc Chem Res 35:218
124. Höhn A, Otto H, Dziallas M, Werner H (1987) J Chem Soc Chem Commun 852
125. Fryzuk M, Huang L, McManus NT, Paglia P, Rettig SJ, White GS (1992) Organometallics 11:2979
126. Werner H, Schulz M, Windmuller B (1995) Organometallics 14:3659
127. Werner H, Ilg K, Lass R, Wolf J (2002) J Organomet Chem 661:137
128. Hou Z, Koizumi T-A, Fujita A, Yamazaki H, Wakatsuki Y (2001) J Am Chem Soc 123:5812
129. Rubio-Pérez L, Iglesias M, Munárriz J, Polo V, Sanz Miguel PJ, Pérez-Torrente JJ, Oro LA (2015) Chem Commun 51:9860
130. Mena I, Casado MA, Polo V, García-Orduña P, Lahoz FJ, Oro LA (2012) Angew Chem Int Ed 51:8259
131. Haack K-J, Hashiguchi S, Fujii A, Ikariya T, Noyori R (1997) Angew Chem Int Ed Engl 36:285
132. Noyori R, Hashiguchi S (1997) Acc Chem Res 30:97
133. López I, Ertem MZ, Maji S, Benet-Buchholz J, Keidel A, Kuhlmann U, Hildebrandt P, Cramer CJ, Batista VS, Llobet A (2014) Angew Chem Int Ed 53:205
134. Sala X, Romero I, Rodríguez M, Escriche L, Llobet A (2009) Angew Chem Int Ed 48:2842
135. Romain S, Vigara L, Llobet A (2009) Acc Chem Res 42:1944
136. Petronilho A, Woods JA, Bernhard S, Albrecht M (2014) Eur J Chem 708

Top Organomet Chem (2016) 59: 59–102
DOI: 10.1007/3418_2015_162

Published online: 23 December 2015

Reactivity and Catalysis at Sites *Trans* to the [Ru–Ru] Bond

Indranil Dutta, Gargi Sengupta, and Jitendra K. Bera

Abstract The reactivity and catalysis at axial sites of [Ru–Ru] bonded compounds are described. Effect of axial donor at axial site of a [Ru–Ru] single bond, having electronic configuration $\sigma^2\pi^4\delta^2\delta^{*2}\pi^{*4}$, is examined. It is shown that the stronger donor leads to longer metal–metal distances. The C–H bond activation and C–C bond formation are studied at axial site of a $[Ru_2(CO)_4]^{2+}$ core. Metal–metal and metal–ligand cooperation is exploited for catalytic alcohol dehydrogenation to aldehyde and subsequent coupling with amine to access imine selectively. Catalytic carbene transfer reactions are discussed for a wide range of diruthenium(I,I) compounds. Catalytic utility of metal–metal multiply bonded diruthenium(II,III) compounds for C–H amination reaction is also discussed.

Keywords Acceptorless alcohol dehydrogenation • Allylic C–H activation • Axial reactivity • Carbenoid C–H insertion • C–H activation • Cycloprpanation • Diruthenium compounds • Metal nitride • Metal–ligand cooperation • Metal–metal bond

Contents

I. Dutta, G. Sengupta, and J.K. Bera (✉)
Department of Chemistry, Indian Institute of Technology Kanpur, Kanpur 208016, India
e-mail: jbera@iitk.ac.in

Abbreviations

AL	Axial ligand
BAr^F	Tetrakis 3,5-bis(tri-fluoromethyl)phenyl borate
BL	Bridging ligand
chp	6-Chloro-2-oxy-pyridinate
DABCO	1,4-Diazabicyclo[2.2.2]octane
DBU	1,8-Diazabicyclo[5.4.0]undec-7-ene
DCE	1,2-Dichloroethane
DCM	Dichloromethane
DFT	Density functional theory
DMSO	Dimethyl sulfoxide
dpa	Di(2-pyridyl) amine
dPhf	*N,N′*-diphenylformamidinate
dppy	2-(diphenylphosphino)pyridine
DSC	Differential scanning calorimetry
EDA	Ethyl diazoacetate
esp	α,α,α′,α′-Tetramethyl-1,3-benzenedipropionate
Et	Ethyl
EXAFS	Extended X-ray absorption fine structure
HOMO	Highest occupied molecular orbital
hp	Hydroxy pyridinate
^{i}Pr	Isopropyl
LUMO	Lowest unoccupied molecular orbital
MDA	Methyl diazoacetate
Me	Methyl
^{n}Bu	*n*-Butyl
NHC	*N*-heterocyclic carbene
Np	Naphthyridine
NPA	Natural population analysis
OAc	Acetate
Ph	Phenyl
py	Pyridine
pz	Pyrazole
^{t}Bu	Tertiary butyl
TFA	Trifluoroacetate
THF	Tetrahydrofuran

1 Introduction

Studies on metal–metal bonded compounds have largely been focused on their structures, bonding, and electronic spectra [1–5]. This class of compounds is increasingly being applied in different fields of research [6–9]. Metal–metal bonded bimetallic complexes are of particular interest due to their applications in catalysis. The bimetal platform provides scope for cooperative action between two metal ions [10–14] and offers prospect for multi-electron redox chemistry [15–19]. Reactivity studies on bimetallic systems provide valuable mechanistic information on chemical reactions catalyzed by metal cluster [20–22], metal nanoparticle [23–27], and reactions occurring on metal surfaces [28–30]. Majority of the reactions on bimetallic complexes occur at equatorial sites [31–34]. Metal–metal singly bonded compounds provide suitable molecular platform for axial site chemistry. The metal–metal single bond allows close approach of the substrate to axial site whereas strong *trans* effect of the metal–metal multiple bonds does not permit strong axial binding.

Dirhodium(II,II) tetraacetate and related complexes are most prominent among bimetallic complexes for their extensive applications as catalysts for a range of organic reactions. Several reviews [35–38] and book chapters [39–42] have appeared recently covering dirhodium(II,II) compounds. Other bimetallic compounds featuring metal–metal single bond include complexes containing [Ir^{II}–Ir^{II}] [43–46] and [Pd^{I}–Pd^{I}] [47–52] bonds. Lack of synthetic procedures for their large scale synthesis, however, has impeded their wider applications.

The isoelectronic [Ru^{I}–Ru^{I}] complexes are relatively more accessible, and such complexes are proving to be useful for a range of chemical reactions. This article collects the chemistry at sites *trans* to the [Ru–Ru] single bond. The C–H activation, C–C bond formation, acceptorless alcohol dehydrogenation, cyclopropanation, carbenoid C–H insertion, and C–H amination reactions are covered. Reactivity studies at axial sites on [Ru–Ru] multiply bonded systems are also included because of their direct relevance in catalytic chemistry. The purpose of this article is to highlight the recent progress on the axial-site chemistry on [Ru^{I}–Ru^{I}] platforms with intent to infuse interests for further development.

2 Diruthenium(I,I) Complexes Bearing Paddlewheel $[Ru_2(CO)_4]^{2+}$ Core

Compounds of general formula $[Ru_2(O_2CR)_2(CO)_4]_n$ and $[Ru_2(O_2CR)_2(CO)_4(AL)_2]$ (Scheme 1) are the commonly used diruthenium(I,I) precursors containing metal–metal single bond [53]. Two acetates bridge between two metals, and four carbonyls bind at equatorial positions to complete the paddlewheel geometry for $[Ru_2(O_2CR)_2(CO)_4]$. Two ligands additionally occupy axial sites for $[Ru_2(O_2CR)_2(CO)_4(AL)_2]$. Polymeric structure is observed for

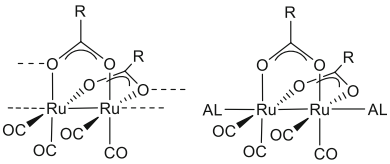

Scheme 1 Diruthenium precursors of general formula $[Ru_2(O_2CR)_2(CO)_4]_n$ and $[Ru_2(O_2CR)_2(CO)_4(AL)_2]$

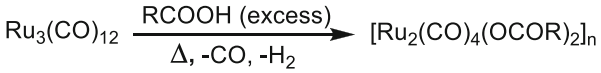

Scheme 2 General synthetic protocol for $[Ru_2(CO)_4(O_2CR)_2]_n$

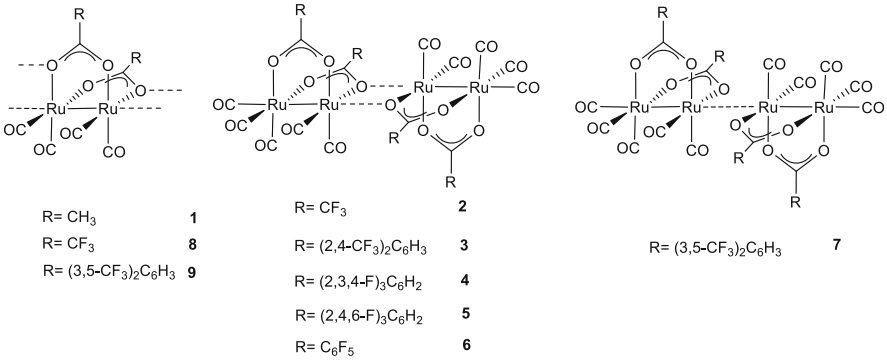

Scheme 3 Diruthenium(I,I) compounds **1–9**

$[Ru_2(O_2CR)_2(CO)_4]_n$ where sites *trans* to [Ru–Ru] bond are occupied by acetate oxygen from neighboring molecule. These compounds are readily synthesized by refluxing $Ru_3(CO)_{12}$ in corresponding carboxylic acids (Scheme 2) [54]. The most common complex in this category is the acetate analogue $[Ru_2(O_2CCH_3)_2(CO)_4]_n$ (**1**). A large number of complexes of general formula $[Ru_2(O_2CR)_2(CO)_4L_2]$ (where R = Me, Ph, Et, ^{t}Bu, CF_3, C_6H_4F, and C_3H_7 and L = $PhCO_2H$, PPh_3, NCMe, P^iPr_3, dpa, CO, P^nBu_3, P^tBu_3, P^tBu_2H, dppy, py, 3-Me-py, HPz, and H_2O) have been synthesized and structurally characterized [55–66]. Similar compounds with carboxylates having bulkier R group, like calix[4]arene-11,23-dicarboxylate, are synthesized by Maas et al. [67]

The trifluoroacetate analogue of $[Ru_2(O_2CR)_2(CO)_4]_n$ was synthesized by Petrukhina et al. [68]. These were obtained by gas phase sublimation of the crude product from the reaction of $Ru_3(CO)_{12}$ and trifluoroacetic acid in a DCM/benzene mixture. The solid state study of $[Ru_2(O_2CCF_3)_2(CO)_5]_2$ (**2**) (Scheme 3) reveals a "dimer of dimer" structure. Petrukhina and Davies also reported a variety of mixed carbonyl/fluorinated benzoates of diruthenium(I,I) obtained via melt reactions of $Ru_3(CO)_{12}$ with appropriate carboxylic acids (**3–9**) [69]. Compounds **3–6** show a

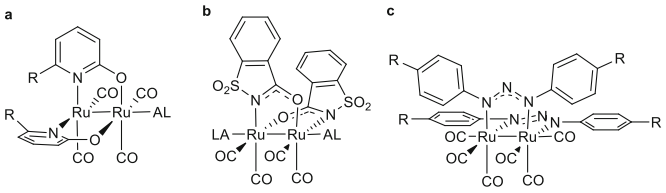

Scheme 4 Diruthenium complexes having N^N, N^O bridging ligands

Scheme 5 Synthesis of $[Ru_2(CO)_4(CH_3CN)_6][PF_6]_2$ [89]

"dimer of dimer" structure analogous to **2**, where two diruthenium units are connected by Ru···O inter-dimer axial contacts. Complex **7** also has a "dimer of dimer" structure, but here two diruthenium units are connected by Ru···Ru interaction. Complexes **8** and **9** exhibit polymeric structures similar to **1**.

The bridging acetates are substituted by different N^N or N^O bridging ligands. The $[Ru_2(CO)_4(BL)_2(AL)_x]$, where BL is 2-pyridonate [70] (Scheme 4a) or saccharinate [71] (Scheme 4b), can be readily synthesized from $Ru_3(CO)_{12}$ by refluxing with 2-hydroxy pyridine and saccharin, respectively [72, 73]. Similar to the carboxylato analogues, these compounds exist as polymers which dissociate in a variety of coordinating solvents or in the presence of Lewis base to provide discrete units of general formula $[Ru_2(CO)_4(BL)_2(AL)_2]$. The triazenido diruthenium(I,I) complexes are synthesized by refluxing a solution of triazene in acetonitrile with $Ru_3(CO)_{12}$ under an atmosphere of carbon monoxide [74]. The precipitate was recrystallized from DCM/ethanol mixture to afford $[Ru_2(CO)_6(ArNNNAr)_2]$ (Scheme 4c).

The unbridged and partially solvated diruthenium(I,I) complex $[Ru_2(CO)_4(CH_3CN)_6](PF_6)_2$ was initially synthesized by Klemperer et al. from $[Ru(CO)_3Cl_2]_2$ (Scheme 5) [75]. Bera et al. made marginal modifications in the procedure and established a pathway for the transformation of $[\{Ru(CO)_3Cl_2\}_2] \rightarrow [Ru^I{}_2(CO)_4]^{2+}$ [76]. The base-promoted reduction involves nucleophilic activation of carbonyls, leading to the μ-hydroxido, μ_2:κ^2-hydroxycarbonyl-bridged diruthenium(II,II) complex. The hydroxycarbonyl complex undergoes decarboxylation on heating to give a dihydrido–diruthenium(II,II) intermediate which readily converts to diruthenium(I,I) complex via a binuclear reductive elimination pathway (Scheme 6). Several of these intermediates have been arrested by employing different functionalized naphthyridine ligands [77]. An improved synthesis of $[Ru_2(CO)_4(CH_3CN)_6](BF_4)_2$ involves heating at reflux of $[Ru(CO)_3Cl_2]_2$ for 4 h in acetonitrile with 4 equiv. of $TlBF_4$ and 2 equiv. of base. The desired product was obtained in high yield (80–85%) with excellent purity where by-products were hydrogen and carbon dioxide (Scheme 7).

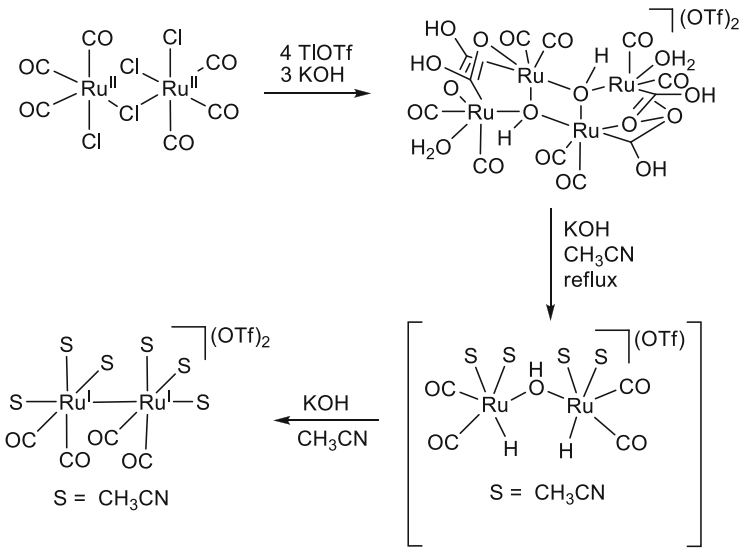

Scheme 6 Proposed reaction pathway for transformation of $[\{Ru(CO)_3Cl_2\}_2]$ to $[Ru^{I}_2(CO)_4]^{2+}$

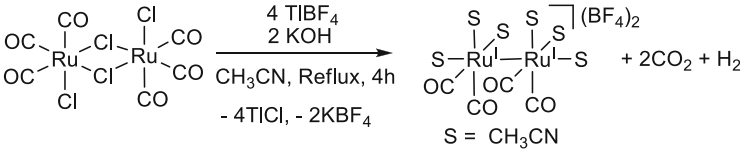

Scheme 7 An improved synthesis of $[Ru^{I}_2(CO)_4]^{2+}$ from $[Ru^{II}(CO)_3Cl_2]$

3 Effect of Axial Donor on the [Ru–Ru] Bond

Substrate coordination to axial site is necessary for its activation. It is therefore important to understand the nature of the interaction between [M–M] bond orbitals and ligand orbital. The metal–metal distance is modulated by the bridging and axial ligands as well [2, 6, 7]. Longer metal–metal distances are observed for unsupported complexes whereas bridging ligands tend to bring the metal ions closer. Quadruple bonds between metal ions are more sensitive to axial ligands than metal–metal bonds of lower bond order. Effects of axial coordination on Cr–Cr [78, 79] and Mo–Mo [80–82] quadruple bonds are well studied. Although the effect is less pronounced, lengthening of Rh–Rh distance by axial coordination is reported in metal–metal singly bonded [Rh–Rh] complexes [83–87]. As a general principle, short metal–metal distance (higher bond order) leads to long metal–ligand distance and vice versa [6, 88]. As a consequence, long metal–ligand (axial) distance is observed for quadruple-bonded $[Mo–Mo]^{4+}$ complexes compared to singly bonded $[Rh–Rh]^{4+}$ analogue for the same ligand. The extent of interaction between the axial ligand with the metal–metal bonded orbital is less than for cases where metal–metal bond is absent.

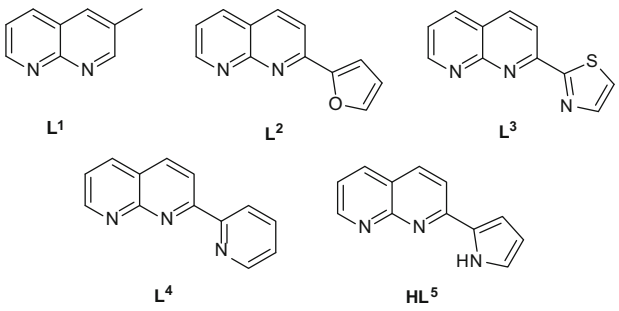

$[Ru_2(CO)_4(CH_3CN)_6](X)_2$ + 2 BL ⟶ $[Ru_2(CO)_4(BL)_2](X)_n$

BL = L^1	X=OTf	n=2	**10**	BL = L^3	X=ClO_4	n=2	**12**
BL = L^2	X=BF_4	n=2	**11**	BL = L^4	X=OTf	n=2	**13**
				BL = L^5		n=0	**14**

Scheme 8 Ligands based on 1,8-naphthyridine and general synthetic scheme for diruthenium(I,I) complexes with general formula $[Ru_2(CO)_4(BL)_2](X)_n$

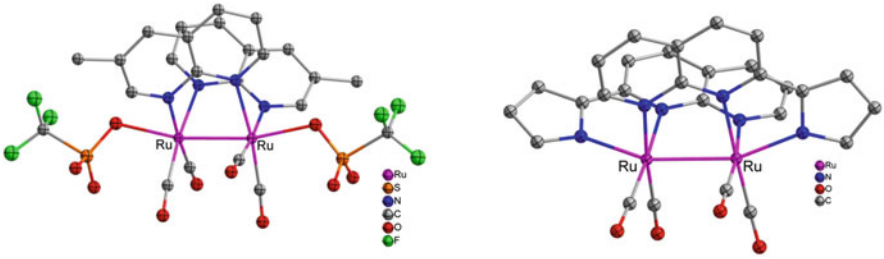

Fig. 1 Molecular structures of **10** and **14**

1,8-Naphthyridine unit bridges between a wide variety of metal ions [89–95]. Ligands with methyl ($\mathbf{L^1}$), furyl ($\mathbf{L^2}$), thiazolyl ($\mathbf{L^3}$), pyridyl ($\mathbf{L^4}$), and pyrrole ($\mathbf{HL^5}$) attachments on the naphthyridine ring, as shown in Scheme 8, allowed a systematic study to understand the effect of axial donors on the [Ru–Ru] single bond [96]. These ligands were synthesized via Friedlander condensation between 2-aminonicotinaldehyde and corresponding acyl derivatives in methanol [97–100]. Reaction of these ligands with $[Ru_2(CO)_4(CH_3CN)_6](X)_2$ (X = BF_4, ClO_4, CF_3SO_3) afforded a series of complexes of general formula $[Ru_2(CO)_4(BL)_2](X)_n$ (**10–14**, Scheme 8). A paddlewheel structure is maintained for all complexes where axial ligands are systematically varied with increasing donor strength. In case of $\mathbf{L^1}$, axial sites are occupied by weakly coordinated triflates. As representative examples, X-ray structures of complexes **10** and **14** containing axial triflate (OTf) and pyrrolyl units are shown in Fig. 1. The [Ru–Ru] single-bond distances increase gradually, although at a smaller extent, when the axial donors are varied in the series – triflates, furyls, thiazolyls, pyridyls, and pyrrolyls (Scheme 9). The shortest and longest

Scheme 9 The lengthening of Ru–Ru distances as a function of the axial donors

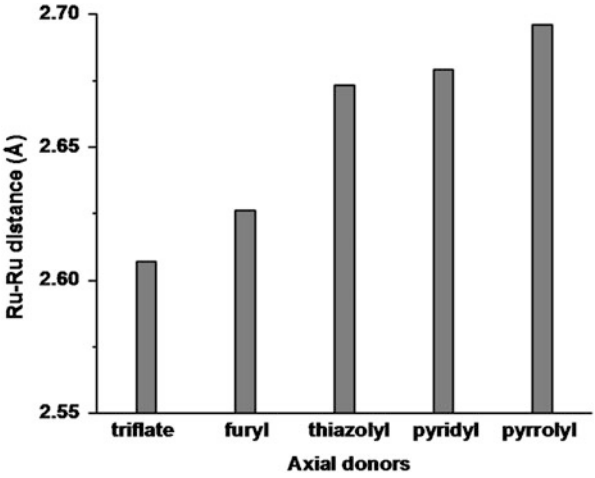

Scheme 10 The energy levels of Ru–Ru bond orbitals in model complexes

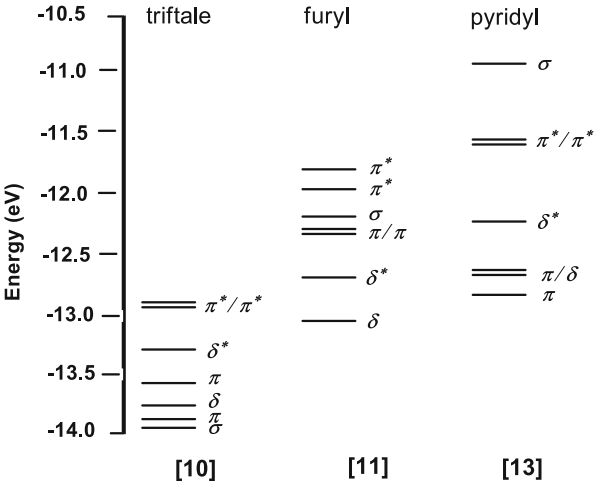

distances were observed for the axially coordinated triflates (2.607(9) Å) and pyrrolyls (2.697(2) Å), respectively. A similar trend was also observed for quadruple-bonded dimolybdenum(II,II) complexes [101]. The metal–metal distance is 2.081(1) Å in *trans*-[{Mo_2(Np-Me_2)$_2$(OAc)$_2$(BF_4)}(BF_4)] (**15**, Np-Me_2 = 2,7 dimethyl 1,8 naphthyridine) where axial ligand is tetrafluoroborate anion whereas longer Mo–Mo distance of 2.124(1) Å is observed for *cis*-[$Mo_2(L^4)_2(OAc)_2$][BF_4]$_2$ (**16**).

The response of the [Ru–Ru] bond to axial donors is rationalized by examining the interaction of ligand orbitals with the metal–metal bond orbitals. The electronic configuration for a paddlewheel $[Ru_2(CO)_4]^{2+}$ core is $\sigma^2\pi^4\delta^2\delta^{*2}\pi^{*4}$ which corresponds to a formal [Ru–Ru] single bond. Ligand coordination raises the energy of both σ and π orbitals of metals but the δ orbitals remain mostly unaffected. The most dramatic effect is observed for σ orbital (Scheme 10). The lone pair of the axial donor

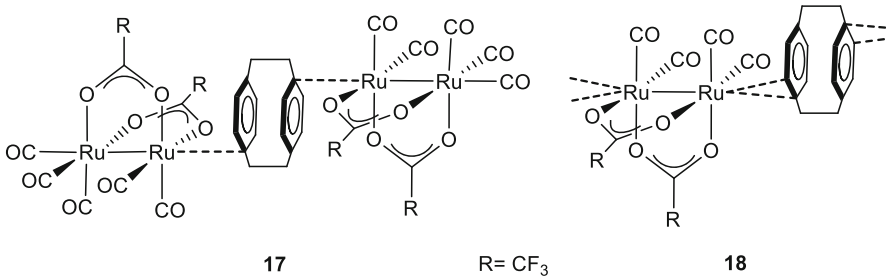

Scheme 11 Structures of **17** and **18**

destabilizes the [Ru–Ru] σ orbital. The extent of destabilization depends on the strength of the donor ligand. DFT calculations show that the [Ru–Ru] σ orbital for furyl complex is destabilized because of the interaction of furyl appendages with O lone pairs, and it lies below the pair of π^* orbitals. The extent of destabilization for axial pyridyl donors is significantly higher, making the [Ru–Ru] σ orbital the HOMO. The same is true for thiazole and pyrrole axial donors. For triflate, the σ orbital is low-lying and LUMO is primarily [Ru–Ru] σ^*. For other complexes, the LUMO is ligand-based π^* orbital. Thus, the lengthening of [Ru–Ru] bond distances as a function of axial donor follows the trend: pyrrolyl > pyridyl ~ thiazolyl > furyl > triflate which agrees well with the calculated destabilization of the [Ru–Ru] σ orbitals.

Axial interaction of an aryl unit with the [Ru–Ru] bond tends to increase the metal–metal distances. Petrukhina et al. isolated two complexes by codeposition of **2** and **8** with [2.2]paracyclophane to yield (**17**) and (**18**), respectively (Scheme 11) [68]. A sandwich structure with the aromatic moiety entrapped between two dimetal units is observed. The [Ru–Ru] distance increases from 2.627(9) Å in **8** to 2.656(3) Å in **18** on axial coordination of the arene moiety. Similarly, a change of [Ru–Ru] distance from 2.673(1) Å in **2** to 2.678(3) Å in **17** was also observed. The inter-centroid distances between the two rings in [2.2]paracyclophane group are shorter (2.974(4) Å in **17** and 2.982(5) Å in **18**) compared to the free [2.2] paracyclophane ligand (3.09 Å). This supports the hypothesis that coordination of aryl group to the electrophilic ruthenium centers allows the aromatic decks to move closer which also increases the [Ru–Ru] bond distances.

Similar to diruthenium(I,I) complexes, axial ligands influence the overall structure and ground-state electronic configuration of diruthenium(II,II) complexes as well [102]. Reduction of $Ru_2(chp)_4Cl$ (**19**) with Zn or $FeCl_2$ in coordinating solvents afforded a series of complexes of general formula $[Ru_2(chp)_4X]$, where X = THF (**20**), DMSO (**21**), py (**22**), CH_3CN (**23**), and PPh_3 (**24**) (Scheme 12). Reduction with Zn in noncoordinating solvents such as toluene or DCM afforded dimeric $[Ru_2(chp)_4]_2$ (**25**) and $[Ru_2(chp)_4](ZnCl_2)$ (**26**). Attempts to incorporate CO at axial site led to the cleavage of the [Ru–Ru] bond similar to diruthenium(II,II) carboxylate analogues [103]. Detailed structural, magnetic, and computational studies revealed that although the basic structures are the same, these complexes are very different with respect to their ground-state electronic configurations. Accordingly, these complexes can be divided into three categories (Scheme 13).

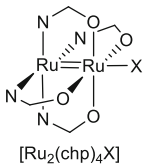

19 X= Cl
20 X= tetrahydrofuran
21 X= dimethyl sulfoxide
22 X= pyridine
23 X= CH_3CN
24 X= PPh_3

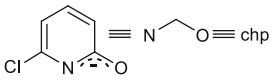

25 $[Ru_2(chp)_4]_2$
26 $[Ru_2(chp)_4](ZnCl_2)$

Scheme 12 Schematic representation of complexes **19–26**

Category	1	2	3
Ground State	^3A	^3A	^3E
Electronic Configuration Structure	$\delta^{*2}\pi^{*2}$ 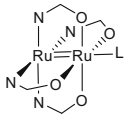	$\delta^{*2}\pi^{*2}$ or $\delta^{*1}\pi^{*3}$ 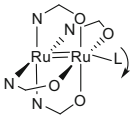	$\delta^{*1}\pi^{*3}$ 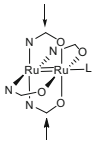
Symmetry	C_4	C_S	C_2
Ru-Ru	2.24-2.28 Å	2.28-2.30 Å	2.34-2.40 Å
Examples	**20**, **21**, **22**, **23**, **25**, **26** $[Ru_2(chp)_4]\cdot X^*$ X=H_2O, NH_3	**24**, $[Ru_2(chp)_4]\cdot CH_2Cl_2^*$	$[Ru_2(chp)_4]\cdot X^*$ X= N_2, CO, S-bound DMSO

* denotes Hypothetical Adduct

Scheme 13 Comparative features of the three categories of $[Ru_2(chp)_4X]$ compounds

Category 1 complexes (**20**, **21**, **22**, **23**, **25**, and **26**) have ^3A ground state with filled δ^* orbital, and each π orbital is filled with one unpaired electron. Category 3 complexes (hypothetical adducts $Ru_2(chp)_4 \cdot X$ (where $X = N_2$, CO, DMSO (S-bound)) have ^3E ground state with one unpaired electron in the δ^* orbital and three electrons distributed over two π orbitals. Category 2 complexes (**24** and hypothetical $[Ru_2(chp)_4] \cdot CH_2Cl_2$) show spectroscopic and structural signature indicative of significant δ^*/π^* orbital mixing. The magnetic data for **24** reveals a ^3A ground state. It has spin configuration similar to category 1 complexes (^3A), but alteration in orbital ordering leads to intermediate properties. The structures of these complexes vary with the identity of the axial ligand. Category 1 complexes adapt a more perfect C_4 symmetry. Category 2 complexes display pseudo Jahn–Teller distortion where axial ligand bends away from [Ru–Ru] axis lowering

the symmetry to C_s. For category 3 complexes, the bridging oxypyridinate ligands bind tighter through the *N*-ends whereas the O-bonded Ru moves toward the axial ligand. The [Ru–Ru] distance increases going from category 1 to category 3. In conclusion, the π acidic character of axial ligand alters heavily the δ^*/π^* ordering and therefore the ground-state electronic configuration. Nevertheless, the extent of axial ligand binding is governed by σ-donor character of the ligand.

4 C–H Bond Activation at Axial Site of a [Ru^I–Ru^I] Bond

C–H bond activation on a metal center is of fundamental interest [104–113]. Several metal catalysts have been developed over the years for C–H functionalization reactions. An extensive range of studies have been undertaken to understand the nature of the metal···C–H interaction. Nearly all studies involve complexes with single metal [114–117]. On the contrary, there are few reports available on C–H activation on a bimetallic complex or metal cluster [118–120]. Orthometalation of aryl phosphines, bis(2-pyridyl)amine, and 2-((α-R-benzylidene)amino)pyridines [R = CH_3, 4-$(CH_3O)C_6H_4$] has been achieved on a [Rh^{II}–Rh^{II}] platform [121–125]. C–H bond activation is also reported on $Ru_3(CO)_{12}$ [126–130]. The Os analogue activated C–H bond of $(Ph_2P)C_{60}H$ [131]. Studies on C–H activation at axial site of a metal–metal bond paved the way for designing catalytic systems based on bimetallic complexes [132].

Suitably designed naphthyridine-based ligands allowed the introduction of aryl C–H bond at axial site of the $[Ru_2(CO)_4]^{2+}$ unit [96]. The ligand systems that were studied are collected in Scheme 14. In noncoordinating solvent DCM, reaction of ligand **HL^6**–**HL^{12}** with $[Ru_2(CO)_4]^{2+}$ core led to a series of complexes, each containing two ligands. One ligand is orthometalated while the *ortho* C–H bond of the second ligand interacts with the metal (Scheme 15a). The isolated complexes are $[Ru_2(HL^6)(L^6)(CO)_4][BF_4]$ (**27**), $[Ru_2(HL^7)(L^7)(CO)_4][BF_4]$ (**28**), $[Ru_2(HL^8)(L^8)(CO)_4][BF_4]$ (**29**), $[Ru_2(HL^9)(L^9)(CO)_4][BF_4]$ (**30**), $[Ru_2(HL^{10})(L^{10})(CO)_4]$

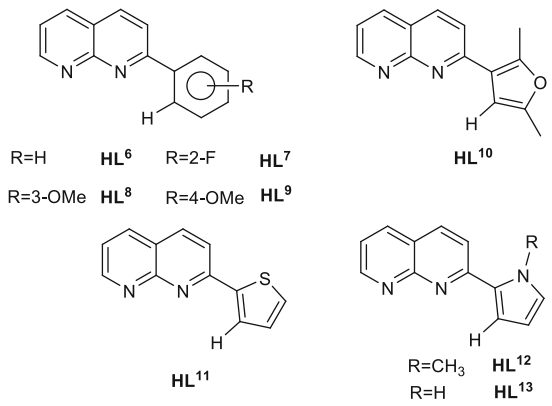

Scheme 14 Ligands used for axial C-H activation on diruthenium(I,I) complexes

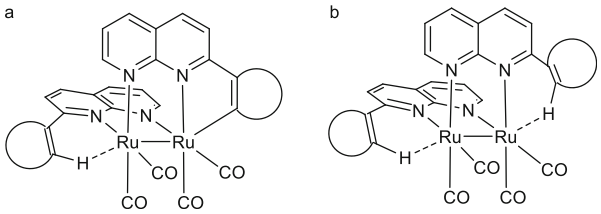

Scheme 15 Schematic representation of diruthenium(I) orthometalated (a) and nonmetalated (b) complexes

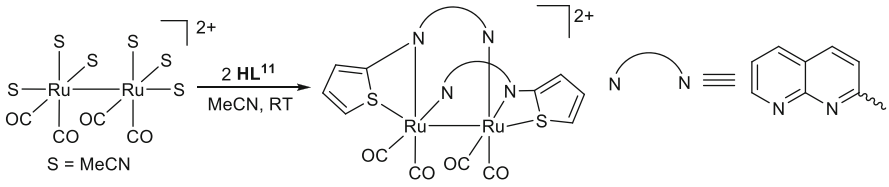

36

Scheme 16 Synthesis of S-coordinated complex **36**

$[BF_4]$ (**31**), $[Ru_2(HL^{11})(L^{11})(CO)_4][BF_4]$ (**32**), and $[Ru_2(HL^{12})(L^{12})(CO)_4][BF_4]$ (**33**) [133]. An interesting chemistry was observed for $\mathbf{HL^{12}}$. Although room-temperature reaction provided the orthometalated compound **33**, reaction at low temperature (4°C) yielded a nonmetalated compound $[Ru_2(HL^{12})_2(CO)_4][BF_4]_2$ (**34**). Here, *ortho* hydrogens of the pyrrolyl group in both ligands were involved in axial interactions with the metal (Scheme 15b). Raising the temperature to room temperature allowed the conversion of **34** to **33**. A nonmetalated complex $[Ru_2(HL^{13})_2(CO)_4][BF_4]_2$ (**35**) was isolated at room temperature which could not be metalated by increasing the temperature.

Interestingly, C–H activation does not occur when the reaction is carried out in coordinating solvent like acetonitrile. An identical reaction with $\mathbf{HL^{11}}$ in acetonitrile afforded sulfur-coordinated complex $[Ru_2(HL^{11})_2(CO)_4](BF_4)_2$ (**36**) (Scheme 16). Moreover the isoelectronic $[Rh–Rh]^{4+}$ system does not cleave C–H bond under identical conditions. Reaction of $Rh_2(OAc)_4$ (**37**) with $\mathbf{HL^6}$ in refluxing DCE, followed by crystallization in DCM, resulted in the formation of $[Rh_2(OAc)_3(HL^6)Cl]$ (**38**) [133].

Most of the complexes (**27**–**33**) are in the orthometalated/nonmetalated (om/nm) category. Complexes **34** and **35** are nonmetalated (nm/nm). As representative examples, X-ray structures of **28**, **33**, and **34** are collected in Fig. 2. Double-orthometalated complexes could not be obtained even under harsh conditions. In all these structures, a $[Ru_2(CO)_4]^{2+}$ unit is spanned by two naphthyridine ligands. For om/nm complexes, e.g., **28**, one of the ligands ($\mathbf{HL^7}$) is orthometalated whereas the second ligand bridges the diruthenium unit. The *ortho* hydrogen H44 is positioned in the vicinity of Ru1. The orthometalated aryl ring is near planar with Np ring (torsional angle ~5°), whereas the nonmetalated ring is characterized by a large torsional angle (~50°) (Fig. 2). For nm/nm complex **34**, both *ortho* hydrogen atoms of the two $\mathbf{HL^{12}}$ ligands are located at sites *trans* to the Ru–Ru bond. The torsional angles confirm that neither of the ligands are orthometalated.

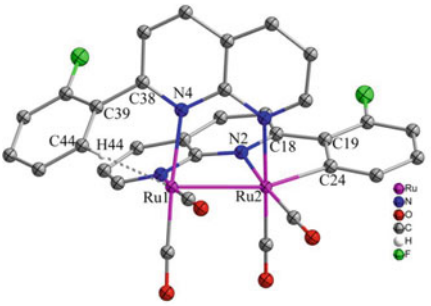

28

Ru1−Ru2 = 2.688(1) Å
Ru1−H44 = 2.540(1) Å
Ru2−C24 = 2.068(4) Å
Angle (N2−C18−C19−C24) = 5.2(5)°
Angle (N4−C38−C39−C44) = 54.0(5)°

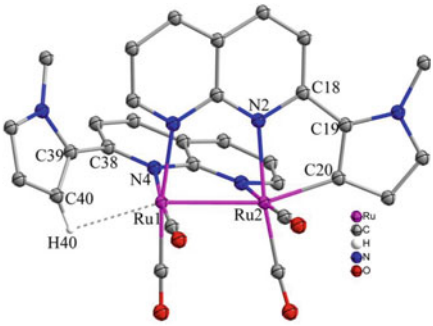

33

Ru1−Ru2 = 2.695(1) Å
Ru1−H40 = 2.503(1)Å
Ru2−C20 = 2.054(6)Å
Angle (N2−C18−C19−C20) = 2.8(9)
Angle (N4−C38−C39−C40) = 49.2(1)

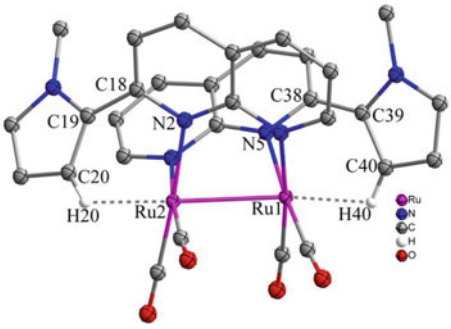

34

Ru1−Ru2 = 2.655(1) Å
Ru1−H40 = 2.301(1)Å
Ru2−H20 = 2.314(1)Å
Angle (N2−C18−C19−C20) = 45.6(9)
Angle (N5−C38−C39−C40) = 46.2(7)

Fig. 2 Molecular structures of **28**, **33**, and **34** with selected bond parameters

^{1}H NMR spectrum of the complex provides valuable information on the structure. This is illustrated by taking complex **28** as an example. Figure 3 depicts the ^{1}H NMR spectra with the assignment. The i proton appears broad, and it shows a downfield shift ($\Delta\delta = 0.57$ ppm, for **28**) relative to the free ligand. This indicates preagostic interaction of proton i with Ru. The a′ proton undergoes a large upfield shift relative to the free ligand ($\Delta\delta = 1.91$ ppm). The a′ proton is located over the phenyl ring of the second ligand. A large upfield shift is attributed to the diamagnetic shielding of the aromatic ring from the second ligand. Similar observations were made for M–M bonded dirhodium(II,II) and dimolybdenum(II,II) complexes [101].

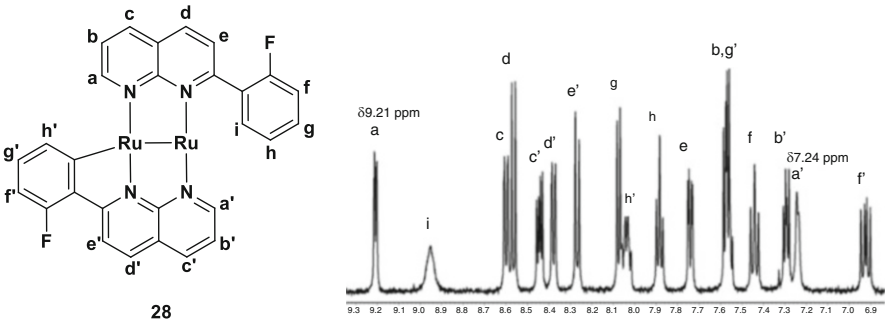

Fig. 3 ^{1}H NMR spectrum of **28**

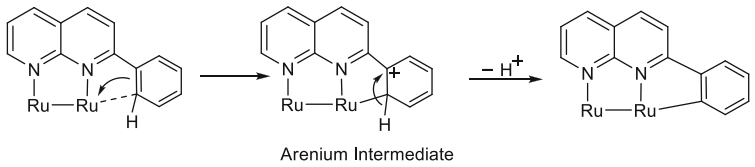

Scheme 17 Proposed electrophilic pathway for the C–H cleavage at axial site

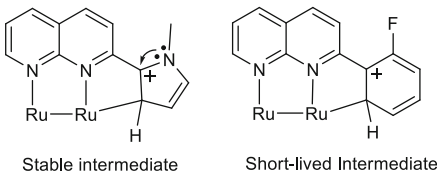

Scheme 18 Heteroatom stabilization in an arenium intermediate for pyrrolyl C–H and the absence of it for a phenyl fragment

It should be noted that the metal–metal bond is intact in the products. The carbonyl ligands around the metal centers do not support the oxidative addition/reductive elimination pathway [111]. Thus, an electrophilic mechanism for C–H cleavage at axial site of the [Ru–Ru] single bond is proposed [134]. The $[Ru_2(CO)_4]^{2+}$ core offers an acceptor [Ru–Ru] σ^* orbital. The π electron density of the axial group is pushed into [Ru–Ru] σ^* orbital. This results in an arenium intermediate. Subsequent release of a proton gives the orthometalated complex (Scheme 17). The relative stability of the arenium intermediate is governed by the nature of the axial group. The intermediate is heteroatom stabilized by the nitrogen lone pair of the heteroarene whereas such stabilization is not possible for the phenyl group. On the contrary, the F substituent renders the arenium species short-lived (Scheme 18). This explains why only orthometalated complexes are obtained for aryl C–H, whereas heteroatom stabilization allows the isolation of nonmetalated complex for pyrrolyl C–H. Now the question arises why double cyclometalation was not observed even under harsher conditions. NPA study of the cyclometalated complexes reveals that the dimetal core is sufficiently electron rich making the

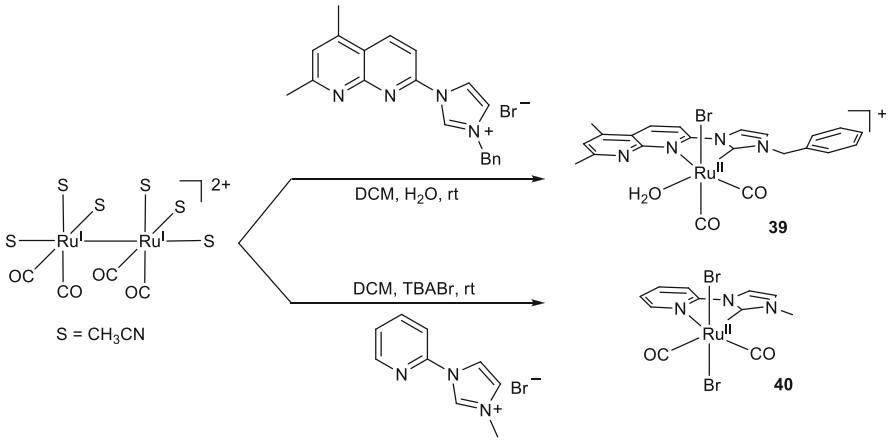

Scheme 19 Oxidative addition of the imidazolium C–H bond to Ru–Ru single bond affording Ru^{II}-NHC compounds

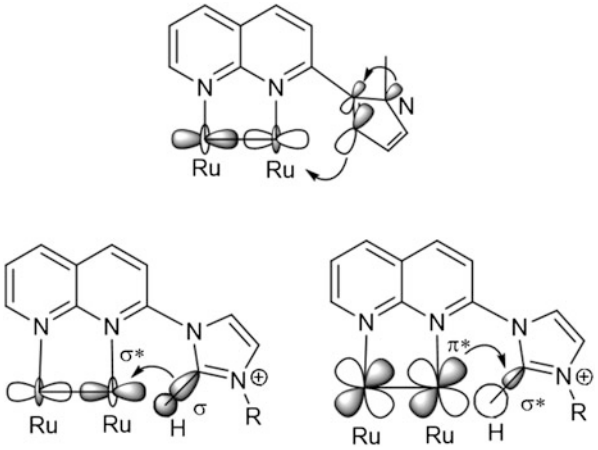

Scheme 20 Proposed mechanism explaining the difference of behavior between pyrrolyl C–H and imidazolium C–H

second cyclometalation difficult. The [Ru–Ru] σ^* orbital is no longer a good acceptor orbital to interact with the second C–H bond [86].

Although the aryl and pyrrolyl C–H bonds undergo electrophilic activation at room temperature, the imidazolium C–H bonds are oxidatively added to [Ru–Ru] single bond providing the corresponding mononuclear Ru(II)–NHC compounds where metal oxidation state is increased by one unit (Scheme 19) (compounds **39** and **40**) [135, 136]. A working mechanism is proposed to explain the difference of behavior between pyrrolyl C–H and imidazolium C–H (Scheme 20) (J.K. Bera et al., unpublished work). The lone pair on pyrrole nitrogen promotes electron donation of *ortho* C(p_π) orbital to [Ru–Ru] σ^* orbital. This interaction polarizes the C–H

σ orbital. Hence, the acidity of the hydrogen atom is increased favoring electrophilic C–H cleavage. The lone pair on imidazole nitrogen is involved in resonance with the Np π cloud. The *ortho* C(p_π) orbital is thus not sufficiently electron rich to interact strongly with [Ru–Ru] σ^* orbital. But, the C–H σ bond interacts with [Ru–Ru] σ^* orbital and back donation occurs from filled [Ru–Ru] π^* to C–H σ^* orbital. The result is the C–H oxidative addition to Ru–Ru resulting in its oxidative cleavage.

5 C–C Bond Formation at Axial Site of a [Ru^I–Ru^I] Bond

The formation of C–C coupled products without the aid of base is highly important [137, 138]. The C–C bond formation reactions were observed at room temperature between an axially coordinated ketone and *ortho* methyl group on the naphthyridine ligand that bridges between the metal centers [139]. Several naphthyridine-derived alcohols (compounds **41**–**43**) were synthesized on the $[Ru_2(CO)_4]^{2+}$ core (Scheme 21). Clearly, the coordination of naphthyridine unit promotes nucleophilic attack of *ortho* methyl group to axially coordinated ketone. Subsequent proton migration affords the C–C coupled alcohol (Scheme 22). Coordination of ketone at axial site is crucial for this reaction. Use of coordinating solvents does not allow the reaction to occur. Diruthenium precursor with triflate anion also makes the reaction

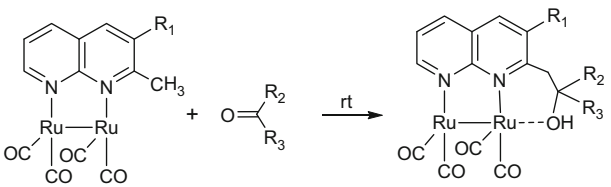

Scheme 21 C–C bond-forming reaction through an aldol-type addition on a $[Ru_2(CO)_4]^{2+}$ core

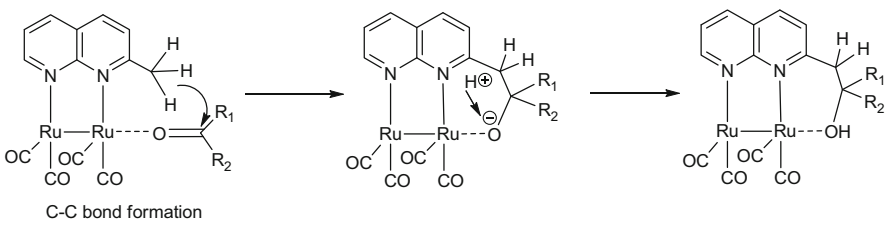

Scheme 22 Proposed mechanism for the formation of C–C coupled alcohol products

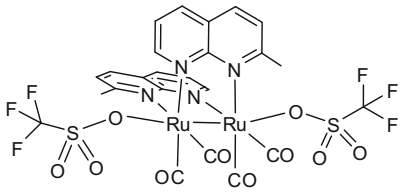

44

Scheme 23 Schematic representation of **44**

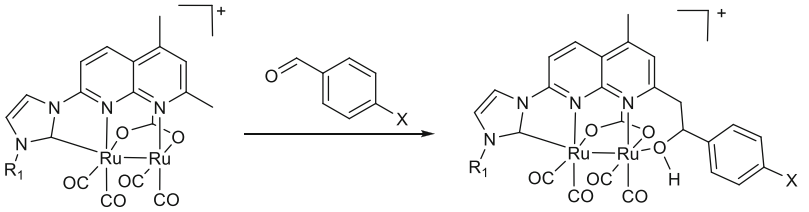

Scheme 24 Syntheses of diruthenium–NHC complexes bearing a protonic arm at the axial site

ineffective, presumably because triflates block the axial sites as it competes with ketone for axial coordination. Structure of $[Ru_2(CO)_4(2\text{-MeNp})(OTf)_2]$ (**44**) confirms the axial coordination of triflate (Scheme 23) [139].

Interestingly, ketones could not be activated when NHC-functionalized naphthyridines are used. However, electron-deficient aromatic benzaldehydes containing electron withdrawing groups ($–NO_2$, –CN, $–CF_3$) at *para* positions underwent C–C coupling reaction between naphthyridine *ortho* methyl substituent and carbonyl compounds with ligand 1-benzyl-3-(5,7-dimethyl-1,8-naphthyrid-2-yl) imidazole (**BIN**) and 1-isopropyl-3-(5,7-dimethyl-1,8-naphthyrid-2-yl)imidazole (**PIN**) (Scheme 40) to give compounds **45**–**48** (Scheme 24). The strength of axial coordination is important which is governed by the second axial ligand. The NHC ligand exerts a strong *trans* influence on the $[Ru^I–Ru^I]$ core unit which does not allow a strong axial binding of the ketone. Consequently, the carbonyl carbon is not electrophilic enough for the methyl carbon to attack. The naphthyridine-bound alcohols are important target compounds for pharmacological applications and are useful ligands as well [140–142]. It should be noted here that pyridine analogues were synthesized from 2-Me-pyridine with ^{n}BuLi (1 eq) and acetone [143]. This work illustrates that the axial site could be useful for organic transformation reactions.

6 Alcohol Dehydrogenation at Axial Site of a [Ru^{I}–Ru^{I}] Bond

Synergic cooperation between two metal ions has been widely recognized to execute a chemical reaction with enhanced rate and selectivity [144–151]. A new class of catalysts is emerging where active participation of ligand in the substrate activation and product elimination steps is observed [152–161]. An eminent example is Noyori's catalyst [162–167] that utilizes metal–amine/metal–amide interconversion to activate dihydrogen and deliver hydrogens of antagonistic properties (hydride and proton) to the carbonyl moiety (Scheme 25a). Milstein introduced the aromatization/dearomatization motif on Ru–PNP and Ru–PNN systems for a wide array of reactions (Scheme 25b) [168–173]. Grützmacher developed Rh–amide system for dehydrogenative coupling of primary alcohols with water, methanol, and amine (Scheme 25c) [174]. Shvo [175–177] and Gelman's [178–183] systems employ –OH unit for alcohol dehydrogenation reactions (Scheme 25d, e).

All these bifunctional catalysts mentioned above involve a single metal ion. There has been a continuing effort to design bifunctional catalysts on new molecular platforms [51, 76, 96, 101, 134, 135, 184–190]. Developing a bifunctional catalyst on a dinuclear platform has the potential to exhibit both metal–metal and metal–ligand cooperation. The design principle involves the introduction of a protonic arm (–OH) at the axial site of the metal–metal bond through the aid of a ligand [191]. A hydroxy unit at the *ortho* position of the NHC–naphthyridine allows metal–ligand interplay at axial site of a diruthenium unit (Scheme 26). Compounds **45**–**48** described earlier meet these criteria as they have an OH appendage at one axial site and NHC binds to ruthenium on the other axial site. The accessible protonic arm

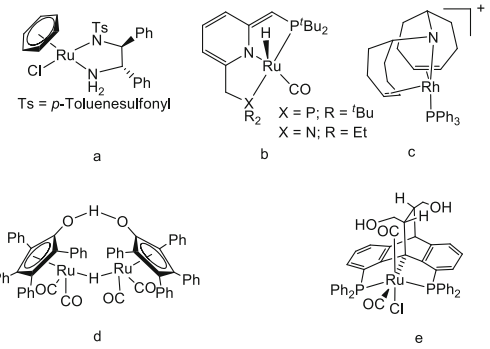

Scheme 25 Catalysts showing metal–ligand cooperativity

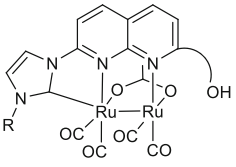

Scheme 26 Metal–ligand interplay through hydroxy arm at axial site of a diruthenium platform

Scheme 27 Imine formation catalyzed by **45**

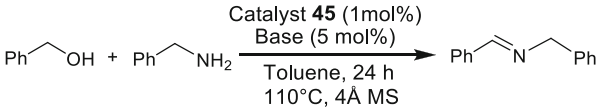

Scheme 28 Catalyst **49** devoid of hydroxy unit

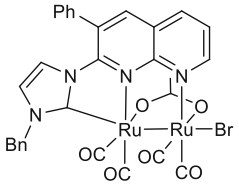

49

allowed acceptorless dehydrogenation of alcohol to aldehyde. In particular, the catalytic utility of **45** was evaluated. Catalyst **45** (1 mol%) afforded 98% conversion of benzyl alcohol to benzaldehyde under reflux in toluene for 24 h. Addition of 1.2 mmol benzylamine in presence of 4 Å molecular sieves provided *N*-benzylidene benzylamine selectively (Scheme 27). The reaction was effective with a range of bases (DBU, DABCO, KOH, KO^{t}Bu, NaH). However, for optimization purpose, DABCO was used. A set of 25 reactions was studied with different combinations of alcohol and amine. The yields varied in the range of 71–96%.

In order to understand the catalytic efficacy of **45**, related but different complexes were also examined. Catalyst **49** (Scheme 28) which does not bear a hydroxy unit afforded benzyl alcohol dehydrogenation product benzaldehyde in lower yield (55%). Similarly, imine conversion was also significantly lower. A lower conversion (68%) was observed for catalyst **45** which has two naphthyridine-based ligands. It is clear that a hydroxy appendage is crucial for the catalyst activity. A bifunctional mechanism is proposed to explain the acceptorless conversion of alcohol to aldehyde. In the presence of base, the active catalyst is the deprotonated form of **45**. The bifunctional addition of alcohol to the [Ru–Ru]–hydroxide forms axial [Ru–Ru]–alkoxide, and the hydroxy arm is opened up (Scheme 29). β-hydride elimination of the alkoxide affords aldehyde, and the [Ru–Ru]–H intermediate is generated (identified in ^{1}H NMR spectrum by a characteristic signal at $\delta = -7.37$ ppm). Liberation of hydrogen leads to the generation of active catalyst, and the extruded aldehyde reacts with amine to give imine as the final product. Kinetic Hammett studies support a β-hydride elimination step for the conversion of alcohol to aldehyde. This bifunctional mechanism is strikingly different from the conventional mechanism which involves oxidative addition of alcohol to a low-valent metal [192]. However, such a pathway would necessarily be accompanied by significant hydrogen scrambling in the product. For example, Madsen et al. observed 42% hydrogen incorporation for the catalyst [$RuCl_2$(I^{i}Pr)(*p*-cymene)] which lacks functional attributes of metal–ligand cooperativity [193]. However, reaction of α,α-[D_2]-benzyl alcohol and benzylamine generated deuterated *N*-benzylidene benzylamine as major product (93:7 D/H observed by GC–MS analysis) (Scheme 30), clearly indicating a bifunctional

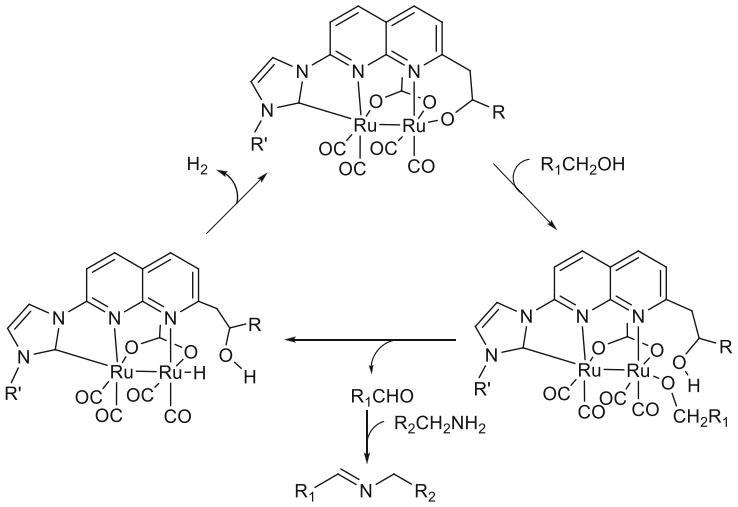

Scheme 29 Proposed mechanism for the imine formation

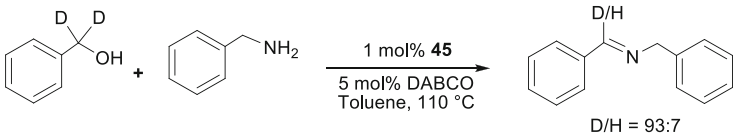

Scheme 30 Deuterium scrambling using α,α-[D_2]-benzyl alcohol for imine formation reaction

mechanism. Although it appears from the mechanism that the reaction occurs at axial site of the [Ru–Ru] single bond, it is shown that the bridging acetate is essential for the increased efficiency. The β-elimination requires an accessible site at the metal. The bridging acetate changes its coordination from μ^2 to η^1 mode providing a vacant site for β-elimination to occur.

The most important aspect is the selective formation of imine in this reaction. In absence of metal catalyst, the reaction of aldehyde and amine invariably gives imine [194]. However, in presence of a metal catalyst, the amine attacks the metal-bound aldehyde generating hemiaminal, which undergoes dehydrogenation to give amide or it simply dehydrates to give imine. Since hydrogen is produced in this reaction (alcohol dehydrogenation), the amine or *N*-alkylated product is also expected. It is thus clear that the outcome of the final product is dictated by the propensity of the metal to bind the intermediate product aldehyde. Coordination of aldehyde to the metal is essential for the amide formation [136, 195]. The ligand architecture in catalyst **45** does not allow the axial binding of the aldehyde. Even if it is allowed, the strong *trans* effect of NHC group at one of the axial sites does not permit strong alcohol binding. The consequence is the metal-free reaction of aldehyde and amine to give imine. Thus, this catalyst displays both metal–ligand and metal–metal cooperation for the selective imine synthesis by dehydrogenative coupling of alcohol with amine.

7 Cyclopropanation

The diruthenium(II,II) complexes $[Ru_2(O_2CR)_4]$ (R = CH_3 (**50**), CF_3 (**51**)) have also been studied for catalytic activity toward cyclopropanation as they are immediate structural analogues of $Rh_2(OAc)_4$ (**37**) (Scheme 31) which is the most effective catalyst in this field [36, 196]. Complex **51** catalyzes cyclopropanation of cyclooctene with EDA quantitatively based on EDA conversion giving *endo*/*exo* ratio 1.65, while **50** is less efficient [197, 198]. Reaction of a mixture of styrene and norbornene with EDA using catalyst **50** at 60°C gave cross-metathesis (major) and cyclopropanated (minor) products. The metathetical activity of the catalyst is governed by the kinetic lability of the acetate bridge [199].

Maas et al. have studied the cyclopropanation reaction using diruthenium(I,I) complexes bearing paddlewheel $[Ru_2(CO)_4]^{2+}$ core, specifically catalysts **1** and **52** (Scheme 31). Before proceeding, the solubility of these compounds should be commented upon. Compound **1** is a coordination polymer and not soluble in noncoordinating solvents, but it dissolves in the reaction mixture during the course of reaction. For axial reactivity, the axial acetonitrile in complex **52** must be removed. Compound **1** catalyzes cyclopropanation of different alkenes with MDA at room temperature in good to high yields (Scheme 32) [200, 201]. The activity is similar to **37** for mono or 1,1-disubstitued alkenes but to some extent lesser for 1,2-disubstitued, trisubstituted, and tetrasubstitued alkenes [202–204]. Steric hindrance at the olefin lowers the yield. The diastereoselectivity for sterically less demanding olefin (1-hexene, cyclohexene, styrene) is similar to those with **37**; however, *syn* selectivity is observed for trisubstituted alkenes [201, 205]. The

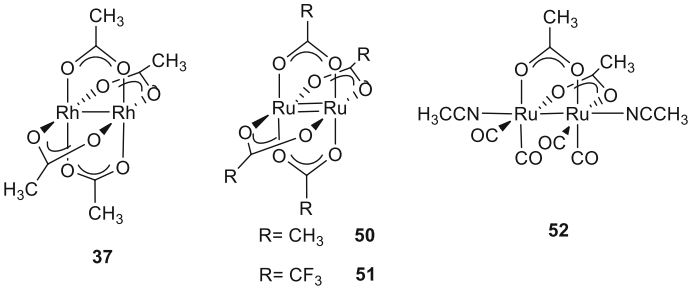

Scheme 31 Schematic representation of complexes **37** and **50**–**52**

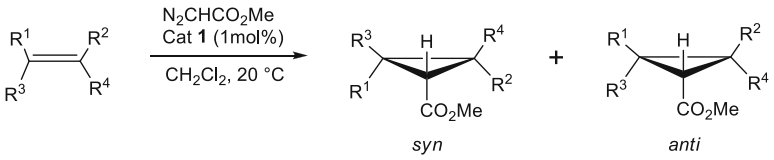

Scheme 32 Cyclopropanation of alkenes with N_2CHCO_2Me (MDA) catalyzed by **1**

Scheme 33 Sawhorse configuration of the dimeric dicarbonylruthenium carboxylate complexes

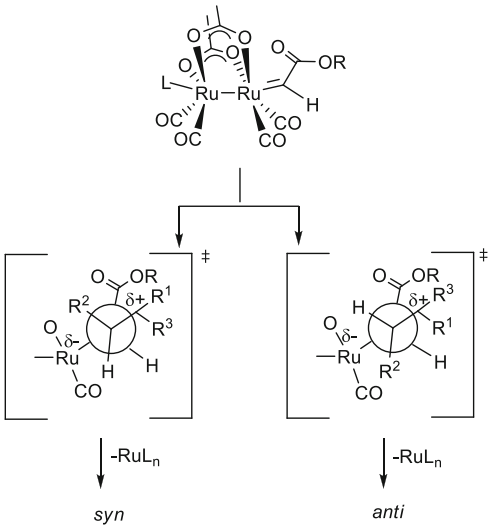

sawhorse configuration of the dimeric diruthenium carboxylate/carbonyl complexes is responsible for the diastereoselectivity as it controls the approach of the alkene as well as the configuration at the Ru=C (carbene) bond (Scheme 33). Compound **1** was also used for alkene cyclopropanation with $N_2CHSiMe_3$ and N_2CHPh [206]. Again, the yields and selectivity are well comparable with **37** [200, 201, 206]. Catalyst **52** exhibited similar activity to **1** at slightly high temperature.

The scope of this reaction was extended to catalysts having different bridging carboxylates. Fluorinated analogues (**2–9**) of carboxylato/carbonyl compounds were also studied for cyclopropanation reaction. The presence of weakly donating carboxylates is likely to increase the electrophilicity of the metal center [207, 208]. But all these compounds (catalyst loading 1 mol%) showed low activity at room temperature for the cyclopropanation reactions between methyl phenyldiazoacetate and styrene [69]. Increasing the temperature to 40°C in DCM gave moderate to good yields (42–69% Scheme 34). The catalytic activity is associated with solubility of the complex and the ease of access to the axial site. The diruthenium catalysts show lower diastereoselectivity compared to dirhodium(II,II) analogues [209]. This is attributed to higher electrophilicity of Ru catalyst which reduces the discriminating abilities of the carbenoid intermediates. Among all the carboxylato/carbonyl ruthenium catalysts studied, compound **1** is the most effective when cyclopropane yields are considered following the trend: acetate > butyrate ~ trifluoroacetates > formate.

The nature of ligand substituent on effectiveness and diastereoselectivity of this reaction was also explored [70]. A number of catalysts of type $[Ru_2(CO)_4(BL)_2]$, where BL are bridging 2-pyridonate ligands (Scheme 35) were synthesized (**53–61**). The 6-halopyridin-2-olato complexes exist in head-to-head (HH) as well as head-to-tail (HT) arrangement. These were employed for the cyclopropanation reaction of MDA with a variety of olefins (Scheme 36) [70]. It was found that 6-bromopyridonate complexes are better than their chloro counterpart, and in some cases, even superior to acetate/carbonyl complexes [200]. X-ray crystal structures

Catalyst	Yield, % (40 °C)	de, % (40 °C)
2	55	50
3	69	83
4	60	51
5	47	59
6	69	72
7	67	69
8	45	59
9	42	64
37	69	>94

Scheme 34 Metal-catalyzed cyclopropanation of styrene

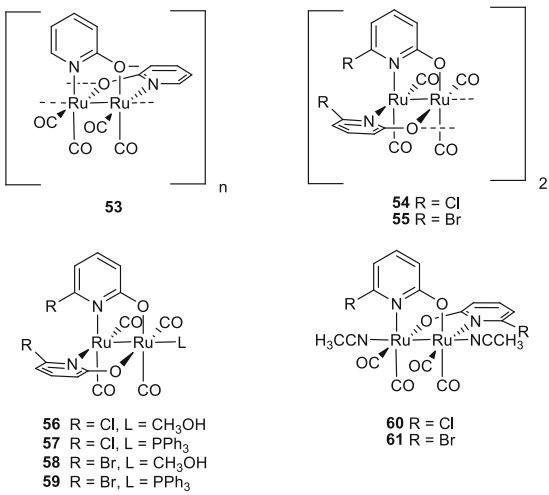

Scheme 35 Diruthenium complexes **53–61** having N^O bridging ligand

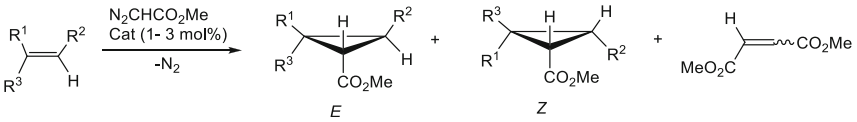

Scheme 36 Cyclopropanation of olefins with methyl diazoacetate

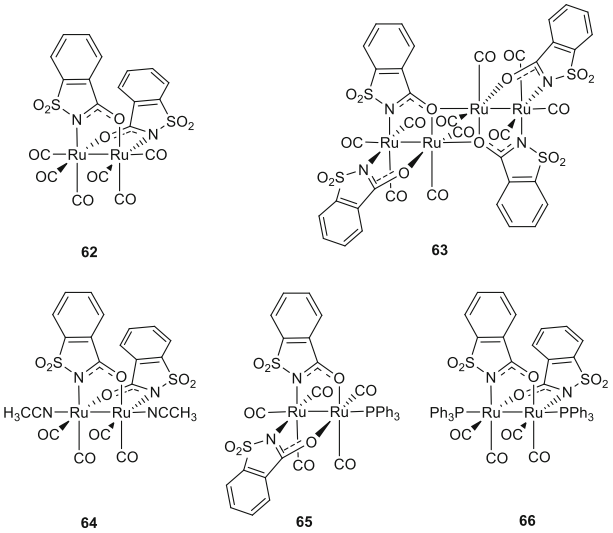

Scheme 37 Diruthenium complexes having bridging saccharinate ligand

of the HH complexes **54–59** [72, 73] revealed that one of the axial sites is inaccessible due to steric crowding of the halides. Hence, the EDA can only approach from the other axial site by replacing the axial ligand. Therefore, the steric crowding does not necessarily lead to diastereoselectivity. A correlation between diastereoselectivity and different bridging ligands could not be obtained due to the fast rearrangement of HT and HH complexes under the reaction conditions [70, 124, 210].

A new set of diruthenium(I,I) complexes containing saccharinate moiety with general formula $[Ru_2(sac)_2(CO)_4(AL)_2]$, where AL represents axial ligands, were designed [71] (**62–66**) (Scheme 37). Complexes **62** and **63** were employed to catalyze transfer of carbene from MDA to olefins (Scheme 38). Initial expectation was that the presence of SO_2 group in the ligand skeleton would increase catalytic activity by increasing the electrophilicity of the catalysts, which in turn would facilitate the faster decomposition of diazoacetate [211]. For the reaction of MDA with alkenes, both **62** and **63** gave moderate yields (45–65%) which are lower compared to catalyst **1** (60–95%). The sluggishness of the reactions is due to catalyst deactivation as the diazoester competes strongly with the olefin. Similar to complex **1**, the saccharinato–ruthenium complexes (**62**, **63**) are not quite efficient for carbene transfer to arenes. With catalyst **63**, MDA in neat benzene did not give

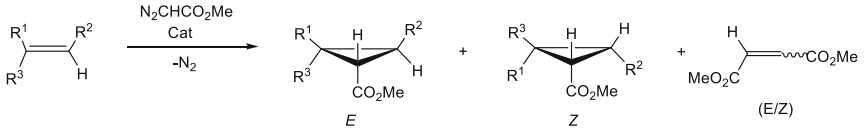

Scheme 38 Carbene transfer from MDA to olefins catalyzed by **62** and **63**

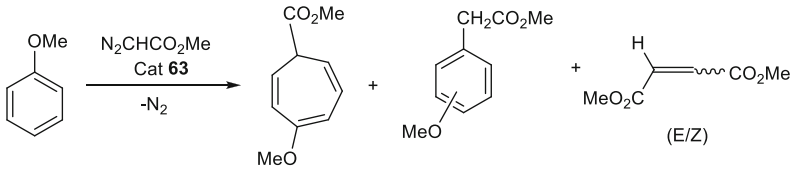

Scheme 39 Carbene transfer from MDA to anisole catalyzed by **63**

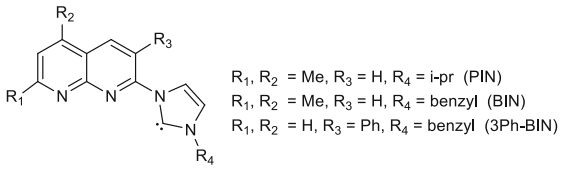

Scheme 40 Naphthyridine-functionalized NHC ligands PIN, BIN, and 3Ph-BIN

any carbene addition products. The use of electron-rich anisole, however, gave cycloheptatrienecarboxylate and the isomeric (methoxyphenyl)acetate in low yields (16%) (Scheme 39). Catalytic activities of **64–66** were not explored.

Introduction of NHC ligands at sites *trans* to the M–M bond tunes the reactivity of dirhodium(II,II) complexes [212–214]. There are several reports where *N*-heterocyclic carbene (NHC) ligands have been incorporated on bimetallic systems [215–219]. Bera et al. synthesized diruthenium(I,I) complexes bearing naphthyridine-functionalized NHC ligands PIN and 3Ph-BIN (Scheme 40) [220]. Room-temperature treatment of the ligand precursor PIN.HBr and 3Ph-BIN.HBr with **1** in acetonitrile provided $Ru_2(CO)_4(\kappa^2C_2,N_1\text{-PIN})_2Br$ (**67**) and $Ru_2(CO)_4(OAc)(\mu^2\text{-}\kappa^2C_2,N_1\text{-3Ph-BIN})Br$ (**68**), respectively (Fig. 4). The PIN ligand provides unbridged chelate complex possibly to avoid steric crowding between *ortho* substituents in the ligand framework. In accordance with this model, 3Ph-BIN afforded a bridged chelate complex.

DFT calculations were performed to understand the effect of NHC anchored to the diruthenium unit. The NPA charge on Ru (−0.12) in the model complex **67** is higher than in **68** (0.00, −0.04). Clearly, the second NHC ligand increases the electron density on the diruthenium core. Initial studies indicated that the presence of bromide in the axial sites suppressed the catalytic aptitude of both complexes. This was resolved by replacing bromides with BAr^F. The catalytic utility of the resulting complexes (**67**-BAr^F) and (**68**-BAr^F) was assessed for carbene-transfer reactions including cyclopropanation, aldehyde olefination, and X–H (X = O, N) insertion reactions (Scheme 41).

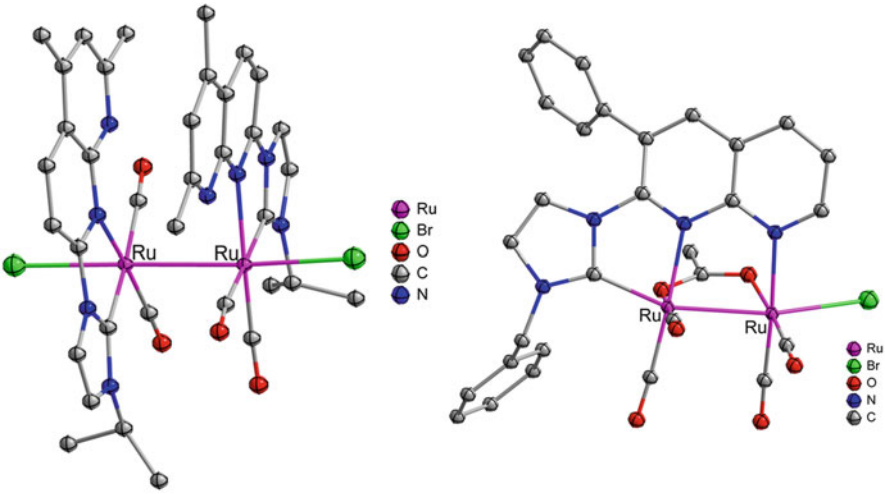

Fig. 4 Molecular structures of **67** and **68**

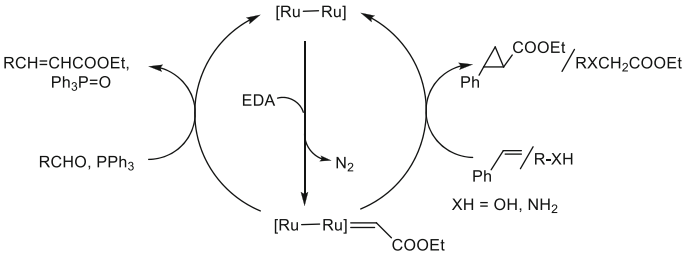

Scheme 41 Carbene-transfer reaction by the diruthenium(I,I) catalyst

Aldehyde olefination reaction was carried out using 1.5 mmol of EDA, 1.2 mmol of PPh_3, and 1 mol% of catalyst in toluene to give excellent to moderate yield. Although the catalyst **68**-BAr^F exhibits lesser reactivity compared to **67**-BAr^F, selectivity is not compromised. The reaction does not occur without PPh_3. The diruthenium catalysts also catalyze cyclopropanation reactions. *Cis* or *trans* cyclopropanes are obtained using 1.5 mmol of EDA as added in a DCM solution of catalyst (0.5 mol%) and olefins (10 mmol) in room temperature. The dimerization of EDA was minimized by its slow addition to an excess of olefin solution. The *trans* to *cis* ratio in all these cases is found to be 75:25. Similar to aldehyde olefination reaction, **67**-BAr^F was found to be superior. Insertion of EDA into N–H and O–H bonds were also studied with amines and alcohols to obtain amino acid derivatives and ethers, respectively. Catalyst **67**-BAr^F affords higher yields than **68**-BAr^F. The reaction of EDA with the diruthenium catalyst is accompanied by the extrusion of N_2, which generates a diruthenium(I,I) species, [Ru^I–Ru^I=CH(COOEt)] (Scheme 41). This species is a common intermediate in all the reactions mentioned above. During aldehyde olefination reaction, the incipient carbene is

transferred to the phosphine to give the phosphorane Ph_3P=CHCOOEt. The olefin is then formed from the reaction of aldehyde and the ylide, accompanied by phosphine oxide. The metal–carbene intermediate may also be attacked by substrates like alkene, amine, or alcohol directly to generate respective products of cyclopropanation, N–C, or O–C bond formation reactions.

Catalyst **67**-BAr^F affords cyclopropanated products with lower catalyst loading and in shorter reaction time compared to **1**. It is important to note that catalyst **67**-BAr^F has two potential catalytic sites whereas **68**-BAr^F offers only one axial site. However, it is unlikely that catalyst **67**-BAr^F utilizes both axial sites during reaction. The formation of the [Ru–Ru]=$CHCO_2Et$ adduct reduces the electrophilicity of the second Ru. This in turn diminishes the possibility of the formation of the bis-carbene adduct. DFT calculations on the model species [**67** · $CHCO_2Me$] and [**68** · $CHCO_2Me$] show that although NPA charges on Ru bonded to $CHCO_2Me$ are similar, carbenoid carbons show very different charges (−0.12 and −0.25). Poor electrophilic nature of the carbenoid carbene in **68** · $CHCO_2Me$ causes the reduced activity of catalyst **68**-BAr^F. Further, this assertion is supported by the higher negative charge on the second Ru (−0.16) in **67** · $CHCO_2Me$. It is thus concluded that the additional reaction site on **67**-BAr^F does not influence its greater reactivity, rather higher electrophilicity of the carbenoid carbon has a more pronounced effect.

8 Carbenoid C–H Insertion

Metal-catalyzed decomposition of α-diazocarbonyls followed by intramolecular carbenoid C–H insertion is an effective means to access important heterocyclic compounds [36, 221–223]. A variety of β- and γ-lactams have been synthesized from α-diazoacetamides. Several dirhodium catalysts are used for this transformation [224–228]. Diruthenium catalysts with acetate (**1**), pyridonate (**60**), saccharinate (**63**), and triazenide (**69**) bridges were employed as potential catalysts for this reaction. A new class of compounds containing calix [4]arenedicarboxylate moiety (**70**–**72**) were also used (Scheme 42) [67]. The catalytic activity of all these diruthenium(I,I) complexes are compared with dirhodium(II,II) complexes **37** and **73** (Scheme 43).

Carbenoid C–H insertion is dependent on the nature of C–H bond, and the reactivity follows the sequence: methine > methylene ≫ methyl [229]. γ-lactam being a five-membered ring is the favored product. β-lactams which are generated by activation of the C–H bond adjacent to the nitrogen atom are also observed [230]. For substrates having aromatic substituents, carbenoid attack at the aromatic ring is preferred over γ-lactam formation [231, 232]. The results of diruthenium(I,I) catalyzed carbenoid C–H insertion of *N*,*N*-diethyldiazoacetamide (**74**), *N*,*N*-dibutyldiazoacetamide (**75**), and *N*,*N*-diisopropyldiazoacetamide (**76**) are shown in Scheme 44. Using diruthenium(I,I) catalysts, **74** and **75** gave only γ-lactam whereas β-lactams are also formed when **76** is used. In fact, β-lactam was the major product for substrate **76**. The dirhodium catalysts **37** and **73** gave higher

Scheme 42 Diruthenium complexes **69**–**72** having triazenide and calixarene moiety

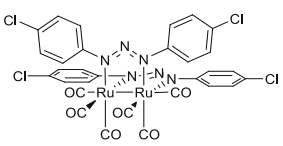

69

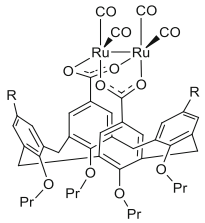

70 R = Br
71 R = ^{t}Bu
72 R = Ph

Scheme 43 Dirhodium complex **73**

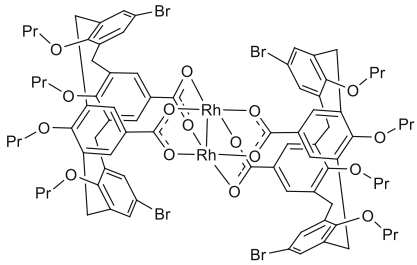

73

yields and higher turnover frequencies compared to all diruthenium catalysts studied. The diruthenium catalysts follow an order of decreasing reactivity with respect to β-lactam formation: **63** > **1** > **69** ~ **60** > **70**, **71**, **72**. Complex **63** having an electron-withdrawing sulfonamide ligand is most electrophilic among them, and thus, this sequence is electronically well justified. In terms of yield, **63** is comparable to **37** [233] while **70**–**72** are least reactive.

Substrates with aryl substitutions were also studied (Scheme 44). *N*,*N*-dibenzyldiazoacetamide (**77**) gave γ-lactam as major product with different catalysts. Here, the γ-lactam has a fused-ring structure formed by intramolecular cyclopropanation of the phenyl ring followed by norcaradiene-to-cycloheptatriene ring expansion. *N*-benzyl-*N*-isopropyldiazoacetamide (**78**) gave four different products by intramolecular carbenoid pathways: carbenoid insertion into an isopropyl CH_3 bond (γ-lactam **79**), the isopropyl CH bond (β-lactam **80**), benzylic CH bond (β-lactam **81**), and carbenoid reaction at the phenyl ring yielding γ-lactam **82**. Using rhodium catalysts **37** and **73**, reaction at the *N*-isopropyl site is favored (**79**, **80**) whereas all diruthenium catalysts favored reactions at the *N*-benzyl substituent (**81**, **82**). However, irrespective of the catalyst used, γ-lactams are preferred over β-lactam. This sharp contrast between **76** and **78** is explained on the basis of the nitrogen substituents. In case of **76**, the methine C–H bond is properly aligned to interact with the metal center, whereas in **78** the methyl C–H bond is in the right position to interact.

The substrate scope was extended to *N*,*N*-disubstituted 2-diazo-acetoacetamides and malonic ester amides. Here, the chosen acetoacetamides contain a second-

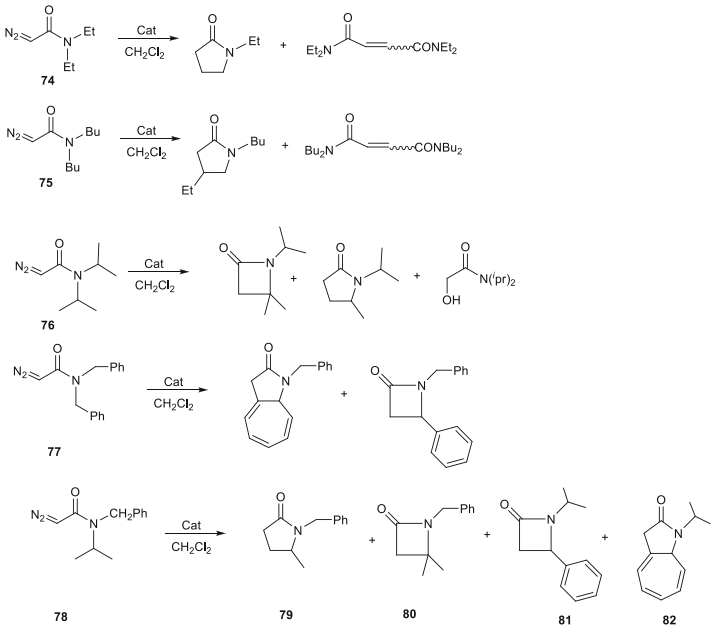

Scheme 44 Catalytic carbenoid C–H insertion of various diazoacetamides

electron-withdrawing substituent at the diazo group making this even less nucleophilic than α-diazoacetamides. Although diruthenium(I,I) catalysts are less reactive compared to dirhodium catalysts, they were still able to generate reactive carbene intermediate during the course of the reaction and catalyze the C–H insertion. Different diazoacetoacetamides (**83**–**86**) are used, and the results are depicted in Scheme 45. The diruthenium catalysts (**1**, **71**, **60**, **63**) show relatively lower yields compared to the two rhodium catalysts (**37**, **73**). But they exhibited similar regioselectivity (formation of β- vs γ-lactam) [225, 230–232], except in the case of diethylamide **83**. Here, the dirhodium catalysts show more γ-selectivity. For substrates **85** and **86**, only β-lactams are formed. The β-lactams in all these cases show complete *trans* selectivity similar to **37**. Contrary to this when the methoxycarbonyl-substituted diazocarboxamides **87** (Scheme 46) was employed, a mixture of *cis* and *trans* products are formed, where *cis*/*trans* ratio depends strongly on nature of catalyst and catalyst concentration.

9 Vinylogous Reactivity

Compounds **2**–**9** were also tested for vinylogous reactivity [69]. Use of vinyldiazoacetates in presence of methanol can give rise to two different types of products arising from nucleophilic attack of methanol at the carbenoid carbon or at the terminal vinyl carbon (Scheme 47). Dirhodium catalysts gave products that result

Scheme 45 Catalytic carbenoid C–H insertion of *N*,*N*-disubstituted 2-diazo-acetoacetamides

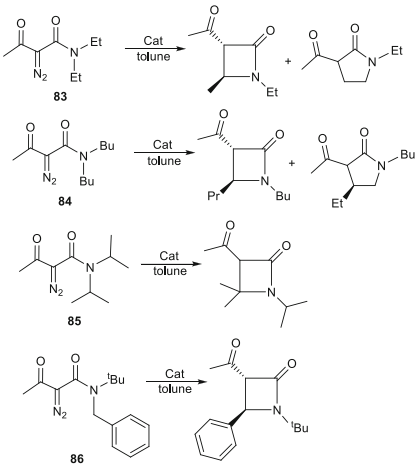

Scheme 46 Catalytic carbenoid C–H insertion of methoxycarbonyl-substituted diazocarboxamides

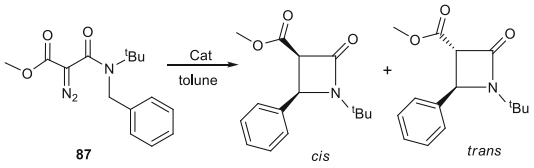

from nucleophilic attack at the carbenoid carbon. Diruthenium catalysts **2**, **3**, and **7** exhibit a shift toward vinylogous reactivity affording more than 80% products. It should be noted here that the yields are lower than the Rh counterparts, but vinylogous reactivity is more pronounced. The diruthenium catalysts gave a 4:1 ratio of product favoring vinylogous reactivity, whereas Rh-catalyzed reaction under the same conditions gave exclusively carbenoid reaction products.

The preferential vinylogous reactivity of diruthenium complexes were also observed for C–C bond-forming reactions. Reaction of methyl vinyldiazoacetate with cyclopentadiene may give rise to product **90** (terminal vinyl reactivity) or **91** (carbenoid reactivity) (Scheme 48). Compound **37** gave major carbenoid products. But diruthenium catalysts gave predominantly bicyclic product although the yields are lower than dirhodium systems. Notably using trifluoroacetate complex $Rh_2(TFA)_4$ (**92**), the selectivity toward vinylogous product was improved [234].

10 Multiply Bonded Diruthenium Systems

Ru_2(II,II) complexes are known to catalyze hydrogenation of alkenes and alkynes [235], cross-metathesis of alkenes [198], and intermolecular insertion of diazo compounds into O–H bond [236]. Ru_2(II,III) complexes catalyze the oxidative transformation of secondary amines to imines [237], aerobic oxidations of alcohols

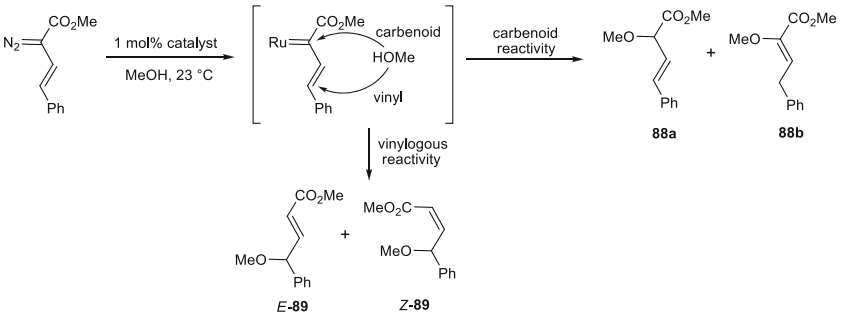

Catalyst	Yield, %	Product ratio			
	(40 °C)	**88**a	**88**b	*E*-**89**	*Z*-**89**
37	85	100	0	0	0
2	45	14	0	11	75
3	26	18	0	15	67
7	28	20	0	18	62

Scheme 47 Carbenoid vs vinylogous reactivity

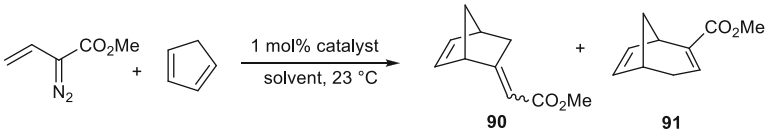

Catalyst	**90**:**91** ratio	*Z*/*E* ratio of **90**	Yield, %
1	>98:2	2:1	54
2	>98:2	2:1	37
6	>98:2	2.4:1	40
37	33:67	2.5:1	81
92	68:32	1.1:1	60

Scheme 48 Vinylogous reactivity in reaction with cyclopentadiene

[238], and carbene insertion into N–H bond of amines [239]. $Ru_2(OAc)_4Cl$ (**93**) and $Ru_2(esp)_2Cl$ (**94**) (Scheme 49) were shown to promote oxidation of organic sulfides by TBHP at ambient condition either in acetonitrile or in neat (solvent-free)

condition [240–243] (Scheme 50). $Ru_2(OAc)_4Cl$ was more selective than $Ru_2(esp)_2Cl$ for the sulfoxide formation. Two possible mechanisms have been suggested. The oxo–sulfur pathway involves the transient formation of $[Ru–Ru]^{7+}=O$ species which transfers oxygen to organic sulfide. The other mechanism involves a concerted pathway involving all three components (diruthenium catalyst, $^tBuO\overline{O}$, organic sulfide) (Scheme 51). For electrophilic $Ru_2(OAc)_4Cl$, the first pathway is likely to be functional whereas the concerted pathway is most suited for bulkier $Ru_2(esp)_2Cl$. Electron-rich diruthenium(II,III) tetramidate compounds $[Ru_2(NHCOC(CH_3)_2)_4Cl]$ (**95**) and $[Ru_2(NHCO(CH_2CH_3))_4Cl]$ (**96**) were also tested for sulfide oxygenation [244]. Initial rate for amidate complexes was found to be comparable with carboxylate analogues. The major product was invariably sulfoxide and solvent-free reactions afforded better conversions.

Although oxo transfer by M–M multiply bonded diruthenium complexes have been reported, the intermediate [M–M]=O has not been characterized. It is proposed that the interplay between metal–metal and metal–oxo multiple bonds would give rise to chemical reactivity that is different from monometal oxo species. In this context, isolation and characterization of $[W_2O]^{6+}$ complex wrapped with four dpa ligands (Scheme 52) was highly significant [245]. Reaction of $W_2(dpa)_4$ (**97**) with

Scheme 49 Schematic representation of complexes **93** and **94**

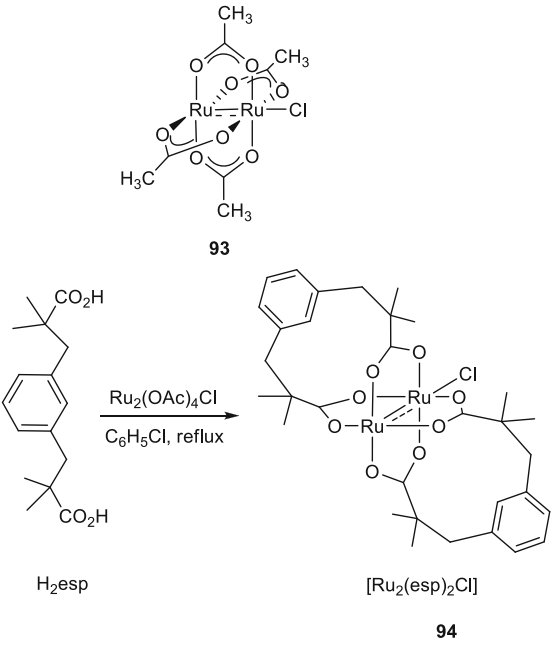

Scheme 50 Catalytic oxidation of organic sulfides

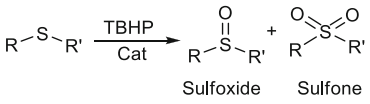

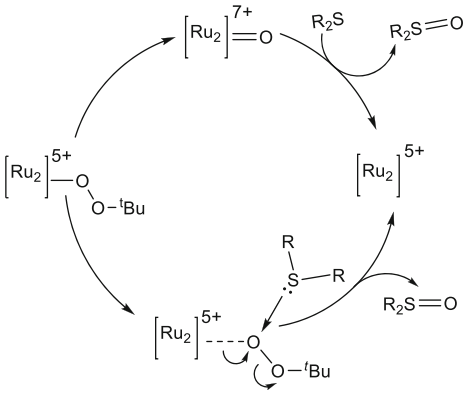

Scheme 51 Proposed mechanism for two possible pathways of oxygen transfer

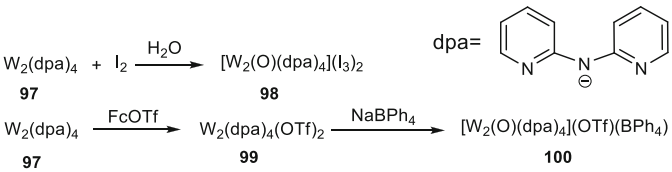

Scheme 52 Formation of the ditungsten terminal oxo complexes

excess iodine in the presence of adventitious water gave $[W_2O(dpa)_4](I_3)_2$ (**98**). In a separate method, oxidation of $W_2(dpa)_4$ with FcOTf gave $[W_2(dpa)_4](OTf)_2$ (**99**) which on further reaction with *m*-chloroperbenzoic acid followed by treatment with BPh_4^- allowed the isolation of $[W_2(O)(dpa)_4][BPh_4][OTf]$ (**100**). X-ray structure indicated a short W–O distance (1.696(2)Å). Interestingly, reaction of $[W_2(dpa)_4O]^{2+}$ (**101**) with excess P^tBu_3 gave back **99**. Reaction of high-valent mononuclear metal–oxo complex with phosphine proceeds via a two-electron reduction with associated oxygen atom transfer. However, the $[W_2(dpa)_4O]^{2+}$ undergoes a four-electron reduction accompanied by oxygen atom transfer to yield quadruple-bonded $[W_2(dpa)_4]$. A detailed mechanistic investigation suggests radical chemistry which could be useful for alkane oxidation chemistry. Clearly, the second metal introduces new chemistry (four-electron reduction) which is not possible for mononuclear metal–oxo complexes.

Metal–metal bonded complexes catalyze the transfer of oxo or nitrene to an organic substrate, but unfortunately, only two [M–M]=E (E = O, N) intermediates containing metal–metal and metal–ligand multiple bonds have been isolated and characterized. In addition to [W–W]=O complex [245], Berry's group trapped a diruthenium–nitride product in frozen matrix and characterized it. Photolytic or thermal treatment of the diruthenium(II,II)–azide [246] (**102**) at low temperature gives $[Ru_2(dPhf)_4N]$ (**103**) (Scheme 53) [247]. The EXAFS measurements reveal a Ru–N bond distance 1.76 Å. The Ru–N stretching frequency is 850 cm^{-1}. These

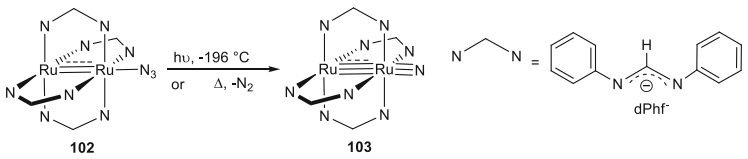

Scheme 53 Formation of nitrido complex **102** from azido complex **103**

values are in between the corresponding values observed for mononuclear $Ru^{VI}{\equiv}N$ complexes [248–252] (Ru–N ~ 1.60 Å, νRu–N ~ 1,000–1,100 cm^{-1}) and triply bridging nitrogen bound on the metal surface (Ru–N ~ 1.93 Å, νRu–N ~ 480–580 cm^{-1}) [253–255]. This indicates that the nature of bond between Ru and N in $[Ru_2(dPhf)_4N]$ is intermediate and resembles more of a double-bond character.

It is worth elaborating the bonding of the [Ru–Ru]≡N system [256]. The $[Ru_2]^{7+}$ core provides nine valence electrons, and nitride unit gives six electrons (three lone pairs, one σ and two π). The formal electron configuration is $\sigma^2\pi^4\delta^2\sigma(nb)^2\pi(nb)^4\delta^{*1}$ which corresponds to $s = 1/2$ ground spin state. The [Ru–Ru] bond order is 3.5 comprising of one σ, two π, and half δ bond. The Ru–N bond order is 3.0. However, because of electron delocalization (3c/4e bond in σ and π framework), the [Ru–Ru] and Ru–N distances are quite long. In fact, [Ru–Ru]–N three-center four-electron bond not only increases the Ru–N distance; the electrophilicity of the nitrogen is also enhanced. A 3c/4e σ bond necessarily makes the Ru–N multiple bond weak. Further, the electron delocalization renders the LUMOs with large N p-orbital character highly susceptible to nucleophilic attack.

As a consequence, the nitride bound to dimetal is more reactive than a nitride bound to a single metal. Indeed, when $Ru_2[d(3,5Cl_2)Phf]N_3$ (**104**) is heated under vacuum in the solid state, N_2 is lost but the corresponding nitride complex could not be identified. Instead, the isolated product reveals insertion of N into one of the aryl C–H bond of the bridging tetramidate ligand [257, 258] (Scheme 54). This reaction also proceeds photolytically. Differential scanning calorimetry (DSC) measurement reveals two distinct steps, suggesting the involvement of [Ru–Ru]≡N species in the reaction. What is most intriguing is the nitrogen transfer mechanism. Several mononuclear nitride complexes are reported to insert N atom into alkyl C–H bond via radical-type reactions [259–263]. Detailed experimental and computational results suggest an electrophilic aromatic substitution mechanism where nitrogen atom is the electrophilic center [264] (Scheme 55). Clearly, the second metal enhances the reactivity of the axial nitride.

11 C–H Amination at Axial Site of a $[Ru–Ru]^{5+}$ Platform

Higher oxidation potential of diruthenium(II,III) system allows the introduction of strong donor ligands such as amidinate on the diruthenium core [265]. But such complexes have found limited application in catalysis. Du Bois' group has

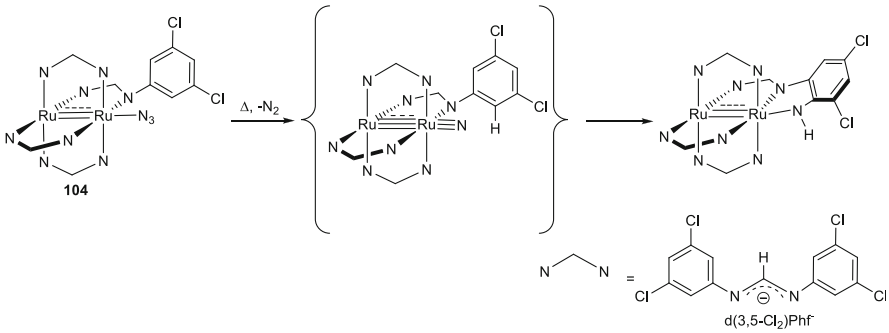

Scheme 54 Nitrogen atom insertion into aryl C–H bond

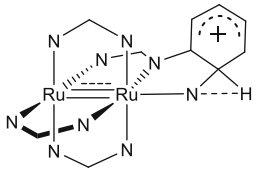

Scheme 55 Proposed intermediate for N insertion into aromatic C–H bond

demonstrated the utility of diruthenium(II,III) catalysts for intra- and intermolecular C–H amination reactions which rivals the performance of dirhodium congeners [265, 266]. The $[Ru_2(esp)_2SbF_6]$ (**105**) efficiently catalyzes intermolecular amination of C–H bonds under oxidative conditions (Scheme 56). Oxidative cyclization of 3-phenylpropyl sulfamate and isoamyl sulfamate proceeds smoothly in refluxing CH_2Cl_2 with soluble oxidant $PhI(O_2C^tBu)_2$ and 5 Å molecular sieves. $Ru_2(OAc)_4Cl$ in combination with $PhI(OAc)_2$ afforded very low conversions.

The tetra-2-oxypyridinate ruthenium dimer $Ru_2(hp)_4Cl$ (**106**) (Scheme 57) promotes the sulfamate cyclization where the dirhodium analogue $Rh_2(hp)_4$ fails possibly due to oxidative degradation under the reaction conditions. The hp system shows a clear selectivity for allylic C–H insertion over the corresponding aziridine formation. For *trans*-4-hexenyl sulfamate, the oxathiazinane heterocycle was isolated in 68% yield with **107/108** 8:1 ratio where **107** is the allylic C–H activated product and **108** is the aziridine product (Scheme 58). $[Ru_2(hp)_4Cl]$ catalyzed the C–H amination for a collection of substrates, giving the oxathiazinane heterocycle as the major (or exclusive) product in moderate to good yields. The activity and selectivity are superior to $[Ru_2(esp)_2(SbF_6)]$ and $Rh_2(S\text{-}nap)_4$ [267]. The $Ru_2(hp)_4Cl$ is the only catalytic system based on diruthenium(II,III) core which performs allylic C–H bond activation better than other bimetallic systems studied including Rh_2 complexes. An array of computational and experimental studies revealed a two-step mechanism that involves homolytic C–H bond cleavage followed by fast radical recombination [268, 269]. Hammett and kinetic studies indicate a different pathway for dirhodium- and diruthenium-catalyzed oxidation

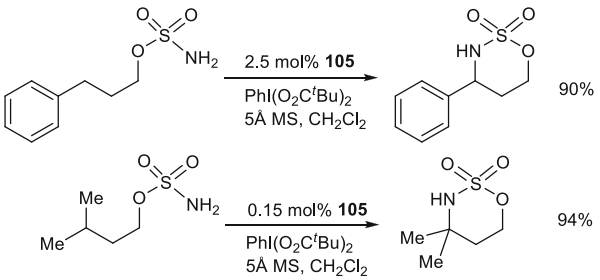

Scheme 56 **105** catalyzed intramolecular amination on benzylic and tertiary centers

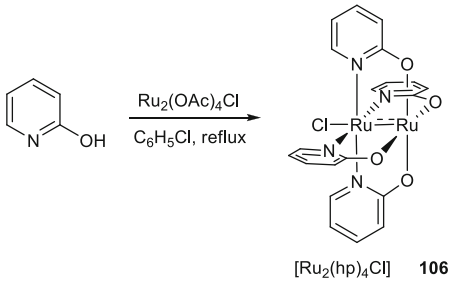

Scheme 57 Schematic representation of complex **106**

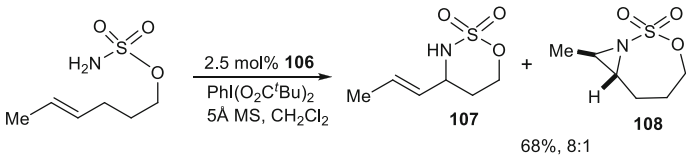

Scheme 58 Selective intramolecular allylic C–H amination catalyzed by **106**

[270]. In fact, the stepwise nature of $[Ru_2(hp)_4Cl]$ catalyzed reaction accounts for preferential allylic C–H bond functionalization over alkene aziridination which is the favored product when dirhodium catalysts are used. The presence of a discrete diradical intermediate further assists the selectivity for allylic C–H amination using a diruthenium catalyst.

12 Concluding Remarks

$Rh_2(OAc)_4$ and its derivatives are well recognized as catalysts for a wide array of organic transformations. The catalytic reactions usually occur at axial site. The isoelectronic $[Ru^{I}–Ru^{I}]$ are relatively less explored. Recent studies have revealed that a multitude of reactions could be executed at sites *trans* to the [Ru–Ru] single

bond. The paddlewheel $[Ru_2(CO)_4]^{2+}$ core is an ideal platform for axial reactivity. A variety of bridging ligands are incorporated at equatorial sites on the $[Ru_2(CO)_4]^{2+}$ core to tune the reactivity and selectivity keeping the axial sites available for reactions. Bera et al. have studied stoichiometric reactions such as C–H activation and C–C bond formation at sites *trans* to the [Ru–Ru] single bond. Mass et al. have explored catalytic cyclopropanation and C–H insertion via carbene-transfer reactions. Introduction of NHC unit in the ligand skeleton increases the catalytic efficiency. Gois et al. have demonstrated that multiply bonded diruthenium compounds are excellent catalysts for catalytic C–H amination. Berry et al. reported electron delocalization on [Ru–Ru]≡N system that makes the N atom highly electrophilic. Metal–metal bonded [Ru–Ru] complexes are beginning to show promise as organometallic catalysts. Further work is needed to realize the full potential of these complexes.

Acknowledgments This work is financially supported by the Department of Science and Technology (DST), India, and the Council of Scientific and Industrial Research (CSIR) of India. J.K.B. thanks Department of Atomic Energy for DAE outstanding investigator award. I.D. thanks CSIR, India, and G.S. thanks IIT Kanpur for fellowships.

References

1. Cotton FA, Walton RA (eds) (1982) Multiple bonds between metal atoms, 1st edn. Wiley, New York
2. Cotton FA, Walton RA (eds) (1993) Multiple bonds between metal atoms, 2nd edn. Oxford University Press, New York
3. Chisholm MH (2007) Proc Natl Acad Sci 104:2563
4. Parkin G (ed) (2010) Metal-metal bonding. Springer, Heidelberg/Berlin
5. Kepert DL, Vrieze K (eds) (1973) Compounds of the transition elements involving metal-metal bonds, vol 27, 1st edn, Pergamon texts in inorganic chemistry. Pergamon, Oxford
6. Cotton FA, Walton RA (eds) (2005) Multiple bonds between metal atoms, 3rd edn. Springer, New York
7. Liddle ST (ed) (2015) Molecular metal-metal bonds: compounds, synthesis, properties . Wiley, Weinheim
8. Lippard SJ, Chisholm MH, Rothwell IP (eds) (2007) Chemical reactions of metal-metal bonded compounds of the transition elements, progress in inorganic chemistry, vol 29. Wiley, New York
9. Shibasaki M, Yamamoto Y (eds) (2004) Multimetallic catalysis in organic synthesis. Wiley, Weinheim
10. Li C, Widjaja E, Garland M (2003) J Am Chem Soc 125:5540
11. Broussard ME, Juma B, Train SG, Peng W-J, Laneman SA, Stanley GG (1993) Science 260:1784
12. Adams RD, Cotton FA (1998) Bimetallic homogeneous hydroformylation. In: Adams RD, Cotton FA (eds) Catalysis by di- and polynuclear metal complexes. Wiley, New York, pp 345–372
13. Parka J, Hong S (2012) Chem Soc Rev 41:6931
14. Matsunaga S, Shibasaki M (2014) Chem Commun 50:1044
15. Esswein AJ, Veige AS, Nocera DG (2005) J Am Chem Soc 127:16641
16. Gray TG, Veige AS, Nocera DG (2004) J Am Chem Soc 126:9760

17. Powers DC, Ritter T (2012) Acc Chem Res 45:840
18. Powers DC, Ritter T (2009) Nat Chem 1:302
19. Teets TS, Cook TR, McCarthy BD, Nocera DG (2011) Inorg Chem 50:5223
20. Braunstein P, Oro LA, Raithby P (eds) (1999) Metal clusters in chemistry. Wiley, Weinheim
21. Adams RD (1990) Clusters and their implications for catalysis. In: Fackler JP (ed) Metal-metal bonds and clusters in chemistry and catalysis. Plenum, New York
22. Lavigne G (2012) Angew Chem Int Ed 51:5794
23. Corain B, Schmid G, Toshima N (2008) Metal nanoclusters in catalysis and materials science: the issue of size control, 1st edn. Elsevier, Amsterdam
24. Tao FF (2012) Chem Soc Rev 41:7977
25. Adams RD, Chen M, Elpitiya G, Potter ME, Raja R (2013) ACS Catal 3:3106
26. Son SU, Jang Y, Park J, Na HB, Park HM, Yun HJ, Lee J, Hyeon T (2004) J Am Chem Soc 126:5026
27. Hermans S, Raja R, Thomas JM, Johnson BFG, Sankar G, Gleeson D (2001) Angew Chem Int Ed 40:1211
28. Kemball C, Dowden DA (1981) Catalysis. Royal Society of Chemistry, Cambridge
29. Yu W, Porosoff MD, Chen JG (2012) Chem Rev 112:5780
30. Ananikov VP, Beletskaya IP (2012) Organometallics 31:1595
31. Nishibayashi Y, Wakiji I, Hidai M (2000) J Am Chem Soc 122:11019
32. Inada Y, Nishibayashi Y, Hidai M, Uemura S (2002) J Am Chem Soc 124:15172
33. Nishibayashi Y, Yamanashi M, Takagi Y, Hidai M (1997) Chem Commun 859
34. Ammal SC, Yoshikai N, Inada Y, Nishibayashi Y, Nakamura E (2005) J Am Chem Soc 127:9428
35. Doyle MP, Duffy R, Ratnikov M, Zhou L (2010) Chem Rev 110:704
36. Doyle MP, Forbes DC (1998) Chem Rev 98:911
37. Chifotides HT, Dunbar KR (2005) Acc Chem Res 38:146
38. Knoll JD, Turro C (2015) Coord Chem Rev 282–283:110
39. Chifotides HT, Saha B, Patmore NJ, Dunbar KR, Bera JK (2015) Group 9 metal–metal bonds. In: Liddle ST (ed) Molecular metal-metal bonds: compounds, synthesis, properties. Wiley, Weinheim
40. Chifotides HT, Dunbar KR (2005) Rhodium compounds. In: Chemical reactions of metal-metal bonded compounds of the transition elements, progress in inorganic chemistry. Chap 12, pp 465–589
41. Timmons DJ, Doyle MP (2005) Chiral dirhodium(II) catalysts and their applications. In: Chemical reactions of metal-metal bonded compounds of the transition elements, progress in inorganic chemistry. Chap 13, pp 591–632
42. Evans PA (ed) (2005) Modern rhodium-catalyzed organic reactions. Wiley, Weinheim
43. Rubio-Pérez L, Iglesias M, Munárriz J, Polo V, Miguel PJS, Pérez-Torrentea JJ, Oro LA (2015) Chem Commun 51:9860
44. Valderrama M, Cuevas J, Boys D, Carmona D, Lamata TMP, Viguri F, Atencio R, Lahoz FJ, Oro LA (1996) J Chem Soc Dalton Trans 2877
45. Brost RD, Bushnell GW, Harrison DG, Stobart SR (2002) Inorg Chem 41:1412
46. Mena I, Casado MA, Polo V, García-Orduña P, Lahoza FJ, Oro LA (2014) Dalton Trans 43:1609
47. Murahashi T, Kurosawa H (2002) Coord Chem Rev 231:207
48. Foo SJL, Jones ND, Patrick BO, James BR (2003) Chem Commun 988
49. Ogura T, Yoshida K, Yanagisawa A, Imamoto T (2009) Org Lett 11:2245
50. Stambuli JP, Kuwano R, Hartwig JF (2002) Angew Chem Int Ed 41:4746
51. Das RK, Saha B, Rahaman SMW, Bera JK (2010) Chem Eur J 16:14459
52. Sarkar M, Doucet H, Bera JK (2013) Chem Commun 49:9764
53. Therrien B, Süss-Fink G (2009) Coord Chem Rev 253:2639
54. Crooks GR, Johnson BFG, Lewis J, Williams IG, Gamlen G (1969) J Chem Soc A 2761
55. Schumann H, Opitz J, Pickardt J (1977) J Organomet Chem 128:253

56. Shiu K-B, Peng S-M, Cheng M-C (1993) J Organomet Chem 452:143
57. Rotem M, Shvo Y, Goldberg I, Shmueli U (1984) Organometallics 3:1758
58. Bruce MI, Skelton BW, White AH, Zaitseva NN (1999) Aust J Chem 52:621
59. Matteoli U, Menchi G, Bianchi M, Piacenti F, Ianelli S, Nardelli M (1995) J Organomet Chem 498:177
60. Kepert CM, Deacon GB, Spiccia L (2003) Inorg Chim Acta 355:213
61. Spohn M, Vogt T, Strähle J (1986) Z Naturforsch B 41:1373
62. Xu L, Sasaki Y (1999) J Organomet Chem 585:246
63. Bright TA, Jones RA, Nunn CM (1988) J Coord Chem 18:361
64. Field JS, Haines RJ, Parry CJ (1997) J Chem Soc Dalton Trans 2843
65. Panneerselvam K, Lu T-H, Huang C-H, Tung S-F, Shiu K-B (1997) Acta Crystallogr C 53:1782–1784
66. Kepert CM, Deacon GB, Spiccia L, Fallon GD, Skelton BW, White AH (2000) J Chem Soc Dalton Trans 2867
67. Grohmann M, Buck S, Schäffler L, Maas G (2006) Adv Synth Catal 348:2203
68. Petrukhina MA, Sevryugina Y, Andreini KW (2004) J Clust Sci 15:451
69. Sevryugina Y, Weaver B, Hansen J, Thompson J, Davies HML, Petrukhina M (2008) Organometallics 27:1750
70. Werle T, Schäffler L, Maas G (2005) J Organomet Chem 690:5562
71. Buck S, Maas G (2006) J Organomet Chem 691:2774
72. Schäffler L, Maas G (2006) Inorg Chim Acta 359:970
73. Schäffler L, Maas G (2008) Inorg Chim Acta 361:109
74. Leger CD, Mass G (2004) Z Naturforsch B 59:573
75. Klemperer WG, Zhong B (1993) Inorg Chem 32:5821
76. Majumdar M, Sinha A, Ghatak T, Patra SK, Sadhukhan N, Rahaman SMW, Bera JK (2010) Chem Eur J 16:2574
77. Ghatak T, Sinha A, Rahaman SMW, Bera JK (2011) Inorg Chim Acta 372:94
78. Cotton FA, Daniels LM, Murillo CA, Pascual I, Zhou HC (1999) J Am Chem Soc 121:6856
79. Cotton FA, Extine MW, Rice GW (1978) Inorg Chem 17:176
80. Cotton FA, Daniels LM, Hillard EA, Murillo CA (2002) Inorg Chem 41:2466
81. Brown-Xu SE, Chisholm MH, Durr CB, Lewis SA, Spilker TF, Young PJ (2014) Chem Sci 5:2657
82. Cotton FA, Thompson JL (1981) Inorg Chem 20:3887
83. Bradley PM, Bursten BE, Turro C (2001) Inorg Chem 40:1376
84. Aullón G, Alvarez S (1993) Inorg Chem 32:3712
85. Bursten BE, Cotton FA (1981) Inorg Chem 20:3042
86. Norman JG, Kolari HJ (1978) J Am Chem Soc 100:791
87. Dubicki L, Martin RL (1970) Inorg Chem 9:673
88. Gracia R, Adams H, Patmore NJ (2009) Dalton Trans 259
89. Collin J-P, Jouaiti A, Sauvage J-P, Kaska WC, McLoughlin MA, Keder NL, Harrison WTA, Stucky GD (1990) Inorg Chem 29:2238
90. Binamira-Soriaga E, Keder NL, Kaska WC (1990) Inorg Chem 29:3167
91. Thummel RP, Lefoulon F, Williamson D, Chavan M (1986) Inorg Chem 25:1675
92. Tikkanen WR, Krüger C, Bomben KD, Jolly WL, Kaska WC, Ford PC (1984) Inorg Chem 23:3633
93. Baker AT, Tikkanen WR, Kaska WC, Ford PC (1984) Inorg Chem 23:3254
94. Tikkanen W, Binamira-Soriaga E, Kaska W, Ford P (1984) Inorg Chem 23:141
95. Tikkanen W, Binamira-Soriaga E, Kaska W, Ford P (1983) Inorg Chem 22:1147
96. Patra SK, Sadhukhan N, Bera JK (2006) Inorg Chem 45:4007
97. Reddy KV, Mogilaiah K, Sreenivasulu B (1986) J Indian Chem Soc 63:443
98. Thummel RP, Lefoulon F, Cantu D, Mahadevan RJ (1984) J Org Chem 49:2208
99. Majewicz TC, Caluwe P (1974) J Org Chem 39:720
100. Hawes EM, Wibberley DG (1966) J Chem Soc C 315

101. Majumdar M, Patra SK, Kannan M, Dunbar KR, Bera JK (2008) Inorg Chem 47:2212
102. Brown TR, Dolinar BS, Hillard EA, Clérac R, Berry JF (2015) Inorg Chem. 10.1021/acs.inorgchem.5b01241
103. Lindsay AJ, Wilkinson G, Motevalli M, Hursthouse MB (1987) J Chem Soc Dalton Trans 2723
104. Arockiam PB, Bruneau C, Dixneuf PH (2012) Chem Rev 112:5879
105. Albrecht M (2010) Chem Rev 110:576
106. Bergman RG (2007) Nature 446:391
107. Labigner JA, Bercaw JE (2002) Nature 417:507
108. Shilov AE, Shul´pin GB (1997) Chem Rev 97:2879
109. Crabtree RH (ed) (2001) The organometallic chemistry of the transition metals, 3rd edn. Wiley, New York
110. Arndtsen BA, Bergman RG, Mobley TA, Peterson TH (1995) Acc Chem Res 28:154
111. Ryabov AD (1990) Chem Rev 90:403
112. Dyker J (1999) Angew Chem Int Ed 38:1698
113. Crabtree RH (1985) Chem Rev 85:245
114. Dupont J, Consorti CS, Spencer J (2005) Chem Rev 105:2527
115. Newkome GR, Puckett WE, Gupta VK, Kiefer GE (1986) Chem Rev 86:451
116. Bruce MI (1977) Angew Chem Int Ed 16:73
117. Omae I (1979) Chem Rev 79:287
118. Huang W, Dulong F, Khan SI, Cantat T, Diaconescu PL (2014) J Am Chem Soc 136:17410
119. Cao W, Liu X, Peng R, He P, Lin L, Feng X (2013) Chem Commun 49:3470
120. Sun S, Sun Q, Zhao B, Zhang Y, Shen Q, Yao Y (2013) Organometallics 32:1876
121. Dowerah D, Radonovich LJ, Woolsey NF (1990) Organometallics 9:614
122. Lloret J, Bieger K, Estevan F, Lahuerta P, Hirva P, Pérez-Prieto J, Sanaú M (2006) Organometallics 25:5113
123. Lloret J, Estevan F, Lahuerta P, Hirva P, Pérez-Prieto J, Sanaú M (2006) Organometallics 25:3156
124. Bieger K, Estevan F, Lahuerta P, Lloret J, Pérez-Prieto J, Sanaú M, Siguero N, Stiriba SE (2003) Organometallics 22:1799
125. Taber DF, Malcom SC, Bieger K, Lahuerta P, da Rocha ZN, Sanaú M, Stiriba SE, Pérez-Prieto J, Monge MA (1999) J Am Chem Soc 121:860
126. Xu K, Li B, Xu S, Song H, Wang B (2009) Organometallics 28:4438
127. Cabeza JA, Damonte M, Garcia-Alvarez P (2011) Organometallics 30:2371
128. Chen D, Xu S, Song H, Wang B (2008) Eur J Inorg Chem 1854
129. Cabeza JA, Río I, Miguel D, Vega MGS (2005) Chem Commun 3956
130. Crittall MR, Ellul CE, Mahon MF, Saker O, Whittlesey MK (2008) Dalton Trans 4209
131. Yeh W, Tsai K (2010) Organometallics 29:604
132. Salvini A, Frediani P, Piacenti F (2000) J Mol Catal A Chem 159:185
133. Patra SK, Bera JK (2006) Organometallics 25:6054
134. Vigalok A, Uzan O, Shimon LJW, Ben-David Y, Martin JML, Milstein D (1998) J Am Chem Soc 120:12539
135. Sinha A, Daw P, Rahaman SMW, Saha B, Bera JK (2011) J Organomet Chem 696:1248
136. Saha B, Sengupta G, Sarbajna A, Dutta I, Bera JK (2014) J Organomet Chem 771:124
137. Sun J-W, Wang X-S, Liu Y (2013) J Org Chem 78:10560
138. Quéguiner G, Marsais F, Snieckus V, Epsztajn J (1991) Adv Heterocycl Chem 52:187
139. Patra SK, Bera JK (2007) Organometallics 26:2598
140. Kuroda T, Suzuki F, Tamura T, Ohmori K, Hosoe H (1992) J Med Chem 35:1130
141. Chen K, Kuo S, Hsiech M, Anthoner K (1997) J Med Chem 40:3049
142. Ferrarini M, Clendio M, Calderone U, Lovella G (1998) Eur J Med Chem 33:383
143. Speiser F, Braunstein P, Saussine L, Welter R (2004) Inorg Chem 43:1649
144. Lippard SJ, Berg JM (eds) (1994) Principles of bioinorganic chemistry. University Science, California

145. Evans DJ, Pickett CJ (2003) Chem Soc Rev 32:268
146. Grotjahn DB, Incarvito CD, Rheingold AL (2001) Angew Chem Int Ed 40:3884
147. Erdogan G, Grotjahn DB (2009) J Am Chem Soc 131:10354
148. Grotjahn DB (2005) Chem Eur J 11:7146
149. Clapham SE, Hadzovic A, Morris RH (2004) Coord Chem Rev 248:2201
150. Zweifel T, Naubron J-V, Büttner T, Ott T, Grützmacher H (2008) Angew Chem Int Ed 47:3245
151. Himo F, Eriksson LA, Maseras F, Siegbahn PEM (2000) J Am Chem Soc 122:8031
152. Dobereiner GE, Crabtree RH (2010) Chem Rev 110:681
153. Gunanathan C, Milstein D (2011) Acc Chem Res 44:588
154. Grützmacher H (2008) Angew Chem 120:1838
155. Maire P, Büttner T, Breher F, Floch PL, Grützmacher H (2005) Angew Chem 117:6477
156. Gelman D, Musa S (2012) ACS Catal 2:2456
157. Cundari RT, Klinckman TR, Wolczanski PT (2002) J Am Chem Soc 124:1481
158. Jiménez MV, Fernández-Tornos J, Pérez-Torrente JJ, Modrego FJ, Winterle S, Cunchillos C, Lahoz FJ, Oro LA (2011) Organometallics 30:5493
159. Musa S, Shaposhnikov I, Cohen S, Gelman D (2011) Angew Chem 123:3595
160. Hetterscheid DGH, van der Vlugt JI, de Bruin B, Reek JNH (2009) Angew Chem 121:8324
161. Scharf A, Goldberg I, Vigalok A (2013) J Am Chem Soc 135:967
162. Haack K-J, Hashiguchi S, Fujii A, Ikariya T, Noyori R (1997) Angew Chem 109:297
163. Ohkuma T, Ooka H, Ikariya T, Noyori R (1995) J Am Chem Soc 117:10417
164. Noyori R, Yamakawa M, Hashiguchi S (2001) J Org Chem 66:7931
165. Noyori R, Ohkuma T (2001) Angew Chem Int Ed 40:40
166. Noyori R (2002) Angew Chem Int Ed 41:2008
167. Noyori R, Sandoval CA, Muňiz K, Ohkuma T (2005) Phil Trans R Soc A 363:901
168. Gunanathan C, Milstein D (2014) Chem Rev 114:12024
169. Zhang J, Leitus G, Ben-David Y, Milstein D (2005) J Am Chem Soc 127:10840
170. Gunanathan C, Shimon LJW, Milstein D (2009) J Am Chem Soc 131:3146
171. Gnanaprakasam B, Zhang J, Milstein D (2010) Angew Chem Int Ed 49:1468
172. Gunanathan C, Milstein D (2008) Angew Chem 120:8789
173. Gunanathan C, Ben-David Y, Milstein D (2007) Science 317:790
174. Zweifel T, Naubron J-V, Grützmacher H (2009) Angew Chem 121:567
175. Shvo Y, Czarkie D, Rahamim Y, Chodosh DF (1986) J Am Chem Soc 108:7400
176. Menashe N, Shvo Y (1991) Organometallics 10:3885
177. Shvo Y, Czarkie D (1986) J Organomet Chem 315:C25
178. Azerraf C, Shpruhman A, Gelman D (2009) Chem Commun 466
179. Musa S, Romm R, Azerraf C, Kozuch S, Gelman D (2011) Dalton Trans 40:8760
180. Azerraf C, Gelman D (2009) Organometallics 28:6578
181. Azerraf C, Gelman D (2008) Chem Eur J 14:10364
182. Gelman D, Romm R (2013) Top Organomet Chem 40:289
183. Oded K, Musa S, Gelman D, Blum J (2012) Catal Commun 20:68
184. Ghatak T, Sarkar M, Dinda S, Dutta I, Rahaman SMW, Bera JK (2015) J Am Chem Soc 19:6168
185. Sinha A, Majumdar M, Sarkar M, Ghatak T, Bera JK (2013) Organometallics 32:340
186. Sinha A, Rahaman SMW, Sarkar M, Saha B, Daw P, Bera JK (2009) Inorg Chem 48:11114
187. Bera JK, Sadhukhan N, Majumdar M (2009) Eur J Inorg Chem 4023
188. Patra SK, Rahaman SMW, Majumdar M, Sinha A, Bera JK (2008) Chem Commun 2511
189. Das RK, Sarkar M, Rahaman SMW, Doucet H, Bera JK (2012) Eur J Inorg Chem 1680
190. Saha B, Rahaman SMW, Sinha A, Bera JK (2011) Aust J Chem 64:583
191. Saha B, Rahaman SMW, Daw P, Sengupta G, Bera JK (2014) Chem Eur J 20:6542
192. Solvhoj A, Madsen R (2011) Organometallics 30:6044
193. Maggi A, Madsen R (2012) Organometallics 31:451
194. Stevens CV, Vekemans W, Moonen K, Rammeloo T (2003) Tetrahedron Lett 44:1619

195. Nova A, Balcells D, Schley ND, Dobereiner GE, Crabtree RH, Eisenstein O (2010) Organometallics 29:6548
196. Lebel H, Marcoux J-F, Molinaro C, Charette AB (2003) Chem Rev 103:977
197. Demonceau A, Noels AF, Saive E, Hubert AJ (1992) J Mol Catal 76:123
198. Noels AF, Demonceau A, Carlier E, Hubert AJ, Marquez-Silva RL, Sanchez-Delgado RA (1988) J Chem Soc Chem Commun 783
199. Noels AF, Demonceau A (1998) J Phys Org Chem 11:602
200. Maas G, Werle T, Alt M, Mayer D (1993) Tetrahedron 49:881
201. Werle T, Maas G (2001) Adv Synth Catal 343:37
202. Anciaux AJ, Hubert AJ, Noels AF, Petiniot N, Teyssie P (1980) J Org Chem 45:695
203. Demonceau A, Noels AF, Hubert AJ (1990) Tetrahedron 46:3889
204. Doyle MP, Dorow RL, Buhro WE, Griffin JH, Tamblyn WH, Trudell ML (1984) Organometallics 3:44
205. Maas G, Alt M, Mayer D, Bergsträsser U, Sklenak S, Xavier P, Apeloig Y (2001) Organometallics 20:4607
206. Maas G, Seitz J (2001) Tetrahedron Lett 42:6137
207. Gray A, Tsybizova A, Roithova J (2015) Chem Sci. doi:10.1039/c5sc01729g
208. Sevryugina Y, Olenev AV, Petrukhina MA (2005) J Clust Sci 16:217
209. Davies HML, Rusiniak L (1998) Tetrahedron Lett 39:8811
210. Estevan F, Lahuerta P, Perez-Prieto J, Pereira I, Stiriba S-E (1998) Organometallics 17:3442
211. Stephenson CJ, McInnis JP, Chen C, Weberski MP, Motta A, Delferro M, Marks TJ (2014) ACS Catal 4:999
212. Snyder JP, Padwa A, Stengel T, Arduengo AJ III, Jockisch A, Kim H-J (2001) J Am Chem Soc 123:11318
213. Gois PMP, Trindade AF, Veiros LF, André V, Duarte MT, Afonso CAM, Caddick S, Cloke FGN (2007) Angew Chem Int Ed 46:5750
214. Trindade AF, Gois PMP, Veiros LF, André V, Duarte MT, Afonso CAM, Caddick S, Cloke FGN (2008) J Org Chem 73:4076
215. Gibson SE, Johnstone C, Loch JA, Steed JW, Stevenazzi A (2003) Organometallics 22:5374
216. van Rensburg H, Tooze RP, Foster DF, Slawin AMZ (2004) Inorg Chem 43:2468
217. Poyatos M, McNamara W, Incarvito C, Peris E, Crabtree RH (2007) Chem Commun 2267
218. Kreisel KA, Yap GPA, Theopold KH (2007) Chem Commun 1510
219. Kreisel KA, Yap GPA, Theopold KH (2006) Organometallics 25:4670
220. Saha B, Ghatak T, Sinha A, Rahaman SMW, Bera JK (2011) Organometallics 30:2051
221. Doyle MP, McKervey MA, Ye T (eds) (1998) Modern catalytic methods for organic synthesis with diazo compounds. Wiley, New York
222. Padwa A, Krumpe KE (1992) Tetrahedron 48:5385
223. Davies HML, Beckwith RE (2003) Chem Rev 103:2861
224. Maas G (1987) Top Curr Chem 137:75
225. Gois PMP, Afonso CAM (2004) Eur J Org Chem 3773
226. Liu W-J, Chen Z-L, Chen Z-Y, Hu W-H (2005) Tetrahedron Asymmetry 16:1693
227. Gois PMP, Candeias NR, Afonso CAM (2005) J Mol Catal A 227:17
228. Merlic CA, Zechman AL (2003) Synthesis 1137
229. Taber DF, Ruckle RE (1986) J Am Chem Soc 108:7686
230. Doyle MP, Shanklin MS, Oon S-M, Pho HQ, Van der Heide FR, Veal WR (1988) J Org Chem 53:3384
231. Padwa A, Austin DJ, Price AT, Semones MA, Doyle MP, Protopopova MN, Winchester WR, Tran A (1993) J Am Chem Soc 115:8669
232. Doyle MP, Pieters RJ, Taunton J, Pho HQ, Padwa A, Hertzog DL, Precedo L (1991) J Org Chem 56:820
233. Doyle MP, Shanklin MS, Pho HQ (1988) Tetrahedron Lett 29:2639
234. Davies HML, Hu B, Saikali E, Bruzinski PR (1994) J Org Chem 59:4535

235. Legzdins P, Mitchell RW, Rempel GL, Ruddick JD, Wilkinson G (1970) J Chem Soc A 1970:3322
236. Cenini S, Cravotto G, Giovenzana GB, Palmisano G, Penonia A, Tollarid S (2002) Tetrahedron Lett 43:3637
237. Murahashi S-I, Okano Y, Sato H, Nakae T, Komiyaa N (2007) Synlett 7:1675
238. Komiya N, Nakae T, Sato H, Naota T (2006) Chem Commun 4829
239. Maidanova AV, Bakeeva AD, Sultanova RM, Biglova RZ, Dokichev VA (2010) Russ J Org Chem 46:1461
240. Lee HB, Ren T (2009) Inorg Chim Acta 362:1467
241. Thompson DJ, Paredes JEB, Villalobos L, Ciclosi M, Elsby RJ, Liu B, Fanwick PE, Ren T (2015) Inorg Chim Acta 424:150
242. Barker JE, Ren T (2008) Inorg Chem 47:2264
243. Villalobos L, Paredes JEB, Cao Z, Ren T (2013) Inorg Chem 52:12545
244. Villalobos L, Cao Z, Fanwick PE, Ren T (2012) Dalton Trans 41:644
245. Nippe M, Goodman SM, Fry CG, Berry JF (2011) J Am Chem Soc 133:2856
246. Chen W-Z, Silva VD, Lin C, Abellard J, Marcus DM, Ren T (2005) J Clust Sci 16:151
247. Pap JS, DeBeer George S, Berry JF (2008) Angew Chem Int Ed 47:10102
248. Leung SKY, Huang JS, Liang JL, Che CM, Zhou ZY (2003) Angew Chem Int Ed 42:340
249. Man WL, Tang TM, Wong TW, Lau TC, Peng SM, Wong WT (2004) J Am Chem Soc 126:478
250. Yip KL, Yu WY, Chan PM, Zhu NY, Che CM (2003) Dalton Trans 3556
251. Chan PM, Yu WY, Che CM, Cheung KK (1998) J Chem Soc Dalton Trans 3183
252. Liang HC, Shapley PA (1996) Organometallics 15:1331
253. Schwegmann S, Seitsonen AP, Dietrich H, Bludau H, Over H, Jacobi K, Ertl G (1997) Chem Phys Lett 264:680
254. Shi H, Jacobi K, Ertl G (1993) J Chem Phys 99:9248
255. Dietrich H, Jacobi K, Ertl G (1997) J Chem Phys 106:9313
256. Berry JF (2012) Dalton Trans 41:700
257. Long AKM, Yu RP, Timmer GH, Berry JF (2010) J Am Chem Soc 132:12228
258. Long AKM, Timmer GH, Pap JS, Snyder JL, Yu RP, Berry JF (2011) J Am Chem Soc 133:13138
259. Schlangen M, Neugebauer J, Reiher M, Schroder D, Lopez JP, Haryono M, Heinemann FW, Grohmann A, Schwarz H (2008) J Am Chem Soc 130:4285
260. Schoffel J, Rogachev AY, George SD, Burger P (2009) Angew Chem Int Ed 48:4734
261. Schoffel J, Susnjar N, Nuckel S, Sieh D, Burger P (2010) Eur J Inorg Chem 4911
262. Thomson RK, Cantat T, Scott BL, Morris DE, Batista ER, Kiplinger JL (2010) Nat Chem 2:723
263. Atienza CCH, Bowman AC, Lobkovsky E, Chirik PJ (2010) J Am Chem Soc 132:16343
264. Timmer GH, Berry JF (2012) Chem Sci 3:3038
265. Harvey ME, Musaev DG, Du Bois J (2011) J Am Chem Soc 133:17207
266. Roizen JL, Harvey ME, Du Bois J (2012) Acc Chem Res 45:911
267. Zalatan DN, Du Bois J (2008) J Am Chem Soc 130:9220
268. Lin X, Zhao C, Che C-M, Ke Z, Phillips DL (2007) Chem Asian J 2:1101
269. Huard K, Lebel H (2008) Chem Eur J 14:6222
270. Williams Fiori K, Espino CG, Brodsky BH, Du Bois J (2009) Tetrahedron 65:3042

Top Organomet Chem (2016) 59: 103–138
DOI: 10.1007/3418_2015_148

Published online: 17 October 2015

Alkyne Activation Using Bimetallic Catalysts

Michael J. Page, D. Barney Walker, and Barbara A. Messerle

Abstract Bimetallic catalysts are capable of activating alkynes to undergo a diverse array of reactions. The unique electronic structure of alkynes enables them to coordinate to two metals in a variety of different arrangements. A number of well-characterised bimetallic complexes have been discovered that utilise the versatile coordination modes of alkynes to enhance the rate of a bimetallic catalysed process. Yet, for many other bimetallic catalyst systems, which have achieved incredible improvements to a reactions rate and selectivity, the mechanism of alkyne activation remains unknown. This chapter summarises the many different approaches that bimetallic catalysts may be utilised to achieve cooperative activation of the alkyne triple bond.

Keywords Alkyne activation · Bimetallic · Catalysis · Catalyst · Cooperativity

Contents

M.J. Page and D.B. Walker
School of Chemistry, The University of New South Wales, Sydney 2052, Australia

B.A. Messerle (✉)
School of Chemistry, The University of New South Wales, Sydney 2052, Australia

Department of Chemistry and Biomolecular Sciences, Macquarie University, North Ryde 2109, Australia
e-mail: barbara.messerle@mq.edu.au

1 Introduction

The use of bimetallic complexes as catalysts for organic transformations is of significant interest because they can dramatically enhance the rate and selectivity of a reaction compared to a monometallic catalysed process. Much early work on bimetallic catalyst design was inspired by the impressive catalytic efficiency of dinuclear metalloenzymes which contain bimetallic active sites [1]. More recently artificial bimetallic catalysts have been developed that offer substantial advantages compared to monometallic catalysts of similar structure [2–7]. This increase in catalyst performance is often attributed to a synergistic or 'cooperative' interaction between the two metals in activating the substrate of interest. Quite often the origin of this cooperativity is poorly understood on a molecular level. How the two metals of a bimetallic catalyst interact with each other and/or the reaction substrate during the catalytic cycle is difficult to determine from direct methods. In general, the second metal in a bimetallic catalyst may participate in a reaction via three possible means:

(a) An *electronic influence*, where the catalytic cycle proceeds solely via interaction of the substrate with one of the metal centres, yet the second metal provides a beneficial electronic influence on the first metal either through direct metal–metal bonding or through a shared ligand group.
(b) A *steric influence*, where the second metal acts to direct the substrate into an advantageous alignment with the first metal centre, without playing a direct role in the bond forming/breaking processes. This is particularly notable in bimetallic catalysts where an enhancement of the reaction selectivity is observed compared to a monometallic catalysed process.
(c) A *concerted activation process*, where both metal centres interact with the substrate(s) to provide a lower activation barrier towards reaction than could be obtained with a single metal centre. This may involve activation of each substrate in a reacting pair of molecules or the combined activation of a single substrate.

Note that these three modes of action are not mutually exclusive, and all processes may take part in the catalytic cycle.

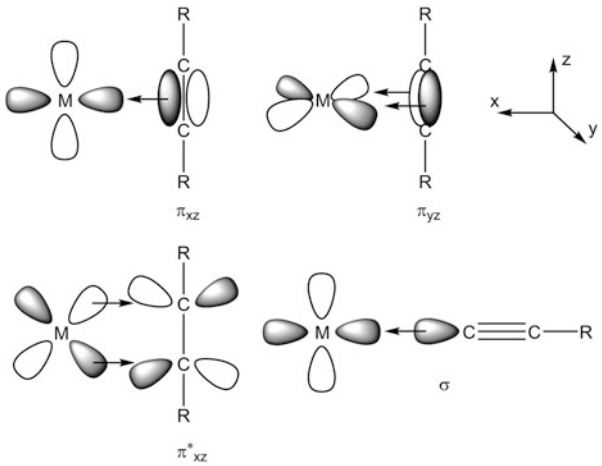

Fig. 1 Types of bonding modes possible between a metal centre and an alkyne

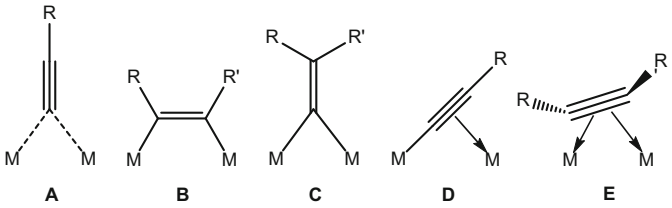

Fig. 2 Types of coordination modes possible for two metal centres binding to a single alkyne moiety

Alkynes are highly versatile building blocks for the synthesis of a wide range of organic molecules. The unsaturated alkyne triple bond can undergo a variety of metal-catalysed reactions, including the inter- or intramolecular addition of carbon or heteroatom nucleophiles; cycloaddition with other π-acidic functional groups such as carbon monoxide, alkenes, other alkynes and nitriles; or the coupling of nucleophilic acetylides with other electrophiles [8–11]. This reactivity is associated with a diverse coordination chemistry of organometallic alkyne species. The alkyne moiety contains two orthogonal π-orbitals that can be involved in its metal coordination chemistry, and in addition the basic acetylide unit contains a stable σ-bonding orbital. The presence of two orthogonal π* antibonding orbitals also allows for back-bonding interactions with π-acidic metal centres, further increasing the complexity of alkyne–metal interactions (Fig. 1).

As a result of the multiple orbitals available for metal–ligand bonding, alkynes readily coordinate with multiple metal centres [12]. Where two metals coordinate to a single alkyne (or acetylide) moiety, a number of different arrangements have been characterised (Fig. 2). An acetylide moiety may coordinate in an end-on fashion via two metal–carbon σ-bonds (structure **A**) with the C ≡ C axis perpendicular to the metal–metal axis ($\mu-\eta^1:\eta^1$). The alkyne can also coordinate parallel to the metal–metal axis (structure **B**), with each alkyne carbon forming a σ-bond to a different

metal centre ($\mu^2-\eta^1:\eta^1$). A 1,2-sigmatropic shift of an alkyne substituent (R in structure **B**) can also yield end-on coordinated vinylidene species (structure **C**, $\mu^2-\eta^2$). For metal acetylide moieties the proximity of a second metal can often yield ($\mu^2-\eta^1:\eta^2$) hybrid structures **D**, where the second metal coordinates in a π-fashion to the σ-bonded metal acetylide. Finally an alkyne may coordinate to two metal centres via its two orthogonal π-bonds, resulting in a tetrahedral C_2M_2 structure (**E**), where the C ≡ C axis lies across the metal–metal axis ($\mu-\eta^2:\eta^2$).

This review is not intended to be fully comprehensive but instead should serve to highlight current understanding of bimetallic cooperative catalysis as it applies to the activation of the alkyne triple bond. We have divided the review into four sections, separated by reaction type, which emphasise different aspects of the bimetallic alkyne activation mechanism. These four sections are as follows:

1. *Cyclotrimerisation, Dimerisation and Nucleophilic Substitution*. These three reactions are promoted by a class of catalysts where the bimetallic mechanism is generally very well understood. In this section the diversity of alkyne activation processes is highlighted through the characterisation of intermediate structures or their analogues.
2. *Cycloaddition with Azides, Alkynes, Alkenes and Allenes*. The copper-catalysed azide–alkyne cycloaddition reaction is typically catalysed by simple, monometallic Cu(I) salts. However, the mechanism of catalysis was recently determined to involve a bimetallic process. Similar bimetallic mechanisms have also been discovered in the cycloaddition of alkynes with alkenes, allenes and other alkynes using Au catalysts. This reaction is discussed for its broad application to many areas of chemistry and for the potential of bimetallic catalyst design to enhance the reaction.
3. *The Pauson–Khand Reaction and Silylformylation*. Perhaps one of the earliest and most widely studied bimetallic alkyne activation processes is the Pauson–Khand Reaction (PKR), which involves the [2 + 2 + 1] cycloaddition of an alkyne, alkene and CO to yield a cyclopentenone product. The key intermediate in both the PKR and the related silylformylation reaction is a ($\mu-\eta^2:\eta^2$)-bonded intermediate of structure E (Fig. 2). Extensive DFT modelling of the catalytic cycles has provided an excellent insight into the electronic changes that occur within the bimetallic unit during the reaction.
4. *Hydroelementation with Silanes, Alcohols, Carboxylic Acids and Amines*. This final class of reaction, involving the addition of Si–H, O–H or N–H bonds across an unsaturated C–C bond, has only recently been explored using bimetallic catalysts. The catalysts used also represent a distinct type of bimetallic design; where two discreet complex fragments are linked by a shared ligand scaffold, but typically do not contain any prearranged metal–metal bonding or bridging atom interactions. Such catalysts can easily be compared to monometallic catalysts of similar structure, thereby allowing a quantitative evaluation of the bimetallic cooperativity.

2 Cyclotrimerisation, Dimerisation and Nucleophilic Substitution

2.1 Cyclotrimerisation of Alkynes

The cyclotrimerisation of alkynes is a useful and atom economical route that enables the formation of substituted benzene derivatives from easily accessible starting materials. The reaction can be catalysed by a wide variety of metals, and, mechanistically, the monometallic catalysed process is very well understood [13–15]. In the first step of the catalytic cycle, a metal complex coordinated by two alkynes (Scheme 1, **A**) undergoes oxidative C–C coupling to yield a metallacyclopentadiene intermediate (**B**). Insertion of a third alkyne yields a transient metallacycloheptatriene intermediate (**C**) which undergoes reductive elimination to yield the substituted benzene product. One of the key challenges of this reaction is to control the regioselectivity of the process across a diverse range of alkyne substituents.

The bimetallic Nb and Ta complexes **1** and **2**, which contain a M–M double bond, were shown to catalyse the cyclotrimerisation of a variety of alkynes with exceptional regioselectivity to yield exclusively 1,3,5-substituted benzene products (Scheme 2) [15, 16]. In comparison the cyclotrimerisation reaction performed using the analogous monometallic catalysts [M(DME)Cl_3] (M = Nb or Ta, DME = 1,2-dimethoxyethane) gave a mixture of 1,3,5- and 1,2,4-substituted benzene products. Exactly how the bimetallic catalyst structure in **1** and **2** influences the regioselectivity of the reaction remains unclear; however, isolation of the Nb(V) intermediate **3** was achieved upon reaction of **1** with a stoichiometric amount of 2-hexyne. Addition of excess 2-hexyne to **3** then afforded the expected 1,3,5-substituted product. These results suggested a mechanism whereby each Nb centre functions separately to couple the alkyne substrates, while the neighbouring metal centre provides an electronic and/or steric influence on the catalytic cycle.

The cyclotrimerisation of electron-rich alkynes is also efficiently catalysed by the bimetallic indenyl complex **4**, which contains Cr(0) and Rh(I) coordinated in a 'transoid' fashion across the indenyl ring (Scheme 3) [17]. Using catalyst **4**, quantitative conversion of methyl propiolate to a mixture of the 1,3,5- and 1,2,4-substituted benzene products is achieved. Of particular note is the fact that **4** can be recovered at the end of the reaction, suggesting that the bimetallic structure remains intact during catalysis. In contrast, the monometallic Rh(I) catalyst

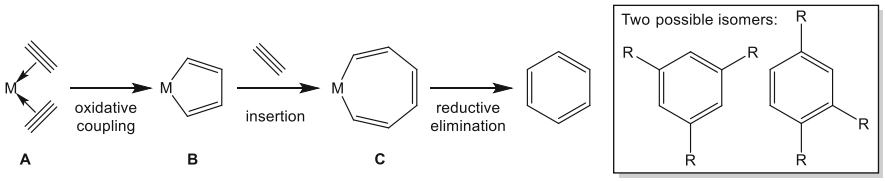

Scheme 1 General metal catalysed cyclotrimerisation reaction of alkynes

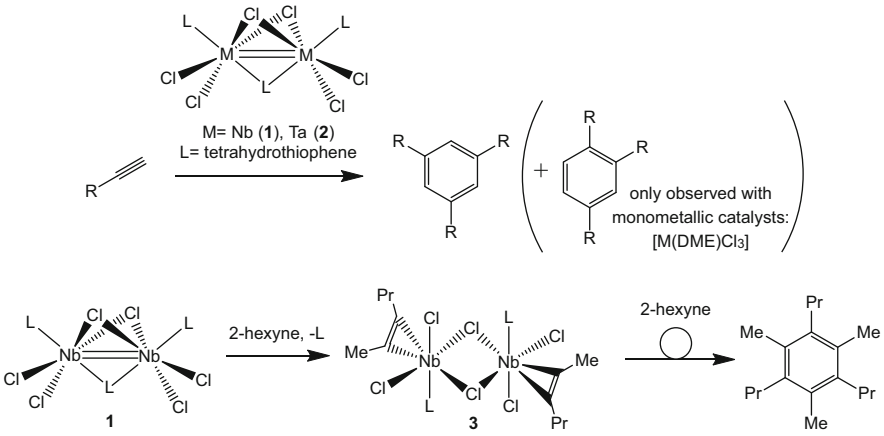

Scheme 2 Catalysed cyclotrimerisation reaction of alkynes using bimetallic Nb (**1**) or Ta (**2**) complexes

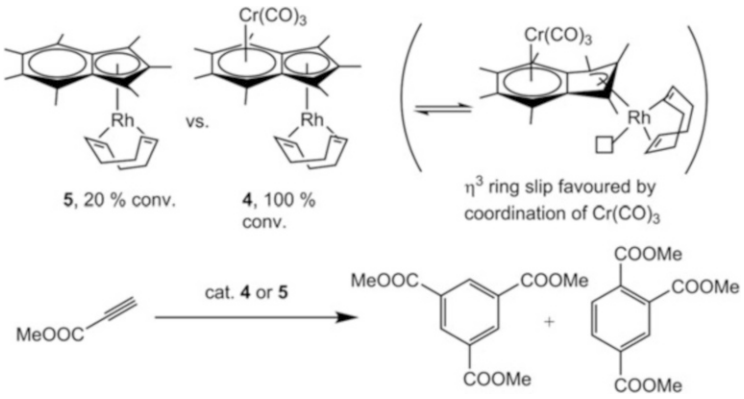

Scheme 3 Catalysed cyclotrimerisation reaction of electron-rich alkynes with a mono- and bimetallic indenyl complex containing both Rh(I) and Cr(0)

5 achieves a maximum conversion of only 20%. To account for this difference in reactivity, it was proposed that the Cr centre electronically impacts the coordination of the indenyl ligand to Rh facilitating an η^5 to η^3 ring slip which exposes the metal towards reaction. This was supported by comparing the kinetics of rotation about the Rh–indenyl bond for both mono- and bimetallic complexes where a larger η^3 component increased the rate of rotation for the bimetallic complex **4** compared to **5**.

The bimetallic complex **6** containing half-sandwich RhCp* fragments (where Cp* = 1,2,3,4,5-pentamethylcyclopentadienyl) bridged by a borohydride scaffold also showed moderate catalytic activity for the cyclotrimerisation of several alkynes (Scheme 4) [18, 19]. **6** was recovered from the reaction mixture unchanged,

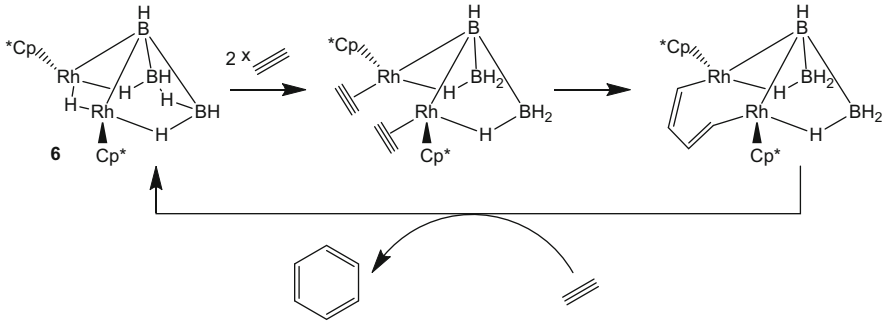

Scheme 4 Bimetallic Rh(III) bridged borohydride complex catalysing the cyclotrimerisation reaction of an alkyne

indicating retention of the bimetallic scaffold. Intriguingly, the authors propose a reaction mechanism whereby the two Rh centres coordinate to each end of the emerging alkyne trimer. It was reasoned that retention of all Rh–B and Rh–H–B interactions was necessary to prevent fragmentation of the rhodaborane cluster, thereby leaving only a single coordination site on each metal vacant. Unfortunately, characterisation of these intermediate species remained elusive.

2.2 Dimerisation of Alkynes

The non-oxidative dimerisation of two terminal alkynes is a practical method for the preparation of enynes. Enynes are present in many natural products and are themselves versatile building blocks in organic synthesis [20, 21]. Bimetallic ruthenium complexes have proven to be particularly useful catalysts for the dimerisation of alkynes due to the high levels of regio- and stereoselectivity they can achieve in product formation. The bimetallic reaction mechanism has been studied in great detail, providing an excellent insight into how the two metals interact during the catalytic cycle.

One of the most well-studied bimetallic catalysts used for the C–C coupling of alkynes are the thiolato-bridged diruthenium complexes **7** (Scheme 5) [22]. In the presence of NH_4BF_4 these complexes catalyse the head-to-head dimerisation of a number of terminal alkynes to selectively yield *Z*-enynes [23]. In contrast, related monometallic Ru catalysts typically yield a mixture of *E*- and *Z*-isomers, with the *E*-isomer more commonly favoured [24–26]. Previous work has shown that diruthenium complexes such as **7** are exceptionally robust due to the strong bridging ability of the thiolate ligands, which results in retention of the dinuclear core during reaction [27]. The proposed mechanism for the dimerisation reaction involves a concerted activation process where both Ru centres activate one alkyne each via the catalytic cycle shown in Scheme 5. Initial coordination of the first alkyne yields the vinylidene intermediate **8**. The second alkyne then coordinates to

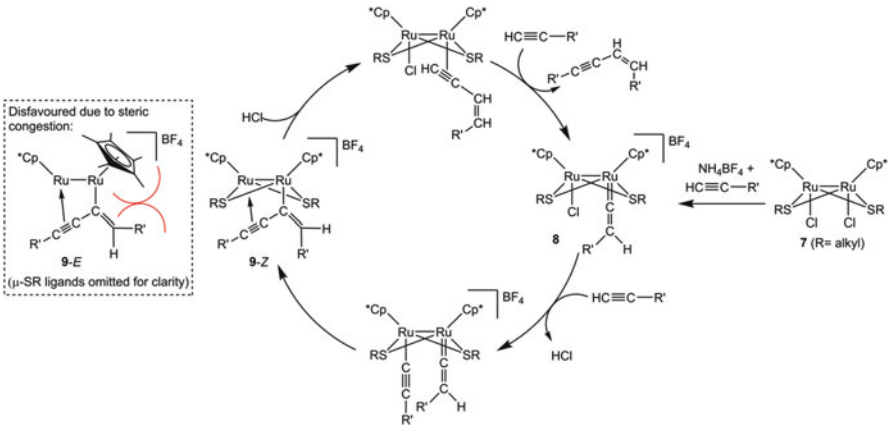

Scheme 5 Bimetallic Ru thiolate complex catalysing the dimerisation of alkynes

the other Ru centre as an acetylide via elimination of HCl. Migration of the acetylide to the η^2-vinylidene carbon yields the butenynyl intermediate **9**-*Z*, where both metals are involved in coordination of the butenynyl unit. The high stereoselectivity of the catalyst for the *Z*-isomer is considered to result from coordination of the alkyne to the second Ru centre in intermediate **9**. This affects an alignment of the vinylidene substituent (=CR′H) with the Cp* ligand and disfavours formation of intermediate **9**-*E* due to steric congestion between the alkyl substituent (R′) and Cp*. Re-addition of HCl affords the coordinated enyne product which is easily displaced by a new equivalent of alkyne, thus restarting the catalytic cycle. Evidence supporting such a mechanism was provided by isolation of the vinylidene complex **8** [28] (R=^{i}Pr, R′ = COOMe) and the butenynyl complex **9** [28] (R=^{i}Pr, R′ = ferrocenyl) from the reaction of **7** with methyl propiolate or ferrocenylacetylene, respectively. Complex **9** itself was shown to be an effective catalyst for the dimerisation reaction, proving its participation within the catalytic cycle. Analogous diruthenium complexes containing end-on coordinated acetylide ligands (i.e. Ru–C ≡ CR) have also been isolated previously [29].

The heterobimetallic Ru–Co complex **10**, which is similar in structure to **7**, catalyses the head-to-head dimerisation of methyl propiolate upon abstraction of a Ru–CO ligand with Me_3NO (Scheme 6) [30]. Evidence for a bimetallic transition state was provided by isolation of the butadiene ruthenacycle **11** from the reaction of **10**, Me_3NO and *p*-tolylacetylene, although a head-to-tail coupling of *p*-tolylacetylene was observed in this case. The role the $Co(CO)_n$ fragment plays in this catalysis is unclear; although the Co should have a strong electronic influence on the Ru centre, the structure of **11** suggests a cooperative interaction between the substrate and both Ru and Co which may also assist the reaction.

The dimerisation of phenylacetylene to yield exclusively the head-to-tail coupling product has been achieved using the diruthenium complex **12** as catalyst (Scheme 7a) [31]. This was the first complex to display such selectivity and remains the only ruthenium complex to do so. Complex **12** contains two bridging

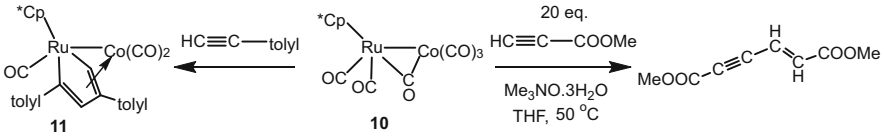

Scheme 6 Head-to-head catalysed dimerisation of alkynes using a Ru-Co bimetallic complex

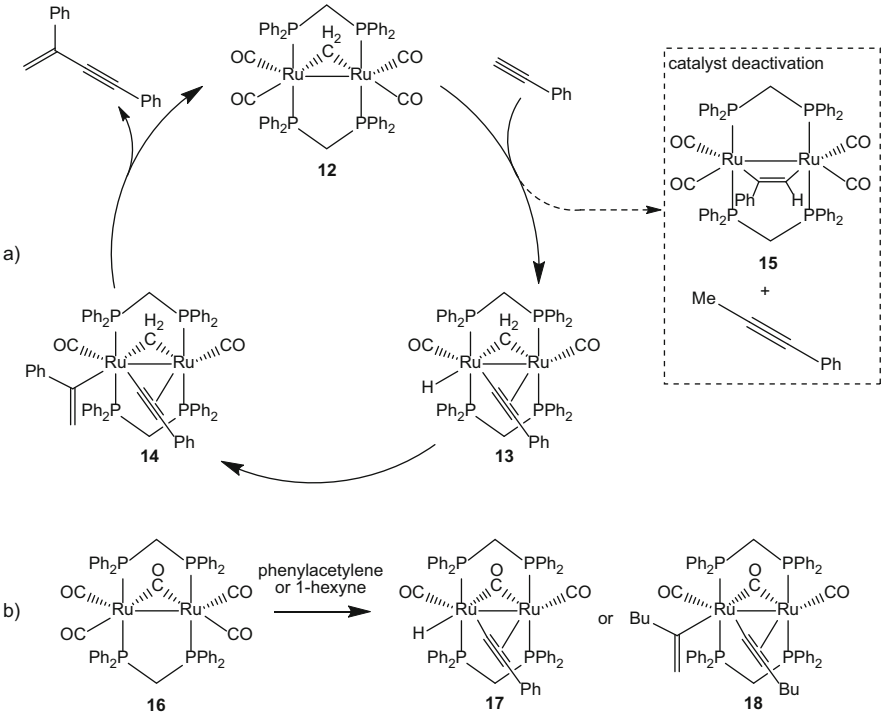

Catalytically inactive complex **16** allows characterisation of compounds **17** and **18**, related to catalytic mechanism

Scheme 7 (**a**) Proposed catalytic cycle for the dimerisation of phenylacetylene using a bimetallic Ru complex (**12**), and (**b**) Isolation of possible intermediates in the catalytic cycle above on using an analogous Ru(CO) complex (**17** and **18**)

bis(diphenylphosphino)methane (dppm) ligands and a bridging methylene moiety, the latter of which was found to be crucial to obtain the desired reactivity. The unusual head-to-tail coupling geometry cannot be achieved via a mechanism involving vinylidene intermediates as was described previously for complex **7**. Rather, the researchers propose an alternative mechanism whereby the alkyne oxidatively adds to one Ru centre to give the acetylide–hydride complex **13**. Insertion of the second alkyne into the Ru–hydride bond affords the alkenyl intermediate **14**, which reductively eliminates the 1,4-diphenylbutenyne product and regenerates the catalyst. Note the acetylide in complexes **13** and **14** is

coordinated by both Ru centres in a $\mu^2-\eta^1:\eta^2$-bonding mode which may stabilise these intermediate structures. Interestingly, upon prolonged reaction of **12** with excess phenylacetylene, the methylene unit is eventually lost through insertion into the alkyne C–H bond to yield 1-phenylpropyne (PhC ≡ CMe) and complex **15**. Complex **15**, which contains a phenylacetylene unit bridging the two Ru centres, is entirely inactive for the dimerisation reaction. Fortunately the researchers were able to characterise a number of related compounds that resemble the intermediate structures **13** and **14** [32, 33]. Complex **16**, which contains a μ–CO ligand in place of the bridging methylene group found in **12**, was found to react with phenylacetylene or 1-hexyne to yield the acetylide–hydride and acetylide–alkenyl complexes **17** and **18**, respectively (Scheme 7b). Compound **16** however was not found to be an effective catalyst for the dimerisation of alkynes, highlighting the crucial role the bridging methylene unit plays in activating catalyst **12**.

2.3 Nucleophilic Substitution of Propargylic Alcohols

The OH group of propargylic alcohols (HC ≡ CCHROH) is readily displaced by a range of nucleophiles, and this enables the facile attachment of an alkyne group to an organic molecule (Scheme 8a) [34]. The alkyne moiety is a versatile entity for further chemical transformations and is itself an important subunit in many fine chemicals and natural products. The bimetallic ruthenium complex **7,** which is an effective catalyst for the dimerisation of alkynes (Scheme 5), also catalyses the nucleophilic substitution of propargylic alcohols using a range of nucleophiles such as alcohols, amines, thiols, ketones and alkenes, among others (Scheme 8a) [35–39]. Unlike the alkyne dimerisation mechanism described above, the propargylic substitution reaction requires only one Ru centre to activate the alkyne, yielding the allenylidene intermediate **19** (Scheme 8b). Complex **19** (where R = Me, CHR′ = C(tolyl)$_2$) was in fact isolated from the reaction of **7** with NH_4BF_4 and HC ≡ CC(tolyl)$_2$OH and was then shown to liberate the propargylic substitution product HC ≡ CC(Tol)$_2$OEt upon treatment with EtOH. Despite only one Ru centre interacting with the substrate in the proposed mechanism, conventional mononuclear ruthenium complexes were not effective catalysts for the propargylic substitution reaction indicating that the diruthenium core was essential for catalysis. Computational investigations show that the π-back-donating ability of the reactive Ru centre is reduced by its bonding to the second Ru centre [40]. This destabilises the vinylidene and allenylidene intermediates and lowers the energy barrier between them. It also labilises the η^2-coordinated alkyne product facilitating its displacement by a second equivalent of substrate in the final turnover step.

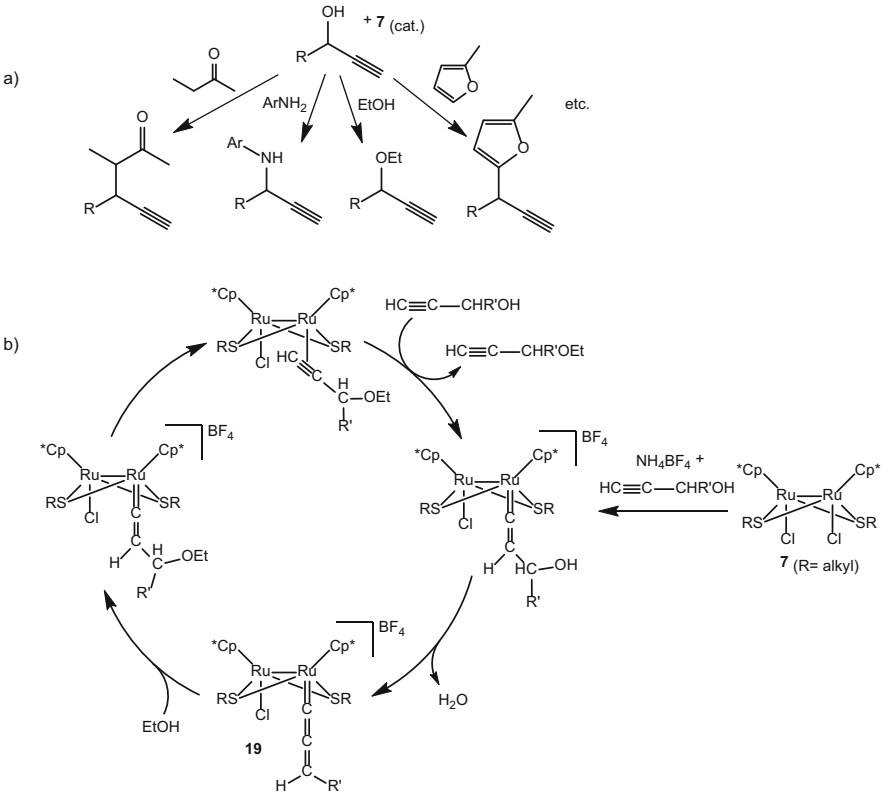

Scheme 8 (**a**) Catalysed nucleophilic substitution of propargylic alcohols with a range of nucleophiles, and (**b**) Proposed catalytic cycle for the nucleophilic substitution of propargylic alcohols using the bimetallic Ru thiolate complex (**7**)

3 Cycloaddition with Azides, Alkynes, Alkenes and Allenes

3.1 Azide–Alkyne Cycloaddition

The copper-catalysed azide–alkyne cycloaddition reaction is a reliable and robust synthetic method for covalently linking a diverse range of molecular building blocks [41, 42], bioconjugation [43] and organic synthesis [44–48]. The reaction proceeds in a highly selective single step, under mild reaction conditions, and is successful in the presence of a wide range of other functional groups. It has only recently been established that this reaction proceeds through the mechanism shown in Scheme 9, whereby η^2-coordination of a second Cu centre to the Cu–acetylide complex forms intermediate **20** [49]. Nucleophilic attack at *N*-3 of the azide by the

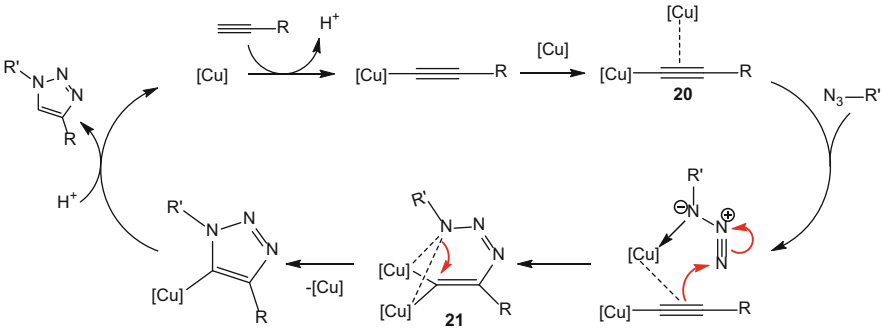

Scheme 9 Cooperatively catalysed azide-alkyne cycloaddition reaction with a second Cu metal centre participating during key intermediate steps

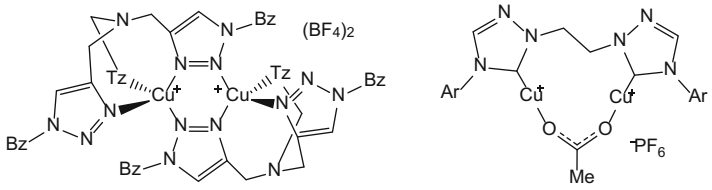

Scheme 10 Highly efficient Cu(I) bimetallic catalysts (**22** and **23**) for the azide-alkyne cycloaddition reaction

C_2-carbon of the acetylide forms the first covalent C–N bond, producing the geminal dicopper intermediate **21**. Formation of the second C–N bond eliminates one Cu centre to generate the Cu-triazolide which is protonated to regenerate the catalyst.

Currently, few examples have been reported of well-defined binuclear Cu complexes that catalyse the click reaction. It has been shown that the use of polytriazolyl ligands can greatly accelerate the rate of Cu-catalysed click reactions compared to reactions catalysed by simple Cu salts [50]. The compound tris (benzyltriazolylmethyl)amine (TBTA) was found to be the most effective ligand for accelerating the Cu-catalysed click reaction. Initially it was assumed that this ligand simply stabilised the catalytically active Cu(I) centre against oxidation; however, attempts to characterise a Cu(I) compound containing TBTA led to the isolation of the bimetallic complex **22** (Scheme 10) [51]. Complex **22**, which

contains two triazolyl moieties bridging the two Cu centres, was then shown to be a highly efficient catalyst for the click reaction. Another example of bimetallic catalyst design leading to cooperative rate enhancement in the Cu-catalysed click reaction was reported by Straub and coworkers [52]. The bis-triazolylidene dicopper(I) complex **23** was synthesised, and its catalytic activity for the coupling of benzyl azide with phenylacetylide was compared to the monometallic *N*-heterocyclic carbene complex $[Cu(ICy)]PF_6$ (ICy = 1,3-bis(cyclohexyl)imidazol-2-ylidene). The cycloaddition of benzyl azide and phenylacetylene catalysed by the bimetallic catalyst **23** was complete within 1.7 h, whereas the monometallic catalyst $[Cu(ICy)]PF_6$ required approximately 4.5 h to reach 60% conversion. It should be noted that this difference in reactivity between **23** and $[Cu(ICy)]PF_6$ is likely to also be affected by the dissimilar carbene ligand properties and the presence of an acetate coligand in **23**.

3.2 *Cycloaddition of Alkynes with Alkynes, Alkenes and Allenes*

The use of homogeneous gold catalysts in synthetic organic chemistry has grown rapidly in recent decades and has proven to be a versatile tool in the total synthesis of natural products among other applications [53, 54]. In the gold-catalysed cycloaddition of alkynes, the participation of bimetallic gold complexes that contain $\mu^2-\eta^1:\eta^2$-acetylide or *gem*-diaurated moieties has been increasingly observed [55]. For example, Corma et al. have observed that $\mu^2-\eta^1:\eta^2$-acetylide catalysts such as **24** are superior to their monometallic analogues for the intermolecular [2 + 2] alkyne–alkene cycloaddition reaction (Scheme 11a) [56]. Hashmi and coworkers have identified the *gem*-diaurated complex **25** as an effective catalyst precursor for the cycloaddition of dialkynes (Scheme 11b) [57]. Toste and coworkers have reported the cycloisomerisation of allenynes using the gold catalyst **26** and determined the involvement of bimetallic $\mu^2-\eta^1:\eta^2$-acetylide and *gem*-digold intermediates (Scheme 11c) [58]. In each of these examples however, the dinuclear catalyst structure is not retained throughout the reaction due to the absence of spectator bridging ligands that can immobilise the two Au centres in close proximity. Although a number of related cycloaddition reactions using chiral bimetallic Au catalysts have been reported [59], the two gold centres are not considered to act through a bimetallic interaction with the substrate as described here. The chemistry of such catalysts is discussed in detail below for the hydrofunctionalisation reactions.

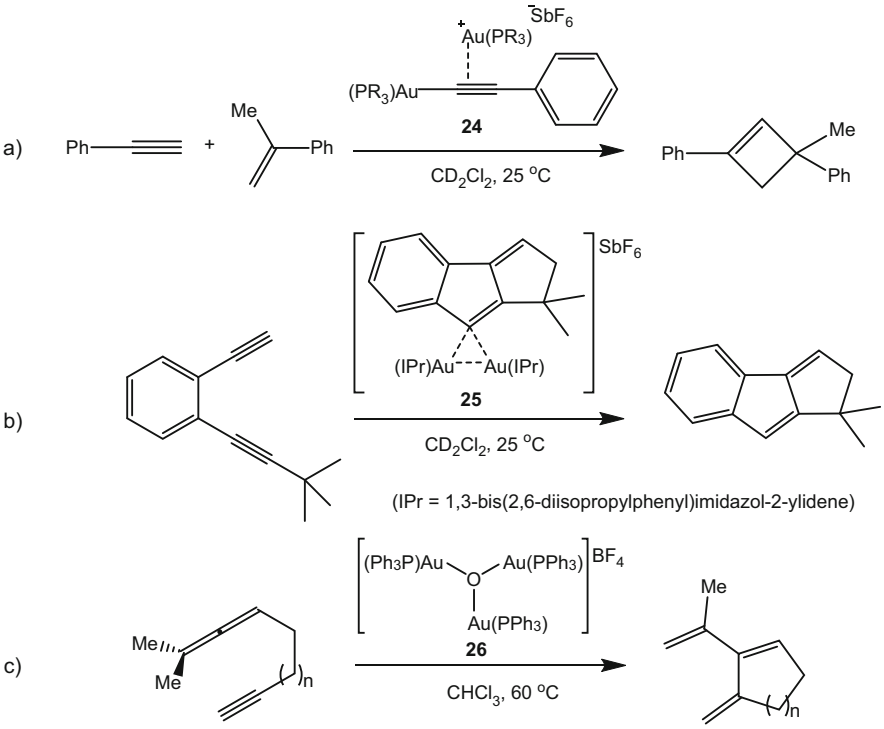

Scheme 11 (**a**) A μ^2-η^1:η^2-acetylide bimetallic Au catalyst (**24**) used in the azide-alkyne cycloaddition, (**b**) a μ^2-η^2 *gem*-diaurated catalyst (**25**) used for the cycloaddition of dialkynes, and (**c**) a trimetallic gold complex (**26**) used in the cycloisomerisation of allenynes

4 The Pauson–Khand Reaction and Silylformylation

4.1 The Pauson–Khand Reaction

The Pauson–Khand reaction is the coupling of an alkyne, alkene and CO to yield a cyclopentenone in an overall [2 + 2 + 1] cycloaddition reaction (Scheme 12) and has proven to be a valuable tool in the total synthesis of various natural products [60, 61]. The reaction was first catalysed by the bimetallic dicobalt complex $[Co_2(CO)_8]$ [62–64], although a number of variations with monometallic cobalt complexes and with different metals have also been reported [61]. The currently accepted mechanism of the $[Co_2(CO)_8]$-catalysed Pauson–Khand reaction involves initial coordination of the alkyne perpendicular to the Co–Co axis through two orthogonal π-bonding interactions to give complex **27**. This is followed by coordination of the alkene and then insertion of the alkene into a Co–C bond. Migratory insertion of a CO ligand and reductive elimination of the product liberates the $[Co_2(CO)_6]$ fragment, which is trapped by a second equivalent of alkyne to renew

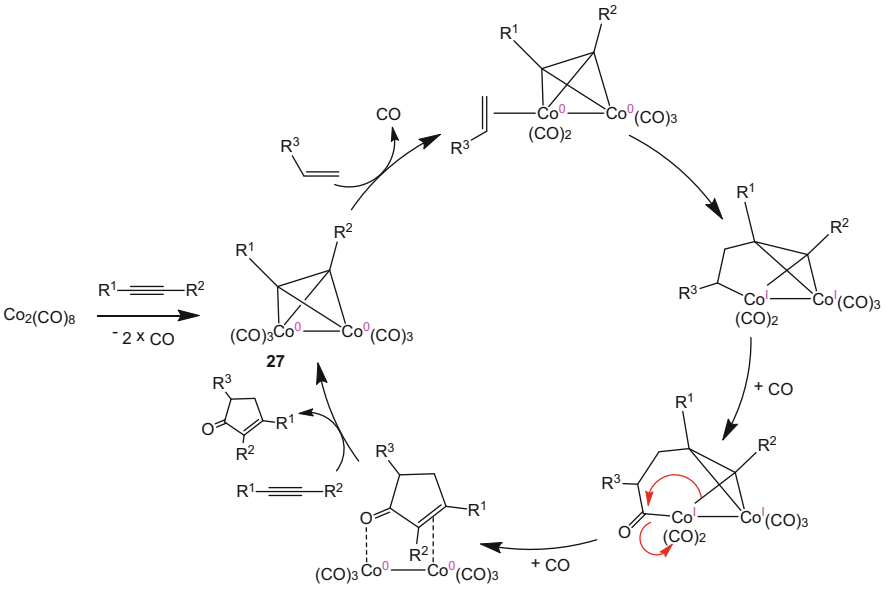

Scheme 12 The currently accepted mechanism for the bimetallic $[Co_2(CO)_8]$ catalysed Pauson–Khand reaction

the catalytic cycle. Unfortunately the only intermediates that have been characterised from this catalytic cycle are $\mu^2-\eta^2:\eta^2$ alkyne complexes such as **27**; however, DFT calculations have been used to support the proposed mechanism [65]. Importantly, these calculations determined that while the C–C bond forming events occur at only one of the two Co centres, the oxidative burden is shared by both metal centres; thus the second Co atom serves as an electron reservoir for the first Co atom. The second Co centre also acts as an anchor to the substrate and remains firmly coordinated to the alkyne throughout the reaction. In reality the above catalytic mechanism only becomes efficient in the presence of certain ligands such as phosphites, phosphines or dimethoxyethane which inhibit the formation of inactive cobalt species and may coordinate to the Co centres in place of one or more CO ligands [60]. Related bimetallic species that facilitate the *stoichiometric* Pauson–Khand reaction include the homobimetallic cyclopentadienyl (Cp) complexes $[MCp(CO)_2]_2(\mu^2-\eta^2:\eta^2$-alkyne) (where M = W or Mo) [66] and the heterobimetallic complex $[MoCp(CO)_2\text{-}Co(CO)_3](\mu^2-\eta^2:\eta^2$-alkyne) [67].

4.2 *Silylformylation of Alkynes*

The silylformylation of alkynes involves the coupling of an alkyne with a silane and carbon monoxide to yield β-silylvinyl aldehydes, which are versatile building

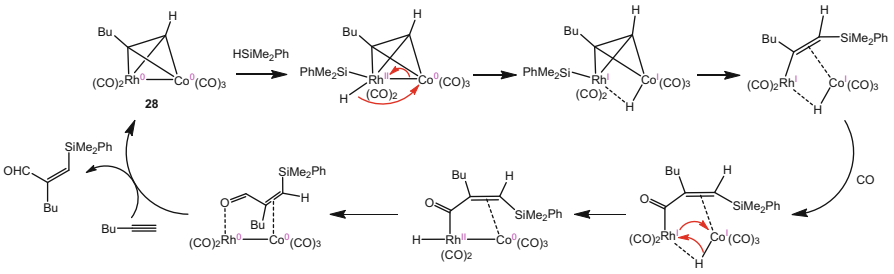

Scheme 13 Proposed reaction mechanism for the silylformylation of alkynes using a heterobimetallic Rh(0)-Co(0) complex (**28**)

blocks in organic synthesis [68]. One of the more effective catalysts for the silylformylation of alkynes is the bimetallic Rh–Co complex **28** (Scheme 13) [69–71]. Complex **28** is directly analogous in structure to the dicobalt Pauson–Khand catalyst **27** (Scheme 12), with the bridging alkyne coordinated perpendicular to the Rh–Co axis via two orthogonal π-bonding interactions ($\mu^2-\eta^2:\eta^2$). Complex **28** was reported to catalyse the silylformylation of 1-hexyne with $HSiMe_2Ph$ and CO under ambient temperature and pressure to yield exclusively the *Z*-isomer of the product. The Rh centre in this case was determined to be the critically important metal for this reaction, with DFT calculations showing that the key C–Si and C–C bond forming reactions both occur at the Rh metal centre [72]. The Co atom plays an important role in binding the alkyne and acting as an electron reservoir to stabilise the Rh-hydride that is formed upon oxidative addition of silane to Rh(0). Experimentally the Co centre has also proven to be crucial in controlling the selectivity of the reaction. For example, analogous monometallic Rh species that catalyse the silylformylation reaction suffer from the formation of hydrosilylated byproducts [73, 74]. Dirhodium(II) complexes have also been employed as efficient silylformylation catalysts; however, it appears likely a bimetallic transition state is not involved in these systems as it has been shown the catalyst is reduced in situ to form monometallic Rh(I) species [75, 76].

5 Hydroelementation with Silanes, Alcohols, Carboxylic Acids and Amines

5.1 Hydrosilylation of Alkynes

The hydrosilylation of alkynes provides facile access to a diverse range of vinyl silane products which are versatile building blocks in organic synthesis [68]. The electrophilic substitution of vinylsilanes is one of the most useful methods for the stereoselective synthesis of substituted alkenes [77, 78]. The effectiveness of

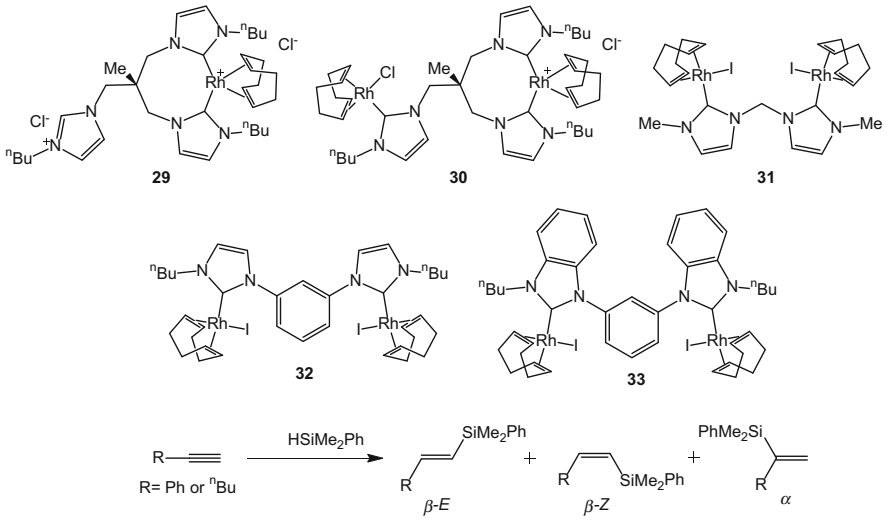

Scheme 14 Rh(I) bimetallic catalysts used for the hydrosilylation of alkynes

monometallic Rh(I) complexes as catalysts for the hydrosilylation of alkynes has been known for several decades [79]; however, only recently have bimetallic Rh(I) catalysts been applied to this reaction [80]. The mono- and bimetallic Rh(I) complexes **29**, **30** and **31** were used to catalyse the hydrosilylation of phenylacetylene and 1-hexyne using dimethylphenylsilane (Scheme 14). For all catalysts the *β-Z*-isomer was formed in preference to either the *β-E*- or α-isomers. The most active catalyst of this series was the bimetallic complex **31**, which achieved quantitative conversion of the substrate within 6 h, while longer reaction times were required to obtain similar conversion with the bimetallic catalyst **30** (24 h) and the monometallic catalyst **29** (72 h). The related bimetallic catalysts **32** [81] and **33** [82] have also been used to catalyse the hydrosilylation reaction (Scheme 14). Under analogous reaction conditions, complex **33** was found to have a similar catalytic activity and selectivity to complex **31** for the hydrosilylation of phenylacetylene with dimethylphenylsilane. Unfortunately comparison of the bimetallic catalysts **31**, **32** and **33** with a suitable monometallic analogue was not attempted [83]; therefore, an evaluation of the bimetallic synergism in this reaction cannot easily be made.[1]

[1] Related monometallic catalysts of the type [Rh(NHC)(COD)Cl] have been used for the hydrosilylation of alkynes; however, the sensitivity of the reaction to conditions of temperature and solvent, and the identity of the silane, halide ligand and NHC substituents, precludes a meaningful comparison of catalyst activity.

5.2 *Hydroalkoxylation of Alkynes*

The *mono*- and *di*hydroalkoxylation of alkynes provides access to enol ether and acetal functional groups, respectively. This reaction is particularly versatile when applied in an intramolecular fashion to yield oxygen containing heterocycles such as furans, pyrans and spiroketals which are essential components of many biologically active compounds. Monometallic Au(I) catalysts are known to be excellent catalysts for the hydroalkoxylation of alkynes [84, 85]. Due to the strong aurophilic interaction that is possible between two gold atoms, bimetallic intermediates have always been suspected to participate in the gold-catalysed hydroalkoxylation reaction (Scheme 15a). In contrast to the general theme of this chapter, it was proposed that the formation of such bimetallic intermediates inhibits the catalytic reaction due to their resistance to protodeauration, a necessary step to eliminate the product and complete the catalytic cycle. Recently, it was discovered that geminal-digold species such as **A** (Scheme 15b) could be isolated from a stoichiometric reaction of

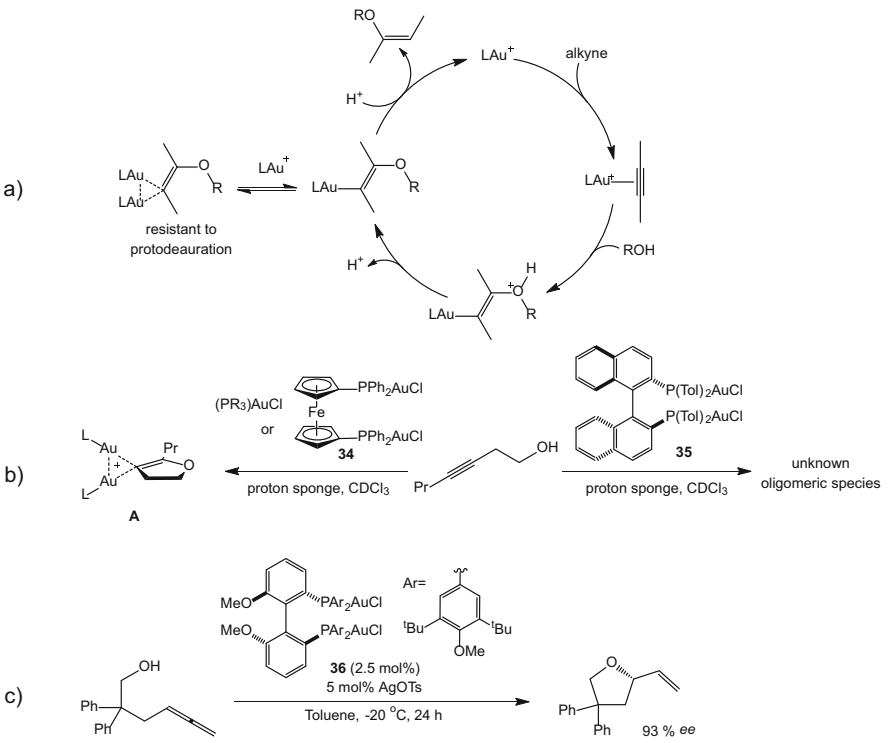

Scheme 15 (**a**) Au(I) catalysed intermolecular hydroalkoxylation reaction, (**b**) attempted isolation of geminal-digold complexes from Au(I) bimetallic complexes during the hydroalkoxylation of alkynols, and (**c**) enantioselective synthesis of O-heterocycles using the chiral bimetallic Au(I) complex (**36**)

3-heptyn-1-ol with a monometallic Au complex in the presence of a proton sponge [86]. The researchers also investigated several bimetallic complexes for this reaction with the expectation that the formation of *gem*-diaurated species may be favoured. Surprisingly a range of coordination modes were characterised depending on the nature of the bridging ligand scaffold. For example, while the ferrocenyl digold complex **34** was shown to yield the expected *gem*-digold intermediate **A**, an analogous structure could not be characterised with the binaphthyl bridged digold complex **35**. The NMR spectra of the reaction containing **35** suggested multiple oligomeric diaurated species of irregular structure might be present. Presumably the helical twist of the binaphthyl unit precludes a simple bimetallic interaction with the substrate in this case. While it has yet to be reported how the different monometallic and bimetallic structures in Scheme 15b affect their efficiency as catalysts for the hydroalkoxylation of alkynes, chiral biaryl catalysts analogous to **35** have been used for the enantioselective hydroalkoxylation of allene substrates [87]. For example, the bimetallic Au catalyst **36** was shown to catalyse the intramolecular hydroalkoxylation of allene alcohols with exceptional enantioselectivity (>93% *ee*) (Scheme 15c).

Moving from Au to other metal centres for promoting C–O bond formation, Messerle and coworkers demonstrated that monometallic Rh(I) and Ir(I) complexes containing bidentate N-donor ligands such as bis(1-pyrazolyl)methane (bpm) are excellent catalysts for the intramolecular dihydroalkoxylation of alkynediols to yield spiroketals, in a one-pot tandem reaction [88]. Recently it was demonstrated that the efficiency of these catalysts could be enhanced by linking two bpm complex fragments by a bridging organic scaffolds to yield a series of bimetallic catalysts (Scheme 16) [89, 90]. An initial investigation showed that the bimetallic complexes **38**, **39** and **40** were all superior catalysts compared to the monometallic analogue **37** for the dihydroalkoxylation of a variety of alkynediol substrates. The reaction rates achieved by catalysts **38**–**40** were also found to increase as the apparent separation between the metal fragments decreased, such that the efficiency of the catalysts could be ordered **38** < **39** < **40**. It was also found that increasing the flexibility of the scaffold, such as in the complexes **41**, **42** and **43** (linked by hexyl, heptyl and ferrocenyl groups, respectively), considerably diminished the bimetallic synergism for these catalysts. The bimetallic complexes **44** and **45** containing a xanthene and dibenzofuran scaffold, respectively, did not achieve catalytic rates as high as the structurally very similar anthracene containing complex **40**. Despite a superficial similarity in structure of the complexes **40**, **44** and **45**, DFT modelling of their structures revealed that the intermetallic distance in their lowest energy conformation differed significantly, which may contribute to their dissimilar reactivity. The weakly basic oxygen heterocycle present in the scaffold of **44** and **45** may also interact with the substrate to alter the reactivity of these catalysts.

To better understand the structure–activity relationship with the bimetallic catalysts **38**–**40**, **44** and **45**, computational modelling of their structural confirmations was performed [90]. A high degree of conformational flexibility existed within the structures due to free rotation of the bpm–arene bond and flipping of the bpm–Rh metallocycle between two possible boat conformations (Fig. 3).

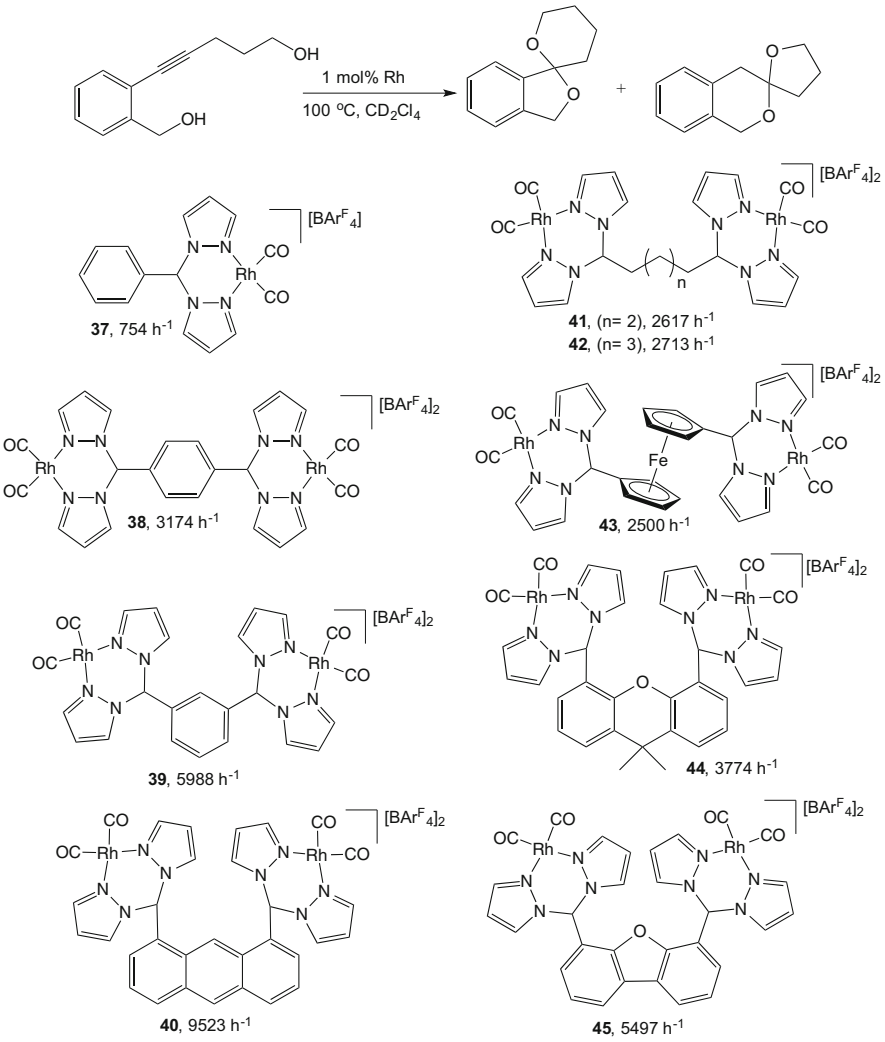

Scheme 16 Rh(I) mono- and bimetallic catalysts containing the bis(1-pyrazolyl)methane ligand used for the intramolecular dihydroalkoxylation reaction

The difference in energy between multiple different conformations was found to be quite small, and as a result the distance between the metal fragments was poorly defined. This result tended to undermine attempts to correlate the activity of the catalysts with their metal−metal separation, and no such correlation could be made (Fig. 3).

In an effort to constrain the flexibility in this type of bimetallic catalyst, complex **46** was synthesised which contains imidazolyl-imine ligands attached directly to the 1,2-phenylene scaffold via the imine nitrogen (Scheme 17) [91]. This arrangement significantly reduces the degree of conformational freedom for complex **46**, which

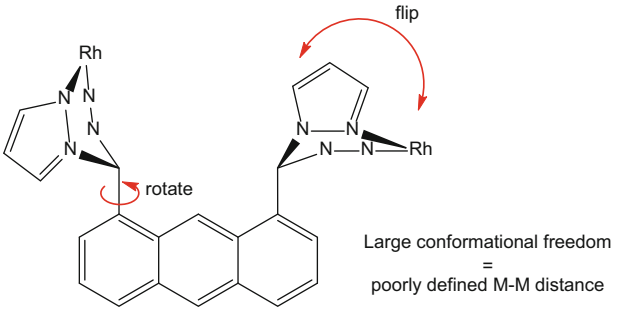

Fig. 3 Conformational flexibility of bimetallic complexes containing the bis(1-pyrazolyl) methane ligand donor

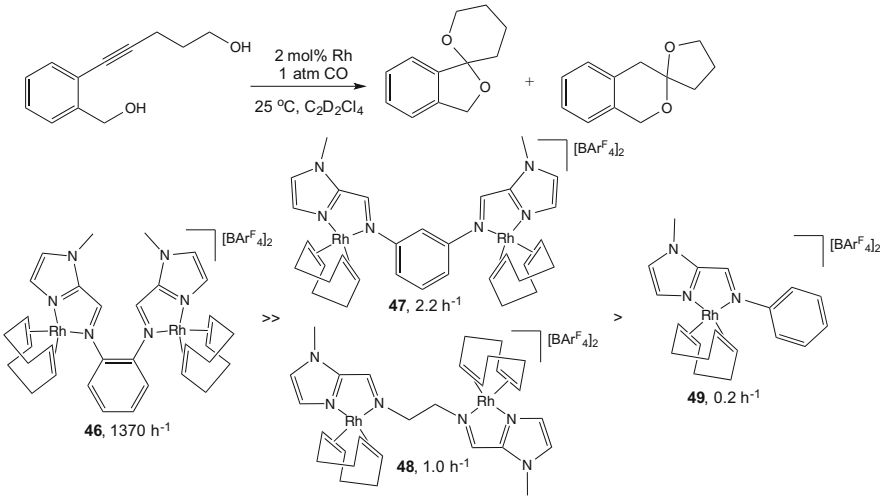

Scheme 17 Rh(I) mono- and bimetallic catalysts containing the imidazolyl-imine ligand (**46**–**49**) used for the intramolecular dihydroalkoxylation reaction

now contains a geometrically flat metallocycle formed by the imidazolyl-imine chelate, and allows for a shorter intermetallic distance through alignment of the complex planes. Complex **46** achieved the highest rate enhancements yet observed for any bimetallic catalysed reaction, over 6,800 times higher turnover frequency than that of the analogous monometallic catalyst **49**. Increasing the Rh···Rh distance (complex **47**) or increasing the flexibility of the C_2 bridge (complex **48**) drastically reduced the effectiveness of the bimetallic catalysts, consistent with previous observations.

5.3 *Hydrocarboxylation of Alkynes*

The hydrocarboxylation of alkynes involves the addition of a carboxylic acid group across the C ≡ C triple bond to yield an enol ester group. While it is superficially similar to the hydroalkoxylation reaction, in that both reactions involve the addition of an O–H bond to the alkyne, the catalysed reaction mechanisms of hydrocarboxylation and hydroalkoxylation can differ substantially [92–94]. The intramolecular hydrocarboxylation also provides access to oxygen heterocycles such as lactones, which are commonly found in flavour and fragrance molecules [95]. To expand on the chemistry of the highly effective bimetallic dihydroalkoxylation catalyst **46**, its potential to catalyse the hydrocarboxylation reaction was investigated [91]. Catalyst **46** was a highly effective catalyst for the hydrocarboxylation of 4-pentynoic acid affording complete conversion to the cyclic lactone within 3 h at 60°C (Scheme 18). In comparison, the monometallic catalyst **49** was entirely inactive under these conditions. The efficiency of the structurally similar indolylimine complexes **50** and **51** as a catalyst for the hydrocarboxylation of 4-pentynoic acid had been investigated previously [96]. The bimetallic complex **50** was also found to be a highly effective catalyst for this reaction; however, no enhancement of reaction rate was obtained relative to its monometallic analogue **51**, with both catalysts achieving complete conversion within 3.5 h. This result is in

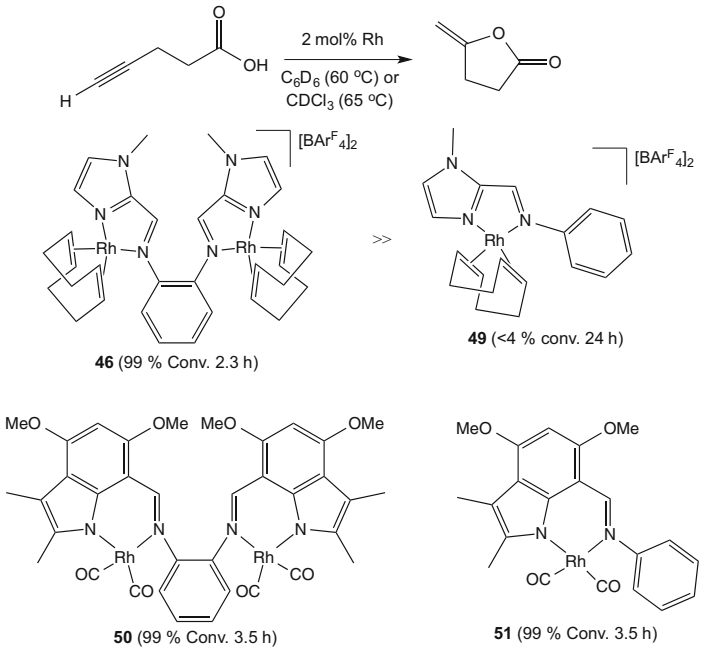

Scheme 18 Rh(I) mono- and bimetallic catalysts (**46**, **49**, **50**, **51**) used for the intramolecular hydrocarboxylation reaction to generate lactones

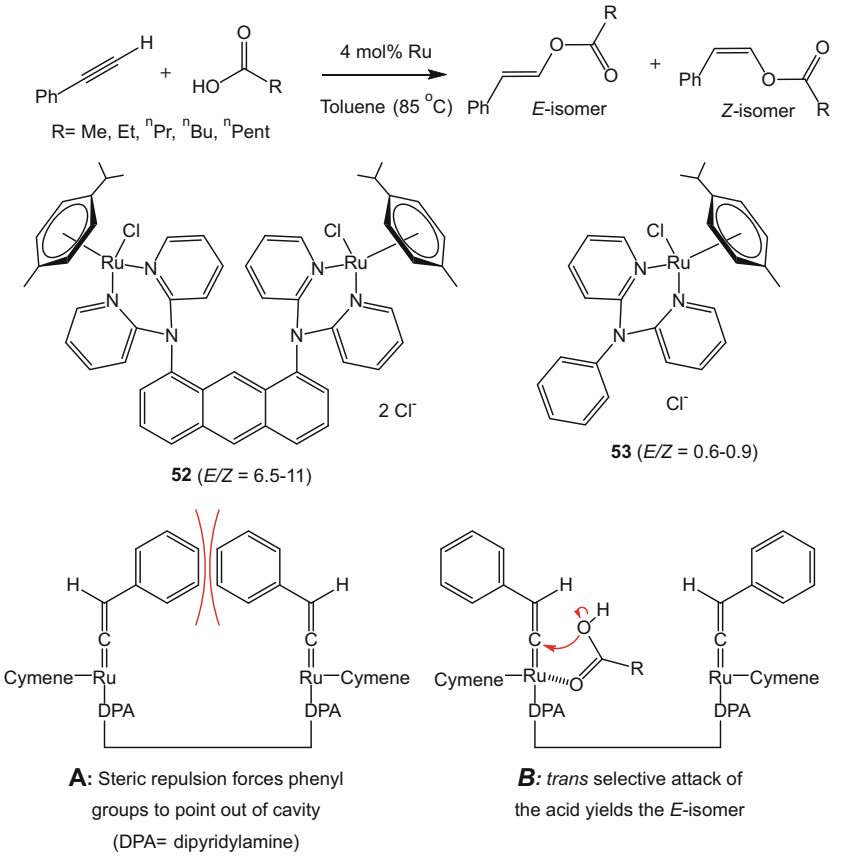

Scheme 19 Ru(II) mono- and bimetallic catalysts (**52**, **53**) used for the intermolecular hydrocarboxylation reaction and the increase in *E*–selectivity on using the bimetallic catalyst **52** due to the steric repulsion of the substrate phenyl groups

stark contrast to the excellent bimetallic rate enhancements obtained with **46** and highlights how small changes in catalyst structure can greatly impact the degree of bimetallic synergism that is obtained.

The intermolecular hydrocarboxylation of phenylacetylene with a range of aliphatic carboxylic acids has been catalysed by the bimetallic Ru complex **52** (Scheme 19) [97]. The bimetallic structure was shown to have a significant impact on the stereoselectivity of the reaction with the anti-Markovnikov *E*-isomer obtained in good preference to the *Z*-isomer. In comparison, the related monometallic catalyst **53** showed a poor stereoselectivity for the hydrocarboxylation of phenylacetylene with the *Z*-isomer product slightly predominant with regard to the *E*-isomer product following catalysis. Similar reaction rates were observed with both catalysts. Analysis of the catalysis reaction by ESI-MS and ^{13}C NMR spectroscopy showed that both Ru centres activate a separate molecule of

phenylacetylene simultaneously to yield a bis-phenylethenylidene complex (structure **A**, Scheme 19). The authors therefore proposed that the selectivity of the bimetallic catalysed reaction is determined by the small size of the cavity between the two Ru complex fragments (Ru···Ru = 9.2 Å). This constrains the phenylethenylidene units to orient in such a manner that the phenyl groups point out of the cavity directing attack by the carboxylic acid towards the *trans* face of the alkylidene to yield the *E*-isomer of the product (structure **B**). Notably, the stereoselectivity of **52** was lost if phenylacetylene was substituted for 1-octyne, which has considerably less steric bulk, or if the steric bulk of the carboxylic acid was increased (R = Ph).

5.4 Hydroamination of Alkynes, Allenes and Alkenes

The hydroamination of alkynes is a highly atom-efficient approach to the synthesis of enamines and imines, as well as to the synthesis of *N*-heterocyclic compounds such as indoles and pyrroles, which are widely occurring functional groups in biologically active molecules. Also included in this section is the hydroamination of allenes and alkenes, as the reaction of these substrates with chiral bimetallic catalysts has been shown to yield the chiral amine products with high enantioselectivity.

A number of reports have demonstrated the utility of monometallic Ir(III) catalysts for the hydroamination of 2-alkynylanilines to yield indole products [98, 99]. In an effort to enhance the efficiency of such catalysts, the bimetallic Ir(III) complex **54** was prepared and investigated as a catalyst for the hydroamination of 2-alkynylanilines (Scheme 20) [100]. During the catalytic cycle it was anticipated that the bridging chlorides of **54** would dissociate to free a vacant coordination site on each metal, through which the alkyne substrate could coordinate. It was hoped that the compact naphthalene scaffold would enforce a close alignment of the two metal fragments and thereby lead to a cooperative enhancement of the reaction rate. While complex **54** was found to be an effective catalyst for this reaction, comparison with an analogous monometallic catalyst (generated in situ by reaction of complex **55** with one equiv. of $AgPF_6$) revealed that no cooperative enhancement of the reaction rate was obtained by the bimetallic system. It is possible that the conformational freedom available to the two Ir fragments upon cleavage of the Ir–μ–Cl bonds prevents a favourable alignment of the metals during catalysis.

Using the bimetallic ruthenium complex **56** as catalyst for the intermolecular hydroamination of phenylacetylene demonstrated that the relative positions of the two Ru fragments must be restricted to achieve effective promotion of the reaction (Scheme 21) [101]. Complex **56** promotes the hydroamination reaction in three steps. Initial protonation of the bridging phenylacetylene unit was shown to yield the isolable vinyl complex **57**, where the vinyl ligand is stabilised by a bimetallic

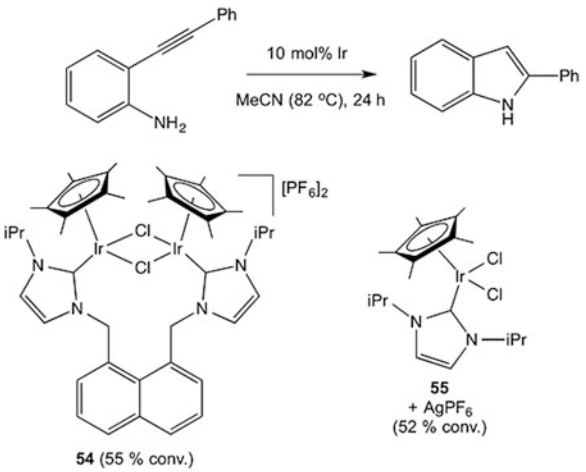

Scheme 20 Ir(III) bi- and monometallic catalysts (**54**, **55**) used for the intramolecular hydroamination reaction

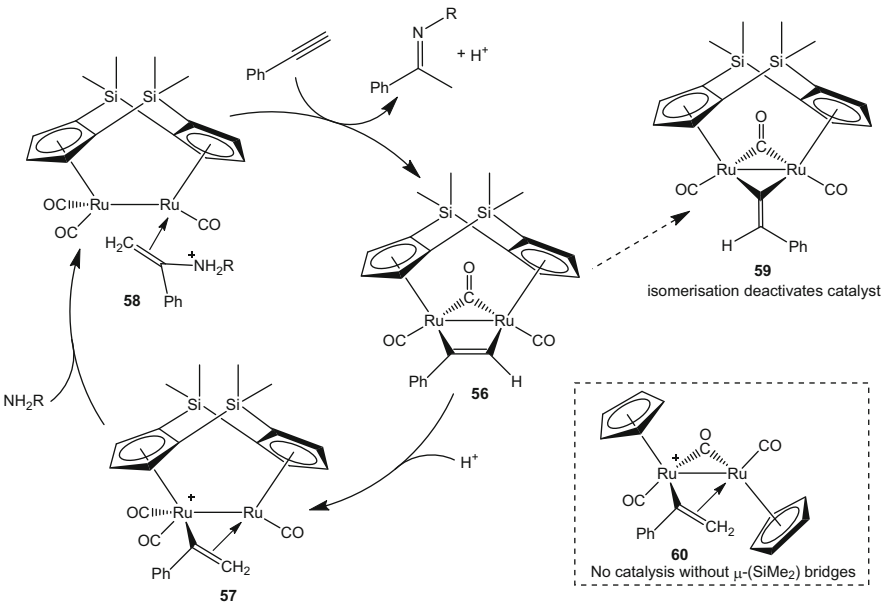

Scheme 21 Bimetallic Ru (**56**) catalysed hydroamination reaction mechanism

$\mu^2-\eta^1:\eta^2$-interaction. Attack of the vinyl group by the amine was proposed to generate the enaminium intermediate **58**, which eliminates the imine product and coordinates phenylacetylene to complete the catalytic cycle. Unfortunately, only a limited number of cycles could be promoted using **56** due to its rapid isomerisation

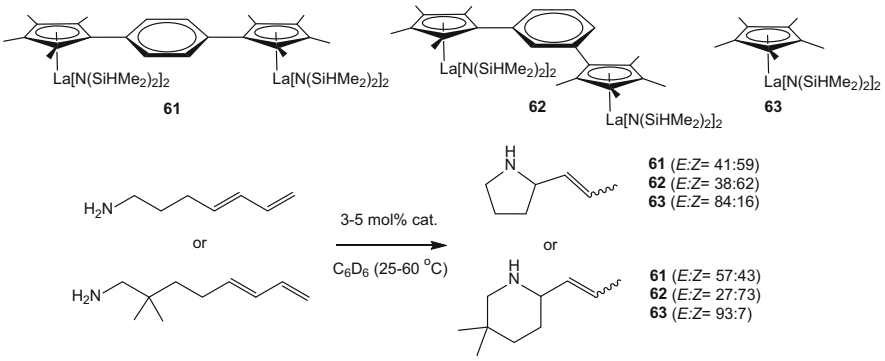

Scheme 22 Intermolecular hydroamination of alkenes using mono- and bimetallic La complexes (**61**–**63**)

to the catalytically inactive vinylidene complex **59**. Crucially the reaction was not catalysed by the bimetallic complex **60**, which is structurally very similar to **57** but contains the cyclopentadienyl ligands oriented in a *trans* arrangement across the Ru–Ru axis [102]. This highlights the importance of the bridging bis(dimethylsilyl) cyclopentadiene ligand in enforcing a catalytically active structure for complex **56**.

The cyclopentadienyl dilanthanum catalysts **61** and **62** that contain a more open bimetallic framework than **56** have also been prepared by Marks and coworkers (Scheme 22) [103]. These complexes were used to catalyse the inter- and intramolecular hydroamination of alkynes, alkenes and allenes. For the most part, no cooperative trends were observed with these catalysts compared to monometallic lanthanum complexes **63** and $La[N(SiHMe_2)_2]_3$, and the steric bulk of the adjacent La containing fragment appeared to dominate what reaction rates were obtained with **61** and **62**. A notable exception to this rule was the hydroamination of amino dienes where a large difference in the *E:Z* selectivity was observed for the bimetallic catalysts **61** and **62** vs the monometallic catalyst **63**. A higher preference for forming the *Z*-isomer products was observed for the bimetallic complexes, with meta-bridged complex **62** exhibiting stronger *Z*-isomer preferences than para-bridged complex **61**. It was suggested that this new selectivity may result from an orientation of the diene by its coordination to the adjacent La centre.

For many bimetallic catalysed systems, the degree of cooperative rate enhancement is highly dependent on a correct alignment of the two complex fragments. A short metal–metal separation is especially important in bimetallic complexes where metal–metal bonding interactions play an essential part in the catalytic cycle. It is particularly important to consider metal–metal bonding interactions in Au-catalysed reactions where the strong aurophilic interaction can often lead to the formation of dinuclear gold species [104]. To investigate the impact of intermetallic distance on the reactivity of bimetallic Au catalysts, Roesky and coworkers synthesised the paracyclophane complexes **64** and **65** (Scheme 23) [105]. In complex **65** the two gold atoms are forced into close proximity resulting in a short Au–Au distance consistent with an intramolecular aurophilic interaction. In contrast the

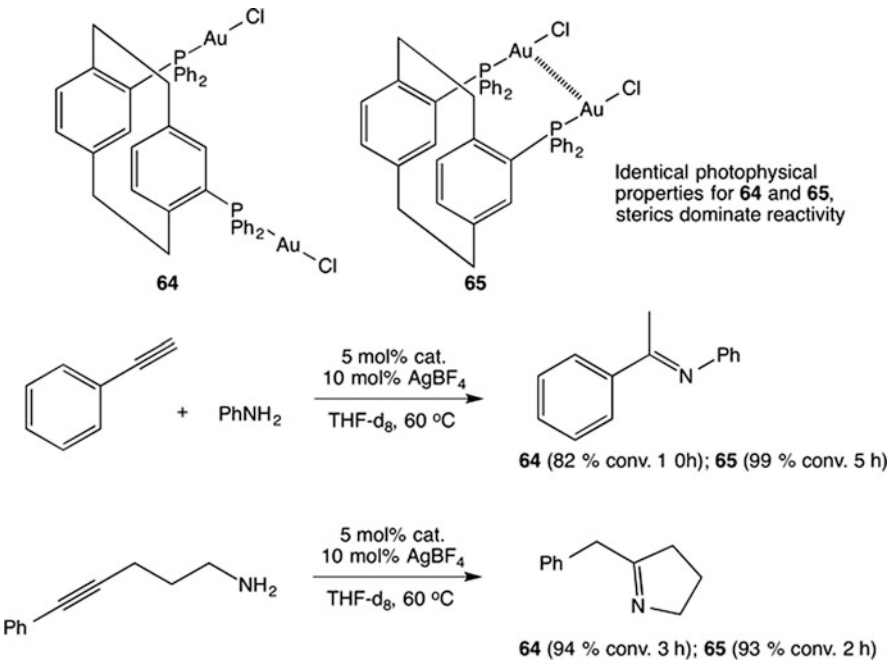

Scheme 23 Inter- and intramolecular hydroamination reaction of alkynes catalysed by the bimetallic Au(I) complexes **64** and **65**

large separation between Au atoms in **64** excludes any Au–Au contact. Both complexes were found to efficiently catalyse the *inter*molecular hydroamination of phenylacetylene and the *intra*molecular hydroamination of 1-phenyl-1-pentyn-5-amine. While complex **65** was found to be a slightly more efficient catalyst than complex **64**, the similar photophysical properties of both complexes suggested this difference in reactivity was mostly due to steric effects.

5.5 *Chiral Bimetallic Catalysts for Hydroamination*

While effective bimetallic catalyst design has the potential to lead to an enhancement of the reaction rate, the use of chiral bimetallic catalysts has also been explored to enhance the enantioselectivity of a reaction. Such bimetallic chiral induction is excellently demonstrated by the use of digold catalysts for the hydroamination of prochiral substrates such as allenes and alkenes [59]. The bimetallic Au catalyst **66**, for example, was shown to be an effective catalyst for the hydroamination of amino-allenes in the presence of a silver salt activator (Scheme 24) [106]. The highest enantioselective induction for this reaction was achieved with a 1:1 ratio of $AgBF_4$ to **66** (51% *ee*) suggesting that the monocationic

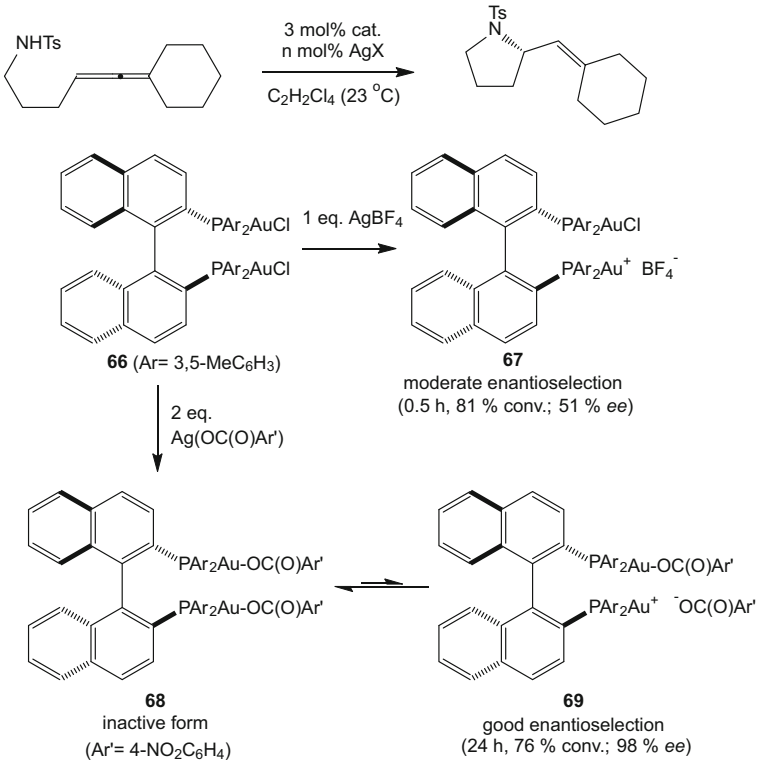

Scheme 24 Different reactivities and selectivities of chiral bimetallic Au complexes used in the enantioselective hydroamination reaction of amino-allenes

species **67** was the active catalyst generated in situ. This would indicate that the catalytic cycle proceeds at only one metal centre and that the second metal provides a steric influence to control the selectivity of the reaction. To further improve the catalyst, two equiv. of a silver salt activator containing the weakly coordinating *p*-nitrobenzoate anion were investigated. It was hypothesised that under these conditions the catalytically active monocationic species **69** would exist in equilibrium with the inactive coordinatively saturated form **68** and that the larger *p*-nitrobenzoate ligand would provide a more sterically demanding chiral environment for the catalyst. Indeed enantioselectivites of up to 98% *ee* were obtained for this reaction using 3 mol% of **66** and 6 mol% Ag(*p*-nitrobenzoate), although longer reaction times were observed due to a lower effective concentration of the catalytically active monocationic species. Note that the chirality of the binaphthyl ligand in complex **66** is locked in place due to restricted rotation of the aryl–aryl bond and that the helical twist of the binaphthyl scaffold prevents formation of an aurophilic interaction between the two Au centres [107].

An alternative approach to chiral complex design has been explored that utilises biphenyl ligands that are sufficiently flexible to allow intramolecular Au–Au

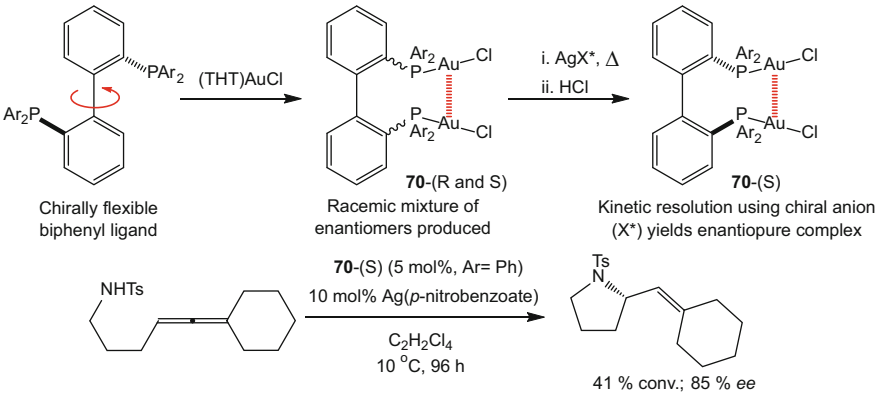

Scheme 25 Kinetic resolution of the Au(I) bimetallic complex **70**-(*R* and *S*) to form **70**-(*S*) which was used in the enantioselective hydroamination of amino-allenes

bonding within their bimetallic complexes. Biphenyl ligands are not inherently chiral due to free rotation of the aryl–aryl bond; however, upon coordination to AuCl the aurophilic interaction locks the chirality of the ligand in place (**70**-*R* and *S*, Scheme 25). Enantiopure digold complexes have been isolated from the resulting racemic mixture via kinetic resolution with a chiral anion [108]. The digold complex **70**-(*S*) (R = Ph) was found to be an effective catalyst for the enantioselective hydroamination of amino-allenes, achieving formation of the amine product in 85% *ee*.

In the hydroamination of *N*-alkenyl ureas, it was shown that the Au–Au bond present in biphenyl complexes such as **70** greatly increased the enantioselectivity of the catalyst relative to binaphthyl complexes such as **66**, which do not contain a Au–Au interaction (Scheme 26a) [109]. For example, an enantiomeric excess of 42% was achieved using catalyst **70**-(*S*) (R = 3,5-$Me_2C_6H_3$), compared to an enantiomeric excess of 17% obtained with catalyst **66**-(*S*). The intramolecular Au–Au bond may enhance the selectivity of **68** by pulling the aryl groups on the phosphine ligands closer to the reaction centre, thereby facilitating discrimination of the diastereotopic intermediates [110]. The bimetallic design of complexes **66** and **70** was also found to dramatically increase the reactivity of these catalysts for the hydroamination of alkenyl ureas compared to the monometallic catalyst **71** [111]. This would indicate a synergistic activation of the substrate by both metals in addition to the stereogenic directing influence. Note the optimal reaction conditions for the hydroamination of *N*-alkenyl ureas using **70** required the use of two molar equivalents of silver triflate to activate the catalyst, which would result in a dicationic catalyst species being generated in situ. It was therefore proposed that both Au centres of **68** actively participate in the catalytic cycle, possibly through coordination of one gold centre to the alkene and coordination of the second gold centre to the urea carbonyl (Scheme 26b). Not only would this accelerate the reaction by bringing the two reacting moieties into close proximity, but the Brønsted acidity of the urea would be increased by its coordination to the

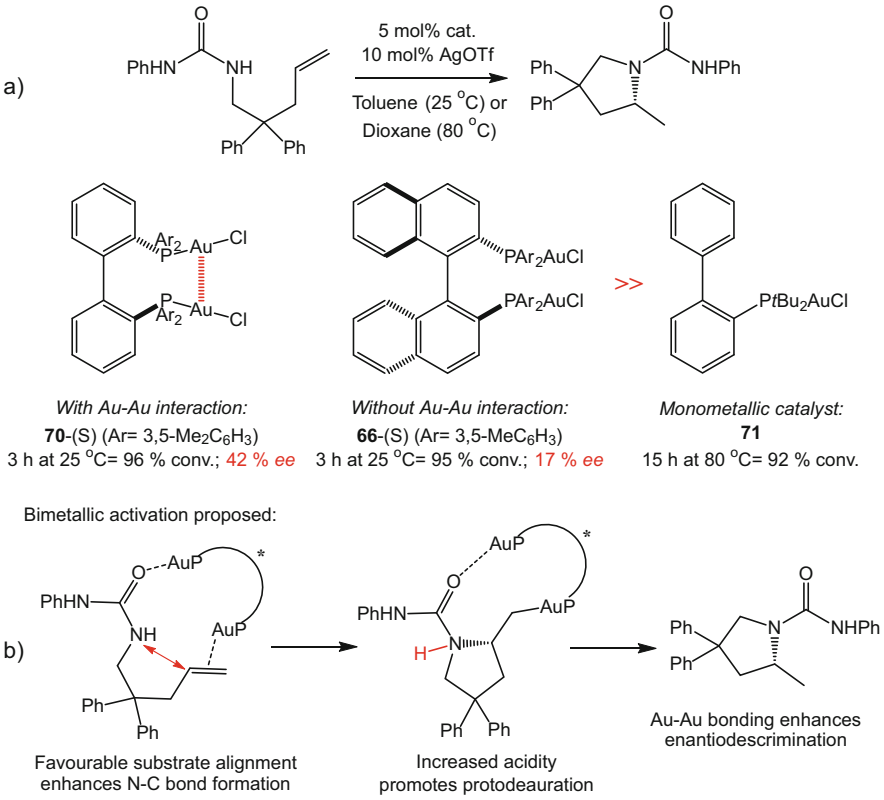

Scheme 26 (**a**) Enhanced stereoselectivity for the hydroamination reaction using the chiral bimetallic Au(I) complex (**70**-(*S*)) containing an Au–Au interaction compared to the non-interacting bi- and monometallic Au complexes (**66** and **71**), and (**b**) proposed bimetallic Au(I) activation of the substrate through favorable alignment

electrophilic Au atom, which would facilitate the final protodeauration step of the catalytic cycle [109].

Attempts to utilise a chiral ligand scaffold to enhance the enantioselectivity of bimetallic Zn complexes have also been explored [112]. The efficiency of the bimetallic complex **72**, which contains a (*S,S*)-1,2-diphenylethane scaffold bridging the two alkyl zinc centres, as a catalyst for the intramolecular hydroamination of aminoalkenes was investigated (Scheme 27). Unfortunately, very poor enantioselectivity (<10% *ee*) was obtained for this reaction. Unrestricted rotation about the C–C bond of the ethane scaffold could lead to a large separation between the two Zn atoms, decreasing the potential for both metals to interact with the substrate. The vigorous reaction conditions (120°C) would also decrease discrimination between similar diastereomeric intermediates.

In an effort to increase the potential for enantioinduction in the hydroamination of amino alkenes, bimetallic complexes of Zn (**73**) and Mg (**74**) have been prepared

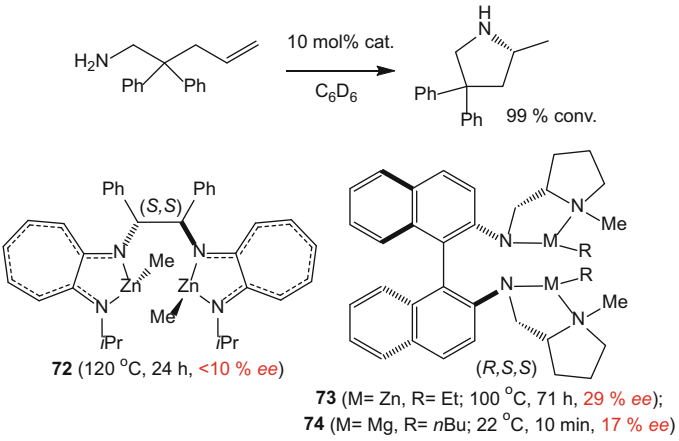

Scheme 27 Intramolecular hydroamination reaction of alkenes using chiral bimetallic Zn and Mg complexes

that contain three chiral centres (Scheme 27) [113]. In addition to the chiral naphthalene scaffold, each metal centre in **73** and **74** is also coordinated by a chiral proline ligand group. The alkyl zinc complex **73** was able to achieve an enantioselectivity of 29% *ee* for the hydroamination reaction, although prolonged reaction times (71 h) and high temperature (100°C) were required to obtain complete conversion. The analogous Mg catalyst **74** was found to be significantly more active achieving 100% conv. within 10 min at 22°C; however, poorer enantioselectivities were obtained (14% *ee*, R′ = Ph). The low chiral induction observed for catalyst **72** was explained by a facile ligand exchange reaction (Schlenk equilibria) and/or protolytic cleavage of the Mg–N bond upon addition of the substrate.

6 Conclusions

The breadth of bimetallic catalyst designs covered above highlights the many different approaches to taking advantage of two metal centres to achieve cooperative alkyne activation. Mechanistic pathways where both metals coordinate and activate the alkyne substrate have been characterised. Nearly all of the bimetallic alkyne coordination modes described in Fig. 1 have been utilised for such concerted activation processes, often with multiple bimetallic coordination modes participating in the catalytic cycle, as well as in the catalyst deactivation steps. Frequently these bimetallic alkyne assemblies involve metal–metal bonding interactions that can strongly influence the electronic properties of the metals and may also assist in the formal transfer of electrons between metals during catalysis.

In using bimetallic catalysts for promoting reactions of alkynes, where only one metal centre is involved in coordination of the alkyne, the role of the second metal

in accelerating the reaction is not always clear. The potential for the second metal to coordinate other functional groups within the substrate and thereby provide a favourable structural or electronic influence on the reaction has been postulated. Equally important is the steric environment created by the bimetallic structure, especially where an enhancement of the reaction selectivity is observed.

No matter what function the bimetallic catalyst fulfils, two key trends of catalyst design emerge from the above examples: (1) a relatively constrained catalyst structure is often essential to ensure a beneficial interaction of both metals; this most likely helps overcome the entropic penalty associated with creating an ordered bimetallic transition state during the catalytic cycle; (2) for catalysts that do not contain any prearranged metal–metal bonding or bridging atom interactions, a relatively short intermetallic distance also appears necessary. Clearly, for many of the catalysts described here, much work remains to understand exactly how the bimetallic structure enhances the catalysts performance.

References

1. Wilcox DE (1996) Chem Rev 96:2435. doi:10.1021/cr950043b
2. van den Beuken EK, Feringa BL (1998) Tetrahedron 54:12985. doi:10.1016/S0040-4020(98)00319-6
3. Gavrilova AL, Bosnich B (2004) Chem Rev 104:349. doi:10.1021/cr020604g
4. Shibasaki M, Matsunaga S (2006) Chem Soc Rev 35:269. doi:10.1039/B506346A
5. Delferro M, Marks TJ (2011) Chem Rev 111:2450. doi:10.1021/cr1003634
6. Park J, Hong S (2012) Chem Soc Rev 41:6931. doi:10.1039/C2CS35129C
7. Bratko I, Gomez M (2013) Dalton Trans 42:10664. doi:10.1039/C3DT50963J
8. Hashmi AS (2003) Gold Bull 36:3. doi:10.1007/BF03214859
9. Beller M, Seayad J, Tillack A, Jiao H (2004) Angew Chem Int Ed 43:3368. doi:10.1002/anie.200300616
10. Omae I (2008) Appl Organomet Chem 22:149. doi:10.1002/aoc.1367
11. Chinchilla R, Nájera C (2013) Chem Rev 114:1783. doi:10.1021/cr400133p
12. Gervasio G, Sappa E, Secco A (2014) J Organomet Chem 751:111. doi:10.1016/j.jorganchem.2013.08.046
13. Galan BR, Rovis T (2009) Angew Chem Int Ed 48:2830. doi:10.1002/anie.200804651
14. Chopade PR, Louie J (2006) Adv Synth Catal 348:2307. doi:10.1002/adsc.200600325
15. Schore NE (1988) Chem Rev 88:1081. doi:10.1021/cr00089a006
16. Matsuura M, Fujihara T, Kakeya M, Sugaya T, Nagasawa A (2013) J Organomet Chem 745–746:288. doi:10.1016/j.jorganchem.2013.07.035
17. Bonifaci C, Ceccon A, Gambaro A, Ganis P, Mantovani L, Santi S, Venzo A (1994) J Organomet Chem 475:267. doi:10.1016/0022-328X(94)84031-8
18. Yan H, Beatty AM, Fehlner TP (2002) Organometallics 21:5029. doi:10.1021/om0205694
19. Yan H, Beatty AM, Fehlner TP (2001) Angew Chem Int Ed 40:4498. doi:10.1002/1521-3773(20011203)40:23<4498::AID-ANIE4498>3.0.CO;2-3
20. Ohshita J, Furumori K, Matsuguchi A, Ishikawa M (1990) J Org Chem 55:3277. doi:10.1021/jo00297a054
21. Trost BM, Kottirsch G (1990) J Am Chem Soc 112:2816. doi:10.1021/ja00163a062
22. Hidai M, Mizobe Y (2005) Can J Chem 83:358. doi:10.1139/v05-016
23. Qü J-P, Masui D, Ishii Y, Hidai M (1998) Chem Lett 27:1003. doi:10.1246/cl.1998.1003

24. Yi CS, Liu N, Rheingold AL, Liable-Sands LM (1997) Organometallics 16:3910. doi:10.1021/om970366t
25. Slugovc C, Mereiter K, Zobetz E, Schmid R, Kirchner K (1996) Organometallics 15:5275. doi:10.1021/om9607816
26. Baratta W, Herrmann WA, Rigo P, Schwarz J (2000) J Organomet Chem 593–594:489. doi:10.1016/S0022-328X(99)00435-0
27. Hidai M, Mizobe Y, Matsuzaka H (1994) J Organomet Chem 473:1. doi:10.1016/0022-328X(94)80099-5
28. Takagi Y, Matsuzaka H, Ishii Y, Hidai M (1997) Organometallics 16:4445. doi:10.1021/om970307f
29. Matsuzaka H, Takagi Y, Ishii Y, Nishio M, Hidai M (1995) Organometallics 14:2153. doi:10.1021/om00005a010
30. Matsuzaka H, Ichikawa K, Ishioka T, Sato H, Okubo T, Ishii T, Yamashita M, Kondo M, Kitagawa S (2000) J Organomet Chem 596:121. doi:10.1016/S0022-328X(99)00608-7
31. Gao Y, Puddephatt RJ (2003) Inorg Chim Acta 350:101. doi:10.1016/S0020-1693(02)01498-6
32. Kuncheria J, Mirza HA, Vittal JJ, Puddephatt RJ (1999) Inorg Chem Commun 2:197. doi:10.1016/S1387-7003(99)00047-7
33. Kuncheria J, Mirza HA, Vittal JJ, Puddephatt RJ (2000) J Organomet Chem 593–594:77. doi:10.1016/S0022-328X(99)00432-5
34. Detz RJ, Hiemstra H, van Maarseveen JH (2009) Eur J Org Chem 2009:6263. doi:10.1002/ejoc.200900877
35. Nishibayashi Y, Wakiji I, Hidai M (2000) J Am Chem Soc 122:11019. doi:10.1021/ja0021161
36. Nishibayashi Y, Wakiji I, Ishii Y, Uemura S, Hidai M (2001) J Am Chem Soc 123:3393. doi:10.1021/ja015670z
37. Nishibayashi Y, Inada Y, Hidai M, Uemura S (2003) J Am Chem Soc 125:6060. doi:10.1021/ja035106j
38. Nishibayashi Y, Inada Y, Hidai M, Uemura S (2002) J Am Chem Soc 124:7900. doi:10.1021/ja026168x
39. Nishibayashi Y, Yoshikawa M, Inada Y, Hidai M, Uemura S (2002) J Am Chem Soc 124:11846. doi:10.1021/ja027023t
40. Ammal SC, Yoshikai N, Inada Y, Nishibayashi Y, Nakamura E (2005) J Am Chem Soc 127:9428. doi:10.1021/ja050298z
41. Golas PL, Matyjaszewski K (2010) Chem Soc Rev 39:1338. doi:10.1039/B901978M
42. Fournier D, Hoogenboom R, Schubert US (2007) Chem Soc Rev 36:1369. doi:10.1039/B700809K
43. Kolb HC, Sharpless KB (2003) Drug Discov Today 8:1128. doi:10.1016/S1359-6446(03)02933-7
44. Fazio F, Bryan MC, Blixt O, Paulson JC, Wong C-H (2002) J Am Chem Soc 124:14397. doi:10.1021/ja020887u
45. Bodine KD, Gin DY, Gin MS (2004) J Am Chem Soc 126:1638. doi:10.1021/ja039374t
46. Seo TS, Li Z, Ruparel H, Ju J (2002) J Org Chem 68:609. doi:10.1021/jo026615r
47. Zhou Z, Fahrni CJ (2004) J Am Chem Soc 126:8862. doi:10.1021/ja049684r
48. Jin T, Kamijo S, Yamamoto Y (2004) Eur J Org Chem 2004:3789. doi:10.1002/ejoc.200400442
49. Worrell BT, Malik JA, Fokin VV (2013) Science 340:457
50. Chan TR, Hilgraf R, Sharpless KB, Fokin VV (2004) Org Lett 6:2853. doi:10.1021/ol0493094
51. Donnelly PS, Zanatta SD, Zammit SC, White JM, Williams SJ (2008) Chem Commun 2459. 10.1039/B719724A
52. Berg R, Straub J, Schreiner E, Mader S, Rominger F, Straub BF (2012) Adv Synth Catal 354:3445. doi:10.1002/adsc.201200734
53. Rudolph M, Hashmi ASK (2012) Chem Soc Rev 41:2448. doi:10.1039/C1CS15279C

54. Li Z, Brouwer C, He C (2008) Chem Rev 108:3239. doi:10.1021/cr0684341
55. Gómez-Suárez A, Nolan SP (2012) Angew Chem Int Ed 51:8156. doi:10.1002/anie.201203587
56. Grirrane A, Garcia H, Corma A, Álvarez E (2011) ACS Catal 1:1647. doi:10.1021/cs2004278
57. Hashmi ASK, Braun I, Nösel P, Schädlich J, Wieteck M, Rudolph M, Rominger F (2012) Angew Chem Int Ed 51:4456. doi:10.1002/anie.201109183
58. Cheong PH-Y, Morganelli P, Luzung MR, Houk KN, Toste FD (2008) J Am Chem Soc 130:4517. doi:10.1021/ja711058f
59. Wang Y-M, Lackner AD, Toste FD (2013) Acc Chem Res 47:889. doi:10.1021/ar400188g
60. Sugihara T, Yamaguchi M, Nishizawa M (2001) Chem Eur J 7:1589. doi:10.1002/1521-3765(20010417)7:8<1589::AID-CHEM15890>3.0.CO;2-1
61. Keun Chung Y (1999) Coord Chem Rev 188:297. doi:10.1016/S0010-8545(99)00032-6
62. Khand IU, Knox GR, Pauson PL, Watts WE (1971) J Chem Soc D Chem Commun 36a. 10.1039/C2971000036A
63. Khand IU, Knox GR, Pauson PL, Watts WE, Foreman MI (1973) J Chem Soc Perkin Trans 1:977. doi:10.1039/P19730000977
64. Khand IU, Knox GR, Pauson PL, Watts WE (1973) J Chem Soc Perkin Trans 1:975. doi:10.1039/P19730000975
65. Yamanaka M, Nakamura E (2001) J Am Chem Soc 123:1703. doi:10.1021/ja005565+
66. Mukai C, Uchiyama M, Hanaoka M (1992) J Chem Soc Chem Commun 1014. 10.1039/C39920001014
67. Rutherford DT, Christie SDR (1998) Tetrahedron Lett 39:9805. doi:10.1016/S0040-4039(98)02178-9
68. Lim DSW, Anderson EA (2012) Synthesis 44:983. doi:10.1055/s-0031-1289729
69. Ojima I, Ingallina P, Donovan RJ, Clos N (1991) Organometallics 10:38. doi:10.1021/om00047a021
70. Ojima I, Donovan RJ, Eguchi M, Shay WR, Ingallina P, Korda A, Zeng Q (1993) Tetrahedron 49:5431. doi:10.1016/S0040-4020(01)87260-4
71. Ojima I, Zhaoyang L, Donovan RJ, Ingallina P (1998) Inorg Chim Acta 270:279. doi:10.1016/S0020-1693(97)05855-6
72. Yoshikai N, Yamanaka M, Ojima I, Morokuma K, Nakamura E (2006) Organometallics 25:3867. doi:10.1021/om060478x
73. Osakada K (2000) J Organomet Chem 611:323. doi:10.1016/S0022-328X(00)00492-7
74. Matsuda I, Fukuta Y, Tsuchihashi T, Nagashima H, Itoh K (1997) Organometallics 16:4327. doi:10.1021/om970549f
75. Biffis A, Conte L, Tubaro C, Basato M, Aronica LA, Cuzzola A, Caporusso AM (2010) J Organomet Chem 695:792. doi:10.1016/j.jorganchem.2009.12.018
76. Doyle MP, Shanklin MS (1994) Organometallics 13:1081. doi:10.1021/om00016a012
77. Fleming I, Dunoguès J, Smithers R (2004) Organic reactions. Wiley, Hoboken
78. Chou SSP, Kuo HL, Wang CJ, Tsai CY, Sun CM (1989) J Org Chem 54:868. doi:10.1021/jo00265a028
79. Ojima I, Kumagai M, Nagai Y (1974) J Organomet Chem 66:C14. doi:10.1016/S0022-328X(00)93873-7
80. Mas-Marzá E, Poyatos M, Sanaú M, Peris E (2004) Inorg Chem 43:2213. doi:10.1021/ic035317p
81. Andavan GTS, Bauer EB, Letko CS, Hollis TK, Tham FS (2005) J Organomet Chem 690:5938. doi:10.1016/j.jorganchem.2005.07.088
82. Huckaba AJ, Hollis TK, Howell TO, Valle HU, Wu Y (2012) Organometallics 32:63. doi:10.1021/om3008037
83. Jiménez MV, Pérez-Torrente JJ, Bartolomé MI, Gierz V, Lahoz FJ, Oro LA (2007) Organometallics 27:224. doi:10.1021/om700728a
84. Teles JH, Brode S, Chabanas M (1998) Angew Chem Int Ed 37:1415. doi:10.1002/(SICI)1521-3773(19980605)37:10<1415::AID-ANIE1415>3.0.CO;2-N
85. Zhdanko A, Maier ME (2014) Chem Eur J 20:1918. doi:10.1002/chem.201303795
86. Zhdanko A, Maier ME (2013) Chem Eur J 19:3932. doi:10.1002/chem.201204491

87. Zhang Z, Widenhoefer RA (2007) Angew Chem Int Ed 46:283. doi:10.1002/anie.200603260
88. Ho JHH, Hodgson R, Wagler J, Messerle BA (2010) Dalton Trans 39:4062. doi:10.1039/B926773E
89. Ho JHH, Choy SWS, Macgregor SA, Messerle BA (2011) Organometallics 30:5978. doi:10.1021/om2007826
90. Timerbulatova MG, Gatus MRD, Vuong KQ, Bhadbhade M, Algarra AG, Macgregor SA, Messerle BA (2013) Organometallics 32:5071. doi:10.1021/om4005059
91. Choy SWS, Page MJ, Bhadbhade M, Messerle BA (2013) Organometallics 32:4726. doi:10.1021/om400613b
92. Messerle BA, Vuong KQ (2007) Organometallics 26:3031. doi:10.1021/om061106r
93. Elgafi S, Field LD, Messerle BA (2000) J Organomet Chem 607:97. doi:10.1016/S0022-328X(00)00233-3
94. Chan DMT, Marder TB, Milstein D, Taylor NJ (1987) J Am Chem Soc 109:6385. doi:10.1021/ja00255a025
95. Chapuis C, Jacoby D (2001) Appl Catal A Gen 221:93. doi:10.1016/S0926-860X(01)00798-0
96. Ho JHH, Black DSC, Messerle BA, Clegg JK, Turner P (2006) Organometallics 25:5800. doi:10.1021/om060591n
97. Cheung K-C, Wong W-L, So M-H, Zhou Z-Y, Yan S-C, Wong K-Y (2013) Chem Commun 49:710. doi:10.1039/C2CC38454J
98. Li X, Chianese AR, Vogel T, Crabtree RH (2005) Org Lett 7:5437. doi:10.1021/ol052186i
99. Gray K, Page MJ, Wagler J, Messerle BA (2012) Organometallics 31:6270. doi:10.1021/om300550k
100. Ogata K, Nagaya T, Fukuzawa S (2010) J Organomet Chem 695:1675. doi:10.1016/j.jorganchem.2010.04.006
101. Klein DP, Ellern A, Angelici RJ (2004) Organometallics 23:5662. doi:10.1021/om049377u
102. Dyke AF, Knox SAR, Morris MJ, Naish PJ (1983) J Chem Soc Dalton Trans 1417. 10.1039/DT9830001417
103. Yuen HF, Marks TJ (2009) Organometallics 28:2423. doi:10.1021/om9000023
104. Schmidbaur H, Schier A (2008) Chem Soc Rev 37:1931. doi:10.1039/B708845K
105. Sarcher C, Lühl A, Falk FC, Lebedkin S, Kühn M, Wang C, Paradies J, Kappes MM, Klopper W, Roesky PW (2012) Eur J Inorg Chem 2012:5033. doi:10.1002/ejic.201200751
106. LaLonde RL, Sherry BD, Kang EJ, Toste FD (2007) J Am Chem Soc 129:2452. doi:10.1021/ja068819l
107. Hashmi ASK, Hamzić M, Rominger F, Bats JW (2009) Chem Eur J 15:13318. doi:10.1002/chem.200901695
108. Aikawa K, Kojima M, Mikami K (2009) Angew Chem Int Ed 48:6073. doi:10.1002/anie.200902084
109. Kojima M, Mikami K (2012) Synlett 2012:57. doi:10.1055/s-0031-1289875
110. Wang M-Z, Zhou C-Y, Guo Z, Wong EL-M, Wong M-K, Che C-M (2011) Chem Asian J 6:812. doi:10.1002/asia.201000651
111. Bender CF, Widenhoefer RA (2006) Chem Commun 4143. 10.1039/B608638A
112. Meyer N, Roesky PW (2008) Organometallics 28:306. doi:10.1021/om800858t
113. Horrillo-Martínez P, Hultzsch KC (2009) Tetrahedron Lett 50:2054. doi:10.1016/j.tetlet.2009.02.069

Top Organomet Chem (2016) 59: 139–186
DOI: 10.1007/3418_2015_161

Published online: 21 November 2015

"Early–Late" Heterobimetallic Catalysis and Beyond

Ewen Bodio, Michel Picquet, and Pierre Le Gendre

Abstract By combining an ever-increasing number of catalysts or catalytic functions, cooperative catalysis is a research area that grows fast. In the field, "early–late" heterobimetallic complexes are rather old objects but they still continue to fascinate chemists because of their latent reactivity. After a brief and concise overview of cooperative catalysis, this review focuses on "early–late" heterobimetallic complexes that were used in catalysis over the last decades. Examples of dual catalysis using early and late metal partners are also described. This chapter ends with an opening towards therapeutic applications of "early–late" heterobimetallic complexes.

Keywords Bifunctional catalysis • Bimetallic complexes • Cooperative catalysis • Dual catalysis • "Early–late" heterobimetallic complexes

Contents

E. Bodio, M. Picquet, and P. Le Gendre (✉)
Institut de Chimie Moléculaire de l'Université de Bourgogne (ICMUB, UMR CNRS 6302), Univ. Bourgogne Franche-Comté, Bât. Sciences de Mirande, Avenue Alain Savary, BP 47870, 21078 Dijon, Cedex, France
e-mail: pierre.le-gendre@u-bourgogne.fr

1 Introduction

Nowadays, homogeneous catalysis has become an indispensable tool for chemists by the variety and selectivity of the reactions it allows [1]. However, the economic development of our society in the context of sustainability pushes the chemists to find novel catalysts more and more efficient able to create high value-added products from abundant and environmentally benign substrates and reagents (or even from wastes) at the minimum energy cost. A source of inspiration for chemists can be found in enzymes which often surpass the most recent man-made catalysts both in activity and selectivity using sustainable substrates and sources of energy [2]. While homogeneous catalysis predominantly involves only one catalytic center which is responsible for the whole transformation of the substrate(s) into the product(s), catalytic sites in enzymes are more sophisticated and are most of the time constituted by two or more catalytic centers or functions which participate together in the reaction [3]. In consequence, it is rather clear that by taking example from nature or by following the intuition that there is strength in numbers, one can hypothesize that the combination of catalysts or of catalytic functions within the same entity constitutes a promising strategy for improving or discovering chemical reactions.

Before focusing on the main topic of this chapter that concerns "early–late heterobimetallic complexes in catalysis," we will present, in a first part, representative examples of cooperative catalysis besides "early–late" heterobimetallic catalysts, which provide some information about which type of catalysts or catalytic functions have been combined to date and illustrate the different cooperative effects that have been observed. The second part is concerned with "early–late" heterobimetallic catalysis and encompasses the period from about 1988 to June 2015. It follows two reviews by Kalck [4] and Thomas [5] which cover the periods 1988–1997 and 2000–2011, respectively, and classified the data according to the catalytic reaction involved. We have chosen to look at this topic from another perspective and categorized the data by group of the late transition metal which often governs the catalytic reaction, by element and finally by the catalytic reaction involved. The reader will thus notice that some bimetallic combinations are much less represented or nonexistent which raises the crucial question of catalyst compatibility. Since the terms "early" and "late" are not strictly defined in the literature, we will first focus on combinations from groups 4 and 5 for early transition metals and groups 8, 9, and 10 for late transition metals. Consequently, the second part of this chapter begins with catalytic reactions promoted by (group 8/groups 4–5) bimetallic complexes followed by (group 9/groups 4–5) and (group 10/groups 4–5) combinations. The third part of this chapter is devoted to dual catalysis from early and late metal complexes and may constitute a source of inspiration for further design of new early–late heterobimetallic catalysts. The last part of this chapter is

dedicated to an overview of another promising use of "early–late heterometallic complexes": medicine and more precisely design of new anticancer agents.

2 Cooperative Catalysis Besides "Early–Late" Heterobimetallic Catalysis

Since the last decades, chemists have described a huge variety of multi-catalytic systems and cooperative effects [6]. First of all, it has been shown that cooperative effects can appear by combining two catalytic functions within the same molecule (bifunctional catalysis) [7] or in two separate molecules (cooperative dual catalysis) [8, 9]. Both can participate to the same catalytic cycle by activating together the same substrate (double-activation catalysis) or its own substrate. The two catalytic centers can also activate simultaneously different substrates in two directly coupled catalytic reactions for giving a product (synergistic catalysis) [10]. Tandem reactions have been also described [11, 12]. In that case, the two catalytic centers operate consecutively in two independent catalytic cycles, the second catalytic cycle using the product of the first one as an intermediate and converts it as final product. The second catalytic function may also not interact with the substrates but contributes to the stability of the active metal center and acts as redox partner (restorative catalysis) [8].

2.1 Bifunctional Organocatalysis, Frustrated Lewis Pairs (FLP), and Organo–Metal Cooperative Catalysis

If we first consider purely organic systems, one can mention the asymmetric reduction of ketones with borane promoted by a chiral oxazaborolidine **1** developed by Corey, Bakshi, and Shibata (CBS reduction, Scheme 1) [13, 14]. In this system, the nitrogen atom of the oxazaborolidine serves as Lewis base and coordinates BH_3 thus improving its nucleophilicity, while the endocyclic boron atom acts as the Lewis acid and activates the ketone toward the reduction. This seminal work constitutes an early example of metal-free catalysis and shows that cooperative effects can emerge from ambiphilic Lewis acid/base catalytic system.

However, mutual affinity between Lewis acid and Lewis base may give rise to self-quenching which precludes further reactivity and makes the development of

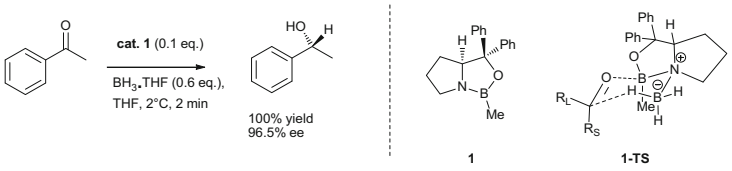

Scheme 1 Corey–Bakshi–Shibata catalyst

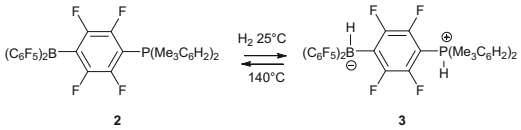

Scheme 2 Reversible activation of H_2 by a nonmetal system

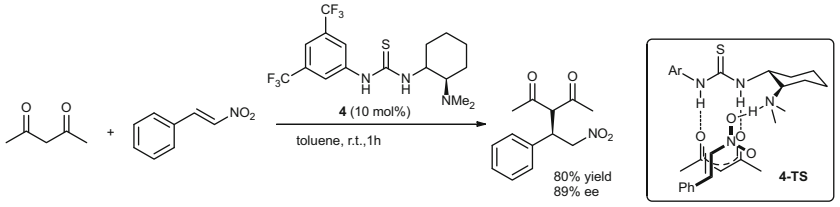

Scheme 3 Addition of acetylacetone to *trans*-β-nitrostyrene by Takemoto's catalyst

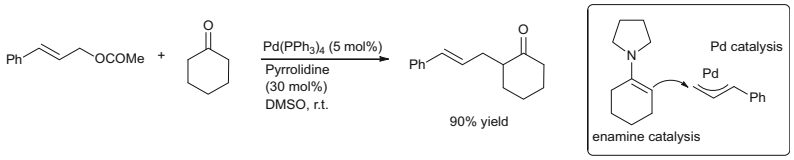

Scheme 4 Catalytic intermolecular α-allylic alkylation of cyclohexanone

analogous catalytic systems challenging. In 2006, a step was taken with the synthesis of a phosphane borane **2** able to realize the ambiphilic activation of H_2 when Stephan has introduced for the first time the notion of Frustrated Lewis Pairs (FLPs) (Scheme 2) [15]. In such systems, steric constraints preclude the formation of a stable unhindered adduct *via* the formation of a formal dative bond giving rise to latent reactivity. In the last years, such FLPs have been extensively studied and have been shown to be able to activate reversibly small molecules (H_2, CO_2, alkenes, alkynes, etc.), to promote metal-free hydrogenation and to reduce carbon dioxide [16].

The roles of the catalytic functions are not necessarily opposite or limited to Lewis acid/base pairs. For example, amine thiourea derivatives like Takemoto's catalyst **4** merge the hydrogen bond donor capability of the thiourea moiety with Brönsted base functionality of the amine function and revealed itself particularly efficient organocatalysts for Michael reactions of various 1,3-dicarbonyl compounds with nitroolefins (Scheme 3) [17–19].

Given recent developments in organocatalysis and the versatility of metal-based catalysis, it is not surprising that chemists have been tempted to combine the two. One can cite the first combination of aminocatalysis and palladium-catalyzed allylic substitution described by Cordova's group which promotes the direct catalytic intermolecular α-allylic alkylation of aldehydes and cyclic ketones (Scheme 4) [20]. Since this pioneering work, almost all types of organocatalysts have been combined with transition metal-based catalyst, and novel or more efficient transformations were discovered [21, 22]. This research area is rapidly expanding and further highlights the potential of catalysts combination.

2.2 Metal–Ligand Bifunctional Catalysis

Focusing on transition metal catalysis and on results which have paved the ways of the above recent developments, key milestones in this area date when Ito [23] and later Shibasaki [24] and Noyori [25] have introduced the concept of metal–ligand bifunctional catalysis and shown that the ligand may interact directly with the substrates in a cooperative manner with the metal. Ruthenium catalyst **5** bearing *N*-sulfonylated 1,2-diamido moiety as chiral ligand developed by Noyori and Ikariya is a representative example of a multicenter catalysts (Scheme 5). In these systems, the diamido ligand cooperates with the metal for the asymmetric transfer hydrogenation of ketones. First, as a Brönsted base, it deprotonates the secondary alcohol which is used as hydrogen source to produce hydrido(amine) complex, and then, as hydrogen bond donor, it coordinates and activates a molecule of ketone [26].

Shibasaki et al. have described heterobi- and polymetallic catalytic systems combining a Lewis acid and Brönsted bases constituted by one cation (Al^{3+}, La^{3+}, etc.), one or three cations (Li^{+}, Na^{+}, etc.), and two or three bridging binaphtolates. The panel of asymmetric reactions catalyzed by such systems is impressive and leads to adducts in very good yields and very high optical purities (for reviews, see [27–29]). For example, in the asymmetric conjugate addition of malonates to cyclic enones promoted by the heterobimetallic Al/Li complex **6**, the Brönsted base generates in situ the nucleophile, while the Lewis acid activates the electrophile, thus facilitating the effective coupling of the substrates in a stereoselective manner (Scheme 6) [30]. Shibasaki's group also described particularly efficient chiral titanium catalyst **7** bearing a phosphane oxide function for the asymmetric

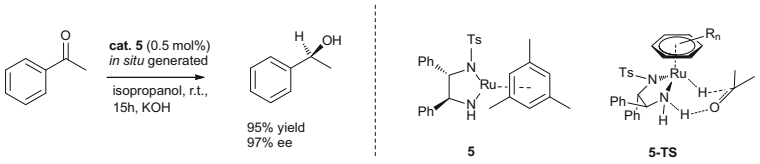

Scheme 5 Noyori's catalyst for asymmetric hydrogen transfer reaction of ketones

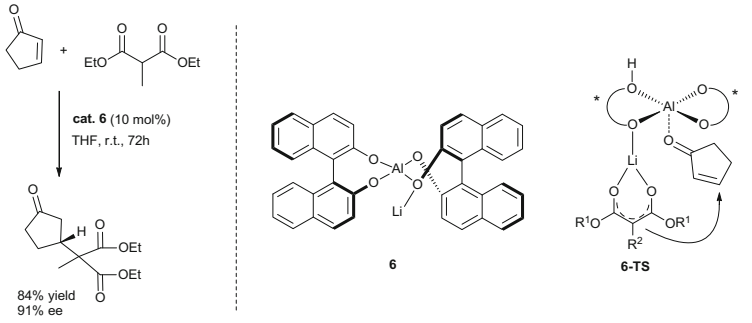

Scheme 6 Shibasaki's heterobimetallic catalyst in asymmetric Michael additions

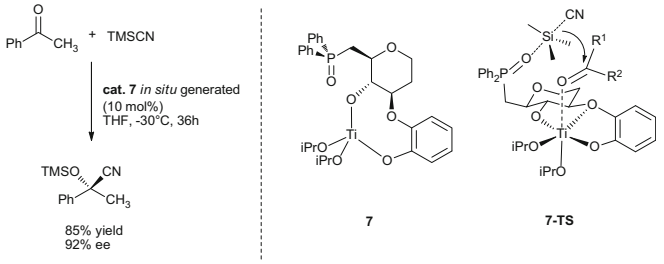

Scheme 7 Shibasaki's catalyst in enantioselective cyanosilylation of ketones

silylcyanation of aldehydes and ketones (Scheme 7) [31, 32]. In these reactions, the carbonyl substrate is activated *via* coordination to titanium, while the silylcyanation reagent is activated through coordination of the phosphane oxide to the silicon atom allowing the formation of cyanohydrin derivatives in stereocontrolled manner. This catalyst constitutes also another example of Lewis acid–Lewis base two-center catalyst. Other catalysts in which metal and ligand cooperate have been described and demonstrate the potential of this approach for a variety of reactions as illustrated by the works of Shvo [33], Milstein [34], Grützmacher [35–37], Ikariya [38], and Bourissou [39].

2.3 *Homobimetallic Catalysis*

The combination of two or more metal centers within the same or in different molecules constitutes also a powerful strategy for developing new or improved synthetic methods [40]. If we first consider homodinuclear complexes, a great variety of bimetallic complexes mimicking metalloenzyme dinuclear active sites has been described. One such example is the bimetallic zinc complex **8** reported by Williams et al. which promotes phosphodiester transesterification of the activated substrate HPNPP (used as a model for RNA cleavage) with very high activity and reveals also very effective for catalyzing the cleavage of uridyl(3′-5′)uridine (UpU) (Scheme 8) [41]. The authors consider that this efficiency comes from the cooperation of double Lewis acid activation through two Zn(II) ions and the hydrogen-bonding environment provided by the ligand.

Besides biomimetic complexes, Jacobsen described particularly efficient bis(chromium–salen) catalyst **9** for the asymmetric ring-opening reaction of epoxides with azide (Scheme 9) [42]. The efficiency of this class of catalysts is attributed to a cooperative mechanism, both substrates being activated toward each other by their respective chromium atom. Of note, a less pronounced cooperative effect was initially demonstrated in an intermolecular manner using monomeric Cr(N_3)–salen catalyst [43]. Jacobsen also showed that an analogous cooperative mechanism takes place using polymer-supported chiral Co(salen) complexes for the hydrolytic kinetic resolution of terminal epoxides [44, 45].

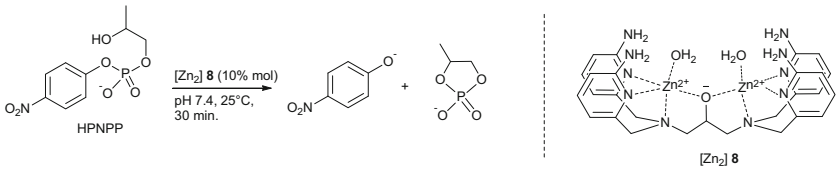

Scheme 8 Catalytic phosphodiester transesterification of HPNPP

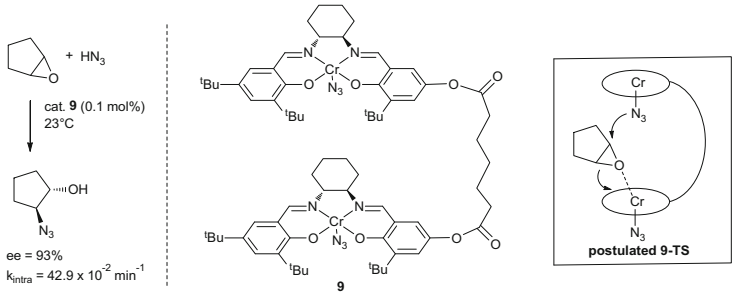

Scheme 9 Jacobsen's catalyst for the ring-opening reaction of epoxides by azide

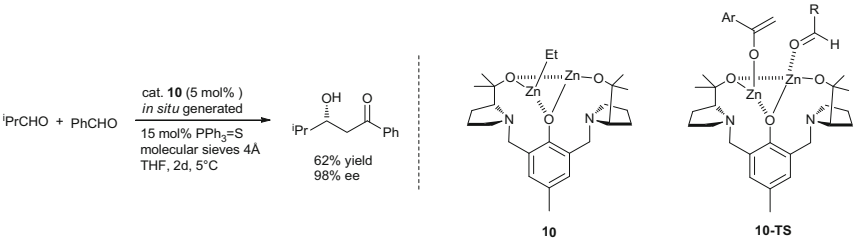

Scheme 10 Catalytic enantioselective aldol reaction by a bimetallic zinc complex

Trost has described very efficient and versatile bimetallic zinc catalyst **10** generated in situ from diethyl zinc and a chiral ligand derived from proline and *p*-cresol (Scheme 10) [46]. For example, this complex can promote catalytic aldol reactions with high enantiomeric excess. The role of two proximal zinc species is for one of them to form the enolate and for the second one to function as a Lewis acid to activate the aldehyde.

One area in which bimetallic catalysis has made greater progress is certainly polymerization catalysis [47, 48]. An illustrative example is the bimetallic titanium complex **11** reported by Marks which exhibits significantly higher activity (≈50 times) in homopolymerization of styrene than its monometallic analogous (Scheme 11) [49]. The role of the second titanium center is thought to coordinate the arene ring of the last inserted styrene thus preventing the deactivation of the active center. The presence of second titanium center not only affects the activity of

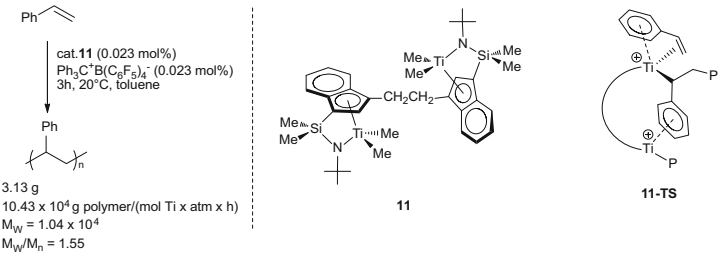

Scheme 11 Marks's catalyst for styrene polymerization

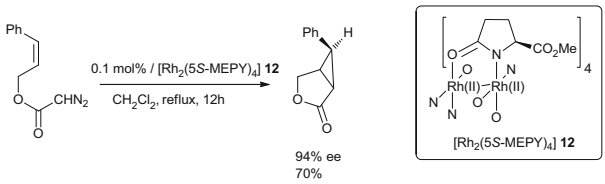

Scheme 12 Catalytic cyclopropanation with Doyle's catalyst

the catalyst but also the regiochemistry of the polymerization for which 1,2-insertion competes with 2,1-insertion to a significant degree.

Introducing a second metal also opens the way to bimetallic redox synergy, which has been observed in paddlewheel binuclear rhodium(II) catalysts. These chiral binuclear complexes are able to promote a variety of catalytic reactions like cyclopropanation [50], cyclopropenation [51], and C–H insertion [52–54] reactions achieving very high enantioselectivities (Scheme 12) (for reviews, see [55–57]). In addition to contributing to the paddle wheel structure of the complex, the role of the second rhodium is to stabilize its rhodium(II) neighbor that accounts for the high catalytic activity.

A parallel can be found in the work of Stanley et al. who described very efficient and selective dinuclear rhodium(I) complex **13** for the hydroformylation of α-olefins (Scheme 13) [58–60]. This bimetallic catalyst in its racemic form is much faster and more selective toward linear products than its monometallic analogues. The enhanced activity is attributed to the formation under catalytic conditions of highly active Rh(II) dimer species **14** with a covalent Rh–Rh bond.

In palladium series, Ritter has described the formation of dinuclear Pd(III) intermediates **15** [61] in Pd-catalyzed aromatic C–H acetoxylation reaction of phenylpyridine previously reported by Sanford [62]. Ritter demonstrated, thanks to a thorough experimental and theoretical investigation, that bimetallic redox synergy between the two metals is responsible for the facility of the reductive elimination step involved in this kind of catalytic reaction (Scheme 14) [63].

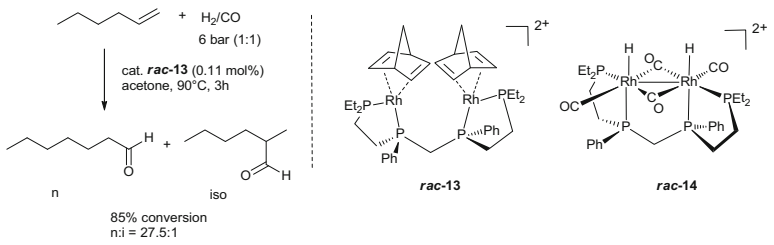

Scheme 13 Stanley's catalyst for hydroformylation

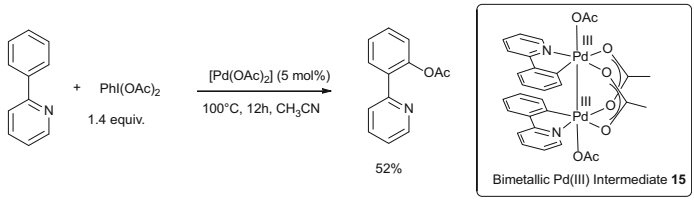

Scheme 14 Catalytic acetoxylation *via* a discrete bimetallic Pd(III) intermediate

2.4 Dual Catalysis from "Neighbor" Metals

Combination of two different metals has a great potential in this field considering that the two metals can produce different and complementary tasks simultaneously or consecutively. If we start with combination from "neighbor" metals, the main progress in this field has been made in using two separate metal-based catalysts. An early example is the Sonogashira reaction which consists in coupling aryl halides with terminal alkynes in the presence of catalytic amount of Pd and Cu (Scheme 15, Eq. 1) [64, 65]. In this cooperative dual catalytic reaction, the palladium catalyzes activation of the aryl halide, while copper activates the alkyne to form an acetylide and transfer it to palladium *via* transmetalation process. Other very elegant examples demonstrate the potential of this research area, among which one can cite the enantioselective allylic alkylation of α-cyanoesters promoted by the Rh/Pd system described by Ito (Scheme 15, Eq. 2) [66]. When in this reaction rhodium was omitted, high yields were obtained but no enantiomeric excess was found, and in the absence of palladium, no conversion was observed. A transition state (**16-TS**), which involves the nucleophilic attack of the rhodium enolate to the π-allylpalladium complex, has been proposed. Goossen has described a Pd/Cu catalyzed decarboxylative biaryl synthesis from aromatic carboxylates and aryl halides or pseudohalides (Scheme 15, Eq. 3) [67]. In this reaction, palladium complex activates aryl triflate, while decarboxylation from the carboxylate is mediated by the copper system, giving rise to aryl palladium and aryl copper species. In a transmetalation step, a diaryl-Pd species is formed that liberates the biaryl product *via* reductive elimination. Synergetic effects have been observed by Hidai using bimetallic Co/Ru system for the hydroformylation of olefins (Scheme 15, Eq. 4) [68]. The rate of the hydroformylation of cyclohexene using a Ru:

Co molar ratio of 1:1 in THF was six times faster than with $[Co_2(CO)_8]$ alone. Conversely, $[Ru_3(CO)_{12}]$ gives rise to cyclohexanecarbaldehyde in only 3% yield in similar conditions. The role of the ruthenium has not been clearly elucidated, but it would be involved in the aldehyde forming step by reacting as a hydride delivering agent on the acyl cobalt intermediate. Combinations of metal-based catalysts have been also used for promoting tandem reactions. One such example is the one-pot preparation of bicyclopentenones reported by Jeong from propargyl malonate and allylic acetate *via* a sequence of Tsuji–Trost allylation and Pauson–Khand reaction promoted by a combination of Pd and Rh catalysts (Scheme 15, Eq. 5) [69]. As in the case of cooperative dual catalysis, such tandem reaction requires testing a wide range of combinations to ensure that both catalytic systems are compatible toward each other and toward the different substrates, intermediates, products, and reagents.

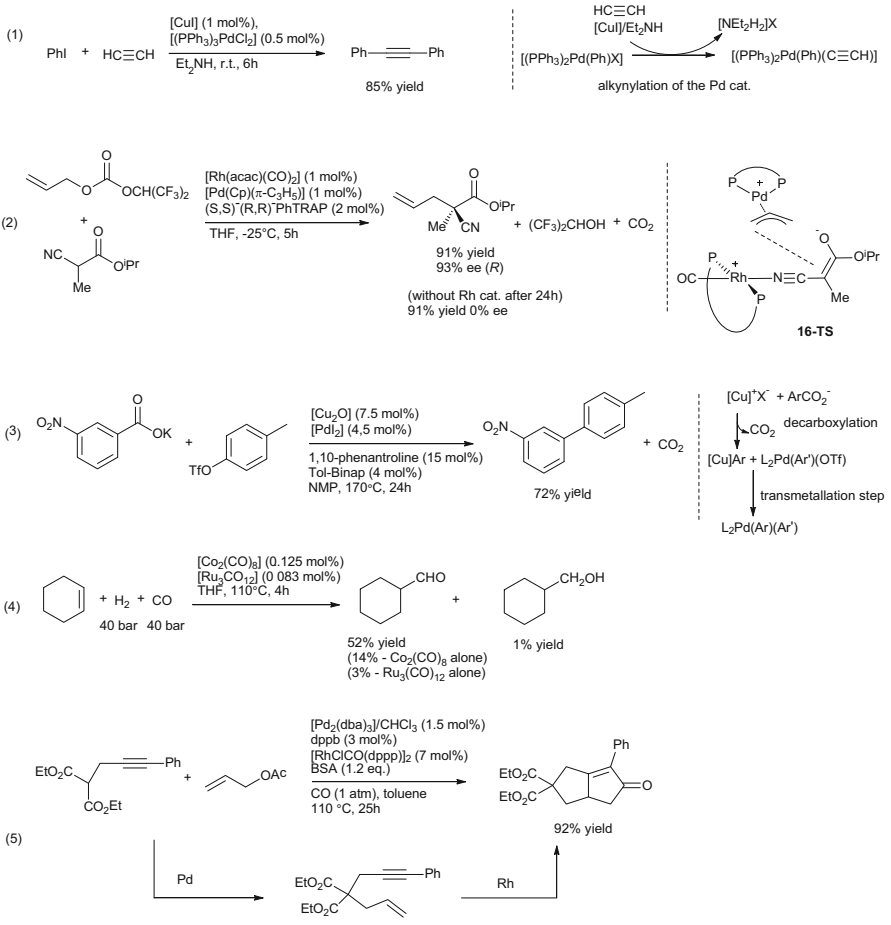

Scheme 15 Examples of two-component catalysis

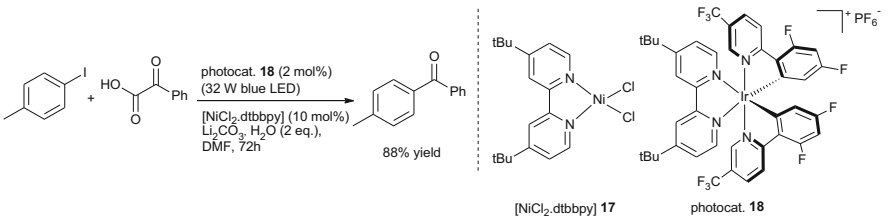

Scheme 16 Metallaphotoredox decarboxylative arylation of α-oxo acids

The role of the second metal may be not to interact directly with the substrates but rather to stabilize or restore the oxidation state of the active metal species. That's the case in the well-known Wacker process, in which $PdCl_2$ promotes catalytic oxidation of ethylene and cupric chloride with oxygen is used for reoxidizing the produced Pd(0) species and maintaining the catalytic cycle of the oxidation [70, 71]. The number of catalyst combinations and of way of cooperating is rapidly growing. Recently, MacMillan has merged iridium-photoredox catalysis with nickel catalysts for the direct decarboxylative cross-coupling of keto acids with aryl halides (Scheme 16) [72]. In the presumed mechanism, Ir photocatalyst **18** both generates acyl radical intermediate from keto acids and restores Ni in zero oxidation state, while Ni catalyst **17** is responsible for aryl halide activation and of the coupling of the acyl and aryl fragments.

2.5 Heterobimetallic Catalysis from "Neighbor" Metals

Surprisingly, only few heterobimetallic complexes combining "neighbor" metals have been described in catalysis [40]. Using an ethylene bis(amido-indenyl) ligand similar to that used in homobimetallic series (see Scheme 11), Marks has described the synthesis of Ti–Zr heterobimetallic complex competent to produce branched polyethylenes in ethylene homopolymerization processes with high selectivity and efficiency [73]. Here, the zirconium center produces octene which is incorporated in the polyethylene chain formed on the titanium center nearby. Late–late heterobimetallic complexes have been synthesized and tested for tandem catalysis by the Peris' group [74, 75]. For example, they described their synthesis of an Ir-Pd heterobimetallic complex **19** using a 1,2,4-triazolyl-3,5-dyilidene bridging ligand and showed that this complex can promote several tandem catalytic reactions such as dehalogenation/transfer hydrogenation, Suzuki–Miyaura coupling/transfer hydrogenation, or Suzuki–Miyaura/α-alkylation of haloacetophenones (Scheme 17). Noteworthy, it has been shown that this complex leads to a better reactivity than the equivalent mixtures of the homobimetallic complexes.

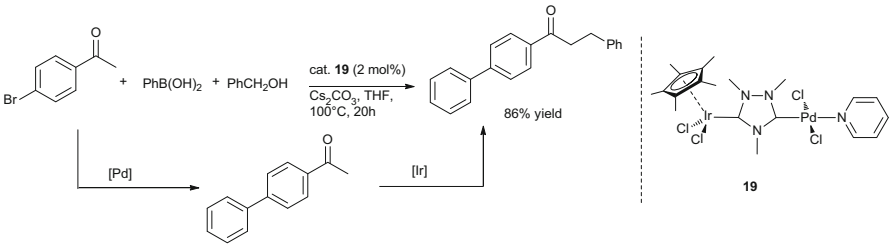

Scheme 17 Tandem catalytic Suzuki–Miyaura coupling/transfer hydrogenation reactions

3 "Early–Late" Heterobimetallic Catalysis

The combination of hard oxophilic early transition metals and soft nucleophilic late transition metals with opposite functionalities, provided they do not inhibit one another, is a priori ideal for promoting cooperative effect. A proof of concept can be found in the stoichiometric reactivity of "early–late" heterobimetallic complexes featuring a metal–metal bond [76]. It has been shown that such complexes are good candidates to realize the heterolytic cleavage of a bond in polar and apolar substrates. An illustrative example by Bergman et al. is the reaction of the Zr–Ir complex **20** with carbon dioxide which leads to the rupture of the metal–metal bond (Scheme 18) [77]. The CO_2 insertion occurs in the expected fashion with the CO_2 bridging the two metals, the carbon atom coordinated to iridium, and the oxygen atom on the zirconium center.

Since the early 1970s, the enthusiasm for this field has never subsided, and a great variety of early–late heterobimetallic complexes has been described over the years allowing a continuous growth in the understanding of the reactivity of these species and of the possible interactions between the two metals [4, 5, 78, 79]. A large panel of "early–late" bimetallic combinations has been tested in catalysis, and several reactions have been thus improved.

3.1 Group 8/Group 4–5 Heterobimetallic Complexes

3.1.1 Fe/Ti and Fe/Zr

M. L. H. Green has shown that the ansa-zirconocene complex **22** with an indenyl moiety connected to a cyclopentadienyl unit by a CMe_2 bridge is a suitable compound for synthesizing a variety of homo- and heterobimetallic complexes (Scheme 19) [80]. Some of these complexes have been used as cocatalysts for ethylene and propylene polymerization. The early–late hetero-trinuclear Fe/Zr complex **23** revealed among the best catalysts giving activities close to $[Cp_2ZrCl_2]$. The role that could play Fe on the activity of Zr was not discussed by the authors.

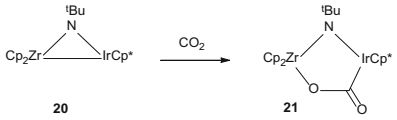

Scheme 18 CO_2 activation by an early–late heterobimetallic Zr–Ir complex

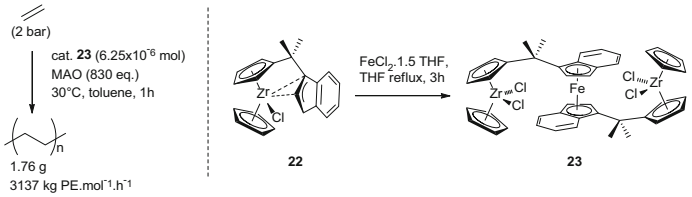

Scheme 19 Ethylene polymerization with a heterotrimetallic Zr/Fe complex

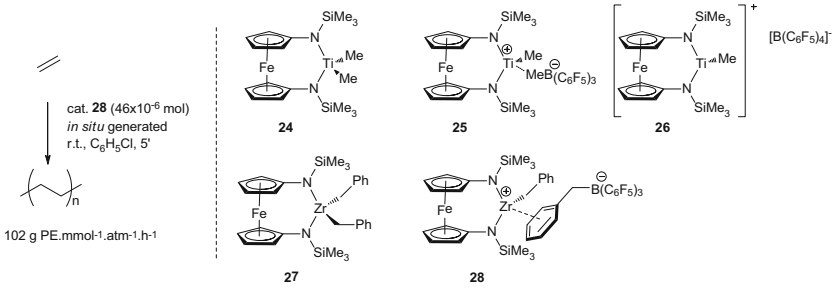

Scheme 20 Ethylene polymerization with heterobimetallic Fe/Zr complexes

Ferrocene has been extensively used as ligand backbone in coordination chemistry. The use of such ligands with early metals constitutes a straightforward route toward early–late heterobimetallic complexes. Moreover, the presence of the electron-rich ferrocenyl moiety can stabilize the neighbor early metal and is particularly relevant in case of cationic species like in Ziegler–Natta olefin polymerization. Arnold has developed this approach and described the synthesis of Fe/Ti **24** and Fe/Zr **27** heterobimetallic complexes using 1,1′-diaminoferrocene ligand (Scheme 20) [81, 82]. The addition of methyl abstractor $B(C_6F_5)_3$ or $[Ph_3C][B(C_6F_5)_4]$ to complex **24** gives the expected cationic species **25** and **26**. The X-ray crystal structure determined for cation **25** shows that the titanium center interacts with both the borate methyl group and iron (distance Fe–Ti = 3.07 Å). The bimetallic cations **25** and **26** were tested for the polymerization of 1-hexene. Both gave short-chain oligomers (5–6 monomer units) with moderate activity (102 g oligomer $mmol^{-1}\ h^{-1}$). Benzyl abstraction of zirconium complex **27** with $B(C_6F_5)_3$ led to ion pairs **28** with an η^6-coordinate benzyl borate anion. The inter distance of 3.2 Å between Fe and Zr observed in the solid structure of **28** precludes any Fe–Zr interaction in this case. The cationic species **28** was found to be moderately active for the polymerization of ethylene.

A series of group 8/group 4 heterobimetallic complexes (Fe/Zr, Ru/Zr, and Ru/Hf) featuring M–M′ bond have been shown to be efficient catalysts for the dehydrogenation of amine boranes (Scheme 21) [83]. The Fe/Zr complex **32** was synthesized from the zirconocenyl diphosphane **29** and [Cp*FeCl(tmeda)]. Reduction of **30** by KC_8 led to the monochloride complex **31** with Fe–Zr bond. The remaining chloride ligand has been exchanged at the last step by addition of MeLi. Catalytic dehydrogenation experiments have been conducted with Me_2NHBH_3 as substrate. Despite complex **32** was not the best of the series, it still gave H_2 gas and cyclic (dimethylamino)borane dimer $(Me_2NBH_2)_2$ with 75% conversion after 3 h. Study on the reaction pathways of this catalytic dehydrogenation reaction has been carried on the most active combination (Ru/Zr) and led the authors to propose a mechanism in which the two metal centers participate in the catalysis. This mechanism will be discussed in the next chapter devoted to Ru/group 4 complexes.

Besides ferrocene being a wonderful backbone for constructing ligands, its redox properties can be used for controlling the reactivity of the early metal center. Gibson and Long have explored this concept and described a redox-switchable catalyst for the ring-opening polymerization of lactides (Scheme 22) [84]. The heterobimetallic complex **33** has been synthesized by reacting a ferrocenyl-substituted salen ligand with $[Ti(O^iPr)_4]$. The reaction of **33** with two equivalents

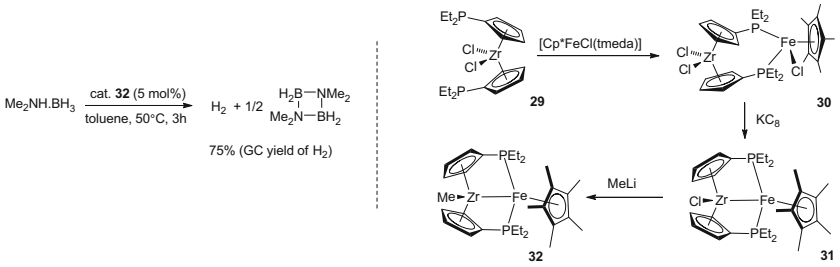

Scheme 21 Catalytic dehydrogenation of amine boranes by a heterobimetallic Fe/Zr complex

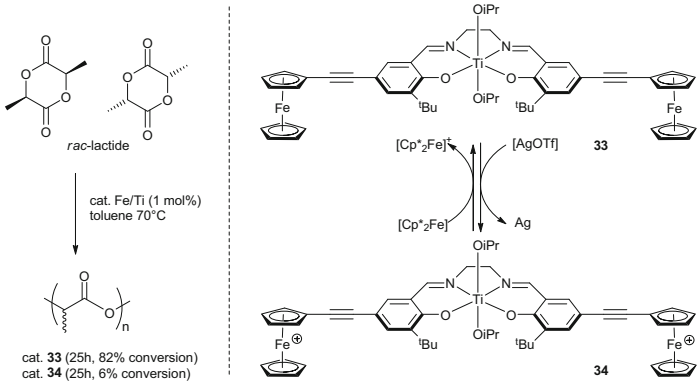

Scheme 22 ROP of *rac*-lactide by a redox-switchable heterobimetallic catalyst

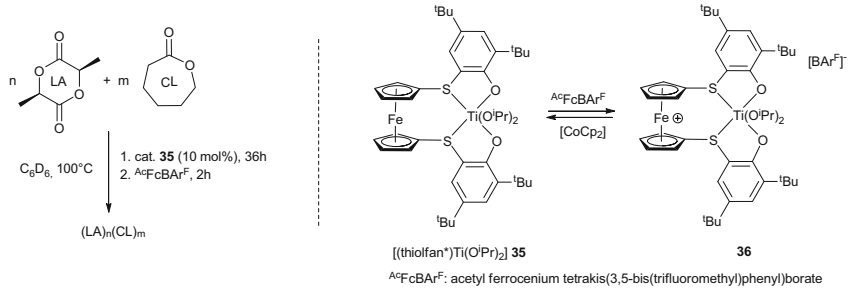

Scheme 23 CoROP of L-lactide and ε-caprolactone by a redox-switchable heterobimetallic catalyst

of [AgOTf] affords the dicationic species **34**, which can be reversibly reduced upon the addition of [Cp*$_2$Fe]. The ROP of *rac*-lactide (LA) was investigated with both complexes and showed that complex with the non-oxidized ligand affords a more rapid polymerization (k_{app}[**33**]/k_{app}[**34**] ≈ 30). The reversible nature of the redox switch was further proved by stopping the ROP of LA by adding [AgOTf] and restoring the activity by addition of [Cp*$_2$Fe].

In 2014, Diaconescu has pushed the concept further and developed redox-switchable catalyst **35** able to promote one-pot copolymerization of L-lactide and ε-caprolactone to give block copolymers (Scheme 23) [85]. This complex has been synthesized by treatment of the corresponding ferrocene-based pro-ligands nicknamed H_2(thiolfan*) with [Ti(O^{i}Pr)$_4$]. Reactivity of **35** and of the oxidized complex **36** toward L-lactide and ε-caprolactone has been studied. Opposite trends were observed for the two complexes. The reduced form is more efficient toward lactide, while the oxidized form is more efficient toward ε-caprolactone. One-pot copolymerization of L-lactide and ε-caprolactone by in situ switching of the redox state of [(thiolfan*)Ti(O^{i}Pr)$_2$] led to the target copolymer poly[block(LA-minor-CL)-block(CL-minor-LA)].

3.1.2 Ru/Ti, Ru/Zr, Ru/Hf, and Ru/Ta

Our group has described the synthesis of a series of Ti/Ru heterobimetallic complexes **37** which feature a titanocene and a (*p*-cymene) $RuCl_2$ fragment (Scheme 24) [86]. These complexes are synthesized by reaction of the corresponding titanocene phosphanes with the binuclear complex [(*p*-cymene)$RuCl_2$]$_2$. Structural diversity has been introduced by replacing the chloroligands at the titanium atom of the organometallic phosphane by benzoate or fluoroligands [87]. The catalytic performances of these complexes have been assessed in ring-closing metathesis (RCM) of *N*,*N*-diallyltosylamide (Scheme 24) [88].

While the monometallic complex [(*p*-cymene)$RuCl_2$(PCy$_3$)] is an efficient metathesis catalyst upon photochemical irradiation [89], the bimetallic complex **37d** in similar conditions shows only poor activity in RCM of *N*,*N*-

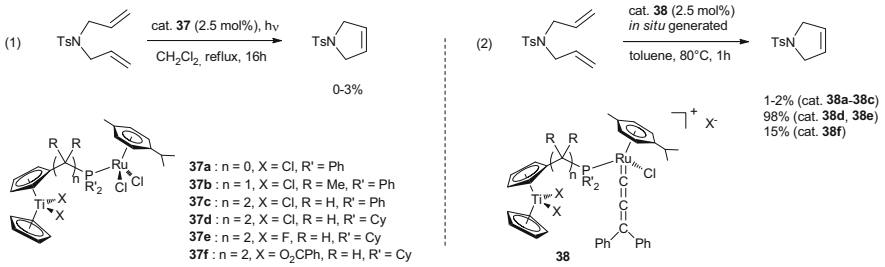

Scheme 24 RCM of *N*,*N*-diallyltosylamide by Ti/Ru heterobimetallic catalysts

diallyltosylamide. Other bimetallic complexes (**37a**–**37c**) show no catalytic activity. It is generally accepted that the photochemical irradiation of (arene)ruthenium complexes induces the decomplexation of the arene ligand, thus generating a highly reactive coordinatively unsaturated species. In the case of the bimetallic complexes **37**, we hypothesized that once the arene ligand is released, both chloride ligands on the titanium atom come to chelate the ruthenium atom and thus inhibit its catalytic properties. A second set of experiments has been carried out using cationic Ti–Ru–allenylidene pre-catalyst **38**. These complexes have been generated in situ by successive addition of silver triflate and diphenylpropynol on **37**. The complexes **38d** and **38e** gave high conversions comparable to [(*p*-cymene)RuCl(PCy_3)(C=C=CPh_2)][OTf], while **38a**–**38c** gave RCM products only as traces [90]. The lower activity of **38a**–**38c** can be attributed to the fact that bulky and basic phosphane is required for the reaction to turnover. It is worth mentioning that the nature of the spacer has a deep impact on the easiness of access to the allenylidene complex: the shorter the alkyl arm is, the slower the dark-violet color of the cumulene complex appears. In the worst case which corresponds to complex **38a**, no change in the coloration of the reaction mixture has been observed. This result can be explained if we consider that the reaction of **38a** with $AgBPh_4$ led to the formation of stable cationic μ-chloro-species whose structure has been determined by X-ray diffraction study [91]. Finally, the nature of the equatorial ligands on titanium atoms was also found to have a deep impact on the activity of the ruthenium complex as attested by the low conversion in dihydropyrrole when using **38f** as catalyst.

Our group has also tested the bimetallic complexes **37a**, **37c**, and **37d** for the synthesis of enol esters (Scheme 25) [92]. The addition of formic acid to 1-hexyne has been carried out in toluene at 90°C in the presence of 1 mol% of bimetallic complexes **37**. Reactions have been also done with complexes [(*p*-cymene)$RuCl_2(PPh_3)$] and [(*p*-cymene)$RuCl_2(PCy_3)$] in similar conditions for comparative purpose. Several remarks can be drawn from this study: the bimetallic compounds **37** were found to be less active than the monometallic counterparts; the bimetallic complex **37a** gave higher conversion and selectivity than **37c** and **37d**, which shows the dramatic influence of the spacer between the Ti and the Ru atoms on the catalytic reaction; formate tetrametallic complexes **39** are formed during the

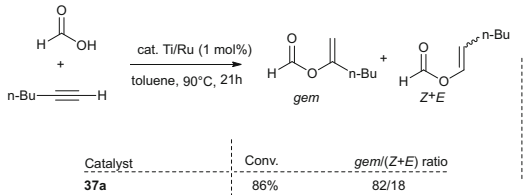

Catalyst	Conv.	*gem*/(*Z*+*E*) ratio
37a	86%	82/18
37c	70%	60/40
37d	66%	66/34
39a (0.5 mol%)	94%	85/15
[(*p*-cymene)$RuCl_2PPh_3$]	92%	80/20
[(*p*-cymene)$RuCl_2PCy_3$]	81%	82/18

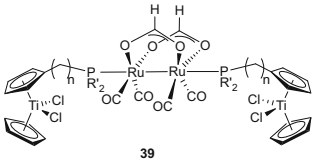

Scheme 25 Enol ester synthesis catalyzed by Ti/Ru heteropolymetallic complexes

reaction and gave once isolated slightly better results for the addition of formic acid to hexyne than their bimetallic counterparts; the ability of the cyclopentadienyl phosphane bridging ligand to maintain tethered the early and late metals in catalytic conditions was thus demonstrated.

The addition of ethyl diazoacetate to styrene catalyzed by heterobimetallic complexes **37** has been also studied (Scheme 26) [93]. Heterobimetallic complex **37** promotes cyclopropanation reaction with comparable activity to those observed with their monometallic counterparts. However, these systems were found more selective toward cyclopropanation reaction inhibiting the competitive metathesis reaction of styrene observed with the monometallic complexes [(*p*-cymene) $RuCl_2(PR_3)$]. This selectivity can be attributed to the early metal fragment which prevents metathesis reaction as already observed in RCM reaction. Similar trend was observed with analogous Ta/Ru heterobimetallic complexes [94].

The catalytic activity of complexes **37** in atom transfer radical polymerization (ATRP) of methyl methacrylate (MMA) was also investigated (Scheme 27) [95]. The polymer yields strongly depend on the titanocene fragment. Indeed, the difluoro-based complex **37e** gave 97% conversion, while complexes **37d** and **37f** gave about 65% conversion. The molecular weight distributions of the polymers were quite narrow in all three cases ($M_W/M_n = 1.2–1.3$), and the living nature of the polymerization was confirmed for complexes **37d** and **37e**.

As mentioned in Sect. 3.1.1, Nishibayashi described a series of group 8/group 4 complexes efficient as catalysts for the catalytic dehydrogenation of amine boranes [83]. Ru/Zr and Ru/Hf complexes (**40**, **41**) were synthesized in three steps from zirconocenyl or hafnocenyl diphosphane and [Cp*Ru(μ_3-Cl)]$_4$ according to a similar procedure as described for Fe/Zr complex **32**. Both complexes were found to promote the dehydrogenation of $HNMe_2BH_3$, the best one being Ru/Zr complex **40** (Scheme 28). Considering that the monomeric species [η^5-$(C_5Me_4H)_2ZrH_2$] and [Cp*RuH(depe)] (depe = $Et_2PCH_2CH_2PEt_2$) are much less active than **40**, the authors concluded that both of the metal centers participate in the catalysis. They propose a mechanism in which a heterobimetallic hydride species **42** is formed by reaction of **40** with $HNMe_2BH_3$. This species would undergo

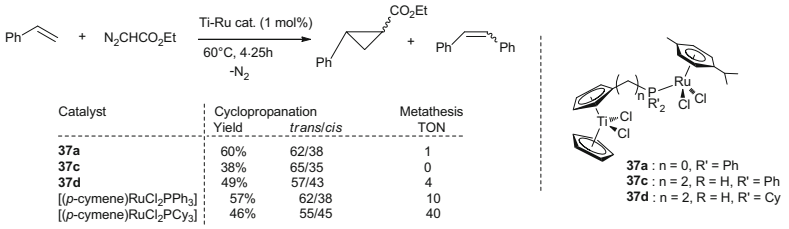

Catalyst	Cyclopropanation Yield	*trans*/*cis*	Metathesis TON
37a	60%	62/38	1
37c	38%	65/35	0
37d	49%	57/43	4
[(*p*-cymene)$RuCl_2PPh_3$]	57%	62/38	10
[(*p*-cymene)$RuCl_2PCy_3$]	46%	55/45	40

Scheme 26 Cyclopropanation of styrene catalyzed by Ti/Ru heterobimetallic complexes

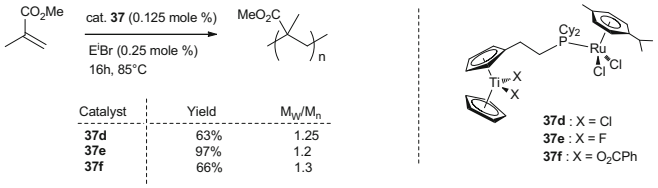

Catalyst	Yield	M_W/M_n
37d	63%	1.25
37e	97%	1.2
37f	66%	1.3

Scheme 27 ATRP of MMA catalyzed by Ti/Ru heterobimetallic complexes

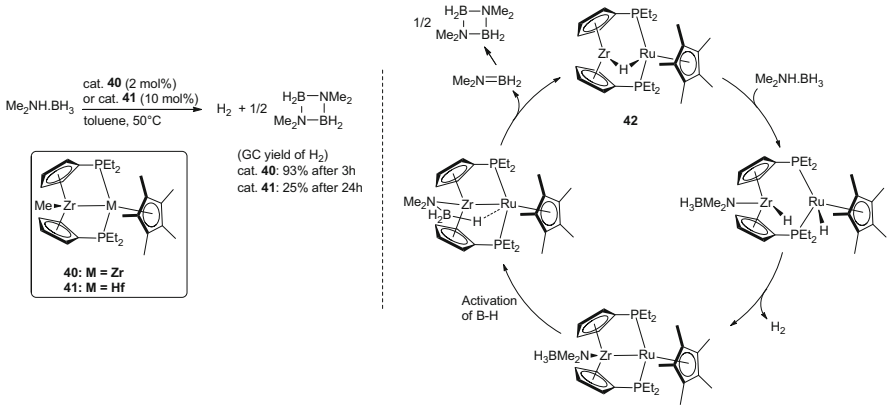

Scheme 28 Dehydrogenation of amine boranes catalyzed by Ti/Ru heterobimetallic complexes and proposed mechanism

successively oxidative addition of the amine borane, reductive elimination of H_2, and activation of the borane–H bond to regenerate **42**.

Nishibayashi has described the etherification of propargylic alcohols using trichloridoheterobimetallic complexes **43** as catalysts (Scheme 29) [96]. The reactions were carried from 1,1-diphenylpropynol and ethanol in the presence of 10 mol% of bimetallic complexes **43** and 10 mol% of $NaB(Ar^F)_4$ at 60°C for 72 h. All three complexes catalyzed the reaction to give propargylic ether in moderate yields, the best combination being Ru/Hf complex **43c**. Although these results are modest, it is much better than with the mononuclear complexes [η^5-$(C_5H_4PEt_2)_2ZrCl_2$], [Cp*RuCl(depe)], or [Cp*RuCl(depf)] (depf=1,1′-bis(diethylphosphino)ferrocene)

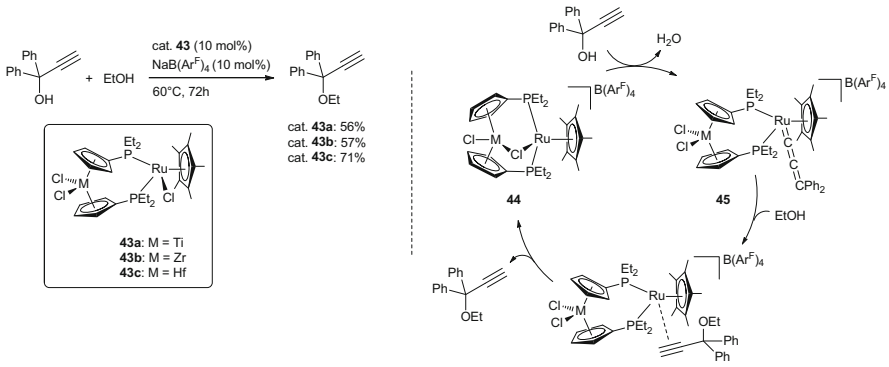

Scheme 29 Etherification of propargylic alcohols catalyzed by heterobimetallic complexes and proposed mechanism

which strongly suggests that the presence of both early and late transition metals is indispensable for the reaction to occur. The stoichiometric reaction of complexes **43b** and **43c** with $NaB(Ar^F)_4$ and propargylic alcohol gave the heterobimetallic allenylidene complexes **45**. These reactions proceed via the formation of chlorido-bridged complexes **44**. The structures of both Ru/Zr complexes **44b** and **45b** have been confirmed by X-ray diffraction study. In the mechanism of the catalytic etherification of propargylic alcohols proposed by the authors, the reaction takes place at the ruthenium center and involves **44** and **45** as key intermediates. The formation of the chlorido-bridged complex **44** during the catalytic reaction would promote the final dissociation of the propargylic ether.

3.2 Group 9/Group 4–5 Heterobimetallic Complexes

3.2.1 Co/Ti, Co/Zr, and Co/Hf

As mentioned in Sect. 3.1.1, Green has described a variety of homo- and heterobimetallic complexes containing a methylene-bridged (cyclopentadienyl)(indenyl) ligand [80]. The Co/Zr heterobimetallic complex **46** has been examined as catalyst precursor for ethylene polymerization with MAO as cocatalyst and shows activities similar to the Fe/Zr complex **22** or $[Cp_2ZrCl_2]$–MAO (Scheme 30).

In a pioneering paper [97], Osakada has reported ethylene polymerization trials with a series of early–late heterobimetallic complexes, including a Co/Zr combination, and showed that some of these complexes enable the enchainment of the α-olefin or of the oligomer formed at the late metal center to the polymer grown at the Zr center. The synthesis of the Co/Zr heterobimetallic complex **49** is elegant and involves as key step the Ru-catalyzed cross metathesis of an *ansa*-zirconocene complex **47** with an allyl substituent and a Co complex **48** having a pendant acrylate (Scheme 31). In the solid state, both Zr and Co atoms were found far away from

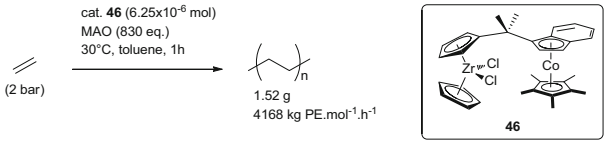

Scheme 30 Ethylene polymerization promoted by Co/Zr heterobimetallic complex

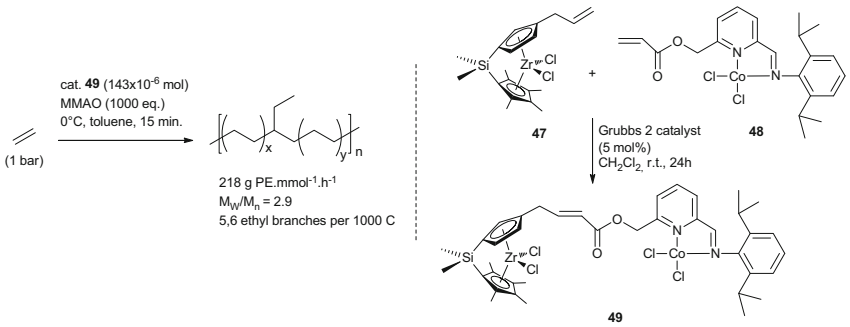

Scheme 31 Ethylene polymerization promoted by Co/Zr heterobimetallic complex

each other at a distance of 9.1 Å. Polymerization initiated by **49** in the presence of MMAO for 15 min at 0°C affords polyethylene with ethyl branches (5.6 branches per 1,000 carbons). Considering that the polymerization initiated by the zirconocene complex **47** leads to linear polyethylene and that the monometallic Co complex **48** produces 1- and 2-butenes, Osakada concludes that the reaction initiated by **49** involves the dimerization of ethylene at the Co center and the copolymerization of ethylene and 1-butene at the Zr center. Of note, a mixture of both monometallic complexes **47** and **48** also provided a polymer with ethyl branches but was less efficient (4.6 branches per 1,000 carbons). If we consider that copolymerization of ethylene and 1-butene (1/1 (v/v)) produces a polymer having much higher incorporation of ethyl branches (131 branches per 1,000 carbons), the kinetic of the dimerization of ethylene at Co center seems rather too slow for producing enough butene for an efficient enchainment to occur.

Despite early/Co heterobimetallic complexes featuring highly polar M–M′ bond being known since several decades [78], there was no example of catalytic application of these complexes until the group of Thomas revisited this chemistry. Her group synthesized a series of heterobimetallic Co/Zr complexes **51** by adding the metalloligands **50** initially designed by Nagashima [98], to CoI_2 (Scheme 32) [99, 100]. The observed concomitant reduction of Co(II) to Co(I) was attributed to the presence of iodide anion as reducing agent assisted in its task by the Lewis acidic zirconium center at proximity to the Co ion. The heterobimetallic complexes **51** have been fully characterized, and the X-ray crystal structures showed Zr–Co interatomic distances ranging from 2.628 to 2.731 Å consistent with the Co→Zr interaction. Upon chemical reduction of **51b** with Na/Hg, two-electron-reduced

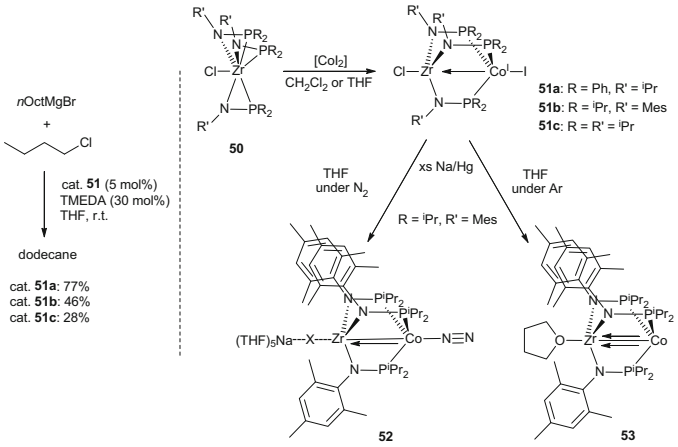

Scheme 32 Kumada coupling catalyzed by Co/Zr heterobimetallic complex

species featuring M–M′ multiple bond have been generated. Depending on the reaction conditions (Ar or N_2, THF or C_6H_6) and on the substituents on the *N*-atoms of the phosphinoamide-bridged ligand, the reduced species can be capped on both sides with either weakly bonded sodium halide (or THF) on Zr and N_2 on Co (complex **52**). Heterobimetallic complexes with an open coordination site either on Zr or on Co (complex **53**) have been also obtained. Theoretical investigation of M–M′ interaction in these systems using DFT has shown that interaction between Co and Zr occurs through a σ overlap in the dihalide complexes and occurs through σ and π overlaps in the reduced species.

The heterobimetallic complexes **51** have been used as catalyst precursors in Kumada cross-coupling reactions with various aryl and alkyl iodides, bromides, and chlorides [101]. Surprisingly, these catalytic systems revealed almost as efficient with chloride substrates as with iodide or bromide substrates. Conversely, the monometallic complexes $[ICo(PPh_2NH^iPr)_3]$ and $[ICo(PPh_3)_3]$ were found ineffective with chloride substrates. This result highlights the beneficial effect of the Zr fragment on the catalytic activity of the cobalt center. The mechanism proposed by Thomas involves first the in situ reduction of complex **51** to **53** by reaction with 2 equiv. of RMgX. The addition of alkyl halide across the multiple M–M′ bonds in **53** would proceed *via* one-electron transfer to the alkyl halide and rapid recombination of the alkyl radical to the Zr/Co species (the formation of alkyl radicals in catalytic conditions has been confirmed by adding the radical-trapping agent TEMPO to the reaction mixture). The resulting complex would undergo successively transmetalation reaction with RMgX followed by reductive elimination. It is at this stage that Zr presumably plays a key role by withdrawing the electron density on the cobalt center, thus facilitating the final reductive elimination step of the catalytic cycle.

The group of Thomas has also shown that apparent minor modification on the phosphinoamide-bridged ligand, that is, replacing *N*-mesityl by *N*-*m*-xylyl substituent, leads to diminished yields in cross-coupling products and favors the formation

of homocoupling by-products [102]. Analogous Co/Hf complexes to **51** have been synthesized and tested in Kumada cross-coupling reaction [103]. Their activity is diminished compared to Zr analogues. This more sluggish reactivity may be explained considering the weakest ability of Hf *vs* Zr to withdraw electron density on Co (Co–Hf bond in analogous complex to **52** is elongated by 0.04 Å from the Co–Zr distance).

The tris(phosphinoamide)-linked heterobimetallic complex **54** was shown to be an efficient catalyst for the hydrosilylation of a variety of aromatic and aliphatic ketones (Scheme 33) [104]. For example, the hydrosilylation of benzophenone with $PhSiH_3$ in the presence of 5 mol% of **54** led after the protic quench to the alcohol with 98% yield. Control reactions with [(^{i}Pr$_2$PNMes)$_3$ZrCl] gave no product, and [ICo(PPh$_2$NH^{i}Pr)$_3$] afforded the product but in 30% yield. These control reactions show that both Zr and Co are involved in the hydrosilylation reaction. Mechanism of this reaction has been investigated by comparing the stoichiometric reaction of **54** with either only $PhSiH_3$ or only benzophenone. Surprisingly no reaction occurred between complex **54** and $PhSiH_3$ which excludes "Chalk–Harrod" mechanism whereby oxidation of silane is the first step. However, **54** in the absence of silane promoted the radical reductive coupling of benzophenone. Based on these observations, Thomas proposed a mechanism where the hydrosilylation reaction takes place at the Zr center. It involves one-electron transfer from Co/Zr complex to the coordinated ketone and subsequent hydrogen transfer from the silane to the Zr-bound ketyl radical. The role of the Co fragment would be to stabilize Zr(III) intermediate *via* M–M bonding thus facilitating radical reactivity at Zr.

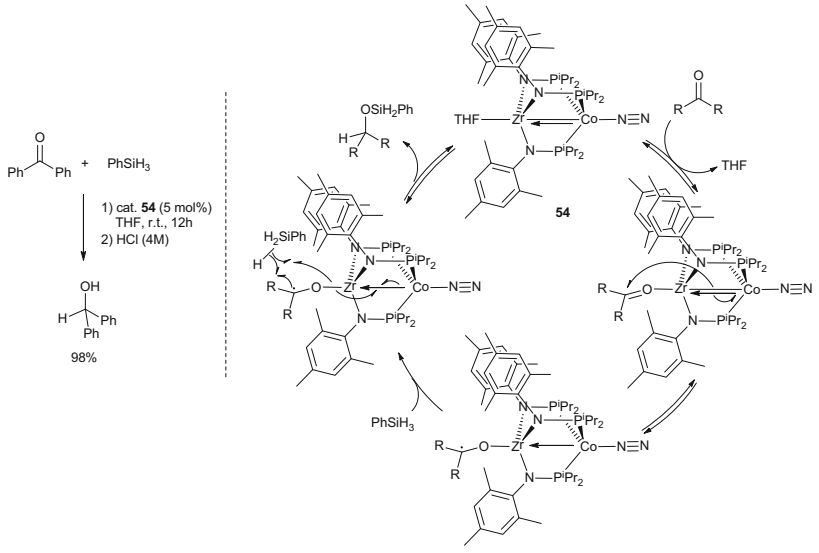

Scheme 33 Hydrosilylation of ketones catalyzed by Co/Zr heterobimetallic complex and proposed mechanism

3.2.2 Rh/Ti, Rh/Zr, and Rh/Hf

The hydroformylation of alkenes involves the activation of the small molecules H_2 and CO and is therefore a relevant reaction for evaluating the performances of early–late heterobimetallic complexes and highlighting synergetic effects. It is therefore understandable that this reaction has been one of the first and most studied reactions in the field. Kalck, Gervais, and Choukroun have greatly contributed to this topic and have reported the first study on hydroformylation of 1-hexene using the Rh/Zr bimetallic complex **56** (Scheme 34) [105]. The latter was obtained by addition of the zirconocene diphosphane $[Cp_2Zr(CH_2PPh_2)_2]$ (**55**) to the μ-thiolato dirhodium complex $[Rh_2(\mu\text{-}S^tBu)_2(CO)_4]$. The structure of **56** has been fully characterized by NMR, IR, and X-ray diffraction studies [106]. In the solid state, the zirconium diphosphane bridges the two rhodium atoms in a *cis* arrangement and one of the sulfur atoms interacts with the zirconium atom. This interaction was also observed by NMR in solution. Hydroformylation of 1-hexene under 5 bar of a 1/1 CO/H_2 mixture in the presence of 0.25 mol% of **56** led after 110 min at 80°C to aldehydes with 90% conversion and a *n*/*iso* ratio (*n*:*i*) equal to 1.9:1. Control reactions done with simple diphosphane ligands like dppb and dppp shown that dppb gave less active rhodium catalyst than Rh/Zr bimetallic complex **56**, whereas dppp gave comparable results [105, 107]. ^{t}Bu-substituted cyclopentadienyl homologue of the metalloligand **55** has been also tested in association with the dinuclear complex $[Rh_2(\mu\text{-}S^tBu)_2(CO)_4]$ for hydroformylation of 1-hexene [108]. Although no zirconium–sulfur interaction was observed in the resulting heterobimetallic complex **57**, the catalytic activities of **57**and **56** were found quite similar.

The catalytic performances in hydroformylation of the metalloligand **55** were further studied along with a series of mononuclear Rh(I) complexes (Scheme 35). The rate of the hydroformylation of hexene and the selectivity toward the linear aldehyde were raised by addition of $[Cp_2Zr(CH_2PPh_2)_2]$ to $[RhH(PPh_3)_4]$ [109]. The isolated complex **58**, which was found less active than its "in situ generated form," features a *trans* arrangement of the chelating diphosphane together with a pentacoordination around zirconium due to a strong interaction between the zirconium metal center and the Rh–H bond [110]. The combination of **55** and $[RhH(CO)(PPh_3)_3]$ and the isolated complex $[Cp_2Zr(CH_2PPh_2)_2RhH(CO)$

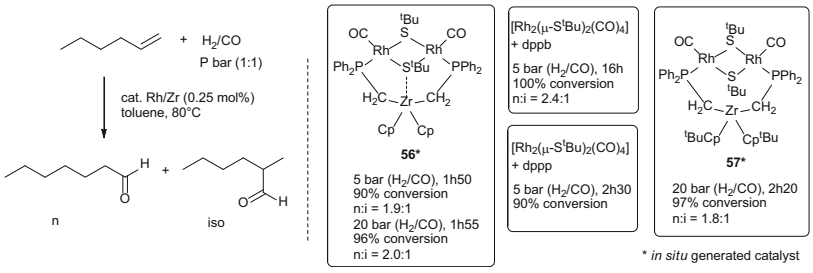

Scheme 34 Hydroformylation of 1-hexene catalyzed by Rh/Zr heterobimetallic complexes

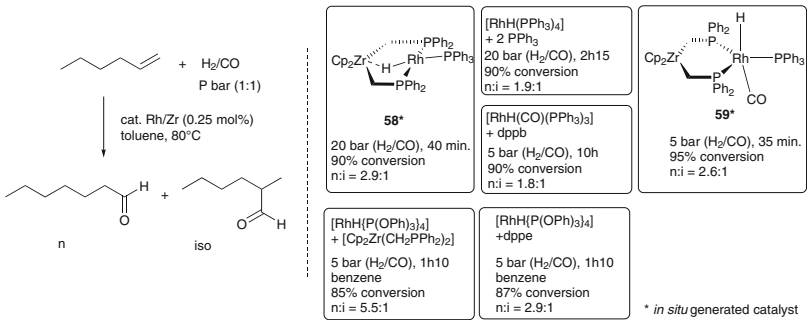

Scheme 35 Hydroformylation of 1-hexene catalyzed by Rh/Zr heterobimetallic complexes

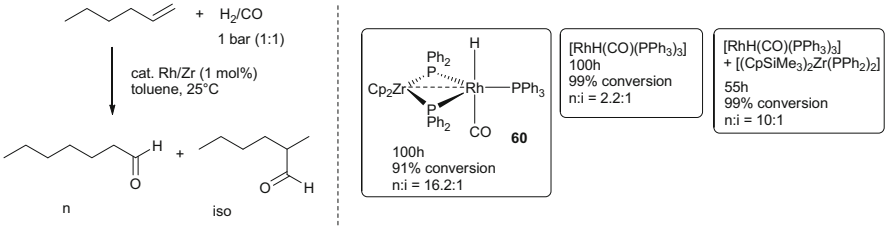

Scheme 36 Hydroformylation of 1-hexene catalyzed by Rh/Zr heterobimetallic complexes

(PPh_3)] **59** were found to be catalytically active for hydroformylation of hexene and more effective than $[RhH(CO)(PPh_3)_3]$ alone or in association with dppb while keeping selectivity toward linear aldehyde around 2.6 [111]. Selectivity was further improved by using the phosphite complex $[RhH\{P(OPh)_3\}_4]$ as late metal partner with **55** despite the fact that the metalloligand was coordinated in a monodentate fashion in this case [112]. The reaction of the metalloligand **55** as well as with its titanium-based analogue with $[Rh(cod)(PPh_3)_2][BPh_4]$ afforded the bimetallic complexes $[Cp_2M(CH_2PPh_2)_2Rh(cod)][BPh_4]$ [113]. In both cases, no improvement in the catalytic performances during hydroformylation of hexene was observed, when compared with the monometallic precursor $[Rh(cod)(PPh_3)_2][BPh_4]$. Catalytic activity of $[Rh(acac)(CO)_2]$ and ligand **55** in hexene hydroformylation has been also studied, but no beneficial effect of the zirconium phosphane ligand on the selectivity or on the conversion has been observed with respect to $[Rh(acac)(CO)_2]$/PPh_3 combination [114].

In 1999, Stephan reported the Zr/Rh bimetallic complex **60** built from a less flexible metalloligand $[Cp_2Zr(PPh_2)_2]$ (Scheme 36) [115]. An X-ray crystallographic study of **60** showed a "butterfly"-shaped ZrP_2Rh core consistent with Rh–Zr interaction ($d_{Rh\text{-}Zr} = 2.980$ Å). Quantum chemical calculations have been carried out on $[Cp_2Zr(PH_2)_2RhH(CO)(PH_3)]$ and confirmed the presence of a Zr–Rh interaction in such structures [116]. The results of the Bader's quantum theory of atoms in molecules (QTAIM) suggest a rather strong polar covalent interaction between the two metal centers. Hydroformylation of 1-hexene has been tested with

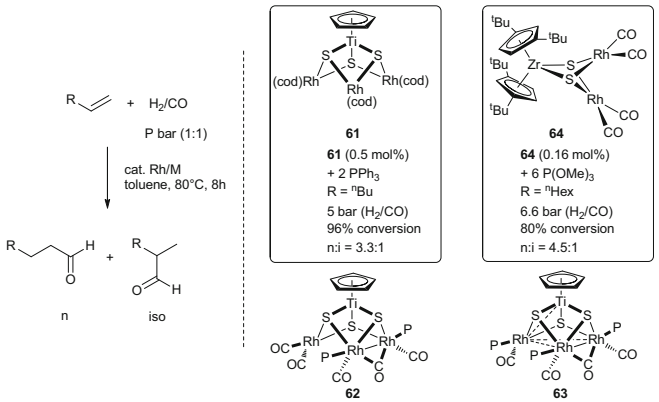

Scheme 37 Hydroformylation of 1-hexene and 1-octene catalyzed by Rh/Zr and Rh/Ti heterobimetallic complexes

60. The rate of catalysis was slower for the bimetallic complex than for [RhH(CO)$(PPh_3)_3$], but the selectivity for the terminal aldehyde was much greater (n:$i = 16$:1 vs 2:1 Rh). Few years later, Choukroun and Royo have shown that the introduction of $SiMe_3$ groups to the cyclopentadienyl rings of the zirconocene diphosphane increased the hydroformylation rate (99% conversion within 55 h) but is less favorable in terms of selectivity (n:$i = 10$) [117]. This result highlights the deep influence of the early metal fragment on the catalytic performances of the late transition metal.

Ciriano and Oro have described a series of Rh/Ti and Rh/Zr heterobimetallic complexes using bridging sulfide ligands and used them as hydroformylation precatalysts (Scheme 37). The heterotetranuclear complex [$CpTi(\mu_3\text{-}S)_3${Rh(cod)}$_3$] (**61**), in the presence of PPh_3, was found to be active catalyst for the hydroformylation of 1-hexene under mild conditions giving linear aldehyde with moderate selectivity [118]. High-pressure NMR spectroscopy experiments have shown that the clusters **62** and **63** are formed under catalytic hydroformylation conditions. In addition NMR analysis of the solution obtained at the end of the hydroformylation reaction indicated that the tetranuclear heterometallic framework is maintained in catalytic conditions. Few years later, the same group has described hydroformylation of 1-octene using the trinuclear $ZrRh_2$ heterobimetallic complex (**64**) [119]. The combination of **64** and $P(OMe)_3$ gave linear aldehydes with 80% conversion and a selectivity toward linear aldehyde of 4.5 under mild conditions. However, investigation of the solution obtained after the reaction has shown that heteronuclear framework is not maintained in catalytic conditions and that the active species are probably monomeric.

In 2000, Erker's group showed that the zirconocenyl diphosphane [$(CpPPh_2)_2ZrMe_2$] reacts with [$HRh(CO)(PPh_3)_3$] with loss of two PPh_3 ligands and liberation of methane to form the Zr/Rh heterobimetallic complex **65** (Scheme 38) [120]. In the solid state, complex **65** features a very short bonding

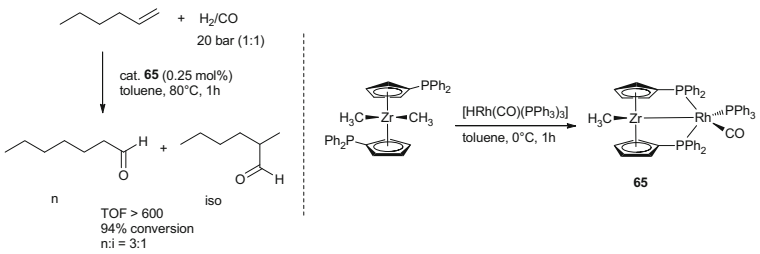

Scheme 38 Hydroformylation of 1-hexene catalyzed by Rh/Zr heterobimetallic complex

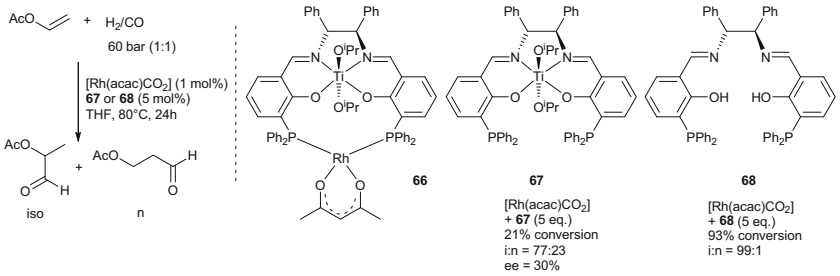

Scheme 39 Hydroformylation of vinyl acetate catalyzed by Rh/Ti heterobimetallic complex

interaction between a pseudo-trigonal bipyramidally coordinated Rh center and a pseudo-tetrahedral Zr center (d(Zr–Rh) = 2.865(1) Å) [121]. This complex is very active for the hydroformylation of 1-hexene giving linear aldehyde with high initial TOF and *n*:*i* ratio of 3. Comparison of this result with some other Rh/chelate phosphane systems suggests that the Zr center alters the electronic features of the Rh center by means of the Zr–Rh bond and is responsible for the improved activity.

The first example of application of a chiral early–late heterobimetallic complex in asymmetric catalysis was reported by Börner in 1999 and deals with hydroformylation of activated olefins (Scheme 39) [122]. The chiral bimetallic complex **66** was generated in situ by reacting the (*R*,*R*)-Diph-salenophos-Ti(O^iPr)$_2$ ligand (**67**) with [Rh(acac)(CO)$_2$]. This complex gives rise to a diminished conversion in aldehyde (21% vs 99%) as well as a lower selectivity (*i*:*n* = 77/23 vs 99/1) with respect to the monometallic salenophos–Rh complex generated in situ from the free-metal ligand **68** and [Rh(acac)(CO)$_2$] but affords the branched aldehyde with 30% *ee*.

In related research, Kalck and Gautheron have been interested in carbonylation of ethylene in the presence of the early–late heterobimetallic complex **69** (Scheme 40) [123]. The latter was synthesized by addition of [Cp*$_2$Zr(SH)$_2$] to [RhCl$_2$(CO)$_2$]. The structure of **69** in the solid state has been determined by X-ray diffraction study. It shows a usual tetrahedral and planar geometry around the Rh and Zr atoms, respectively, a planar ZrS_2Rh core, and a rather long Rh–Zr distance of 3.161(3) Å. Complex **69** promoted the direct carbonylation of ethylene with low efficiency (TON = 2) in the presence of PPh_3 and triethyl orthoformate. The analogous reaction in the absence of triethyl orthoformate gave acrolein in

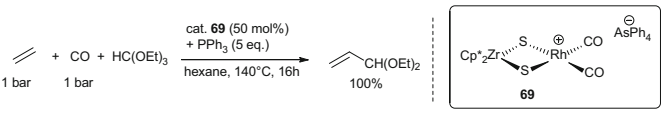

Scheme 40 Carbonylation of ethylene catalyzed by Rh/Zr heterobimetallic complex

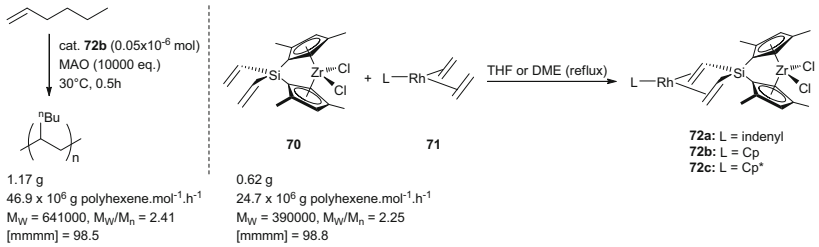

Scheme 41 Polymerization of 1-hexene catalyzed by Rh/Zr heterobimetallic complex

stoichiometric amount. Of note, the rhodium precursor $[Rh_2(\mu\text{-S-}^tBu)_2(CO)_4]$ was found totally inactive in these conditions, while $[Cp^*_2Zr(SH)_2]$ gave a small amount of acrolein but rapidly decomposed. These results strongly suggest that both metals are required for the reaction to occur.

Group 9/group 4 heterobimetallic complexes have been also used for polymerization of olefins. For such a purpose, Suzuki and coworkers have designed a series of *ansa*-zirconocene/rhodium heterobimetallic complexes **72** which allow potential bimetallic effects to be examined with exclusion of any steric factors (Scheme 41) [124]. These complexes have been synthesized by olefin exchange from the divinylsilylene *ansa*-zirconocene complex **70** and bis(ethylene)rhodium complexes **71**. The X-ray diffraction study of complex **72b** reveals that the coordination of the Rh in the back side of the metallocene does not affect the structure of the zirconocene moiety. However, the electronic features of the Zr center are affected by the presence of Rh as attested by the more negative potentials of reduction of Zr(IV) in the bimetallic complexes **72** with respect to those of the corresponding monometallic ones. The catalytic activities of **72** for hexene polymerization were assessed and found to be higher than that of the parent zirconocene complex **70** giving isotactic polymers of high molecular weights. This trend was also observed for propylene. Conversely, similar polymerization rates were obtained for ethylene when using mono- or bimetallic complexes. A possible explanation of the "bimetallic effect depending on the monomer substrate" advanced by Suzuki is that the electron-donating ability of the rhodium unit facilitates the insertion step which is the rate-determining step for 1-hexene and propylene but has a smaller effect for ethylene polymerization for which olefin coordination is the rate-limiting step [125]. Of note, comparison of the Mulliken population on the Zr center based on *ab initio* MO calculation of the cationic Zr^+–H species derived from **72b** and **70** showed that the Zr center of the Zr^+–Rh complex had a smaller positive charge than the corresponding mononuclear complex ($\Delta = -0.0179$). These results demonstrate how the judicious design of the bridging

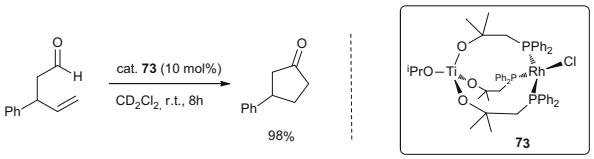

Scheme 42 Intramolecular hydroacylation catalyzed by Rh/Ti heterobimetallic complex

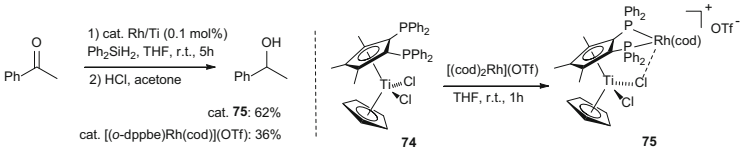

Scheme 43 Hydrosilylation of acetophenone catalyzed by Rh/Ti heterobimetallic complex

ligand can allow the subtle electronic effects of the late transition metal on the Zr catalytic activity to be highlighted.

In 2005, inspired by the pioneering works of Wolczanski [126], Morgan and Kundu reported the synthesis of the Rh/Ti heterobimetallic complex **73** in two steps *via* the addition of $[Ti(O^iPr)_4]$ to three equivalents of $HOCMe_2CH_2PPh_2$ and the subsequent addition of $[Rh(cod)Cl]_2$ (Scheme 42) [127]. Complex **73** was found to decompose in the solid state but was stable in solution for 36 h which allowed its rough characterization. This complex performed the intramolecular hydroacylation of 3-phenyl-4-pentenal at room temperature to give exclusively cyclopentanone in 98% yield. In similar conditions, none of $[Rh(cod)Cl]_2$, the ligand, or $[Ti(O^iPr)_4]$ can individually or in pairwise combination catalyze the reaction. Conversely, it was previously shown that $[Rh(S\text{-}BINAP)]^+$ at 1 mol% catalyst loading gave cyclopentanone in 51% yield after only 45 min but accompanied with two other side products [128]. Similarly trend was observed for the intramolecular hydroacylation of styrene-2-carboxaldehyde. A mechanism involving the activation of the aldehydic C–H bond by the Rh center assisted by the Lewis acidic titanium center was considered by the authors, but it was rejected taken into account that the catalytic system $[RhCl(PPh_3)_3]/[Ti(O^iPr)_4]$ was inefficient in hydroacylation. Computational studies have been undertaken to get insights into this cooperative bimetallic effect and suggested that titanium activates the rhodium center toward the final reductive elimination step of the catalytic cycle by space charge–charge repulsion rather than by direct orbital interaction, both metallic centers lying rather far from each other ($d_{Ti\text{-}Rh} = 3.1$ Å).

In our own laboratory, we have reported the synthesis of a new Rh/Ti heterobimetallic complex **75** by reacting the 1,2-titanocenyl diphosphane ligand **74**, nicknamed TiPHOS, with $[Rh(cod)_2](OTf)$ (Scheme 43) [129, 130]. The structure of **75** was determined by X-ray diffraction study and dynamic NMR studies. A weak bonding interaction between one of the two chloride atoms of the TiPHOS ligand and the Rh center has been observed both in solution and in the solid state. The catalytic activity of complex **75** has been tested for the hydrosilylation of aromatic and aliphatic

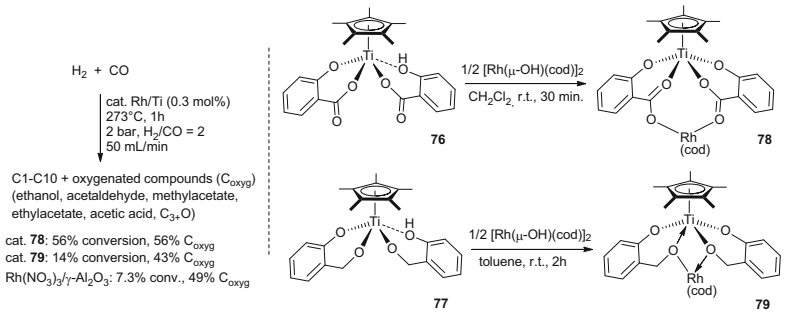

Scheme 44 Hydrogenation of CO catalyzed by Rh/Ti heterobimetallic complex

ketones with Ph_2SiH_2 as stoichiometric reducing agent. Control reactions have been performed with the monometallic [(*o*-dppbe)Rh(cod)](OTf) complex (*o*-dppbe=*ortho*-diphenylphosphinobenzene). With acetophenone, the more active catalyst was found to be the bimetallic complex **75**. This supremacy was further confirmed with two other substrates (propiophenone and tetralone). The reason of the "bimetallic effect" was not established, but we hypothesized that the oxophilic titanium ion assists the Rh center in the activation of the carbonyl substrate.

Otero and Terreros have described interesting heterobimetallic complexes **78** and **79** with the aim of mimicking rhodium catalyst supported on titania and have studied their activity in CO hydrogenation (Fischer–Tropsch synthesis) (Scheme 44) [131, 132]. The heterobimetallic complexes **78** and **79** have been synthesized by reacting either the titanium salicylate [Cp*Ti(Sal)(SalH)] ($SalH_2$=salicylic acid) **76** or [TiCp*(O_2Bn)(OBnOH)](HOBnOH=2-hydroxybenzyl alcohol) **77** with [Rh(μ-OH)(cod)]$_2$. For comparative purposes, Rh-based catalysts prepared by impregnation on γ-Al_2O_3 or SiO_2 support have been tested in parallel. The heterobimetallic complex **78** displayed the highest CO conversion (56%) and selectivity for the desired oxygenated compounds (56% oxygenated products/ethanol 24.6%, ethyl acetate 18.4%) than the silica- or alumina-supported rhodium catalyst (7.3% CO conversion, 49.1% oxygenated products, ethanol 20.8%, ethyl acetate 13.5%). Although the comparison is clearly in favor of the bimetallic complex **78**, no explanation of the role that could play the titanium center in these Fischer–Tropsch reactions was provided by the authors.

In 2011, van Leeuwen has described the synthesis of a library of over 100 chiral Ti-based metalloligands by self-assembling and has screened the catalytic performances of these ligands in association with [Rh(nbd)$_2$](BF_4) for the catalytic asymmetric hydrogenation of (*Z*)-methyl-2-acetamido-3-phenylacrylate (Scheme 45) [133]. The library of diphosphanes was obtained by reacting subsequently 10 different chiral diols and 8 ditopic Schiff bases with [Ti(OiPr)$_4$]. The resulting diphosphanes were next added to [Rh(nbd)$_2$](OTf). The best system was identified as complex **80**, which gave hydrogenated product with 100% conversion after 3 h and 92% *ee*. This study, which did not target M–M′ cooperative effects, clearly showed that the use of Ti as assembling metal is a powerful strategy for designing libraries of chiral ligands and for asymmetric synthesis.

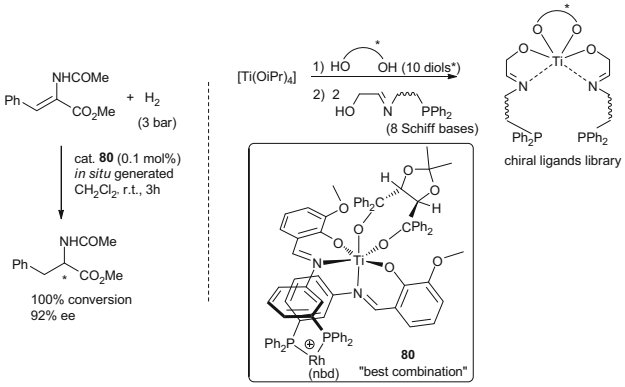

Scheme 45 Asymmetric hydrogenation catalyzed by Rh/Ti heterobimetallic complex

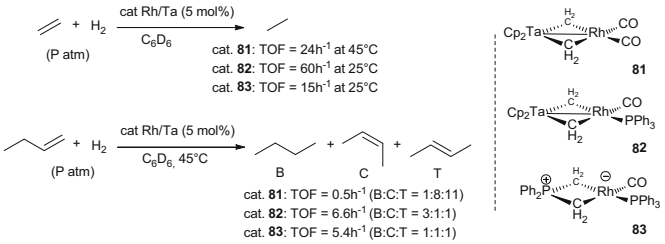

Scheme 46 Hydrogenation and isomerization of alkenes catalyzed by Rh/Ta heterobimetallic complexes

To date, there are very few examples of early–late heterobimetallic catalysts with a group 5 element. This might be explained considering the weaker Lewis acid character of group 5 *vs* group 4 metal complexes which limits the possibility of dual activation of polar substrates. First examples appeared in the early 1990s in the group of Bergman who described the synthesis of a series of bis-bridging methylene Ir/Ta complexes (see Sect. 3.2.3) and Rh/Ta complexes and reported their catalytic performances for alkene hydrogenation, isomerization, and hydrosilylation [134]. The Rh/Ta complexes **81** and **82** were synthesized by reaction of $[Cp_2Ta(CH_2)(CH_3)]$ with $LiN(TMS)_2$ and addition of the resulting deprotonated complex to $[Rh(CO)_2Cl]_2$ or $[RhCl(CO)(PPh_3)_2]$ [135]. The Rh/Ta complexes **81** and **82** were tested for the catalytic hydrogenation in a variety of alkenes in parallel with a phosphorus-ylide analogue **83** for comparative purposes (Scheme 46). Both complexes catalyzed hydrogenation of ethylene under atmospheric pressure with a TOF of 24 h^{-1} for complex **81** (at 45°C) and 60 h^{-1} for complex **82** (at 25°C). With 1-butene as substrate, butane (noted B) and *cis*- and *trans*-2-butene (noted C and T) were formed at much slower rates (complex **81**, TOF = 0.5 h^{-1}; complex **82**, TOF = 6.6 h^{-1}). These performances are much better than the ones with the parent Ir/Ta complexes (*vide infra*) but comparable to those reported with the phosphorus-

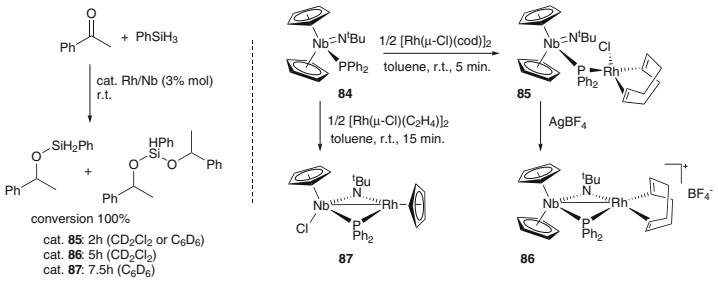

Scheme 47 Hydrosilylation of acetophenone catalyzed by Rh/Nb heterobimetallic complexes

ylide rhodium complexes **83**. Therefore, the role of the early metal in these complexes seems rather limited. However, a particularity of both Ir/Ta and Zr/Ta complexes versus the parent monometallic phosphorus-ylide derivatives is that they can incorporate D_2 into the bridging methylene positions. This reaction plays a crucial role in Ir/Ta series for the catalytic hydrogenation takes place by opening coordination sites on the Ir center but seems in Rh series less energetically favorable than PPh_3 or CO dissociation (*vide infra*).

Much later, Nikonov has become interested in catalytic hydrosilylation of acetophenone and benzaldehyde with Rh/Nb heterobimetallic complexes **85** and **87** (Scheme 47) [136]. The latter were synthesized by addition of the phosphido/imidoniobiocene ligand **84** either to $[Rh(\mu\text{-}Cl)(C_2H_4)_2]_2$ or to $[Rh(\mu\text{-}Cl)(cod)]_2$. Surprisingly Cp/Cl exchange occurred with the chlorobis(ethylene)rhodium dimer but not with the analogous cyclooctadiene derivative. The structure of both complexes has been confirmed by X-ray diffraction studies and showed Rh–Nb distances of 4.266 Å and 2.6744(2) Å for **85** and **87**, respectively. The bimetallic complex **85** was found to catalyze hydrosilylation of acetophenone with $PhSiH_3$ and performed better than the parent Rh complex $[Rh(\mu\text{-}Cl)(cod)]_2$ in the absence of any added phosphide. This trend was opposite when a secondary silane ($PhMeSiH_2$) was used. Complex **85** catalyzed also hydrosilylation of benzaldehyde with $PhSiH_3$. A cationic complex formulated as **86** was generated in situ by addition of $AgBF_4$ to **85**. Both complexes **86** and **87** showed lower activity than **85**. Of note, stoichiometric reactions of **85** with $PhSiH_3$ or benzaldehyde in a 1:1 ratio led to the decomposition of the bimetallic complex.

3.2.3 Ir/Zr and Ir/Ta

Suzuki's group has described bimetallic Ir/Zr hydrido complexes capable of promoting stoichiometric and catalytic C–H activation (Scheme 48) [137]. These complexes were synthesized by reaction of *ansa*-zirconium dichloride with Li[Cp*IrH_3] and subsequent treatment with equimolar amount of RLi. The use of PhLi led to complex **88**. The latter undergoes ligand exchange with C_6D_6 and a variety of aromatic, aliphatic, and organometallic compounds at 70–100°C. It catalyzes also the isotopic exchange between arenes and C_6D_6 as solvent at 120°C.

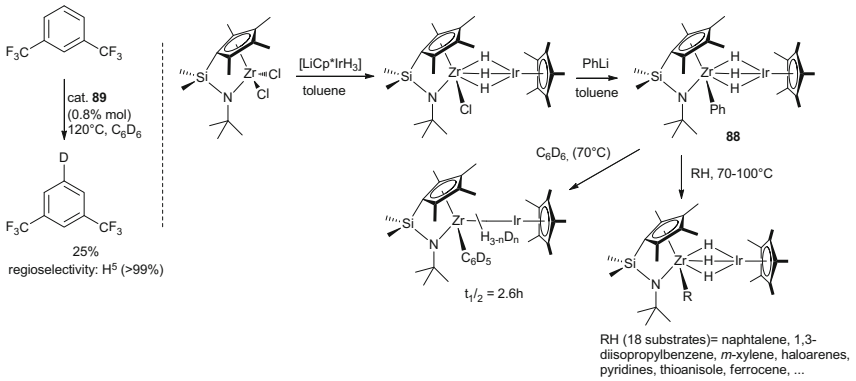

Scheme 48 Isotopic exchange catalyzed by Ir/Zr heterobimetallic complex

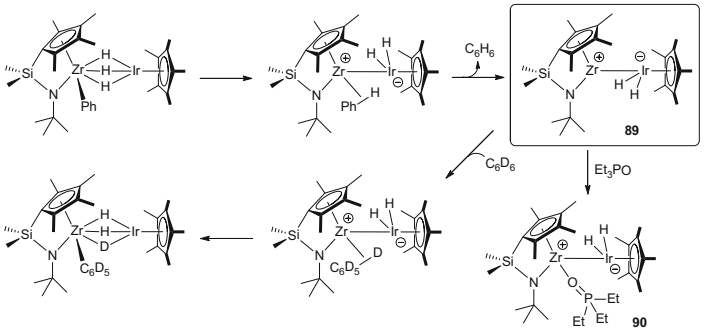

Scheme 49 Mechanism proposed by Suzuki for the ligand exchange and isotopic exchange

The catalytic isotopic exchange gives rise to regioselectivities fairly consistent with those observed in stoichiometric ligand exchange reactions and proceeds probably through common intermediates. One mechanistic scenario proposed by Suzuki involves as key steps the in situ generation of the Lewis acid intermediate **89** followed by the addition of the C–H(D) bond across the M–M′ bond (Scheme 49). The existence of the intermediate **89** was demonstrated by isolation of the $Et_3P{=}O$ adduct **90**. NBO analysis conducted on this complex revealed that the Zr–Ir interaction involves one single covalent bond and a secondary ionic interaction. Although the catalytic C–H activation was limited to isotopic exchange in this study, these results clearly show that early–late heterobimetallic complexes with unsupported multiple M–M′ bond can activate C–H bond without extensive complex decomposition.

A benchmark publication in the field of early–late heterobimetallic catalysis is certainly the study reported by Bergman in 1990 about catalytic hydrogenation, isomerization, and hydrosilylation of alkenes by $[Cp_2Ta(\mu\text{-}CH_2)_2Ir(CO)_2]$(**91**)

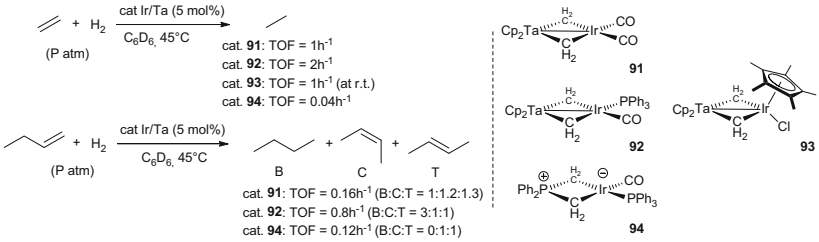

Scheme 50 Hydrogenation and isomerization of alkenes catalyzed by Ir/Ta heterobimetallic complexes

(Scheme 50) [134]. This publication has been completed by other studies few years later including mechanistic studies and complementary results with [$Cp_2Ta(\mu\text{-}CH_2)_2Ir(CO)(PPh_3)$] (**92**), [$Cp_2Ta(\mu\text{-}CH_2)_2IrH(Cp^*)$](**93**), and analogous rhodium complexes (*vide supra*) [135, 138, 139]. The heterobimetallic complex **91** has been obtained by treating [$Cp_2Ta(CH_2)(CH_3)$] with [(η^5-indenyl)$Ir(CO)_2$], which results in the loss of one equivalent of indene and the formation of two methylene bridges. The X-ray crystal structure of the related complex [$Cp(\eta^5\text{-}C_9H_7)Ta(\mu\text{-}CH_2)_2Ir(CO)_2$] has been determined and shows a Ta–Ir bond length of 2.858(1) Å consistent with the presence of a metal–metal bond. Complex **92** was obtained by addition PPh_3 to **91**. Ethylene and mono- and disubstituted alkenes have been used as substrates for evaluating the catalytic performances of the bimetallic complexes **91** and **92** in hydrogenation. For comparative purposes, an analogous monometallic phosphorus-ylide iridium complex **94** has been synthesized and tested in parallel. The reactions were run at 45–66°C in benzene under atmospheric pressure of H_2 with 5% of catalyst. Complexes **91** and **92** were found to catalyze the hydrogenation of ethylene in ethane with low TOF of 1 and 2 h^{-1}, respectively. However, these complexes were found to be robust allowing 40 TON (in the case of **91**) for several runs to be proceeded. Despite these modest performances, the hydrogenation operates much faster than with the parent phosphorus-ylide iridium complexes **94**. For complex **91**, hydrogenation of 1-butene proceeds slower than hydrogenation of ethylene in similar conditions and is accompanied by a partial isomerization in a mixture of *cis*- and *trans*-2-butene. Reaction of complex **91** with D_2 gave rise to incorporation of D_2 into the bridging methylene units at a much faster rate than hydrogenation. Conversely, the monometallic Ir complexes **94** cannot incorporate D_2 into the $\mu\text{-}CH_2$ groups. Bergman proposed therefore that the early metal plays a key role in both mechanisms of isotopic exchange and catalytic hydrogenation by inducing the methylene bridge reductive elimination and the reverse oxidative addition of the Ta–CH_3(D) group across the iridium metal

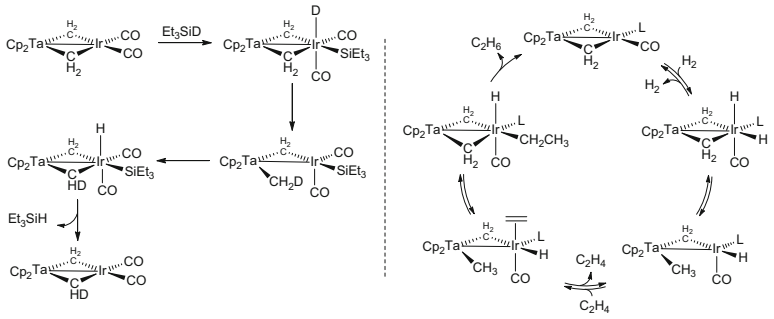

Scheme 51 Proposed mechanisms for the isotopic exchange and catalytic hydrogenation of ethylene with complexes **91** and **92**

center (Scheme 51). In the case of the catalytic hydrogenation of olefins, the reductive elimination of the methylene bridge assisted by the early metal would offer more favored route toward unsaturated coordinated Ir center than PPh_3 or CO dissociation.

Complex **91** was also found to catalyze hydrosilylation of ethylene with a variety of silanes (Me_3SiH, Et_3SiH, Ph_3SiH). Kinetic studies have been undertaken on this reaction and have shown that the rate of this reaction depends upon the concentration of complex and ethylene but is independent of the concentration of silane. In the absence of alkene, the reaction of complex **91** with Et_3SiD results in the incorporation of deuterium into the methylene bridges as what has been observed with D_2. However, the addition of an overpressure of CO to a hydrosilylation reaction inhibits considerably the rate of the reaction. Therefore, Bergman proposed that the necessary creation of open coordination site on Ir center operates by simple CO ligand dissociation and not by Ta-induced methylene bridge elimination as in the hydrogenation reaction. Hydrogenation experiments have been also conducted with $[Cp_2Ta(\mu\text{-}CH_2)_2IrH(Cp^*)]$(**93**). This complex promotes hydrogenation of ethylene in ethane at room temperature with TOF equal to 1 h^{-1}. Under D_2, complex **93** promotes also the reduction of ethylene in deuterated ethane but without incorporation of D in the μ-CH_2 bridge. This can be correlated to the fact that the opening of the methylene bridge in complex **93** occurred under H_2 atmosphere, as it has been observed with complex **91** but at a much higher temperature (105°C). In addition, it was shown that the hydrogenation of ethylene in the presence of **93** was inhibited by adding PMe_3, whereas PMe_3 does not react with **93**. All these data led Bergman to propose that complex **93** is not itself the real catalyst but in situ produces a very active species (*i.e.*, monometallic rhodium complex) whose activity is blocked by PMe_3.

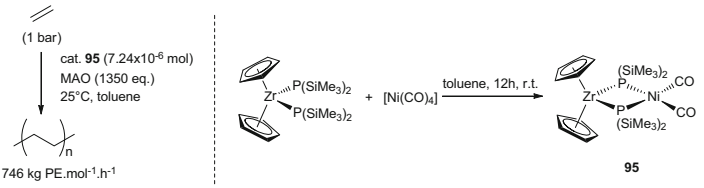

Scheme 52 Polymerization of ethylene catalyzed by a heterobimetallic Ni/Zr complex

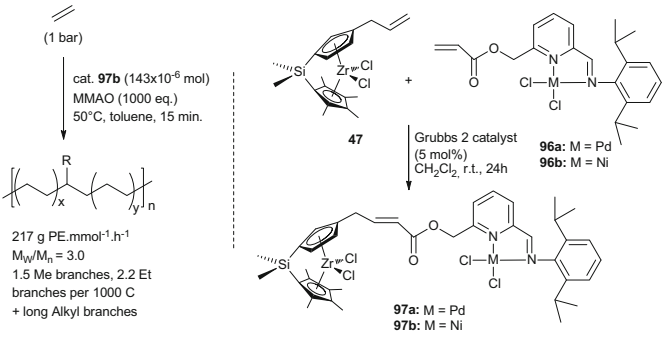

Scheme 53 Polymerization of ethylene catalyzed by a heterobimetallic Ni/Zr complex

3.3 Group 10/Group 4–5 Heterobimetallic Complexes

Despite group 10 metal complexes being extensively used in catalysis, examples of early–late bimetallic catalysis with group 10 metals are rare. Hey-Hawkins and Eisen have assessed the catalytic performances of the heterobimetallic Ni/Zr complex **95** associated with MAO in polymerization of ethylene and propylene (Scheme 52) [140, 141]. The bimetallic complex was synthesized *via* the reaction of the zirconocene diphosphido ligand $[Cp_2Zr(PSiMe_3)_2]$ with $[Ni(CO)_4]$. The X-ray crystal structure of **95** shows a Zr–Ni distance of 3.038(1) Å larger than the sum of the covalent radii precluding Zr–Ni bond. Complex **95**, in the presence of a large excess of MAO, was found to be active for the polymerization of ethylene and propylene. However, higher catalytic activity was obtained with an analogous Zr–Mo bimetallic complex. The authors suggest that a strong donor interaction takes place between Ni and the Zr center which slow down the polymerization catalytic activity.

Osakada has tested in parallel to Co/Zr complexes **49** described in Sect. 3.2.1, an analogous system with Pd and Ni as late metal partners [97]. Palladium was found to have no effect on the catalytic activity of zirconium, while the Ni/Zr complex **97b** enables concomitant oligomerization at the nickel center and enchainment of the resultant branched oligomers to the polymer grown at the Zr center giving rise to polyethylene with methyl, ethyl, and long alkyl branches. A control reaction performed with a mixture of the mononuclear complexes **47** and **96b** gave also polymers but with almost no alkyl branches (Scheme 53).

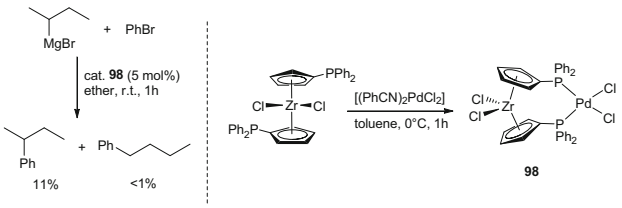

Scheme 54 Cross-coupling reaction catalyzed by a heterobimetallic Pd/Zr complex

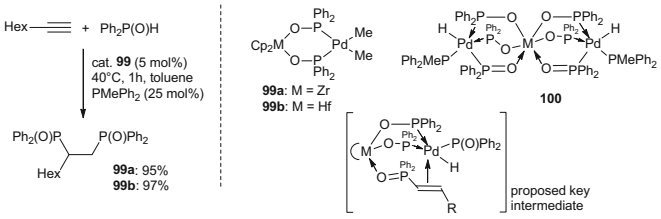

Scheme 55 Hydrophosphinylation reaction catalyzed by heterobimetallic Pd/Zr and Pd/Hf complexes

The Pd/Zr complex **98** reported by Erker was assessed as catalyst for Kumada cross-coupling reaction [120]. This complex was synthesized by addition of the metalloligand $[(CpPPh_2)_2ZrCl_2]$ to $[PdCl_2(PhCN)_2]$ (Scheme 54). Complex **98** was found to be a better catalyst in cross-coupling reaction of *sec*-butylmagnesium bromide with bromobenzene or *p*-bromoanisole with respect to activity and regioselectivity than conventional catalysts that are $[PdCl_2(PPh_3)_2]$ or $[PdCl_2(dppp)_2]$. However, comparison with $[PdCl_2(dppf)]$ (dppf=1,1′-diphenylphosphinoferrocene) shows that the latter gives coupling products with analogous selectivity but is much more active (35% yield after 0.5 h). This last result suggests that the catalytic behaviors of **98** are rather due to the metallocene skeleton of the diphosphane ligand than the early metal center itself and to a potent "bimetallic effect."

In 2008, Mizuta has shown that the binuclear complexes **99** with added $PMePh_2$ can promote the double hydrophosphinylation of 1-octyne under milder reaction conditions than $[Pd(PPh_3)_4]$ which required enforcing conditions (refluxing toluene, 24 h) for getting similar results (Scheme 55) [142] (for hydrophosphinylation with $Pd(PPh_3)_4$, see [143, 144]). They have shown that the reaction of the bimetallic complexes **99** with $PPh_2(O)H$ and $PMePh_2$ led to trinuclear complexes **100** with liberation of the cyclopentadienyl ligand. A mixture of mononuclear $[Cp_2MCl_2]$ and $[PdMe_2(tmeda)]$ complexes with $PMePh_2$ gave rise also to the formation of the trinuclear complexes **100** and gave comparable results in catalytic hydrophosphinylation of 1-octyne to those obtained with the bimetallic complexes **99** and $PMePh_2$. The authors propose therefore a mechanism in which the trinuclear complexes **100** are the active catalysts and where the coordination of the phosphane oxide function of the monohydrophosphinylated product interacts with the early metal, thus facilitating the second hydrophosphinylation at the Pd center.

4 Dual Catalysis from Early and Late Metal Complexes

As we already mentioned earlier in this chapter, there have been a huge variety of multi-catalytic systems and cooperative effects that have been described. Among them, examples of the simultaneous use of separated early and late transition metal catalysts however remain somewhat scarce. Nonetheless one could use these examples as an inspiration to design early–late heterobimetallic complexes with the hope to encompass performances of separated systems.

Olefin polymerization is an obvious field to apply dual catalysis from early and late metal complexes owing to the well-recognized olefin polymerization properties of group 4/5 metal complexes (*Ziegler-type catalysts*) and oligomerization or polymerization ability of some late transition metals. As an example, Bianchini et al. reported the use of Zr/Co or Ti/Co tandem polymerization systems for the homogeneous surface coating of multiwalled carbon nanotubes with linear low-density polyethylene (*LLDPE*) [145]. In these systems, the role devoted to the cobalt catalyst is to produce α-olefins from ethylene (mainly 1-butene and 1-hexene) which are subsequently incorporated in the polyethylene chain during the zirconium- or titanium-catalyzed ethylene polymerization process (Scheme 56). Thus, using the same 6-thienyl-2-(imino)pyridine cobalt complex **101**, LLDPE-coating containing only ethyl branching was obtained with [Cp_2ZrCl_2] **102**, while a non-negligible amount of butyl branching was observed with the hemititanocene complex **103**. It is noteworthy that the total branch content, as well as the Et/Bu branching ratio for the Ti/Co system, was found to be dependent on the early–late complex ratio, a parameter that of course would not be tunable if using a predefined heterobimetallic complex. It should be also mentioned that incorporating Zr and Co in the same heterobimetallic catalyst for ethylene polymerization to LLDPE was already exploited by Osakada as mentioned above (see complex **49** Scheme 31).

Less refined metallic species can be employed to perform dual polymerization processes. In 2007, Kong and Pan described the use of a simple [Cp_2TiCl]/$CuBr_2$

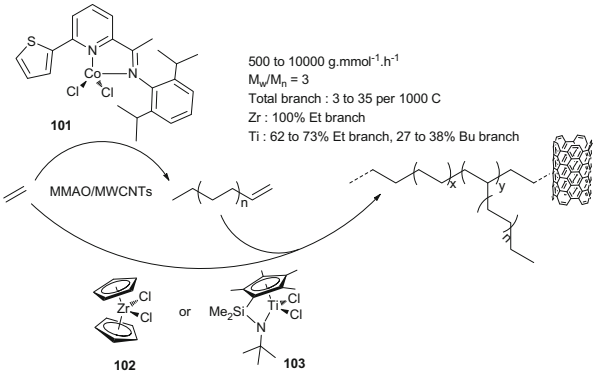

Scheme 56 Tandem multiwalled carbon nanotubes (MWCNTs) coating through in situ copolymerization catalysis of ethylene with Zr/Co or Ti/Co systems

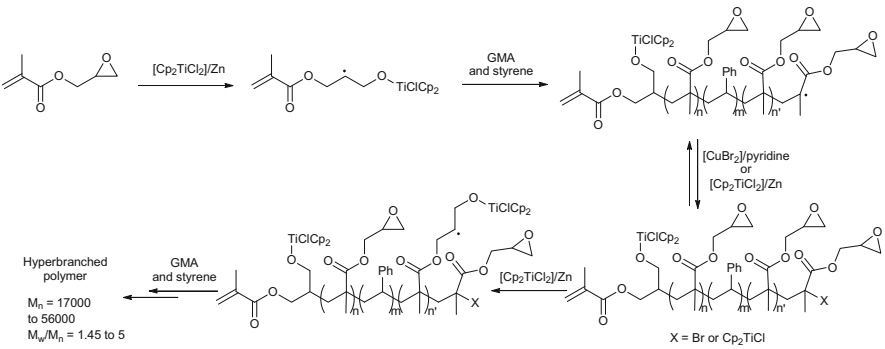

Scheme 57 Glycidyl methacrylate/styrene copolymerization promoted by a Ti/Cu combination

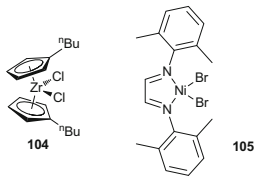

Scheme 58 Example of a Zr/Ni combination used for reactor blending in ethylene polymerization

mixture in the presence of bipyridine to perform the controlled radical polymerization of glycidyl methacrylate (GMA) and styrene and to form hyperbranched polymers (Scheme 57) [146]. The Ti(III) species was simply obtained by in situ reduction of $[Cp_2TiCl_2]$ with zinc. It should be pointed out that in this case the Ti (III) and Cu(II) complexes do not act as catalysts but serve as radical initiator and living radical polymerization mediator, respectively.

Frontier with the subject of this paragraph, the use of early and late metal complexes combinations for reactor blending during ethylene polymerization can also be mentioned. In such a process, known since the 1980s, the early and late catalysts polymerize ethylene independently to afford an intimate mixture of polyethylene (*PE*) chains of different structure. Although in this case there is no cooperative effect of the two metals from a molecular or mechanistic point of view, the beneficial simultaneous use of the two catalysts, such as a dichlorozirconocene and a diimine nickel complex (Scheme 58) ([147] and references therein), is found in the bulk physicochemical properties of the obtained PE.

If one thinks about a cooperative effect between early and late transition metals, an obvious idea is to take advantage of their electrophilic and nucleophilic properties. This concept was used by Sisak and Halmos for the ring opening of oxiranes using combinations of group 4 metal derivatives and cobalt carbonyl [148]. Using different well-chosen titanium, zirconium, hafnium, and cobalt precursors, they showed that it is possible to generate in situ a bimetallic complex with a M–Co bond (M=Ti, Zr, Hf). However, this bond splits when the complex reacts with oxiranes, the electropositive early metal reacts with the Lewis basic oxygen of the substrate,

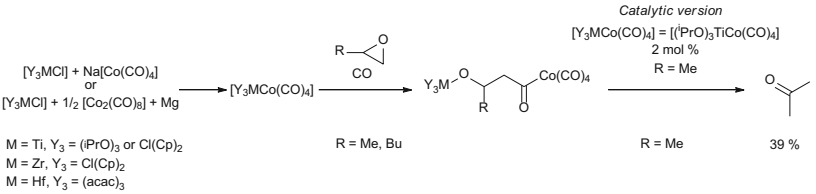

Scheme 59 Oxirane ring opening with early–late combinations

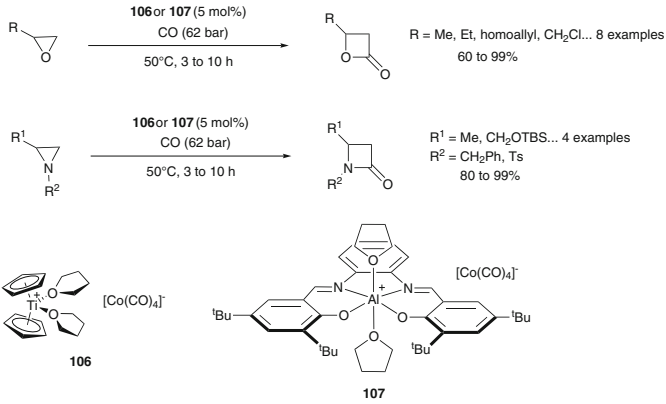

Scheme 60 Catalytic oxirane and aziridine carbonylative ring expansion

and the cobalt moiety performs a nucleophilic attack on a carbon center (Scheme 59). A CO molecule, originating from partial decomposition of starting materials, is then subsequently inserted in the Co–C bond. A catalytic version was attempted using [TiCl(*i*PrO)$_3$] and Na[Co(CO)$_4$] (2 mol%) as precatalysts. Acetone, resulting from carbonyl disinsertion from the acylcobalt intermediate and subsequent β-hydride elimination, was obtained in 39% yield.

With the same concept, but using the more reactive Ti(III) cationic radical [Cp$_2$TiCl(THF)$_2$]$^+$or a cationic salphen aluminum complex in combination with the cobalt anion [Co(CO)$_4$]$^-$, Coates et al. succeeded to make the epoxide or aziridine carbonylative ring expansion reaction catalytic (Scheme 60) [149]. For both substrates, it is proposed a nucleophilic attack of the cobalt anion at the least-substituted carbon atom of the three-membered ring, the latter being activated by the Lewis acidic part of the catalyst. Of note, catalysts **106** and **107** used in this reaction are described as ion pairs rather than M–Co bond containing complexes.

In a series of papers, Bercaw et al. recently described a very elegant tantalum/iridium tandem alkane/alkene coupling ([150] and references therein). Especially exemplified with 1-hexene and heptane, this process involves the dimerization of two different alkenes (here 1-hexene and 1-heptene) catalyzed by the hemitantallocene **108**, while an iridium pincer complex **109** dehydrogenates the

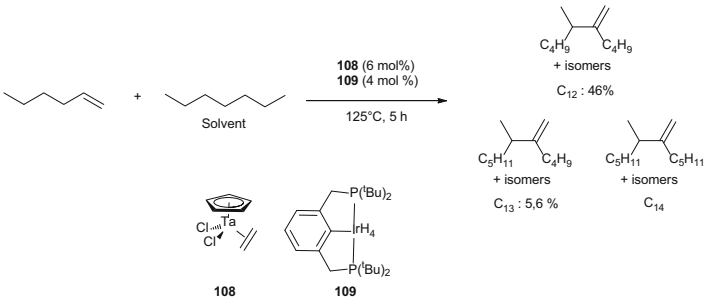

Scheme 61 Tandem catalyzed alkane/alkene coupling

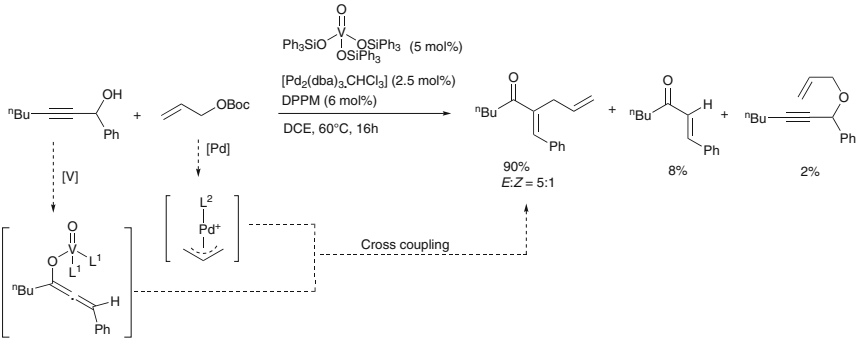

Scheme 62 Synthesis of α-allylated α,β-unsaturated ketones promoted by Pd/V catalytic combination

alkane (heptane) to produce more of one of the alkene (1-heptene) to be dimerized (Scheme 61). Although a large amount of C_{12} compound was obtained through the tantalum-catalyzed dimerization of 1-hexene, the presence of detectable amounts of C_{13} and C_{14} dimerization products indicates the formation of 1-heptene *via* the iridium-catalyzed dehydrogenation of heptane prior to alkene dimerization. Moreover, substantial amounts of hexane (45%) were also observed, thus indicating transfer hydrogenation from heptane to sacrificial 1-hexene. Thorough kinetic studies were conducted to optimize the tandem system. However, they revealed very different kinetics for the two catalysts, leading to the conclusion that "ideal" reaction conditions could only be a compromise.

Synergistic catalysis constitutes a powerful strategy for discovering new reactions. However, the implementation of such processes is highly challenging. Indeed, it involves the coupling of two reactive intermediates which belong to their own catalytic process and are therefore present in low concentrations with respect to other substrates and reagents. In 2011, Trost has developed this approach and described the synthesis of a great variety of α-allylated α,β-unsaturated ketones, esters, and amides from propargylic alcohols and allyl carbonates using a catalyst combination of $[O{=}V(OSiPh_3)_3]$ and a [Pd(dppm)] complex (Scheme 62)

[151]. The products have been obtained in moderate to excellent isolated yields with good chemo- and stereoselectivities. These results are all the more remarkable given that in optimized conditions the percentages of undesired Meyer–Schuster or *O*-allylation products are very low, while they are majority products when V or Pd catalyst are taken alone. The mechanism proposed by Trost for this reaction involves as key step the coupling of a vanadium allenoate and a π-allylpalladium intermediate, the rate of this bimolecular coupling being much faster than the competitive protonation or *O*-alkylation of the intermediates.

5 Early–Late Heterobimetallic Complexes as New Anticancer Agents

In this chapter, the interests of gathering an early metal with a late one were clearly put forward concerning the field of catalysis. Catalysis is not the only field using metals. Indeed, they are widely used in medicine as for treating stomach ulcers (bismuth) [152], diabetes (vanadium) [153], rheumatoid arthritis (gold) [154], cancer (platinum and others) [155], etc. As a consequence, early–late heterobimetallic complexes seem to be interesting objects to be investigated for their biological properties. Surprisingly, as far as we are aware, only two research groups published significant results on this subject [91, 156, 157, 158, 159]. The reasons may be the reputed instability of the early metal complexes in aqueous media. Indeed, for biological applications the compound should be stable enough in physiological media to reach its target.

Today, the only early metal integrated in heterobimetallic complexes for anticancer purposes is titanium. That might be explained considering that titanocene dichloride was the first organometallic complex which entered clinical trials in 1993 [160]. Its activity in vitro and in vivo in experimental models was really promising [161, 162] even in tumors difficult to treat [163]. Unfortunately, due to its lack of efficacy in patients, [Cp_2TiCl_2] did not fulfill the criteria required in phase II clinical trials. To tackle this problem, some researchers as Tacke [164] or Tshuva [165] designed specific titanium complexes which gave very promising results. Our group and Maria Contel's one chose another strategy: adding at least one late metal. Obviously, the choice of the second metal was made in the most promising metals in oncology: platinum, ruthenium, and gold [166]. Indeed, nowadays cisplatin and platinum derivatives are used in clinics in more than 50% of anticancer chemotherapeutic cocktails [167]. Several ruthenium complexes entered clinical trials such as NAMI-A, KP1019, or NKP1339. Concerning gold derivatives, two drugs used previously for rheumatoid arthritis – auranofin and sodium aurothiomalate – are now investigated in clinical trials for the treatment of cancer. Titanium and platinum are thought to enter nucleus of the cell and target DNA or chromatin, while most of ruthenium and gold complexes seem to accumulate in the cytoplasm and target

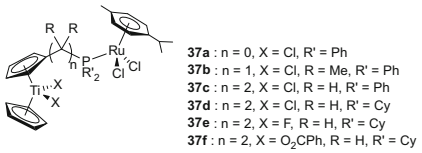

Fig 1 First early–late heterometallic complexes developed for an anticancer application

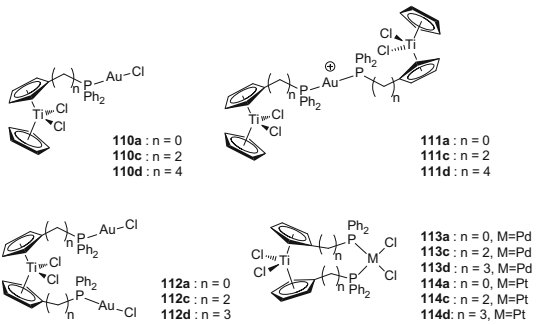

Fig. 2 Examples of Au/Ti, Pd/Ti, and Pt/Ti heterometallic complexes displaying interesting cytotoxic properties

enzymes, proteins, RNA, etc. Consequently, combining two metals with different targets should prevent resistance phenomena and may induce synergistic effects.

We published the first potential anticancer early–late complexes in 2010 (Fig. 1) [91]. The chosen combination was Ti–Ru. The ruthenium was bound to a titanocene dichloride *via* a phosphane introduced on a modified Cp. All the heterobimetallic complexes **37** were found to be considerably more active than the parent mononuclear titanocene dichloride and [(arene)$RuCl_2PR_3$] complexes or than the mixture of both of them. Moreover, the results suggested no cross-resistance with cisplatin. Cathepsin B inhibition was hypothesized as a possible mechanism of action.

These promising results drove us to study other combinations such as Au/Ti. The reaction of titanocenyl phosphanes with gold(I) ion complex led to the formation of neutral binuclear Au/Ti complexes **110** and cationic trinuclear complexes **111** (Fig. 2) [156]. In parallel, Contel's group developed Au/Ti (**112**), Pd/Ti (**113**), and Pt/Ti (**114**) complexes using similar synthetic strategy (Fig. 2) [157]. The conclusions of both studies are similar, and linking both metal ions clearly improves the cytotoxicity more than the simple cumulative effect. It was also shown that the heterobimetallic complexes can interact with DNA without claiming that it is their ultimate biomolecular target.

Contel's group then chose to focus on the stabilization of the bimetallic complex toward hydrolysis by using carboxylates bearing either phosphine [158] or thiolate [159] to bind the second metal (Fig. 3). The resulting complexes were found to be significantly more stable and more cytotoxic against human renal cancer cell lines than cisplatin and titanocene Y, which are benchmarks of the field. Undoubtedly, it means that the two metal centers induced synergistic effects. Biological experiments suggest that their mechanism of action put at stake pathways that involve the inhibition of thioredoxin reductase and decreased expression of protein kinases that drive cell migration. Moreover, in vivo trials with mice revealed a tumor reduction of about 67%.

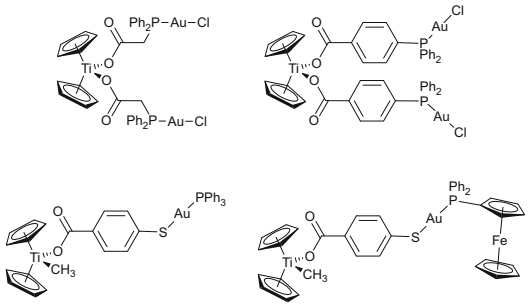

Fig. 3 Examples of Au/Ti displaying good stability in water

Overall, these different studies strongly support the efficacy of early–late complexes. Thus, when designing a new heterobimetallic complex, researchers should think to test its biological properties.

6 Conclusion

Since several decades, chemists are fascinated by "early–late" heterobimetallic complexes for their latent reactivity which makes them particularly promising candidates for catalysis. After an introductive part which aims at putting this topic in the broader context of cooperative catalysis, we identified several "early–late" combinations that have been used as catalyst. It appears that (group 9/groups 4–5) combinations have been far more studied than (group 8/group 4–5) or (group 10/group 4–5) combinations. This disparity is probably due to one of the main issues of bimetallic or dual catalysis that is the compatibility of the metal partners. Both electron-rich and electron-poor metals should indeed "tolerate" each other within the complex in its initial form but also throughout the catalytic process while their respective oxidation state and ligands are subject to change many times. Nevertheless, overall a wide range of catalytic reactions and "early–late" bimetallic complexes have yet been studied, and it appears in certain cases that bimetallic complexes surpass the performances of their monometallic counterparts or even are able to promote reactions which are not possible or difficult in monometallic series. Rather surprisingly and despite intensive research efforts, the development of a catalytic process which involves the double activation of an apolar substrate like dihydrogen and/or polar substrates like carbon monoxide or dioxide for which "early–late" heterobimetallic complexes have been originally designed remains challenging. The ways of cooperating for the two metals, when understood, were instead shown diverse, often complex, and difficult to foresee. If one takes a step back and looks at this topic objectively, it is clear that "early–late" bimetallic catalysis has lagged a little behind the global advance in cooperative catalysis. However, the recent progress registered in related multi-catalytic systems such as FLP catalysts clearly encourages chemists to persist in developing such "unnatural" combinations for developing new and challenging catalytic transformations. One

way for a more rational and efficient design of such species may consist in testing first a series of mononuclear early and late complexes in dual catalysis and then synthesizing the heterobimetallic complex with the hope that by bringing both metals closer, a better reactivity would be observed for kinetic reasons. Finally, cooperative effects or synergetic effects are not limited to catalysis, and the use of early–late bimetallic complexes for other purposes such as therapy constitutes also wonderful opportunity to widen the scope of this research.

References

1. Beller M, Bolm C (eds) (2004) Transition metals for organic synthesis, 2nd edn. Wiley-VCH, Weinheim, p 1344
2. Steinhagen H, Helmchen G (1996) Angew Chem Int Ed 35:2339–2342
3. Drauz K, Waldmann K (eds) (2002) Enzyme catalysis in organic synthesis, vols 1–3, 2nd edn. Wiley-VCH, Weinheim, p 1556
4. Wheatley N, Kalck P (1999) Chem Rev 99:3379–3419
5. Cooper BG, Napoline JW, Thomas CM (2012) Catalysis Reviews: Science and Engineering 54:1–40
6. Peters R (2015) Cooperative catalysis: designing efficient catalysts for synthesis. Wiley-VCH, Weinheim
7. Rowlands GJ (2001) Tetrahedron 57:1865–1882
8. Lee JM, Na Y, Han H, Chang S (2004) Chem Soc Rev 33:302–312
9. Shinde VS, Gajula B, Patil NT (2012) Org Biomol Chem 10:211–224
10. Allen AE, MacMillan DWC (2012) Chem Sci 3:633–658
11. Fogg D, Santos E (2004) Coord Chem Rev 248:2365–2379
12. Lohr TL, Marks TJ (2015) Nat Chem 7:477–482
13. Corey EJ, Bakshi RK, Shibata S, Chen C-P, Singh VK (1987) J Am Chem Soc 109:7925–7926
14. Corey EJ, Halal CJ (1998) Angew Chem Int Ed 37:1986–2012
15. Welch GC, Juan RRS, Masuda JD, Stephan DW (2006) Science 314:1124–1126
16. Stephan DW, Erker G (2010) Angew Chem Int Ed 49:46–76
17. Okino T, Hoashi Y, Takemoto Y (2003) J Am Chem Soc 125:12672–12673
18. Hamza A, Schubert G, Soós T, Pápai I, Am J (2006) Chem Soc 128:13151–13160
19. Siau W-Y, Wang J (2011) Catal Sci Technol 1:1298–1310
20. Ibrahem I, Cordova A (2006) Angew Chem Int Ed 45:1952–1956
21. Shao Z, Zhang H (2009) Chem Soc Rev 38:2745–2755
22. Du Z, Shao Z (2013) Chem Soc Rev 42:1337–1378
23. Ito Y, Sawamura M, Hayashi T (1986) J Am Chem Soc 108:6405–6406
24. Sasai H, Suzuki T, Arai S, Arai T, Shibasaki M (1992) J Am Chem Soc 114:4418–4420
25. Hashiguchi S, Fujii A, Takehara J, Ikariya T, Noyori R (1995) J Am Chem Soc 117:7562–7563
26. Yamakawa M, Ito H, Noyori R (2000) J Am Chem Soc 122:1466–1478
27. Shibasaki M, Sasai H, Arai T (1997) Angew Chem Int Ed Engl 36:1236–1256
28. Shibasaki M, Yoshikawa N (2002) Chem Rev 102:2187–2209
29. Shibasaki M, Kanai M, Matsunaga S, Kumagai N (2009) Acc Chem Res 42:1117–1127
30. Arai T, Sasai H, Aoe K-I, Okamura K, Date T, Shibasaki M (1996) Angew Chem Int Ed Engl 35:104–106
31. Hamashima Y, Kanai M, Shibasaki M (2000) J Am Chem Soc 122:7412–7413
32. Shibasaki M, Kanai M, Funabashi K (2002) Chem Comm 1989–1999

33. Shvo Y, Czarkie D, Rahamim Y (1986) J Am Chem Soc 108:7400–7402
34. Gunanathan C, Milstein D (2013) Science 341:249–260
35. Maire P, Buttner T, Breher F, Le Floch P, Grützmacher H (2005) Angew Chem Int Ed 44:6318–6323
36. Zweifel T, Naubron JV, Grützmacher H (2009) Angew Chem Int Ed 48:559–563
37. Grützmacher H (2008) Angew Chem Int Ed 47:1814–1818
38. Kashiwame Y, Kuwata S, Ikariya T (2012) Organometallics 31:8444–8455
39. Nebra N, Monot J, Shaw R, Martin-Vaca B, Bourissou D (2013) ACS Catal 3:2930–2934
40. Bratko I, Gómez M (2013) Dalton Trans 42:10664–10681
41. Feng G, Natale D, Prabaharan R, Mareque-Rivas JC, Williams NH (2006) Angew Chem Int Ed 45:7056–7059
42. Konsler RG, Karl J, Jacobsen EN (1998) J Am Chem Soc 120:10780–10781
43. Larrow JF, Schaus SE, Jacobsen EN (1996) J Am Chem Soc 118:7420–7421
44. Tokunaga M, Larrow JF, Kakiuchi F, Jacobsen EN (1997) Science 277:936–938
45. Annis DA, Jacobsen EN (1999) J Am Chem Soc 121:4147–4154
46. Trost BM, Ito H (2000) J Am Chem Soc 122:12003–12004
47. Li H, Marks TJ (2006) Proc Nat Acad Sci 103:15295–15302
48. Delferro M, Marks TJ (2011) Chem Rev 111:2450–2485
49. Guo N, Li L, Marks TJ (2004) J Am Chem Soc 126:6542–6543
50. Doyle MP, Austin RE, Bailey AS, Dwyer MP, Dyatkin AB, Kalinin AV, Kwan MMY, Liras S, Oalmann CJ (1995) J Am Chem Soc 117:5763–5775
51. Goto T, Takeda K, Shimada N, Nambu H, Anada M, Shiro M, Ando K, Hashimoto S (2011) Angew Chem Int Ed 50:6803–6808
52. Hashimoto S, Watanabe N, Ikegami S (1990) Tetrahedron Lett 31:5173–5174
53. Doyle MP, Westrum LJ, Wolthuis WNE, See MM, Boone WP, Bagheri V, Pearson MM (1993) J Am Chem Soc 115:958–964
54. Davies HML, Hutcheson DK (1993) Tetrahedron Lett 34:7243–7246
55. Doyle MP, Duffy R, Ratnikov M, Zhou L (2010) Chem Rev 110:704–724
56. Colacot TJ (2000) Proc Indian Acad Sci (Chem Sci) 112:197–207
57. Lebel H, Marcoux J-F, Molinaro C, Charette AB (2003) Chem Rev 103:977–1050
58. Broussard ME, Juma B, Train SG, Peng WJ, Laneman SA, Stanley GG (1993) Science 260:1784–1788
59. Matthews RC, Howell DK, Peng W-J, Train SG, Treleaven WD, Stanley GG (1996) Angew Chem Int Ed Engl 35:2253–2256
60. Aubry DA, Bridges NN, Ezell K, Stanley GG (2003) J Am Chem Soc 125:11180–11181
61. Powers DC, Geibel MAL, Klein JEMN, Ritter T (2009) J Am Chem Soc 131:17050–17051
62. Dick AR, Hull KL, Sanford MS (2004) J Am Chem Soc 126:2300–2301
63. Powers DC, Benitez D, Tkatchouk E, Goddard WA III, Ritter T (2010) J Am Chem Soc 132:14092–14103
64. Sonogashira K, Tohda Y, Hagihara N (1975) Tetrahedron Lett 16:4467–4470
65. Sonogashira K (2002) In: Handbook of organopalladium chemistry for organic synthesis, vol 1, Chap III.2.8. Wiley-Interscience: New-York, pp 493–529
66. Sawamura M, Sudoh M, Ito Y (1996) J Am Chem Soc 118:3309–3310
67. Goossen LJ, Rodríguez N, Linder C (2008) J Am Chem Soc 130:15248–15249
68. Hidai M, Fukuoka A, Koyasu Y, Uchida Y (1986) J Mol Cat 35:29–37
69. Jeong N, Seo SD, Shin JY (2000) J Am Chem Soc 122:10220–10221
70. Smidt J, Hafner W, Jira R, Sedlmeier J, Sieber R, Rüttinger R, Kojer H (1959) Angew Chem 71:176–182
71. Jira R (2009) Angew Chem Int Ed 48:9034–9037
72. Chu L, Lipshultz JM, MacMillan DWC (2015) Angew Chem Int Ed 54:7929–7933
73. Wang J, Li H, Guo N, Li L, Stern CL, Marks TJ (2004) Organometallics 23:5112–5114
74. Zanardi A, Mata JA, Peris E (2009) J Am Chem Soc 131:14531–14537
75. Mata JA, Ekkerhardt Hahn F, Peris E (2014) Chem Sci 5:1723–1732

76. Gade LH (2000) Angew Chem Int Ed 39:2659–2678
77. Hanna TA, Baranger AM, Bergman RG (1995) J Am Chem Soc 117:11363–11364
78. Bullock RM, Casey CP (1987) Acc Chem Res 20:167–173
79. Stephan DW (1989) Coord Chem Rev 95:41–107
80. Green MLH, Popham NH (1999) J Chem Soc Dalton Trans 1049–1059
81. Shafir A, Arnold J (2001) J Am Chem Soc 123:9212–9213
82. Shafir A, Arnold J (2003) Organometallics 22:567–575
83. Miyazaki T, Tanabe Y, Yuki M, Miyake Y, Nishibayashi Y (2011) Organometallics 30:2394–2404
84. Gregson CKA, Gibson VC, Long NJ, Marshall EL, Oxford PJ, White AJP (2006) J Am Chem Soc 128:7410–7411
85. Wang X, Thevenon A, Brosmer JL, Yu I, Khan SI, Mehrkhodavandi P, Diaconescu PL (2014) J Am Chem Soc 136:11264–11267
86. Le Gendre P, Richard P, Moïse C (2000) J Organomet Chem 605:151–156
87. Bareille L, Comte V, Le Gendre P, Richard P, Moïse C (2005) Eur J Inorg Chem 2451–2456
88. Le Gendre P, Picquet M, Richard P, Moïse C (2002) J Organomet Chem 643–644:231–236
89. Fürstner A, Ackermann L (1999) Chem Commun 95–96
90. Fürstner A, Liebl M, Lehmann CW, Picquet M, Kunz R, Bruneau C, Touchard D, Dixneuf PH (2000) Chem Eur J 6:1847–1857
91. Pelletier F, Comte V, Massard A, Wenzel M, Toulot S, Richard P, Picquet M, Le Gendre P, Zava O, Edafe F, Casini A, Dyson PJ (2010) J Med Chem 53:6923–6933
92. Le Gendre P, Comte V, Michelot A, Moïse C (2003) Inorg Chim Acta 350:289–292
93. Goux J, Le Gendre P, Richard P, Moïse C (2005) J Organomet Chem 690:301–306
94. Goux J, Le Gendre P, Richard P, Moïse C (2006) J Organomet Chem 691:3239–3244
95. Borguet Y, Delfosse S, Sauvage X, Delaude L, Demonceau A, Bareille L, Le Gendre P, Moïse C (2008) PolymerPreprint 49:24–25
96. Miyazaki T, Tanabe Y, Yuki M, Miyake Y, Nishibayashi Y (2011) Organometallics 30:3194–3199
97. Kuwabara J, Takeuci D, Osakada K (2006) Chem Commun 3815–3817
98. Sue T, Sunada Y, Nagashima H (2007) Eur J Inorg Chem 2897–2908
99. Greenwood BP, Forman SI, Rowe GT, Chen C-H, Foxman BM, Thomas CM (2009) Inorg Chem 48:6251–6260
100. Greenwood BP, Rowe GT, Chen C-H, Foxman BM, Thomas CM (2010) J Am Chem Soc 132:44–45
101. Zhou W, Napoline JW, Thomas CM (2011) Eur J Inorg Chem 2029–2033
102. Zhou W, Saper NI, Krogman JP, Foxman BM, Thomas CM (2014) Dalton Trans 1984–1989
103. Setty VN, Zhou W, Foxman BM, Thomas CM (2011) Inorg Chem 50:4647–4655
104. Zhou W, Marquard SL, Bezpalko MW, Foxman BM, Thomas CM (2013) Organometallics 32:1766–1772
105. Senocq F, Randrianalimanana C, Thorez A, Kalck P, Choukroun R, Gervais D (1984) Chem Commun 1376–1377
106. Choukroun R, Gervais D, Jaud J, Kalck P, Senocq F (1986) Organometallics 5:67–71
107. Senocq F, Randrianalimanana C, Thorez A, Kalck P (1986) J Mol Catal 35:213–219
108. Choukroun R, Dahan F, Gervais D, Rifai C (1990) Organometallics 9:1982–1987
109. Choukroun R, Iraqi A, Gervais D (1986) J Organomet Chem 311:C60–C62
110. Choukroun R, Iraqi A, Gervais D, Daran J-C, Jeannin Y (1987) Organometallics 6:1197–1201
111. Choukroun R, Gervais D, Kalck P, Senocq F (1987) J Organomet Chem 335:C9–C12
112. Trzeciak AM, Ziólkowski JJ, Choukroun R (1991) J Organomet Chem 420:353–358
113. Choukroun R, Iraqi A, Rifai C, Gervais D (1988) J Organomet Chem 353:45–52
114. Trzeciak AM, Ziólkowski JJ, Choukroun R (1996) J Mol Catal 110:135–139
115. Gelmini L, Stephan DW (1988) Organometallics 7:849–855
116. Gogoi U, Guha AK, Phukan AK (1991) Organometallics 30:5991–6002

117. Larsonneur A-M, Choukroun R, Daran J-C, Cuenca T, Flores JC, Royo P (1993) J Organomet Chem 444:83–89
118. Casado MA, Pérez-Torrente JJ, Ciriano MA, Oro LA, Orejón A, Claver C (1999) Organometallics 18:3035–3044
119. Hernandez-Gruel MAF, Pérez-Torrente JJ, Ciriano MA, Rivas AB, Lahoz FJ, Dobrinovitch IT, Oro LA (2003) Organometallics 22:1237–1249
120. Bosch BE, Brümmer I, Kunz K, Erker G, Fröhlich R, Kotila S (2000) Organometallics 19:1255–1261
121. Cornelissen C, Erker G, Kehr G, Fröhlich R (2005) Organometallics 24:214–225
122. Quirmbach M, Kless A, Holz J, Tararov V, Börner A (1999) Tetrahedron Asymmetry 10:1803–1811
123. Kalck P, Serra C, Machet C, Broussier R, Gautheron B, Delmas G, Trouvé G, Kubicki M (1993) Organometallics 12:1021–1022
124. Yoshitaka Y, Suzuki N, Mise T, Wakatsuki Y (1999) Organometallics 18:996–1001
125. Takayama C, Yamaguchi Y, Mise T, Suzuki N (2001) J Chem Soc Dalton Trans 948–953
126. Slaughter LM, Wolczanski PT (1997) Chem Commun 2109–2110
127. Morgan JP, Kundu K, Doyle MP(2005) Chem Commun 3307–3309
128. Barnhart RW, Bosnich B (1995) Organometallics 14:4343–4348
129. Le Gendre P, Maubrou E, Blacque O Boni G, Moïse C (2001) Eur J Inorg Chem 1437–1440
130. Comte V, Le Gendre P, Richard P, Moïse C (2005) Organometallics 24:1439–1444
131. Fandos R, Hernández C, Otero A, Rodríguez A, Ruiz MJ, Terreros P (2003) Chem Eur J 9:671–677
132. Ojeda M, Fandos R, Fierro JLG, Otero A, Pastor C, Rodríguez A, Ruiz MJ, Terreros P (2006) J Mol Catal A Chem 44–51
133. van Leeuwen PWNM, Rivillo D, Raynal M, Freixa Z (2011) J Am Chem Soc 133:18652–18665
134. Hostetler MJ, Bergman RG (1990) J Am Chem Soc 112:8621–8623
135. Hostetler MJ, Butts MD, Bergman RG (1993) J Am Chem Soc 115:2743–2752
136. Leelasubcharoen S, Zhizhko PA, Kuzmina LG, Churakov AV, Howard JAK, Nikonov GI (2009) Organometallics 28:4500–4506
137. Oishi M, Oshima M, Suzuki H (2014) Inorg Chem 53:6634–6654
138. Hostetler MJ, Butts MD, Bergman RG (1993) Organometallics 12:65–75
139. Butts MD, Bergman RG (1994) Organometallics 13:2668–2676
140. Lindenberg F, Shribman T, Sieler J, Hey-Hawkins E, Eisein MS (1996) J Organomet Chem 515:19–25
141. Shribman T, Kurz S, Senff U, Lindenberg F, Hey-Hawkins E, Eisein MS (1998) J Mol Catal A Chem 129:191–198
142. Mizuta T, Miyajima C, Katayama T, Ushio J-I, Kubo K, Miyoshi K (2009) Organometallics 28:539–546
143. Han L-B, Choi N, Tanaka M (1996) Organometallics 15:3259–3261
144. Allen A Jr, Ma L, Lin W (2002) Tetrahedron Lett 43:3707–3710
145. Toti A, Giambastiani G, Bianchini C, Meli A, Bredeau S, Dubois P, Bonduel D, Claes M (2008) Chem Mater 20:3092–3098
146. Kong L-Z, Pan C-Y (2007) Macromol Chem Phys 208:2686–2697
147. Mecking S (1999) Macromol Rapid Commun 20:139–143
148. Sisak A, Halmos E (2007) J Organomet Chem 692:1817–1824
149. Mahadevan V, Getzler YDYL, Coates GW (2002) Angew Chem Int Ed 41:2781–2784
150. Labinger JA, Leitch DC, Bercaw JE, Deimund MA, Davis ME (2015) Top Catal 58:494–501
151. Trost BM, Luan X, Miller Y (2011) J Am Chem Soc 133:12824–12833
152. Sun HZ, Zhang L, Szeto KY (2004) Met Ions Biol Syst 41:333–378
153. Thompson KH, Orvig C (2000) J Chem Soc Dalton Trans 2885–2892

154. Ward JR, Williams HJ, Egger MJ, Reading JC, Boyce E, Altz-Smith M, Samuelson CO Jr, Willkens RF, Solsky MA, Hayes SP, Blocka KL, Weinstein A, Meenan RF, Guttadauria M, Kaplan SB, Klippel J (1983) Arthritis Rheumatism 26:1303–1315
155. Rosenberg B, Vancamp L, Krigas T (1965) Nature 205:698–699
156. Wenzel M, Bertrand B, Eymin M-J, Comte V, Harvey JA, Richard P, Groessl M, Zava O, Amrouche H, Harvey PD, Le Gendre P, Picquet M, Casini A (2011) Inorg Chem 50:9472–9480
157. González-Pantoja JF, Stern M, Jarzecki AA, Royo E, Robles-Escajeda E, Varela-Ramírez A, Aguilera RJ, Contel M (2011) Inorg Chem 50:11099–11110
158. Fernández-Gallardo J, Elie BT, Sulzmaier FJ, Sanaú M, Ramos JW, Contel M (2014) Organometallics 33:6669–6681
159. Fernández-Gallardo J, Elie BT, Sadhukha T, Prabha S, Sanaú M, Rotenberg SA, Ramos JW, Contel M (2015) Chem Sci 6:5269–5283
160. Korfel A, Scheulen ME, Schmoll HJ, Gründel O, Harstrick A, Knoche M, Fels LM, Skorzec M, Bach F, Baumgart J, Sass G, Seeber S, Thiel E, Berdel WE (1998) Clin Cancer Res 4:2701–2708
161. Abeysinghe PM, Harding MM (2007) Dalton Trans 3474–3482
162. Olszewski U, Hamilton G (2010) Anticancer Agents Med Chem 10:302–311
163. Lümmen G, Sperling H, Luboldt H, Otto T, Rübben H (1998) Cancer Chemother Pharmacol 42:415–417
164. Strohfeldta K, Tacke M (2008) Chem Soc Rev 37:1174–1187
165. Tshuva EY, Ashenhurst JA (2009) Eur J Inorg Chem 2203–2218
166. Muhammad N, Guo Z (2014) Curr Opin Chem Biol 19:144–153
167. Klein AV, Hambley TW (2014) In: Storr T (ed) Platinum-based anticancer agents in ligand design in medicinal inorganic chemistry. Wiley, Chichester, pp 9–10

Top Organomet Chem (2016) 59: 187–232
DOI: 10.1007/3418_2015_151

Published online: 17 December 2015

The Catalytic Binuclear Elimination Reaction: Importance of Non-linear Kinetic Effects and Increased Synthetic Efficiency

Marc Garland

Abstract In the context of metal-mediated organic synthesis, cooperativity and synergism are rather broad terms which are often used to denote systems where unusual rate or selectivity effects are observed. These effects can be exhibited by monometallic, heterobimetallic and even multimetallic systems. The present contribution looks exclusively at one of the simplest cases, namely, systems possessing simultaneously both mononuclear and dinuclear complexes (hence both monometallic and heterobimetallic are included, but multimetallic systems are excluded). In Sect. 1, a brief introduction to the general area and a working definition for catalytic binuclear elimination reaction (CBER) is provided. In Sect. 2, we step back and classify the broad range of systems under consideration in order to enumerate the host of reaction networks considered, the potential for non-linear kinetic effects and how this relates to concepts of synthetic efficiency. In Sect. 3, we return to specific examples of CBER, how they fit into the overall context of the systems classification and how they can be identified in an unambiguous manner using in situ spectroscopic techniques. Indeed, tests can be constructed which permit the experimentalist to check crucial features and characteristics consistent with CBER. The present contribution focuses on the subarea in which CBER systems exist and hence CBER's scope for organic syntheses.

Keywords Catalytic binuclear elimination reaction (CBER), Hydroformylation, In-situ spectroscopy, Rhodium

Contents

M. Garland (✉)
Institute of Chemical and Engineering Sciences (ICES), Agency for Science Technology and Research (A*STAR), 1 Pesek Rd, Jurong Island 627833, Singapore
e-mail: marc_garland@ices.a-star.edu.sg

1 Introduction

1.1 Catalytic Syntheses, Cooperativity and Synergism

In the catalytic sciences, and specifically in the context of organic synthesis, it is common to represent the catalytic transformation of reactants, namely, reagents (substrate(s)) to product(s) as shown in Fig. 1a. This simplified representation puts emphasis on the net transformation of reactants, which is indeed the proper emphasis for the vast majority of synthetic situations. In Fig. 1a, the details of the catalysis are embedded in the term [cat], and the details are in no manner explicit. Therefore, in fine heterogeneous catalysis [cat] is simply understood to be a heterogeneous catalyst, perhaps a supported metal added to the system [1], in enzymatic catalysis [cat] is usually understood to be a protein or metalloprotein added to the system [2], in organocatalysis [cat] is often understood to be an organic amine or phosphine added to the system [3], in acid/base catalysis [cat] may refer to H^+ or OH^- in the system or Lewis acids/bases [4], and in metal-mediated homogeneous catalysis, [cat] often refers to an inorganic or organometallic precursor added to the system [5].

On occasion, there is a secondary interpretation or meaning used for [cat] and that is the actual catalytic mechanism by which the reaction is effected or accelerated. It is this secondary meaning that will form the basis for the present exposition. In order to keep the reaction diagrams as simple and clear as possible in the present contribution, green boxes will always represent reagents (substrate(s)) and red

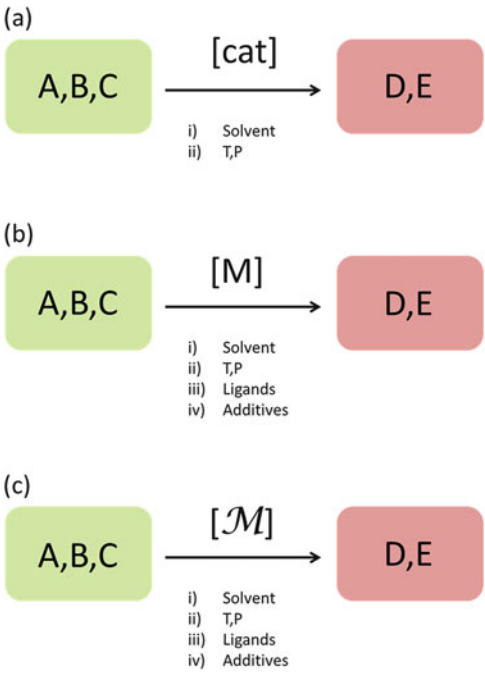

Fig. 1 (**a**) Perhaps the generically most common notation to denote a catalysed reaction of substrates A, B and C to products D and E throughout the catalytic sciences. (**b**) The most common notation for denoting a metal-mediated homogeneous catalytic reaction. (**c**) The stylized notation adopted in the present work to highlight that the cooperative or synergistic catalysis arises from an important structural feature in the underlying reaction mechanism

boxes will always represent product(s) even if there is no chemical formula or structure explicitly entered.

In metal-mediated homogeneous catalysis, the term [cat] is often focused on the metallic element involved. Thus, for example, in palladium-mediated C–C cross-coupling reactions [6], one typically simply sees the representation [Pd]. In generic terms, and particularly for the case of metal-mediated homogeneous organic synthesis, this representation becomes [M] as shown in Fig. 1b where M stands for the metallic element. In Fig. 1a, b, for metal-mediated homogeneous organic synthesis, the primary meaning of the argument within the brackets, namely, "M", becomes somewhat blurred (at least more so than in other catalytic chemistries). It could mean the precursor containing the mentioned metallic element; however, since in some respects the molecular understanding of catalysis is frequently more well defined in the case of homogeneous catalysis, [M] frequently signifies that emphasis is not on the precursor used but rather on the set of intermediates and hence mechanism that is operating. Indeed, it is widely appreciated by most practitioners that more than one precursor containing metallic element M is often effective in facilitating a specified reaction with similar rate and selectivity. As a consequence, for many chemists, the precursor that they use is often not of paramount importance, just as long as it contains metallic element M and consequently gives rise to the same mechanism.

Some homometallic and heterobimetallic metal-mediated homogeneous catalytic syntheses exhibit markedly unusual rate and/or selectivity patterns due to the underlying mechanism. Such systems will be distinguished by the stylized notation

[$\mathcal{M}$] as shown in Fig. 1c. Since the present book is dedicated to cooperativity or synergism [7] in metal-mediated *homogeneous* catalysis, the term [$\mathcal{M}$] in this chapter will possess four interrelated characteristics, and [$\mathcal{M}$] will:

(1) Denote a reaction mechanism.
(2) This reaction mechanism will arise from the application of one or two metallic elements in the catalytic system.
(3) The system will exhibit either an unusual rate dependence and/or an unusual selectivity pattern that has its origin(s) in the structure of the reaction mechanism and not in some secondary effect due to physico-chemical issues such as transport [8].
(4) Finally, all overall reactants for the organic reaction and all organometallic intermediates for this organic reaction are solvated during all individual reaction steps present in the catalytic reaction mechanism.

The motivation for stating point (4) arises from the fact that many so-called homogeneous catalytic reactions are actually present in multiphase slurries and these slurries arise, for example, and, in some cases, due to the addition of various insoluble additives or auxiliaries or the formation of precipitates. For the present chapter, point (4) explicitly excludes surface-mediated reaction steps in the homogeneous catalytic reaction mechanism.

The expression *unusual* has been deliberately been left open ended or ill defined since the effect will almost certainly differ between systems having different phenomenological bases for cooperativity or synergism. Nevertheless, a rather useful working definition might be *a rate or selectivity dependence which cannot be explained as a strictly additive effect of the metal*(*s*) *used*. Having said that, the homometallic and heterobimetallic catalytic binuclear elimination reactions (CBERs) which are the focus of this chapter have very well-defined rate dependences which can be traced back to the topology of the reaction mechanisms.

1.2 Stoichiometric Binuclear Elimination

Heck and Breslow [9] observed that the addition of $HCo(CO)_4$ to a solution of $CH_3COCo(CO)_4$ resulted in the formation of the corresponding aldehyde CH_3CHO and the *homometallic* dinuclear carbonyl $Co_2(CO)_8$. They postulated that such a reaction might be operating under alkene cobalt-mediated hydroformylation reaction conditions and thus contribute to aldehyde product formation. This observed stoichiometric reaction is apparently the first documented case of a well-defined reaction between two organometallic complexes RML_n and $R'M'L_m$, leading to the formation of an organic product and a dinuclear complex. This class of stoichiometric reactions became known as binuclear eliminations [10]. The generic representation for a stoichiometric *homometallic* binuclear elimination is shown in (Eq. 1) where $M = M'$ and where the Greek letter α will be used to denote the bimolecular reaction between mononuclear organometallics throughout the remainder of this chapter. Clearly Eq. 1 is not in general elementary, and it is not

immediately apparent at which step the bimolecular reaction really takes place. The genuine elementary α step might be the reaction of $HCo(CO)_4$ with coordinately unsaturated $CH_3COCo(CO)_3$:

$$\alpha\{\mathrm{RML}_n + \mathrm{R}'\mathrm{M}'\mathrm{L}_m \rightarrow \mathrm{RR}' + \mathrm{MM}'\mathrm{L}_{n+m}, \quad \mathrm{M} = \mathrm{M}' \tag{1}$$

Stoichiometric *heterobimetallic* binuclear eliminations are also known. Kovak et al. [11, 12] extensively studied a class of reactions closely related to the Heck and Breslow chemistry. Specifically, they studied the addition of $HMn(CO)_5$ with $EtOC(O)CH_2Co(CO)_4$ and $EtOC(O)Co(CO)_4$ yielding the corresponding products and heterobimetallic carbonyls. The generic representation for a stoichiometric *heterobimetallic* binuclear elimination is shown in Eq. 2 where $\mathrm{M} \neq \mathrm{M}'$, and again the Greek letter α will be used to denote the bimolecular reaction between mononuclear organometallics. Equation 2 is not in general elementary. The genuine elementary α step might be the reaction of $HMn(CO)_5$ with coordinately unsaturated $EtOC(O)CH_2Co(CO)_3$ and $EtOC(O)Co(CO)_3$:

$$\alpha\{\mathrm{RML}_n + \mathrm{R}'\mathrm{M}'\mathrm{L}_m \rightarrow \mathrm{RR}' + \mathrm{MM}'\mathrm{L}_{n+m}, \quad \mathrm{M} \neq \mathrm{M}' \tag{2}$$

Circa 35 rather well-defined stoichiometric homometallic and heterobimetallic binuclear elimination reactions have been identified to date. The synthetic products range from molecular hydrogen to hydrocarbons and even more functionalized organics.

1.3 The Catalytic Binuclear Elimination Reaction (CBER)

Considerable effort, often involving in situ spectroscopies, has been invested into identifying the catalytic analogues of stoichiometric binuclear elimination. Collectively, these synthetic and in situ studies, which will be discussed in greater detail in Sects. 2 and 3, have confirmed the existence of CBER. This catalytic reaction mechanism necessitates the simultaneous existence of two very special steps. The first step to mention is an α step between mononuclear organometallics leading to product formation and a dinuclear organometallic. The second crucial step will be denoted β, and this involves the fragmentation of the dinuclear organometallic back to mononuclear species.

The catalytic binuclear elimination reaction is now accepted as a recognized and defined term in the field of homogeneous catalysis [13]. The CBER reaction mechanism may be defined to be *a synthetic system possessing simultaneously both mononuclear and dinuclear organometallic intermediates, acting in a synchronized and bicyclic reaction topology, where each set of mononuclear intermediates carry an organic moiety which will eventually be part of the organic product*. Both the monometallic and heterobimetallic cases can be visualized using similar

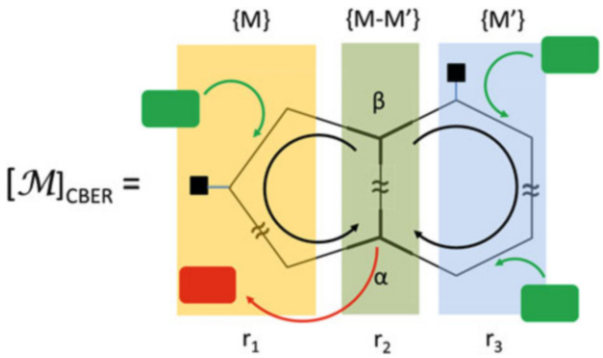

Fig. 2 The general structure of a single-product mechanism for a heterobimetallic catalytic binuclear elimination where {M} represents the set of mononuclear intermediates possessing metal M, {M′} represents the set of mononuclear intermediates possessing metal M′ and {M–M′} presents the set of heterobimetallic intermediates. The all-important steps α and β which transform mononuclear species to dinuclear species and dinuclear species to mononuclear species are highlighted for emphasis. The symbol ≈ allows each sequence to possess an arbitrary non-zero number of intermediates

representations as shown in Fig. 2. In this figure, (a) all nodes represent soluble organometallic intermediates; (b) all edges represent reactions; (c) there are two sequences of mononuclear intermediates highlighted in orange and light blue, and each sequence carries out a set of elementary transformations involving one or more substrates; (d) the sequence of dinuclear species is highlighted in grey–green; (e) the all important α and β steps are prominently displayed with bold edges; (f) reservoirs are present as black squares; and (g) the direction for the net flux of transformation is indicated by black arrows.

The nodes and hence intermediates represented in a CBER mechanism may or may not be unique. For example, in the heterobimetallic case shown in Fig. 2, the intermediates belonging to metal M in the orange sequence must all be distinct from the intermediates longing to metal M′ in the blue sequence. In the case of monometallic CBER, the mononuclear intermediates may not be distinct. If one demands that an intermediate appear exactly only one time in a graph, too many visually different types of representations can arise due to the variety of branching points. This causes considerable difficulties in visualizing the omnipresent bicyclic structure of CBER and in keeping track of the distinction between CBER and other topologies.

The bicyclic structure in Fig. 2 is extremely special and helps with one additional and very important concept, namely, rationalizing the rate of substrate consumption and product formation at steady state. Inspection indicates that the net r in moles of each sequence of transformations at steady state is identical (Fig. 2). Thus, in the heterobimetallic case, the net rate r_1 of reaction along the orange {M} sequence exactly equals the net rate r_3 along the blue {M′} sequence, and both of these net rates of reaction exactly equal the net rate r_2 along the grey–green dinuclear {M–M′} sequence. This situation exists regardless of any changes in the amounts of M or M′

in the system. The reaction network simply relaxes to a new steady state since the α and β steps control the ratios M:M–M′:M′. The same arguments exist for the various monometallic cases where M = M′, and this is treated in Sect. 2 in more detail.

The structure shown in Fig. 2 hints at the potential for spectacular rate increases with metal loading when the α step is rate determining. Since the general structure of a single-product mechanism allows only one route to product(s), issues concerning selectivity cannot be addressed by this structure alone (Fig. 2). Selectivity issues will be reserved for Sects. 2 and 3.

1.4 In Situ Spectroscopic Investigations, Specialized Experimental Set-Ups, Chemometrics

Understanding of the speciation under catalytic reaction conditions and hence confirmation of the catalytic binuclear elimination demonstrated in this chapter required detailed in situ (operando) techniques. These areas are simply not under the purview and scope of this chapter. Therefore it will be just briefly mentioned that two excellent textbooks on this subject, one focusing on the special case of homogeneous mechanisms [14] and the other general catalysis [15], exist and should be consulted. Moreover, there are reviews available which specifically focus on in situ FTIR in homogeneous catalysis [16], signal processing and chemometrics in homogeneous catalysis [17] and the concurrent use of combined in situ spectroscopy, chemometrics and DFT for confirming the identity of intermediates [18]. Information contained in the latter two reviews as well as on specialized hermetically sealed recirculating experimental instrumentation to conduct experiments with various types of reaction perturbations [19] will be of special importance to understanding the methods used in this chapter.

1.5 Brief Comment: Graph Theory and Flows in Networks

The literature related to graph theoretic representations of chemical reactions is vast [20], and there are numerous classes of representations which have been used. By far, the most frequent convention is to represent a reaction sequence with nodes representing species and arrows or edges of the graph representing a single elementary reaction step (note: sometimes authors use an arrow for a nonelementary reaction, or a set of nested arrows to do the same). Bipartite and multipartite graphs are another very useful class of representations; however, the cyclic connectivity of intermediates is much more difficult to visualize. Considering the importance of visualizing the cyclical nature of catalysis, the classic convention will be adopted throughout.

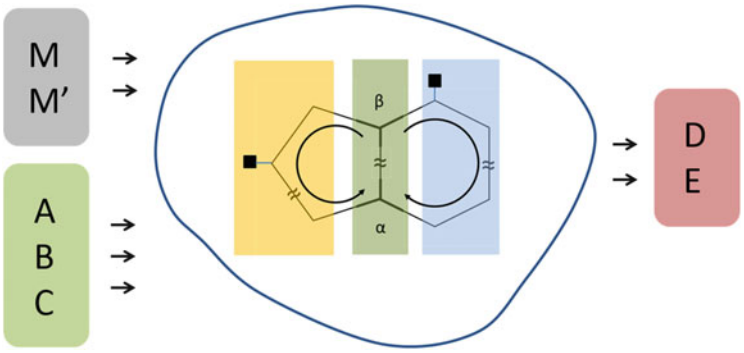

Fig. 3 The non-linear reaction mechanism $[\mathcal{M}]_{\mathrm{CBER}}$ in a pseudo-network representation, emphasizing that the inputs can be independently varied or perturbed in order to induce transients in the individual reaction rates and the concentration of intermediates. Such issues assist in verifying the underlying structure and characteristic of the system

Graph theoretic representations form the basis for evaluating individual fluxes, but moreover generating relationships for the overall flow through the graph or network [21]. Indeed, the most important global theorem for electrical flows through arbitrarily complex electrical networks is the Tellegen theorem [22]. The Tellegen theorem not only encompasses all known steady-state electrical engineering laws (Kirchhoff voltage law and Kirchhoff current law) but also captures the transient behaviour of all parts of the network. Recently, it has been shown that stoichiometric chemical reaction networks and even catalytic reactions can be appropriately represented in equivalent graph theoretic terms such that the Tellegen theorem can be applied [23]. One of the major applications of this new and exciting development is to verify that individual steps are self-consistent with the overall flux generated by the overall organic transformation (in other words, verify that the hypothesized catalytic reaction mechanism is indeed realistic). In the future, complex non-linear, cooperative/synergistic metal-mediated homogeneous systems will require sophisticated tools in order to verify individual steps and to verify consistency with the overall proposed reaction mechanisms (here, in situ spectroscopic information will be invaluable). This will probably lead to a better understanding of what cooperativity and synergism really mean. Work is currently going on in our laboratory to characterize the response of generic CBER networks, in terms of individual and overall fluxes, and to establish further characteristics of such systems (Fig. 3).

2 Connectivity of Catalytic Reaction Networks

This section will review the connectivity of some catalytic reaction networks starting from isolated one-product unicyclic mechanisms, connected unicyclic mechanisms showing selectivities (regio-, chemo- and stereoselectivities) and systems possessing more than one uncoupled unicyclic mechanisms. All of these systems exhibit various forms of *linear rate increases* versus *metal loading*. Subsequently, mechanisms exhibiting quadratic, linear–quadratic, bilinear and linear–bilinear rate dependences will be explored. CBER systems can exhibit any one of these four complex rate dependences.

2.1 Variations on Unicyclic Mechanisms

Maintaining the notation and convention introduced in Sect. 1, two simple single-product unicyclic catalytic reaction mechanisms possessing reservoirs are shown in Fig. 4a, b. A unicyclic catalytic reaction mechanism will be one where each and every intermediate possesses the same nuclearity [24]. Thus Fig. 4a represents a unicyclic reaction mechanism possessing just mononuclear intermediates, and Fig. 4b represents a unicyclic reaction mechanism possessing just dinuclear intermediates. Although the reaction in Fig. 4a, b is unicyclic, e.g. there is at least one continuous path or sequence of steps leading from organic reactant to product, this does not negate the possibility of closed loops adjacent to the main cyclic. Such closed loops adjacent to a cycle certainly exist. A good example is the CO insertion into an alkyl-metal bond in either a two-step sequence, i.e. $RML_n \rightarrow RMCOL_{n-1} \rightarrow RCOML_{n-1} \rightarrow RCOML_n$, or in a concerted manner $RML_n + CO \rightarrow RCOML_n$.

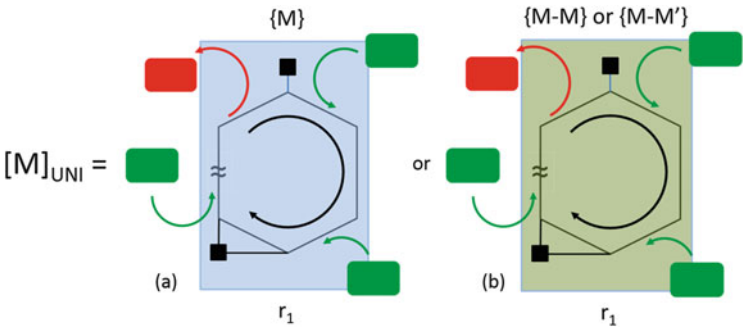

Fig. 4 Two unicyclic catalytic reaction mechanisms, one based on mononuclear intermediates {M} and one based on binuclear intermediates either {M–M} or {M–M′}. Again, *black squares* indicate reservoirs and the *closed loop triangle* suggests that many catalytic cycles have complex branches along the main synthetic sequence. The directed graph has a net rate of r_1 moles per time through the mechanism

King and Altman [25] were apparently the first to provide an analytic rate expression for a unicyclic catalytic mechanism. They performed this analysis in the context of homogeneous enzymatic catalysis, but the main result carries over directly to the case of metal-mediated homogeneous catalysis. Accordingly, for a mechanism possessing intermediates of one and the same nuclearity, the analytic rate expression in terms of the total steady-state concentrations of intermediates $\Sigma[I_i]$ is given by Eq. 3 where the turnover frequency term TOF contains terms in just rate constants k and steady-state concentrations of reactants (but no intermediates). The approach introduced by King and Altman has been verified and extended by others [26], particularly for developing rate expressions in terms of any individual intermediate I_i. As a consequence, it can be shown that the rate of product formation is a linear function of each intermediate concentration (Eq. 4). The importance of the analytical results is straightforward (Fig. 4a, b); regardless of the nuclearity of the intermediates, the rate is a linear function of the intermediate concentrations (at least this is the case observed with multimetallic metalloproteins). A unicyclic catalytic reaction mechanism possessing dinuclear intermediates does not exhibit a non-linear rate expression.

$$r_1 = \mathrm{TOF}\sum [I_i] \tag{3}$$

$$r_1 = k_i^{\mathrm{app}}[I_i] \tag{4}$$

More complex branching occurs in mechanisms where selectivities arise. Therefore, consider as an example the overall transformation of a symmetric alkene cyclopentene in the presence of CO and H_2 to both cyclopentane carboxaldehyde and cyclopentane, facilitated by the addition of a Group 9 (or CAS systems VIIIB) metal hydride complex HML_n capable of performing both hydroformylation [27, 28] and hydrogenation [29]. Upon addition of the metal hydride to the system, one would expect the steps $HML_n \rightarrow \mathbf{HML_{n-1}} \rightarrow \mathbf{H(\pi\text{-}cyclopentene)ML_{n-1}} \rightarrow \mathbf{C_5H_9ML_{n-1}}$ where the bold intermediates should be common to both unicyclic catalytic sequence of steps. At this point there is a branching in the network of intermediates, and one of either two paths is followed:

1. Molecular hydrogen activation occurs at the metal centre, eventually resulting in cyclopentane and HML_{n-1}.
2. CO association and then CO insertion occur, followed by molecular hydrogen activation at the metal centre, eventually resulting in cyclopentane carboxaldehyde and HML_{n-1}.

A possible graph representation for this interconnected unicyclic catalytic mechanism, possessing only mononuclear intermediates, which exhibits chemoselectivity resulting in two distinct products, is shown in Fig. 5. Again, the mechanism is colour-coded, representing the three distinct linear sequences of mononuclear intermediates. The light blue is strictly associated with those intermediates which produce aldehyde, the dark blue is associated strictly with those

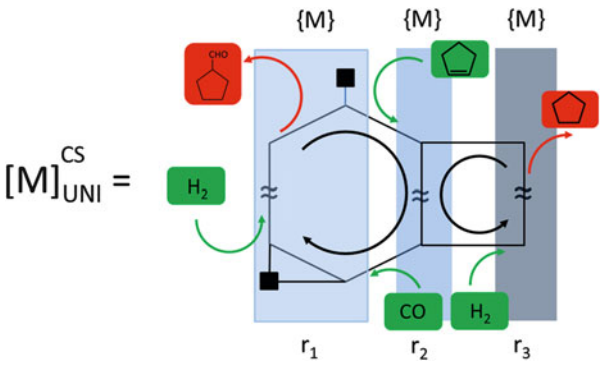

Fig. 5 A chemoselective (CS) unicyclic (UNI) mechanism which exhibits both hydrogenation and hydroformylation activities. A symmetric alkene, cyclopentene, is chosen as the substrate in order to reduce branching points and the number of cycles that can potentially arise. *Different shades of blue* are used to help to distinguish different sets of mononuclear intermediates

intermediates which produce alkane, and the medium blue represents intermediates common to both closed sequences.

If r_1 represents the rate of net reaction through the light blue path leading to aldehyde formation and if r_3 represents the rate of net reaction through the dark blue path leading to alkane formation, then the rate r_2 of net reaction through the medium blue pathway must be $r_2 = r_1 + r_3$. Stated in a language similar to King and Altman, there is a unique constant associated with each synthetic pathway, which relates the rate of each product formation for that pathway with the sum total concentration of all intermediates in the network (Eqs. 5 and 6). Moreover, the sum total productivity of the network (or more accurately said – the consumption of substrate) is also linear in the sum total concentration of all intermediates (Eq. 7).

$$r_1 = \mathrm{TOF}_1 \sum [I_\mathrm{i}] \tag{5}$$

$$r_3 = \mathrm{TOF}_3 \sum [I_\mathrm{i}] \tag{6}$$

$$r_2 = (\mathrm{TOF}_1 + \mathrm{TOF}_3) \sum [I_\mathrm{i}] \tag{7}$$

The above analysis and the above conclusions concerning rate linearity exist even if simultaneous and concurrent regioselectivity, stereoselectivity/stereodifferentiation [30] and chemoselectivity all occur together. Therefore, very briefly consider the overall transformation of styrene + CO + H_2 into *n*-aldehyde, (+) branched aldehyde, (−) branched aldehyde and ethylbenzene in a single system. Assume as before that a precursor HML_n is added to the system and that this precursor can effect both hydroformylation and hydrogenation. Then the species HML_{n-1} is the only intermediate common to all reaction pathways. In fact, it can be shown that there are eight synthetic pathways (taking into account enantiofaces) involving five interconnected unicyclic sequences resulting in four distinct products. Moreover, there are five overall rate expressions, one for each of the four

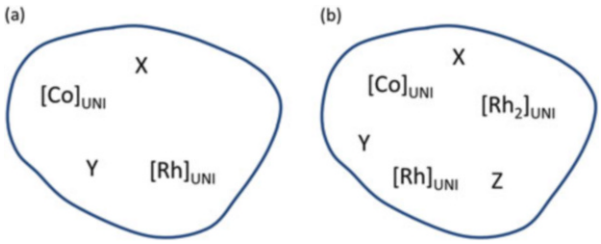

Fig. 6 (**a**) A homogeneous catalytic system containing exactly two independent unicyclic mechanisms for hydroformylation of a symmetric alkene. *X*, *Y*, *Z* are organometallic present which do not participate in a catalytic mechanism and do not interact with any intermediates. They are just spectator species. (**b**) The system after addition of a chelated dinuclear rhodium complex which also performs hydroformylation

distinct products plus one rate expression for consumption of styrene. The take-home message is that all five rate expressions are linear in the concentrations of intermediates. No intrinsic rate non-linearities exist in spite of the network complexity. The systematic evaluation of the number of independent synthetic routes in an arbitrary network was clearly developed in a mathematical framework by Horiuti [31].

In the context of unicyclic networks, one further case must be considered for completeness and this is the case of disjoint unicyclic mechanisms. In this case, assume that there are two precursors which independently and selectively effect alkene hydroformylation and that the mechanisms do not share any common intermediates whatsoever. Perhaps the first precursor is a bidentate phosphine-substituted mononuclear cobalt complex, and the second precursor is a mononuclear rhodium complex. This situation can be represented in shorthand notation as shown in Fig. 6a.

The consequence (Fig. 6a) is that the rate(s) can be expressed as a multilinear summation in the sum total of intermediates in each disjoint unicyclic mechanism (Eq. 8). Next assume one more precursor, for example, a chelated dinuclear rhodium complex [32], is added to the system. This dinuclear rhodium complex has been shown to facilitate hydroformylation via a unicyclic mechanism having exclusively dinuclear intermediates. This new system is illustrated in Fig. 6b where again it is assumed that the individual mechanisms do not have common intermediates and the intermediates in different mechanisms do not interact. In terms of canonical variables in the system, the rate(s) is still multilinear as shown in Eq. 9:

$$r_{\text{tot}} = \text{TOF}_{\text{Co}} \sum [I_{\text{i}}]_{\text{Co}} + \text{TOF}_{\text{Rh}} \sum [I_{\text{i}}]_{\text{Rh}} \tag{8}$$

$$r_{\text{tot}} = \text{TOF}_{\text{Co}} \sum [I_{\text{i}}]_{\text{Co}} + \text{TOF}_{\text{Rh}} \sum [I_{\text{i}}]_{\text{Rh}} + \text{TOF}_{\text{Rh}_2} \sum [I_{\text{i}}]_{\text{Rh}_2} \tag{9}$$

From an exploratory viewpoint and without detailed in situ information on the systems mentioned above, the experimentalist might be falsely led to believe that there is an intrinsic non-linear effect and non-linear cooperativity or synergism is

occurring in the system. Indeed, without in situ spectroscopic information and without proper mass balances, the experimentalist has just the nominal additions of metal complexes on which to base conclusions and the nominal loading are not the canonical variables for the system. The remainder of this chapter occasionally emphasizes this very important observation concerning the ease by which misleading conclusions can be obtained when supporting in situ spectroscopic information is not available.

2.2 *Monometallic and Heterobimetallic CBER: The Core Mechanisms*

2.2.1 Monometallic Case

The monometallic CBER mechanism $[\mathcal{M}]_{\mathrm{CBER}}$ occurs when $\mathrm{M} = \mathrm{M}'$ and hence only one metal is present. Figure 7 shows this case. There are two sequences of mononuclear intermediates from the set {M} and these are distinguished by the use of different shades of blue. One reason for representing these sequences in the same colour arises from the possibility that some of the organometallic intermediates in each sequence are not uniquely present in just one sequence. The sequence consisting of homometallic dinuclear complexes is colour-coded in grey–green. As before, there are two very special reactions α and β, and these transform mononuclear species into homometallic dinuclear complexes and homometallic dinuclear complexes into mononuclear species.

The rates in each sequence follow the rules set out in Sect. 1, namely, r in moles/time of each sequence of transformations is identical. Thus, in the homometallic case, the net rate r_1 of reaction along the light blue {M} sequence exactly equals the net rate r_3 along the medium blue {M} sequence, and both of these net rates of

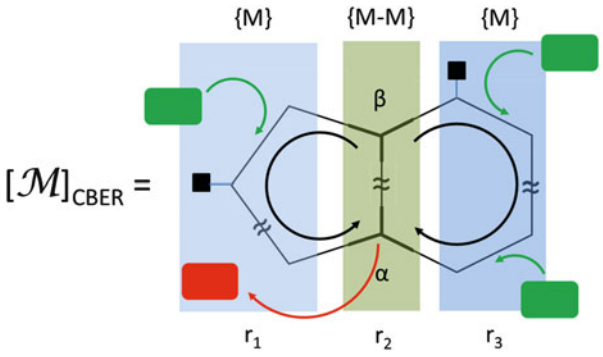

Fig. 7 The monometallic CBER mechanism $[\mathcal{M} = \{\mathrm{M}\}, \{\mathrm{M}-\mathrm{M}\}]_{\mathrm{CBER}}$. The all-important steps α and β which transform mononuclear species to dinuclear species and dinuclear species to mononuclear species are highlighted for emphasis. The symbol ≈ allows each sequence to possess an arbitrary non-zero number of intermediates

reaction exactly equal the net rate r_2 along the grey–green dinuclear {M–M} sequence.

The monometallic CBER mechanism $[\mathcal{M} = \{M\}, \{M - M\}]_{CBER}$ in Fig. 7 has two limiting kinetic scenarios, and these can arise for a number of reasons.

Limit of Linear Rates

a. Can occur if a rate limiting step exists in the light blue sequence {M}
b. Can occur if a rate limiting step exists in the medium blue sequence {M}
c. Can occur if a rate limiting step exists in the grey–green sequence {M–M} and the equilibria favour the formation of dinuclear species

Limit of Quadratic Rates

d. Can occur if step α is rate limiting step
e. Can occur if step β is rate limiting step and the equilibria do not favour the formation of dinuclear species
f. Can occur if a rate limiting step exists in the grey–green sequence {M–M} and the equilibria do not favour the formation of dinuclear species

Much of the conditional phasing used above arises from the complication associated with whether the equilibria favour the mononuclear or dinuclear species. From an encounter probability viewpoint alone, at typical loadings of 1–100 ppm metal, the bimolecular α step may frequently become rate determining.

Jacobsen's group has shown two interesting systems which have strictly quadratic rate kinetics. In the one case, a chromium–salen complex is used to catalyse the asymmetric ring opening of epoxides by trimethylsilyl (TMS) azide [33], and in the other case, a (pybox)$YbCl_3$complex is used to catalyse the ring opening of epoxides with TMSCN [34]. In both cases the authors propose mechanisms in which there is bimolecular reaction between mononuclear complexes and where each mononuclear species brings with it a moiety which is eventually incorporated in the final organic product. In the first mechanism, a dinuclear complex is explicitly proposed as is a step for fragmentation. In situ spectroscopic data is not reported. However formally, there does not seem to be α and β steps per se. Therefore, although there are quite a few similarities between these two systems and the bicyclic structure in Fig. 7, the final reaction network may or may not be somewhat different to a monometallic CBER definition.

A special case of the monometallic CBER mechanism $[\mathcal{M}]_{CBER}$ arises when the light blue sequence {M} and the medium blue sequence {M} are forced to be disjoint. This could occur if the two pools of intermediates are not permitted to interchange. Therefore, as one example, assume that all ligands in the light blue sequence {M} are labile and can dissociate, and assume further that at least one ligand in the medium blue sequence cannot dissociate. If, for example, a carbene or tridentate ligand is attached to $\{M^{\#}\}$, then the moles $\{M\} + \{M - M^{\#}\}$ and $\{M^{\#}\} + \{M - M^{\#}\}$ can be varied independently, and a different experimental situation arises. There are a few reasons to suspect that a quadratic limiting case

for $[\mathcal{M} = \{M\}, \{M^{\#}\}, \{M - M^{\#}\}]_{CBER}$ might be more likely or made to be more likely to occur.

2.2.2 Heterobimetallic Case

The heterobimetallic CBER mechanism $[\mathcal{M}]_{CBER}$ occurs when $[M] \neq [M']$ as previously shown in Fig. 2. The heterobimetallic CBER mechanism in Fig. 2 has two limiting kinetic scenarios, and these arise for a number of reasons.

Limit of Linear Rates

a. Can occur if a rate limiting step exists in the light blue sequence {M}
b. Can occur if a rate limiting step exists in the medium blue sequence {M′}
c. Can occur if a rate limiting step exists in the grey–green sequence {M–M′} and the equilibria favour the formation of dinuclear species

Limit of Quadratic Rates

d. Can occur if step α is rate limiting step
e. Can occur if step β is rate limiting step and the equilibria do not favour the formation of dinuclear species
f. Can occur if a rate limiting step exists in the grey–green sequence {M–M′} and the equilibria do not favour the formation of dinuclear species

As mentioned above, much of the conditional phasing arises from the complication associated with whether the equilibria favour the mononuclear or dinuclear species. From an encounter probability viewpoint alone, at typical loadings of 1–100 ppm metal, the bimolecular α step may frequently become rate determining.

2.3 Monometallic and Heterobimetallic CBER: The Extended Mechanisms

There is a possibility, even a non-negligible probability, that a core CBER mechanism does not exist in isolation.

2.3.1 Homometallic Case

A non-disjoint mechanism, which at least in principle allows simultaneous linear–quadratic kinetics, is shown in Fig. 8. This arises exclusively in the monometallic case that $M = M'$ when the core CBER structure is shared with a unicyclic mechanism. In this case, there are two pathways for product formation, and this arises

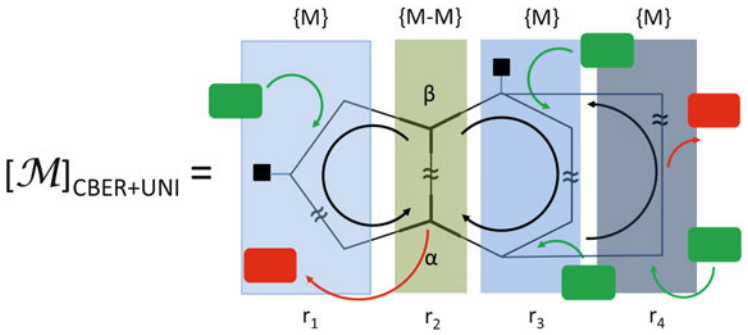

Fig. 8 A monometallic non-disjoint mechanism arising when a core CBER structure is shared with a unicyclic mechanism. *Three shades of blue* are used to represent the mononuclear sequences

from three interconnected cycles. There is one set of all important steps α and β, and there are four sequences of intermediates. Three of these sequences are mononuclear and one is dinuclear.

In a non-disjoint homometallic $[\mathcal{M}]_{\text{CBER+UNI}}$ mechanism, the relationships between steady-state rates are (1) $r_1 = r_2$ (2) $r_3 = r_2 + r_4$.[1] If $r_3 \ll r_4$, the unicyclic mechanism dominates and the rate of product formation becomes linear in {M}. If $r_3 \gg r_4$, the CBER mechanism dominates and the rate of product formation can be either linear in {M} or quadratic in {M} as limiting cases. A special expression for the total rate of product formation from a non-disjoint $[\mathcal{M}]_{\text{CBER+UNI}}$ mechanism would allow a fit to both terms, and it would take a form similar to Eq. 10. The term k_1 accommodates the linear part either in terms of a formal summation over mononuclear intermediates or as a summation of spectroscopically observable mononuclear during the catalysis. The term k_2 accommodates the quadratic part where focus at the moment will be placed on the bimolecular reaction between mononuclear complexes, namely, the α step.

$$r_{\text{tot}} = k_1 \sum [I_i \in \text{ML}_n] + k_2([\text{ML}_n][\text{ML}_m])_\alpha \tag{10}$$

In the decades following the identification of the stoichiometric cobalt binuclear elimination reaction by Heck and Breslow, a number of researchers set out to verify the catalytic analogue. In particular, Whyman [35, 36], Alemdaroglu et al. [37] and Mirbach [38] conducted in situ spectroscopic analyses using high-pressure infrared spectroscopy. All groups observed the simultaneous presence of the mononuclear species $HCo(CO)_4$ and $RCOCo(CO)_4$ with simple alkenes (i.e. R = octyl, cyclohexyl) and the dinuclear complex $Co_2(CO)_8$ under catalytic alkene hydroformylation conditions. The general conclusion from Whyman and Mirbach was that

[1] The rate r has taken a product-centric perspective throughout. However, there are many levels of interpretation, and they serve different purposes. Taking a metal-centric perspective, the rate relationships take the form (1) ${}^{\text{M}}r_1 = 1/2\ {}^{\text{M}}r_2$ and (2) ${}^{\text{M}}r_3 = (1/2){}^{\text{M}}r_2 + {}^{\text{M}}r_4$.

the experimentally found value of the quadratic $k_2[\mathrm{Co}]^2$term was small but not entirely negligible, i.e. on the order of 10% (first term greater than second term in Eq. 11). The studies of Alemdaraglu et al. suggested that the contribution of the quadratic $k_2[\mathrm{Co}]^2$ term was considerably greater. Hence, the in situ experimental studies support the contention that a Heck and Breslow binuclear mechanism indeed existed under genuine hydroformylation conditions, although most researchers contend that this mechanism is the minor pathway.

$$r_{\mathrm{tot}} = k_1\left[\mathrm{RCOCo(CO)_4}\right] + \; k_2\left(\left[\mathrm{HCo(CO)_4}\right]\left[\mathrm{RCOCo(CO)_4}\right]\right)_{\alpha} \qquad (11)$$

A short historical chronology of crucial events in unmodified cobalt carbonyl chemistry as well as cobalt-catalysed hydroformylation should be taken into account in order to better understand the context for the above observations. The first two cobalt clusters to be isolated and identified were $Co_2(CO)_8$ and $Co_4(CO)_{12}$ [39, 40]. Bor and Noack [41] and Bor et al. [42] using FTIR then confirmed that in solution two isomers of $Co_2(CO)_8$ were observable, the all-terminal and the more favoured di-bridging. $HCo(CO)_4$ was discovered by Hieber et al. [43]. The first hydroformylation or oxo products were identified by Roelen [44] at Ruhrchemie when a cobalt containing heterogeneous catalyst was used. Pino et al. [45] carried out the first stoichiometric hydroformylation of alkenes using $Co_2(CO)_8$ and this was followed by the stoichiometric hydroformylation of alkenes using $HCo(CO)_4$ [46]. The unmodified catalysis and kinetics were extensively studied by the Natta group [47] including the negative order in $[\mathrm{CO}]^{-1}$. After their paper of 1960 dealing with binuclear elimination, Heck and Breslow [9] published a second paper dealing more with a unicyclic mechanism for cobalt-catalysed hydroformylation. This latter mechanism is that which is usually, but not always, referred to as the Heck–Breslow mechanism [48]. Thus circa 40–50 years were spanned between the identification of aldehydes in cobalt-catalysed hydroformylation and then in situ spectroscopic and modelling evidence that two mechanisms are present and operating together and that catalytic binuclear elimination is one of the mechanistic reasons.

A similar in situ spectroscopic strategy was undertaken to determine if a Heck and Breslow binuclear elimination mechanism might be present in the unmodified rhodium-catalysed hydroformylation of alkenes. In one study alone, over 15 substrates were investigated where the acyl species $RCORh(CO)_4$ was always observed, but under the conditions used, only the linear term was statistically supported [49]. However, hydroformylation of two substrates, namely, cyclohexene and cyclooctene, exhibited outlier behaviour. With these two substrates, full conversion of the catalyst precursor $Rh_4(CO)_{12}$ was never observed. Further detailed study of cyclohexene could not verify a statistically supported quadratic contribution [50, 51]. The in situ study of cyclooctene at much lower CO partial pressure was more fruitful, as $RCORh(CO)_4$, $HRh(CO)_4$ and $Rh_2(CO)_8$ were all observed simultaneously [52]. At the mean reaction conditions used in this study, 40% of product formation arose from the quadratic term $k_2[\mathrm{Rh}]^2$. Therefore, it appears that

a CBER mechanism is operating in the unmodified rhodium case, at least when some special substrates are used at appropriate reaction conditions.

$$r_{\text{tot}} = k_1\left[\text{RCORh(CO)}_4\right] + k_2\left(\left[\text{HRh(CO)}_4\right]\left[\text{RCORh(CO)}_4\right]\right)_{\alpha} \qquad (12)$$

A short historical chronology of unmodified rhodium carbonyl chemistry as well as rhodium-catalysed hydroformylation should be taken into account in order to better understand the context for the above developments. The first two rhodium clusters to be isolated and positively identified were $Rh_4(CO)_{12}$ [53] and $Rh_6(CO)_{16}$ [54]. The solid state structure of $Rh_4(CO)_{12}$ exhibited C_{3v} symmetry with three bridges. In solution, fluxionality of all COs was observed, and this leads to numerous experimental and theoretical studies. The long sought all-terminal variety of $Rh_4(CO)_{12}$ was not identified until after the advent of the latest generation of signal processing techniques [55]. The dinuclear $Rh_2(CO)_8$ is also non-isolatable and was first observed under hundreds of bar CO partial pressure [56]. This assignment was then confirmed by Hanlan and Ozin [57]. Experimental in situ FTIR evidence for the existence of $HRh(CO)_4$, with bands at 2,070, 2,039 and 2,008 cm^{-1}under circa 1,600 bar of syngas, was initially reported [58], but this result remained inconclusive due to the extreme overlap of peaks. After the advent of the latest generation of signal processing techniques, $HRh(CO)_4$ was identified at 2,124, 2,072 and 2,042 cm^{-1} and its deuterated analogue $DRh(CO)_4$ was identified at 2,124, 2,072 and 2,042 cm^{-1}under circa 50 bar of syngas [59]. An alkylrhodium tetracarbonyl $RRh(CO)_4$ ($R = C_2H_5$) was tentatively reported using high-pressure in situ FTIR [60], but it is now known that the reported bands are due to the acylrhodium tetracarbonyl $RCORh(CO)_4$($R = C_2H_5$) [61–63]. The acylrhodium tetracarbonyl $RCORh(CO)_4$ was first reported by Garland and Bor [64] and since then a few dozen different R groups have been used and the spectra reported. The Nottingham in situ spectroscopy group has confirmed the aforementioned results concerning existence of $RCORh(CO)_4$ using matrix techniques [65].

The first indications of rhodium as an outstanding hydroformylation metal are attributed to the unmodified patents filed by Shell and Esso in the early 1950s. The group which perhaps contributed most to kinetic and mechanistic investigations in the early years was at Vesprem [66] and they confirmed a $[CO]^{-1}[H_2]$ dependency for the catalysis. However, many groups, but particularly Wender and Pino, contributed greatly to the scope of the synthetic potential [67, 68]. An elegant isotopic labelling experiment by [69] put an end to the speculation concerning cluster catalysis with $Rh_4(CO)_{12}$ as precursor and firmly shifted emphasis to mononuclear catalysis mechanisms. After the discovery of acyl rhodium carbonyl $RCORh(CO)_4$, detailed in situ spectroscopy and chemometrics were combined to better understand the catalysis. Unicyclic mechanisms, at least for 3,3-dimethybut-ene [70], cyclohexene [71] and styrene [50, 51] were firmly established where the $[CO]^{-1}[H_2]$ rate dependency exists. Thus again, circa 50 years were spanned between the first identification of the rhodium carbonyls as catalyst precursors in

hydroformylation and finally until experimental evidence for catalytic binuclear elimination was obtained.

In both the unmodified cobalt and rhodium carbonyl cases, the β step will be fast. Indeed, Ungvary [72] extensively studied molecular hydrogen activation on $Co_2(CO)_8$ to give $HCo(CO)_4$. The stoichiometric sequence involves the formation of the hepta-carbonyl, followed by oxidative addition of hydrogen on the dinuclear centre resulting in the mononuclear species. In the case of mixtures of rhodium carbonyls in the presence of molecular hydrogen, it is clear that system $Rh_4(CO)_{12}$, $Rh_2(CO)_8$ and $HRh(CO)_4$ redistribute to a new equilibrium on a very fast timescale when the hydrogen partial pressure is changed, even under considerable CO [59].

Returning to the monometallic non-disjoint mechanism in Fig. 8 and starting with the α step, the following step takes place: the bimolecular reaction between mononuclear species ($HCo(CO)_4 + RCOCo(CO)_3$ or $HRh(CO)_4 + RCORh(CO)_3$) to give aldehyde and the coordinately unsaturated species $Co_2(CO)_7$ and $Rh_2(CO)_7$ (which are in equilibrium exchange with their respective coordinately saturated carbonyls $M_2(CO)_8$). Then in the sequence involving r_2, hydrogen activation on the dinuclear species occurs and the mononuclear species $HCo(CO)_3$/$HCo(CO)_4$ and $HRh(CO)_3$/$HRh(CO)_4$ are generated at the β step. The sequence involving r_1 possesses only the coordinately saturated hydrides $HM(CO)_3$/$HM(CO)_4$. The sequence involving r_3 possesses $HM(CO)_3$/$HM(CO)_4$, the coordinated alkene H (π-alkene)$M(CO)_3$, the alkyls $RM(CO)_3$/$RM(CO)_4$ and finally the acyls $RCOM(CO)_3$/$RCOM(CO)_4$. At the branch point, either the acyl proceeds to the α step, or molecular hydrogen activation directly occurs along the r_4 sequence yielding aldehyde and $HM(CO)_3$/$HM(CO)_4$. All sequences are at this point connected. It is worth emphasizing again that in the CBER mechanism, each mononuclear sequence picks up or carries with it a moiety which will eventually become part of the organic product.

2.3.2 Heterobimetallic Case

A non-disjoint mechanism, which at least in principle allows simultaneous linear–bilinear kinetics, is shown in Fig. 9. This arises exclusively in the bimetallic case $\{M\} \neq \{M'\}$ when the core CBER structure is shared with a unicyclic mechanism. In this case, there are two pathways for product formation, and this arises from three interconnected cycles. There is one set of all important steps α and β, and there are four sequences of intermediates. Three of these sequences are mononuclear and one is dinuclear.

In a non-disjoint heterobimetallic $[\mathcal{M} = \{M\}, \{M'\}, \{M - M'\}]_{CBER+UNI}$ mechanism, the relationships between rates are (1) $r_1 = r_2$ (2) $r_3 = r_2 + r_4$.[2] If $r_3 \ll r_4$, the unicyclic mechanism dominates and the rate of product formation becomes linear in

[2] Taking a metal-centric perspective, the rate relationships take the form (1) ${}^{M}r_1 = {}^{M}r_2$ and (2) ${}^{M'}r_3 = {}^{M'}r_2 + {}^{M'}r_4$.

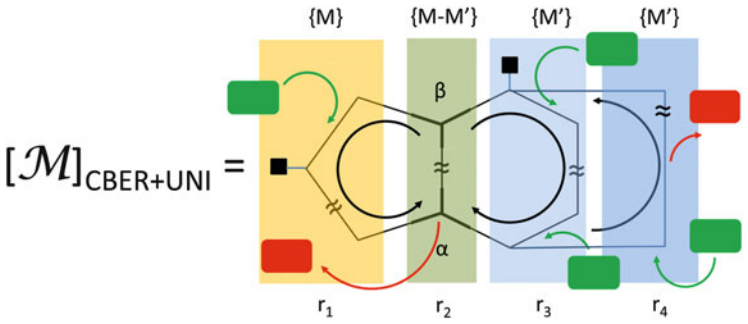

Fig. 9 A heterobimetallic non-disjoint mechanism arising when a core CBER structure is shared with a unicyclic mechanism. The *orange shaded region* involves mononuclear species of M, and the *two shades of blue* are used to represent the mononuclear sequences involving M′

{M′}. If $r_3 \gg r_4$, the CBER mechanism dominates and the rate of product formation can be either linear in {M} or {M′} or bilinear in the product of {M} and {M′}as limiting cases. A general expression for the total rate of product formation from a non-disjoint heterobimetallic $[\mathcal{M} = \{\mathrm{M}\}, \{\mathrm{M}^{'}\}, \{\mathrm{M}-\mathrm{M}^{'}\}]_{\mathrm{CBER+UNI}}$ mechanism would allow a fit to three terms, and it would take a form similar to Eq. 13. The term k_1 accommodates the linear part either in terms of a formal summation over mononuclear intermediates {M′} or as spectroscopically observable mononuclear during the catalysis. The term k_2 accommodates the bilinear part where focus at the moment will be placed on the bimolecular reaction between mononuclear complexes, namely, the α step.

$$r_{\mathrm{tot}} = k_1 \sum \left[I_{\mathrm{i}} \in \mathrm{M}^{'}\mathrm{L}_n\right] + k_2\left(\left[\mathrm{ML}_n\right]\left[\mathrm{M}^{'}\mathrm{L}_m\right]\right)_{\alpha} \tag{13}$$

One of the earliest indications that the heterobimetallic $[\mathcal{M}]_{\mathrm{CBER+UNI}}$ catalytic mechanism may exist came from the work on the addition of lanthanide complexes to unmodified cobalt-catalysed alkene hydroformylation [73]. Upon addition of the lanthanide complexes, a dramatic rate increase was observed. Lanthanides are known to readily generate highly reactive hydrides, and this would support the supposition that lanthanide hydrides are attacking the acyl cobalt complex $RCOCo(CO)_3$/$RCOCo(CO)_4$. In situ spectroscopic analysis was not available/reported.

In a series of studies, $HMn(CO)_5$ [61–63, 74], $HRe(CO)_5$ [75–78], $HMoCp(CO)_3$ [77, 78] and $HWCp(CO)_3$ [79] the complexes were added individually to unmodified rhodium-catalysed alkene hydroformylations. In situ FTIR spectroscopy was performed on all systems, and detailed modelling was performed on the more well-behaved systems containing $HMn(CO)_5$ and $HRe(CO)_5$. Additional isotopic approaches were used to verify that a CBER mechanism was involved (see Sect. 3 for details). A number of different substrates were used. Both the $HMn(CO)_5$ and $HRe(CO)_5$ containing systems provided unambiguous support for a two-term expression (Eq. 14) where the bilinear term contributed up to circa 90% of the product formation (note: M = Mn, Re).

$$r_{\text{tot}} = k_1\left[\text{RCORh(CO)}_4\right] + k_2\left(\left[\text{HM(CO)}_5\right]\left[\text{RCORh(CO)}_4\right]\right)_\alpha \qquad (14)$$

Relating these results (Fig. 9) and starting with the α step, it is inferred that there is bimolecular reaction between mononuclear species ($HM(CO)_5 + RCORh(CO)_3$) to give aldehyde and the coordinately unsaturated species $MRh(CO)_8$ (which are in equilibrium exchange with their respective coordinately saturated and observed carbonyls $MRh(CO)_9$). Then in the sequence involving r_2, hydrogen activation on the dinuclear species occurs and the mononuclear species $HM(CO)_5$ and $HRh(CO)_3$ are generated at the β step. The sequence involving r_1 possesses only the coordinately saturated hydrides $HM(CO)_5$. The sequence involving r_3 possesses $HRh(CO)_3$/$HRh(CO)_4$, the coordinated alkene $H(\pi\text{-alkene})Rh(CO)_3$, the alkyls $RRh(CO)_3$/$RRh(CO)_4$ and finally the acyls $RCORh(CO)_3$/$RCORh(CO)_4$. At the branch point, either the acyl proceeds to the α step, or molecular hydrogen activation directly occurs along the r_4 sequence yielding aldehyde and $HRh(CO)_3$/$HRh(CO)_4$. All sequences are at this point connected.

2.4 *Disjoint CBER + Unicyclic Mechanisms*

The mechanisms discussed in Sects. 2.3.1 and 2.3.2 arose spontaneously upon the addition of just one or at most two organometallic precursors without modifiers (phosphine-free, carbene-free etc.). Briefly, it is important to mention that *disjoint CBER + unicyclic mechanisms* might arise given the correct circumstances; however, it appears that many of these systems will not arise spontaneously with a minimum of reagents but rather would probably require deliberate intervention and planning by the experimentalist in order to achieve. The main message is that with planning, it is probable that *disjoint CBER + unicyclic mechanisms* could be constructed which would possess linear, bilinear and/or quadratic terms, more or less simultaneously similar to Eqs. 10 and 13. For example, in Fig. 10 the non-linear mechanism may be the known and unmodified $[\mathcal{M} = \{\text{Re}\}, \{\text{Rh}\}, \{\text{Re} - \text{Rh}\}]_{\text{CBER+UNI}}$ for hydroformylation and the linear mechanism might be a tridentate modified $[\text{M} = \{\text{Rh}\}]_{\text{UNI}}$ also for hydroformylation. Hence caution will be needed when deciding what types of mechanism are operating when exotic recipes using simultaneously different metals and different modifying ligands are implemented.

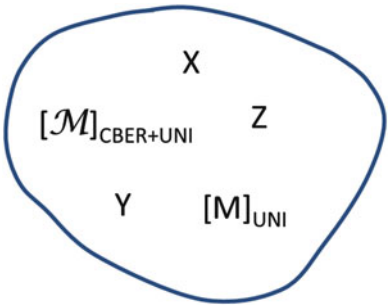

Fig. 10 A hypothetical catalytic system for hydroformylation, which simultaneously possesses both an unmodified $[\mathcal{M} \in \{Re\}, \{Rh\}, \{Re - Rh\}]_{CBER+UNI}$ and a tridentate modified $[M \in \{Rh\}]_{UNI}$. The kinetics of such systems using simultaneously multiple metals and multiple modes of modification will require considerable care when interpreted, due to the very real potential for multiple linear, bilinear and quadratic terms

2.5 Increased Synthetic Efficiency

In the day-to-day practice of performing reactions, experimentalists make repeated use of some basic definitions and guidelines. In terms of definitions, conversion of substrate, selectivity to a specific product and yield of the target molecule are the most common and essential for quantifying the syntheses. In terms of guidelines, simple reaction design considerations are used to decide (a) what order to add reagents and (b) how to add organic reagents, i.e. dropwise, or all at one time. On a more advanced level and focused on catalytic syntheses, two definitions are frequently used:

1. The definition of turnover number TON (moles product/mole metal)
2. The definition of atom economy [80]

The existence of non-linear catalytic mechanisms provides the opportunity to expand on the concepts associated with synthetic efficiency. The well-defined cases of quadratic, bilinear, linear–quadratic and linear–bilinear kinetics rates with respect to intermediates, illustrated in Sects. 2.3.1 and 2.3.2, suggest that new possibilities for extending the scope of increased synthetic efficiency exist.

Assume that there are five different mechanisms for the same overall syntheses and that these mechanisms are unicyclic, quadratic, bilinear, linear–quadratic and linear–bilinear. Furthermore, assume that at a concentration of 1 mmol/L metal loading, each system has the same rate, namely, 1 mmol/min. Holding the amount of metal at a constant 1 mmol, these five systems are expected to show rates similar to that in Fig. 11a as a function of volume. In other words, simply by changing the volume, the metals in the non-linear systems are being utilized in a far more efficient manner. In the real world, there will be limits due to transport control and formation of higher nuclear species as the volume decreases, and there will be

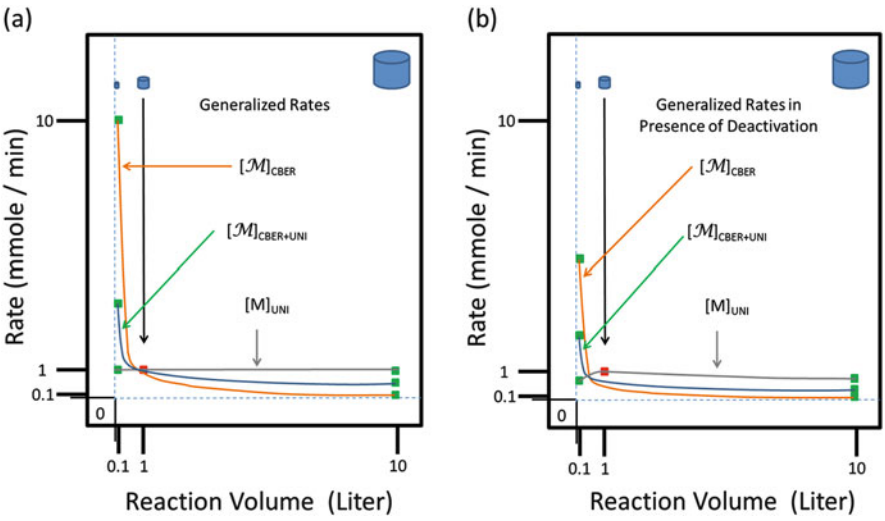

Fig. 11 A comparison of rates from linear and non-linear mechanisms. (**a**) A generalized case in the absence of deactivation. (**b**) A generalized case in the presence of deactivation

more and more metal consumed by impurities as the volume increases, and many real-world scenarios would look more like that presented in Fig. 11b.

Next, compare just a bilinear and quadratic mechanism, where M is a cheaper base metal and M′ is a precious metal. In the case of the bilinear system, the amount of precious metal M′ will be held constant and the amount of base metal M will be increased ten times. In the case of the quadratic system, the amount of precious metal will be increased ten times. The corresponding rates are shown in Fig. 12. In the bilinear system, without the use of more precious metal, substantial increases in rate can be achieved. At some point, the addition of the base metal M to the systems $[\mathcal{M} = \{\mathrm{M}\}, \{\mathrm{M}'\}, \{\mathrm{M} - \mathrm{M}'\}]_{\mathrm{CBER}}$ will result in the r_3 sequence becoming rate limiting; however, until that point is reached, a bilinear advantage would control product formation. In an age when the supply of precious metals is not expanding and in many instances is dwindling and given the ever-increasing demand for fine and speciality chemicals, bilinear kinetics $[\mathcal{M} = \{\mathrm{M}\}, \{\mathrm{M}'\}, \{\mathrm{M} - \mathrm{M}'\}]_{\mathrm{CBER}}$ or $[\mathcal{M} = \{\mathrm{M}\}, \{\mathrm{M}'\}, \{\mathrm{M} - \mathrm{M}'\}]_{\mathrm{CBER+UNI}}$ offer possibilities to use the available precious metal in a more economic or prudent manner. To truly extract the potential of non-linear mechanisms, there should be reconsideration of continuous rather than batch modes of synthesis as well.

In summary for this section, it would appear that at least a third advanced concept for homogeneous catalytic synthetic efficiency can be stated:

3. Prudent use of mechanisms $[\mathcal{M}]$ which exhibit intrinsic non-linear kinetics so that the yield of product with respect to precious metal can be maximized

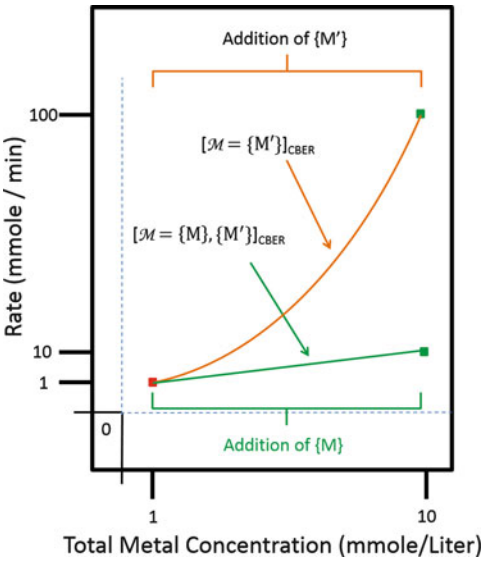

Fig. 12 A comparison of quadratic (*orange*) versus bilinear (*green*) rates as a function of total metal loading at a fixed reaction volume

2.6 Regio-, Chemo- and Stereoselectivities

Presently, there is very little known concerning selectivity patterns in $[\mathcal{M}]_{CBER}$ and $[\mathcal{M}]_{CBER+UNI}$. There were attempts in our laboratory to detect regioselective changes in unmodified $[\ \mathcal{M} = \{Mn\},\{Rh\},\{Mn-Rh\}\ ]_{CBER+UNI}$ and $[\mathcal{M} = \{Re\},\{Rh\},\{Re-Rh\}]_{CBER+UNI}$, but these studies were inconclusive. Additionally, bidentate phosphines were used in conjunction with $[\ \mathcal{M} = \{Re\},\{Rh\},\{Re-Rh\}\ ]_{CBER+UNI}$ as a prelude to stereoselective studies, but at the typical room temperatures used for previous unmodified $[\ \mathcal{M} = \{Re\},\{Rh\},\{Re-Rh\}]_{CBER+UNI}$, the systems did not appear to turnover. It would appear that more work in this area is needed in order to better understand the potential for $[\mathcal{M}]_{CBER}$ and $[\mathcal{M}]_{CBER+UNI}$ to control selectivity. A cursory inspection suggests that severe steric constraints in the α step may direct preferential regioselectivity towards terminal products. Furthermore, the idea that not just one but two metals could be simultaneously modified using chiral ligands suggests that if an α step exists in such systems, then given the chirality on {M} and the chirality on {M′}, perhaps the energetics are such that very high stereoselectivities might arise in some types of reactions (think of the diastereomeric pocket in enzymes as perhaps a similar example). Therefore, this area looks potentially fruitful for dramatic selectivity increases due to the above-mentioned reasons. Due to considerable branching of the main reaction pathways, such systems are expected to be difficult to represent and visualize diagrammatically.

2.7 *Feinberg, Horiuti and Wegscheider Criterion*

2.7.1 The Feinberg Deficiency Theorems and Stability

In the physical sciences, many natural and man-made systems exhibit instabilities, in particular, dampened, indefinitely periodic and undampened oscillations. Such oscillations are found in mechanical systems, electrical systems, biological systems and indeed chemical systems. Perhaps the most well-known chemical oscillations are those associated with the liquid phase redox systems, the Belousov–Zhabotinsky system which is cerium catalysed and the Briggs–Rauscher system which is manganese catalysed and their related chemistries [81], which, in addition to showing temporal oscillations, may show spatio-temporal oscillations as well in both 3D and 2D environments. Most of the conceptual foundations for this area can be traced back to the mathematician and computer scientist Alan Turing and his seminal paper in which he proposed the existence of all these classes of chemical oscillations [82].

Given the non-linear structure of the CBER mechanisms $[\mathcal{M}]_{\mathrm{CBER}}$ and $[\mathcal{M}]_{\mathrm{CBER+UNI}}$ and given the pronounced rate enhancements that can take place, their stability should be questioned. Said another way, is it possible that such mechanisms contribute to product formation from repeated fast and slow rate intervals, or is it possible that such mechanisms contribute to product formation for a brief time but then decay?

Over a three-decade period, Feinberg [83] developed the criteria for answering chemical network stability questions, given any reaction with any given number of reactants. The basis for the so-called deficiency theorems is rooted in topology (structure), but in short summary, one takes each reaction with each set of inputs and outputs and defines new quantities called *complexes*. After summing over all individual reactions, all reactants and all complexes, one obtains the criterion.

Our group has applied the Feinberg deficiency criteria for quadratic, bilinear, linear–quadratic and linear–bilinear CBER systems for both realized and hypothesized hydroformylations and hydrogenations with varying degrees of complexity/selectivity. As far as we can tell, there is no fundamental reason that CBER systems should be unstable. The important converse conclusion is that CBER systems are synthetically useful in the generalized case since they are kinetically stable.

2.7.2 Enumeration of Synthetic Pathways: The Horiuti Criteria

For symmetric substrates in hydroformylation, the non-linear structure of the CBER mechanisms $[\mathcal{M}]_{\mathrm{CBER}}$ and $[\mathcal{M}]_{\mathrm{CBER+UNI}}$ are visually, diagrammatically and conceptually rather straightforward to follow. When considerations of selectivity are included, be these considerations regio-, chemo- and stereoselective or a combination thereof, issues rapidly become very complex. A question that one may ask is this: given a CBER mechanism with simultaneous regio-, chemo- and stereo-

aspects, resulting in PR products, how many pathways PW are there for these product syntheses? One could try to draw out the entire network and then trace out all independent pathways, but errors are likely to occur for very complex networks.

Horiuti was faced with a similar problem, but arguably, on a more difficult scale. He was trying to figure out the number of independent pathways in *heterogeneous systems* [31]. The Horiuti criteria are also based on topological arguments, and therefore, the conclusions obtained can be taken with a great deal of confidence. The Horiuti criteria are straightforward to implement after writing all the assumed individual steps in any order. They do not have to be structured. After entering all the needed information on steps and reactants, an integer number is obtained. This is the number of independent pathways. The Horiuti criteria seems to be the most rational approach to take with non-linear and selective reaction mechanisms in order to understand how many independent pathways PW to the multiple products PR occur. The most important consequence of PW > PR in complex systems is that, in the construction of any truly accurate kinetic model, expressions to account for PW independent pathways and not just the PR products need to be developed.

The unicyclic graphs possessing {M} and {M–M}/{M–M′} containing loops in Fig. 4 have PR = 1 product and PW = 2 independent paths. The chemoselective graph [M] in Fig. 5 has PR = 2 products and PW = 2 independent paths. The CBER mechanisms $[\mathcal{M}]_{\mathrm{CBER}}$ in Figs. 2 and 7 have PR = 1 product and PW = 1 independent paths, and the CBER mechanisms $[\mathcal{M}]_{\mathrm{CBER+UNI}}$ in Figs. 8 and 9 have PR = 1 product and PW = 2 independent paths.

2.7.3 Detailed Balance, Cycles and Constraints

Wegscheider is generally credited with developing the first detailed balancing for complex chemical systems and more specifically catalytic systems [84]. In distilled form, all the steps in a mechanism are constrained, in a non-trial manner, to the overall organic reaction involved and particularly the $\Delta_r G$ of the organic reaction. Hence for a simple unicyclic network, the product of all the forward rate constants are related to the product of all reverse rate constants for all times. This holds from reaction start up to end of the reaction when the entire system is equilibrated. The arguments in the rate constant exponentials sum up to $+/-(\Delta_r G/\mathrm{RT})$. If the forward product and reverse product are equal, then all rate constants cannot be independent. Since the metal-mediated homogeneous mechanisms mentioned in this chapter are fairly complex and since there are a number of simultaneous *material* and *kinetic* constraints operating, it is worthwhile to briefly review two cases, one from [M] and one from $[\mathcal{M}]$.

In Sect. 2.1 a chemoselective unicyclic mechanism was presented for a simultaneous hydroformylation and hydrogenation of cyclopentene. This mechanism, by definition, possesses intermediates of only mononuclear intermediates. The updated figure which provides emphasis to constraints is shown in Fig. 13 where additional

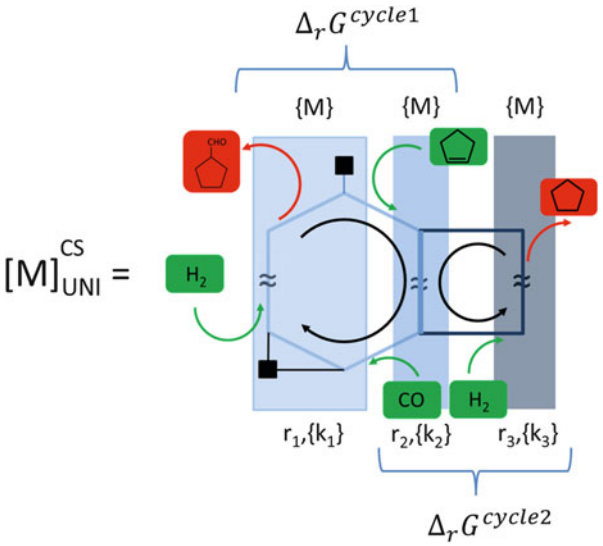

Fig. 13 A representation of a chemoselective unicyclic mechanism for aldehyde and alkane formation, as clarification for the multiple constraints enumerated in Sect. 2.7.3

notation for Gibbs energy of reaction and sets of rate constants $\{k_i\}$ on the cycle associated with each group are provided.

If in situ spectroscopy is available for (i) identifying intermediates, (ii) establishing mass balances and (iii) developing rate expressions, then in an ideal world, an attempt to address at least the following constraints should be performed:

1. Total and partial mass balances on metal in moles N:
   a. Total mass balance : $N^{sys} = N^{[M]} + N^{spectator} + N^{insoluble}$
   b. conversion $= N(t)^{precursor}/N(0)^{precursor}$
      selectivity $= N(t)^{[M]}/(N(t)^{precursor} - N(0)^{precursor})$
      yield $= N(t)^{[M]}/N(0)^{precursor}$
   c. partial mass balances : $N^{[M]} = N^{r_1} + N^{r_2} + N^{r_3}$
   d. Let s denote the instantaneous selectivity for hydroformylation, then
      $N^{cycle\ 1} = N^{r_1} + sN^{r_2}$, moles of metal doing work in cycle 1, and
      $N^{cycle\ 2} = (1-s)N^{r_2} + N^{r_3}$, moles of metal doing work in cycle 2.

2. Concerning total rates and partial rates, let (i) the rate of aldehyde production be r^{ald} and the rate of alkane production be r^{alk}, (ii) the free energy of aldehyde formation be $\Delta_r G^{ald}$ and the free energy of alkane formation be $\Delta_r G^{alk}$ and (iii) the corrected and exact turnover frequency of aldehyde formation be TOF^{ald} and the corrected and exact turnover frequency of alkene formation be TOF^{alk}.
   a. $-r^{cyclopentene} = r^{ald} + r^{alk}$
      $-r^{cyclopentene} = r_2 = r_1 + r_3$
   b. $\Delta_r G^{ald} = \Delta_r G^{cycle1}$

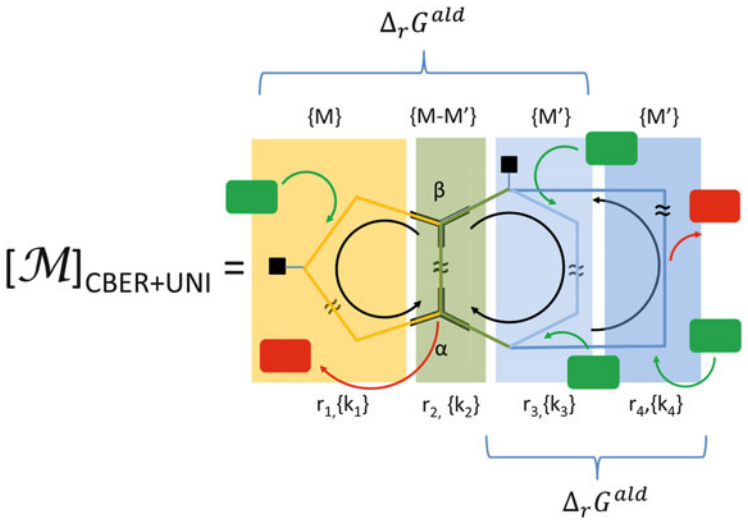

Fig. 14 A representation of the PW = 2 pathway, single-product heterobimetallic $[\mathcal{M} \in \{\mathrm{M}\}, \{\mathrm{M}'\}, \{\mathrm{M}-\mathrm{M}'\}]_{\mathrm{CBER+UNI}}$ mechanism, as clarification for the multiple constraints enumerated in Sect. 2.6.3

$$\Delta_r G^{\mathrm{alk}} = \Delta_r G^{\mathrm{cycle2}}$$

So the free energies of the two cycles (and by inference rate constants) are related since the $\{k_2\}$ sequence is common.

c. corrected $\mathrm{TOF}^{\mathrm{ald}} = r^{\mathrm{ald}}/N^{\mathrm{cycle1}} = r_1/N^{\mathrm{cycle1}}$
corrected $\mathrm{TOF}^{\mathrm{alk}} = r^{\mathrm{alk}}/N^{\mathrm{cycle2}} = r_3/N^{\mathrm{cycle2}}$

In Sect. 2.3.2 a single-product heterobimetallic $[\mathcal{M} = \{\mathrm{M}\}, \{\mathrm{M}'\}, \{\mathrm{M}-\mathrm{M}'\}]_{\mathrm{CBER+UNI}}$ mechanism was presented for a hydroformylation where PW = 2 simultaneous pathways exist. The updated figure which provides emphasis to constraints is shown in Fig. 14 where additional notation for Gibbs energy of reaction and sets of rate constants $\{k_i\}$ on the cycle associated with each group are provided.

If in situ spectroscopy is available for (i) identifying intermediates, (ii) establishing mass balances and (iii) developing rate expressions, then in an ideal world, an attempt to address at least the following constraints should be performed:

1. Total and partial mass balances on metal M and M′ in moles N:

   a. Total mass balances:

$$N^{\text{M-sys}} = N^{\{\mathrm{M}\}} + N^{\{\mathrm{M}-\mathrm{M}'\}} + N^{\text{M-spectator}} + N^{\text{M-insoluble}}$$
$$N^{\text{M}'\text{-sys}} = N^{\{\mathrm{M}'\}} + N^{\{\mathrm{M}-\mathrm{M}'\}} + N^{\text{M}'\text{-spectator}} + N^{\text{M}'\text{-insoluble}}$$
$$N^{\mathrm{T}} = N^{\text{M-sys}} + N^{\text{M}'\text{-sys}}$$

b. $\text{conversion}^{\text{M-sys}} = N\ (t)^{\text{M-precursor}}/N(0)^{\text{M-precursor}}$

$\text{selectivity}^{\text{M-sys}} = \left(N(t)^{\{\text{M}\}} + N(t)^{\{\text{M}-\text{M}'\}}\right)/\left(N(t)^{\text{M-precursor}} - N(0)^{\text{M-precursor}}\right)$

$\text{yield}^{\text{M-sys}} = \left(N(t)^{\{\text{M}\}} + N(t)^{\{\text{M}-\text{M}'\}}\right)/N(0)^{\text{M-precursor}}$

$\text{conversion}^{\text{M}'\text{-sys}} = N(t)^{\text{M}'\text{-precursor}}/N(0)^{\text{M}'\text{-precursor}}$

$\text{selectivity}^{\text{M}'\text{-sys}} = \left(N(t)^{\{\text{M}'\}} + N(t)^{\{\text{M}-\text{M}'\}}\right)/\left(N(t)^{\text{M}'\text{-precursor}} - N(0)^{\text{M}'\text{-precursor}}\right)$

$\text{yield}^{\text{M}'\text{-sys}} = \left(N(t)^{\{\text{M}'\}} + N(t)^{\{\text{M}-\text{M}'\}}\right)/N(0)^{\text{M}'\text{-precursor}}$

c. Partial mass balances:

$N^{\text{M}} = N^{\{\text{M}\}} + N^{\{\text{M}-\text{M}'\}} = N^{r_1} + N^{r_2}$

$N^{\text{M}'} = N^{\{\text{M}'\}} + N^{\{\text{M}-\text{M}'\}} = N^{r_2} + N^{r_3} + N^{r_4}$

d. Let Φ^1 denote the instantaneous fraction of hydroformylation product arising from cycle 1 = CBER, and let Φ^2 denote the instantaneous fraction of hydroformylation product arising from cycle 2 = UNI; then

$N^{\text{CBER}} = N^{r_1} + 2N^{r_2} + \Phi^1 N^{r_3}$, moles of metal doing work in cycle 1, and

$N^{\text{UNI}} = \Phi^2 N^{r_3} + N^{r_4}$, moles of metal doing work in cycle 2

2. Concerning total rates and partial rates, let (i) the rate of aldehyde production from the CBER mechanism be r^{ald1} and the rate of aldehyde production from the unicyclic mechanism be r^{ald2}, (ii) the free energy of aldehyde formation be $\Delta_r G^{\text{ald}}$ and (iii) the corrected and exact turnover frequency of aldehyde formation be TOF^{ald1} from the CBER mechanisms and the corrected and exact turnover frequency of aldehyde formation be TOF^{ald2} from the unicyclic mechanism.

a. $-r^{\text{cyclopentene}} = r^{\text{ald1}} + r^{\text{ald2}}$

b. $\Delta_r G^{\text{ald}} = \Delta_r G^{\text{CBER}}$

$\Delta_r G^{\text{ald}} = \Delta_r G^{\text{cycle2}}$

So the free energies of the left-hand and the right-hand side in Fig. 14 (and by inference rate constants) are related by the interesting result:

$\Delta_r G^{\text{CBER}} - \Delta_r G^{\{k_3\}} = \Delta_r G^{\text{cycle2}} - \Delta_r G^{\{k_3\}}$

c. $\text{corrected TOF}^{\text{ald-CBER}} = r^{\text{ald1}}/N^{\text{CBER}} = r_1/N^{\text{CBER}} = r_2/N^{\text{CBER}}$

$\text{corrected TOF}^{\text{ald-UNI}} = r^{\text{ald2}}/N^{\text{UNI}} = r_4/N^{\text{UNI}}$

The corresponding results for the remaining three mechanisms in this chapter, namely, the monometallic and heterobimetallic CBER mechanisms $[\mathcal{M}]_{\text{CBER}}$ and the monometallic CBER mechanism $[\mathcal{M} = \{\text{M}\}, \{\text{M}-\text{M}\}]_{\text{CBER+UNI}}$, are readily obtained from the methods derived above. Each provides a new set of relationships, previously unreported for catalytic systems.

2.8 Other Systems, Other Non-linear Mechanisms

2.8.1 Importance of Pre-catalytic Stoichiometric Transformations

There is a class of stoichiometric reactions which exacerbate the interpretation of catalytic rates and which must be mentioned. This class of stoichiometric reactions confound not only the novice in catalytic sciences but occasionally seasoned practitioners as well, since extremely dramatic effects on catalytic reaction rates can arise – and of course, these may then be misinterpreted as suggesting some sort of cooperativity or synergism in the catalytic mechanism.

This class of stoichiometric reactions are those associated with the conversion of the catalyst precursor to intermediates. The half-lives for conversion can easily vary over many orders of magnitude – seconds to days (especially when inorganic salts or micronized metal is used). Moreover, depending on the ligands present, their concentrations, the auxiliaries used and the sequence of additions, the selectivity to spectator species rather than intermediates may be favoured and the ultimate yield of intermediates is severely affected. This idea is presented in Fig. 15.

Two examples supported by detailed in situ spectroscopic studies will highlight the above problem.

System 1 A variety of monometallic rhodium complexes and heterobimetallic cobalt–rhodium carbonyl complexes were used as catalyst precursors for the room

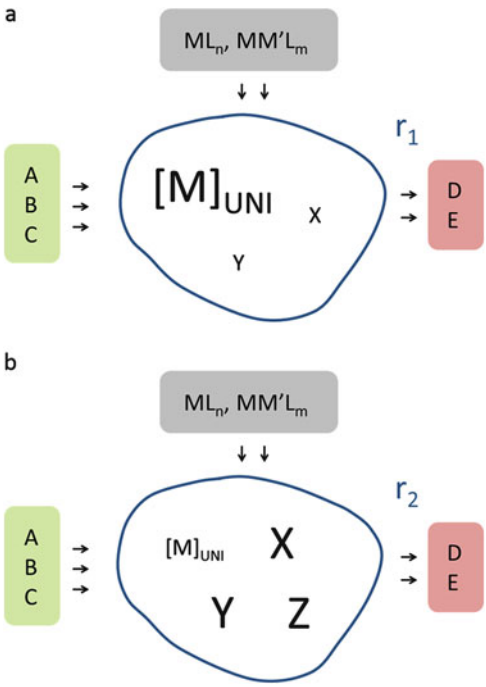

Fig. 15 An illustration of the effect of pre-catalytic transformations on the ultimate performance of a system. (**a**) A system where most of the metal M in the catalytic precursor is transformed to intermediates in a unicyclic mechanism $[M]_{UNI}$. (**b**) A system where little of the metal M in the catalytic precursor is transformed to intermediates in a unicyclic mechanism $[M]_{UNI}$. Accordingly, holding everything else equal, the maximum observable rates are $\max\{r_1\} \gg \max\{r_2\}$

temperature unmodified catalytic hydroformylation of 3,3-dimethybut-1-ene [85]. The dinuclear heterobimetallic cobalt–rhodium carbonyl complex $CoRh(CO)_7$ disappeared completely from solution in circa 5 min. The yield of rhodium intermediates, specifically the observable $RCORh(CO)_4$, was basically 100%. The system exhibited a very high rate of reaction after the 5 min induction period. The observable $RCOCo(CO)_4$ was found to contribute no statistically significant amount of product formation at the conditions used. The other monometallic rhodium complexes exhibited half-lives to $RCORh(CO)_4$ on the order of 1 h to circa 8 h. Moreover, the selectivity to $RCORh(CO)_4$ was in some cases significantly less than unity (particularly when using $RhCl_3$), and hence the yield of $RCORh(CO)_4$ was seriously diminished. As expected, these latter systems exhibited considerably lower rates than the system generated from $CoRh(CO)_7$. To make sure that no inadvertent error was made with the mass balances, the turnover frequencies TOF based on instantaneous $RCORh(CO)_4$ in each system were evaluated and were found to be the same.

System 2 The polynuclear precursor $Ru_3(CO)_{12}$ can be used to carbonylate piperidine under CO with 100% selectivity. The system is particularly sensitive to the sequence of additions and holding times of the reagents, or in other words, the start up [86]. Thus, if $Ru_3(CO)_{12}$ is added to piperidine under 1 bar CO, a very gradual disappearance of $Ru_3(CO)_{12}$ occurs, almost no detectable new mononuclear species can be observed, and the rate of product formation is negligible. If, however, $Ru_3(CO)_{12}$ is added to piperidine under 50 bar CO, a very rapid disappearance of $Ru_3(CO)_{12}$ occurs, with nearly quantitative formation of $Ru(CO)_5$. Under these conditions the rate of product is negligible. However, then by lowering the system pressure to say 5 bar, a very active system is created where the concentration of mononuclear intermediates appears entirely stable in time. Thus System 2 illustrates the stunning difference between circa 0% and 100% yield of intermediates using exactly the same set of reagents.

2.8.2 Other Non-linear Systems and Another Possible Non-linear Mechanism

As mentioned in Sect. 1, the field of cooperative or synergistic behaviour is very broad and this chapter is certainly not the appropriate place to survey the area. Having said that, mention was made of Jacobsen's quadratic systems in Sect. 2.2.1 although there are some dissimilarities with monometallic CBER. Other groups of reactions which have attracted this author's attention are the Pt–Sn hydroformylation systems and the Ir–Ru Cativa process for acetic acid [87]. A common theme in the Pt–Sn and Ir–Ru systems appears to be the need of the second metal (Sn or Ru) in order to abstract a halogen from the first metal, thereby freeing a coordination site. Catalytic bimetallic systems where a second metal is needed to abstract a halogen should, at some level, exhibit a bilinear term to reflect the abstraction.

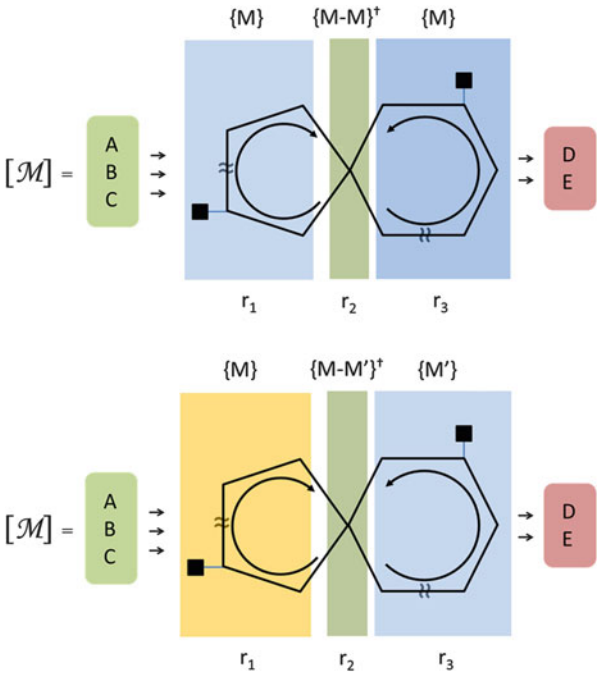

Fig. 16 Illustration of two possible inherently non-linear mechanisms involving only mononuclear intermediates and a dinuclear transition state

Therefore, this author started to consider the possibility of a non-linear mechanism where there are two sets of mononuclear intermediates and no dinuclear intermediates. Instead of a set of dinuclear intermediates, there is just one transition state. If such systems were to exist, namely, a homometallic $[\mathcal{M} = \{\mathrm{M}\}, \{\mathrm{M} - \mathrm{M}\}^{\dagger}]$ or heterobimetallic $[\mathcal{M} = \{\mathrm{M}\}, \{\mathrm{M}'\}, \{\mathrm{M} - \mathrm{M}'\}^{\dagger}]$ mechanism, then they might have structures that have some similarity to that presented in Fig. 16.

The essence of the above argument can be easily concluded. The limiting rate expressions for the non-linear mechanisms in Fig. 16 will be linear in M, linear in M′, quadratic in M and bilinear in MM′ and resemble in large part the generalized forms present for the non-linear CBER mechanisms in Sects. 2.2 and 2.3. Therefore there might be quite a variety of non-linear mechanisms which can give rise to linear in M, linear in M′, quadratic in M and bilinear in MM′ rate kinetics. Considerable attention will need to be given in the future a classification so that the field of cooperativity and synergism can develop in a structured manner.

3 The Catalytic Binuclear Elimination Reaction

3.1 Chemistry, Structure

This section will concentrate on the single-product heterobimetallic hydroformylation $[\mathcal{M} = \{\text{Re}\}, \{\text{Rh}\}, \{\text{Re} - \text{Rh}\}]_{\text{CBER+UNI}}$ mechanism, although the analogous Mn–Rh, Mo–Rh and W–Rh systems will be selectively used to emphasize various issues.

The single-product heterobimetallic hydroformylation $[\mathcal{M} = \{\text{Re}\}, \{\text{Rh}\}, \{\text{Re} - \text{Rh}\}]_{\text{CBER+UNI}}$ mechanism is typically initiated by the combined application of $HRe(CO)_5$ and $Rh_4(CO)_{12}$ as catalyst precursors to a *n*-hexane solution containing an alkene, hydrogen and CO at ambient temperature [75–78]. The structure of the system is shown in Fig. 17 where the original form of representation is retained. As mononuclear observable intermediates in the system, both coordinately saturated $HRe(CO)_5$ and $RCORh(CO)_4$ have been quantified, and as dinuclear observable intermediate in the system, coordinately saturated $RhRe(CO)_9$ has been quantified, by in situ FTIR spectroscopy.

Unfolding the mechanism and re-representing it in the newer format introduced in this chapter, $[\mathcal{M} = \{\text{Re}\}, \{\text{Rh}\}, \{\text{Re} - \text{Rh}\}]_{\text{CBER+UNI}}$ takes the form of that in Fig. 18. At this point it is possible to readily identify the aforementioned

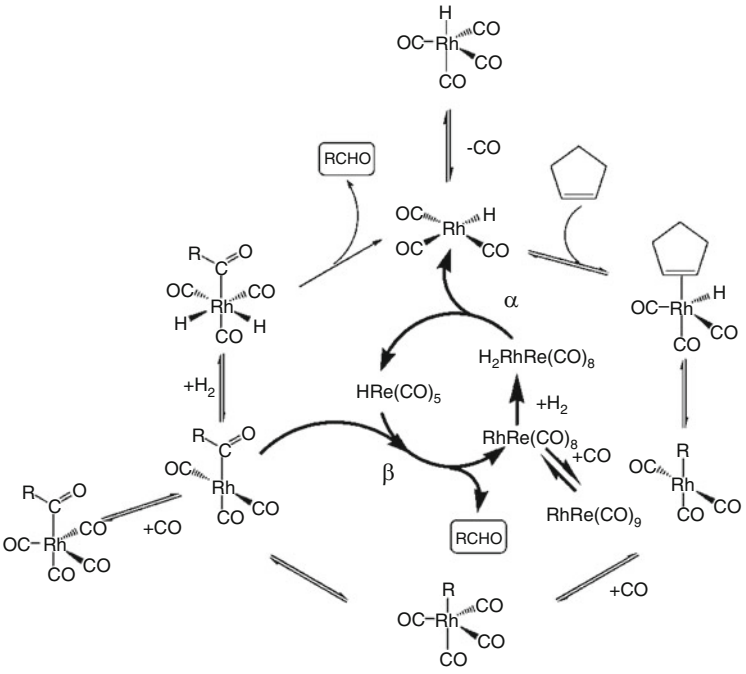

Fig. 17 The original representation of the Rh–Re CBER catalysis (reprinted with permission from Li et al. [75]. Copyright (2007) American Chemical Society)

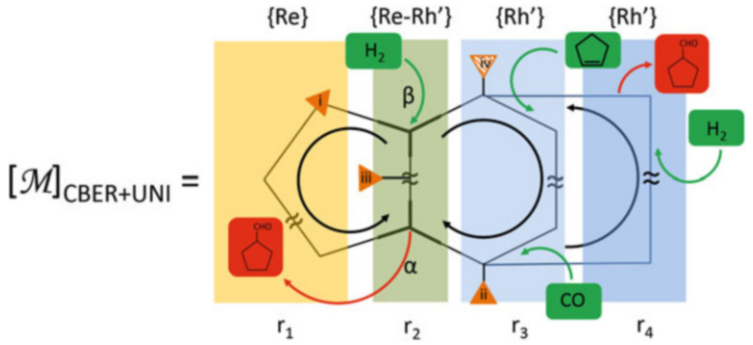

Fig. 18 The Rh–Re CBER mechanism for hydroformylation $[\mathcal{M} = \{\mathrm{Re}\}, \{\mathrm{Rh}\}, \{\mathrm{Re-Rh}\}]_{\mathrm{CBER+UNI}}$ presented in the format introduced in this chapter with additional annotation for the coordinately saturated and observable intermediates (*i*) $HRe(CO)_5$, (*ii*) $RCORh(CO)_4$, (*iii*) $RhRe(CO)_9$ and (*iv*) $HRh(CO)_4$ (a thatched representation is used for the hydride as it was only clearly identified in a homometallic CBER). For visual clarity, the additional reagents which enter and exit from line segments connecting reservoirs have been omitted

observables and more easily assign them to their roles. The α step is the bimolecular reaction of $HRe(CO)_5$ and $RCORh(CO)_4$ to yield the aldehyde and an unsaturated Rh–Re carbonyl. The β step involves hydrogen activation on the saturated Rh–Re carbonyl $RhRe(CO)_9$ after CO dissociation to give $HRe(CO)_5$ and the coordinately unsaturated $HRh(CO)_3$. $HRe(CO)_5$ is present in the r_1 sequence, both as reagent for the α step and as product of the β step. The observable dinuclear species is present in the r_2 sequence. $HRh(CO)_3$ and $RCORh(CO)_4$ are present in the r_3 sequence. The coordinately unsaturated $HRh(CO)_3$ is in equilibrium exchange with $HRh(CO)_4$. The intermediates $RCORh(CO)_4$ and $RCORh(CO)_3$ may proceed to the step α or may enter the r_4 sequence. If it proceeds through the r_4 sequence, then the unicyclic mechanism is completed and aldehyde and $HRh(CO)_3$ are produced in a second pathway.

3.2 In Situ FTIR Spectra and Kinetics

In situ FTIR spectroscopy was used to study all the $[\mathcal{M}]_{\mathrm{CBER+UNI}}$ systems mentioned in this Sect. 3. Advanced signal processing was used in all of these studies. The foundations for the mathematics used as well as details on the chemometric procedures used have been summarized elsewhere (see Sect. 1.4). Here it is sufficient just to mention the main algorithm by name, band-target entropy minimization (BTEM), which untangles large sets of raw experimental spectra into the individual pure component spectra, using no a priori information. Thus, in the case of $[\mathcal{M} = \{\mathrm{Re}\}, \{\mathrm{Rh}\}, \{\mathrm{Re-Rh}\}]_{\mathrm{CBER+UNI}}$, the pure component spectra obtained included the alkene and aldehyde as well as the organometallics shown in Fig. 19. Hundreds of raw spectra were used as input to achieve the results in Fig. 19.

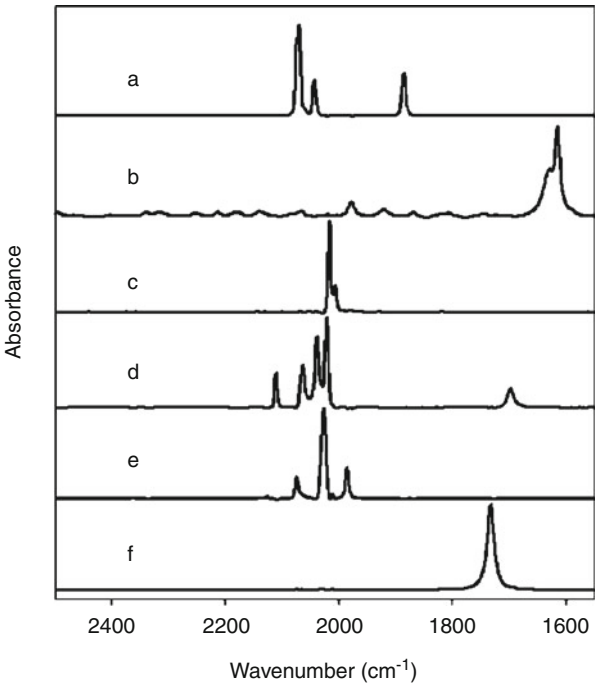

Fig. 19 The pure component spectra obtained from the Rh–Re hydroformylation of cyclopentene (reprinted with permission from Li et al. [75]. Copyright (2007) American Chemical Society)

Approximately 99% of the spectroscopic signals in the raw spectra can be accounted for by the six pure component spectra in Fig. 19 (the dissolved CO and the solvent *n*-hexane are excluded).

The pure component spectra were then fit back onto the original raw multicomponent reaction spectra in order to get the signal contribution of each pure component spectra, and calibration was achieved using the known quantities of Rh and Re moles used in each experiment. The results are sets of smooth concentration profiles in time. A typical profile for a 300 min hydroformylation experiment is shown in Fig. 20. As this figure shows, there is a fast nearly step change in the concentration of $HRe(CO)_5$ after addition, with the immediate formation of significant amounts of $RhRe(CO)_9$. The concentration of the observable precursor $Rh_4(CO)_{12}$ approaches zero at circa 150 min, and at the same time the concentration of $RCORh(CO)_4$ has been attained at maximum. The induction period (initial curvature) in the profile of aldehyde is minimal. Care was taken to ensure that experiments reported are free from transport control in either H_2 or CO.

It was possible to model the rate of aldehyde formation with exactly two terms, one term being linear in the concentration of $RCORh(CO)_4$ and the second being bilinear in $RCORh(CO)_4$ and $HRe(CO)_5$ (Eq. 15a). The expanded rate constant k_1 for the linear term is entirely consistent with the kinetics of the simple rhodium unicyclic hydroformylation of alkenes as studied using in situ spectroscopic data [75]. The expanded bilinear rate constant k_2 clearly shows that molecular hydrogen

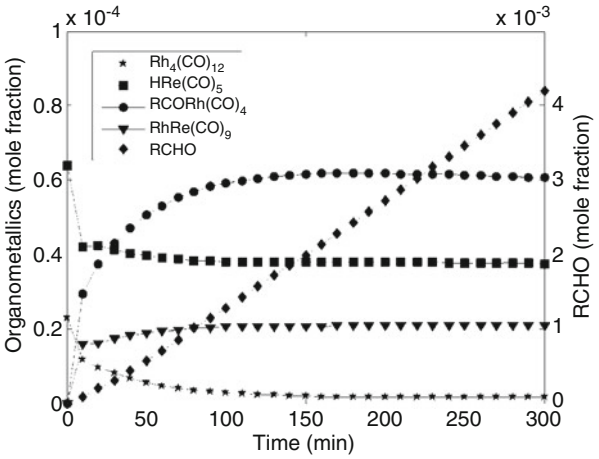

Fig. 20 Typical concentration profiles from a bimetallic Rh–Re CBER hydroformylations (reprinted with permission from Li et al. [75]. Copyright (2007) American Chemical Society)

is not involved. The unusual exponent for CO of circa −1.5 is highly reproducible and has been consistently observed for Rh–Mn and Rh–Re systems.

$$r = \left(k_1 + k_2\left[\mathrm{HRe(CO)_5}\right]\right)\left[\mathrm{RCORh(CO)_4}\right] \tag{15a}$$

$$k_1 = k_1^{'}[(\mathrm{CO})]^{-1}[\mathrm{H_2}] \tag{15b}$$

$$k_2 = k_2^{'}[(\mathrm{CO})]^{-1.5} \tag{15c}$$

In the case of the Rh–Mn systems modelled, circa 10–40% of the product formation arose from a bilinear term; in the case of Rh–Re systems, up to circa 90% of the product formation arose from the bilinear term. This situation existed in spite of the fact that on a mole-to-mole ratio, the ratio of Mn:Rh and Re:Rh was <1, and blank experiments run with just $HMn(CO)_5$ or $HRe(CO)_5$ confirm that neither metal alone shows any measurable activity at the conditions used. At the partial pressures of hydrogen used, the mole fraction of dissolved H_2 was on the order of 0.01. The typical mole fraction of Re used was 10^{-5}. Therefore, on a mole-to-mole basis, $HRe(CO)_5$ is circa 1,000 times more effective than molecular hydrogen towards attack on $RCORh(CO)_4$.

3.3 Isotopic Labelling

In order to make sure under catalytic hydroformylation conditions that the H in $HRe(CO)_5$ was incorporated into the product aldehyde, deuteroformylations were conducted with D_2 and then $HRe(CO)_5$ was injected into the system. These experiments showed that the H label in $HRe(CO)_5$ was exclusively incorporated in the formyl group of the organic product [75].

The ease with which bimolecular reactions between mononuclear species were occurring in the mechanisms $[\mathcal{M} = \{M\}, \{M'\}, \{M - M'\}]_{CBER+UNI}$ leads to some concern about potential for partial product formation reversibility. Therefore, a triply labelled cyclopentane carboxaldehyde was prepared $(C_5H_8D)^{13}CDO$. This triply labelled product was then injected under hydroformylation conditions where H_2 and natural abundance CO were used. There was no indication whatsoever over the circa 4 h reaction that any $(C_5H_8D)^{13}CDO$ was incorporated into the mechanism $[\mathcal{M} = \{M\}, \{M'\}, \{M - M'\}]_{CBER+UNI}$ and then converted back to product either as $(C_5H_8D)^{12}CDO$ or $(C_5H_8D)^{12}CHO$ or $(C_5H_8D)^{13}CHO$ by a partially reversible network.

3.4 From Stoichiometric to Catalytic Binuclear Reaction

The work on stoichiometric binuclear elimination by Heck and Breslow in the homometallic case and the extensive work by Unvary and Kovak in the heterobimetallic case were the primary drivers for encouraging the search by Penninger, Mirbach and others for the catalytic cases.

Now with the identification of clear-cut $[\mathcal{M} = \{M\}, \{M - M\}]_{CBER+UNI}$ and $[\mathcal{M} = \{M\}, \{M'\}, \{M - M'\}]_{CBER+UNI}$ hydroformylation systems, the issues come full circle. So the question arises: can one start with a stoichiometric binuclear elimination reaction and let it run until it has exhausted its potential and then restart it by application of hydrogen and at the end obtain a fully functioning $[\mathcal{M} = \{M\}, \{M - M\}]_{CBER+UNI}$ and $[\mathcal{M} = \{M\}, \{M'\}, \{M - M'\}]_{CBER+UNI}$ system?

The question can be answered in the affirmative. Thus, $HWCp(CO)_3$ and $Rh_4(CO)_{12}$ were introduced as precursors to a solution containing *n*-hexane as solvent and cyclopentene and CO. Various perturbations were made by introducing additional aliquots of $HWCp(CO)_3$ and cyclopentene during the first 160 min. At each perturbation, there was a very fast redistribution of organometallics with additional formation of aldehyde. The concentration of the dinuclear species $RhW(CO)_7Cp$ increased at each perturbation. At circa 160 min, H_2 was introduced. A marked transition to catalytic behaviour occurred with an increase in the concentration of $HWCp(CO)_3$ and decrease in the concentrations of $Rh_4(CO)_{12}$ and $RhW(CO)_7Cp$. The results are shown in Fig. 21.

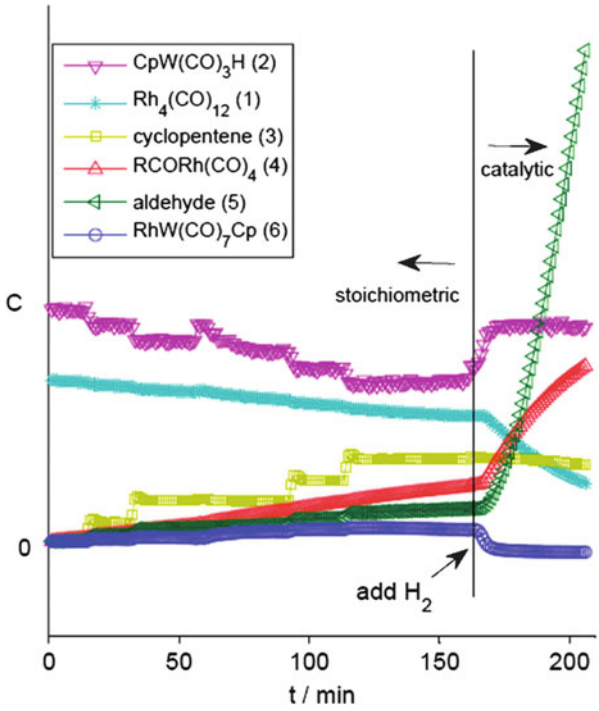

Fig. 21 An example of stoichiometric binuclear elimination to CBER using $HWCp(CO)_3$ and $Rh_4(CO)_{12}$ as precursors (reprinted with permission from Li et al. [79]. Copyright (2011) American Chemical Society)

3.5 Miscellaneous Mechanistic Issues

3.5.1 More on the β Step

Molecular hydrogen activation, into homolytically (or heterolytically) split hydrogen, is usually considered a very difficult step to achieve. Indeed, a significant portion of the mechanistic work on organometallics and homogeneous catalysis by James [88] and others clearly shows the usually high activation barriers and general difficulty encountered when other strongly binding ligands like CO are present to fill coordination sites. Although mononuclear organometallics were used in the vast majority of studies, it had been widely surmised that dinuclear centres and particularly heterobimetallic dinuclear centres might yield lower activation energies and potential new opportunities.

One of the earliest well-defined examples of very facile hydrogen activation on a dinuclear complex occurs with $CoRh(CO)_7$, a formally coordinately unsaturated semi-bridged species first tentatively reported by Spindler et al. [89] and then confirmed by Horvath et al. [90]. Although crystallisable under CO at cryogenic temperatures, it was never isolated. This species remains coordinately unsaturated even under tens of bars of CO pressure. The equilibrium is shifted to the coordinately saturated and all-terminal $CoRh(CO)_8$ in the range of 100 bar [70]. In situ hydrogen activation studies showed that molecular hydrogen was split on CoRh

$(CO)_7$ in the presence of substantial concentrations of CO to yield $HCo(CO)_4$ and $Rh_4(CO)_{12}$ [91]. Importantly, the hydrogen activation kinetics are zero order in CO – no dissociation step is needed prior to H_2 oxidative addition [92]. The typically observed half-life of the reaction in the range of 250–293 K is 1–2 min which corresponds to the mixing time of the reagents used.

The above reaction suggested that it would be instructive to mix $HRe(CO)_5$ and $Rh_4(CO)_{12}$ in *n*-hexane solvent both in the presence and absence of dissolved CO. In both cases, reaction occurred on the timescale of mixing, and the product was all-terminal $RhRe(CO)_9$ [61–63]. By varying the hydrogen partial pressure, it was possible to show that the reaction is reversible and very rapid, again on the mixing timescale, pushing the organometallics back towards $HRe(CO)_5$ and $Rh_4(CO)_{12}$. As of the present writing, direct hydrogen activation experiments on pure $RhRe(CO)_9$ in *n*-hexane have not been performed, since no attempts to isolate $RhRe(CO)_9$ have ever been made.

3.5.2 Hydride Pools and Minimal Cluster Concentrations

From an in situ spectroscopic and chemometric view point, the lack of measurable quantities of $Rh_2(CO)_8$ and $Rh_6(CO)_{16}$ in heterobimetallic CBERs is one of the most obvious differences with homometallic rhodium hydroformylations. This is clearly related to the very aggressive nature of the hydrides $HMn(CO)_5$, $HRe(CO)_5$, $HWCp(CO)_3$ and $HMoCp(CO)_3$ towards higher nuclearity rhodium carbonyls. It also suggests that in the heterobimetallic systems, there is slightly better utilization of rhodium due to the deduced concentrations of these di- and multinuclear reservoirs.

3.5.3 Hydrogen Bonding and Deactivation

There are many other details to explain in the CBER systems $[\mathcal{M} = \{\mathrm{M}\}, \{\mathrm{M}-\mathrm{M}\}]_{\mathrm{CBER+UNI}}$ and $[\ \mathcal{M} = \{\mathrm{M}\}, \{\mathrm{M}'\}, \{\mathrm{M}-\mathrm{M}'\}\ ]_{\mathrm{CBER+UNI}}$, but we will end with just one of these. In the $[\mathcal{M} = \{\mathrm{Mo}\}, \{\mathrm{Rh}\}, \{\mathrm{Mo}-\mathrm{Rh}\}]_{\mathrm{CBER+UNI}}$ and $[\mathcal{M} = \{\mathrm{W}\}, \{\mathrm{Rh}\}, \{\mathrm{W}-\mathrm{Rh}\}]_{\mathrm{CBER+UNI}}$ systems, additional dinuclear organometallics without M–M′ bonds were observed. These new complexes $RCORh(CO)_4$–$HWCp(CO)_3$ and $RCORh(CO)_4$–$HMoCp(CO)_3$ existed due to hydrogen bonding between the Cp moieties and the carbonyls on rhodium. This example is noted just as a further justification for in situ studies and signal processing. The chemistry of catalytic systems is usually so very complex and there are often new exciting results if one is able to investigate in an in situ manner.

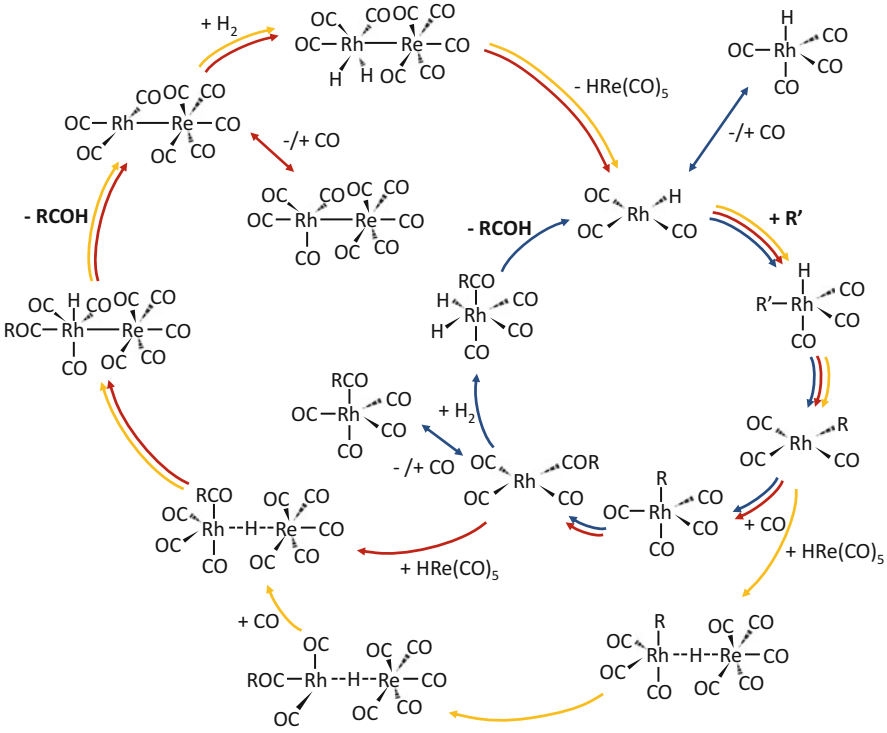

Fig. 22 Two interlocking CBER systems in the $[\mathcal{M} \in \{\text{Re}\},\{\text{Rh}\},\{\text{Re}-\text{Rh}\}]_{\text{CBER+UNI}}$ for hydroformylation (reprinted with permission from Klähn and Garland [93]. Copyright (2015) American Chemical Society)

3.6 *Possible Future Applications*

The most obvious chemistries to try next are chemistries closely related to hydroformylation, for example, the hydroaminations, hydrosilations, hydrocyanations, etc., using the metals noted throughout this chapter. The extension of CBER mechanisms to regio-, chemo- and stereoselective hydroformylation systems as well as the aforementioned chemistries should produce an incredibly rich variety of new results and go a long way towards classifying the scope of non-linear CBER mechanisms.

In terms of connectivity of intermediates in CBER systems, new possibilities may also arise. Indeed, very recently [93], it was found that the $HRe(CO)_5$ actually attacks two different rhodium intermediates in the $[\mathcal{M} = \{\text{Re}\},\{\text{Rh}\},\{\text{Re}-\text{Rh}\}]_{\text{CBER+UNI}}$ for hydroformylation. Specifically, using computational chemistry techniques, it was found that $HRe(CO)_5$ actually attacks both $RCORh(CO)_4$ and $RRh(CO)_3$. This situation thus explains the unusual rate dependence on CO, namely, $[CO]^{-1.5}$. From a connectivity viewpoint, the important issue is that there are two interlocking CBER systems operating simultaneously Fig. 22.

4 Conclusions

Monometallic and heterobimetallic CBER mechanisms are a specific class of synthetic systems which permit linear, quadratic and bilinear reaction rate terms. It is possible to classify the basic structures. CBER mechanisms possess mononuclear sequences and a dinuclear sequence of intermediates. In addition there are steps to transform mononuclear intermediates into dinuclear intermediates and dinuclear intermediates back into mononuclear intermediates. One of the main synthetic advantages of a CBER mechanism is associated with the potential for tremendous rate increases due to the binuclear elimination step. This in turn can lead to much more efficient synthetic use of a precious metal, either by taking advantage of bilinear kinetics or quadratic kinetics.

A considerable emphasis of this chapter was to highlight the need for in situ spectroscopic measurements in order to confirm the observable speciation present and hence reaction network. Another strong emphasis was given to the fact that the non-linear CBER mechanism provides a fertile area to apply quite advanced and seldom used mathematical tools to catalysis. Thus the Feinberg criteria indicate that these systems are stable and not oscillatory, the Horiuti criteria will help to decide how many terms needed to be included in any comprehensive model by enumerating all independent pathways to products, and the Wegschieder criteria help to clarify that the cycles in the CBER are not, by any means, independent. As catalysis moves from simple unicyclic mechanisms to more complex and potentially non-linear mechanisms, additional tools will be needed to meet the challenges of better understanding these systems and to make better use of these systems synthetically.

Acknowledgement The author would like to thank the Agency for Science Technology and Research for generous support of this research. The author would also like to thank Dr Marco Klähn for his recent and extensive computational work concerning CBER and allowing the inclusion of Fig. 22.

References

1. van Santen RA, Neurock M (2006) Molecular heterogeneous catalysis: a conceptual and computational approach. Wiley-VCH, Weinheim
2. Illanes A (ed) (2008) Enzyme biocatalysis: principles and applications hardcover. Springer, Heidelberg
3. Waser M (2012) Asymmetric organocatalysis in natural product syntheses. Springer, Heidelberg
4. Erker G, Stephen DW (2013) Frustrated Lewis Pairs II: expanding the scope. Springer, Heidelberg
5. Parshall GW, Ittel SD (1992) Homogeneous catalysis: the applications and chemistry of catalysis by soluble transition metal complexes. Wiley-Intersceince, New York
6. Molnar A (2013) Palladium-catalyzed coupling reactions: practical aspects and future developments. Wiley-VCH, Weinheim

7. Jenner G (1988) Hydrocarbonylation of linear and branched aliphatic C2–C4 alcohols catalyzed by cobalt-ruthenium systems. A comparative study. J Organomet Chem 346(2):237–251
8. Garland M (2002) Transport effects in homogeneous catalysis. In: Horvath IT (ed) Encyclopedia of catalysis. Wiley, New York
9. Breslow DS, Heck RF (1961) The reaction of cobalt hydrotetracarbonyl with olefins. J Am Chem Soc 83(19):4023–4027
10. Norton JR (1979) Organometallic elimination mechanisms: studies on osmium alkyls and hydrides. Acc Chem Res 12:139–145
11. Kovacs I, Hoff CD, Ungvary F, Marko L (1985) Kinetic investigation of the mixed-metal bimolecular reductive eliminations in the reactions of $EtOC(O)CH_2M(CO)_n$ or $EtOC(O)M(CO)_n$ ($M = Co$, $n = 4$; $M = Mn$, $n = 5$) with $HCo(CO)_4$ or $HMn(CO)_5$. Organometallics 4:1347–1350
12. Kovacs I, Ungvary F, Marko L (1986) Kinetic investigation of the cleavage of n-butyryl- or isobutyrylcobalt tetracarbonyl with hydridocobalt tetracarbonyl or dihydrogen. Organometallics 5(2):209–215
13. Li CZ, Garland M (2013) Catalytic binuclear elimination. In: Cornils B, Herrmann WA, Wong CH, Zanthoff HW (eds) Catalysis from A to Z: a concise encyclopedia, 4th edn. Wiley, Weinheim, pp 434–435
14. Heaton B (ed) (2005) Mechanisms in homogeneous catalysis: a spectroscopic approach. Wiley, Germany
15. Niemantsverdriet JW (2007) Spectroscopy in catalysis. Weinheim, Wiley VCH
16. Haynes A (2005) The use of high pressure infrared spectroscopy to study catalytic mechanisms. In: Heaton B (ed) Mechanisms in homogeneous catalysis: a spectroscopic approach. Wiley, Weinheim, pp 107–150
17. Garland M (2005) Processing spectroscopic data. In: Heaton B (ed) Mechanisms in homogeneous catalysis: a spectroscopic approach. Wiley, Weinheim, pp 151–193
18. Garland M, Li CZ, Guo LF (2012) Four criteria for evaluating pure component spectral estimates and the subsequent identification of intermediates in homogeneous catalysis. ACS Catal 2:2327–2334
19. Gao F, Ng K, Li C, Krummel K, Allian A, Garland M (2006) A versatile and compact experimental apparatus for the on-line spectroscopic study of liquid-phase heterogeneous catalytic systems. J Catal 237:49–57
20. Temkin ON, Zeiggarnik AV, Bonchev DG (1996) Graph chemical reaction networks: a graph-theoretical approach. CRC, Boca Raton
21. Ford LR, Fulkerson DR (2010) Flows in networks. Princeton University Press, Princeton
22. Penfield P, Spencer R, Duinker S (1970) Tellegen's theorem and electrical networks. MIT, Boston
23. Fishtik I, Callaghan CA, Datta R (2004) Reaction route graphs. I. Theory and algorithm. J Phys Chem B 108(18):5671–5682
24. Masters C (2013) Homogeneous transition-metal catalysis: a gentle art paperback. Springer, Heidelberg
25. King EL, Altman C (1956) A schematic method of deriving the rate laws for enzyme-catalyzed reactions. J Phys Chem 60(10):1375–1378
26. Chou KC (1989) Graphic rules in steady and non-steady state enzyme kinetics. J Biol Chem 264:12074–12079
27. van Leeuwen PWNM, Claver C (2002) Rhodium catalyzed hydroformylation. Springer, Heidelberg
28. Taddei M, Mann A (eds) (2014) Hydroformylation for organic synthesis. Springer, Heidelberg
29. de Vries JG, Cornelis J (eds) (2007) Handbook of homogeneous hydrogenation. Elsevier, Amsterdam
30. Izumi A, Tai Y (1977) Stereo-differentiating reactions: the nature of asymmetric reactions. Academic, San Diego

31. Horiuti J (1973) Theory of reaction rates as based on the stoichiometric number concept. Ann N Y Acad Sci 213:5
32. Broussard ME, Juma B, Train SG, Peng WJ, Laneman SA, Stanley GG (1993) A bimetallic hydroformylation catalyst: high regioselectivity and reactivity through homobimetallic cooperativity. Science 260:1784–1788
33. Hansen KB, Leighton JL, Jacobsen EN (1996) On the mechanism of asymmetric nucleophilic ring-opening of epoxides catalyzed by (salen)CrIII complexes. J Am Chem Soc 118:10924–10925
34. Schaus SE, Jacobsen EN (2000) Asymmetric ring opening of meso epoxides with TMSCN catalyzed by (pybox)lanthanide complexes. Org Lett 2:1001–1004
35. Whyman R (1974) In situ infrared spectral studies on the cobalt carbonyl-catalysed hydroformylation of olefins. J Organomet Chem 66(1):C23–C25
36. Whyman R (1974) The hydroformylation of olefins catalysed by cobalt carbonyls: a high pressure infrared spectral study. J Organomet Chem 81(1):97–106
37. Alemdaroğlu NH, Penninger ML, Oltay E (1976) Study of the mechanism of hydroformylation at industrial reaction conditions. Monatsh Chem 107(4):1153–1165
38. Mirbach MF (1984) On the mechanism of the $Co_2(CO)_8$ catalyzed hydroformylation of olefins in hydrocarbon solvents. A high pressure UV and IR study. J Organomet Chem 265 (2):205–213
39. Mond L, Hirzt H, Cowap MD (1910) Einige neue metallkarbonyle. Z Anorg Allg Chem 68:207–219
40. Mond L, Hirzt H, Cowap MD (1910) LIV.—some new metallic carbonyls. J Chem Soc Trans 97:798–810
41. Bor G, Noack K (1974) On the infrared spectrum of dicobalt octacarbonyl. Results of ^{13}CO enrichment studies. J Organomet Chem 64:367–373
42. Bor G, Dietler UK, Noack K (1976) High temperature infrared spectrum of dicobalt octacarbonyl: predominance of the third isomer. J Chem Soc Chem Commun 914–916
43. Hieber W, Mühlbauer F, Ehmann EA (1932) Derivate des Kobalt- und Nickelcarbonyls. Ber Dtsch Chem Ges 65(7):1090
44. Roelen O (1938) Process for preparing valuable oxo products. Patent Germany, 849.548
45. Pino P, Ercoli R, Calderazzo F (1955) Sinntesi di aldeidid a temperature ambiente per reazione fra olefin dicobalto-ottacarrbonile e idrogeno. Chim Ind 37:782
46. Kirch L, Orchin M (1959) On the mechanism for the Oxo reaction. J Am Chem Soc 81:3597–3599
47. Natta G, Ercoli R, Castelano S (1955) Cinetica dell'ossosintesi. Chim Ind 37:6
48. Falbe J (ed) (1980) New syntheses with carbon monoxide. Springer, Heidelberg
49. Liu G, Volken R, Garland M (1999) Unmodified rhodium-catalyzed hydroformylation of alkenes using tetrarhodium dodecacarbonyl. The infrared characterization of 15 acyl rhodium tetracarbonyl intermediates. Organometallics 18(17):3429–3436
50. Feng J, Garland M (1999) Unmodified homogeneous rhodium-catalyzed hydroformylation of styrene. The detailed kinetics of the regioselective synthesis. Organometallics 18(3):417–427
51. Feng J, Garland M (1999) The unmodified homogeneous rhodium-catalyzed hydroformylation of cyclohexene and the search for monometallic catalytic binuclear elimination. Organometallics 18(8):1542–1546
52. Liu G, Li CZ, Guo LF, Garland M (2006) Experimental evidence for a significant homometallic catalytic binuclear elimination reaction: Linear-quadratic kinetics in the rhodium catalyzed hydroformylation of cyclooctene. J Catal 237(1):67–78
53. Wei CH, Dahl LF (1966) Molecular structures of triiron dodecacarbonyl and tetracobalt dodecacarbonyl. J Am Chem Soc 88:1821–1822
54. Corey ER, Dahl LF, Beck W (1963) Rh6(CO)16 and its identity with previously reported Rh4 (CO)11. J Am Chem Soc 85:1202–1203
55. Allian AD, Garland M (2005) Spectral resolution of fluxional organometallics. The observation and FTIR characterization of all-terminal $Rh_4(CO)_{12}$. Dalton Trans 1957–1965

56. Whyman R (1970) Dirhodium octacarbonyl. J Chem Soc D 1194–1195
57. Hanlan LA, Ozin GA (1974) Synthesis using transition metal diatomic molecules. Dirhodium octacarbonyl and diiridium octacarbonyl. J Am Chem Soc 96(20):6324–6329
58. Vidal JL, Walker WE (1981) Rhodium carbonyl cluster chemistry under high pressure of carbon monoxide and hydrogen. 3. Synthesis, characterization, and reactivity of $HRh(CO)_4$. Inorg Chem 20(1):249–254
59. Li CZ, Widjaja E, Chew W, Garland M (2002) Rhodium tetracarbonyl hydride: the elusive metal carbonyl hydride. Angew Chem 114(20):3939–3943
60. King RB, King AD Jr, Iqbal MZ (1979) Alkylrhodium tetracarbonyl derivatives as catalytic intermediates in homogeneous hydroformylation reactions. An infrared spectroscopic study. J Am Chem Soc 101(17):4893–4896
61. Li CZ, Guo LF, Garland M (2004) Homogeneous hydroformylation of ethylene catalyzed by $Rh_4(CO)_{12}$. The application of BTEM to identify a new class of rhodium carbonyl spectra: RCORh(CO)3(π-C2H4). Organometallics 23(9):2201–2204
62. Li CZ, Guo LF, Garland M (2004) Identification of rhodium − rhenium nonacarbonyl $RhRe(CO)_9$. Spectroscopic and thermodynamic aspects. Organometallics 23(22):5275–5279
63. Li CZ, Widjaja E, Garland M (2004) $Rh_4(CO)_{12}$-catalyzed hydroformylation of cyclopentene promoted with $HMn(CO)_5$. Another example of $Rh_4(CO)_{12}/HMn(CO)_5$ bimetallic catalytic binuclear elimination. Organometallics 23:4131–4138
64. Garland M, Bor G (1989) Infrared spectroscopic studies on metal carbonyl compounds. 24. Observation of the infrared spectrum of an acylrhodium tetracarbonyl during the hydroformylation of olefins with rhodium-containing catalyst precursors. Inorg Chem 28(3):410–413
65. Zhang J, Poliakoff M, George MW (2003) Rhodium-catalyzed hydroformylation of alkenes using in situ high-pressure IR and polymer matrix techniques. Organometallics 22 (8):1612–1618
66. Csontos S, Heil B, Marko L (1974) Hydroformylation of olefins with rhodium carbonyls as catalysts. IV. Mechanism of the reaction. Ann N Y Acad 239:47–54
67. Wender I, Pino P (1968) Organic syntheses via metal carbonyls, vol 1. Wiley, New York
68. Wender I, Pino P (1977) Organic syntheses via metal carbonyls, vol 2. Wiley, New York
69. Pino P, Oldani F, Consiglio G (1983) On hydrogen activation in the hydroformylation of olefins with $Rh_4(CO)_{12}$ or $Co_2(CO)_8$ as catalyst precursors. J Organomet Chem 250:491–497
70. Garland M, Horvath IT, Bor G, Pino P (1991) Thermodynamic parameters for the formation of cobalt-rhodium heptacarbonyl and cobalt-rhodium octacarbonyl. Organometallics 10 (3):559–567
71. Fyhr C, Garland M (1993) Phenomenological aspects of homogeneous catalysis. The case of equilibrium-controlled precursor conversion. Organometallics 12(5):1753–1764
72. Ungvary F (1972) Kinetics and mechanism of the reaction between dicobalt octacarbonyl and hydrogen. J Organomet Chem 36:363
73. Beletskaya IP, Magomedov GK, Voskoboinikov AZ (1990) Heterometallic catalysts. Cobalt carbonyl derivatives of lanthanides in catalysis of octene-1 hydroformylation. J Organomet Chem 385:289–295
74. Li CZ, Widjaja E, Garland M (2003) The $Rh_4(CO)_{12}$-catalyzed hydroformylation of 3,3-dimethylbut-1-ene promoted with $HMn(CO)_5$. Bimetallic catalytic binuclear elimination as an origin for synergism in homogeneous catalysis. J Am Chem Soc 125:5540–5548
75. Li CZ, Chen L, Garland M (2007) Synchronicity of mononuclear and dinuclear events in homogeneous catalysis. Hydroformylation of cyclopentene using $Rh_4(CO)_{12}$ and $HRe(CO)_5$ as precursors. J Am Chem Soc 129:13327–13334
76. Li CZ, Chen L, Garland M (2008) Synthetic applications of synergism using catalytic binuclear elimination reactions. Further examples of rhodium-manganese and rhodium-rhenium-catalyzed hydroformylations. Adv Synth Catal 350:679–690
77. Li CZ, Cheng S, Tjahjono M, Schreyer M, Garland M (2010) Concurrent synergism and inhibition in bimetallic catalysis: catalytic binuclear elimination, solute-solute interactions and

a hetero-bimetallic hydrogen-bonded complex in Rh-Mo hydroformylations. J Am Chem Soc 2010:4589–4599
78. Li CZ, Chen L, Widjaja E, Garland M (2010) The catalytic binuclear elimination reaction: confirmation from in situ FTIR studies of homogeneous rhodium catalyzed hydroformylation. Catal Today 155:261–265
79. Li CZ, Gao F, Cheng S, Tjahjono M, van Meurs M, Tay BY, Jacob C, Guo LF, Garland M (2011) From stoichiometric to catalytic binuclear elimination in Rh–W hydroformylations. Identification of two new heterobimetallic intermediates. Organometallics 30:4292–4296
80. Trost B (1991) The atom economy – a search for synthetic efficiency. Science 254:1471–1477
81. Noyes RM, Furrow SD (1982) The oscillatory Briggs–Rauscher reaction. 3. A skeleton mechanism for oscillations. J Am Chem Soc 104(1):45–48
82. Turing AM (1952) The chemical basis of morphogenesis. Philos Trans R Soc B 237:37–72
83. Feinberg M (1995) The existence and uniqueness of steady states for a class of chemical reaction networks. Arch Ration Mech Anal 132:311–370
84. Wegscheider R (1901) Über simultane Gleichgewichte und die Beziehungen zwischen Thermodynamik und Reactionskinetik homogener Systeme. Monatsh Chem 32(8):849–906
85. Garland M (1993) Heterometallic clusters as catalyst precursors. Synergism arising from the facile generation of a reactive fragment. Organometallics 12(2):535–543
86. Liu G, Hakimifard M, Garland M (2001) An in situ spectroscopic study of the ruthenium catalyzed carbonylation of piperidine starting with triruthenium dodecacarbonyl: the importance of path dependence in homogeneous catalysis. J Mol Catal A Chem 168:33–37
87. Haynes A, Maitlis PM, Morris GE, Sunley GJ, Adams H, Badger PW, Bowers CM, Cook DB, Elliott PIP, Ghaffar T, Green H, Griffin TR, Payne M, Pearson JM, Taylor JM, Vickers PW, Watt RJ (2004) Mechanistic studies of the cativa process. J Am Chem Soc 2004 (126):2847–2861
88. James BR (1973) Homogeneous hydrogenation. Wiley, New York
89. Spindler F, Bor G, Dietler UK, Pino P (1981) The formation of a new mixed cobalt rhodium carbonyl from $Co_2(CO)_8$ and $Rh_4(CO)_{12}$: infrared spectroscopic characterization under carbon monoxide pressure. J Organomet Chem 213:303–312
90. Horvath IT, Bor G, Garland M, Pino P (1986) Cobalt-rhodium heptacarbonyl: a coordinatively unsaturated dinuclear metal carbonyl. Organometallics 5(7):1441–1445
91. Horvath IT, Bor G, Garland M, Pino P (1988) Low temperature activation of molecular hydrogen in CO/H_2 mixtures in the presence of $CoRh(CO)_7$. J Organomet Chem 358:C17–C22
92. Garland M, Pino P (1990) Kinetics of molecular hydrogen activation by cobaltrhodium heptacarbonyl. Organometallics 9(6):1943–1949
93. Klähn M, Garland M (2015) On the mechanism of the catalytic binuclear elimination reaction in hydroformylation systems. ACS Catal 5:2301–2316

Top Organomet Chem (2016) 59: 233–272
DOI: 10.1007/3418_2015_146

Published online: 16 September 2015

Biomimetic Complexes for Production of Dihydrogen and Reduction of CO_2

Lu Gan, David Jennings, Joseph Laureanti, and Anne Katherine Jones

Abstract The active sites of several bioenergetically important metalloenzymes that perform multielectron redox reactions feature heterobimetallic complexes. Herein, we review recent understanding of the structure and mechanisms of hydrogenases, formate dehydrogenases, and carbon monoxide dehydrogenases. Then we evaluate progress toward creating functional, small-molecule complexes that reproduce the activities of these active sites. Particular emphasis is placed on comparing catalytic properties including turnover number, turnover frequency, required overpotential, and catalyst stability. Opportunities and challenges for future work are also considered.

Keywords Bio-inspired metallocomplexes • Biomimicry • Carbon monoxide dehydrogenase • Catalysis • Energy • Formate dehydrogenase • Hydrogenase

Contents

L. Gan, D. Jennings, J. Laureanti, and A.K. Jones (✉)
Department of Chemistry and Biochemistry, Arizona State University, Tempe, AZ 85287, USA
e-mail: jonesak@asu.edu

Abbreviations

adt^{Bn}	$(SCH_2)_2NBn$
bdt	benzene-1,2-dithiolate
bpy	bipyridyl
CB	conduction band
CODH	carbon monoxide dehydrogenase
Cy	cyclohexyl
DFT	density functional theory
dmg	dimethylgloxime
dppe	1,2-bis(diphenylphosphino)ethane
dppf	1,1′-bis(diphenylphosphino)ferrocene
dppv	*cis*-1,2-bis(diphenylphosphino)ethylene
EXAFS	Extended X-ray Absorption Fine Structure
FDH	formate dehydrogenase
Gly	glycine
HER	hydrogen evolution reaction
HOMO	highest occupied molecular orbital
LUMO	lowest unoccupied molecular orbital
MeCN	acetonitrile
pdt	1,3-propanedithiol
$PFc^{*Et}{}_2$	$Et_2PCH_2C_5Me_4FeCp^*$
$P^RN^{Ph}{}_2$	1,5-diaza-3,7-diphosphaoctane
RHE	reversible hydrogen electrode
TD-DFT	time-dependent density functional theory
TFA	trifluoroacetic acid
VB	valence band

1 Introduction

Enzymes have long been known to be efficient catalysts [1–3]. In particular, they are admired for selectivity, fast rates, and low activation energies. When considering applications that require sustainability and scalability, enzymes also have the advantage of being constructed exclusively from earth-abundant, bioavailable materials. Thus metalloenzymes typically employ only earth-abundant metals

such as first row transition metals, although industrial catalysts for the same reaction often require precious metal catalysts based on Pt, Pd, or Ru. Moreover, using modern molecular biological techniques, enzymes can often be cheaply produced with microbial overexpression systems. However, enzymes function ordinarily only over the limited range of conditions in which the protein remains correctly folded. Thus, they are not ideal for use directly in all applications. Instead, in many cases, enzymes serve as inspiration to uncover underlying principles of fast catalysis that can be implemented in simple, synthetic molecules.

Biological inspiration has proven particularly important in energy research. Human-driven production of greenhouse gases and their resulting impact on global processes including climate has increased awareness of the need to develop catalysts for carbon-neutral production of fuels [4]. Hydrogen and carbonaceous fuels derived from carbon dioxide reduction are the most desirable targets, and many metalloenzymes catalyzing production of these fuels are well known. In fact, the only catalytic process for carbonaceous fuel production that has been successful on the global scale is biological, i.e., photosynthesis. Remarkably, many fuel production enzymes feature unique heterobimetallic active sites for substrate activation. These unusual inorganic structures serve both as templates and as aspirational goals for development of robust catalysts.

In this chapter, we survey recent efforts to produce biologically inspired catalysts for proton and CO_2 reduction. First, we introduce the biological catalysts that underpin this research: hydrogenases, carbon monoxide dehydrogenases, and formate dehydrogenases. Then, we describe some of the most catalytically successful synthetic molecules that have been inspired by these biological catalysts, paying particular attention to catalytic properties and mechanism.

2 Biological Catalysts

2.1 Hydrogenases

Hydrogen and protons have been utilized for bioenergetic processes in organisms for billions of years. Hydrogenases are the enzymes responsible for hydrogen oxidation and production. These proteins turnover at high rates ($k_{cat} \sim 10^4\ s^{-1}$) and are highly reversible, i.e., operate with minimal electrochemical overpotential [5]. There are three types of hydrogenase, distinguished by the metal content of their active sites: [Fe]-, [FeFe]-, and [NiFe]-hydrogenase. Figure 1 shows the active sites of these enzymes. Unlike the other hydrogenases, the [Fe]-hydrogenase contains a monometallic, as opposed to bimetallic, active site and no accessory [FeS] clusters. Furthermore, it only performs the hydrogenase reaction in the presence of an additional organic cofactor [6]. Thus, this type of hydrogenase will not be discussed further here. The bimetallic hydrogenases, [FeFe] and [NiFe], have been more extensively characterized. They catalyze the reaction

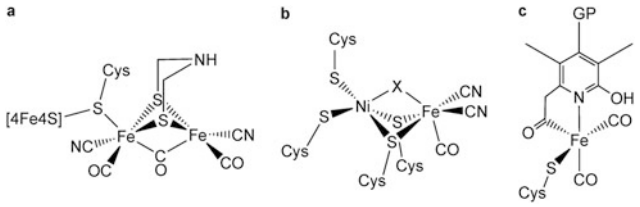

Fig. 1 Active sites of the (**a**) [FeFe]-hydrogenase, (**b**) [NiFe]-hydrogenase, and (**c**) [Fe]-hydrogenase. X represents an exogenous ligand such as H^-, OH^-, or OOH^-. GP is guanylpyridinol

shown in Eq. (1). In the following sections, these two bimetallic types of hydrogenases will be introduced with particular attention paid to structural and mechanistic features relevant to the design of functional models.

$$2H^+ + 2e^- \rightleftharpoons H_2 \tag{1}$$

2.1.1 [FeFe]-Hydrogenases

The active site of [FeFe]-hydrogenases is called the H-cluster (Fig. 1a). It is a unique six-iron metallocenter consisting of a standard [4Fe4S] cubane bridged via a single cysteine residue to a diiron subsite. Functionally, the cubane serves as an electron reservoir that provides (or removes) reducing equivalents from the diiron center, itself the primary site of catalysis. The diiron center contains ligands that, although common in organometallic chemistry, are unprecedented in biology outside of hydrogenases: CO and CN^-. As we will describe below, these ligands are also found in the [NiFe]-hydrogenases, which are functionally, but not evolutionarily, related enzymes. Thus, it appears that these ligands are essential for biological hydrogen activation. Both irons of the active site cycle through the Fe(II)/Fe(I) couple under physiological conditions. This is aided by the π-acceptor ligands which stabilize the low valent oxidation states [7]. These ligands may also be important in stabilizing a metallocenter basic enough for reaction with protons at near neutral pH. The irons are also bridged by an organic, nonproteinaceous azapropanedithiolate ligand [8]. The nitrogen at the bulkhead position of this ligand has been shown to be essential for catalytic activity [9] and, by analogy to organometallic model complexes [10, 11], is believed to serve as a proton transfer relay site. In addition to the first coordination sphere of the H-cluster, the protein is believed to provide a number of outer coordination sphere contacts that are essential for both active site structure and reactivity. For example, the π-acceptor ligands form hydrogen bonds to amino acids in the active site pocket [12]. These outer coordination sphere interactions limit the conformational flexibility of the metallocenter, especially the distal Fe (defined as the Fe atom farthest from the attached [4Fe4S] cluster). The result is a conformation that has come to be known as the "rotated" structure, and this unusual conformation is thought to be key in promoting high catalytic activity [13]. This conformation creates a vacant, terminal coordination site on the distal Fe

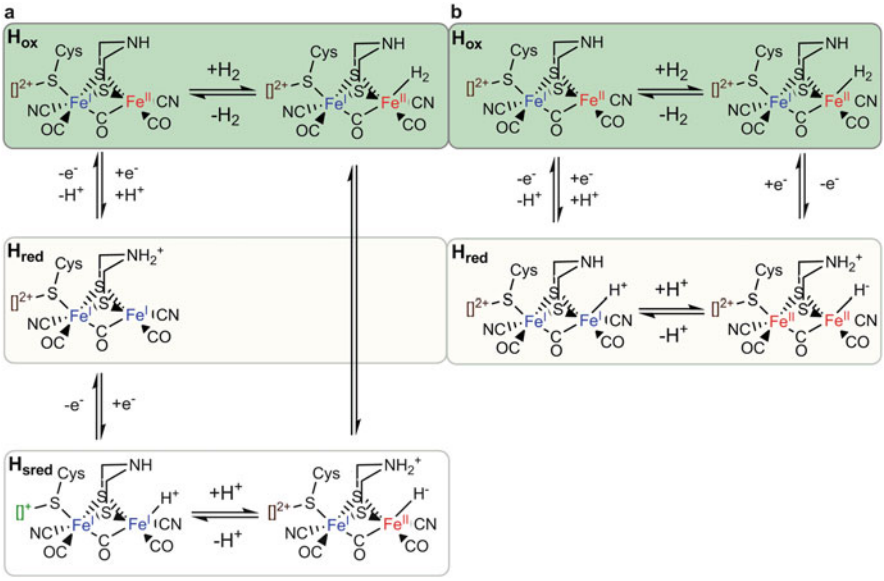

Fig. 2 Proposed mechanisms for [FeFe]-hydrogenase that (**a**) include H_{sred} and (**b**) exclude H_{sred}. The rectangle on the far left of each structure and associated charge represents the [4Fe4S] cluster of the H-cluster

where substrate or other exogenous species can bind. In contrast, small model complexes usually adopt an "eclipsed" conformation that promotes binding of ligands in a bridging mode and results in lower catalytic activity.

The redox chemistry of [FeFe]-hydrogenases is extensive. Although only three oxidation states are strictly necessary for the two-electron reaction catalyzed by hydrogenases, the presence of six metals creates the possibility of many stable states, and the enzyme has been isolated with the H-cluster in five distinct redox or spectroscopic states [14]. Two inactive states have been identified. The first, H_{ox}^{inact} [Fe(II)Fe(II)], is formed by oxidative inactivation. The second, H_{ox}–CO [Fe(I)Fe(II)], forms when CO binds to the vacant site on the distal Fe. There are also two known active states: H_{ox} [Fe(I)Fe(II)] and H_{red} [Fe(I)Fe(I)]. A fifth state, H_{sred}, [Fe(I)Fe(I)] with the [4Fe4S] cubane also reduced, has been observed, but the catalytic relevance of this state is still under debate [15, 16].

Figure 2 shows two different hypothetical catalytic cycles for [FeFe]-hydrogenases; these two cycles differ primarily in whether the H_{sred} state is included as a catalytically relevant state [16, 17]. Despite this, there are a number of commonalities shared by both schemes. First, for proton reduction, both cycles start with a one-electron reduction of H_{ox} to form H_{red} followed by protonation. It is unknown whether, during this step, the electron transfer or the proton transfer occurs first, or if they happen simultaneously. Second, both involve formation of a terminal hydride on the distal iron. Third, dihydrogen forms via combination of this hydride with a proton associated with the bulkhead nitrogen atom. Finally, in both cases, the H_2 then dissociates to regenerate the H_{ox} state and complete the

catalytic cycle. However, there are also differences between the two schemes, primarily in the stable sites of protonation. Figure 2a, the cycle including H_{sred}, suggests that the organic ligand is protonated first. Then, following the second reduction, the proton is ambiguously associated with the H-cluster until a second protonation event. In contrast, Fig. 2b, depicting the cycle without H_{sred}, suggests that the first proton coordinates directly to the distal Fe.

2.1.2 [NiFe]-Hydrogenases

[NiFe]- and [FeFe]-hydrogenases are not evolutionarily related, but the need to perform the same catalysis has resulted in closely related active sites in an example of convergent evolution. Most obviously, the Fe in the [NiFe]-hydrogenase active site is also coordinated by CO and CN^- ligands (Fig. 1b). Second, both sites are bimetallic. In addition, in both cases, the two metals are also bridged by thiolate ligands. In the [NiFe] enzyme, these are provided by cysteine side chains. The distal iron of the [FeFe]-hydrogenase can be thought of as substituted by the Ni of [NiFe]-hydrogenases, but then the similarities start to break down. The primary coordination sphere of the nickel is completed by two terminal cysteine thiolate ligands. Although [NiFe]-hydrogenases do not feature a coordinated cubane cluster, it is worth noting that all hydrogenases of this type include an [FeS] cluster, referred to as the proximal cluster when other [FeS] clusters are present, near the [NiFe] active site. The [FeS] clusters present in both [NiFe]- and [FeFe]-hydrogenases are essential for providing an electrical linkage between the buried active site and the surface of the protein at which the physiological partner can give or receive reducing equivalents. In some [NiFe]-hydrogenases, the proximal cluster may also play a role in protecting the active site from irreversible reactions with oxygen [18]. Finally, although extrinsic ligands coordinate the H-cluster at a terminal position, spectroscopic evidence has shown that many extrinsic ligands coordinate the [NiFe]-site in a bridging mode [19, 20].

Using primarily EPR signals associated with paramagnetic Ni states and the FTIR signals associated with the vibrations of the diatomic ligands, a number of different redox states of the [NiFe] active site have been identified [21]. Evidence suggests that the Fe atom remains in a low spin Fe(II) state and all redox transitions occur at the Ni ion which cycles between the Ni(II) and Ni(III) states. Under high potential (oxidizing) or aerobic conditions, two different inactive Ni(III) states, both spectroscopically and kinetically distinguishable, are formed. The Ni-A state is reactivated on long timescales, whereas Ni-B requires shorter timescales to reactivate. Crystal structures have suggested that both states contain a bridging ligand derived from oxygen, but the chemical difference between these two states remains unclear [20, 22]. Three catalytically competent states have also been identified: Ni–Si_a, Ni–C, and Ni–R. As shown in Fig. 3, the two most reduced, Ni–C and Ni–R, are thought to contain a bridging hydride ligand.

Figure 3 shows a proposed catalytic mechanism for [NiFe]-hydrogenases. For hydrogen oxidation, the catalytic cycle starts at the Ni–SI_a state, a Ni(II) state with no bridging ligand. Hydrogen binds the active site and is heterolytically cleaved to produce the Ni–R state, a Ni(II) species with a bridging hydride and likely a

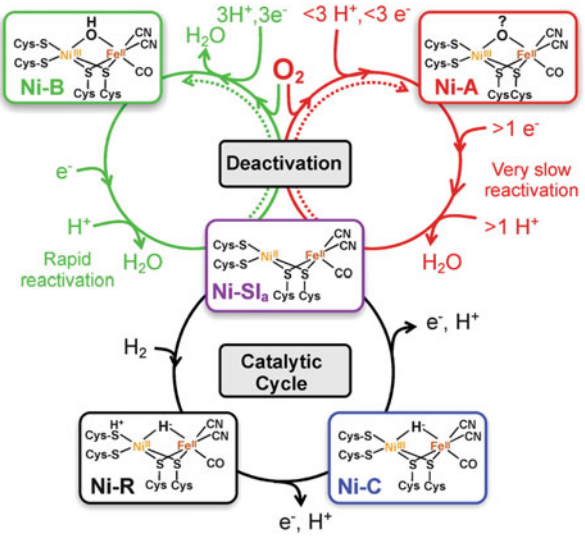

Fig. 3 The catalytic cycle of [NiFe]-hydrogenases. Reprinted with permission from Lubitz et al. [5]. Copyright 2014 American Chemical Society

protonated terminal thiolate ligand. This state is then oxidized and deprotonated to yield Ni–C, a Ni(III) state with a bridging hydride. It is worth noting that formally, Ni(I) coordinated to a proton is electronically equivalent. A further oxidation and deprotonation results in regeneration of the Ni–SI_a state to close the cycle [5]. As for [FeFe]-hydrogenases, the precise order of proton and electron transfer events is not yet entirely clear, and some may be concerted.

Like the [FeFe]-hydrogenases, the protein component of [NiFe]-hydrogenases is thought to play a number of crucial roles in tuning the reactivity of the metallocenter active site for fast catalysis. First, exposure of protein crystals to high pressure xenon has revealed gas channels that can concentrate substrate, product, or inhibitors and influence diffusion to the active site [23]. Site-directed mutations that narrow these channels have led to decreased reactivity of the enzyme with oxygen, also known as "oxygen tolerance" [24]. Second, the proximal [FeS] cluster is also thought to play a key role in imparting oxygen tolerance to some [NiFe]-hydrogenases. Crystal structures of oxygen-tolerant [NiFe]-hydrogenases from *Escherichia coli* and *Ralstonia eutropha* revealed an unprecedented [4Fe3S] cluster at the proximal position (Fig. 4) [25]. Spectroscopic results have suggested that this unusual cluster can undergo two different one-electron reactions, allowing it to provide an additional reducing equivalent to the active site when compared to a standard cubane [26]. Thus, enzymes with the [4Fe3S] cluster may be able to react with oxygen to uniquely produce water, i.e., to avoid production of reactive oxygen species. Third, the polypeptide provides a proton relay from the active site to the outside of the enzyme. It has been shown that mutations of residues in this pathway lead to reduced enzymatic activity presumably via disruption of proton transport [27].

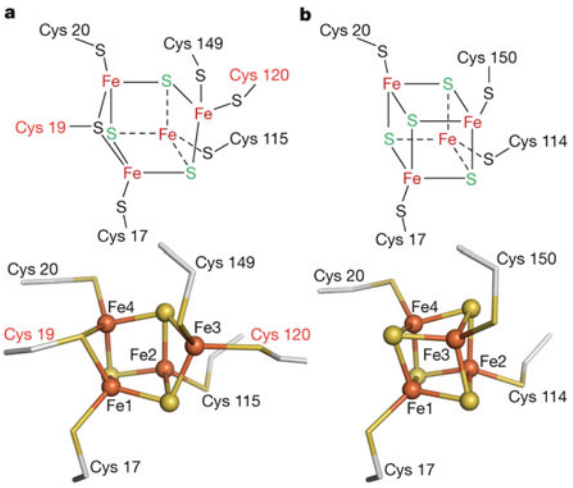

Fig. 4 Structures of the (**a**) [4Fe3S] proximal cluster found in oxygen-tolerant [NiFe]-hydrogenases and (**b**) [4Fe4S] proximal cluster found in oxygen-sensitive [NiFe]-hydrogenases. Reprinted with permission from Macmillan Publishers Ltd: Nature 479(7372): 249–252, copyright 2011

2.2 Carbon Monoxide Dehydrogenases (CODHs)

Biological systems fix CO_2 through a variety of pathways employing an array of enzymes. One of these enzymes is carbon monoxide dehydrogenase (CODH). Physiologically, these proteins catalyze the oxidation of CO to CO_2, and, in some cases, they can perform the reverse reaction (Eq. 2) [28]. There are two types of CODHs that are distinguished by the metal in the active site: MoCu and Ni. MoCu-CODHs are found in aerobic bacteria, whereas the oxygen-sensitive Ni-CODHs are found only in anaerobic bacteria [29]. Both enzymes have a bimetallic active site; however, the structures differ significantly, as shown in Fig. 5. Ni-CODHs have high k_{cat} values for CO oxidation of approximately 4×10^4 s^{-1}. CO_2 reduction has also been observed with this type of CODH, albeit with much lower turnover frequency of 45 s^{-1} [30]. In contrast, MoCu-CODHs turnover more slowly (circa 100 s^{-1}), and no activity for CO_2 reduction has been detected [31]. The following sections will discuss each type of CODH with a focus on structural and mechanistic features key to the function of these enzymes.

$$CO + H_2O \rightleftharpoons CO_2 + 2e^- + 2H^+ \tag{2}$$

2.2.1 MoCu-CODH

The MoCu-CODH active site is shown in Fig. 5a. The bimetallic structure consists of Mo and Cu ions connected by a bridging sulfide. The Cu ion is in a linear coordination geometry with the sulfide and a cysteinyl thiolate as ligands. The five-coordinate geometry about the molybdenum ion is distorted square pyramidal. In addition to the bridging sulfide, the molybdenum ligand set consists of an oxo group, a hydroxyl group, and bidentate coordinated pterin [32]. During catalysis, the Cu remains in a Cu(I) state, and the Mo changes from Mo(VI) to Mo(IV).

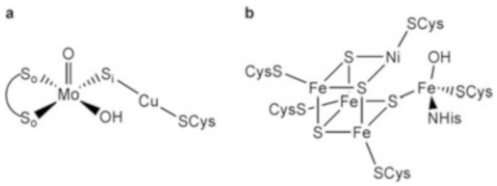

Fig. 5 Active site of MoCu-CODH (**a**) and Ni-CODH (**b**). The bidentate sulfur ligands of the MoCu-CODH denoted by S_o are part of a molybdopterin cytosine dinucleotide cofactor. S_i denotes an inorganic sulfide ligand

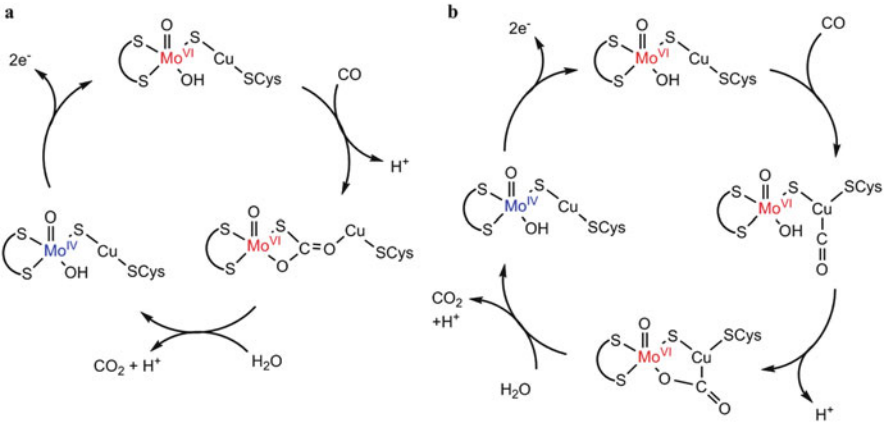

Fig. 6 Proposed mechanism of MoCu-CODH from (**a**) X-ray data [32] and (**b**) DFT calculations [33]

As shown in Fig. 6, two distinct mechanisms have been proposed for MoCu-CODH. The first mechanism (Fig. 6a) is inspired by the crystal structure of the *n*-butylisonitrile inhibited form of the enzyme [32]. This mechanism starts with CO insertion into the Cu–S bond. The coordinated hydroxyl group then attacks the CO forming CO_2 which dissociates, resulting in reduced Mo(IV) species. The cycle is closed by oxidation of the Mo to Mo(VI) and addition of a hydroxyl ligand derived from a water molecule. The second mechanism (Fig. 6b) is derived from DFT calculations that suggest that the large geometry change associated with insertion of CO into the Cu–S bond is unfavorable [33]. These calculations imply that it is more likely that CO binds directly to Cu(I). The rest of the cycle then proceeds analogously to the first mechanism: the hydroxyl attacks and CO_2 is released followed by reoxidation of Mo(IV) to Mo(VI) and addition of a hydroxyl ligand. Both the X-ray and DFT studies suggest an important role for the polypeptide in this enzyme. X-ray data suggest that a nearby glutamate is essential for stabilization of the Mo (VI) state. In addition, DFT results suggest that attack of CO by the hydroxyl ligand is more favorable after deprotonation, likely facilitated by a nearby, conserved glutamate residue [32].

2.2.2 Ni-CODHs

Ni-CODHs contain a unique cluster in the active site, called the C-cluster (Fig. 5b). The structure is a distorted [4Fe4S] cluster with a nickel replacing one of the traditional irons and an iron pendent to the cluster; this atom is referred to as the "dangling iron." All of the metal atoms in the cubane are ligated by cysteine and inorganic sulfide, as in an ordinary [4Fe4S] cluster. In addition to a cysteine and a cluster sulfide, the dangling iron is ligated by a histidine and a hydroxyl ligand [34]. Spectroscopic studies have identified four states of the C-cluster [35]. C_{ox} is an inactive, oxidized state of the cluster. C_{red1} and C_{red2} are believed to be the active states of the enzyme. These states are one and three electrons more reduced than C_{ox}, respectively. C_{int} is two electrons more reduced than C_{ox}, i.e., a state between C_{red1} and C_{red2}. Figure 7 shows a proposed mechanism that has several similarities to those proposed for MoCu-CODH. The site of catalysis is thought to be between the Ni and the dangling Fe. First, CO binds to Ni in the C_{red1} state causing a two-electron reduction. Second, the bound CO is attacked by the hydroxyl group coordinating the Fe before both leave as CO_2. Third, the starting state of the enzyme is regenerated by oxidation of C_{red2} to C_{red1} and addition of a hydroxyl ligand. Structural data suggests that nearby amino acid residues provide hydrogen bonds to CO and CO_2 to stabilize the intermediate steps, again suggesting a crucial role for the protein environment in promoting catalysis. Furthermore, no structural changes of the C-cluster have been observed in different oxidation states. This suggests that the cluster provides a rigid support which may minimize the reorganization energy associated with the redox events of the catalytic cycle [34].

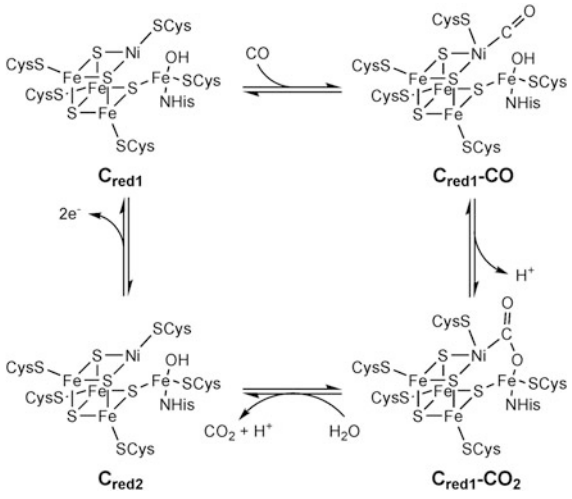

Fig. 7 Proposed mechanism of Ni-CODH [34]

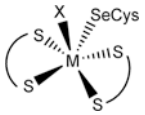

Fig. 8 Structure of the FDH active site. M=Mo or W, X=O or S ligand. The bidentate sulfur ligands represent molybdopterin guanine dinucleotide

2.3 Formate Dehydrogenase (FDH)

Another important enzyme in biological carbon dioxide fixation is formate dehydrogenase (FDH). This enzyme reversibly catalyzes the two-electron reduction of CO_2 to formate. Like hydrogenases and CODHs, there are several classes of FDH; the two main types are the NAD^+-dependent FDHs and the NAD^+-independent FDHs [36]. In general, the former do not contain redox-active cofactors and will, therefore, not be discussed further. The latter are oxygen-sensitive, [FeS] cluster-containing enzymes with a molybdenum or tungsten active site. Both X-ray crystallography and EXAFS have been essential in determining the active site structure shown in Fig. 8 [37, 38]. The metal is coordinated in a triangular prism geometry by two molybdopterin guanine dinucleotides bound via dithiolene moieties, an inorganic S or O ligand, and, in some oxidation states, a selenocysteine [37]. Like the MoCu-CODHs, the active states of the FDHs are Mo/W(VI) and Mo/W (IV) species. An additional Mo/W(V) state has been observed with EPR, but it is not believed to be part of the catalytic cycle [39]. Three conserved amino acid residues near the active site are proposed to be very important in catalysis [40]. First, a mobile selenocysteine ligand binds to the metal in the oxidized form but dissociates and shifts 9 Å in the reduced form [41]. This large conformational change is known as the sulfur shift and has also been observed for other members of the protein superfamily containing FDHs [42]. Replacement of this selenocysteine with a standard cysteine via site-directed mutagenesis results in enzyme with much lower catalytic ability, confirming the importance of this residue for catalysis [43]. Second, an arginine residue has been shown to form a hydrogen bond with the selenocysteine in the reduced state, suggesting that the arginine is also crucial in facilitating movement of the peptide chain. Third, computational studies have suggested that a histidine residue near the selenocysteine in the reduced form is also essential for stabilizing the sulfur shift [44].

The mechanism of this enzyme is the subject of active debate, but one proposed mechanism is shown in Fig. 9. Starting from the oxidized state of the enzyme with the selenocysteine bound, the selenocysteine residue shifts to leave a vacant site to which formate binds. The formate α proton is abstracted by the selenide, and CO_2 leaves generating a reduced Mo/W(IV) state. After two-electron oxidation of the metal to Mo/W(VI) and deprotonation of the Se atom, the selenocysteine shifts back to bind the Mo/W and closes the catalytic cycle. In addition to the conserved residues, DFT studies have suggested that the pyranopterin groups are also key to

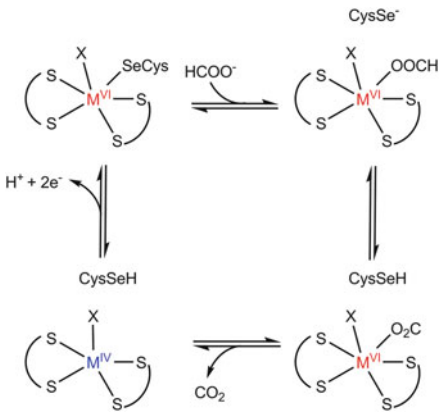

Fig. 9 Proposed mechanism for FDH. M=Mo or W, X=O or S [41, 45]

the function of the enzyme. These groups are proposed to play two roles. First, they aid in the shuttling of electrons to and from the active site. Second, they share some of the negative charge density that arises from formate binding, decreasing the electrostatic penalty associated with ligand binding [44].

3 Hydrogen Production Catalysts

On a per active site basis, hydrogenases have turnover frequencies approaching or matching that of platinum [46, 47]. However, despite these exceptional activities, they present a number of challenges for successful utilization in industrial applications. For example, they are rapidly inactivated by molecular oxygen. With that in mind and inspired by similarities between the hydrogenase active sites and well-known organometallic iron and nickel complexes, considerable research has been devoted to construction of synthetic models with structural or functional similarity to the enzyme active sites. In this section, we focus on functional models, considering not only structurally closely related compounds but also mononuclear catalysts that incorporate particular mechanistic features of hydrogenases to achieve fast catalysis at a non-precious metal site. Finally, we consider incorporation of some of these catalysts into functional photocatalytic systems, a first step toward artificial photosynthetic production of fuels using water-derived electrons.

3.1 Bimetallic Hydrogen Production Electrocatalysts Featuring Nickel

Although a number of close structural mimics of [NiFe]-hydrogenases have been reported, very few of these models are catalytically active. Figure 10 shows a

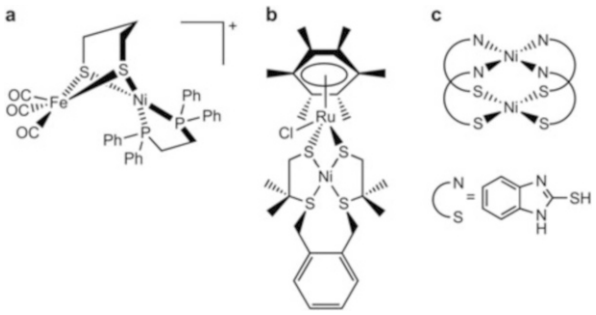

Fig. 10 Select [NiM] complexes that catalyze proton reduction to evolve hydrogen. (**a**) NiFe(pdt)(dppe)$(CO)_3$ for pdt = 1,3-propanedithiol and dppe = 1,2-bis(diphenylphosphinoethane), (**b**) [Ni(xbsms)RuCp*Cl]$^+$ for H_2xbsms = 1,2-bis(4-mercapto-3,3-dimethyl-2-thiabutyl)benzene, and (**c**) Ni_2(MBT) for MBT = 2-mercaptobenthiazole [48–50]

collection of multimetallic model complexes featuring nickel together with a different metal that are active proton reduction electrocatalysts. The [NiFe] complex NiFe(pdt)(dppe)$(CO)_3$ (for pdt=1,3-propanedithiol and dppe=1,2-bis(diphenylphosphino)ethane) electrocatalytically reduces protons in the presence of TFA at rates of 50–75 s^{-1} with overpotentials of approximately 400 mV [48, 51, 52]. However, catalysis by the complex is likely mechanistically quite distinct from the enzyme. Recent computational work in combination with the experimental evaluation of Ni–Pd and Ni–Pt analogues suggests that protonation occurs at the Fe site of the reduced, mixed valence Fe(0)–Ni(II) complex, whereas interaction with substrate in the enzyme takes place at the nickel [53]. This iron protonation is thought to be induced by a large geometry change at the nickel site from tetrahedral to square planar. It is worth noting that the enzyme active site is relatively rigid because of the protein scaffold surrounding it, and this may be a crucial factor in the high activity of the enzyme. This rigidity can be difficult to reproduce in small-molecule mimics.

3.2 Bimetallic Hydrogen Production Electrocatalysts Featuring Only Iron

Early work showed that complexes of the type $Fe_2(\mu\text{-}SR)_2(CO)_6$, which are relatively good structural mimics of [FeFe]-hydrogenases, are also electrocatalysts for hydrogen evolution from acidic solutions [54]. For catalysis to occur in weak acids, a conformational change from the symmetric eclipsed form to a state that has been referred to as “rotated” or “inverted square pyramidal” is also necessary, creating a bridging CO ligand and weakening the Fe–Fe bond (Fig. 11, panels a and b). Darensbourg was the first to refer to this rotated structure as an entatic state and hypothesized that the protein scaffold plays a crucial role in stabilizing the unusual

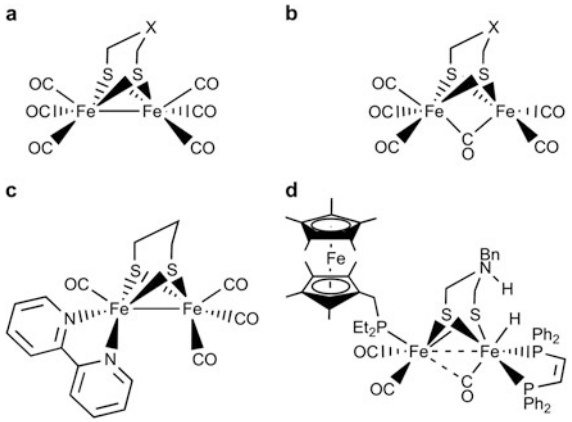

Fig. 11 Structures of selected diiron complexes capable of proton reduction to generate hydrogen. (**a**) Eclipsed and (**b**) rotated conformers of $Fe_2(\mu\text{-}SR)_2(CO)_6$. X can be CH_2, NH, or O. (**c**) The compound $(\mu\text{-}S(CH_2)_3S)Fe_2(CO)_4(\kappa^2\text{-bpy})$ is derived from the hexacarbonyl by substitution of carbonyls. (**d**) $Fe_2(adt^{Bn})(CO)_3(dppv)(PFc^{*Et}{}_2)$ [55–58]

coordination geometry within the enzyme [55]. Two design strategies have successfully yielded related complexes with rotated structures: incorporation of steric bulk into a terminal ligand, the bridge, or both [59–62] and replacement of CO with the isoelectronic NO^+ [63, 64]. Nonetheless, synthesis of a complex with a stable rotated structure suitable for catalysis has proven challenging, and development of supramolecular scaffolds that could stabilize the geometry remains an important area of research [65–68].

One or more of the CO ligands in these complexes can be substituted by more electron-donating ligands such as phosphines, bipyridine, or *N*-heterocyclic carbenes (Fig. 11c). These electron-rich complexes tend also to be electrocatalysts, but as a consequence of the higher electron density at the metals, they require substantial overpotential for catalysis [56].

Rauchfuss and coworkers were the first to describe a bimetallic model of [FeFe]-hydrogenases capable of both catalytic hydrogen oxidation and proton reduction [58]. As shown in Fig. 11d, the complex, $Fe_2(adt^{Bn})(CO)_3(dppv)(PFc^{*Et}{}_2)$ for adt^{Bn}=$(SCH_2)_2NBn$, dppv=*cis*-1,2-bis(diphenylphosphino)ethylene, and $PFc^{*Et}{}_2$=$Et_2PCH_2C_5Me_4FeCp^*$, features not only the classic diiron motif of other models but also a redox-active ferrocenylphosphine ligand. There are two notable features to this complex: the nitrogen atom in the bridging ligand and the ferrocene appended to the diiron core. Removal of the nitrogen, i.e., by using pdt as a ligand, results in a catalytically inactive complex. This may indicate that the bulkhead nitrogen plays a role in transferring or positioning protons to the irons during catalysis. Similarly, an analogous complex without the ferrocenyl ligand has a similar reduction potential but is not as catalytically active, since an inactive bridging hydrido complex forms. This suggests crucial functional roles both for the azadithiolate and the [4Fe4S] cluster of the enzyme active site. Additional evidence for the importance of the nitrogen in the bridging ligand in the enzyme has been provided by incorporating synthetic diiron clusters into the empty active site of partially matured enzyme. Compounds with an oxygen or carbon at the bulkhead position had only very limited activity, whereas the complex with nitrogen resulted in native-like activity [69].

3.3 Monometallic Proton Reduction Electrocatalysts

3.3.1 Mononuclear Iron Proton Reduction Catalysts

Several groups have sought to overcome the challenges of creating diiron complexes with rotated structures by instead constructing monoiron catalysts with an open coordination site already present in the structure. Interestingly, Sellman and coworkers prepared the 18-electron complex $[Fe(bdt)(PMe_3)_2(CO)_2]$ and noted that it had an unexpected tendency to lose a CO to form a 16-electron complex [70]. Rauchfuss and coworkers used the work as inspiration to create $(Et_4N)_2[Fe(bdt)(CN)_2(CO)]$, a relatively good spectroscopic model of [FeFe]-hydrogenases [71]. Ott and coworkers combined the use of bdt with chelating phosphine ligands to generate catalytically active complexes of the type $[Fe(X\text{-}bdt)(P^R{}_2N^{Ph}{}_2)(CO)]$ for $P^RN^{Ph}{}_2$=1,5-diaza-3,7-diphosphaoctane, and R=Ph, Bn, Cyc, or *tert*-Bu and the benzene dithiolate substituted with X as H, Cl_2, or Me (Fig. 12a) [72–74]. These complexes feature not only an open coordination site but also a pendent base meant to facilitate proton transfer to the active site metal. These authors found that the use of a chelating phosphine was critical for generating complexes with an open coordination site. Using computational methods, they also suggested a role for large geometric rearrangements in catalysis. Five-coordinate complexes can have geometries on the spectrum from trigonal bipyramidal (Fig. 12b) to square pyramidal (Fig. 12c). Roy and coworkers used the 1,1′-bis(diphenylphosphino)ferrocene (dppf) ligand to create the analogous $[(\kappa^2\text{-dppf})Fe(CO)(\kappa^2\text{-bdt})]$ complex (Fig. 12b) [57]. The dppf ligand is unique in that, due to the geometric constraints and rigidity of the ferrocene, it has a larger bite angle than most chelating phosphines. In the solid state, the complex is trigonal bipyramidal, and the geometry predicted to be less active toward proton reduction. However, the complex catalyzed proton reduction from acetic acid with an overpotential of only 0.17 V. The rate of 10 s^{-1} is unfortunately very low and reminds us that catalysis at low overpotentials is usually paid for by a low turnover frequency. Decoupling these two properties is one of the greatest challenges facing chemists. It is worth noting that this last complex does not have a pendent amine, and DFT calculations suggest that both protonations occur at the iron site.

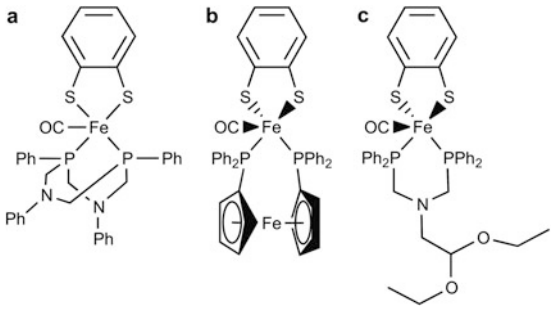

Fig. 12 Structures of key mononuclear, five-coordinate iron complexes capable of proton reduction. (**a**) Fe(CO)(bdt)(PPh_2NPh_2), (**b**) (bdt)Fe(CO)(dppf), and (**c**) (bdt)Fe$(CO)(P_2)$ for P_2 is *O*,*O*′-$(CH_3CH_2)_2$-2-{bis-(diphenylphosphinomethyl)amino}-acetate [57, 72, 73]

3.3.2 Mononuclear Cobalt Proton Reduction Catalysts

Efforts to use cobalt complexes as homogeneous hydrogen production catalysts started more than 30 years ago primarily with the work of Eisenberg and Sutin [75, 76]. Although cobalt is not one of the metals employed in biological hydrogen production, cobalt complexes with a wide variety of ligand sets have proven exceptional in both electrocatalytic and photocatalytic systems. Herein, we describe some of the most important types of compounds with an emphasis on recent, biologically inspired work.

Multidentate phosphine and pyridyl ligands have garnered significant attention for creating Co proton reduction catalysts. For example, the polypyridyl complex $[(PY_5Me_2)Co(MeCN)](CF_3SO_3)_2$ for PY_5Me_2=2,6-bis(1,1-bis(2-pyridyl)ethyl) pyridine has proven very active for proton reduction in aqueous solutions with a turnover number approaching 55,000 moles of hydrogen per mole of catalyst and stability for longer than 60 h (Fig. 13a) [77]. Related compounds have also been shown to be active in three-component photocatalytic systems using a sacrificial electron donor [78, 79].

Cobalt phosphine complexes of the type CpCo(diphosphine) have been known since 1986 to be molecular electrocatalysts for hydrogen production [80]. Catalysis by this family of compounds occurs through a $[CpCo^{III}(diphosphine)H]^+$ intermediate that is only reduced at relatively large overpotentials. This limitation has led to

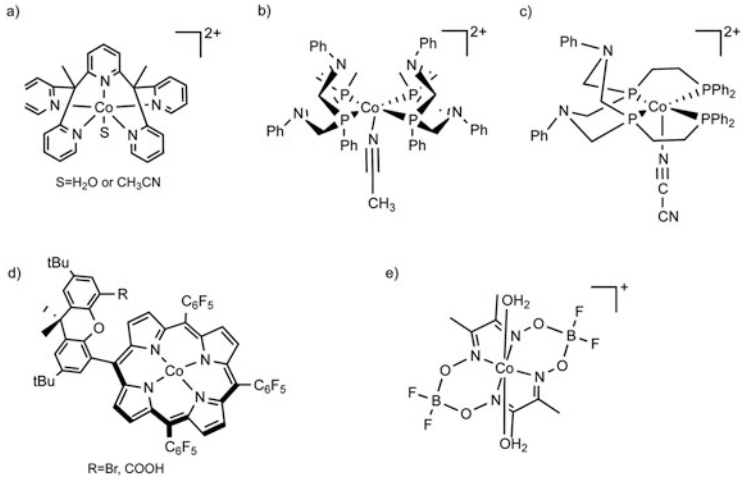

Fig. 13 Structures of selected cobalt complexes that catalyze proton reduction to generate hydrogen. (**a**) $[(Py_5Me_2)Co(MeCN)](CF_3SO_3)_2$ in which Py_5Me_2 is 2,6-bis(1,1-bis(2-pyridyl) ethyl)pyridine, (**b**) $[Co(P^R{}_2N^{R'}{}_2)_2(CH_3CN)](BF_4)_2$ in which $P^R{}_2N^{R'}{}_2$ represents 1,5-diaza-3,7-diphosphacyclooctane, (**c**) $[Co^{II}(L2)(CH_3CN)](BF_4)_2$ in which L2 is 1,5-diphenyl-3,7-bis ((diphenylphosphino)$(CH_2)_2$)-1,5-diaza-3,7-diphosphacyclooctane, (**d**) CoHPX-R in which HPX-R is 5-(4-(5-R-2,7-di-*tert*-butyl-9,9-dimethyl-xanthene))-10,15,20-tris(pentafluorophenyl)-porphyrin and R is a variable organic group, and (**e**) $[Co(dmgBF_2)_2(OH_2)_2]$ for dmg representing dimethyl-glyoxime

variations of both the Cp, to make it more electron withdrawing and facilitate catalysis [81], and the diphosphine. By analogy to the Ni family (see Sect. 3.3.3), Bullock and coworkers have described a number of Co complexes with pendent amines incorporated into the phosphine backbone to facilitate proton transfer [82–84]. Initial complexes based on the $P^R{}_2N^{R'}{}_2$ (1,5-diaza-3,7-diphosphacyclooctane) ligand had modest turnover frequencies, circa 100 s^{-1}, at moderate overpotentials of approximately 400 mV (Fig. 13b). However, these compounds are unstable in acidic media. Thus complexes including tetradentate phosphines were created (Fig. 13c). Although more stable compounds, the increased turnover frequency of these catalysts comes at the price of high, more than 1 V, overpotential. This is another reminder that decoupling turnover frequency and overpotential is nontrivial.

Cobalt macrocyclic, or pseudo-macrocyclic, complexes have proven among the most widespread cobalt-based proton reduction catalysts. For example, Fisher and Eisenberg demonstrated in 1980 that some cobalt tetraazamacrocyclic complexes are active in both CO_2 and H^+ reduction [75]. Similarly, porphyrins have been extensively investigated. Nocera and coworkers showed that cobalt(II) hangman porphyrins can catalyze proton reduction with less overpotential and weaker acids than their standard porphyrin cousins (Fig. 13d) [85, 86]. Both features are thought to be a result of the enhanced proton donation by the carboxylic acid of the hangman substituent. Bren and coworkers showed that the biologically derived cobalt-substituted microperoxidase-11 is stable with a turnover number of 25,000, but the catalytic rate is relatively low at 6.7 s^{-1} [87].

The pseudo-macrocyclic diimine and dioxime complexes of cobalt were also already recognized in the mid-1980s as proton reduction catalysts [88], and the groups of Artero, Fontecave, and Peters have extensively investigated the catalytic properties of this family [89]. Using $[Co(dmgBF_2)_2(OH_2)_2]$ (for dmg=dimethylglyoxime) (Fig. 13e) as a starting point, they have described variants for hydrogen evolution from both aqueous and organic solutions, either electrocatalytically or photocatalytically [90–92]. These complexes are both fast and efficient with some reported to have turnover frequencies in excess of 1,000 s^{-1} and most with overpotentials of approximately 200 mV. Like the phosphine-coordinated complexes described above, enhanced stability has been achieved using tetradentate ligands [93]. Importantly, systematic study of these compounds has shown that although modifications of the equatorial ligand can be used to tune the reduction potential, there is not a concomitant effect on overpotential for catalysis. The problem is that reduction potential and nucleophilicity, i.e., ability to be protonated, are tightly linked [91, 92, 94]. However, modifications of the axial ligand have been used to tune the rate of catalysis without significant impact on overpotential [90]. Finally, taking advantage of its ability to coordinate planar macrocyclic complexes, apomyoglobin has been used as a scaffold to coordinate $[Co(dmgBF_2)_2(OH_2)_2]$ and $[Co(dmgH)_2(OH_2)_2]$. In this arrangement, the protein provides the axial ligand [95], and the reduction potential is 100 mV more negative than the compound free in solution. Although catalytic activity was detected, it is

less efficient than the free compounds. Unfortunately, stability of the system is also clearly a problem with turnover numbers on the order of five reported.

Finally, we offer a word of caution. A number of different groups have shown that heterogeneous proton reduction or water oxidation catalysts, formed in situ from bio-inspired Ni and Co complexes in electrochemical experiments, can be deposited on the electrode surface [96–100]. Thus it is essential that researchers take every effort to ensure that the species they believe they are studying is indeed the active catalyst.

3.3.3 Mononuclear Nickel Proton Reduction Catalysts

Many of the ligand sets that have been used to create cobalt complexes have also been used to produce nickel-based hydrogen evolution catalysts. For example, mononuclear nickel complexes employing bidentate phosphine, thiolate, and amine ligands have been reported to be excellent proton reduction complexes. The groups of Bullock, DuBois, and Helm have prepared a large family of nickel complexes supported by phosphines that contain amines in the second coordination sphere intended to facilitate proton transfer to and from the active site (Fig. 14). Using the $P^{R}{}_{2}N^{R'}{}_{2}$ ligand 1,5-diaza-3,7-diphosphacyclooctane which is functionalizable at both the phosphorous and nitrogen substituents, they have created proton reduction, hydrogen oxidation, and bidirectional catalysts [101]. These compounds have proven appealing for several reasons. First, the ligand is readily functionalizable, offering a handle to control the electronic properties of the complex [102, 103]. Second, systematic studies have been undertaken

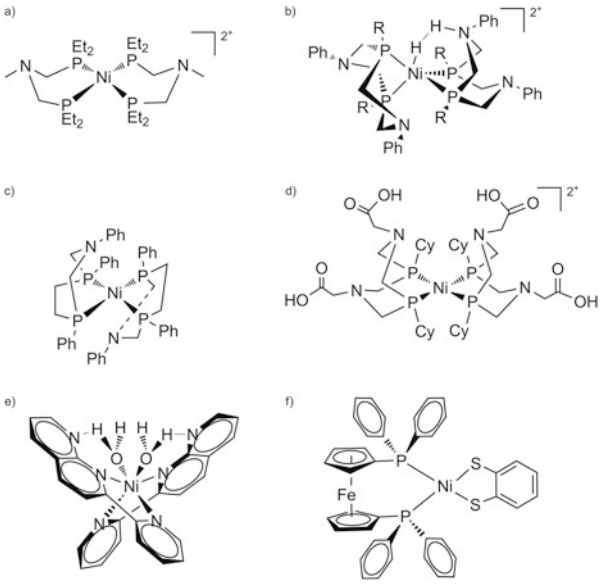

Fig. 14 Structures of selected mononuclear nickel complexes for proton reduction to generate hydrogen. (**a**) $Ni(P^{Et}{}_{2}N^{Me})_{2}$. (**b**) $Ni(P^{R}{}_{2}N^{Ph}{}_{2})_{2}(H_{2})$. (**c**) $Ni(P^{Ph}{}_{2}N^{Ph})_{2}$. (**d**) $[Ni(P^{Cy}{}_{2}N^{Gly}{}_{2})_{2}]$. (**e**) $[Ni(L)_{2}(H_{2}O)](BF_{4})_{2}$ for L of 2-(2-pyridyl)-1,8-naphthyridine. (**f**) Ni(bdt)(dppf)

to map structure–function relationships [104, 105]. Third, extraordinarily high turnover frequencies exceeding 10^4 s^{-1} have been reported [106–108]. As a substitute for the eight-membered diphosphine, the seven-membered ligand $P^{Ph}{}_2N^{Ph}$=1,3,6-triphenyl-1-aza-3,6-diphosphacycloheptane has also been employed as a means to prevent formation of an unproductive isomer in which a proton is pinched between the two amines of a single ligand (Fig. 14b,c). The compound $[Ni(P^{Ph}{}_2N^{Ph})_2]$ is reported to have a turnover frequency of more than 100,000 s^{-1} under optimal conditions [106]. However, the change from an eight-membered ligand to a seven-membered one also has an impact on coordination geometry, enforcing a more planar geometry about the nickel (Fig. 14c). The change in geometry is likely to be the cause of the increase in required overpotential that accompanies the increase in rate for the $P^{Ph}{}_2N^{Ph}$ complex. This is a reminder that changing one aspect of a complex can, and often does, have unintended consequences on other properties, and predictive design of molecular catalysts is by no means a mature field.

Due to their exceptional turnover frequencies as homogeneous electrocatalysts, several groups have reported efforts to immobilize mononuclear nickel catalysts on electrodes to create heterogeneous systems. The Bullock group recently reported an ester-functionalized variant of $P^{R}{}_2N^{R'}{}_2$ which they could use as a handle to covalently functionalize glassy carbon electrodes. Although the functionalized electrodes have catalytic properties similar to related compounds in solution, electrode immobilization results in markedly increased instability under acidic conditions [109]. Promisingly, Artero and coworkers reported the non-covalent immobilization of a pyrene-functionalized version of a member of this family on carbon nanotubes resulting in electrodes with current densities of 20 mA cm^{-2} for hydrogen evolution [110]. In related work, covalent attachment to the carbon nanotubes resulted in exceptionally stable catalysts, and turnover number reported to be more than 100,000, requiring only 10s of mV of overpotential, but the current density was relatively low [111]. Thus, it remains a challenge to translate the knowledge from homogeneous catalysis to create a related heterogeneous system that is fast, efficient, and stable.

Shaw and coworkers have explored the ability to tune proton reduction catalysis by modifications of the second coordination sphere starting from the nickel phosphine complexes of DuBois described above. They have demonstrated that modification of the outer coordination sphere of $[Ni((P_2N_2R)\text{-}N\text{-}R')_2]^{2+}$ complexes with amino acids can significantly modify catalytic properties (Fig. 14d) [112, 113]. Remarkably, several derivatives are capable of fully reversible H_2 production and oxidation in aqueous solutions with pH values in the range of 0–6 [114]. By comparing the rates of complexes with various amino acids, they have hypothesized that a carboxylic acid in the outer coordination sphere may enhance catalysis, much like proton transfer residues in natural enzymes [115].

First coordination spheres including nitrogen and sulfur donors have also been used to construct highly active nickel proton reduction catalysts. Employing a polypyridyl ligand framework, Sun and coworkers have created the complex $[Ni(L)_2(H_2O)_2](BF_4)_2$ for L=2-(2-pyridyl)-1,8-naphthyridine, which, under optimal, basic, photocatalytic conditions, has a remarkable turnover number of 3230

(Fig. 14e) [116]. However, under acidic conditions, the ligand is protonated and the complex rapidly decomposes. Taking a cue from the coordination of hydrogenases, a P_2S_2-coordinated complex [Ni(bdt)(dppf)] that catalyzes hydrogen evolution at a rate in excess of 10^3 s^{-1} with only 265 mV of overpotential [117] and stability on the timescale of hours was reported (Fig. 14f).

By analogy to results obtained from cobalt complexes, recent work has focused on using macrocyclic ligands to create more stable nickel-based electrocatalysts. For example, Lau, Robert, and coworkers have created a collection of complexes employing related N_4, N_3S, and N_3P ligands. Surprisingly, in many cases, the active catalyst is a nickel nanoparticle, and the active catalyst sometimes depends whether the experiment is photocatalytic or electrocatalytic. For example, the N_3P ligand 2,12-dimethyl-7-phenyl-3,11,17-triaza-7-phospha-bicyclo[11,3,1]heptadeca-1(17),13,15-triene supported the most active complex [99]. This compound is active as a homogeneous catalyst in electrocatalytic experiments but converts to nickel nanoparticles under photocatalytic conditions. The reason for the change in mechanism may be that solution conditions such as pH differ between the two types of experiments. This will be crucial to take into account as researchers begin to translate basic gains in molecular hydrogen production catalyst synthesis to larger-scale applications.

3.4 Photocatalytic Production of Hydrogen

Photosynthesis directly converts solar energy to chemical energy. The process essentially consists of photon capture to generate a charge-separated state and coupling of this state to catalysts. A number of cyanobacteria and algae are known to produce hydrogen photosynthetically, but the efficiency and yields are relatively low [118–122]. This may be because competing metabolic pathways vie for solar-derived reducing equivalents. Metabolic engineering efforts such as eliminating competing sinks have resulted in modest improvements [120], and Golbeck and coworkers have demonstrated that directly tethering the electron-donating FeS cluster of Photosystem I to the accepting cluster of an [FeFe]-hydrogenase in vitro increases the rate of hydrogen evolution [123].

This understanding of natural photosynthesis and attempts to reengineer it have served as inspiration for artificial photosynthetic systems [124]; see Fig. 15 for a schematic view of the components and functional requirements for an artificial photosynthetic system. Although artificial constructs capable of emulating certain aspects of photosynthesis, such as light-driven generation of a long-lived charge-separated state, have been described [124–127], developing complete systems for efficient utilization of light energy to produce fuel remains a significant challenge. More than a hundred molecular catalysts for electrocatalytic proton reduction have been described; in contrast, relatively few molecular systems for photocatalytic hydrogen production have been reported [128]. The challenge is that a functional photocatalytic system requires more than just a good catalyst. In most cases, i.e., when the catalyst is not itself photochemically active, the catalyst must interact

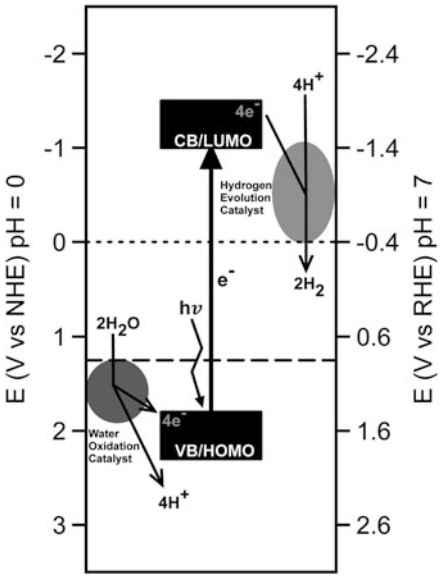

Fig. 15 Schematic overview of artificial photosynthesis employing water as electron source and producing hydrogen as fuel product. The valence band (VB, for a semiconducting material) or the highest occupied molecular orbital (HOMO, for a molecular photosensitizer) must have a reduction potential more positive than the water oxidation catalyst to promote efficient electron transfer. Likewise, the hydrogen evolution catalyst must have a reduction potential more positive than the conduction band (CB, for a semiconducting material) or the lowest unoccupied molecular orbital (LUMO, for a molecular photosensitizer; since this molecular orbital is the most likely to be occupied by an electron upon excitation) for electron transfer to be thermodynamically favorable. Water, a coordinating ligand, can have a significant impact on catalysts with an open coordination site. Thus the RHE scale has been included

with a photosensitizer. This means that the catalyst requires a mild reduction potential, since extreme potentials cannot be generated by typical photosensitizers. This requirement eliminates many standard hydrogenase-inspired models such as phosphine-substituted variants of diironhexacarbonyl complexes and highlights the importance of overpotential. In addition, low overpotential for the catalytic reaction is also highly desirable so that catalysis can be driven by visible, as opposed to ultraviolet, light. It is also worth noting that the electrons for the reduction are usually provided by a sacrificial reductant and poor interactions between the reductant and the photosensitizer can also limit catalytic performance. Finally, many reported systems are limited not by the rates of the catalysts but rather by catalyst and photosensitizer stability. Essentially, the entire system must be stable in the harsh conditions of constant illumination and acidity. This is a challenge both for the traditional ironcarbonyl catalysts, since the CO ligands tend to be photolabile, and for commonly used Ru polypyridyl photosensitizers.

The first three-component hydrogen production systems, i.e., catalyst, photosensitizer, and sacrificial electron donor, employing a diiron dithiolate-type catalyst were reported by Song and coworkers [129, 130]. Drawing from the extensive

electrocatalytic literature surrounding these complexes, they prepared the complexes $[\{(\mu\text{-}SCH_2)_2NCH_2C_6H_5\}\{Fe(CO)_2L^1\}\{Fe(CO)_2L^2\}]$ in which L^1 and L^2 are CO or $P(Pyr)_3$ because they have modest reduction potentials but are highly basic. In concert with $[Ru(bpy)_3]^{2+}$ as photosensitizer and ascorbic acid as electron donor, hydrogen evolution with a turnover number of 4.3 (based on catalyst) or 86 (based on photosensitizer) over a period of 3 h was observed. Spectroscopic investigation showed that the catalyst decomposed completely during the course of the experiment. Ott and coworkers showed that a simple modification of the bridging ligand to Cl_2bdt=3,6-dichlorobenzene-1,2-dithiolate and an excess of photosensitizer significantly improved catalysis, even using only the hexacarbonyl derivative [131]. They achieved TON of 200 with TOF of 2.7 min^{-1}. For this second system, reductive quenching of the ruthenium excited state is rate limiting. Comparison of these systems reminds us that they are multicomponent systems involving a number of elementary reactions. Even when the components are similar, different rate-limiting steps and decomposition pathways may be accessible, making optimization of each system unique and challenging. For more information, Sun and coworkers have carefully reviewed this early diiron-based photocatalysis [128].

Catalytically, the most impressive photocatalytic hydrogen evolution systems with diiron carbonyl catalysts have employed nanoparticulate photosensitizers. These semiconductor particles are more robust than the precious metal-based molecular photosensitizers, often resulting in higher TONs. Pickett and coworkers reported intercalating $Fe_2S_2(CO)_6$ into an indium phosphide nanocrystal array on an electrode surface to generate a photoelectrode capable of hydrogen production with circa 60% faradaic efficiency. The addition of light to the electrocatalytic system provides enough energy to drive catalysis at potentials approximately 250 mV less reducing than in the dark [132]. Wu and coworkers employed CdSe quantum dots instead and achieved hydrogen production with a TON of 8781 and an initial TOF of approximately 10 s^{-1} in completely aqueous conditions [133]. Analogous systems have been constructed using other catalysts, and the results were recently reviewed [134]. The most impressive TON is 22,200, with a TOF = 120 min^{-1}, in a system employing a large dendrimer encapsulating the diiron catalyst [135].

Although most of the photocatalytic systems reported fall clearly in the traditional category of artificial, meaning they employ synthetic chemical components, a number of hybrid systems in which a synthetic component is combined with a natural biological component have been reported recently. Our own group was the first to develop synthetic means to immobilize $Fe_2(\mu\text{-}pdt)(CO)_6$-related compounds in a peptide scaffold [68, 136]. This synthetic approach was used by Hayashi and coworkers to embed the classic $Fe_2(\mu\text{-}pdt)(CO)_6$ catalyst in protein scaffolds including cytochrome *c*, the C-terminal segment of cytochrome c_{556}, and the β-barrel protein nitrobindin, creating aqueous photocatalytic systems in combination with a Ru-photosensitizer and ascorbate [66, 137, 138]. The systems have TONs in the range of 9–120 over the course of hours. In related work, Wu and coworkers demonstrated that confinement of the catalyst in a chitosan network, a naturally occurring polysaccharide, results in significant stabilization. They employed a CdTe quantum dot as photosensitizer, and the system is stable for

40 h with a turnover number of up to 52,000, a factor of 4,000 higher than the same components simply free in solution [139]. Unfortunately, the TOF is very low with an initial value of 1 s^{-1}. For comparison, Armstrong and coworkers reported that *Desulfomicrobium baculatum* [NiFeSe]-hydrogenase immobilized on Ru-sensitized TiO_2 particles using triethanolamine as sacrificial electron donor has a TOF of 50 s^{-1} [140]. However, the enzyme system undergoes O_2-dependent photodecomposition in air in less than 2 min. For other examples of photocatalytic systems employing natural hydrogenases, King has recently reviewed constructs for immobilization of hydrogenases at semiconductor particles [141]. Hybrid systems are not limited to the diiron family of catalysts. Bren and coworkers demonstrated that cobalt-microperoxidase 11 is an HER electrocatalyst with a TOF of 6.7 s^{-1} at an overpotential of 850 mV and TON of 25,000 [142]. Ghirlanda and coworkers extended this result to photocatalysis using Co-protoporphyrin IX embedded in myoglobin [143], but the TON was unfortunately only 520 and TOF <1 min^{-1}. Thus, to date, the biohybrid iron system remains far superior catalytically.

Although most molecular hydrogen-producing catalysts are not inherently photocatalysts, i.e., they require a photosensitizer, the asymmetric complex $[(\mu\text{-pdt})(\mu\text{-H})\text{-}Fe_2(CO)_4(dppv)]^+$ (for pdt=1,3-propanedithiolate and dppv=*cis*-1,2-$C_2H_2(PPh_2)_2$) has been reported to catalyze evolution of hydrogen gas under sensitizer-free conditions (Fig. 16) [144]. This is a particularly exciting result because the need for a precious metal-based photosensitizer is eliminated. Unfortunately, only four turnovers were achieved in this system during continuous irradiation. Two fundamentally different mechanisms have been proposed to account for this catalysis. Rauchfuss and coworkers hypothesized that irradiation generates an excited state which is a stronger base. Thus, it can be protonated by strong acids, creating an unstable dication and releasing hydrogen. However, TD-DFT work suggested that excitation was more likely to result in photolysis or gross deformation of the core geometry leading to a more terminal Fe–H species [145]. Based on this theoretical work and their own time-resolved infrared spectroscopic investigation, Hunt, Pickett, and coworkers suggested that a CO is photolabile [146]. The CO-depleted photoproduct may be the active catalyst. Alternatively, a short-lived photoexcited state may encounter by chance either acid or the sacrificial reductant, octamethylferrocene, leading to catalysis. This last option is exciting because it suggests a means to improve the catalysis by tethering an acid or reductant to the catalyst.

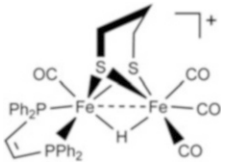

Fig. 16 Structure of the asymmetric complex $[(\mu\text{-pdt})(\mu\text{-H})\text{-}Fe_2(CO)_4(dppv)]^+$ that has been reported to catalyze photocatalytic evolution of hydrogen gas under sensitizer-free conditions [144]

4 Carbon Dioxide Reduction Catalysts

A number of products including CO, formate, methanol, and methane can be formed by carbon dioxide reduction. Furthermore, since the potential for reduction of protons to hydrogen is typically 100 mV more favorable, hydrogen evolution usually competes with CO_2 reduction at transition metal sites. Thus, development of selective, fast, and efficient carbon dioxide reduction catalysts has proven a challenging research area. Enzymes carefully couple proton and electron movement to generate multielectron-reduced states and catalysts specific for one product. Control of proton movement has also proven an important theme in preparation of synthetic catalysts. In this section, we start by considering some of the better precious metal-based CO_2 reduction catalysts and then describe how these have been modified to generate catalysts based on more abundant metals by incorporating bio-inspired features.

4.1 Structural Models of CODHs

Structural models of both aerobic (MoCu) and anaerobic Ni–CODHs have recently been reviewed by Majumdar (see Fig. 5 for active site structures) [147]. The groups of Holm, Tatsumi, and Young [148–150] have developed several new synthetic approaches to create sulfide-bridged binuclear MoCu complexes as models for the aerobic enzymes, and, as a result of this work, two significant challenges have come to light. First, the formation of a $Mo(\mu_2\text{-}S)_2Cu$ rhomb is highly favored so that forming singly bridged complexes is difficult. Second, Mo(VI) is unstable to autoreduction, especially in the presence of anionic sulfur ligands. The latter problem can be overcome by working with W complexes, but these seldom have the same reactivity as the Mo analogues. With respect to the anaerobic CODHs, attempts to mimic the spectroscopic properties of the NiFeS active site with synthetic complexes were underway even before the determination of the active site structure. There have been two major approaches: construction of $[NiFe_3S_4]$ clusters, spearheaded largely by the Holm group [151–155], and efforts to make heterobimetallic [NiFe] complexes, research closely related to the modeling of [NiFe]-hydrogenases (see Sect. 3). Unfortunately, none of the complexes produced in these efforts are reported to either reduce CO_2 or oxidize CO.

4.2 Functional Models of CODH: Molecular Electrocatalysts for Reduction of CO_2 to CO

Functional models of CODH, i.e., molecular catalysts for CO_2 reduction to CO, have been constructed using the precious metals Re and Ru as well as the first row transition metals Co, Fe, Mn, and Ni.

4.2.1 Transition Metal Phosphine Complexes

The history of synthetic metal phosphine complexes as CO_2 reduction catalysts begins more than three decades ago when Slater and Wagenknecht demonstrated the stoichiometric electrochemical reduction of CO_2 to formate using a [Rh(diphosphine)$_2$]$^+$ complex [156]. This Rh complex is not a catalyst, but it improves the thermodynamics of reduction of CO_2 by approximately 700 mV. Shortly thereafter, Darensbourg and coworkers showed that CO_2 could be inserted into *trans*-[(H)$_2$Ni(PCy$_3$)$_2$] to form *trans*-[(H)(HCO$_2$)Ni(PCy$_3$)$_2$] [157], an important step in understanding possible intermediates of CO_2 reduction by transition metal phosphine complexes. Simultaneously, DuBois and coworkers reported a series of transition metal phosphine complexes based on Fe, Ni, and Pd with weakly bound solvent molecules; some of these are electrocatalytically active for CO_2 reduction. The [Pd(triphosphine)(CH$_3$CN)](BF$_4$)$_2$ (triphosphine=RP(CH$_2$CH$_2$PR′$_2$)$_2$ where R and R′ can be alkyl or aryl substituents) complexes are the best catalysts in this class [158, 159]. They catalyze reduction of CO_2 to CO in acidic solution under 1.0 atm of CO_2 with TONs up to 130 at an overpotential of only 0.3 V. The mechanism of this class of catalysts has been studied in detail. As shown in Fig. 17, reduction of Pd(II) to Pd(I) is followed by coordination and protonation of CO_2. A second reductive step then occurs before loss of the coordinated solvent and a second protonation. The vacant coordination site generated is crucial in cleaving the CO bond. In fact, in the presence of a strongly coordinating ligand such as dimethyl sulfoxide or a monodentate phosphine ligand, catalysis is inhibited. Finally, the CO bond is broken in the rate-determining step leaving coordinated water and CO. Release of these products regenerates the catalyst. This release is facile since

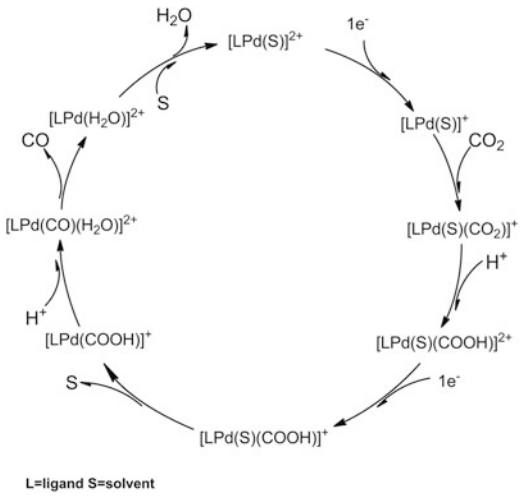

Fig. 17 Mechanism of [Pd(triphosphine)(CH$_3$CN)](BF$_4$)$_2$ for reduction of CO_2

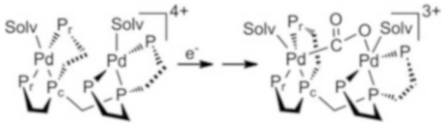

Fig. 18 Homobimetallic analogue of [Pd(triphosphine)(CH_3CN)]$^{2+}$ featuring a bifunctional active site to enhance CO_2 binding

the metal has low affinity for CO, but this is the rate-determining step for several complexes involving other metals.

Building on the success of the [Pd(triphosphine)(CH_3CN)]$^{2+}$ catalyst and inspired by the bimetallic active site of CODHs, homobimetallic analogues such as shown in Fig. 18 were designed to create a bifunctional active site and enhance CO_2 binding [160]. In fact, the bimetallic complex has a second-order catalytic rate constant greater than 2.5×10^4 M^{-1} s^{-1}, much higher than its monometallic analogues. However, rapid formation of a Pd–Pd bond inactivates the catalyst, resulting in a relatively low TON. The enzyme is less likely to undergo this type of inactivation since it contains only first row transition metals that have a weaker tendency to form metal–metal bonds, highlighting an advantage of moving away from precious metals.

4.2.2 Re(bpy-R)(CO_3)X Family of CO_2 Reduction Catalyst

Bipyridyl metal carbonyls have proven to be effective catalysts for photo- and electrocatalytic reduction of CO_2 to CO. Of these, the rhenium complexes have been the most widely studied [161–163]. Lehn and coworkers [161] showed already in the early 1980s that Re(bpy)($CO)_3$Cl (bpy=2,2′-bipyridyl) electrocatalytically reduces CO_2 to CO in DMF-H_2O solution with a faradaic efficiency reaching 91%. This result has inspired the synthesis of a number of related compounds, especially with modified bipyridyl ligands. Of particular note are improvements in catalytic properties afforded by complexes incorporating a bipyridyl ligand with a functional group handle that allows for polymerization and formation of heterogeneous catalytic films on electrode surfaces. For example, O'Toole et al. [164] modified the bipyridyl ligand via incorporation of a vinyl group to generate vbpy=4-vinyl-4′-methyl-2,2′-bipyridine. Immobilization of the Re complex generated from this ligand in a polymer results in a 20–30 times enhancement of the TON compared to the homogeneous analogue. TONs are reported to be as high as *ca*. 600 [165] on certain surfaces, and the effects of electrode material, film thickness, and the structure of bipyridyl ligands have been investigated [166, 167]. In another example, polymerization via a pyrrole-substituted bipyridyl ligand generates poly-Re(LX)($CO)_3$Cl (L=pyrrole-substituted bpy, $X = 3,4,5$, numbers of pyrrole groups). These films catalyze CO_2 reduction with less electrochemical overpotential but have lower rates.

4.2.3 Manganese as an Alternative to Rhenium

Manganese is approximately one million times more abundant than rhenium in the earth's crust [168], making it a much better candidate for catalyst design with future large-scale applications. The complexes $Mn_2(CO)_{10}$ and $Mn(CO)_5I$ were first reported in the 1950s [169], and *fac*-Mn(bpy-R)$(CO)_3$X, where X is a halogen, complexes have been known since 1959 [170]. However, their catalytic properties were not described until much later. In 1996, Hartl and coworkers concluded from an IR spectroelectrochemical study that $[Mn(bpy)(CO)_3]^{1-}$ does not react with CO_2 [171]. Further, IR studies showed that air stable *fac*-Mn(bpy)$(CO)_3$Br quickly forms a dimer under reducing conditions [172] and further reduction formed the $[Mn(bpy)(CO)_3]^{1-}$ anion. The X-ray crystal structure of the two-electron-reduced $[Mn(bpy)(CO)_3]^{1-}$ was reported in 2007 by the same group [173]. The breakthrough did not come until 2011 when Deronzier et al. [174] reported that a proton source is the missing ingredient. Both *fac*-Mn(bpy-R)$(CO)_3$Br and $[Mn(bpy\text{-}R)(CO)_3]_2$ (R=H, Me) electrocatalytically reduce CO_2 to CO in acetonitrile with water as a proton source. The catalysis occurs at the potential at which $[Mn(bpy)(CO)_3]^{1-}$ is formed, suggesting that the two-electron-reduced anion promotes the catalysis. Inspired by Deronzier's work, related Mn(bpy-R)$(CO)_3$X complexes with different substitution of the bipyridyl ligand were also shown to electrocatalytically reduce CO_2 in solution with a proton source. In particular, Kubiak et al. [175] observed similar behavior with *tert*-butyl-substituted manganese complex. Upon reduction, dimerization occurs followed by formation of the catalytically active anion. Remarkably, the activity of the *tert*-butyl derivative approaches that of the rhenium analogs and exceeds them in the presence of water. It is also important to note that the activity increases with increasing strength of the Brönsted acid. Several groups have explored the idea of replacing the bipyridyl ligand. Hartl and coworkers [176] reported a related manganese catalyst with a diimine ligand, $Mn(CO)_3$(R-DAB)X (R-DAB=*N*,*N*′-Di-R-1,4-diazabuta-1,3-diene). Although formation of dimer was not observed, as for the bipyridyl complexes, the catalyst has been identified as the reduced anion, $Mn(CO)_3(R\text{-}DAB)^{1-}$. Catalysis is thought to follow an ECE mechanism, and an extra 100 mV of overpotential is required relative to the bipyridyl analogue.

4.2.4 Metal Complexes with Macrocyclic Ligands: Role of the Outer Coordination Sphere

A number of different metallocomplexes supported by macrocyclic ligands have been shown to reduce CO_2 to CO. A common theme seen in many of these complexes is hydrogen bonding between ligand protons and bound CO_2 or transfer

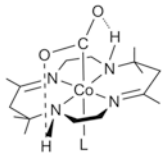

Fig. 19 Co(I) macrocyclic complex in which bound CO_2 forms an intramolecular hydrogen bond with a ligand N–H proton

of a proton to bound substrate by a Brönsted base in the secondary coordination sphere. One early example, as shown in Fig. 19, is Co(I) macrocyclic complexes in which bound CO_2 forms an intramolecular hydrogen bond with a ligand N–H proton [177–179].

4.2.5 Fe(0) Porphyrins

The most catalytically active example of a macrocyclic metal CO_2 reduction catalyst reported to date is electrocatalytically generated Fe(0) porphyrin catalysts. Initially, Savéant and coworkers showed that these complexes are good catalysts in the presence of Brönsted or Lewis acids [180–182]. Modification of the porphyrin macrocycle with peripheral phenol groups (see Fig. 20) resulted in a catalyst with a faradaic yield for CO in excess of 90% and an improvement of the catalytic rate by approximately two orders of magnitude with a modest overpotential of less than 0.5 V [183]. The authors estimate that the addition of these intramolecular phenol groups is analogous to creating a local concentration of phenol equivalent to a 150 M solution, a concentration that could never be achieved in a bulk, bimolecular experiment. The chemical role of the phenols is twofold [184]. First, the large local proton concentration favors proton transfer to the bound CO_2 at the catalytic metal center. Second, the phenols stabilize the Fe(0)–CO_2 adduct via hydrogen bonding. In the next generation, two of the four phenol groups were replaced by perfluorinated phenyl rings, to explore the hypothesis that these electron-withdrawing substituents would ease the reduction of the complex to the Fe (0) state, i.e., decrease the overpotential necessary for catalysis. This may seem obvious, but it is actually a gamble since decreased electron density may also decrease reactivity toward the CO_2 ligand. The gamble paid off [185]. The so-called FCAT molecule converts CO_2 to CO with nearly quantitative faradaic efficiency with a TOF in bulk electrolysis experiments of 240 s^{-1} and an overpotential of 0.39 V, i.e., a TOF 1.4 times that of the derivative with only phenol substituents. Furthermore, the FCAT molecule is more stable under persistent electrocatalytic conditions.

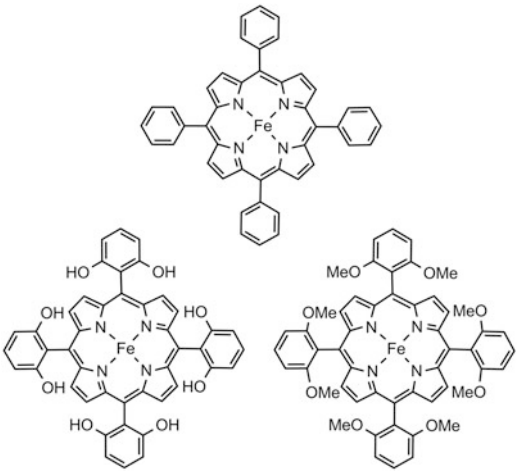

Fig. 20 Fe(0) porphyrins with and without prepositioned phenol functionalities to facilitate CO_2 reduction to CO

5 Conclusions and Outlook

As described herein, metalloenzymes offer blueprints for production of sustainable molecular catalysts for fuel production. Although substantial progress has been made toward this goal, several important objectives remain. First, the stability of catalysts, especially under operating conditions, must be dramatically improved. Second, catalysts will need to be modified for use in specific electrocatalytic or photocatalytic applications. This likely means immobilization at electrode surfaces or tethering to photosensitizers. In both cases, synthetic methods for stable, long-term covalent immobilization must be developed, and studies of catalyst behavior at interfaces will need to be undertaken. Third, both the turnover numbers and turnover frequencies of CO_2 reduction catalysts need to be improved. Fourth, the specificity of CO_2 reduction catalysts must be improved. These last two objectives will likely require development of new ligand sets, syntheses, and complexes. In closing, we note that biological systems have solved analogues of all of these challenges. Thus although our goal is not to recreate biology, we hope that research in this area will continue to benefit from biological inspiration.

Acknowledgments This work was supported as part of the Biological Electron Transfer and Catalysis Energy Frontier Research Center funded by the US Department of Energy, Office of Science, Basic Energy Sciences under Award # DE-SC0012518. Research on hydrogen production catalysis was funded by the Department of Energy, Office of Basic Energy Sciences under contract #DE-FG02-12ER16303. JL is supported by an IGERT-SUN fellowship funded by the National Science Foundation (Award 1144616). AKJ thanks the Institut D'Etudes Avancées Exploratoire Méditerranéen de l'Interdisciplinarité for sabbatical support in research on carbon dioxide reduction.

References

1. Dewar MJ, Storch DM (1985) Alternative view of enzyme reactions. Proc Natl Acad Sci U S A 82(8):2225–2229
2. Warshel A, Sharma PK, Kato M, Xiang Y, Liu H (2006) Electrostatic basis for enzyme catalysis. Chem Rev 106(8):3210–3235. doi:10.1021/cr0503106
3. Albery WJ, Knowles JR (1976) Free-energy profile of the reaction catalyzed by triosephosphate isomerase. Biochemistry 15(25):5627–5631. doi:10.1021/bi00670a031
4. Rockström J, Steffen W, Noone K, Persson Å, Chapin FS, Lambin EF, Lenton TM, Scheffer M, Folke C, Schellnhuber HJ, Nykvist B, de Wit CA, Hughes T, van der Leeuw S, Rodhe H, Sörlin S, Snyder PK, Costanza R, Svedin U, Falkenmark M, Karlberg L, Corell RW, Fabry VJ, Hansen J, Walker B, Liverman D, Richardson K, Crutzen P, Foley JA (2009) A safe operating space for humanity. Nature 461 (7263):472–475. doi:10.1038/461472a
5. Lubitz W, Ogata H, Ruediger O, Reijerse E (2014) Hydrogenases. Chem Rev 114:4081–4148. doi:10.1021/cr4005814
6. Hiromoto T, Warkentin E, Moll J, Ermler U, Shima S (2009) The crystal structure of an [Fe]-hydrogenase-substrate complex reveals the framework for H_2 activation. Angew Chem Int Ed 48:6457–6460. doi:10.1002/anie.200902695
7. Fontecilla-Camps JC, Volbeda A, Cavazza C, Nicolet Y (2007) Structure/function relationships of [NiFe]- and [FeFe]-hydrogenases. Chem Rev 107(10):4273–4303. doi:10.1021/cr050195z
8. Silakov A, Wenk B, Reijerse E, Lubitz W (2009) ^{14}N HYSCORE investigation of the H-cluster of [FeFe]-hydrogenase: evidence for a nitrogen in the dithiol bridge. Phys Chem Chem Phys 11:6592–6599. doi:10.1039/b905841a
9. Esselborn J, Lambertz C, Adamska-Venkatesh A, Simmons T, Berggren G, Nothl J, Siebel J, Hemschemeier A, Artero V, Reijerse E, Fontecave M, Lubitz W, Happe T (2013) Spontaneous activation of [FeFe]-hydrogenases by an inorganic [2Fe] active site mimic. Nat Chem Biol 9:607–609. doi:10.1038/nchembio.1311
10. Liu T, DuBois DL, Bullock RM (2013) An iron complex with pendent amines as a molecular electrocatalyst for oxidation of hydrogen. Nat Chem 5:228–233. doi:10.1038/nchem.1571
11. Wilson AD, Newell RH, McNevin MJ, Muckerman JT, DuBois MR, DuBois DL (2006) Hydrogen oxidation and production using nickel-based molecular catalysts with positioned proton relays. J Am Chem Soc 128:358–366. doi:10.1021/ja056442y
12. Nicolet Y, Lemon BJ, Fontecilla-Camps JC, Peters JW (2000) A novel [FeS] cluster in Fe-only hydrogenases. Trends Biochem Sci 25:138–143. doi:10.1016/s0968-0004(99)01536-4
13. Schilter D, Rauchfuss TB, Stein M (2012) Connecting [NiFe]- and [FeFe]-hydrogenases: mixed-valence nickel-iron dithiolates with rotated structures. Inorg Chem 51:8931–8941. doi:10.1021/ic300910r
14. Hexter SV, Grey F, Happe T, Climent V, Armstrong FA (2012) Electrocatalytic mechanism of reversible hydrogen cycling by enzymes and distinctions between the major classes of hydrogenases. Proc Natl Acad Sci U S A 109:11516–11521. doi:10.1073/pnas.1204770109
15. Hajj V, Baffert C, Sybirna K, Meynial-Salles I, Soucaille P, Bottin H, Fourmond V, Léger C (2014) [FeFe]-hydrogenase reductive inactivation and implication for catalysis. Energy Environ Sci 7:715–719. doi:10.1039/c3ee42075b
16. Adamska A, Silakov A, Lambertz C, Rudiger O, Happe T, Reijerse E, Lubitz W (2012) Identification and characterization of the "super-reduced" state of the H-cluster in [FeFe]-hydrogenase: a new building block for the catalytic cycle? Angew Chem Int Ed 51:11458–11462. doi:10.1002/anie.201204800
17. Mulder DW, Ratzloff MW, Shepard EM, Byer AS, Noone SM, Peters JW, Broderick JB, King PW (2013) EPR and FTIR analysis of the mechanism of H_2 activation by [FeFe]-

hydrogenase HydA1 from *Chlamydomonas reinhardtii*. J Am Chem Soc 135:6921–6929. doi:10.1021/ja4000257
18. Evans RM, Parkin A, Roessler MM, Murphy BJ, Adamson H, Lukey MJ, Sargent F, Volbeda A, Fontecilla-Camps JC, Armstrong FA (2013) Principles of sustained enzymatic hydrogen oxidation in the presence of oxygen - the crucial influence of high potential Fe-S clusters in the electron relay of [NiFe]-hydrogenases. J Am Chem Soc 135:2694–2707. doi:10.1021/ja311055d
19. Lemon BJ, Peters JW (1999) Binding of exogenously added carbon monoxide at the active site of the iron-only hydrogenase (CpI) from *Clostridium pasteurianum*. Biochemistry 38 (40):12969–12973. doi:10.1021/bi9913193
20. Pandelia ME, Ogata H, Lubitz W (2010) Intermediates in the catalytic cycle of [NiFe] hydrogenase: functional spectroscopy of the active site. ChemPhysChem 11:1127–1140. doi:10.1002/cphc.200900950
21. Shafaat HS, Rudiger O, Ogata H, Lubitz W (2013) [NiFe]-hydrogenases: a common active site for hydrogen metabolism under diverse conditions. Bioenergetics 1827:986–1002. doi:10.1016/j.bbabio.2013.01.015
22. Ogata H, Hirota S, Nakahara A, Komori H, Shibata N, Kato T, Kano K, Higuchi Y (2005) Activation process of [NiFe]-hydrogenase elucidated by high-resolution X-Ray analyses: conversion of the ready to the unready state. Structure 13:1635–1642. doi:10.1016/j.str.2005.07.018
23. Montet Y, Amara P, Volbeda A, Vernede X, Hatchikian EC, Field MJ, Frey M, Fontecilla-Camps JC (1997) Gas access to the active site of [NiFe]-hydrogenases probed by X-Ray crystallography and molecular dynamics. Nat Struct Mol Biol 4:523–526. doi:10.1038/nsb0797-523
24. Liebgott PP, de Lacey AL, Burlat B, Cournac L, Richaud P, Brugna M, Fernandez VM, Guigliarelli B, Rousset M, Léger C, Dementin S (2011) Original design of an oxygen-tolerant [NiFe]-hydrogenase: major effect of a valine-to-cysteine mutation near the active site. J Am Chem Soc 133:986–997. doi:10.1021/ja108787s
25. Volbeda A, Amara P, Darnault C, Mouesca J-M, Parkin A, Roessler MM, Armstrong FA, Fontecilla-Camps JC (2012) X-Ray crystallographic and computational studies of the O_2-tolerant [NiFe]-hydrogenase 1 from *Escherichia coli*. Proc Natl Acad Sci U S A 109:5305–5310. doi:10.1073/pnas.1119806109
26. Pandelia M-E, Bykov D, Izsak R, Infossi P, Giudici-Orticoni M-T, Bill E, Neese F, Lubitz W (2013) Electronic structure of the unique [4Fe-3S] cluster in O_2-tolerant hydrogenases characterized by ^{57}Fe mössbauer and EPR spectroscopy. Proc Natl Acad Sci U S A 110:483–488. doi:10.1073/pnas.1202575110
27. Dementin S, Burlat B, De Lacey AL, Pardo A, Adryanczyk-Perrier G, Guigliarelli B, Fernandez VM, Rousset M (2004) A glutamate is the essential proton transfer gate during the catalytic cycle of the [NiFe]-hydrogenase. J Biol Chem 279:10508–10513. doi:10.1074/jbc.M312716200
28. Appel AM, Bercaw JE, Bocarsly AB, Dobbek H, DuBois DL, Dupuis M, Ferry JG, Fujita E, Hille R, Kenis PJA, Kerfeld CA, Morris RH, Peden CHF, Portis AR, Ragsdale SW, Rauchfuss TB, Reek JNH, Seefeldt LC, Thauer RK, Waldrop GL (2013) Frontiers, opportunities, and challenges in biochemical and chemical catalysis of CO_2 fixation. Chem Rev 113:6621–6658. doi:10.1021/cr300463y
29. Can M, Armstrong FA, Ragsdale SW (2014) Structure, function, and mechanism of the nickel metalloenzymes, CO dehydrogenase, and acetyl-CoA synthase. Chem Rev 114:4149–4174. doi:10.1021/cr400461p
30. Svetlitchnyi V, Peschel C, Acker G, Meyer O (2001) Two membrane-associated [NiFeS]-carbon monoxide dehydrogenases from the anaerobic carbon-monoxide-utilizing eubacterium *Carboxydothermus hydrogenoformans*. J Bacteriol 183:5134–5144. doi:10.1128/jb.183.17.5134-5144.2001

31. Zhang B, Hemann CF, Hille R (2010) Kinetic and spectroscopic studies of the [molybdenum-copper] CO dehydrogenase from *Oligotropha carboxidovorans*. J Biol Chem 285:12571–12578. doi:10.1074/jbc.M109.076851
32. Dobbek H, Gremer L, Kiefersauer R, Huber R, Meyer O (2002) Catalysis at a dinuclear CuSMo(==O)OH cluster in a CO dehydrogenase resolved at 1.1-angstrom resolution. Proc Natl Acad Sci U S A 99:15971–15976. doi:10.1073/pnas.212640899
33. Hofmann M, Kassube JK, Graf T (2005) The mechanism of Mo-/Cu-dependent CO dehydrogenase. J Biol Inorg Chem 10:490–495. doi:10.1007/s00775-005-0661-5
34. Jeoung J-H, Dobbek H (2007) Carbon dioxide activation at the Ni, Fe-cluster of anaerobic carbon monoxide dehydrogenase. Science 318:1461–1464. doi:10.1126/science.1148481
35. Russell WK, Lindahl PA (1998) CO/CO_2 potentiometric titrations of carbon monoxide dehydrogenase from *Clostridium thermoaceticum* and the effect of CO_2. Biochemistry 37:10016–10026. doi:10.1021/bi980149b
36. Majumdar A, Sarkar S (2011) Bioinorganic chemistry of molybdenum and tungsten enzymes: a structural-functional modeling approach. Coord Chem Rev 255:1039–1054. doi:10.1016/j.ccr.2010.11.027
37. Jormakka M, Tornroth S, Byrne B, Iwata S (2002) Molecular basis of proton motive force generation: structure of formate dehydrogenase-N. Science 295:1863–1868. doi:10.1126/science.1068186
38. George GN, Costa C, Moura JJG, Moura I (1999) Observation of ligand-based redox chemistry at the active site of a molybdenum enzyme. J Am Chem Soc 121:2625–2626. doi:10.1021/ja9841761
39. Rivas MG, Gonzalez PJ, Brondino CD, Moura JJG, Moura I (2007) EPR characterization of the molybdenum(V) forms of formate dehydrogenase from *Desulfovibrio desulfuricans* ATCC 27774 upon formate reduction. J Inorg Biochem 101:1617–1622. doi:10.1016/j.jinorgbio.2007.04.011
40. Bevers LE, Hagedoorn PL, Hagen WR (2009) The bioinorganic chemistry of tungsten. Coord Chem Rev 253:269–290. doi:10.1016/j.ccr.2008.01.017
41. Raaijmakers HCA, Romao MJ (2006) Formate-reduced *E. coli* formate dehydrogenase H: the reinterpretation of the crystal structure suggests a new reaction mechanism. J Biol Inorg Chem 11:849–854. doi:10.1007/s00775-006-0129-2
42. Cerqueira NMFSA, Fernandes PA, Gonzalez PJ, Moura JJG, Ramos MJ (2013) The sulfur shift: an activation mechanism for periplasmic nitrate reductase and formate dehydrogenase. Inorg Chem 52:10766–10772. doi:10.1021/ic3028034
43. Axley MJ, Bock A, Stadtman TC (1991) Catalytic properties of an *Escherichia coli* formate dehydrogenase mutant in which sulfur replaces selenium. Proc Natl Acad Sci U S A 88:8450–8454. doi:10.1073/pnas.88.19.8450
44. Mota CS, Rivas MG, Brondino CD, Moura I, Moura JJG, Gonzalez PJ, Cerqueira NMFSA (2011) The mechanism of formate oxidation by metal-dependent formate dehydrogenases. J Biol Inorg Chem 16:1255–1268. doi:10.1007/s00775-011-0813-8
45. Raaijmakers H, Macieira S, Dias JM, Teixeira S, Bursakov S, Huber R, Moura JJG, Moura I, Romao MJ (2002) Gene sequence and the 1.8 angstrom crystal structure of the tungsten-containing formate dehydrogenase from *Desulfovibrio gigas*. Structure 10:1261–1272. doi:10.1016/s0969-2126(02)00826-2
46. Jones AK, Sillery E, Albracht SPJ, Armstrong FA (2002) Direct comparison of the electrocatalytic oxidation of hydrogen by an enzyme and a platinum catalyst. Chem Commun 8:866–867. doi:10.1039/b201337a
47. Madden C, Vaughn MD, Díez-Pérez I, Brown KA, King PW, Gust D, Moore AL, Moore TA (2012) Catalytic turnover of [FeFe]-hydrogenase based on single-molecule imaging. J Am Chem Soc 134(3):1577–1582. doi:10.1021/ja207461t
48. Barton BE, Whaley CM, Rauchfuss TB, Gray DL (2009) Nickel-iron dithiolato hydrides relevant to the [NiFe]-hydrogenase active site. J Am Chem Soc 131(20):6942–6943. doi:10.1021/ja902570u

49. Canaguier S, Field M, Oudart Y, Pecaut J, Fontecave M, Artero V (2010) A structural and functional mimic of the active site of NiFe hydrogenases. Chem Commun 46(32):5876–5878. doi:10.1039/c001675f
50. Cui H-H, Wang J-Y, Hu M-Q, Ma C-B, Wen H-M, Song X-W, Chen C-N (2013) Efficient photo-driven hydrogen evolution by binuclear nickel catalysts of different coordination in noble-metal-free systems. Dalton Trans 42(24):8684–8691. doi:10.1039/c3dt50140j
51. Barton BE, Rauchfuss TB (2010) Hydride-containing models for the active site of the nickel-iron hydrogenases. J Am Chem Soc 132(42):14877–14885. doi:10.1021/ja105312p
52. Carroll ME, Barton BE, Gray DL, Mack AE, Rauchfuss TB (2011) Active-site models for the nickel–iron hydrogenases: effects of ligands on reactivity and catalytic properties. Inorg Chem 50(19):9554–9563. doi:10.1021/ic2012759
53. Huynh MT, Schilter D, Hammes-Schiffer S, Rauchfuss TB (2014) Protonation of nickel–iron hydrogenase models proceeds after isomerization at nickel. J Am Chem Soc 136 (35):12385–12395. doi:10.1021/ja505783z
54. Tard C, Pickett CJ (2009) Structural and functional analogues of the active sites of the [Fe]-, [NiFe]-, and [FeFe]-hydrogenases. Chem Rev 109(6):2245–2274. doi:10.1021/cr800542q
55. Darensbourg MY, Lyon EJ, Zhao X, Georgakaki IP (2003) The organometallic active site of [Fe]-hydrogenase: models and entatic states. Proc Natl Acad Sci U S A 100(7):3683–3688. doi:10.1073/pnas.0536955100
56. Roy S, Groy TL, Jones AK (2013) Biomimetic model for [FeFe]-hydrogenase: asymmetrically disubstituted diiron complex with a redox-active 2,2′-bipyridyl ligand. Dalton Trans 42 (11):3843–3853. doi:10.1039/c2dt32457a
57. Roy S, Mazinani SKS, Groy TL, Gan L, Tarakeshwar P, Mujica V, Jones AK (2014) Catalytic hydrogen evolution by Fe(II) carbonyls featuring a dithiolate and a chelating phosphine. Inorg Chem 53(17):8919–8929. doi:10.1021/ic5012988
58. Lansing JC, Camara JM, Gray DE, Rauchfuss TB (2014) Hydrogen production catalyzed by bidirectional, biomimetic models of the [FeFe]-hydrogenase active site. Organometallics 33 (20):5897–5906. doi:10.1021/om5004013
59. Liu T, Darensbourg MY (2007) A mixed-valent, Fe(II)Fe(I), diiron complex reproduces the unique rotated state of the [FeFe]-hydrogenase active site. J Am Chem Soc 129 (22):7008–7009. doi:10.1021/ja071851a
60. Justice AK, Rauchfuss TB, Wilson SR (2007) Unsaturated, mixed-valence diiron dithiolate model for the H-ox state of the [FeFe]-hydrogenase. Angew Chem Int Ed 46(32):6152–6154. doi:10.1002/anie.200702224
61. Singleton ML, Bhuvanesh N, Reibenspies JH, Darensbourg MY (2008) Synthetic support of *de novo* design: sterically bulky [FeFe]-hydrogenase models. Angew Chem Int Ed 47 (49):9492–9495. doi:10.1002/anie.200803939
62. Munery S, Capon J-F, De Gioia L, Elleouet C, Greco C, Pétillon FY, Schollhammer P, Talarmin J, Zampella G (2013) New Fe(I)-Fe(I) complex featuring a rotated conformation related to the [2Fe](H) subsite of [FeFe]-hydrogenase. Chemistry 19(46):15458–15461. doi:10.1002/chem.201303316
63. Olsen MT, Bruschi M, De Gioia L, Rauchfuss TB, Wilson SR (2008) Nitrosyl derivatives of diiron(I) dithiolates mimic the structure and Lewis acidity of the [FeFe]-hydrogenase active site. J Am Chem Soc 130(36):12021–12030. doi:10.1021/ja802268p
64. Hsieh C-H, Erdem OF, Harman SD, Singleton ML, Reijerse E, Lubitz W, Popescu CV, Reibenspies JH, Brothers SM, Hall MB, Darensbourg MY (2012) Structural and spectroscopic features of mixed valent Fe(II)Fe(I) complexes and factors related to the rotated configuration of diiron hydrogenase. J Am Chem Soc 134(31):13089–13102. doi:10.1021/ja304866r
65. Singleton ML, Reibenspies JH, Darensbourg MY (2010) A cyclodextrin host/guest approach to a hydrogenase active site biomimetic cavity. J Am Chem Soc 132(26):8870–8871. doi:10.1021/ja103774j

66. Sano Y, Onoda A, Hayashi T (2011) A hydrogenase model system based on the sequence of cytochrome *c*: photochemical hydrogen evolution in aqueous media. Chem Commun 47 (29):8229–8231. doi:10.1039/c1cc11157d
67. Caserta G, Roy S, Atta M, Artero V, Fontecave M (2015) Artificial hydrogenases: biohybrid and supramolecular systems for catalytic hydrogen production or uptake. Curr Opin Chem Biol 25:36–47. doi:10.1016/j.cbpa.2014.12.018
68. Jones AK, Lichtenstein BR, Dutta A, Gordon G, Dutton PL (2007) Synthetic hydrogenases: incorporation of an iron carbonyl thiolate into a designed peptide. J Am Chem Soc 129 (48):14844–14845. doi:10.1021/ja075116a
69. Berggren G, Adamska A, Lambertz C, Simmons TR, Esselborn J, Atta M, Gambarelli S, Mouesca JM, Reijerse E, Lubitz W, Happe T, Artero V, Fontecave M (2013) Biomimetic assembly and activation of [FeFe]-hydrogenases. Nature 499(7456):66–69. doi:10.1038/nature12239
70. Sellmann D, Kleine-Kleffmann U, Zapf L, Huttner G, Zsolnai L (1984) Übergangsmetall-Komplexe mit Schwefelliganden: VII. Synthese und Struktur der Benzoldithiolato-Eisen-Komplexe $[AsPh_4]_2[Fe(S_2C_6H_4)_2]$ und $[Fe(S_2C_6H_4)(PMe_3)_3]$. J Organomet Chem 263 (3):321–331. doi:10.1016/0022-328X(84)85035-4
71. Rauchfuss TB, Contakes SM, Hsu SCN, Reynolds MA, Wilson SR (2001) The influence of cyanide on the carbonylation of iron(II): synthesis of Fe – SR – CN – CO centers related to the hydrogenase active sites. J Am Chem Soc 123(28):6933–6934. doi:10.1021/ja015948n
72. Orthaber A, Karnahl M, Tschierlei S, Streich D, Stein M, Ott S (2014) Coordination and conformational isomers in mononuclear iron complexes with pertinence to the [FeFe]-hydrogenase active site. Dalton Trans 43:4537–4549. doi:10.1039/c3dt53268b
73. Beyler M, Ezzaher S, Karnahl M, Santoni M-P, Lomoth R, Ott S (2011) Pentacoordinate iron complexes as functional models of the distal iron in [FeFe]-hydrogenases. Chem Commun 47:11662–11664. doi:10.1039/c1cc14449a
74. Gardner JM, Beyler M, Karnahl M, Tschierlei S, Ott S, Hammarström L (2012) Light-driven electron transfer between a photosensitizer and a proton-reducing catalyst Co-adsorbed to NiO. J Am Chem Soc 134(47):19322–19325. doi:10.1021/ja3082268
75. Fisher BJ, Eisenberg R (1980) Electrocatalytic reduction of carbon dioxide by using macrocycles of nickel and cobalt. J Am Chem Soc. doi:10.1021/ja00544a035
76. Creutz C, Sutin N (1985) Photogeneration and reactions of cobalt(I) complexes. Coordin Chem Rev 64:321–341. doi:10.1016/0010-8545(85)80058-8
77. Sun Y, Bigi JP, Piro NA, Tang ML, Long JR, Chang CJ (2011) Molecular cobalt pentapyridine catalysts for generating hydrogen from water. J Am Chem Soc 133 (24):9212–9215. doi:10.1021/ja202743r
78. Rodenberg A, Orazietti M, Probst B, Bachmann C, Alberto R, Baldridge KK, Hamm P (2015) Mechanism of photocatalytic hydrogen generation by a polypyridyl-based cobalt catalyst in aqueous solution. Inorg Chem 54(2):646–657. doi:10.1021/ic502591a
79. Khnayzer RS, Thoi VS, Nippe M, King AE, Jurss JW, El Roz KA, Long JR, Chang CJ, Castellano FN (2014) Towards a comprehensive understanding of visible-light photogeneration of hydrogen from water using cobalt(II) polypyridyl catalysts. Energy Environ Sci 7(4):1477–1488. doi:10.1039/C3EE43982H
80. Koelle U, Paul S (1986) Electrochemical reduction of protonated cyclopentadienylcobalt phosphine complexes. Inorg Chem 25(16):2689–2694. doi:10.1021/ic00236a007
81. Fang M, Wiedner ES, Dougherty WG, Kassel WS, Liu T, DuBois DL, Bullock RM (2014) Cobalt complexes containing pendant amines in the second coordination sphere as electrocatalysts for H_2 production. Organometallics 33(20):5820–5833. doi:10.1021/om5004607
82. Jacobsen GM, Yang JY, Twamley B, Wilson AD, Bullock RM, DuBois MR, DuBois DL (2008) Hydrogen production using cobalt-based molecular catalysts containing a proton relay in the second coordination sphere. Energy Environ Sci 1(1):167–174. doi:10.1039/B805309J

83. Wiedner ES, Yang JY, Dougherty WG, Kassel WS, Bullock RM, DuBois MR, DuBois DL (2010) Comparison of cobalt and nickel complexes with sterically demanding cyclic diphosphine ligands: electrocatalytic H_2 production by $[Co(PtBu_2NPh_2)(CH_3CN)_3](BF_4)_2$. Organometallics 29(21):5390–5401. doi:10.1021/om100395r
84. Wiedner ES, Roberts JAS, Dougherty WG (2013) Synthesis and electrochemical studies of cobalt(III) monohydride complexes containing pendant amines. Inorg Chem 52(17):9975–9988. doi:10.1021/ic401232g
85. Lee CH, Dogutan DK, Nocera DG (2011) Hydrogen generation by hangman metalloporphyrins. J Am Chem Soc 133(23):8775–8777. doi:10.1021/ja202136y
86. Roubelakis MM, Bediako DK, Dogutan DK, Nocera DG (2012) Proton-coupled electron transfer kinetics for the hydrogen evolution reaction of hangman porphyrins. Energy Environ Sci 5(7):7737–7740. doi:10.1039/c2ee21123h
87. Kleingardner JG, Kandemir B, Bren KL (2014) Hydrogen evolution from neutral water under aerobic conditions catalyzed by cobalt microperoxidase-11. J Am Chem Soc 136(1):4–7. doi:10.1021/ja406818h
88. Connolly P, Espenson JH (1986) Cobalt-catalyzed evolution of molecular hydrogen. Inorg Chem 25(16):2684–2688. doi:10.1021/ic00236a006
89. Artero V, Chavarot-Kerlidou M, Fontecave M (2011) Splitting water with cobalt. Angew Chem Int Ed 50(32):7238–7266. doi:10.1002/anie.201007987
90. Razavet M, Artero V, Fontecave M (2005) Proton electroreduction catalyzed by cobaloximes: functional models for hydrogenases. Inorg Chem 44(13):4786–4795. doi:10.1021/ic050167z
91. Baffert C, Artero V, Fontecave M (2007) Cobaloximes as functional models for hydrogenases. 2. Proton electroreduction catalyzed by difluoroborylbis(dimethylglyoximato)cobalt (II) complexes in organic media. Inorg Chem 46(5):1817–1824. doi:10.1021/ic061625m
92. Hu X, Brunschwig BS, Peters JC (2007) Electrocatalytic hydrogen evolution at low overpotentials by cobalt macrocyclic glyoxime and tetraimine complexes. J Am Chem Soc 129(29):8988–8998. doi:10.1021/ja067876b
93. Jacques PA, Artero V, Pecaut J, Fontecave M (2009) Cobalt and nickel diimine-dioxime complexes as molecular electrocatalysts for hydrogen evolution with low overvoltages. Proc Natl Acad Sci U S A 106(49):20627–20632. doi:10.1073/pnas.0907775106
94. Hu X, Cossairt BM, Brunschwig BS, Lewis NS, Peters JC (2005) Electrocatalytic hydrogen evolution by cobalt difluoroboryl-diglyoximate complexes. Chem Commun 37:4723–4725. doi:10.1039/b509188h
95. Bacchi M, Berggren G, Niklas J, Veinberg E, Mara MW, Shelby ML, Poluektov OG, Chen LX, Tiede DM, Cavazza C, Field MJ, Fontecave M, Artero V (2014) Cobaloxime-based artificial hydrogenases. Inorg Chem 53(15):8071–8082. doi:10.1021/ic501014c
96. Fang M, Engelhard MH, Zhu Z, Helm ML, Roberts JAS (2014) Eelectrodeposition from acidic solutions of nickel Bis(benzenedithiolate) produces a hydrogen-evolving Ni-S film on glassy carbon. ACS Catal 4:90–98. doi:10.1021/cs400675u
97. Wang D, Ghirlanda G, Allen JP (2014) Water oxidation by a nickel-glycine catalyst. J Am Chem Soc 136(29):10198–10201. doi:10.1021/ja504282w
98. Cobo S, Heidkamp J, Jacques P-A, Fize J, Fourmond V, Guetaz L, Jousselme B, Ivanova V, Dau H, Palacin S, Fontecave M, Artero V (2012) A Janus cobalt-based catalytic material for electro-splitting of water. Nat Mater 11(9):802–807. doi:10.1038/nmat3385
99. Chen L, Chen G, Leung C-F, Yiu S-M, Ko C-C, Anxolabéhère-Mallart E, Robert M, Lau T-C (2015) Dual homogeneous and heterogeneous pathways in photo- and electrocatalytic hydrogen evolution with nickel(II) catalysts bearing tetradentate macrocyclic ligands. ACS Catal 5 (1):356–364. doi:10.1021/cs501534h
100. Cherdo S, El Ghachtouli S, Sircoglou M, Brisset F, Orio M, Aukauloo A (2014) A nickel dimethyl glyoximato complex to form nickel based nanoparticles for electrocatalytic H_2 production. Chem Commun 50(88):13514–13516. doi:10.1039/C4CC05355A

101. Shaw WJ, Helm ML, DuBois DL (2013) A modular, energy-based approach to the development of nickel containing molecular electrocatalysts for hydrogen production and oxidation. Bioenergetics 1827(8–9):1123–1139. doi:10.1016/j.bbabio.2013.01.003
102. Kilgore UJ, Roberts JAS, Pool DH, Appel AM, Stewart MP, DuBois MR, Dougherty WG, Kassel WS, Bullock RM, DuBois DL (2011) $[Ni(PPh_2NC_6H_4X_2)_2]^{2+}$ complexes as electrocatalysts for H_2 production: effect of substituents, acids, and water on catalytic rates. J Am Chem Soc 133(15):5861–5872. doi:10.1021/ja109755f
103. Kilgore UJ, Stewart MP, Helm ML, Dougherty WG, Kassel WS, DuBois MR, DuBois DL, Bullock RM (2011) Studies of a series of $[Ni(Pr_2NPh_2)_2(CH_3CN)]^{2+}$ complexes as electrocatalysts for H_2 production: substituent variation at the phosphorous atom of the P_2N_2 ligand. Inorg Chem 50(21):10908–10918. doi:10.1021/ic201461a
104. DuBois DL, Bullock RM (2011) Molecular electrocatalysts for the oxidation of hydrogen and the production of hydrogen - the role of pendant amines as proton relays. Eur J Inorg Chem 2011(7):1017–1027. doi:10.1002/ejic.201001081
105. O'Hagan M, Shaw WJ, Raugei S, Chen S (2011) Moving protons with pendant amines: proton mobility in a nickel catalyst for oxidation of hydrogen. J Am Chem Soc 133 (36):14301–14312. doi:10.1021/ja201838x
106. Helm ML, Stewart MP, Bullock RM, DuBois MR, DuBois DL (2011) A synthetic nickel electrocatalyst with a turnover frequency above 100,000 s^{-1} for H_2 production. Science 333 (6044):863–866. doi:10.1126/science.1205864
107. Pool DH, Stewart MP, O'Hagan M, Shaw WJ, Roberts JAS, Bullock RM, DuBois DL (2012) Acidic ionic liquid/water solution as both medium and proton source for electrocatalytic H_2 evolution by $[Ni(P_2N_2)_2]^{2+}$ complexes. Proc Natl Acad Sci U S A 109(39):15634–15639. doi:10.1073/pnas.1120208109
108. Hoffert WA, Roberts JAS, Bullock RM, Helm ML (2013) Production of H_2 at fast rates using a nickel electrocatalyst in water–acetonitrile solutions. Chem Commun 49(71):7767–7769. doi:10.1039/C3CC43203C
109. Das AK, Engelhard MH, Bullock RM (2014) A hydrogen-evolving Ni(P2N2)2 electrocatalyst covalently attached to a glassy carbon electrode: preparation, characterization, and catalysis. Comparisons with the homogeneous analogue. Inorg Chem 53(13):6875–6885. doi:10.1021/ic500701a
110. Tran PD, Le Goff A, Heidkamp J, Jousselme B, Guillet N, Palacin S, Dau H, Fontecave M, Artero V (2011) Noncovalent modification of carbon nanotubes with pyrene-functionalized nickel complexes: carbon monoxide tolerant catalysts for hydrogen evolution and uptake. Angew Chem Int Ed 50(6):1371–1374. doi:10.1002/anie.201005427
111. Le Goff A, Artero V, Jousselme B, Tran PD, Guillet N, Metaye R, Fihri A, Palacin S, Fontecave M (2009) From hydrogenases to noble metal-free catalytic nanomaterials for H_2 production and uptake. Science 326(5958):1384–1387. doi:10.1126/science.1179773
112. Dutta A, Lense S, Hou J, Engelhard MH, Roberts JAS, Shaw WJ (2013) Minimal proton channel enables H_2 oxidation and production with a water-soluble nickel-based catalyst. J Am Chem Soc 135(49):18490–18496. doi:10.1021/ja407826d
113. Ginovska-Pangovska B, Dutta A, Reback ML, Linehan JC, Shaw WJ (2014) Beyond the active site: the impact of the outer coordination sphere on electrocatalysts for hydrogen production and oxidation. Acc Chem Res 47(8):2621–2630. doi:10.1021/ar5001742
114. Dutta A, Roberts JAS, Shaw WJ (2014) Arginine-containing ligands enhance H2 oxidation catalyst performance. Angew Chem Int Ed Engl 53(25):6487–6491. doi:10.1002/anie.201402304
115. Dutta A, DuBois DL, Roberts JAS, Shaw WJ (2014) Amino acid modified Ni catalyst exhibits reversible H_2 oxidation/production over a broad pH range at elevated temperatures. Proc Natl Acad Sci U S A 111(46):16286–16291. doi:10.1073/pnas.1416381111
116. Yang Y, Wang M, Xue L, Zhang F, Chen L, Ahlquist MSG, Sun L (2014) Nickel complex with internal bases as efficient molecular catalyst for photochemical H_2 production. ChemSusChem 7(10):2889–2897. doi:10.1002/cssc.201402381

117. Gan L, Groy TL, Tarakeshwar P, Mazinani SKS, Shearer J, Mujica V, Jones AK (2015) A nickel phosphine complex as a fast and efficient hydrogen production catalyst. J Am Chem Soc 137(3):1109–1115. doi:10.1021/ja509779q
118. Happe RP, Roseboom W, Pierik AJ, Albracht SP, Bagley KA (1997) Biological activation of hydrogen. Nature 385(6612):126. doi:10.1038/385126a0
119. Ghirardi ML, Zhang L, Lee JW, Flynn T, Seibert M (2000) Microalgae: a green source of renewable H_2. Trends Biotechnol 18:506–511. doi:10.1016/S0167-7799(00)01511-0
120. Rumpel S, Siebel JF, Fares C, Duan J, Reijerse E, Happe T, Lubitz W, Winkler M (2014) Enhancing hydrogen production of microalgae by redirecting electrons from photosystem I to hydrogenase. Energy Environ Sci 7(10):3296–3301. doi:10.1039/C4EE01444H
121. Winkler M, Kuhlgert S, Hippler M, Happe T (2009) Characterization of the key step for light-driven hydrogen evolution in green algae. J Biol Chem 284(52):36620–36627. doi:10.1074/jbc.M109.053496
122. Leino H, Shunmugam S, Isojärvi J, Oliveira P, Mulo P, Saari L, Battchikova N, Sivonen K, Lindblad P, Aro E-M, Allahverdiyeva Y (2014) Characterization of ten H_2 producing cyanobacteria isolated from the Baltic Sea and Finnish lakes. Int J Hydr Energy 39 (17):8983–8991. doi:10.1016/j.ijhydene.2014.03.171
123. Lubner CE, Applegate AM, Knörzer P, Ganago A, Bryant DA, Happe T, Golbeck JH (2011) Solar hydrogen-producing bionanodevice outperforms natural photosynthesis. Proc Natl Acad Sci U S A 108(52):20988–20991. doi:10.1073/pnas.1114660108
124. Sherman B, Vaughn M, Bergkamp J, Gust D, Moore A, Moore T (2014) Evolution of reaction center mimics to systems capable of generating solar fuel. Photosynth Res 120(1–2):59–70. doi:10.1007/s11120-013-9795-4
125. Megiatto JD, Antoniuk-Pablant A, Sherman BD, Kodis G, Gervaldo M, Moore TA, Moore AL, Gust D (2012) Mimicking the electron transfer chain in photosystem II with a molecular triad thermodynamically capable of water oxidation. Proc Natl Acad Sci U S A 109 (39):15578–15583. doi:10.1073/pnas.1118348109
126. Gust D, Moore TA, Moore AL (2009) Solar fuels via artificial photosynthesis. Acc Chem Res 42(12):1890–1898. doi:10.1021/ar900209b
127. Gust D, Moore TA, Moore AL (2012) Realizing artificial photosynthesis. Faraday Discuss 155:9. doi:10.1039/c1fd00110h
128. Wang M, Chen L, Li X, Sun L (2011) Approaches to efficient molecular catalyst systems for photochemical H_2 production using [FeFe]-hydrogenase active site mimics. Dalton Trans 40 (48):12793–12800. doi:10.1039/C1DT11166C
129. Na Y, Pan J, Wang M, Sun L (2007) Intermolecular electron transfer from photogenerated $[Ru(bpy)_3]^{3+}$ to [2Fe2S] model complexes of the iron-only hydrogenase active site. Inorg Chem 46(10):3813–3815. doi:10.1021/ic070234k
130. Na Y, Wang M, Pan J, Zhang P, Åkermark B, Sun L (2008) Visible light-driven electron transfer and hydrogen generation catalyzed by bioinspired [2Fe2S] complexes. Inorg Chem 47(7):2805–2810. doi:10.1021/ic702010w
131. Streich D, Astuti Y, Orlandi M, Schwartz L, Lomoth R, Hammarström L, Ott S (2010) High-turnover photochemical hydrogen production catalyzed by a model complex of the [FeFe]-hydrogenase active site. Chem Eur J 16(1):60–63. doi:10.1002/chem.200902489
132. Nann T, Ibrahim SK, Woi P-M, Xu S, Ziegler J, Pickett CJ (2010) Water splitting by visible light: a nanophotocathode for hydrogen production. Angew Chem Int Ed 49(9):1574–1577. doi:10.1002/anie.200906262
133. Li C-B, Li Z-J, Yu S, Wang G-X, Wang F, Meng Q-Y, Bin C, Feng K, Tung C-H, Wu L-Z (2013) Interface-directed assembly of a simple precursor of [FeFe]–H_2ase mimics on CdSe QDs for photosynthetic hydrogen evolution in water. Energy Environ Sci 6(9):2597–2602. doi:10.1039/C3EE40992A
134. Wen F, Li C (2013) Hybrid artificial photosynthetic systems comprising semiconductors as light harvesters and biomimetic complexes as molecular cocatalysts. Acc Chem Res 46 (11):2355–2364. doi:10.1021/ar300224u

135. Yu T, Zeng Y, Chen J, Li Y-Y, Yang G, Li Y (2013) Exceptional dendrimer-based mimics of diiron hydrogenase for the photochemical production of hydrogen. Angew Chem Int Ed 52 (21):5631–5635. doi:10.1002/anie.201301289
136. Roy S, Shinde S, Hamilton GA, Hartnett HE, Jones AK (2011) Artificial [FeFe]-hydrogenase: on resin modification of an amino acid to anchor a hexacarbonyldiiron cluster in a peptide framework. Eur J Inorg Chem 7:1050–1055. doi:10.1002/ejic.201000979
137. Sano Y, Onoda A, Hayashi T (2012) Photocatalytic hydrogen evolution by a diiron hydrogenase model based on a peptide fragment of cytochrome c_{556} with an attached diiron carbonyl cluster and an attached ruthenium photosensitizer. J Inorg Biochem 108:159–162. doi:10.1016/j.jinorgbio.2011.07.010
138. Onoda A, Kihara Y, Fukumoto K, Sano Y, Hayashi T (2014) Photoinduced hydrogen evolution catalyzed by a synthetic diiron dithiolate complex embedded within a protein matrix. ACS Catal 4(8):2645–2648. doi:10.1021/cs500392e
139. Jian J-X, Liu Q, Li Z-J, Wang F, Li X-B, Li C-B, Liu B, Meng Q-Y, Chen B, Feng K, Tung C-H, Wu L-Z (2013) Chitosan confinement enhances hydrogen photogeneration from a mimic of the diiron subsite of [FeFe]-hydrogenase. Nat Commun 4:2695. doi:10.1038/ncomms3695
140. Reisner E, Powell DJ, Cavazza C, Fontecilla-Camps JC, Armstrong FA (2009) Visible light-driven H_2 production by hydrogenases attached to dye-sensitized TiO_2 nanoparticles. J Am Chem Soc 131(51):18457–18466. doi:10.1021/ja907923r
141. King PW (2013) Designing interfaces of hydrogenase–nanomaterial hybrids for efficient solar conversion. Bioenergetics 1827(8–9):949–957. doi:10.1016/j.bbabio.2013.03.006
142. Kleingardner JG, Kandemir B, Bren KL (2013) Hydrogen evolution from neutral water under aerobic conditions catalyzed by cobalt microperoxidase-11. J Am Chem Soc 136(1):4–7. doi:10.1021/ja406818h
143. Sommer DJ, Vaughn MD, Ghirlanda G (2014) Protein secondary-shell interactions enhance the photoinduced hydrogen production of cobalt protoporphyrin-IX. Chem Commun 50 (100):15852–15855. doi:10.1039/C4CC06700B
144. Wang W, Rauchfuss TB, Bertini L, Zampella G (2012) Unsensitized photochemical hydrogen production catalyzed by diiron hydrides. J Am Chem Soc 134(10):4525–4528. doi:10.1021/ja211778j
145. Bertini L, Fantucci P, De Gioia L, Zampella G (2013) Excited state properties of diiron dithiolate hydrides: implications in the unsensitized photocatalysis of H_2 evolution. Inorg Chem 52(17):9826–9841. doi:10.1021/ic400818t
146. Frederix PWJM, Adamczyk K, Wright JA, Tuttle T, Ulijn RV, Pickett CJ, Hunt NT (2014) Investigation of the ultrafast dynamics occurring during unsensitized photocatalytic H_2 evolution by an [FeFe]-hydrogenase subsite analogue. Organometallics 33(20):5888–5896. doi:10.1021/om500521w
147. Majumdar A (2014) Bioinorganic modeling chemistry of carbon monoxide dehydrogenases: description of model complexes, current status and possible future scopes. Dalton Trans 43 (32):12135–12145. doi:10.1039/c4dt00729h
148. Gourlay C, Nielsen DJ, White JM, Knottenbelt SZ, Kirk ML, Young CG (2006) Paramagnetic active site models for the molybdenum – copper carbon monoxide dehydrogenase. J Am Chem Soc 128(7):2164–2165. doi:10.1021/ja056500f
149. Takuma M, Ohki Y, Tatsumi K (2005) Sulfido-bridged dinuclear molybdenum – copper complexes related to the active site of CO dehydrogenase: [(dithiolate)Mo(O)S2Cu(SAr)] 2− (dithiolate=1,2-S2C6H4, 1,2-S2C6H2-3,6-Cl2, 1,2-S2C2H4). Inorg Chem 44 (17):6034–6043. doi:10.1021/ic050294v
150. Groysman S, Majumdar A, Zheng S-L, Holm RH (2009) Reactions of monodithiolene tungsten(VI) sulfido complexes with copper(I) in relation to the structure of the active site of carbon monoxide dehydrogenase. Inorg Chem 49(3):1082–1089. doi:10.1021/ic902066m

151. Ciurli S, Ross PK, Scott MJ, Yu SB, Holm RH (1992) Synthetic nickel-containing heterometal cubane-type clusters with $NiFe_3Q_4$ cores (Q=sulfur, selenium). J Am Chem Soc 114(13):5415–5423. doi:10.1021/ja00039a063
152. Zhou J, Raebiger JW, Crawford CA, Holm RH (1997) Metal ion incorporation reactions of the cluster $[Fe_3S_4(LS_3)]^{3-}$, containing the cuboidal $[Fe_3S_4]^0$ core. J Am Chem Soc 119 (27):6242–6250. doi:10.1021/ja9704186
153. Panda R, Zhang Y, McLauchlan CC, Venkateswara Rao P, Tiago de Oliveira FA, Münck E, Holm RH (2004) Initial structure modification of tetrahedral to planar nickel(II) in a nickel – iron – sulfur cluster related to the C-cluster of carbon monoxide dehydrogenase. J Am Chem Soc 126(20):6448–6459. doi:10.1021/ja030627s
154. Panda R, Berlinguette CP, Zhang Y, Holm RH (2005) Synthesis of $[MFe_3S_4]$ clusters containing a planar MII site (M=Ni, Pd, Pt), a structural element in the C-cluster of carbon monoxide dehydrogenase. J Am Chem Soc 127(31):11092–11101. doi:10.1021/ja052381s
155. Sun J, Tessier C, Holm RH (2007) Sulfur ligand substitution at the nickel(II) sites of cubane-type and cubanoid $[NiFe_3S_4]$ clusters relevant to the C-clusters of carbon monoxide dehydrogenase. Inorg Chem 46(7):2691–2699. doi:10.1021/ic062362z
156. Slater S, Wagenknecht JH (1984) Electrochemical reduction of carbon dioxide catalyzed by $Rh(diphos)_2Cl$. J Am Chem Soc 106(18):5367–5368. doi:10.1021/ja00330a064
157. Darensbourg DJ, Darensbourg MY, Goh LY, Ludvig M, Wiegreffe P (1987) Reaction of $(Cy_3P)_2Ni(H)(CH_3)$ with carbon dioxide. Formation of an hydridonickel formate complex, $HNi(O_2CH)(Cy_3P)_2$. J Am Chem Soc 109(24):7539–7540. doi:10.1021/ja00258a053
158. DuBois DL, Miedaner A (1987) Mediated electrochemical reduction of CO_2. Preparation and comparison of an isoelectronic series of complexes. J Am Chem Soc 109(1):113–117. doi:10.1021/ja00235a019
159. DuBois DL, Miedaner A, Haltiwanger RC (1991) Electrochemical reduction of carbon dioxide catalyzed by [Pd(triphosphine)(solvent)]$(BF4)_2$ complexes: synthetic and mechanistic studies. J Am Chem Soc 113(23):8753–8764. doi:10.1021/ja00023a023
160. Steffey BD, Curtis CJ, DuBois DL (1995) Electrochemical reduction of CO_2 catalyzed by a dinuclear palladium complex containing a bridging hexaphosphine ligand: evidence for cooperativity. Organometallics 14(10):4937–4943. doi:10.1021/om00010a066
161. Hawecker J, Lehn J-M, Ziessel R (1983) Efficient photochemical reduction of CO_2 to CO by visible light irradiation of systems containing $Re(bipy)(CO)_3X$ or $Ru(bipy)_3^{2+}$-Co^{2+} combinations as homogeneous catalysts. Chem Commun 9:536–538. doi:10.1039/c39830000536
162. Hawecker J, Lehn J-M, Ziessel R (1984) Electrocatalytic reduction of carbon dioxide mediated by $Re(bipy)(CO)_3Cl$ (bipy=2,2′-bipyridine). Chem Commun 6:328–330. doi:10.1039/c39840000328
163. Hawecker J, Lehn J-M, Ziessel R (1986) Photochemical and electrochemical reduction of carbon dioxide to carbon monoxide mediated by (2,2′-bipyridine)tricarbonylchlororhenium (I) and related complexes as homogeneous catalysts. Helv Chim Acta 69(8):1990–2012. doi:10.1002/hlca.19860690824
164. O'Toole TR, Margerum LD, Westmoreland TD, Vining WJ, Murray RW, Meyer TJ (1985) Electrocatalytic reduction of CO_2 at a chemically modified electrode. Chem Commun 20:1416–1417. doi:10.1039/c39850001416
165. Cabrera CR, Abruña HD (1986) Electrocatalysis of CO_2 reduction at surface modified metallic and semiconducting electrodes. J Electroanal Chem Interfacial Electrochem 209 (1):101–107. doi:10.1016/0022-0728(86)80189-9
166. Cosnier S, Deronzier A, Moutet J-C (1986) Electrochemical coating of a platinum electrode by a poly(pyrrole) film containing the *Fac*-Re(2,2′-bipyridine)$(CO)_3Cl$ system application to electrocatalytic reduction of CO_2. J Electroanal Chem Interfacial Electrochem 207 (1–2):315–321. doi:10.1016/0022-0728(86)87080-2
167. Cosnier S, Deronzier A, Moutet J-C (1988) Electrocatalytic reduction of CO_2 on electrodes modified by Fac-Re(2,2′-bipyridine)$(CO)_3Cl$ complexes bonded to polypyrrole films. J Mol Catal 45(3):381–391. doi:10.1016/0304-5102(88)80070-1

168. Yaroshevsky AA (2006) Abundances of chemical elements in the Earth's crust. Geochem Int 44(1):48–55. doi:10.1134/s001670290601006x
169. Brimm EO, Lynch MA, Sesny WJ (1954) Preparation and properties of manganese carbonyl. J Am Chem Soc 76(14):3831–3835. doi:10.1021/ja01643a071
170. Abel EW, Wilkinson G (1959) Carbonyl halides of manganese and some related compounds. J Chem Soc 1501–1505. doi:10.1039/jr9590001501
171. Johnson FPA, George MW, Hartl F, Turner JJ (1996) Electrocatalytic reduction of CO_2 using the complexes [Re(bpy)$(CO)_3$L]n (n = +1, L = $P(OEt)_3$, CH_3CN; n = 0, L = Cl−, Otf−; bpy = 2,2′-bipyridine; Otf − = CF_3SO_3) as catalyst precursors: infrared spectroelectrochemical investigation. Organometallics 15(15):3374–3387. doi:10.1021/om960044+
172. Hartl F, Rossenaar BD, Stor GJ, Stufkens DJ (1995) Role of an electron-transfer chain reaction in the unusual photochemical formation of five-coordinated anions [Mn$(CO)_3$(-α-diimine)]- from *Fac*-[Mn(X)$(CO)_3$(α-diimine)] (X=halide) at Low temperatures. Recl Trav Chim Pays Bas 114(11–12):565–570. doi:10.1002/recl.19951141123
173. Hartl F, Rosa P, Ricard L, Le Floch P, Záliš S (2007) Electronic transitions and bonding properties in a series of five-coordinate "16-electron" complexes [Mn$(CO)_3(L_2)$]$^-$ (L_2=chelating redox-active π-donor ligand). Coord Chem Rev 251(3–4):557–576. doi:10.1016/j.ccr.2006.09.003
174. Bourrez M, Molton F, Chardon-Noblat S, Deronzier A (2011) [Mn(bipyridyl)$(CO)_3$Br]: an abundant metal carbonyl complex as efficient electrocatalyst for CO_2 reduction. Angew Chem Int Ed 50(42):9903–9906. doi:10.1002/anie.201103616
175. Smieja JM, Sampson MD, Grice KA, Benson EE, Froehlich JD, Kubiak CP (2013) Manganese as a substitute for rhenium in CO_2 reduction catalysts: the importance of acids. Inorg Chem 52(5):2484–2491. doi:10.1021/ic302391u
176. Zeng Q, Tory J, Hartl F (2014) Electrocatalytic reduction of carbon dioxide with a manganese (I) tricarbonyl complex containing a nonaromatic α-diimine ligand. Organometallics 33 (18):5002–5008. doi:10.1021/om500389y
177. Fujita E, Creutz C, Sutin N, Szalda DJ (1991) Carbon dioxide activation by cobalt (I) macrocycles: factors affecting carbon dioxide and carbon monoxide binding. J Am Chem Soc 113(1):343–353. doi:10.1021/ja00001a048
178. Fujita E, Creutz C, Sutin N, Brunschwig BS (1993) Carbon dioxide activation by cobalt macrocycles: evidence of hydrogen bonding between bound CO_2 and the macrocycle in solution. Inorg Chem 32(12):2657–2662. doi:10.1021/ic00064a015
179. Fujita E, Furenlid LR, Renner MW (1997) Direct XANES evidence for charge transfer in Co − CO_2 complexes. J Am Chem Soc 119(19):4549–4550. doi:10.1021/ja970151a
180. Bhugun I, Lexa D, Savéant J-M (1994) Ultraefficient selective homogeneous catalysis of the electrochemical reduction of carbon dioxide by an iron(0) porphyrin associated with a weak broensted acid cocatalyst. J Am Chem Soc 116(11):5015–5016. doi:10.1021/ja00090a068
181. Bhugun I, Lexa D, Savéant J-M (1996) Catalysis of the electrochemical reduction of carbon dioxide by iron(0) porphyrins: synergystic effect of weak brönsted acids. J Am Chem Soc 118 (7):1769–1776. doi:10.1021/ja9534462
182. Bhugun I, Lexa D, Savéant J-M (1996) Catalysis of the electrochemical reduction of carbon dioxide by iron(0) porphyrins. Synergistic effect of Lewis acid cations. J Phys Chem 100 (51):19981–19985. doi:10.1021/jp9618486
183. Costentin C, Drouet S, Robert M, Savéant J-M (2012) A local proton source enhances CO_2 electroreduction to CO by a molecular Fe catalyst. Science 338(6103):90–94. doi:10.1126/science.1224581
184. Costentin C, Passard G, Robert M, Savéant J-M (2014) Pendant acid–base groups in molecular catalysts: H-bond promoters or proton relays? mechanisms of the conversion of CO_2 to CO by electrogenerated iron(0)porphyrins bearing prepositioned phenol functionalities. J Am Chem Soc 136(33):11821–11829. doi:10.1021/ja506193v
185. Costentin C, Passard G, Robert M, Savéant J-M (2014) Ultraefficient homogeneous catalyst for the CO_2-to-CO electrochemical conversion. Proc Natl Acad Sci U S A 111 (42):14990–14994. doi:10.1073/pnas.1416697111

Index